

# Technical Report

## TR-11-04

### Site description of the SFR area at Forsmark at completion of the site investigation phase

#### SDM-PSU Forsmark

Svensk Kärnbränslehantering AB

May 2013

**Svensk Kärnbränslehantering AB**

Swedish Nuclear Fuel  
and Waste Management Co

Box 250, SE-101 24 Stockholm  
Phone +46 8 459 84 00



ISSN 1404-0344

SKB TR-11-04

ID 1288472

# **Site description of the SFR area at Forsmark at completion of the site investigation phase**

## **SDM-PSU Forsmark**

Svensk Kärnbränslehantering AB

May 2013

*Keywords:* Kravdatabas SFR-utbyggnad (N2-272).

A pdf version of this document can be downloaded from [www.skb.se](http://www.skb.se).

# Preface

The Swedish Nuclear Fuel and Waste Management Company (SKB) has undertaken site characterisation in the SFR area at Forsmark in order to identify a suitable location for a planned extension of the existing final repository for short-lived radioactive waste (SFR). An integrated component of the characterisation work is the development of a site descriptive model (SDM) constituting a description of the site. The model describes the current state of the geosphere and the ongoing natural processes that influence its long-term evolution.

The site descriptive model concluding the site investigations for the extension of SFR, SDM-PSU, is compiled in the present report. A synthesis of the SDM report, focusing on model integration and the current model of the site, is presented in Chapter 9. This chapter serves as an executive summary.

The overall objective of the site descriptive modelling work at SFR is to develop and document an integrated description of the site, based on data from the site investigation work, as a basis for a site-adapted design of the extension and assessment of the repository's long-term radiological safety (SR-PSU).

The site descriptive modelling work performed within the site characterisation project was conducted by a multi-disciplinary project group. All individuals contributing to the project are gratefully acknowledged for making this report possible. Specifically, the following individuals contributed to this final report:

Magnus Odén – SDM PSU project leader.

Sven Follin – editor and site synthesis.

Kristina Skagius – co-editor.

Jakob Levén and Jesper Petersson – site investigation data.

Björn Söderbäck – site evolutionary aspects.

Kent Werner – surface system and surface-bedrock interactions.

Philip Curtis and Jesper Petersson – geology.

Eva Hakami – rock mechanics.

Johan Öhman and Sven Follin – hydrogeology.

Ann-Chatrin Nilsson, John Smellie and Eva-Lena Tullborg – hydrogeochemistry.

Ulf Brisning – production of maps and figures.

The report has been formally reviewed by the following members of the SFR extension project's own expert group SARG (SFR extension Application Review Group): Jordi Bruno (Chairman, Amphos 21); Michael C. Thorne (Mike Thorne and Associates Ltd); Alan Geoffrey Milnes (GEA consulting Rock Engineering); Derek Martin (University of Alberta); Russell Alexander (Bedrock Geosciences); Tommy Olsson (I&T Olsson AB); Kastriot Spahiu (SKB).

In addition, the report has been reviewed by the following people outside of SKB: Michael Stephens (SGU); Lee Hartely (Serco); Johan Holmén (Golder).

The reviewers provided many valuable comments and suggestions for this work. However, they are not to be held responsible for any remaining shortcomings of the report.

Magnus Odén

Project leader SDM-PSU

# Summary

The Swedish Nuclear Fuel and Waste Management Company (SKB) has undertaken site characterisation in the SFR area at Forsmark in order to identify a suitable location for a planned extension of the existing final repository for short-lived radioactive waste (SFR). The site investigation has been conducted mainly from the surface, and modelling has been carried out for the overall purpose of developing a descriptive model (SDM). The site descriptive model forms a basis for repository engineering aimed at designing the underground extension facility and developing a repository layout adapted to the site. It is also essential for safety assessment, since the model is a vital source of site-specific input. Another important use of the site descriptive model is in the environmental impact assessment.

The site descriptive model (SDM) presented in this report is an integrated model for bedrock geology, rock mechanics, bedrock hydrogeology and bedrock hydrogeochemistry of the site investigated in the SFR extension project (PSU). A description of the surface system is also included in the report. However, the surface system is not integrated with the other disciplines as new data regarding the surface system will not be available until after the completion of SDM-PSU. It is noted that SDM-PSU does not include all disciplines handled in SDM-Site Forsmark (SKB 2008b), the focus is to produce a site description that meets the needs of the SFR extension project. The overall objective of the SFR extension project is to have the application for the extension ready by 2013.

This report presents an integrated site model incorporating the historic data acquired from the investigations for and construction of the existing SFR facility (1980–1986), as well as from the recent investigations for the planned extension of SFR (2008–2009). It also provides a summary of the abundant underlying data and the discipline-specific models that support the integrated site model. The description relies heavily on background reports concerning detailed data analyses and modelling in the different disciplines. It is noteworthy that the investigations conducted during the SFR extension project were guided by the choice of site prior to the investigations, which was based on the experience gained during the construction of the existing SFR facility.

The modelling work prior to the site descriptive model, SDM-PSU, has involved four different model versions: 0, 0.1, 0.2 and 1.0. Version 0 (SKB 2008a) was based on the information available at the start of the site investigation programme for the SFR extension. This information mainly includes data from the preceding Forsmark site investigation (SKB 2008b), along with documentation from the construction of the existing SFR facility. Each of the subsequent versions was planned to include models for geology, hydrogeology and hydrogeochemistry. A primary function of the initial model versions (0.1 and 0.2) was feedback to the ongoing site investigations. However, due to the rapid progress of the investigations, it was decided to omit the intermediate geological model version (0.2) and instead focus on the final version 1.0. For each of the disciplines, the version 1.0 model reports are the main background reports.

Primary data have been evaluated to devise an integrated conceptual model of the investigation area with regard to bedrock geology, rock mechanics, bedrock hydrogeology, and bedrock hydrogeochemistry. Although confidence in the occurrence of steeply dipping deterministic deformation zones in the target volume intended for the SFR extension facility is high and the occurrence of undetected steeply dipping deformation zones longer than 300 m is judged unlikely, the sub-horizontal to gently dipping structures above –200 m elevation make a much more significant contribution to the pattern of local groundwater flow in the upper part of the bedrock than the steeply dipping deformation zones. These structures include several possible deformation zones recognised in the boreholes that were not possible to model deterministically using the procedures adopted in the geological modelling work and were judged to be minor structures with a size below the level of resolution adopted for this work. In conclusion, the principal remaining uncertainty in SDM-PSU concerns the occurrence, size, nature and transmissivity of sub-horizontal to gently dipping structures in the uppermost part of the bedrock. Additional boreholes and hydraulic testing together with a geological discrete fracture network (DFN) model could possibly have improved the structural-hydraulic modelling in this regard.

In SDM-PSU, the issue was handled in the hydrogeological modelling work by including a shallow bedrock aquifer (SBA) concept for some of the unresolved possible deformation zones together with a conditional hydrogeological DFN model for the remaining unresolved possible deformation zones, similar to that used in SDM-Site Forsmark. Eight so-called SBA-structures have been inferred from the acquired structural and/or hydraulic data. In the context of data support and interpreted spatial extent in 3D space, the confidence in existence of the deterministically modelled SBA-structures varies. A primary idea with their present interpretation in the hydrogeological model is to allow for a discussion about their potential importance for safety assessment since current data suggest that transmissive, sub-horizontal to gently dipping structures may intersect the rock vaults of the planned extension of the existing SFR facility depending on the decided location.

# Contents

<b>1</b>	<b>Introduction</b>	11
1.1	Background	11
1.2	Final disposal of short-lived radioactive waste at SFR	11
1.3	The scope and role of the site description	12
1.4	Setting	12
1.5	Objectives and strategy of the site descriptive modelling work at SFR	13
1.6	Methodology and organisation of the work	16
	1.6.1 Methodology	16
	1.6.2 Interfaces between disciplines	16
	1.6.3 Organisation of work	16
	1.6.4 Quality assurance aspects	17
	1.6.5 Nomenclature	17
1.7	This report and supporting documents	19
<b>2</b>	<b>Investigations, available data and other prerequisites for the modelling</b>	21
2.1	Overview of investigations	21
2.2	Surface-based investigations	23
2.3	Tunnel investigations in the SFR facility	25
2.4	Borehole investigations	28
	2.4.1 Geophysical borehole investigations	31
	2.4.2 Geological borehole investigations	31
	2.4.3 Hydrogeological borehole investigations	32
	2.4.4 Hydrogeochemical borehole investigations	33
2.5	Monitoring	34
2.6	Geographical data	35
2.7	Model domains, volumes and areas	35
2.8	Model versions	36
	2.8.1 Version 0.1	37
	2.8.2 Version 0.2	37
	2.8.3 Version 1.0	37
2.9	Design of the existing SFR facility and the extension, preliminary layout L0	38
	2.9.1 The existing SFR facility	38
	2.9.2 The SFR extension, preliminary layout L0	38
<b>3</b>	<b>Evolutionary aspects</b>	41
3.1	Bedrock evolution during the Proterozoic and Phanerozoic eons	41
	3.1.1 Bedrock evolution in southeastern Sweden	41
	3.1.2 Bedrock evolution in the Forsmark area	44
3.2	Palaeoclimate and geological evolution during the Quaternary period	46
3.3	Seismicity during the Quaternary period	49
3.4	Groundwater evolution during the Quaternary period	50
3.5	Evolution of ecosystems during the late Quaternary period	52
3.6	Human population and land use	53
<b>4</b>	<b>Surface system and surface-bedrock interactions</b>	55
4.1	Abiotic characteristics	56
	4.1.1 Topography	56
	4.1.2 Regolith	57
	4.1.3 Meteorology, hydrology and near-surface hydrogeology	59
	4.1.4 Coastal oceanography	60
	4.1.5 Hydrogeochemistry	62
4.2	Ecosystems	62
	4.2.1 Terrestrial ecosystems	62
	4.2.2 Limnic ecosystems	63
	4.2.3 Marine ecosystems	65

4.3	Human utilisation and natural resources	65
4.4	Surface-bedrock interactions	65
4.4.1	Hydrology and hydrogeology	65
4.4.2	Hydrogeochemistry and solute transport	66
4.5	Confidence and uncertainties	67
<b>5</b>	<b>Bedrock geology</b>	<b>69</b>
5.1	Overview	69
5.2	Evaluation of primary data	71
5.2.1	Geological tunnel data from SFR	71
5.2.2	Rock units and possible deformation zones in boreholes	73
5.2.3	Major groups and types of rocks – properties, alteration and volumetric proportions	73
5.2.4	Ductile deformation	75
5.2.5	Brittle deformation	77
5.2.6	Identification, character and geological significance of lineaments	81
5.2.7	Character and geological significance of seismic data	82
5.2.8	Inversion modelling of ground magnetic data	83
5.3	Rock domain model	84
5.3.1	Conceptual understanding of the rock domains	84
5.3.2	Methodology and assumptions	85
5.3.3	Geometric model and property assignment	85
5.3.4	Character of rock domains	87
5.4	Deformation zone model	89
5.4.1	Conceptual understanding of the deformation zone model	89
5.4.2	Methodology and assumptions	91
5.4.3	Geometric models and property assignment	92
5.4.4	Character of different sets of zones	95
5.5	Confidence and remaining uncertainties	103
5.5.1	Deterministic model for rock domains	103
5.5.2	Deterministic model for deformation zones	104
<b>6</b>	<b>Rock mechanics</b>	<b>107</b>
6.1	Intact rock properties	107
6.1.1	Compressive strength	107
6.1.2	Tensile strength	111
6.1.3	Deformation properties	111
6.2	Single fracture properties	112
6.2.1	Normal and shear stiffness	113
6.2.2	Hydraulic normal stiffness	117
6.2.3	Single fracture strength parameters	118
6.2.4	Single fracture property model	118
6.3.	Rock mass mechanics properties	118
6.3.1	Rock domains	118
6.3.2	Deformation zones	120
6.4	<i>In situ</i> state of stress	121
6.4.1	Primary data	121
6.4.2	Rock stress magnitude	122
6.4.3	Rock stress orientation	124
6.4.4	Rock stress model for SFR	126
6.5	Confidence and remaining uncertainties	126
6.5.1	Intact rock mechanics properties	126
6.5.2	Single fractures mechanics properties	126
6.5.3	Rock mass mechanics properties	126
6.5.4	<i>In situ</i> stress conditions	127

<b>7</b>	<b>Bedrock hydrogeology</b>	129
7.1	Overview of hydrogeological modelling	129
7.2	Evaluation of primary data	132
7.2.1	Observations from the existing SFR facility	133
7.2.2	Measured heads in 2010	137
7.2.3	Interference tests and hydraulic responses during drilling	140
7.2.4	Integration with geology and hydrogeochemistry	146
7.2.5	Orientation and intensity of open fractures	148
7.2.6	Single-hole hydraulic tests	150
7.3	Hydrogeological model for the bedrock – conceptualisation and modelling methodology	154
7.3.1	Inflow and groundwater levels	154
7.3.2	Transmissivity in the bedrock along HCDs	154
7.3.3	Transmissivity of fractures in the bedrock outside HCDs	156
7.3.4	Summary	166
7.4	Parameterisation of hydraulic domains	166
7.4.1	Hydraulic conductor domains	166
7.4.2	Hydraulic rock mass domains	167
7.4.3	Shallow bedrock aquifer structures	168
7.5	Groundwater flow modelling	170
7.6	Confidence and remaining uncertainties	179
7.6.1	Integration with geology and hydrogeochemistry	179
7.6.2	Discipline-specific issues	179
<b>8</b>	<b>Bedrock hydrochemistry</b>	181
8.1	Overview	181
8.1.1	Palaeohydrochemistry	181
8.1.2	Investigation prerequisites	181
8.1.3	Interpretation and modelling	182
8.1.4	Integration with geology and hydrogeology	183
8.2	Methodology	184
8.3	Groundwater type categorisation and groundwater origins	186
8.3.1	Present conceptual model	186
8.3.2	Groundwater types	188
8.3.3	Groundwater residence time	188
8.4	Groundwater composition and reactions	190
8.4.1	Major ion trends and behaviour	190
8.4.2	Redox geochemical systems and redox-buffering capacity	194
8.4.3	Uranium, radium and radon	196
8.5	Hydrogeochemical site description and visualisation	196
8.5.1	Structural and hydrochemical considerations	196
8.5.2	Possible pore water trends	198
8.5.3	The influence of the SFR on groundwater chemistry	199
8.5.4	Hydrogeochemical conceptual model	202
8.6	Confidence and uncertainty in the hydrogeochemical model	204
8.6.1	Measured and modelled uncertainties	204
8.6.2	General confidence level	206
<b>9</b>	<b>Current understanding of the site</b>	207
9.1	Introduction	207
9.2	Surface system	207
9.3	Rock domain model and general fracture characteristics	209
9.4	Current stress field	213
9.5	Deformation zones and their transmissivity	213
9.5.1	Geological data and modelling	213
9.5.2	Hydraulic properties	216



9.6	Hydrogeological model of the rock mass between deformation zones	218
9.6.1	Open fractures	218
9.6.2	Flowing fractures	218
9.6.3	Shallow bedrock aquifer concept	220
9.6.4	Delineation of discrete features for stochastic modelling	222
9.6.5	Modelling of residual HRDs	224
9.7	Groundwater – composition and flow	227
9.7.1	Hydrogeochemical data and modelling	227
9.7.2	Integrated conceptual model	230
9.7.3	Flow to the existing SFR facility	232
9.8	Remaining key uncertainties	236
9.9	Groundwater flow modelling in SR-PSU	237
9.9.1	Hydrogeological base case	237
9.9.2	Model variants	238
<b>10</b>	<b>Conclusions</b>	<b>239</b>
	<b>References</b>	<b>241</b>
<b>Appendix 1</b>	Map of the Forsmark and SFR area	251
<b>Appendix 2</b>	List of abbreviations	253
<b>Appendix 3</b>	Tables with references to primary data	255
<b>Appendix 4</b>	Properties of deformation zones modelled to intersect the SFR local model volume	261
<b>Appendix 5</b>	DFN parameters suggested for usage in the SFR extension project	417
<b>Appendix 6</b>	Final deformation-zone parameterisation	419

# 1 Introduction

## 1.1 Background

Radioactive waste from nuclear power plants is managed by the Swedish Nuclear Fuel and Waste Management Co, SKB. The first stage of the final repository for short-lived radioactive waste (SFR) was constructed and taken into operation in 1988. During 2008, SKB initiated an investigation programme for a future extension of the facility. This extension of SFR is required due to the upcoming decommissioning of the closed reactors (Barsebäck, Studsvik, and Ågesta), the increased amounts of operational waste resulting from the extended operating time of the remaining nuclear power plants, and the future decommissioning of the remaining nuclear power plants (SKB 2008a). The overall objective of the SFR extension project (PSU) is to have the application for the extension finalised at 2013, and the site descriptive model (SDM) presented in this report will support the application.

The site investigation was conducted between April 2008 and January 2010. The quality-assured site data have then been analysed and modelling has been carried out for the overall purpose of developing a site descriptive model. The SDM for the SFR extension project, SDM-PSU, is an integrated model for geology, rock mechanics, hydrogeology and hydrogeochemistry. A description of the surface system is also included in the report. However, the surface system is not integrated with the other disciplines as new data regarding the surface system will be available first after the completion of SDM-PSU. The site investigations did not include investigations into the mechanical properties (e.g. *in situ* stress or strength) of the rock, since adequate information existed from the investigations for the existing SFR facility and the experience gained during its construction. In this report, a rock mechanics site descriptive model of the SFR area is presented based partly on data from the existing SFR facility and partly on data collected during the Forsmark site investigations.

It is important to notice that the objective of SDM-PSU is not to produce a site description covering all disciplines in SDM-Site Forsmark (SKB 2008b). Rather, the focus is to produce a site description that meets the needs of the PSU project. Hence, not all disciplines that were covered in SDM-Site Forsmark are relevant for SDM-PSU.

This report presents an integrated model of the site and provides a summary of the models and the underlying data supporting the current site understanding.

## 1.2 Final disposal of short-lived radioactive waste at SFR

SKB manages and disposes of three types of nuclear waste: operational waste, decommissioning waste and spent nuclear fuel. The level of radioactivity and its physical and chemical form determine how the waste is handled.

Short-lived, low- and intermediate-level operational waste – such as used ion exchange resins, protective clothing and replaced parts from the power plants – constitutes over 80% (by volume) of all nuclear waste. This waste is deposited in rock vaults in the existing SFR facility.

When the nuclear power plants are decommissioned, it will also be necessary to manage the radioactive waste (such as scrap metal and structural material) that is generated. Like operational waste, all of this waste is short-lived, low- and intermediate-level. This waste must be isolated from human beings and the environment in the same way as operational waste.

Because of the decommissioning waste and the additional amount of operational waste caused by the extended operational time of the existing nuclear power plants, an extension of the SFR facility is needed and is expected to be operational by 2020.

### 1.3 The scope and role of the site description

Site characterisation should provide all the site-specific data required for an integrated evaluation of the suitability of the investigated site for a geological repository, and a fundamental component of the characterisation work is the development of a site descriptive model. As stated in Section 1.1, SDM-PSU is an integrated model mainly for geology, rock mechanics, hydrogeology and hydrogeochemistry. Full integration with the surface system will be done in the safety assessment (SR-PSU). Since no new rock mechanics data have been acquired during the SFR extension investigation, the existing data have been evaluated with regard to the new geological model.

The objective of SDM-PSU is not to produce a site description covering all disciplines in SDM-Site Forsmark (SKB 2008b). Rather, the focus is to produce a site description that meets the needs of the SFR extension project. Hence, not all disciplines that were covered in SDM-Site Forsmark are relevant for SDM-PSU. At an early stage of PSU it was decided that no additional data or modelling regarding transport properties or thermal properties were needed from SDM-PSU. Another important decision was that a geological DFN model for all fractures was not needed, i.e. the rock mass between deformation zones is described only by a hydrogeological DFN model for open and flowing fractures.

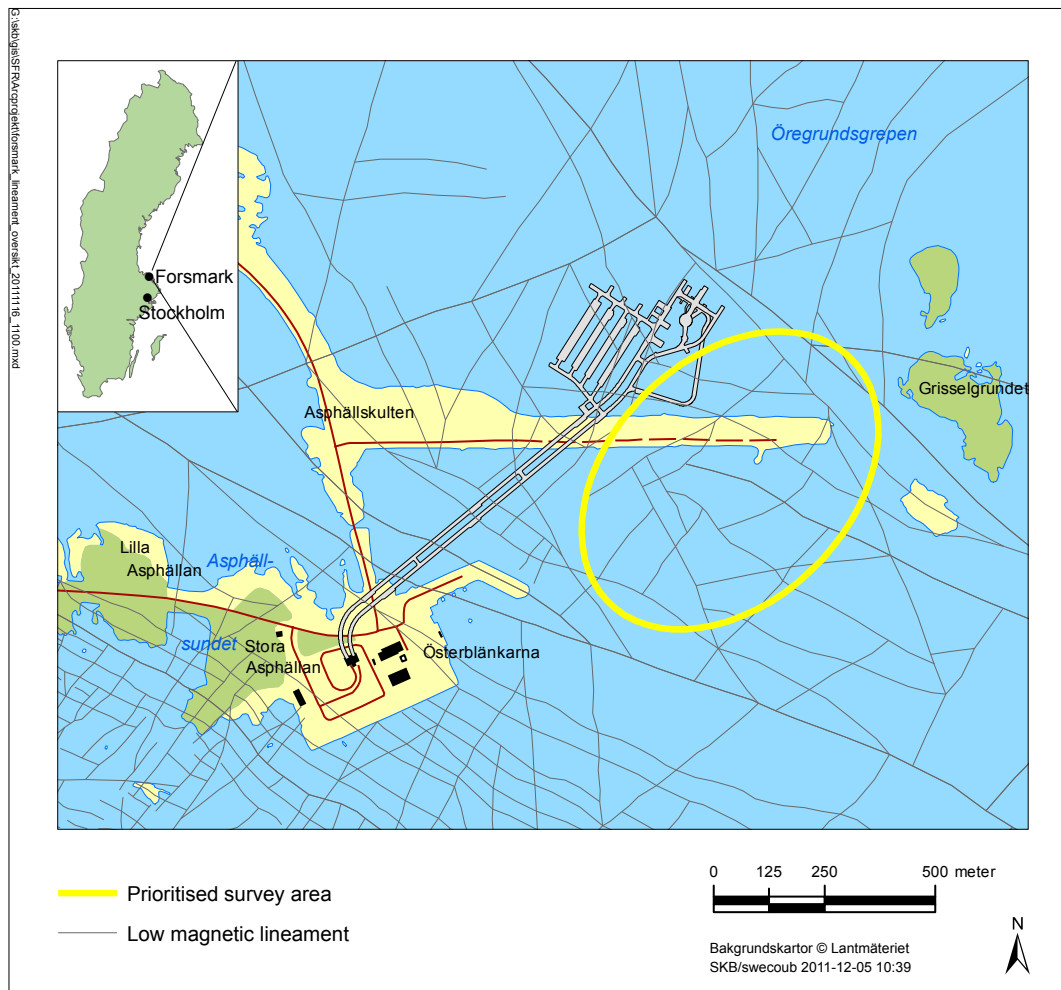
Quality-assured site characterisation data stored in the SKB database Sicada and in the SKB geographic information system (GIS) comprise the input to site descriptive modelling. The results of the site descriptive model are used to adapt the repository layout to site conditions, and as input to the design of the underground facility. They are also essential for the safety assessment. Another important use of the site descriptive model is in the environmental impact assessment. Furthermore, it helps to provide a general site understanding to various stakeholder groups.

In the SKB programme, a site description is a description of the site including the current state of the geosphere and the biosphere as well as descriptions of ongoing natural processes that can influence their long-term evolution. However, it is not the task of the site description to make any predictions regarding the future evolution of site conditions. This is done within safety assessment based on the understanding of current conditions and past evolution compiled in the site description. It is also not the task of site descriptive modelling to evaluate the impact on current site conditions of the excavation or operation of a repository extension at the site. This is carried out within the framework of repository engineering and as part of the environmental impact assessment, but again based on input from the site description.

### 1.4 Setting

The Forsmark area is located in northern Uppland within the municipality of Östhammar, about 120 km north of Stockholm. The prioritised survey area for the SFR site investigation is located north of the area selected for the final repository for spent nuclear fuel, in an area that is below the sea and southeast of the existing SFR (Figure 1-1). The prioritised survey area for the site investigations was selected prior to the start of the investigations, and the reasons for selecting this area are presented in SKB (2008a). The main reason is that this area was deemed more favourable than the other alternatives listed in SKB (2008a) due to the following factors:

- Existing knowledge of geological conditions prior to the SFR site investigations indicated a suitable rock mass.
- No need to construct tunnels through the deformation zones ZFMNW805A and –B (Northern boundary belt).
- Boreholes can be drilled from the pier.
- Minimal disturbance of the operation of the existing SFR facility.



*Figure 1-1. Location of the prioritised survey area for the site investigations.*

The current ground surface in the Forsmark region forms a part of the sub-Cambrian peneplain in southeastern Sweden. This peneplain represents a relatively flat topographic surface with a gentle dip towards the east that formed more than 540 million years ago. The Forsmark area is characterised by a small-scale topography at low elevation (Figure 1-2). The most elevated areas to the southwest are located at c. 25 m above current sea level. The whole area is located below the highest coastline associated with the last glaciation, and large parts of the area emerged from the Baltic Sea only during the last 2,000 years. Both the flat topography and the still ongoing shoreline displacement of c. 6 mm per year strongly influence the current landscape. Sea bottoms are continuously transformed into new terrestrial areas or freshwater lakes, and lakes and wetlands are successively covered by peat. Most of the prioritised survey area is covered by sea water at present (Figure 1-2), but the seabed will continue to rise and the seabed above the prioritised survey area will be at the shoreline within approximately 1,000 years (3000 AD).

## 1.5 Objectives and strategy of the site descriptive modelling work at SFR

The overall objective of the current site descriptive modelling work (SDM-PSU) is to develop and document an integrated description of the area surrounding the existing SFR facility, i.e. the SFR regional model domain (see Figure 1-3), that meets the needs of the PSU project. The local model domain has a higher data intensity and covers the volume that hosts the existing SFR facility and that is expected to also host the planned extension, whereas the regional model domain covers a larger volume that places the description of the local volume in a larger context.



**Figure 1-2.** Photographs from Forsmark showing a) the prioritised survey area (yellow) together with the existing SFR facility, and b) the flat topography and the low-gradient shoreline with recently isolated bays due to land uplift.

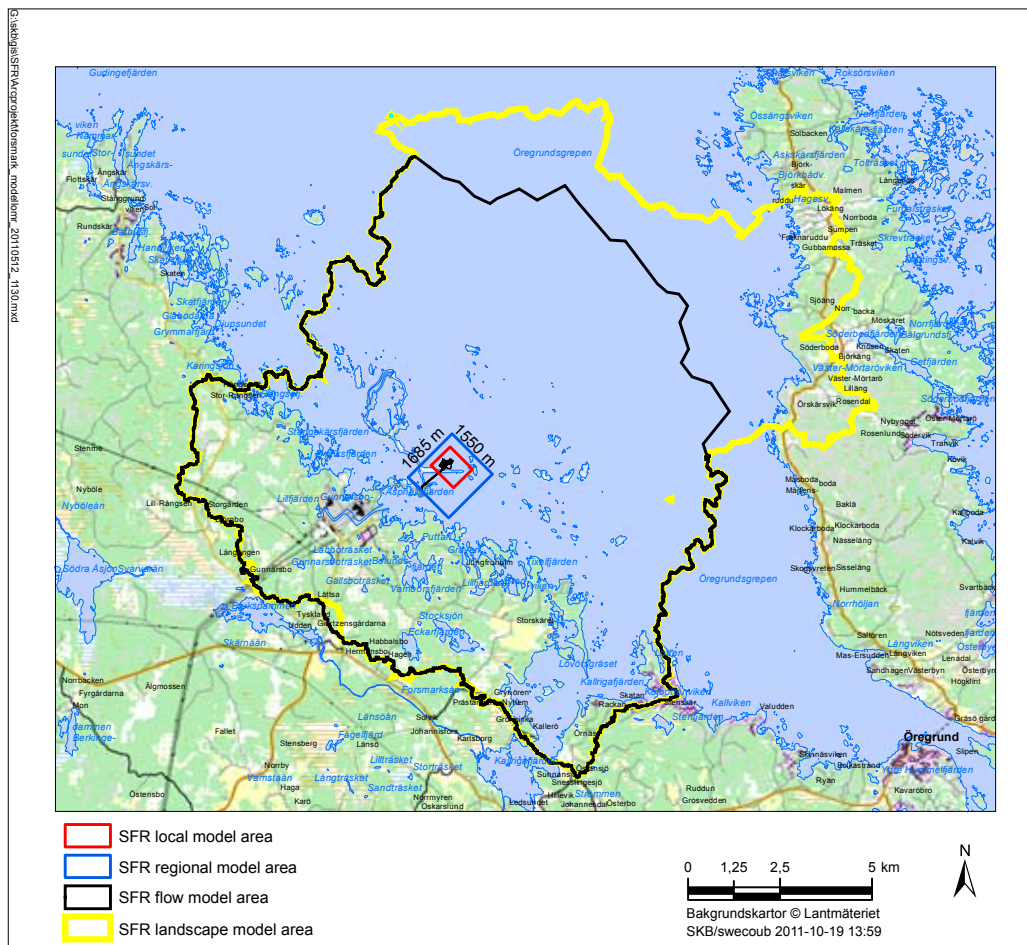
The strategy for the site descriptive modelling is described in more detail in SKB (2008a). The description is based on historic data as well as on data from the site investigation work conducted for the planned extension of the existing SFR facility. SDM-PSU is intended to be a basis for a site-adapted design of this extension as well as for an assessment of the entire repository's long-term radiological safety (SR-PSU).

The description has to be based on a fundamental understanding of the bedrock and surface systems. To demonstrate that this understanding is sufficient, the reliability and reasonability of the assumptions made with respect to the current state and naturally ongoing processes have to be assessed. Furthermore, the work must utilise all knowledge and understanding built into previous model versions and the feedback obtained from the safety assessment SAR08 (SKB 2008c).

The specific objectives of the work are to:

- analyse the primary site characterisation data produced within the recently concluded site investigation and the historic data available at the start of this investigation,
- describe the evolution of the site from the time the bedrock formed to the current day,
- develop a three-dimensional integrated site descriptive model including geology, rock mechanics, hydrogeology and hydrogeochemistry, and
- perform an overall confidence assessment including an evaluation of alternative interpretations.

The strategy applied for achieving the stated objectives is to base the site descriptive model on the quality-assured, geoscientific field data in the SKB databases Sicada and GIS. The methodology is described in more detail in Section 1.6.



**Figure 1-3.** Regional (blue) and local (red) model areas for SFR model version 1.0 relative to the flow model area SFR (black) defined by surface water divides, as well as the model area for the landscape model (yellow).

## **1.6 Methodology and organisation of the work**

### **1.6.1 Methodology**

The project is multi-disciplinary in that it covers potential properties of the site that are of importance for its overall understanding, for the design of the extension to the SFR repository, for the safety assessment and for the environmental impact assessment. The overall strategy employed in the work has been to develop discipline-specific models by interpretation and analyses of the quality-assured primary data that are stored in the SKB databases Sicada and GIS, and then to integrate these discipline-specific models into a unified site description. The quantitative, discipline-specific models are stored in the SKB database SKBdoc, from where quality-assured versions of the models can be accessed by the users of the site description. Quality assurance aspects of the modelling procedure are further described in Section 1.6.4.

The site descriptive modelling comprises the iterative steps of evaluation of primary data, descriptive and quantitative modelling in 3D, and evaluation of the confidence in the resulting models. Data are first evaluated within each discipline and then the evaluations are cross-checked between the disciplines. This is followed by three-dimensional modelling for the purpose of estimating the distribution of parameter values in space as well as their uncertainties. In this context, the geological models provide the geometrical framework for all discipline-specific modelling. The three-dimensional description presents the parameters with their spatial variability over a relevant and specified scale, with the uncertainty included in this description. If required, different alternative descriptions are provided.

The modelling work conducted during the SFR extension project followed the guidelines in the following reports:

- Geological site descriptive modelling (Munier et al. 2003).
- Hydrogeological site descriptive modelling (Rhén et al. 2003).
- Hydrogeochemical site descriptive modelling (Smellie et al. 2002).

New experience of methodology issues was also gained during the course of the iterative process of site descriptive modelling for a spent fuel repository at Forsmark (SKB 2008b) and Laxemar (SKB 2009). When appropriate, this experience has been adopted into the methodologies employed and has also, in some cases, resulted in updates to, or amendments of, the strategy reports.

### **1.6.2 Interfaces between disciplines**

The geological model is central to the description of the bedrock and provides the geometrical context in terms of the characteristics of the deterministically modelled deformation zones. Using the deterministic geological model as a basis, descriptive and quantitative models for the other geoscientific disciplines (rock mechanics, hydrogeology and hydrogeochemistry) have been developed for the bedrock. In the work reported here, the rock mechanics modelling is limited to an analysis of historic data with regard to the updated deterministic geological model.

Development of these models has, in turn, highlighted issues of potential importance for the bedrock geological model. Another important interface is that between hydrogeology and hydrogeochemistry, which has been handled, for example, by producing combined descriptions of flow paths and water types in different zones.

The handling of the interfaces between disciplines is described in more detail in Chapter 4 (surface system) and Chapters 5 through 8 (bedrock system).

### **1.6.3 Organisation of work**

The work has been conducted by a project group containing representatives of the disciplines geology, hydrogeology, hydrogeochemistry and surface systems. In addition, certain group members have specific qualifications of importance in this type of project for example expertise in RVS (Rock Visualisation System) modelling, GIS modelling and statistical data analysis.

Each discipline representative in the project group was given responsibility for the assessment and evaluation of primary data and for the modelling work concerning his or her specific discipline. This task was then carried out either by the representatives working alone or together with other experts or groups of experts outside the project group.

#### **1.6.4 Quality assurance aspects**

In order to ensure that the site descriptive model is based on qualified data and that the model and sub-models derived from these qualified data are correct and are the models that are delivered to, and employed by, the users, a number of quality assurance (QA) procedures and instructions in the SKB quality assurance system have been followed. The process used to progress from collection of primary data to models available to the downstream users, as defined by the QA procedures and applied in the site modelling, is summarised briefly below.

All primary data collected in the field and from laboratory measurements are stored in the SKB databases Sicada and GIS. Before delivery to the database operator, the data are reviewed and approved by the person responsible for the field activity furnishing the data (activity leader). The database operator transfers the data to the database and then exports the same data from the database. The data exported from the database are then checked by the database operator and the activity leader to ensure that no mistakes are made in transferring the data to the database. When everything is found to be in order, the activity leader approves the data by his or her signature. The execution of this process is specified in the SKB QA document SDK-508.

Primary data collected at the site and used in the site descriptive modelling are only extracted from the databases Sicada and GIS. Information regarding the procedures for data collection and factors of importance in the interpretation of data is provided in the documentation (SKB's P report series) of the data collection activity, but the primary data have to be ordered from the databases. Only approved (signed) data may be delivered to users of the data. All orders and deliveries of data from the databases are registered, making it possible to trace all data deliveries. The execution of the process of order and delivery of data from the databases is specified in the SKB QA documents SDVI-200 (Sicada) and SDVI-203 (GIS).

Errors in data identified during the subsequent analytical and modelling work are reported by the modeller. The errors are compiled in a list that is published on SKB's internal website. It is the responsibility of the users of the data to report all errors found and to keep up-to-date on the data errors reported. For all errors reported, the type of error is identified and corrective actions are taken. The actions taken are documented in the data error list and corrected data are transferred to the databases according to the procedure described above. The procedure for handling errors in primary data is specified in the SKB QA document SD-141.

The discipline-specific models developed within site modelling, using quality-assured data according to the procedures described above, are stored in the SKB database SKBdoc. In this context, the term "models" refers to, for example, 3D models of the geometry of deformation zones, 2D models of surface objects, and DFN model parameters. Before the models are officially released to downstream users, they are approved by the person who is responsible for a specific discipline at SKB. The only models that are allowed to be used by e.g. repository engineering and safety assessment are the approved versions downloaded from SKBdoc. The model database is also used for internal deliveries within the site modelling project. Instructions for the use of the model database are compiled in the SKB QA document SDU-203.

The peer review of previous and current model versions conducted by SFR extension project's own expert group SARG (SFR extension Application Review Group) is also important in a quality assurance context. The work of SARG focuses on reviewing main reports essential for the application, but also on providing guidance to the project management on vital issues.

#### **1.6.5 Nomenclature**

Some definitions are provided here for terms that are of basic importance for the modelling and description. Most of these are geological terms that are related to the geometrical framework of the modelling and are, as a consequence, common to all disciplines. Definitions of abbreviations are provided in Appendix 2.



<b>Fracture (broken, unbroken, sealed, open and partly open)</b>	A natural break in the rock. In drill cores, there are broken and unbroken fractures, depending on whether the core is split or not. Broken fractures include both open fractures and originally sealed fractures which were broken during the drilling or the following treatment of the drill core. To decide if a fracture was open, partly open or sealed <i>in situ</i> , SKB has developed a classification system. A broken fracture is classified as open if it fulfils one of the following criteria: (1) distinguishable aperture in the borehole image, (2) weathered or altered fracture surfaces or (3) a poor fit of the fracture planes. Otherwise it is mapped as sealed. Unbroken fractures are generally classified as sealed, except in those cases where they display macroscopically distinguishable apertures and consequently are classified as partly open.
<b>Crush zone</b>	Shattered rock with a very high frequency of open fractures.
<b>Sealed fracture network</b>	In drill cores, a length interval where the intensity of sealed fractures is too high and/or where the fractures are too irregular to allow mapping of individual fractures. Generally the distance between individual fractures is less than 3 cm. In the case of a very high intensity of sealed fractures with concomitant rotation of rock fragments, the term breccia is used.
<b>Deformation zone</b>	Deformation zone is a general term that refers to an essentially 2D structure along which there is a concentration of brittle, ductile or combined brittle and ductile deformation. Brittle deformation zones generally consist of one or several zones of crushed and/or intensely fractured material (core zones) surrounded by zones of fractured and/or hydrothermally altered rock (damage zones). Deformation zones at Forsmark are denoted ZFM followed by two to eight letters or digits. An indication of the orientation of the zone is included in the identification code (e.g. ZFMNNW1209).
<b>Possible deformation zone</b>	Possible deformation zone (often labelled PDZ) is a term used by SKB to designate structures observed in boreholes which possess deformation-zone-type properties and thus may represent deformation zones in 3D. In the single-hole interpretation work, PDZs are identified on the basis of fracture frequency, rock alteration and focused resistivity along a borehole. Other data that have assisted in their identification include the occurrence of low radar amplitude anomalies in the borehole radar data, low magnetic susceptibility and caliper anomalies. Confidence in their existence is assigned to three classes: high, medium and low.
<b>Tunnel deformation zone</b>	In the present report, tunnel deformation zones (often labelled tDZ) refer to structures with a concentration of brittle deformation (i.e. fracture zones) that are presented in drawing -103 by Christiansson and Bolvede (1987).
<b>Rock unit</b>	A rock unit is defined in single-hole interpretation on the basis of the composition, grain size and inferred relative age of the dominant rock type. Other geological features include the degree of bedrock homogeneity, the degree and style of ductile deformation, and the occurrence of early-stage alteration (albitization) that affects the composition of the rock. Anomalous fracture frequency also helps define and distinguish some rock units.
<b>Rock domain</b>	A rock domain refers to a rock volume in which rock units that show specifically similar composition, grain size, degree of bedrock homogeneity, and, to some extent, degree and style of ductile deformation have been combined and distinguished from each other. In addition, the magnetic signature of the rock domain has been important in distinguishing SFR area. Different rock domains in the SFR local model volume are referred to as RFRxxx.
<b>Southern boundary belt</b>	A group of deformation zones including the regionally dominant Singö deformation zone (ZFMWNW0001) that can be said to define the southern boundary of the SFR Central Block (cf. Figure 5-2 and Figure 7-2). The belt consists of ZFMWNW0001 along with ZFMWNW0813, ZFMWNW3259, ZFMNW0002 and, to a lesser extent, ZFMWNW1035. In the SFR area, these zones merge to comprise a complex broad deformation "belt" of concentrated ductile and brittle deformation. The belt has an overall thickness of c. 200–400 m and a length of over 30 km.
<b>Northern boundary belt</b>	Deformation zone ZFMNW0805A and a smaller splay ZFMNW0805B that can be said to define the northern boundary of the SFR Central Block (cf. Figure 5-2 and Figure 7-2). It has a similar orientation and character as the Southern boundary belt, but is much smaller with a length of between 3 and 4 km and a thickness of c. 50–100 m. On a larger regional scale, the magnetic data suggest that it is probably a splay from the main Singö deformation zone. It has the same sequence of ductile deformation followed by brittle reactivation that is seen in the Southern boundary belt.
<b>Central block</b>	A tectonic block that is bounded to the northeast and southwest by two broad belts of concentrated ductile and brittle deformation. The Central block is less affected by deformation than the bounding belts.

## 1.7 This report and supporting documents

This report presents the integrated site model of the SFR regional model domain on completion of the site investigations and provides a summary of the models and the underlying data supporting the site understanding. The report is intended to describe the properties and conditions at the site and to provide information essential for demonstrating this understanding, but relies heavily on background reports concerning details of data analyses and modelling.

The version 1.0 model reports are the main background report for each of the disciplines to the SDM-PSU report. These background reports are listed below.

- Bedrock Geology, Site investigation SFR (Curtis et al. 2011).
- Bedrock Hydrogeology, Site investigation SFR (Öhman et al. 2012).
- Bedrock Hydrogeology – Groundwater flow modelling, Site investigation SFR (Öhman et al. 2013).
- Bedrock Hydrogeochemistry, Site investigation SFR (Nilsson et al. 2011).

The site descriptive modelling resulting in the final site description, SDM-PSU, has involved several modelling stages/versions. These are briefly described in Section 2.8.

The content of the remaining chapters of this report is as follows.

Chapter 2 summarises available primary data and provides an overview of previous model versions and other prerequisites for the modelling.

In Chapter 3, the current understanding of the evolution of the geosphere and the surface system over time is described.

Chapter 4 describes the surface system, with a focus on aspects of importance for the bedrock system.

Chapters 5 to 8 provide summaries of the modelling of bedrock geology, rock mechanics, hydrogeology and hydrogeochemistry, respectively.

In Chapter 9, the current model of the SFR regional model domain is summarised. It focuses on an integrated description that demonstrates consistency and, as such, it also functions as an executive summary for the SDM-PSU report.

Chapter 10 provides the conclusions from the work in terms of fulfilment of objectives and a look at the most important issues judged to merit further study prior to and during the underground construction phase in order to reduce remaining uncertainties in the description of the local model volume.

Finally, a geographical map of the Forsmark area is provided in Appendix 1, where the location of different local geographical names that are referred to in the site description can be found.

## 2 Investigations, available data and other prerequisites for the modelling

Since the start of the site investigations for the planned extension of SFR in 2008, more data have successively been added to the databases used in site descriptive modelling. The modelling has now reached the final integrated model version. This chapter provides a summary of the investigations behind the databases used for modelling.

The strategy for the site investigations (described in SKB 2008a) has been to characterise a pre-defined rock volume close to the existing SFR repository large enough to accommodate a repository with a storage capacity of at least 140 000 m<sup>3</sup>. Key issues for the investigation to address have been:

- the geological character of magnetic lineaments (as deformation zones, anisotropy related to rock type and/or ductile strain in the bedrock),
- the occurrence of highly transmissive fractures and fracture zones, and
- the mechanical properties of the bedrock as a basis for forthcoming repository engineering work.

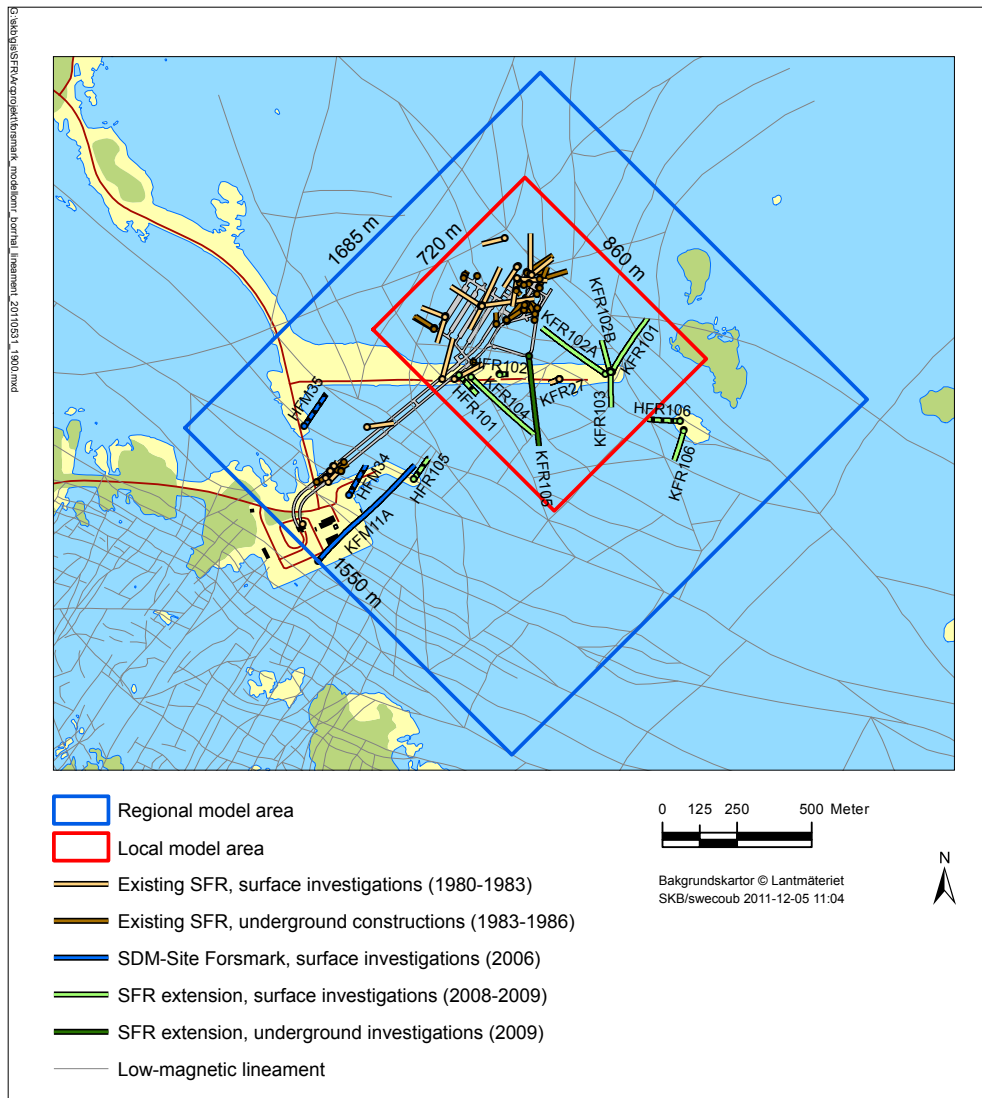
### 2.1 Overview of investigations

The data upon which the SFR site descriptive model (SDM) is based were acquired mainly during three different investigations. Figure 2-1 shows the boreholes from the different stages in relation to the regional and local model areas.

1. Investigations prior to and during the construction of the existing SFR facility, from 1980 to 1986, and the following monitoring programme relating to geoscientific parameters. This includes investigations for the construction of discharge tunnels from units 1–3 of the Forsmark nuclear power plant.
2. The site investigation at Forsmark for a final repository for spent nuclear fuel, which was undertaken from January 2002 to March 2007, along with associated monitoring of geoscientific parameters and ecological objects.
3. Site investigations for the planned extension of SFR, which were undertaken from April 2008 to January 2010.

There is a considerable quantity of geological documentation from the pre-investigations and construction of SFR. During the pre-investigation phase 1980 to 1983, surface boreholes were drilled from offshore platforms, from ice-cover, and from land. During the SFR construction phase, from 1983 to 1986, subsurface boreholes were drilled from underground openings and access tunnels. Totally, 60 cored boreholes were drilled. In addition, extensive geological information was obtained from the SFR access tunnels and underground openings.

Although the older data were quality assured by the standards used at the time of acquisition, they do not comply with current SKB standards of the SFR extension and Forsmark site investigations, in terms of investigation methodology, definitions and quality assurance. An important part of the work has therefore been to review and identify which of the older data could be the subject of further processing and quality checks, with the aim of reaching a level where they can be included in the SKB databases for use in the modelling work. Data from the later SFR extension and Forsmark site investigations have generally been given precedence over data from SFR construction. However, some older qualitative data, such as the geological tunnel mapping, have been considered key data of particular value in the modelling work.



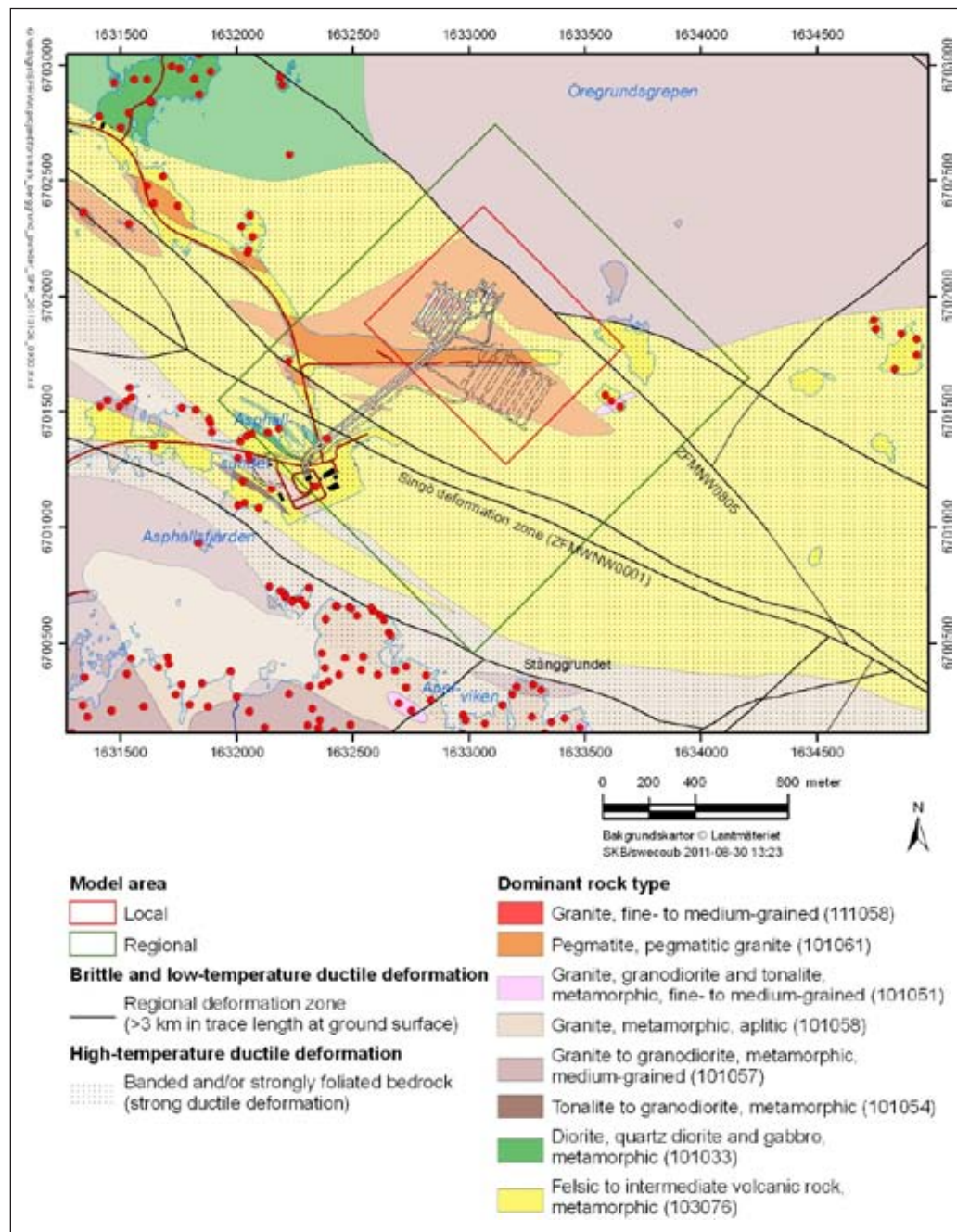
**Figure 2-1.** Map visualising the borehole coverage within the model area showing the horizontal component of inclined boreholes. Boreholes are colour coded by investigation project/period. Cored boreholes (KFRXX) are solid colour; percussion (HFRXX) boreholes have black dots.

The data acquisition during the three investigation programmes can be divided into a number of investigation categories, where boreholes and tunnel documentation are of key importance due to the sea coverage in the SFR area.

- Surface based geoscientific investigations. The majority of these data were acquired during the Forsmark site investigation and include ground geophysics and compilations in terms of bedrock and Quaternary geological maps.
- Tunnel investigations from the SFR construction phase along with an updated mapping of the lower construction tunnel (NBT) during the SFR extension project.
- Borehole investigations, comprising drilling, drilling measurements, logging, geological mapping and sampling of water and drill cores. The boreholes of relevance from the Forsmark site investigation are one telescopic borehole (see Section 2.4) and two percussion-drilled boreholes.
- Monitoring of geoscientific parameters, especially during and subsequent to the Forsmark site investigation, but also the SFR monitoring programme, which has generated data on inflows, groundwater levels and groundwater chemistry for some 25 years.
- Results and interpretations included in the various older SFR investigation and construction reports.

## 2.2 Surface-based investigations

A bedrock map over the mainland and archipelago at Forsmark, at the scale 1:10,000, was generated during the Forsmark site investigation, primarily on the basis of outcrop data and the interpretation of airborne (helicopter) magnetic data (Figure 2-2). The results of modal and geochemical analyses of surface samples as well as the analysis of structural data from the outcrops were presented in Stephens et al. (2003, 2005) and Stephens and Forsberg (2006). Geochronological data were compiled and evaluated in Söderbäck (2008). The description of the map, including the rock type distribution and the ductile structures, was presented initially in SKB (2005) and, in more detail, in Stephens et al. (2008).

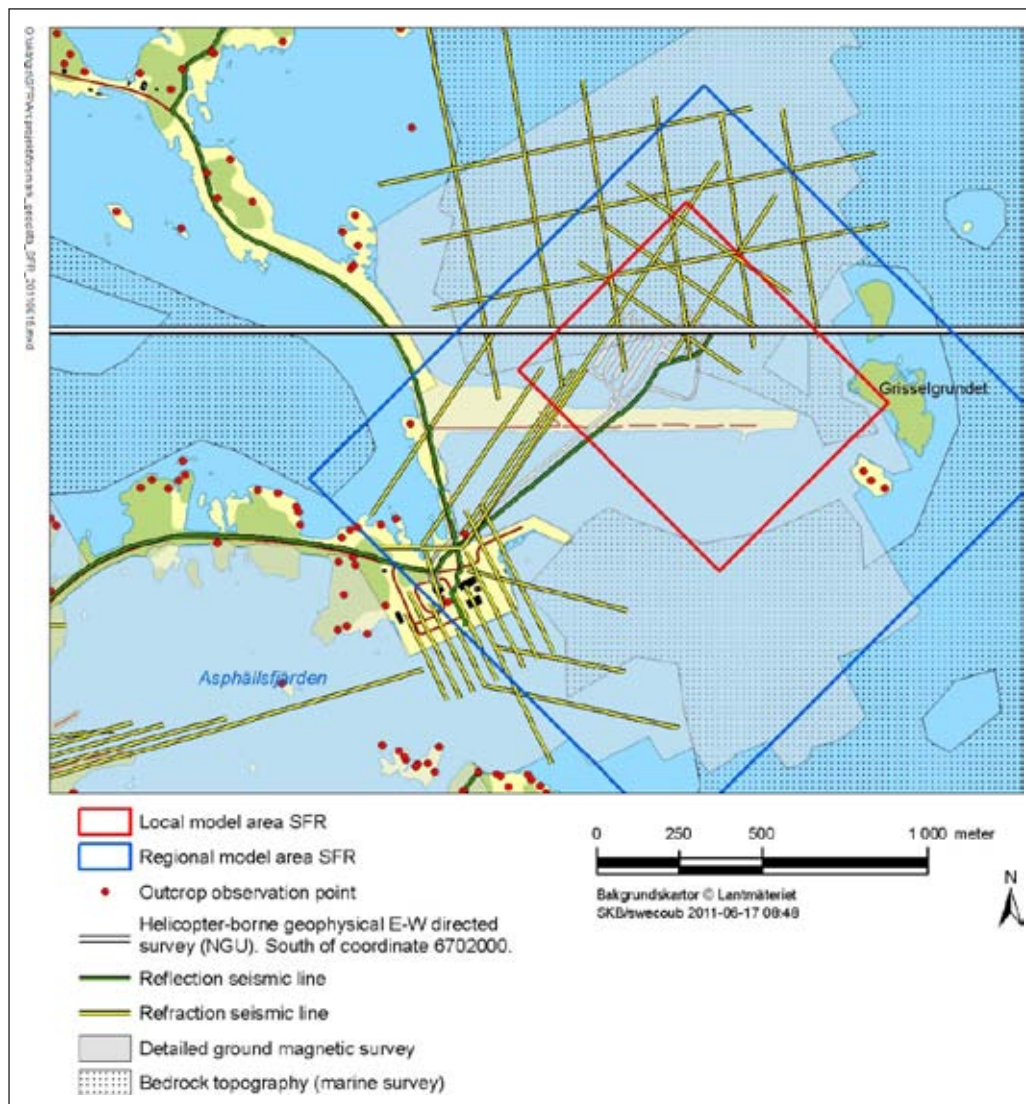


**Figure 2-2.** Bedrock geological map of the area around SFR based on the bedrock geological map, Forsmark stage 2.3 Stephens et al. (2008) produced during the Forsmark site investigation. Local and regional SFR model areas are also shown. The paler shades for each colour on the map indicate that the corresponding rock unit is covered by water. The outline of the existing SFR tunnel system is shown by solid lines and a possible configuration of the planned facility is shown by dashed lines.

Both the regional and local SFR model areas are located in an area where the quality of the map is judged as ‘variable but generally low’ (cf. SKB 2008b). No outcrops exist in the local SFR model area and the observation points in the regional SFR model area are limited to the small island south of Grisselgrundet and outcrops along the road to Biotestsjön (Figure 2-3).

All outcrops within and in proximity to the regional SFR model area were revisited for brief inspection during the SFR site investigation. However, no new surface geological data have been produced since the Forsmark site investigation.

An overview of the geophysical data gathered and used during the Forsmark site investigation is provided in Stephens et al. (2007), and the surface coverage of the available geophysical data in the SFR area is shown in Figure 2-3. No new surface-based geophysical investigations have been carried out during the SFR extension site investigation. However, a revised interpretation of lineaments and connections defined by magnetic minima inside the SFR regional model area has been completed. Reprocessing and review of earlier surface-based seismic reflection data covering the SFR regional model area has been performed by Juhlin and Zhang (2010) with a focus on the shallow depth relevant to the SFR storage level.



**Figure 2-3.** Outcrop observation points from the geological bedrock mapping, along with the coverage of available geophysical data around the SFR model areas. The whole area is covered by the Geological Survey of Sweden (SGU) fixed-wing airborne survey and the Geological Survey of Norway (NGU) helicopter-borne NS-directed survey. Note that all bedrock exposures have been visited and islands with no outcrop observation points have a cover comprising of Quaternary deposits dominated by till.

The main source of the magnetic data is dense measurements from the ground survey on land, sea and lakes with a grid resolution of approximately 4 by 4 m. A less resolved data set is provided by a helicopter-borne survey. At sea, and also quite near the shore, a marine geological survey provided data on the bedrock topography. Campaigns with refraction seismics, both on land and in the sea, resulted in models for the bedrock topography and the P-wave velocity distribution in the bedrock. Only two of the reflection seismic profiles (profiles 5b and 8) cover part of the SFR model areas (Juhlin and Palm 2005). It is data associated with these two profiles that have been subject to reprocessing and review during the preparation of version 1.0 (Juhlin and Zhang 2010).

Except for a new digital elevation model (DEM), no new investigations concerning the surface system have been carried out during the SFR extension site investigation. Chapter 4 provides a brief description of the surface system and the interactions between the surface system and the bedrock.

## 2.3 Tunnel investigations in the SFR facility

The geological and hydrogeological documentation of the underground openings compiled during the construction of SFR is extensive. A summary of the engineering geology is presented in the final construction report of Christiansson and Bolvede (1987), which is based on geological mapping of underground openings, geohydrological surveys, cored boreholes and probe drilling. Detailed geological maps at the scale 1:200 that provide information on rock type, fractures, fracture zones and water seepage for all underground openings are included. All these drawings have been digitally scanned, geo-referenced in the ArcGis software and attached to the RVS model (stored in the SKB database SDE GIS as Field note SFR 146). These drawings have been used in combination with as-built tunnel centre-line and laser scanned tunnel section survey data to estimate the zone tunnel intersection positions in 3D.

In addition, Christiansson and Bolvede (1987) provided four overview drawings of (1) lithology in the access tunnels (drawing –101) and storage area (drawing –102) at the scale 1:1,000, (2) structures (drawing –103) and (3) water-bearing structures and grouting (drawing –104) at the scale 1:2,000. The overview structural drawing focuses on brittle structures distinguished according to the nomenclature in Figure 2-4. As a key input to the DZ modelling work, intercept positions and orientations for all brittle structures marked on the overview drawing were extracted from the detailed drawings and listed in Appendix 2 of Curtis et al. (2011), where these features are referred to as ‘possible tunnel deformation zones’ (tDZ).

Fracture trace data in the detailed drawings and stereographic projections (see Appendix 4 for details regarding their construction) included in the structural overview (drawing –103; cf. Figure 2-4) provide the only source of fracture orientation information. Since none of the data are available numerically, it has not been possible to apply the data directly in quantitative modelling. Overall approximately 600 water-bearing traces have been mapped on the walls and ceiling of different tunnel sections of the existing SFR facility (Christiansson and Bolvede 1987); inflow has been described as “locally flowing” inside deformation zones, and as “moisture” or “dripping” outside zones. These traces are reported in terms of 389 orientations that may represent packages or sequences of fractures and, therefore, fracture sets cannot be directly compared, for example in terms of intensity.

Drawing –104 in Christiansson and Bolvede (1987) summarises the grouting performed during tunnel construction and information on the spatial location of large tunnel inflows. The largest grouting efforts were made in the passage through the zones ZFMWNW0001 (Singö zone), ZFMNNE0869 (zone 3) and ZFM871 (zone H2), whereas only minor grouting was performed in the storage facilities (Figure 2-5). The Silo was not grouted at all despite its proximity to ZFMNW805A and B (zone 8).

An updated mapping of the lower construction tunnel (NBT) in SFR was performed by Berglund (2008) (delivery Sicada\_11\_015). The mapping was based on a template of the laser-scanned tunnel geometry and consists of three-dimensional graphical elements related to a database with geological properties. Fractures, lithology, rock contacts, minor deformation zones and obvious water seepage have been recorded according to the geological nomenclature used by SKB. Details regarding the minor deformation zones are presented in Appendix 2 of Curtis et al. (2011).

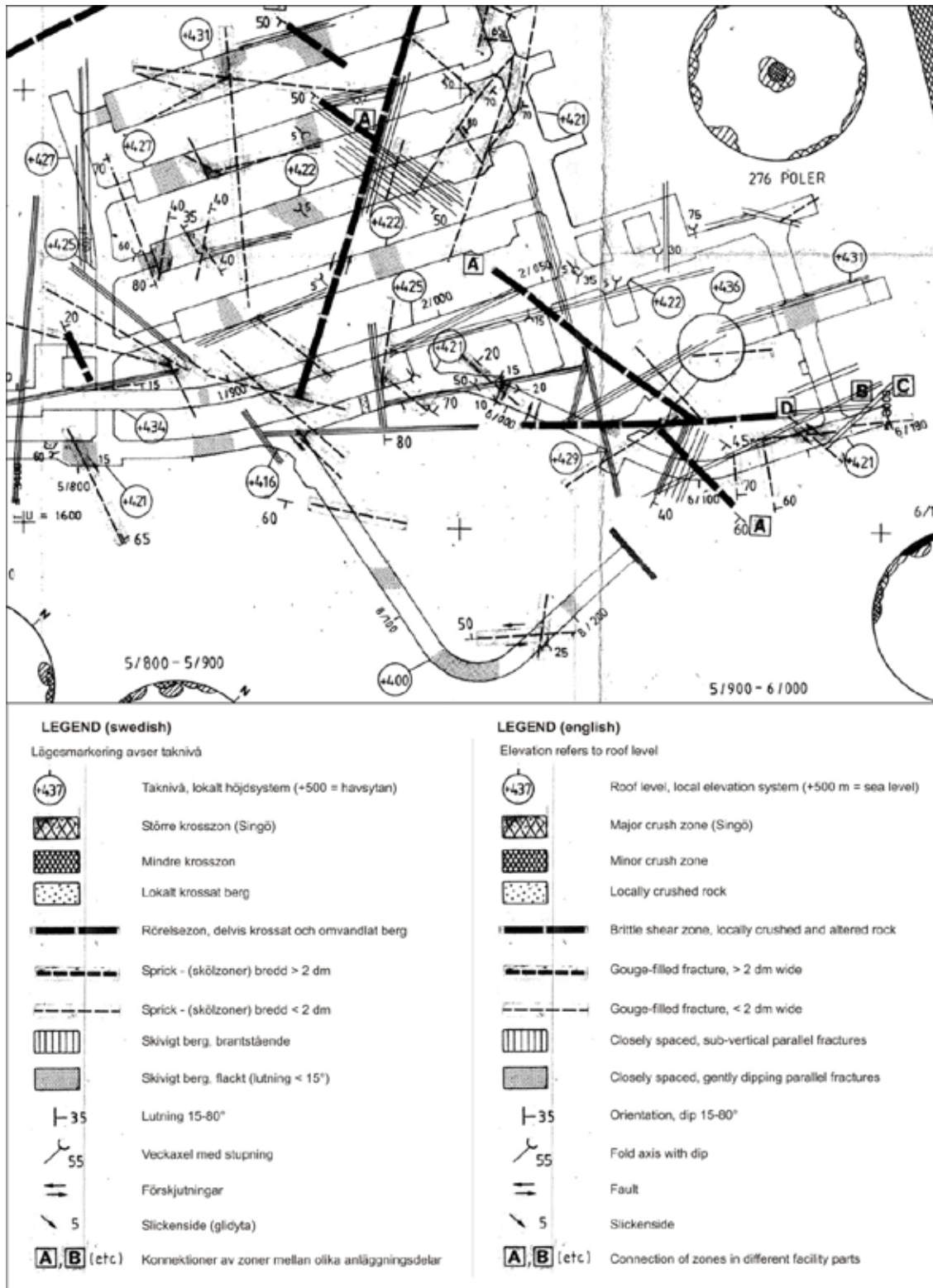
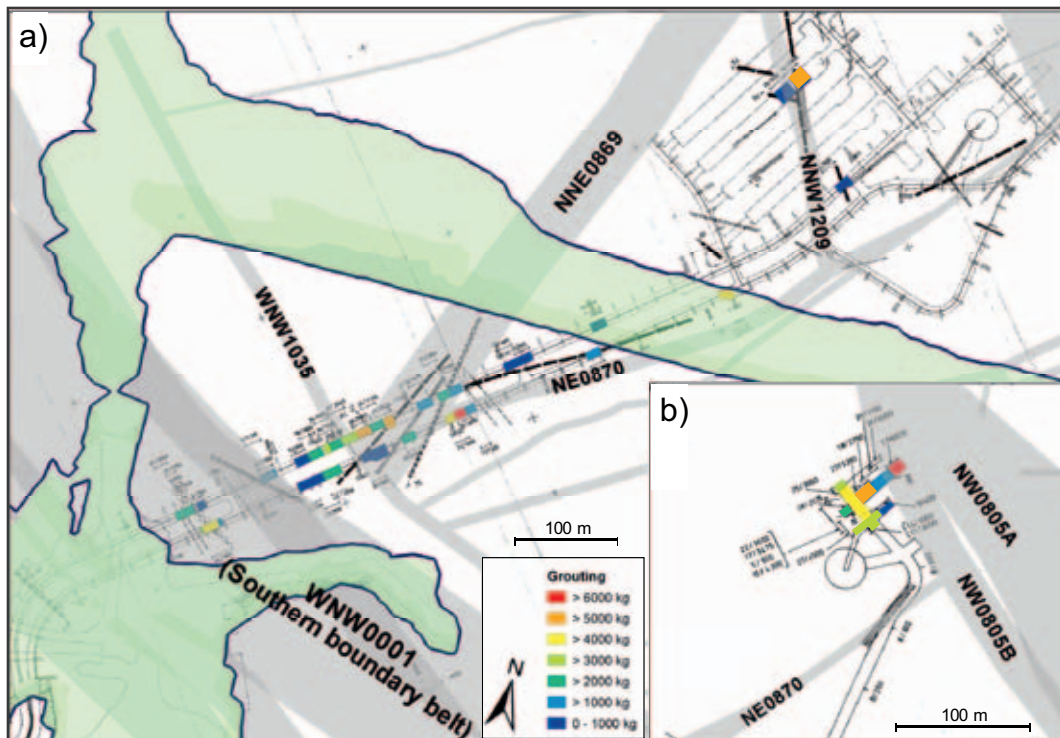


Figure 2-4. Detail of the structural overview drawing (-103) in Christiansson and Bolvede (1987). English legend translated from Swedish.

To facilitate the rock domain modelling, a further integration of earlier SFR tunnel mapping results has been completed by (1) translation of the different rock types defined by Christiansson and Bolvede (1987) into the bedrock nomenclature introduced during the Forsmark site investigation (cf. Stephens et al. 2003), and by (2) colour coding of the rock types in all detailed drawings at the scale 1:200 according to SKB standards (stored in SDE GIS database as Field note SFR 146).

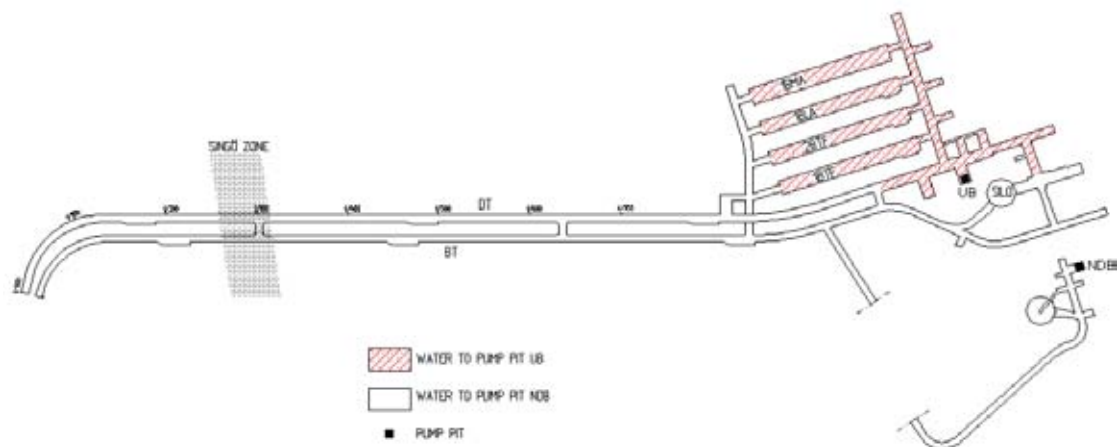




**Figure 2-5.** Grouted tunnel sections in the existing SFR. For readability, the original sketch 104 by Christiansson and Bolvede (1987) has been coloured by injected mass of cement and placed in the context of the ground traces of the steeply dipping deformation zones of the geological model SFR v. 1.0. The insert, b) illustrates the lower level of the SFR tunnels that intersect ZFM871 (zone H2).

The basis for the translation is primarily the updated mapping of NBT by Berglund (2008), but also visits to other areas of the facility with focus on specific lithological issues. A compilation showing an example of the available geological data for a section of NBT is presented in Figure 5-3.

Measurements of the inflow to the SFR facility have been carried out regularly since January 1988 (Carlsson and Christiansson 2007, SKBdoc 1233642). The drainage from the operational area is collected in pump pit UB, the rest of the drainage is collected in pump pit NDB in the lower construction tunnel (Figure 2-6). In addition, there is a pump pit in connection to the entrance gates to the SFR tunnel system at an elevation of about -12 m (RHB 70), which collects the drainage water and precipitation from the open uppermost part of the SFR ramp.



**Figure 2-6.** The locations of measuring points for groundwater inflow to the SFR underground facility. From Carlsson and Christiansson (2007).

## 2.4 Borehole investigations

Borehole data from the following three drilling campaigns in the area have been used in the current modelling work.

- The investigation and construction of the existing SFR facility resulted in a total of 60 cored boreholes. During the pre-investigation phases prior to the construction of SFR, 1980 to 1983, surface boreholes were drilled from offshore platforms, from ice-cover, and from land. During the construction phase of SFR, 1984 to 1986, subsurface boreholes were drilled from underground constructions and access tunnels, to explore and verify locations of deformation zones.
- The Forsmark site investigation. The relevant boreholes include one cored borehole (KFM11A) and two percussion boreholes (HFM34 and HFM35) all of which were drilled within or in close proximity to zone ZFMWNW0001 and penetrate the western part of the SFR regional model volume.
- The current site investigation for a future extension of SFR. The drilling campaign yielded seven cored boreholes (KFR101, KFR102A, KFR102B, KFR103, KFR104, KFR105 and KFR106) and four percussion boreholes (HFR101, HFR102, HFR105 and HFR106) situated south to south-east of the existing SFR facility, predominantly inside the local model volume selected prior to the investigations. The location and orientations of the boreholes were chosen so that information of the prioritised survey area could be provided without penetrating a possible repository volume, and thereby creating shortcuts to the surface. The drilling also included an extension of the existing cored borehole KFR27. All drilling, except for that of KFR105, was performed from the ground surface. That is, no boreholes were drilled from offshore platforms or from ice-cover.

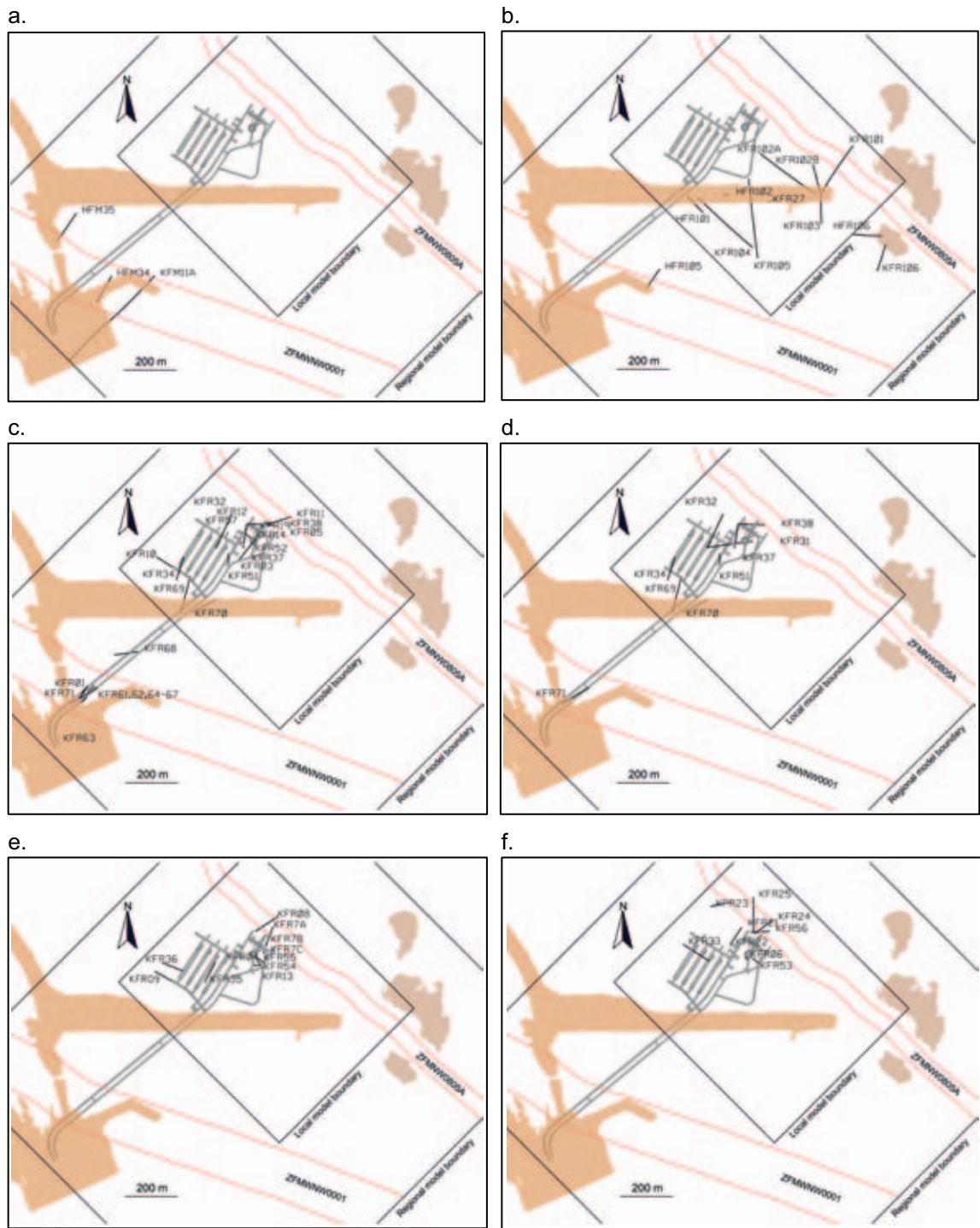
The boreholes from the investigation and construction of SFR range between 15 and 242 m in length. All percussion-drilled boreholes from the recent SFR site investigation, except for HFR102 (55 m), are approximately 200 m in length, whereas the cored boreholes range between 180 and 601 m. Only three of the boreholes, KFR27, KFR102A and KFR104 reach below -300 m elevation, which is the bottom of the local SFR model domain. The percussion-drilled boreholes HFM34 and HFM35, included from the Forsmark site investigation, are both approximately 200 m in length, whereas the core-drilled borehole KFM11A is 851 m in length.

The performance and technical design of different types of boreholes drilled during the Forsmark and SFR site investigations, comprising telescopic boreholes, core-drilled boreholes of standard type and percussion-drilled boreholes, are fully described in SKB's method documents SKB MD 620.003 and 610.003. More details for individual boreholes are provided in the associated P-reports.

The available technical documentation of the boreholes drilled during the construction of SFR is basically limited to three data reports (Hagkonsult 1982, 1983, Carlsson et al. 1986). During the Forsmark site investigation, all these boreholes were renamed by Keisu and Isaksson (2004) to harmonise with the current SKB nomenclature. In addition, the borehole positions in the local SFR coordinate system were transformed into the national RT90-RHB 70 system.

The locations of all boreholes used in the SFR modelling work are shown in Figure 2-7, whereas geometrical borehole information is provided in Table 2-1.

Down-hole deviation measurements have been conducted in all boreholes from the Forsmark and SFR site investigations according to SKB's method document SKB MD 224.001. Although deviation measurements also were carried out for most boreholes drilled during the construction of SFR (e.g. Hagkonsult 1982, 1983), there are no calculated deviations available in the SKB database Sicada. Instead, the orientations of the boreholes have been defined at the top-of-casing. However, it must be emphasised that none of these boreholes exceeds 250 m in length and that the deviations given in Hagkonsult (1982, 1983) are all less than one metre from the theoretical orientation.



**Figure 2-7.** The general position of boreholes within the regional model volume relative to the SFR underground facility, coastline and ground surface trace of ZFMWNW0001 (Singö) and ZFMNW0805A. a) Forsmark site investigation boreholes, b) boreholes from the current SFR extension drilling campaign and c–f) old boreholes from the construction of SFR. The latter are divided into c) boreholes where existing lithological logs have been translated into current SKB nomenclature and subjected to a simplified single-hole interpretation (SHI; as defined in Section 2.4.2), d) boreholes that were subjected to lithological overview mapping and a simplified SHI, e) boreholes that were remapped by the Boremap-system and subjected to SHI and f) boreholes that contain no available drill core and, consequently, no available geological information. Note that designations are placed at the end of the boreholes.

**Table 2-1. Borehole ID, length, location, inclination and bearing of all boreholes used in the SFR modelling work. Note that three of the boreholes lack spatial information (i.e. KFR72, KFR89 and SFR (Silo1)) and were therefore not considered in the geometric models. The heading 'BH group' refers to the maps of Figure 2-7 denoted a-f.**

BH ID	Old ID	Length (m)	Northing (m)	Easting (m)	Inclination (°)	Bearing (°)	BH group
HFM34	n/a	200.75	6701325.06	1632470.21	-58.6	030.5	a
HFM35	n/a	200.75	6701555.86	1632320.51	-59.3	033.0	a
HFR101	n/a	209.30	6701725.15	1632838.91	-60.0	150.0	b
HFR102	n/a	55.04	6701728.55	1632974.54	-59.1	085.0	b
HFR105	n/a	200.50	6701376.55	1632686.82	-63.0	034.5	b
HFR106	n/a	190.40	6701574.11	1633579.85	-59.8	269.4	b
KFM11A	n/a	851.21	6701103.82	1632366.75	-60.9	040.2	a
KFR01	HK1	62.30	6701434.83	1632453.42	-60.0	230.5	c
KFR02	HK2	116.80	6701770.05	1632887.78	-90.0	000.0	c
KFR03	HK3	101.60	6701908.96	1632997.74	-90.0	000.0	c
KFR04	HK4	100.50	6701946.04	1633055.96	-75.0	098.2	e
KFR05	HK5	131.40	6701946.04	1633056.58	-70.0	009.1	c
KFR06	HK6	39.00	6701961.50	1633059.01	-63.0	315.6	f
KFR08	HK8	104.40	6702071.23	1633066.45	-05.0	056.4	e
KFR09	HK9	80.24	6701881.83	1632755.38	-05.0	299.9	e
KFR10	HK10	107.28	6701882.58	1632755.89	-45.0	302.5	c
KFR11	HK11	98.07	6702046.91	1633110.05	-10.0	072.5	c
KFR12	HK12	50.26	6702057.64	1632899.87	-90.0	000.0	c
KFR13	HK13	76.60	6701910.29	1633092.89	-90.0	000.0	e
KFR14	HK14	29.10	6702010.36	1633031.74	-45.0	135.1	c
KFR19	KB19	110.17	6701908.32	1633000.46	13.8	038.2	c
KFR20	KB20	109.70	6701909.55	1632998.33	10.4	056.4	c
KFR21	KB1	250.80	6702093.30	1633037.21	-90.0	230.5	f
KFR22	KB2	160.10	6702087.50	1633033.17	-60.0	213.0	f
KFR23	KB3	160.20	6702184.17	1632993.04	-60.0	257.0	f
KFR24	KB4	159.20	6702062.95	1633083.74	-57.0	051.5	f
KFR25	KB5	196.50	6702065.30	1633077.79	-46.0	000.0	f
KFR27	KB7	501.64	6701714.42	1633175.52	-87.4	248.2	b
KFR31	KB11	242.10	6701959.66	1632915.47	-43.2	082.1	d
KFR32	KB12	209.70	6701956.59	1632915.67	-46.5	024.9	d
KFR33	KB13	167.00	6701958.73	1632912.61	-43.8	302.5	d
KFR34	KB14	142.00	6701923.75	1632794.20	-49.0	198.1	d
KFR35	KB15	140.20	6701956.28	1632915.93	-51.5	208.1	e
KFR36	KB16	123.90	6701922.23	1632792.99	-46.0	291.7	e
KFR37	KB17	204.90	6702050.31	1633033.49	-62.5	188.5	d
KFR38	KB18	185.40	6702048.62	1633035.53	-57.6	092.2	d
KFR51	KB21	46.85	6701898.12	1632963.47	35.0	358.8	d
KFR52	KB22	29.95	6701963.94	1633066.31	10.0	230.5	c
KFR53	KB23	40.60	6701947.78	1633100.54	-27.4	312.6	f
KFR54	KB24	53.30	6701949.71	1633102.00	-47.7	310.0	e
KFR55	KB25	61.89	6701930.05	1633094.49	-11.0	329.0	e
KFR56	KB26	81.73	6702069.46	1633067.51	26.0	087.9	f
KFR57	KB27	25.38	6702050.77	1632854.91	-90.0	230.5	c
KFR61	DS1	70.90	6701382.45	1632391.99	-44.0	038.4	c
KFR62	DS2	82.80	6701368.43	1632401.86	-45.0	042.9	c
KFR63	DS3	15.08	6701226.87	1632315.81	-90.0	230.5	c
KFR64	DS4	54.17	6701406.16	1632407.71	-60.0	033.9	c
KFR65	DS5	39.68	6701403.62	1632406.04	-90.0	230.5	c
KFR66	DS6	29.17	6701420.17	1632417.16	-90.0	230.5	c
KFR67	DS7	48.95	6701419.85	1632419.75	-65.0	034.6	c
KFR68	DS8	128.03	6701552.67	1632530.76	-45.0	082.0	c

BH ID	Old ID	Length (m)	Northing (m)	Easting (m)	Inclination (°)	Bearing (°)	BH group
KFR69	DS9	201.20	6701713.56	1632783.24	-45.4	014.5	d
KFR70	DS10	172.50	6701712.85	1632823.74	-51.3	061.8	d
KFR71	DS101	120.90	6701367.83	1632363.08	02.0	059.5	d
KFR72	DS102	100.53	n/a	n/a	n/a	n/a	-
KFR80	INJ	20.00	6702028.08	1633056.22	-70.0	196.0	f
KFR83	SH3	20.00	6702061.20	1632857.98	-35.0	032.5	f
KFR84	BT 5/241	29.50	6701409.24	1632432.52	25.0	308.8	f
KFR85	BT 5/247 1	12.20	6701406.24	1632443.03	-05.0	115.3	f
KFR86	BT 5/247 2	14.70	6701406.94	1632443.09	-90.0	230.5	f
KFR87	NBT 1	15.10	6702035.75	1633042.79	-05.0	212.5	f
KFR88	NBT 2	30.00	6702058.78	1633063.72	20.0	338.5	f
KFR89	SFR1/177	17.00	n/a	n/a	n/a	n/a	-
KFR101	n/a	341.76	6701736.32	1633351.40	-55.5	028.8	b
KFR102A	n/a	600.83	6701730.30	1633330.21	-65.4	302.3	b
KFR102B	n/a	180.08	6701740.53	1633343.91	-54.1	344.9	b
KFR103	n/a	200.50	6701737.13	1633347.20	-53.9	179.9	b
KFR104	n/a	454.57	6701719.45	1632879.34	-53.8	133.8	b
KFR105	n/a	306.8	6701789.85	1633072.96	-10.1	174.5	b
KFR106	n/a	300.13	6701541.19	1633592.14	-69.9	195.1	b
KFR7A	HK7A	74.70	6702020.20	1633107.36	-02.0	020.8	e
KFR7B	HK7B	21.10	6702017.62	1633109.54	-75.0	011.5	e
KFR7C	HK7C	34.00	6701999.29	1633100.63	-70.0	196.0	e
n/a	SFR(Silo1)	45.12	n/a	n/a	n/a	n/a	-

#### 2.4.1 Geophysical borehole investigations

A standard geophysical borehole logging programme was generally performed in the boreholes produced during the Forsmark and SFR site investigations. This comprised density (gamma-gamma), magnetic susceptibility, natural gamma radiation, focused resistivity (127 and 300 cm), caliper mean, fluid resistivity, fluid temperature and borehole radar. Radar logging was not conducted in HFR101, HFR102, HFR105, HFR106, KFR102B and KFR103. The logging of KFM11A, HFM34 and HFM35 was more extensive and included also single point resistance and P-wave velocity. Furthermore, oriented image logs were generated along each borehole by the Borehole Image Processing System (BIPS), though the image quality in the deeper parts of HFM34 was too poor to allow Boremap mapping.

Geophysical borehole logging was performed in seven boreholes (KFR01, KFR02, KFR03, KFR04, KFR05, KFR19, KFR20) drilled during the investigation and construction of the SFR facility. Natural gamma radiation and single point resistivity were logged in all seven boreholes, whereas fluid temperature, magnetic susceptibility, neutron and normal resistivity logging were conducted in only some of them. Note that none of the old boreholes have been BIPS-logged, due to technical complications, associated with the removal of casing and chemical precipitation that requires broaching. Hence, fracture data from old boreholes lack orientations.

Petrophysical laboratory data from the SFR area are limited to 57 drill core samples analysed for density and, in some cases, magnetic susceptibility. Gamma spectrometry measurements to obtain the distribution of K, U and Th do not exist.

#### 2.4.2 Geological borehole investigations

All cored and percussion boreholes from the SFR site investigation, as well as KFM11A, HFM34 and HFM35 from the Forsmark site investigation, were subjected to geological mapping using the BIPS-based Boremap system. A combination of some of the geophysical data (e.g. density, natural gamma radiation and single point resistivity) provided support to the geological mapping, especially in the percussion boreholes.

Data acquisition from the cored boreholes drilled during the construction of SFR deviated from the standard SKB procedure, mainly due to the lack of BIPS-images, but also due to the general absence of radar data and geophysical logs, as well as a lower quality in available data and drill cores. This has required a reassessment of the data together with a renewed examination of all available drill cores from 43 old cored boreholes. To allow integration with data from later drilling campaigns, the following activities have been completed for these older cored boreholes.

- Drill cores from eleven of these boreholes have been subjected to renewed mapping by use of the Boremap-system. The prime criterion for the selection of the boreholes was a distinct cross-cutting relationship with inferred deformation zones in the earlier structural model of SFR (cf. Axelsson and Mærsk Hansen 1997). Since no BIPS images are available for the boreholes, it has not been possible to obtain absolute orientations of the geological features and the mapping is a simplified version of the established SKB methodology.
- Data acquisition from the remaining 32 boreholes, for which there are drill cores available was focused on lithological documentation, consisting of (1) translation of original bedrock mapping into established SKB rock nomenclature and (2) if such information did not exist, overview mapping where rock types exceeding 1 m in drill core length were recorded along with information on ductile and brittle-ductile deformation and alteration. Thus, no primary data for the brittle structures in these drill cores were obtained. Details of the activities are provided in Stephens et al. (2008) and Petersson et al. (2011).

### 2.4.3 Hydrogeological borehole investigations

All percussion-drilled boreholes from the SFR site investigation, including HFM34 and HFM35 from the Forsmark site investigation, were flow logged with the so-called HTHB-equipment, designed to perform combined pump tests and impeller flow logging in open percussion-drilled boreholes. However, only a single 44 m scale injection test is available in HFR102, as no impeller flow logging was performed.

The cored boreholes from the SFR site investigation, as well as the telescopic boreholes KFM11A and KFR102A, were all subjected to difference flow logging with the Posiva Flow Log (PFL) device, developed to detect continuously flowing features, i.e. flow paths that are connected to a positive hydraulic boundary. After an initial overlapping/sequential PFL flow logging in 5 m sections under natural flow conditions, detected flow anomalies were re-examined with the PFL Difference Flow logging method under pumped conditions. Flow logging of KFM11A did not reach beyond approximately 500 m borehole length and the outcome of the hydraulic test in the upper 99.3 m of KFR27 is restricted to sequential 5 m PFL data.

The single-hole transmissivity data available for the boreholes from the construction of SFR have been measured by four different methods:

- falling head (FH),
- pressure build-up (BU),
- steady state injection (PH), and
- transient injection (TI).

Altogether, there are 1,122 tested sections distributed among 45 boreholes, but the data are of varying quality; they have been evaluated with different test methods, at different test-scales, and under different test durations. Consequently, the data have different detection limits. However, most transmissivity data are measured over 3 m borehole sections and have a high detection limit, around  $5 \cdot 10^{-8}$  m<sup>2</sup>/s. Pressure build-up tests and transient injection tests have the longest durations (several hours) resulting in lower detection limits; unfortunately such data are relatively rare and have large variation in test scale. The falling-head and steady-state injection data had test durations of a few minutes only; they comprise a large sample size of consistent test scale (3 m sections). Falling-head data have an overall low confidence in relation to the other data types (Carlsson et al. 1986). In total, about 40% of the tested sections fall below the detection limit. The hydraulic data set underwent a screening process, in which 179 overlapping data, erroneous data, and inconsistent data were excluded, as described in Öhman and Follin (2010a).

Two short interference tests were performed in the site investigation for the SFR extension; a pumping test in HFR101 and opening of the underground borehole KFR105. In addition to these tests, interferences from borehole activities that cause hydraulic responses, like drilling and nitrogen flushing, were analysed and evaluated by Walger et al. (2011). The evaluation of interference tests involved estimations of hydraulic diffusivity, normalised drawdown and boundary-condition interpretations for responding observation sections. The evaluation of drilling responses involved a qualitative classification of the responses at different drilling depths and a quantitative estimation of hydraulic diffusivity between the drilled borehole and the observation section.

A number of interference tests were also performed during 1985 to 1987 in the boreholes from the investigation and construction of SFR, to provide insight into the connectivity between zones (Axelsson et al. 2002). The responses have only been used qualitatively; classed as direct response, indirect response and no response.

#### 2.4.4 Hydrogeochemical borehole investigations

The hydrogeochemical characterisation programme within the SFR site investigation included sampling in; a) the telescopic cored borehole KFR102A, the three conventional cored boreholes KFR101, KFR104 and KFR106 from the ground surface, and the conventional borehole KFR105 from the lower construction tunnel in the SFR repository, b) the three percussion-drilled boreholes HFR101, HFR105 and HFR106, as well as c) complementary investigations (Oct. 2010) in most of the early boreholes drilled from the SFR facility.

- **Cored boreholes:** This entailed eleven sampled borehole sections in pre-installed fixed borehole sections for pressure monitoring and groundwater sampling. Borehole KFR102A was well suited for groundwater sampling with two installed circulation sections allowing traditional pumping. In addition, borehole KFR105, drilled from the SFR facility, allowed sampling with little risk of contamination from drilling and drilling water, since the groundwater flow (under drawdown pressure) is directed towards the tunnel and no pumping was needed. Five delimited borehole sections were sampled simply by opening the valves. In the conventional boreholes (KFR101, KFR104 and KFR106) drilled from the surface, air lift pumping using nitrogen gas was the only possible technique to pump the groundwater to the surface. This may have affected especially trace metals, sulphide and parameters related to gas phases (e.g. radon). Furthermore, sampling of relatively long borehole sections reduces the possibility to resolve the groundwater composition along the boreholes due to mixing from different groundwater sources and possibly greater contamination from residual water present in the borehole section prior to sampling. Generally, groundwater sampling in the SFR investigation boreholes was performed within two to three months after completion of the borehole. Time series of three to five samples were collected during continuous discharge (days to weeks), and generally the time series sampling was not repeated more than once.
- **Percussion boreholes:** This entailed sampling of the entire boreholes HFR101 and HFR105, as well as two delimited sections in HFR106, during hydraulic tests using the HTHB equipment. In common with the cored boreholes, sampling from entire percussion boreholes can reduce the possibility to resolve the water composition along the borehole. However, in this case the flow anomalies in these short boreholes were few and therefore the representative sample lengths from boreholes HFR101 and HFR105 could be reduced. Generally, groundwater sampling was performed within two to three months after completion of the borehole. Time series of three to four samples were collected during continuous discharge (days) and time series sampling was not repeated more than once.
- **Complementary sampling in old SFR boreholes in October 2010:** This entailed the sampling of approximately 40 borehole sections in 18 cored boreholes drilled from the SFR tunnels (KFR01 to 05, KFR08 to 13, KFR19 and 20, KFR55 and 56 and KFR7A to 7C). The sampling and analysis programme was more extensive compared to the extensive monitoring programme conducted each fifth year, cf. Section 2.5, and included carbon and uranium isotopes as well as <sup>36</sup>Cl isotopes and on line measurements of Eh in selected borehole sections. Furthermore, fracture mineral investigations were performed on drillcores from borehole sections with Eh measurements.

The hydrochemical investigation programme did not include studies on porewater or colloids, and microbe investigations, gas sampling and redox measurements were conducted in a few selected borehole sections only.

Besides the data obtained from these recent hydrochemical investigations associated with the SFR extension phase, the description of the SFR site has benefited also from earlier investigations at Forsmark (Smellie et al. 2008, Laaksoharju et al. 2008), i.e. from boreholes HFM34, HFM35 and KFM11. This in addition to the previous investigations in boreholes in SFR during the construction phase (1983–1987) and the ongoing monitoring during the operational phase which commenced in 1989 (cf. Section 2.5).

Online Eh measurements exist for seven sections in boreholes KFR01, KFR08, KFR10, KFR19, KFR105 and KFR7A, and other available redox sensitive data include total Fe, Fe(II), S(-II), Mn, N(III), N(V), N(III)+N(V), N(-III) and U concentrations for a limited number of groundwater samples.

Gas analyses, which include N<sub>2</sub>, H<sub>2</sub>, CO<sub>2</sub>, O<sub>2</sub>, Ar, CH<sub>4</sub>, He, CO, C<sub>2</sub>H<sub>2</sub>, C<sub>2</sub>H<sub>4</sub>, C<sub>2</sub>H<sub>6</sub>, C<sub>3</sub>H<sub>8</sub> and total gas volume, have been performed in year 2000 and more recently in boreholes KFR01, KFR08, KFR10, KFR19, KFR105 and KFR7A.

Microbiological investigations, conducted in two sections of borehole KFR105, included determinations of total number of cells, concentration of adenosine-tri-phosphate (ATP), number of cultivable, heterotrophic aerobic bacteria, and most probable number of cultivable metabolic groups, i.e. iron, manganese, sulphate and nitrate reducing bacteria, as well as acetogens and methanogens. For borehole sections in KFR01, KFR10 and KFR7A, data corresponding to the total number of cells are available from year 2000.

Most pH data consist of laboratory measurements; field pH data were measured only in boreholes from the recent Forsmark and SFR site investigations and during the complementary groundwater sampling in the early SFR boreholes in October 2010. A sensitivity analysis of the effect of pH on solubility-, speciation- and redox modelling is presented in Gimeno et al. (2011).

## 2.5 Monitoring

A number of geoscientific parameters with a certain degree of time-dependent and site-specific variability have been monitored with the objectives of (1) establishing 'undisturbed' conditions, (2) recognising changes caused by the SFR construction and (3) gaining knowledge of the underlying, often complex processes that govern the time-dependent variations. A routine groundwater control or monitoring programme for SFR has been ongoing since 1989. An extensive monitoring programme, which includes a number of different parameters and objects in the environment, was initiated during the Forsmark site investigation. This programme continued with a few modifications after completion of the site investigations and the full extent from July 2007 and onwards is described in SKB (2007). A control programme with a focus on hydrogeological and hydrogeochemical monitoring in boreholes was also performed during the site investigations for the SFR extension.

The long-term groundwater pressure evolution around the SFR facility has been monitored in tunnel boreholes since the construction phase in 1985. In total, 38 sections in 12 boreholes (KFR01, KFR03–05, KFR08–09, KFR13, KFR19, KFR55–56, KFR7A–7B) are monitored and the results have been reported on a yearly basis (e.g. SKBdoc 1233647).

Groundwater levels were monitored in all relevant boreholes from the Forsmark site investigation (HFM34, HFM35 and KFM11A) and the site investigation for the SFR extension, after completion of each borehole.

Hydrogeochemical data have been acquired from the SFR groundwater monitoring programme since 1989. Annual sampling has been conducted in four boreholes and approximately each fifth year (1995, 2000, 2006 and 2010) the monitoring programme included also the other boreholes and a more extensive analytical protocol. To ensure selection of reliable groundwater data covering the time span representing the hydraulic conditions during the SFR excavation and construction phases, and presently during the operational phase, careful consideration was given to the variation in sampling quality during this long period of time.



## 2.6 Geographical data

The coordinate system used is:

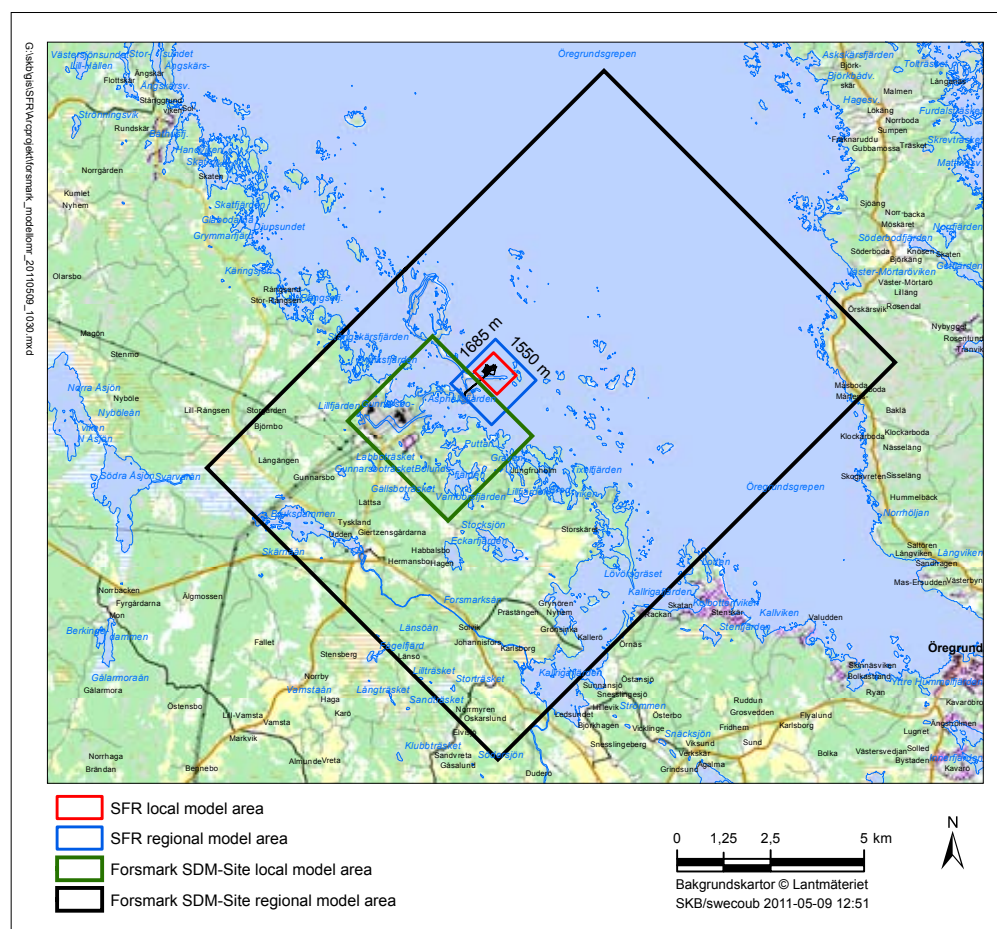
X/Y (N/E): the national 2.5 gon V 0:–15, RT 90 system (“RAK”),

Z (elevation): the national RHB 70 levelling system.

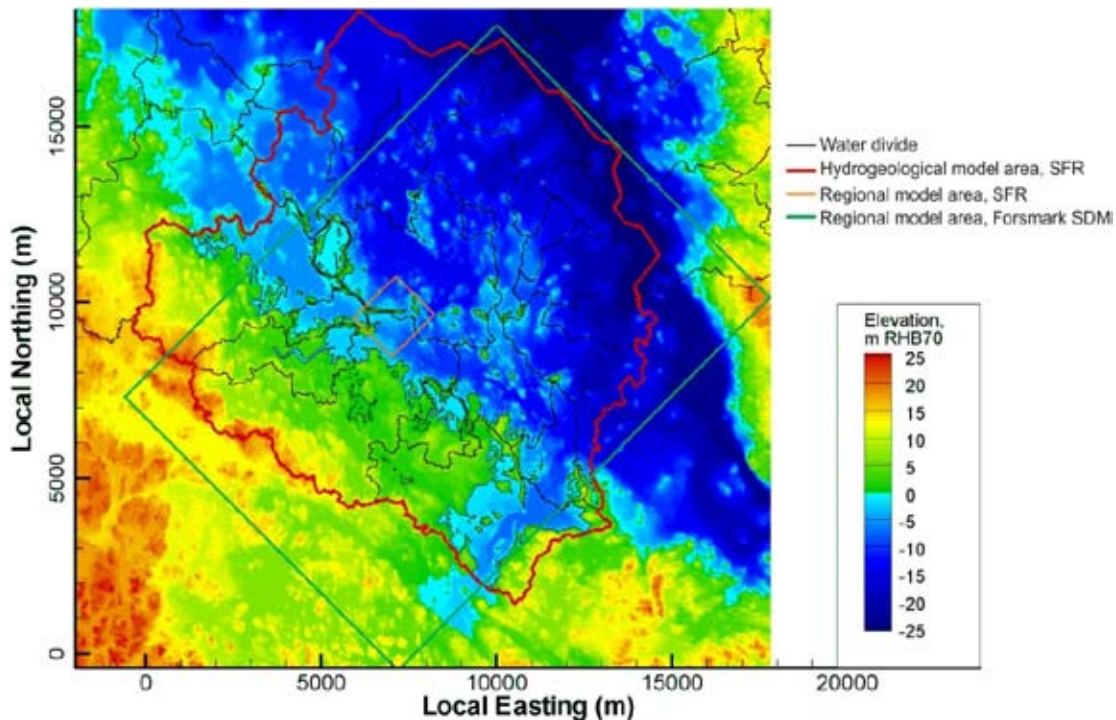
## 2.7 Model domains, volumes and areas

Two different model domains for the site descriptive modelling have been defined by the geo-scientific programme (SKB 2008a): a local model domain and a regional model domain. The local model domain covers the volume which is expected to host the existing SFR facility and the planned extension, whereas the regional model domain covers a larger volume that places the description of the local volume in a larger context. The relationship between the SFR model areas and the model areas used in the Forsmark site investigation is shown in Figure 2-8. The SFR model areas are smaller than the model areas used in the Forsmark site investigation because of the fact that the SFR site investigation is a detailed site investigation with an already defined prioritised survey area, see Chapter 1. The SFR local model volume extends from elevation +100 m RHB 70 to –300 m RHB 70, whereas the regional model volume extends from +100 m RHB 70 to –1,100 m RHB 70. The coordinates defining the horizontal extent of the model volumes are provided in Table 2-2.

A separate hydrogeological model area was defined for groundwater flow and solute transport modelling using DarcyTools (Svensson et al. 2010). The hydrogeological model area was defined from surface water divides that were interpreted from topographic data (Figure 2-9).



**Figure 2-8.** Regional (blue) and local (red) model areas for SFR model version 1.0 relative to the local (green) and regional (black) model areas used in the Forsmark SDM-Site (SKB 2008b).



**Figure 2-9.** Hydrogeological model area SFR (red) defined by surface water divides. The regional model area in the SFR structural model (orange) is a sub-volume of the regional model area used in the Forsmark site investigation, SDM-Site. Local origin set to Northing = 6692000, Easting = 1626000.

**Table 2-2. Coordinates defining the model areas for SFR in metres. RT90 (RAK) system.**

Regional model volume		Local model volume	
Easting	Northing	Easting	Northing
1631920.0000	6701550.0000	1632550.0000	6701880.0000
1633111.7827	6702741.1671	1633059.2484	6702388.9854
1634207.5150	6701644.8685	1633667.2031	6701780.7165
1633015.7324	6700453.7014	1633157.9547	6701271.7311

The parts of the model area that are currently below sea have been chosen with respect to future topographical divides, as well as the deep seafloor trench (the so-called Gräsörännan). The topographic data are available as a Digital Elevation Model (DEM) with a spatial resolution of 20 m scale in the horizontal plane. The hydrogeological model volume extends vertically from +100 m RHB 70 to -1,100 m RHB 70.

## 2.8 Model versions

The modelling work prior to the site descriptive model, SDM-PSU, has involved four different model versions: versions 0, 0.1, 0.2 and 1.0. Version 0 (SKB 2008a) was completed from the information available at the start of the site investigation programme for the SFR extension. This information includes mainly data from the preceding Forsmark site investigation (SKB 2008b), along with documentation from the construction of the existing SFR facility, which to some extent had been systematised and evaluated by Keisu and Isaksson (2004) and Carlsson and Christiansson (2007). The choice of a priority area south-east of the current SFR facility took place at this stage.

Each of the subsequent versions was planned to include models for geology, hydrogeology and hydrogeochemistry. A primary function of the initial model versions (0.1 and 0.2) was feedback to the ongoing site investigations. However, because of the rapid investigation progress, it was not

possible to provide feedback to the site investigations from model version 0.2. Hence, it was decided to omit the intermediate geological model version (0.2), and instead focus on the final version, v. 1.0. Consequently, the hydrogeological and hydrogeochemical models version v. 0.2 could not be developed according to the SKB methodology. However, the final hydrogeological model v. 1.0 reported in Chapter 7 is based on the final geological model v. 1.0. The same holds for the hydrogeochemical model v. 1.0 reported in Chapter 8.

### **2.8.1 Version 0.1**

The SFR geology model version 0.1 (Curtis et al. 2009) is based on additional evaluation of older geological data from SFR and a revision of the interpretation of lineaments defined by magnetic minima based on the high-resolution measurements of the magnetic total field covering most of the SFR area (Isaksson et al. 2007). Only a deterministic deformation zone model was produced during version 0.1. In this model version, the regional volume contains all modelled deformation zones that have a trace length on the ground surface of  $\geq 1,000$  m, whereas the local model contains all  $\geq 300$  m. A combined model that contained modelled deformation zones of all sizes was also delivered. The combined format was selected to facilitate further work by the hydrogeological modelling group who were the primary end users of version 0.1. No rock domain or geological DFN (discrete fracture network) modelling work was undertaken.

The hydrogeological model version 0.1 (Öhman and Follin 2010a) was a review of historic (old) hydraulic data related to SFR with respect to the geological model version v. 0.1 (Curtis et al. 2009). In other words, the hydrogeological model v.0.1 was based on hydraulic data available prior to the initiation of the SFR extension investigation, the same hydraulic data as used by Holmén and Stigsson (2001), but an updated model of the geological structures (Curtis et al. 2009). The associated flow modelling is reported in Öhman (2010).

Version 0.1 of the hydrogeochemical model presented in Nilsson A-C (2009), comprised a systematic data evaluation and retrospective QA of data from the early SFR boreholes, including the period 1984 to 2007, rather than the establishment of a hydrogeochemical model. The main purpose was to become acquainted with the dataset and groundwater variability, as well as to discover inconsistencies and outliers among the data. The revealed errors were subsequently corrected in Sicada and questionable data were highlighted in the report.

### **2.8.2 Version 0.2**

There exists no intermediate version of the geological and hydrogeological models. Instead, the focus of the hydrogeological modelling shifted to analyse the recent data outside possible deformation zones and to examine the hydrogeological DFN concept since there was no geological DFN modelling carried out (Öhman and Follin 2010b).

The specific aim with the hydrogeochemical model version 0.2 was to produce a preliminary hydrogeochemical site descriptive model based on both the old SFR data and most of the new data from the SFR extension project. Explorative analyses using traditional geochemical approaches were performed to describe the data and to provide an early insight and understanding of the site, i.e. to construct a preliminary conceptual model. The report (Nilsson et al. 2010) was a progress report, documenting the initial achievements in the interpretation and modelling work, rather than a complete hydrogeochemical site description.

### **2.8.3 Version 1.0**

The final geological model version 1.0 (Curtis et al. 2011) provides the framework for the modelling work by other disciplines, including hydrogeology and hydrogeochemistry, as well as a foundation for the detailed design and the long-term safety assessment. For version 1.0 separate local and regional deformation zone models as well as a combined model have been delivered. In addition, a local rock domain model has been developed. In the deformation zone model, the regional volume contains all modelled deformation zones that have a trace length on the ground surface of  $\geq 1,000$  m, whereas the local model contains all  $\geq 300$  m. The development of a geological discrete fracture network (DFN) model or fracture domain model, covering smaller structures, was not included in

the scope of the geological model. That is, for the SFR extension project, a hydrogeological DFN model was deemed sufficient to describe the rock mass between deformation zones. In addition, the aim of the final geological model version 1.0 has not been to provide an engineering description of the rock mass, but rather to establish a strictly geological description of the deformation zones at the predefined resolution (cf. above).

The final hydrogeological model v. 1.0 is described in Öhman et al. (2012). The model is based on a compilation and interpretation of all relevant data with respect to the final SFR geologic model v.1.0. It provides a hydraulic parameterisation of both deformation zones and the rock mass between these zones as defined by the deterministic geological model.

The final hydrogeochemical model version 1.0 (Nilsson et al. 2011) developed further the palaeohydrogeochemical conceptual model and the explorative analyses included in version 0.2. Additional modelling approaches and techniques have been used and the modelling of the data have been mainly centred on four identified main groundwater types by consideration of for example: a) the groundwater composition of different bedrock features, b) changes in water composition since the construction of the SFR, c) mixing calculations, d) descriptions of groundwater mineral systems and redox systems and e) groundwater residence times.

For each of the disciplines, the version 1.0 model reports are the main background reports for these disciplines to the SDM-PSU report.

## **2.9 Design of the existing SFR facility and the extension, preliminary layout L0**

### **2.9.1 The existing SFR facility**

The existing SFR facility (SFR 1) is located at a depth of approximately 60 m beneath the Baltic Sea and is reached from a surface facility via two, 1 km long access tunnels. The existing repository consists of several facility areas designed to meet the requirements for waste with different activity levels and packaging types. These include four rock vaults, each approximately 160 m in length, and an upright, cylindrical rock cavern denoted 'silo' (Figure 2-10). The deepest part of the facility is the end of the lower construction tunnel (NBT) at -140 m RHB 70, close to the base of the silo.

The silo is constructed of *in situ* cast concrete, which is founded on a bed of sand and bentonite. The bottom slab and parts of the walls in the rock vault BMA are made of *in situ* cast reinforced concrete, whereas the other rock vaults (1BTF, 2BTF and BLA) have concrete floors; remaining parts of the rock vaults are lined with shotcrete. Most other underground openings in the SFR facility are covered by shotcrete, which prohibits direct observations of the bedrock, especially in highly fractured tunnel sections. The NBT is the only part of the facility that is at least to some extent free from shotcrete.

The capacity of the facility is approximately 63,000 m<sup>3</sup> and the total volume of excavated rock is about 400,000 m<sup>3</sup>. The waste deposited in SFR 1 is short-lived and comes mainly from operation and maintenance of nuclear reactors and the interim storage of spent nuclear fuel. The waste consists primarily of spent organic ion exchange resins from cleaning of reactor water and mechanical components. A smaller quantity consists of similar waste from other industrial and medical activities and research. The silo and the BMA were constructed for storage of intermediate-level, solidified waste and contain about 80% and 20%, respectively, of the total activity in SFR 1. The other three rock vaults contains low-level waste in the form of solid scrap and trash, in addition to dewatered ion exchange resin and drums of ashes from trash incineration.

Closure measures have been planned since the design of SFR 1. Some measures are carried out during the operating period, for example closure of boreholes and filled disposal chambers. Complete sealing and facility closure is assumed to take place after all waste has been deposited.

### **2.9.2 The SFR extension, preliminary layout L0**

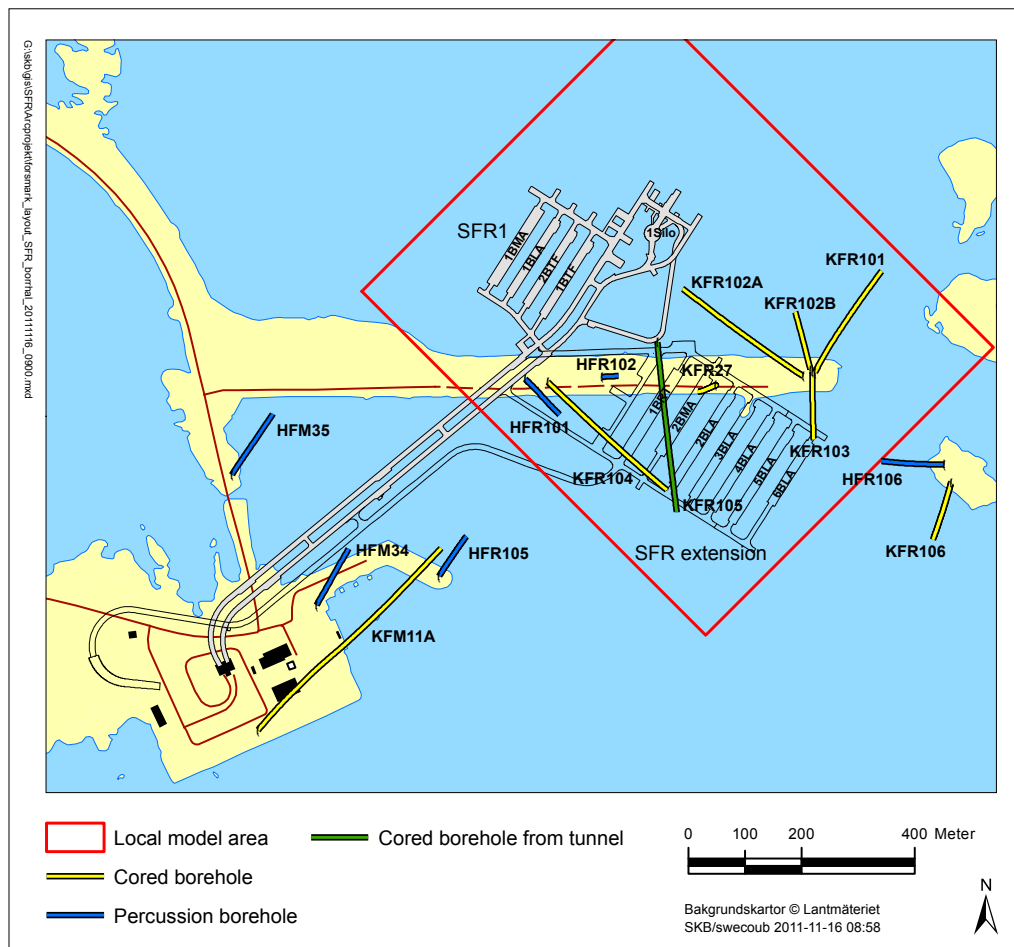
The layout of the extended SFR facility is not yet finalised. The layout, as it is described below, is an option that has been developed within the framework of the feasibility studies that have been undertaken, see Chapter 1. The SFR extension is planned to an area south-east of the current facility,

at the same level at approximately  $-60$  m RHB 70 (Figure 2-10). The analysis of the results from the geological and hydrogeological investigations and the long-term safety assessment will probably change the layout, both in design and in space, but the depth of the facility will probably not exceed an elevation of  $-200$  m RHB 70.

To enable reactor vessels to be brought into the SFR extension in one piece, a new opening may be constructed on Stora Asphällan, from where a new approximately 1.1 km long tunnel parallel to the existing repository access to SFR 1 may be built. In the current layout, the SFR extension connects to the existing SFR facility in two locations along the access tunnels (Figure 2-10).

The rock excavation work for the SFR extension will consist of five rock vaults for low-level waste (BLA), one rock vault for short-lived intermediate-level waste (BMA), and one rock vault for storage of reactor vessels (BRT; Figure 2-10). In addition to this, transportation tunnels and a separate tunnel for technical installations, electrical equipment and ventilation will be constructed. Overall, the layout of the extension is similar to the existing facility logistically. The main differences are the layout of the tunnels and the rock vaults required for the reactor vessels.

The excavated volume of rock is expected to be about  $500,000$  m<sup>3</sup> and the area of the rock mass where the rock vaults will be placed is expected to be approximately  $200 \times 300$  m. The SFR extension is planned to be built over a period of 3–4 years, starting at the turn of 2016/2017. The ordinary operation of SFR will continue during the construction period, although at a reduced rate. When the SFR extension is completed, it will be fully incorporated with the existing facility and the facility will work as one unit with merged systems. The design lifetime with normal operating and maintenance work is 100 years.



**Figure 2-10.** Preliminary layout of the SFR extension relative to the existing SFR 1 and the local model area together with the Forsmark site investigation boreholes and the boreholes from the SFR extension drilling campaign.

## 3 Evolutionary aspects

This chapter is a brief summary of the SKB report (Söderbäck 2008), which provides a comprehensive account of the geological evolution, palaeoclimate and historical development of the Forsmark and the Laxemar-Simpevarp areas. The report constituted a background report to SDM-Site Forsmark, the site description published on completion of the site investigation stage (SKB 2008b). A detailed reference list is provided in that report, and only a few key references are included in the text here. In this chapter, the Forsmark area refers to the region in southeastern Sweden where Forsmark is situated, without any specified delimitation, since information on evolutionary aspects in most cases is not specific to the restricted modelling area.

### 3.1 Bedrock evolution during the Proterozoic and Phanerozoic eons

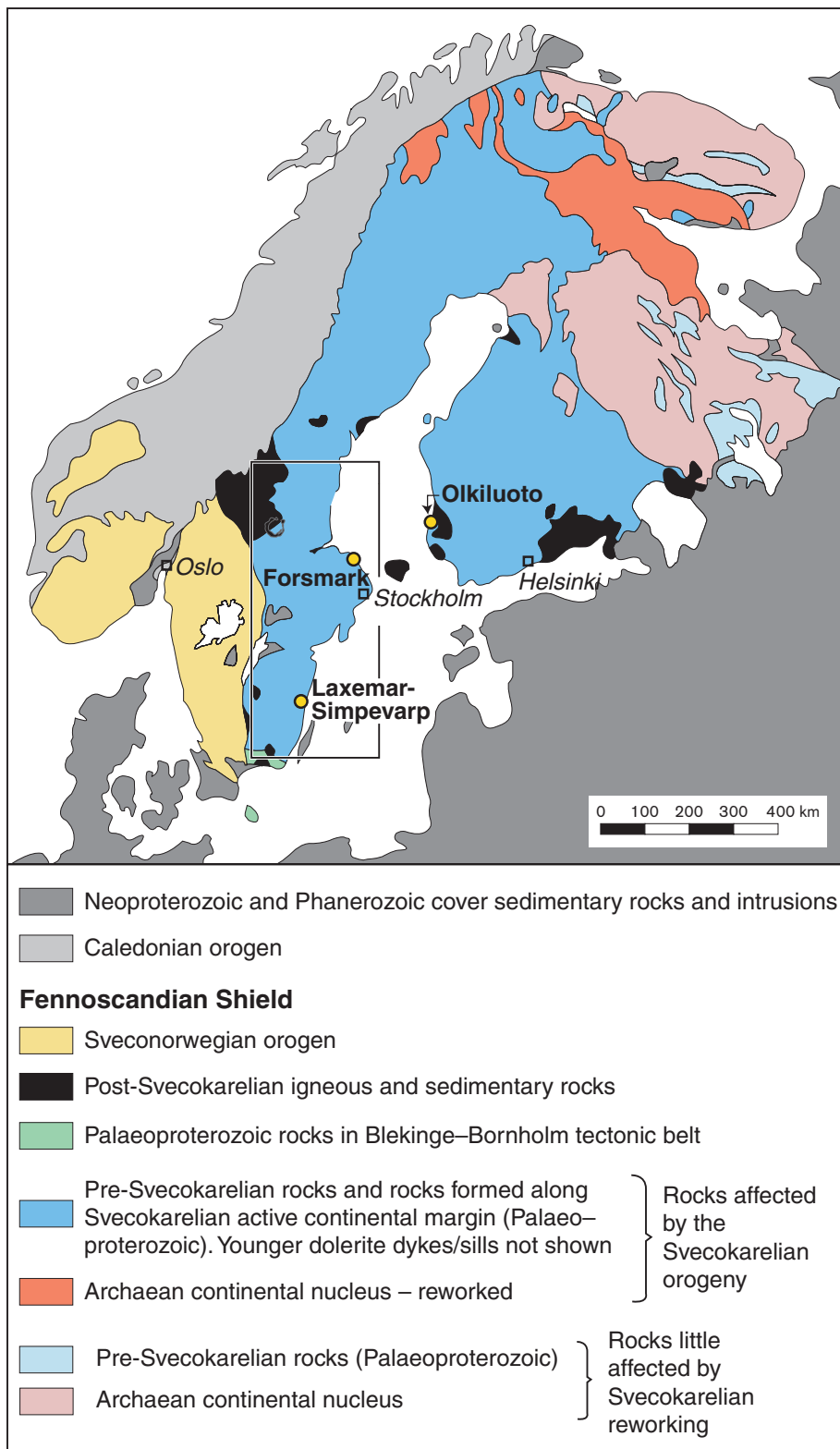
The Forsmark area is situated in the southwestern part of one of the Earth's ancient continental nucleus, referred to as the Fennoscandian Shield (Koistinen et al. 2001). This part of the shield belongs predominantly to the Svecokarelian (or Svecofennian) orogen (Figure 3-1). The bedrock in the Svecokarelian orogen is dominated by Proterozoic igneous rocks that were affected by complex ductile strain and metamorphism at predominantly mid-crustal levels, prior to later exhumation to the current level of erosion.

In order to provide the necessary boundary conditions for an understanding of the geological evolution of both the Forsmark and Laxemar-Simpevarp areas (Söderbäck 2008), these areas were viewed in a broader geological perspective. For this purpose, attention has been focused on an area in the southern and eastern part of Sweden, referred to as the geological reference area (Figure 3-1).

#### 3.1.1 Bedrock evolution in southeastern Sweden

The bedrock geology at the current level of erosion in the geological reference area in southeastern Sweden (Figure 3-1) can be divided into several major tectonic domains. These domains trend WNW more or less parallel to an older, Archaean continental nucleus to the northeast (Figure 3-1). The predominantly igneous bedrock in all these domains was formed between 1.91 and 1.75 billion years ago (1.91–1.75 Ga). This bedrock was also affected by a variable degree of deformation in a hot, ductile regime and the various domains amalgamated more or less into their current geometric configuration during the same time interval. A remarkably thick continental crust throughout most of the Fennoscandian Shield (up to c. 60 km) is a heritage from the dramatic tectonic evolution during the later part of the Palaeoproterozoic era. The geological time scale that has been used for assessing the bedrock evolution is shown in Figure 3-2.

Although the bedrock in southeastern Sweden had already started to stabilise after 1.75 Ga, tectonic activity that involved continued crustal growth and crustal reworking continued during the remainder of the Proterozoic to the west and south (Gothian, Hallandian and Sveconorwegian orogenies). By c. 900 Ma, the bedrock in the northern part of Europe had collided with other continental segments to form the supercontinent Rodinia. Break-up of Rodinia, drift of the newly-formed continent Baltica from cold latitudes in the southern hemisphere over the equator to northerly latitudes, and amalgamation of the new supercontinent Pangaea occurred between c. 600 and 300 Ma. Rifting of the continental crust, and opening and spreading of the North Atlantic Ocean dominated the subsequent geological evolution to the south and west of the geological reference area. This long period of extensional tectonic activity was interrupted during the Late Cretaceous and early Palaeogene by a more compressive tectonic regime, which can be related to the collision of Eurasia and Africa.



**Figure 3-1.** Map showing the major tectonic units in the northern part of Europe at the current level of erosion (modified after Koistinen et al. 2001). The area referred to in Section 3.1.1 and used to provide a regional geological perspective for both the Forsmark and Laxemar-Simpevarp areas is outlined by the rectangle. This area is referred to as the geological reference area (Söderbäck 2008).

Geological time units				
MILLION YEARS	EON	ERA	PERIOD	AGE
2	PHANEROZOIC	CENO-ZOIC	PLEISTOCENE / HOLOCENE IN QUATERNARY	1.635 or older
			PALAEOGENE / NEOGENE IN TERTIARY	65
100		MESOZOIC	CRETACEOUS	144
200			JURASSIC	206
			TRIASSIC	248
300		PALAEOZOIC	PERMIAN	290
400			CARBONIFEROUS	360
			DEVONIAN	417
			SILURIAN	443
500			CAMBRIAN	490
543		PRECAMBRIAN	NEO	VENDIAN
				650
1000	MESO		LATE	1000
			MIDDLE	1400
			EARLY	1600
1600	PALAEO			1600
2500				2500
3000	ARCHAEAN			
3500				
4000				4000

**Figure 3-2.** Geological time scale based on the compilation used in Koistinen et al. (2001). Age is given in million years (Ma). In the main text and some later figures, the symbol Ga is used, whereby 1 Ga = 1,000 Ma.

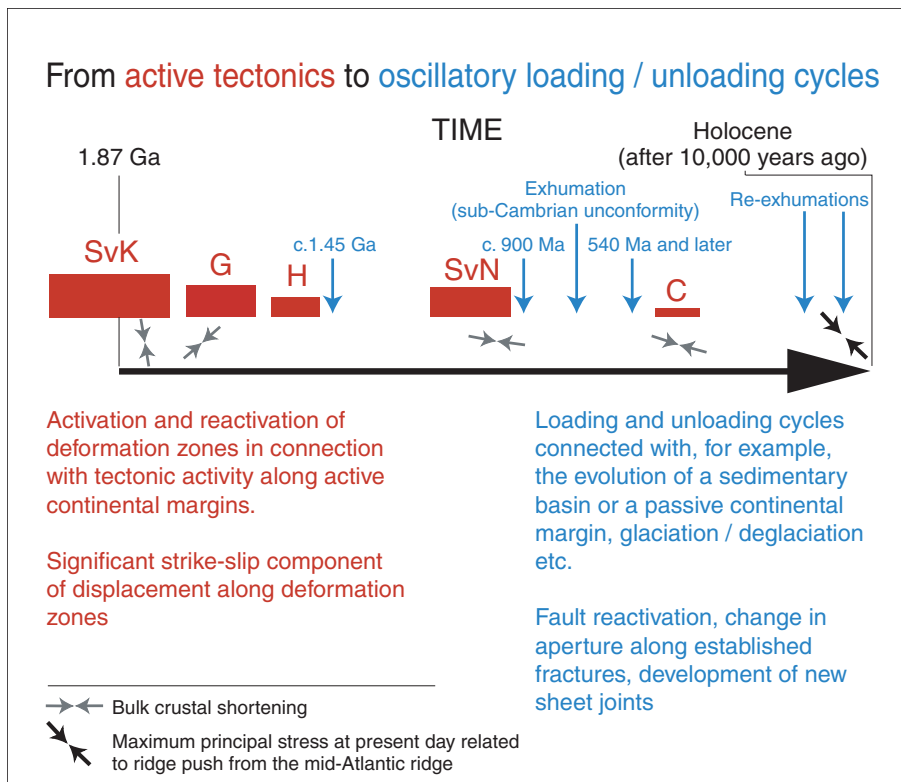
An overview of the effects of these different, far-field tectonic events in the near-field realm represented in southeastern Sweden is described in Söderbäck (2008). These effects gave rise to local igneous activity during the Proterozoic, burial and denudation of sedimentary cover rocks during the Proterozoic and Phanerozoic, and predominantly brittle deformation in the bedrock at different times throughout this long time interval. At least two episodes of pre-Quaternary exhumation of the ancient crystalline bedrock can be inferred, one prior to the Cambrian and the other after the Cretaceous, probably during the Neogene. The current ground surface corresponds to the sub-Cambrian unconformity that morphologically is referred to as the sub-Cambrian peneplain.

In conclusion, it appears that two fundamental types of geological process have made a profound impact on the geological evolution of the geological reference area in southeastern Sweden (Figure 3-3).

- Igneous activity and crustal deformation along an active continental margin at different time intervals mostly during Proterozoic time.
- Loading and unloading cycles in connection with the burial and denudation, respectively, of sedimentary rocks, around and after c. 1.45 Ga.

As the effects of regional tectonic activity mostly waned in southeastern Sweden and became prominent solely in the far-field realm, the effects of loading and unloading related to the burial and denudation of sedimentary rocks, respectively, increased in significance (Figure 3-3).



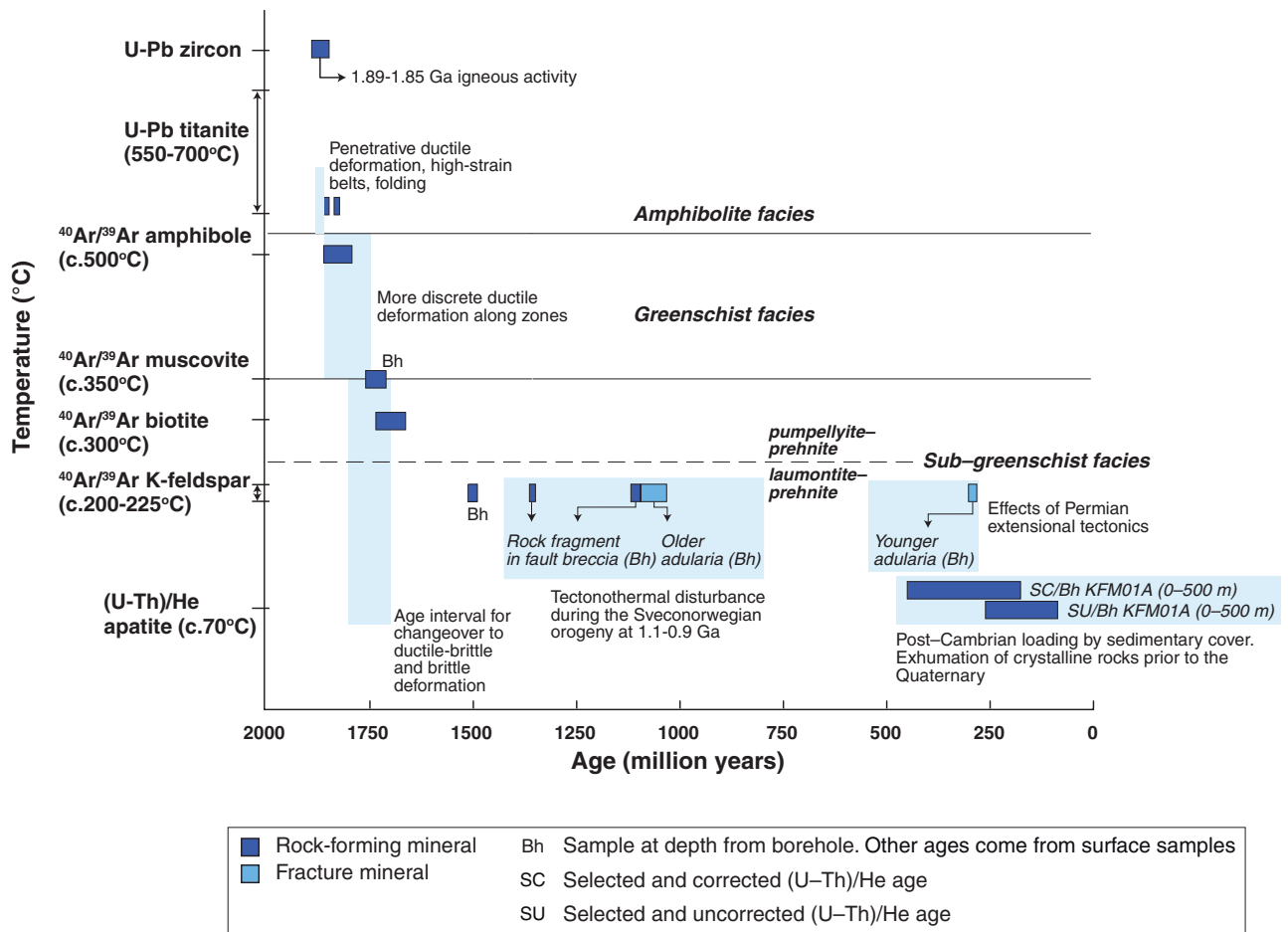


**Figure 3-3.** Active tectonics (red) and oscillatory loading and unloading cycles (blue) during geological time in the geological reference area (modified after Stephens et al. 2007). The detailed evolution during the Quaternary period with several glaciations (loading) and deglaciations (unloading) is not shown. SvK = Svecokarelian orogeny, G = Gothian orogeny, H = Hallandian orogeny, SvN = Sveconorwegian orogeny, C = Caledonian orogeny.

### 3.1.2 Bedrock evolution in the Forsmark area

The bedrock evolution of the Forsmark area has been evaluated with the aid of surface and borehole observational data as well as geochronological data (Söderbäck 2008). The geochronological data are summarised in Figure 3-4. In this area, an older suite of plutonic, calc-alkaline intrusive rocks formed between 1.89 and 1.87 Ga, and the metagranite inside the tectonic lens, where the deep repository for spent nuclear fuel is planned to be located, is included within this suite. Amphibolites that intrude into the metagranite and a younger suite of calc-alkaline rocks and granites formed between 1.87 Ga and 1.85 Ga. These two suites of intrusive rocks (Figure 3-4) have been included in separate Svecokarelian tectonic cycles at 1.91–1.86 Ga and 1.87–1.82 Ga, respectively, that have been recognised in southeastern Sweden (Söderbäck 2008).

Deformation in the Forsmark area initiated between 1.87 and 1.86 Ga (Figure 3-4) with the development of a penetrative grain-shape fabric, with planar and linear components, that formed under amphibolite-facies metamorphic conditions and at mid-crustal depths. Development of broad WNW-ESE to NW-SE belts with higher ductile strain surrounding tectonic lenses with generally lower ductile strain also occurred around 1.86 Ga. The amphibolites and other intrusive rocks that belong to the younger suite intruded during the waning stages of and after the development of the penetrative, ductile strain in the area. Regional folding of the variably intense, planar grain-shape fabric also affected the amphibolites. Ductile deformation after 1.85 Ga occurred predominantly inside the high-strain WNW-ESE to NW-SE belts. It became increasingly focused along ductile high-strain zones within these belts, and cooling ages indicate that ductile strain along these zones probably occurred until at least 1.8 Ga. A combination of dextral strike-slip displacement along the belts and shortening across them, so-called dextral transpressive deformation, has been inferred. This deformation is related to bulk crustal shortening in an approximately northward direction during oblique subduction of the oceanic lithosphere. Subduction occurred beneath the ancient continental margin to the northeast (Figure 3-1).



**Figure 3-4.** Summary of the geochronological data that constrain bedrock evolution in the Forsmark area (from Söderbäck 2008).  $^{40}\text{Ar}/^{39}\text{Ar}$  biotite data from depth in boreholes are not shown here. As expected, these data are somewhat younger than the equivalent surface data. Only a selection of (U-Th)/He data are shown. The procedure adopted concerning the interpretation of all the (U-Th)/He data, both corrected and uncorrected, is discussed in Söderbäck (2008). Important geological events that have been recognised in the Forsmark area are shown in pale blue rectangles with accompanying text on the figure.

The brittle deformational history of Forsmark, which initiated sometime between 1.8 and 1.7 Ga (Figure 3-4), has been evaluated with the aid of three approaches.

- The use of low-temperature geochronological data to shed light on the exhumation and cooling history of the area (Figure 3-4).
- The relative time relationships between different fracture minerals and the absolute ages of the low-temperature variant of the mineral K-feldspar, referred to as adularia (Figure 3-4 and Sandström et al. 2009).
- A comparison of kinematic data from brittle structures along deformation zones (Section 5.2.6 in SKB 2008b and Saintot et al. 2011) with the tectonic evolution in a regional perspective (Section 3.1.1).

Different generations of fracture minerals have been recognised in the Forsmark area. An early period of precipitation of a high-temperature mineral assemblage, which includes epidote, was followed by a period of hydrothermal precipitation of different, lower temperature minerals, including adularia (older generation), hematite, prehnite, laumontite and calcite. The fractures that bear epidote formed prior to 1.1 Ga are pre-Sveconorwegian in age. The importance of Sveconorwegian tectonothermal activity for the evolution of fracture mineral assemblages is evident (Figure 3-4). However, the close relationship between the stability field for the laumontite-prehnite mineral assemblage and the closure temperature at c. 200 to 225°C for the  $^{40}\text{Ar}/^{39}\text{Ar}$  K-feldspar isotope system (Figure 3-4) illustrates the

sensitivity of this system to resetting during growth of, for example, laumontite. For this reason, it is not clear whether the older generation of adularia formed during or prior to the Sveconorwegian tectonothermal event. The integrated evaluation that makes use of the different lines of approach outlined above suggests that the different sets and sub-sets of deformation zones in the Forsmark area had formed and had already reactivated during Proterozoic time, in connection with the late Svecokarelian, Gothian and Sveconorwegian tectonic events (see also Stephens et al. 2007).

On the basis of the (U-Th)/He apatite data from boreholes, some constraints on when different segments of the bedrock at different crustal levels passed through the c. 70°C geotherm have been specified (Figure 3-4). These data indicate that a sedimentary cover was situated on top of the crystalline basement rocks throughout much of the Phanerozoic. At Forsmark, this cover was possibly c. 3 km thick during the Silurian. A generally slow exhumation rate in the order of 3 to 10 m/Ma occurred during the Late Palaeozoic and Mesozoic and resulted in a reduction in the thickness of the cover to c. 2 km by the Early Jurassic (Söderbäck 2008). Some evidence for an increase in exhumation rate during the Permian is apparent.

Several lines of evidence indicate faulting after the establishment of the sub-Cambrian unconformity in the Forsmark area. Furthermore, precipitation of younger low-temperature minerals – including sulphides, clay minerals and calcite – occurred during and probably after Palaeozoic era. Both growth of adularia (younger generation) during the Permian (Figure 3-4) and migration of fluids downwards from the sedimentary cover into the crystalline bedrock have been established. Examples of downward fluid migration include the precipitation of oily asphaltite along fractures in the upper part of the bedrock. The asphaltite was derived from overlying Cambrian to Lower Ordovician oil shale that has now been eroded away. Furthermore, fluids that transported glacial sediment migrated downwards and filled new or reactivated fractures during the later part of the Quaternary period. The downward migration of different types of water during the Quaternary is addressed in greater detail in Section 3.4.

## **3.2 Palaeoclimate and geological evolution during the Quaternary period**

The Quaternary climate has been characterised by large and sometimes rapid changes in global temperature. The current warm period was preceded by recurring colder periods, during which ice sheets covered larger areas than at present. There are likely to have been ten or more glaciations during the Quaternary as determined from palaeoclimatic records such as ice and sediment cores, and the Forsmark area has been covered by glacier ice at least three times during the period. It is worth noting that each glacial episode tends to remove the evidence of the previous episode.

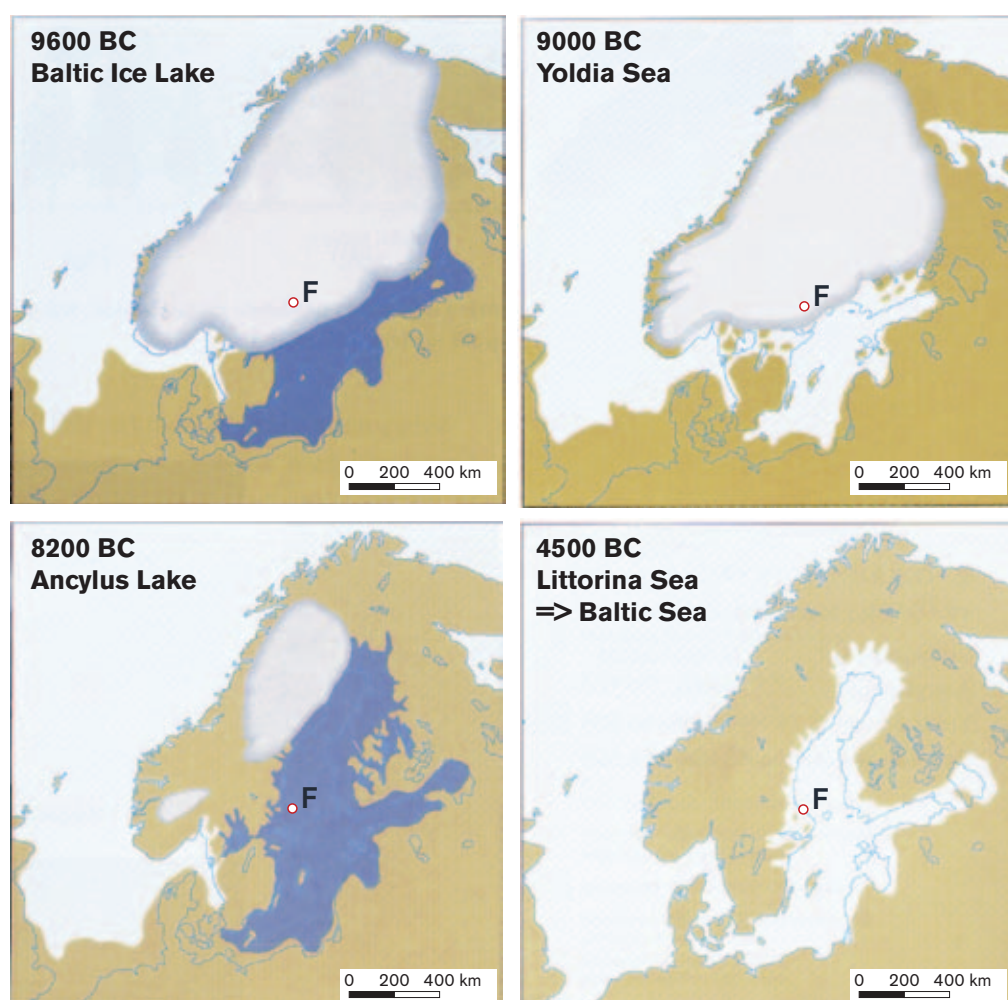
The cold glacial periods during the Quaternary were much longer than the warmer interglacial periods, which were characterised by a climate similar to the present. However, long ice-free periods have also occurred during the glacials. During these ice-free periods, the climate was colder than today and tundra conditions probably prevailed in large parts of Sweden. Consequently, it can be assumed that permafrost has prevailed in the Forsmark area for long periods. The latest glaciation (Weichselian) started c. 115,000 years ago, and there is geological evidence for at least two periods during the Weichselian when a large part of Sweden was free of ice. However, the onset of the latest glacial coverage at Forsmark and the exact timing and duration of the ice-free periods at the site are unknown. By contrast, the timing of the latest deglaciation is rather well established along the coast of the Baltic Sea, including the Forsmark area.

The present interglacial, the Holocene, started during the deglaciation of Mid-Sweden when the ice margin had not yet retreated as far as Forsmark. The climate during the deglaciation became successively warmer, although some periods with colder climate did occur. In southern Sweden, the warmer climate caused a gradual change from tundra vegetation to forest dominated by deciduous trees. The Mid-Holocene climate was characterised by temperatures a few degrees higher than today. The forests in southern Sweden have subsequently become dominated by coniferous forest. The areas covered by forest began to decrease c. 3000 BC due to the introduction of agriculture. However, the areas used as arable land are decreasing today and the forested areas are increasing.

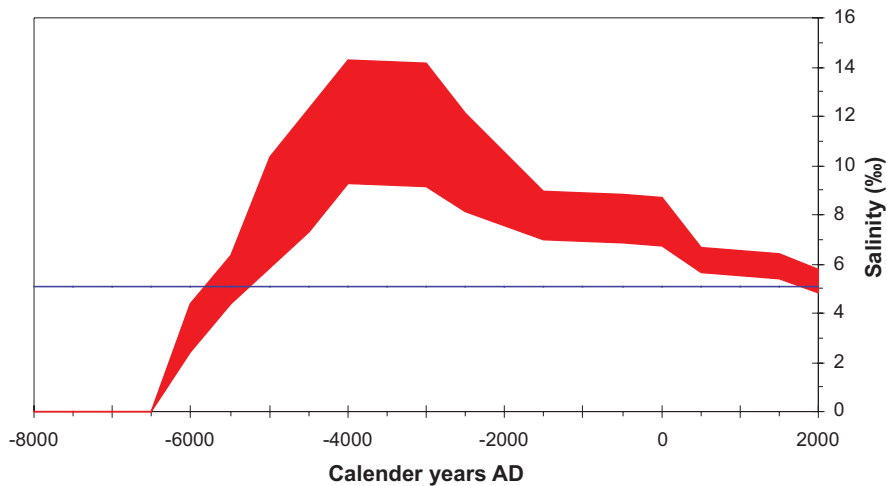
The evolution of the Baltic Sea since the latest deglaciation has been characterised by ongoing shoreline displacement. The interaction between isostatic recovery related to the removal of ice and unloading along with eustatic sea level variations has caused variable depth in the straits connecting the Baltic Sea with the Atlantic Ocean in the west. This in turn has caused variable salinity in the Baltic throughout the Holocene. The evolution of the Baltic Sea since the latest deglaciation has been divided into four main stages (Figure 3-5). Three of these stages; Yoldia, Ancylus and Littorina, are named after molluscs, which reflect the salinity of the stages. The salinity variations in the open Bothnian Sea during the last c. 9,000 years is shown in Figure 3-6. During the period 4500–3000 BC, the salinity was almost twice as high as it is today.

The Forsmark area is situated below the highest shoreline. During the deglaciation at c. 8800 BC, Forsmark was situated c. 150 m below the current sea level, and the first parts of the area at Forsmark emerged from the sea around 500 years BC (Figure 3-7).

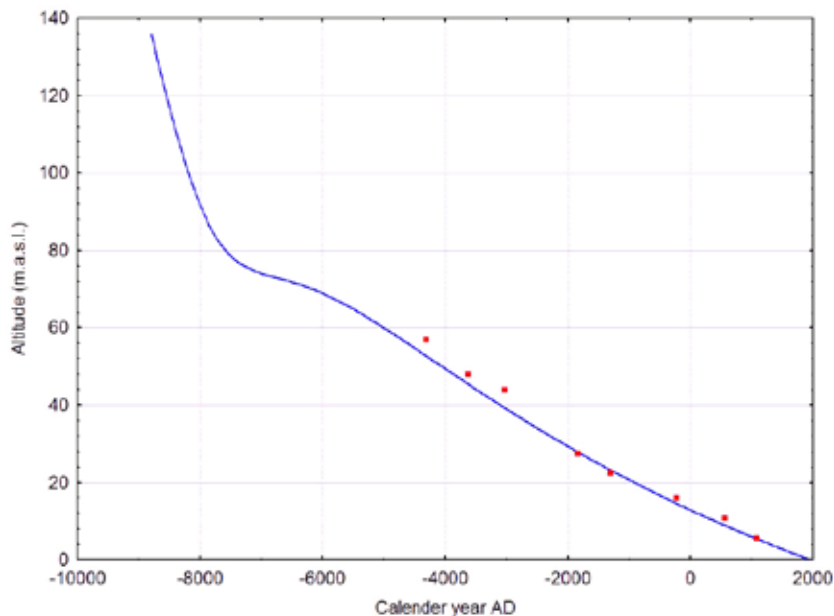
It is suggested that all known unconsolidated deposits at Forsmark were deposited during the last phase of the latest glaciation and after the following deglaciation (see Chapter 4 in Söderbäck 2008). A till unit consisting of over-consolidated silty-clayey till was deposited during an earlier phase of the latest glaciation. However, the possibility of the occurrence of older deposits cannot be excluded and there are indications of older deposits in adjacent areas in the region.



**Figure 3-5.** Four main stages characterise the evolution of the Baltic Sea since the latest deglaciation modified after Fredén (2002): A) the Baltic Ice Lake (13,000–9500 BC), B) the Yoldia Sea (9500–8800 BC), C) the Ancylus Lake (8800–7500 BC) and D) the Littorina Sea (7500 BC-present). Fresh water is symbolised by dark blue and marine/brackish water by pale blue. “F” indicates the location of Forsmark.



**Figure 3-6.** Estimated range for the salinity of sea water in the open Bothnian Sea during the last c. 9,000 years. Maximum and minimum estimates are derived from Westman et al. (1999) and Gustafsson (2004a, b). The present salinity in the area is shown as a horizontal reference line.



**Figure 3-7.** Shoreline displacement curve for the Forsmark area after the latest deglaciation. The red symbols are from dating of the isolation of lakes and mires (Hedenström and Risberg 2003). The blue solid curve was calculated using a model from Pässe (2001).

Till and glaciofluvial material were deposited directly by the ice sheet and by glacial meltwater, respectively. During the deglaciation, glacial clay was deposited in the lowest topographical areas. The subsequent shoreline displacement had a major impact on the distribution and relocation of fine-grained Quaternary deposits. The most exposed areas were affected by wave washing and bottom currents. Sand and gravel were consequently eroded from older deposits, transported and deposited at more sheltered locations. Periods of erosion also occurred at sheltered locations, which caused erosion of fine-grained deposits such as glacial clay. Shoreline displacement is an ongoing process and new areas are currently exposed to erosion, whereas sheltered bays, with conditions favourable for deposition of clay gyttja, have formed elsewhere.

### 3.3 Seismicity during the Quaternary period

An earthquake is the result of a sudden release of energy through movement (faulting) along a deformation zone, resulting in the emission of seismic waves. This movement is normally the result of stresses that have accumulated over a given time interval in a particular volume of the Earth's crust. Overviews of palaeoseismic activity in Sweden during the most recent part of and after the Weichselian glaciation, with a special focus on the Forsmark and Laxemar-Simpevarp areas, as well as of seismic activity in historical time from 1375 up to 2005 AD in northern Europe, are presented in Söderbäck (2008).

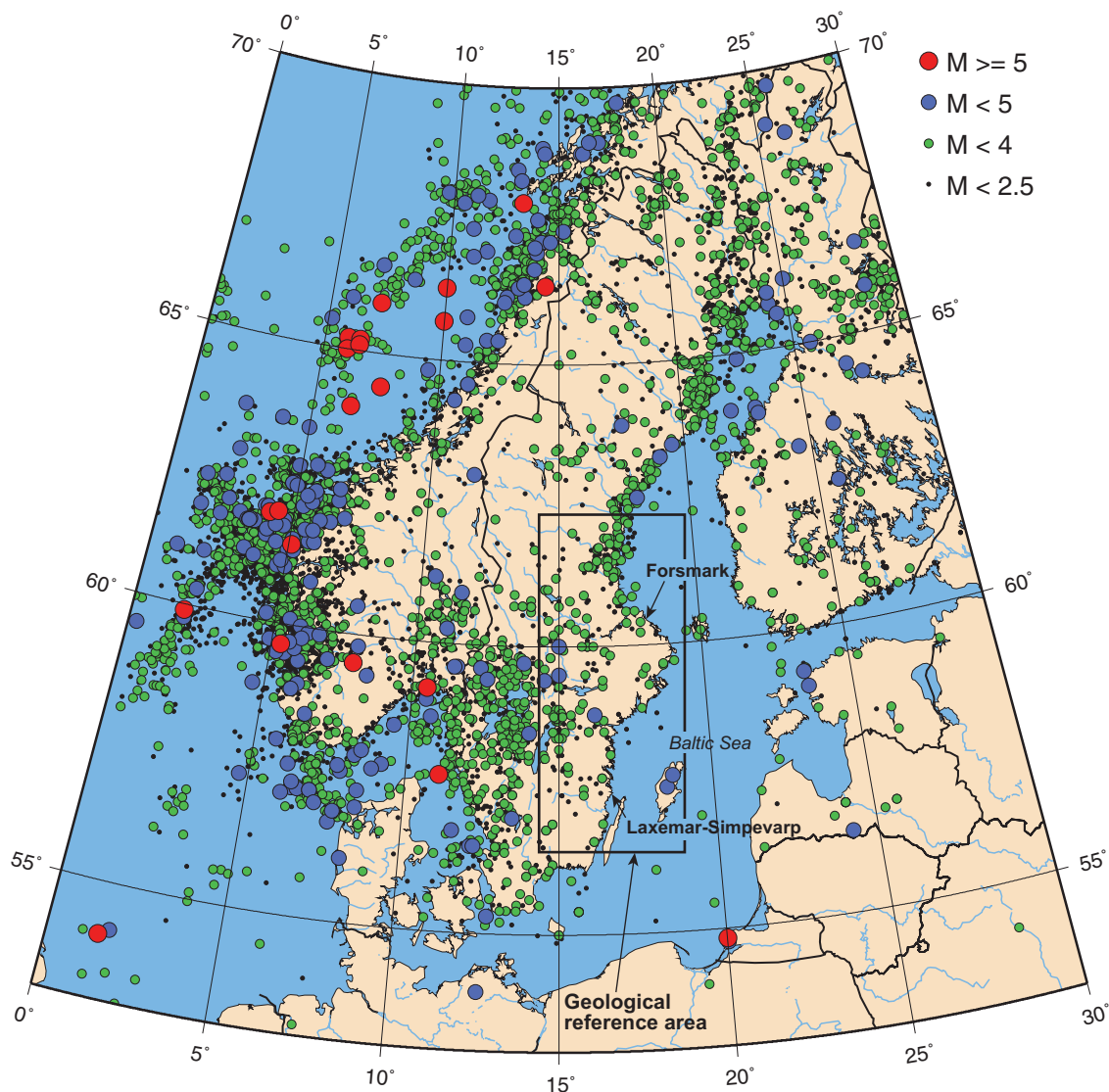
Palaeoseismic activity has been inferred directly by, for example, observations of distinct displacement of the surface that separates the crystalline bedrock from the Quaternary cover or indirectly by observations of seismically derived deformation of Quaternary sediments. The interpretation of aerial photographs provides a tool for identifying morphologically conspicuous lineaments that are candidates for late- or post-glacial faults. A significant number of late- or post-glacial reverse fault scarps have been identified in the northern part of Sweden and it has been inferred that the accompanying earthquakes reached magnitudes of up to M8 or even larger on the Richter magnitude scale. As yet, conclusive evidence for such fault movements is lacking in the southern part of Sweden.

With the aid of a methodology similar to that used in the northern part of the country, detailed investigations have been carried out in the context of the site investigation work to evaluate the occurrence of palaeoseismic activity in and around the Forsmark area. None of the morphological lineaments that have been recognised have been interpreted as representing late- or post-glacial faults. Furthermore, no deformational features in Quaternary sediment have been unambiguously related to seismic activity. On the basis of these results, evidence in the geological record for major (magnitude > M7 on the Richter scale) earthquakes in the Forsmark area is lacking.

Compared with other parts of the world, especially close to plate boundaries, there is generally a low frequency of registered earthquakes throughout historical time in the northern part of Europe, and an absence of earthquakes with a magnitude  $\geq$  M6 on the Richter scale (Figure 3-8). However, seismic activity in Sweden throughout historical time is not evenly distributed over the country (Figure 3-8). Areas of relatively high activity are conspicuous along linear alignments in the northern part of the country, in a broader region in southwestern Sweden and, less conspicuously, in the southernmost part of the country (Skåne). By contrast, much of the geological reference area in southeastern Sweden, including the Forsmark area, shows relatively little seismic activity (Figure 3-8).

The relatively high level of seismicity along the Baltic Sea coast is not an artefact of station distribution or some other factor. The linear alignments of earthquakes, at least in the northernmost part of the country and in adjacent areas in Finland and Norway, have been related to the late- or post-glacial faults that have been recognised with the aid of palaeoseismic studies. The linear alignment along the Baltic Sea coast in Norrland occurs where both land uplift related to post-glacial isostatic rebound is greatest and there is also a tendency towards a decrease in crustal thickness. A correlation between an increased frequency of seismic events and crustal thinning is apparent in southwestern and southernmost Sweden. The crustal thinning occurs in areas where Late Palaeozoic and younger extensional tectonics has taken place. The crust in Sweden below c. 35 km is seismically quiet and this changeover is most probably related to the more ductile character of the crust beneath this depth. Although strike-slip movement is the dominant focal mechanism, irrespective of where in Sweden the seismic event occurred, reverse dip-slip or oblique-slip fault plane solutions are also present. Since seismic events predominantly occur along geologically ancient fractures or planes of weakness in the bedrock, the orientation of these structures has an influence on the focal mechanism. It is also important to keep in mind that the fault plane solutions discussed above pertain to crustal stress at depths affected by seismic activity. Considerable evidence points to a reverse sense of movement in the uppermost part of the crust (c. 1,000 m) in large parts of Sweden, with a vertical or sub-vertical minimum principal stress.

The maximum horizontal stress, as inferred from the seismic data, is oriented WNW-ESE. This direction is in accordance with that expected from plate tectonics with ridge push forces from the mid-Atlantic ridge. These considerations give support to the hypothesis that ongoing plate tectonic processes are important for an understanding of recent seismic activity. Palaeoseismic activity has been explained by the release of stress that accumulated earlier during glacial loading in association with long-term tectonic plate motions. An alternative mechanism that involves the release of high horizontal stresses induced by flexure during loading, in combination with the ambient plate tectonic stresses, has also been discussed. The release of stress and fault instability occurred during unloading and the rapid removal of the ice.



**Figure 3-8.** Epicentre and magnitude of earthquakes on the Richter scale ( $M$ ) in the northern part of Europe between 1375 and 2005 AD. There is no lower limit to the magnitude of the earthquakes shown in the figure. However, since the ability to detect smaller events has changed and gradually improved over time, no precise level of completeness for such data can be provided. Note that earthquake data for the neighbouring countries to the south of the Baltic Sea are also not complete. Modified after Böldvarsson et al. (2006).

### 3.4 Groundwater evolution during the Quaternary period

The groundwater evolution in the Forsmark area has been strongly affected by climate changes in the past. Investigations have shown that the groundwaters observed today have different origins, including glacial meltwater, meteoric water and marine water, depending on the prevailing conditions (e.g. SKB 2008b, Nilsson et al. 2011). Shoreline displacement plays an important role in understanding the infiltration mechanism for these waters. It is particularly important for the intrusion of the saline Littorina Sea water into the bedrock, as well as for the subsequent flushing processes in the upper, more permeable bedrock horizons. It seems that the most recently recharged water tends to flush out older water types, especially in the upper permeable part of the bedrock. However, hydraulic conditions vary over time, and remnants of hydrogeochemical signatures of earlier climatic fluctuations can be preserved in localised areas of low permeability. Thus, palaeohydrogeochemistry provides an important framework for understanding the hydrogeochemical evolution of the bedrock, which is in turn important for a hydrogeochemical and hydrogeological understanding of the site. Hydrogeological changes that have already occurred may be repeated during the lifespan of a repos-

itory (thousands to hundreds of thousands of years). As a result, water types such as brine, glacial water, marine and meteoric waters will intrude and be mixed in a complex manner at various levels in the bedrock.

When the continental ice melted and retreated from the Forsmark area around 8800 BC, glacial meltwater was hydraulically forced under considerable pressure into the bedrock. This took place before the appearance of the Ancylus Lake in the area. The exact penetration depth is unknown and is dependent on the geometry and heterogeneity of the system. However, chemical and isotopic data from rock matrix pore water and from fracture groundwater at Forsmark indicate that the penetration depths of a glacial component are about 400 m and 1,000 m, respectively (Laaksoharju et al. 2008). In the latter case, however, the data, particularly from depths greater than 600 m, do not necessarily reflect the latest deglaciation; they could indicate a cumulative effect over several glaciations.

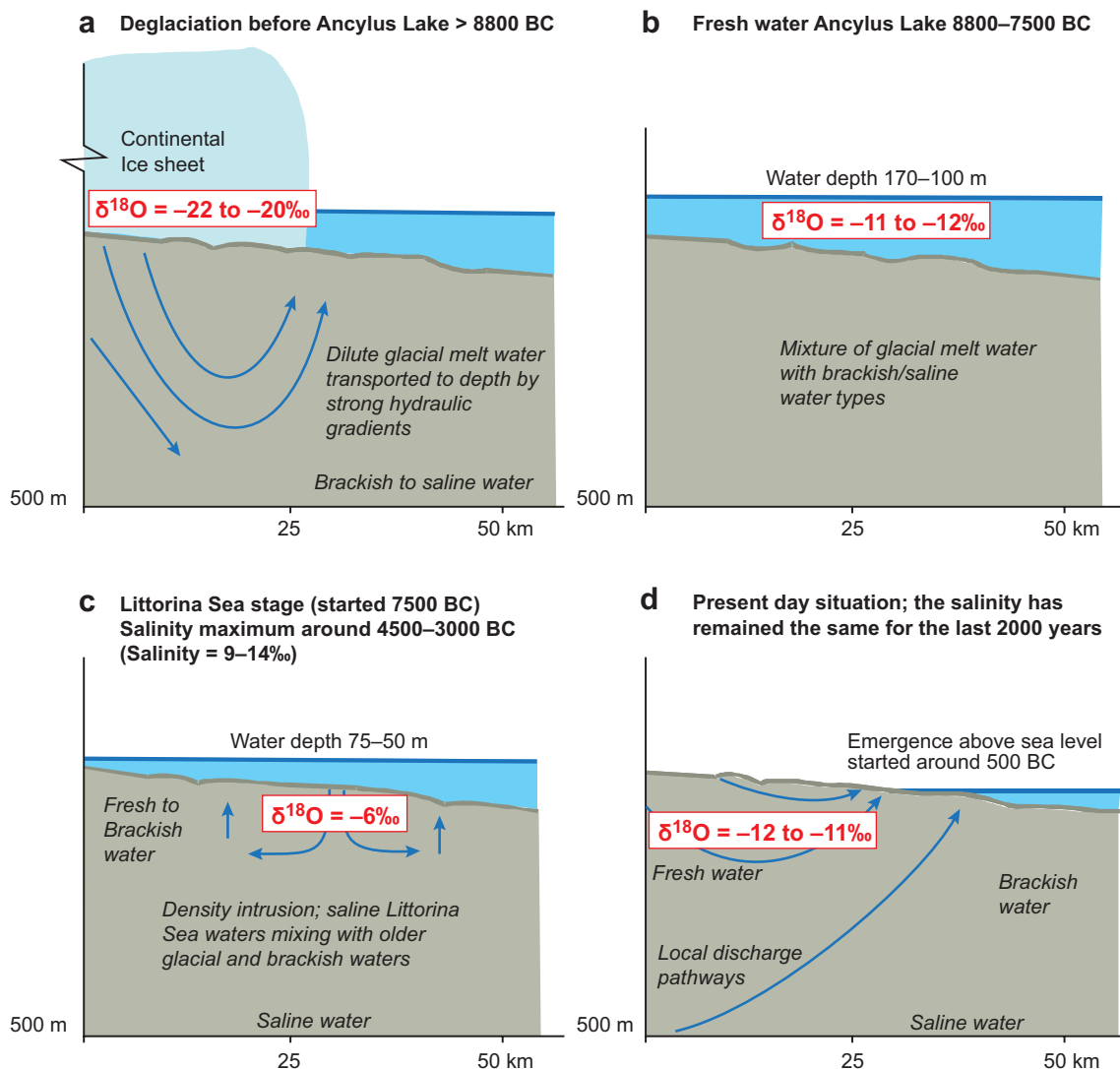
As described in Section 3.2, the post-glacial evolution of the area close to the Baltic Sea can be divided into a number of non-saline and brackish lake/sea stages. Two stages with brackish water can be recognised: the Yoldia Sea (9500 to 8800 BC) and the Littorina Sea (7500 BC to the present). Since the deglaciation of the Forsmark region coincided with the end of the Yoldia Sea stage, there are no signs of water related to the Yoldia Sea in the bedrock. In contrast, the freshwater Ancylus Lake came into being after the deglaciation, followed by the Littorina Sea (see Figure 3-5). During the Littorina Sea stage, the salinity of the water was considerably higher than at the present day, reaching a maximum around 915‰ between 4500 and 3000 BC. Dense brackish seawater from the Littorina Sea was able to penetrate the bedrock, resulting in a density intrusion that affected the groundwater in the more conductive parts of the bedrock. The density of the intruding seawater in relation to the density of the existing groundwater, together with the hydraulic properties of the bedrock, determined the final penetration depth. As the Littorina Sea stage provided the most saline groundwater, it is assumed to have had the deepest penetration depth, eventually mixing with the groundwater mixtures already present in the bedrock, e.g. deep saline water, old meteoric-glacial waters, and Holocene glacial meltwater. The salinity of the sea water has remained relatively constant during the past 2,000 years (cf. Figure 3-6).

When the Forsmark area subsequently emerged from the sea, starting around 500 BC in the western part of the area near Forsmark church, meteoric recharge water formed a layer on top of the saline water due to its low density. As a result of the flat topography of the Forsmark area and of the short period that has elapsed since the area emerged from the sea, the out-flushing of saline water has been limited. For this reason, a freshwater layer is restricted to shallow depth, from the surface down to 25–100 m, depending on hydraulic conditions.

As a result of late- and post-glacial developments, groundwater components of five different origins can be identified in the groundwaters in the Forsmark area (SKB 2008b). The origins of the SFR groundwaters are mainly the same. However, fresh meteoric water components of present precipitation type have not been identified at SFR and are suggested to be of minor significance due to the location of this facility below the Baltic Sea. On the basis of hydrogeochemical data from the SFR regional model area, the groundwater components are, in relative chronological order: Deep saline water (oldest) > Old non-marine brackish waters > Glacial melt water from the last deglaciation > Littorina Sea water > Present Baltic Sea water (recent, probably present due to drawdown effects from the SFR facility). A detailed description of the origins of the groundwaters in the SFR regional model area is given in Chapter 8 in this report.

In order to aid in understanding the step-by-step evolution of groundwater in the Forsmark area during the post-glacial period, i.e. during the Holocene, a conceptual model is presented in Figure 3-9. The palaeohydrological conditions in the area have changed rapidly over time and, as can be seen, the major driving mechanism behind the flow lines is shoreline displacement due to land uplift. Some uncertainties remain in this conceptual model, and these uncertainties are greater further back in time. Hence, the greatest uncertainties are associated with the stage during which injection and subsequently flushing of glacial meltwater took place.





**Figure 3-9.** Conceptual model for groundwater evolution in the Forsmark area during the post-glacial period a) the deglaciation before the Ancylus Lake (> 8800 BC), b) stagnant conditions during the freshwater Ancylus Lake stage between 8800 and 7500 BC, c) density-driven intrusion of Littorina sea water between 7500 BC and 0 AD, and d) the present-day situation. Blue arrows indicate groundwater flow pattern. The existing SFR facility is situated at a depth of  $-60$  to  $-140$  m RHB 70 and the present-day sea water depth is approximately 6 m.

### 3.5 Evolution of ecosystems during the late Quaternary period

Long-term ecosystem evolution in near-coastal areas of Fennoscandia is driven mainly by two different factors: climate change and shoreline displacement. In addition, human activities have strongly influenced the evolution of both terrestrial and aquatic ecosystems, especially during the past millennium.

Shortly after the most recent ice retreat, which started in southernmost Sweden c. 15,000 BC, the landscape was free of vegetation and can be characterised as polar desert. Relatively soon after the deglaciation, the ice-free areas were colonised and in southern Sweden the landscape was covered by a sparse birch forest. Since then, the climate has oscillated between colder and warmer periods. During the cold period called the Younger Dryas (c. 11,000–9500 BC), large areas of the deglaciated parts of Sweden were again affected by permafrost and much of the previously established flora and fauna disappeared. From the onset of the Holocene (c. 9500 BC) and thereafter, southern Sweden has been more or less covered by forests, although the species composition has varied due to climatic changes. Most of the present mammal fauna was established in southern Sweden during the early

Holocene. During the past few thousand years, the composition of the vegetation has changed due not only to climatic changes, but also to human activities which have reduced the areas covered by forest. In southern Sweden, the introduction of agriculture and the subsequent opening of the landscape started c. 3000 BC.

In coastal areas like Forsmark, shoreline displacement has strongly affected ecosystem evolution and is still causing changes in the abiotic environment. As a result of an overall regressive shoreline displacement, the sea floor is being uplifted and transformed into new terrestrial areas or to fresh-water lakes. The initial conditions for ecosystem succession from the original near-shore seafloor are strongly dependent on the topographical conditions. Sheltered bays accumulate organic and fine-grained inorganic material, while the finer fractions are washed out from more wave-exposed shorelines with a large fetch. During the process of shoreline displacement, a sea bay may either be isolated from the sea at an early stage and thereafter gradually turn into a lake as the water becomes fresh, or it may remain a bay until shoreline displacement turns it into a wetland.

After isolation from the sea, the lake ecosystem gradually matures in an ontogenetic process that includes subsequent sedimentation and deposition of substances originating from the surrounding catchment or produced within the lake. Hence, the long-term ultimate fate of all lakes is infilling and transformation to either a wetland or a drier land area, the final result depending on local hydrological and climatic conditions. In Forsmark, all present-day lakes have developed into oligotrophic hardwater lakes that are characteristic of the area. These lakes are slightly alkaline (pH 7.8), with a low total phosphorus concentration (P-tot often lower than 0.015 mg/L), high concentrations of major ions and therefore a high electrical conductivity (often exceeding 35 mS/m). This is a combined effect of the calcium-rich Quaternary deposits, recent emergence from the Baltic Sea and the shallow lake depths, resulting in high primary production at the light-illuminated sediment surface and very low production in the water mass. The high primary production at the sediment surface results in high benthic pH, which in turn causes benthic precipitation of  $\text{CaCO}_3$  and co-precipitation of phosphate. Much of the precipitated phosphorus is more or less permanently locked in the sediments by high pH and high  $\text{O}_2$  concentration.

Mires are formed basically by three different processes: terrestrialisation, paludification and primary mire formation. Terrestrialisation is the filling-in of shallow lakes by sedimentation and establishment of vegetation. Paludification, which is the dominant process of mire formation in Sweden, is an ongoing waterlogging of more or less water-permeable soils, mainly by expanding mires. Primary mire formation is when peat is developed directly on fresh soils after their emergence from water or from under ice. All three processes have likely occurred in the Forsmark area, but infilling of lakes (terrestrialisation) is probably the most common way for peatland to develop in the area. The richer types of mires, which are typical of the Forsmark area, will undergo a natural long-term acidification when they turn into more bog-like mires.

### **3.6 Human population and land use**

The human prehistoric period in the Forsmark region, which is an investigation area around Forsmark including six parishes together covering c. 1,000 km<sup>2</sup> (Berg et al. 2006), is relatively short, since Forsmark was covered with water until c. 500 years BC. Accordingly, the Forsmark region was not permanently settled until the end of the prehistoric period. In the register of prehistoric remains kept by the National Heritage Board, there are about 30 places with one or more prehistoric or cultural remains registered in the investigated region. However, there are many prehistoric settlements further inland in the northern parts of Uppland. The oldest known remains in the Forsmark region are graves from the older Iron Age (300 BC–400 AD), currently situated 10 to 15 m above sea level. These graves were originally situated along the coastline.

The oldest information on settlements in the region is the tax register from 1312 AD, which includes three of the investigated parishes. This source indicates that the region was relatively densely populated in the early medieval period. Between 1312 and 1550 AD, there seems to have been a substantial decrease in the number of settlement units in the region, probably as an effect of the recurrent plague epidemics after 1349 AD (Berg et al. 2006). During the medieval period, the Forsmark region was characterised by small villages, and new settlements were created in the peripheral areas of the older

ones. At the end of the medieval period, the investigated parishes showed a dominance of freeholders and the proportion of farms belonging to the nobility was small.

During the early modern period (i.e. 1550–1750 AD), the establishment of the iron industry in the Forsmark region dramatically affected the surrounding landscape. Production was geared towards the needs of the industry: charcoal production, mining and the production of fodder for animals used in the industry. The ownership structure also changed abruptly with the establishment of large estates. As at many other places in Sweden, there was a substantial population expansion. Many crofts were established in the forested areas around Forsmark, inhabited by people involved in the production of charcoal. The population doubled or increased at an even faster rate between the 1570s and the 1750s.

The large estates in the Forsmark region expanded during the 18<sup>th</sup> century and the number of freehold farms decreased accordingly. The population increased dramatically from the 1780s up to the late 19<sup>th</sup> century. This increase ceased at the turn of the century, and the rural population decreased during the latter part of the 20<sup>th</sup> century. The number of people involved in agriculture has declined, while the number of people employed in industry and crafts is greater than before.

The extent of arable land in the region increased continuously from the colonisation of the area until around 1950 AD. To increase the amount of hay that was fed to the farm animals, small farms and individual families carried out hay-making using the reeds and grasses on wetland areas. Since these areas were often distant and hard to reach, they were mainly used by poor families that needed to feed their animals. Until the middle of the 19th century, there were large wetland areas in the woodlands. From the beginning of the 18th century onwards, much of the new agricultural land was gained by draining wetlands. Some of these areas are still cultivated, whereas others are now deserted and have in some cases been turned into woodlands. Between the early 1900s and the 1950s there was little change in arable land use in the Forsmark region. However, since the 1950s, a significant portion of the former open land has been abandoned and current land use is completely dominated by forestry. During the last few decades, the establishment of the Forsmark nuclear power plant has resulted in substantial changes in land use, transforming parts of the area from relatively pristine, rural conditions to an industrial park and a semi-urban society.

## 4 Surface system and surface-bedrock interactions

This chapter provides a brief description of the surface system, i.e. topography, regolith, hydrology and near-surface hydrogeology, hydrogeochemistry, terrestrial, limnic and marine ecosystems, and the interactions between the surface system and the bedrock. The surface system description concerns an area that is larger than the SDM-PSU regional model area, which under present-day conditions is located almost completely below the sea (cf. landscape model area in Figure 1-3). Ongoing shoreline displacement (Chapter 3) entails that the regional model area eventually will rise above sea level and become land. One reason for including present land areas in the description in this chapter is that it is reasonable to expect that such future land areas will resemble the present-day land areas. Moreover, radionuclides that are released from the SFR facility in the future will be transported to downstream areas, currently located below the sea and outside of the SDM-PSU regional model area. In the following, the area included in the description of the surface system is, for simplicity's sake, referred to as the Forsmark area, even though the actual area differs somewhat between different surface system disciplines.

The description is based on data and modelling within several scientific disciplines concerning properties and processes on various spatial and temporal scales. The main purpose of this chapter is to identify important aspects and main background reports, which provide details and also contain references to further supporting reports. The description of the historic evolution of the site forms a basis for the understanding of present-day conditions. This description is provided in Chapter 3 and in Söderbäck (2008).

Previous descriptions of the surface system at Forsmark have been presented in connection with the SFR safety assessment project SAFE (Kautsky 2001), whereas the most recent description in the context of SDM-Site (Lindborg 2008) provided input to the safety assessment (SR-Site) related to the planned repository for spent nuclear fuel at Forsmark (SKB 2010). Investigations, available data and other prerequisites for the present site description are summarised in Chapter 2. As regards the surface system, the following are examples of supplementary investigations and modelling activities that provide input to the present site description and/or the safety assessment SR-PSU (i.e. the assessment of the long-term radiological safety of the entire SFR facility).

- Supplementary investigations of the bathymetry (bottom level) in marine areas close to the SFR facility, and development of a new digital elevation model (DEM, now available) and a new model of regolith depth and stratigraphy (will be reported for SR-PSU).
- Evaluation of additional time series of hydrogeological, hydrological and meteorological monitoring data (will be reported for SR-PSU).
- Updated numerical modelling of hydrology and near-surface hydrogeology, including boreholes at and close to the SFR facility (will be reported for SR-PSU).
- Supplementary regolith and sediment sampling for analysis of solute transport properties (e.g.  $K_d$ ), to be reported for SR-PSU.

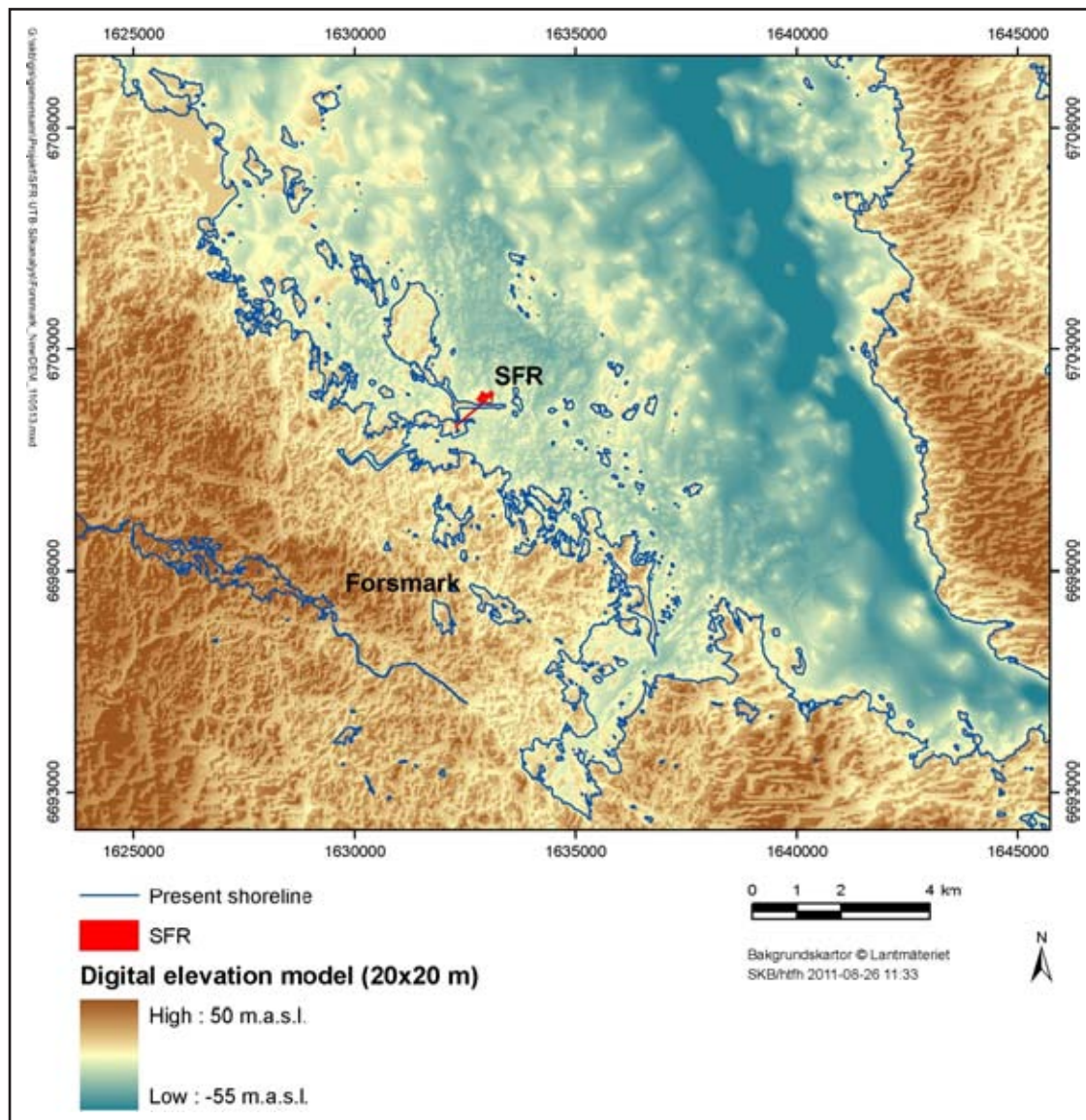
The present description is divided into abiotic characteristics (Section 4.1), ecosystems (4.2), human utilisation and natural resources (4.3) and surface-bedrock interactions (4.4). Abiotic characteristics (e.g. topography, hydrology, climate, and physical and chemical properties of the regolith) determine the limits for development of ecosystems and human utilisation of the landscape. Moreover, there is an interdependency between abiotic factors, ecosystem development and the resulting chemical environment; formation of ecosystems influences abiotic factors (e.g. soil properties and hydrochemical characteristics of surface waters), whereas abiotic factors provide the conditions for the formation of specific ecosystems.

## 4.1 Abiotic characteristics

### 4.1.1 Topography

A new DEM (digital elevation model) has recently been developed to describe the topography of the Forsmark area (Figure 4-1). The DEM, which has a resolution of 20 m, is an important input to other models for projections of past and future conditions, and it is used as input to most descriptions and models mentioned in this chapter. The topography of Forsmark is characterised by low relief. The marine areas have a gentle slope towards the northwest. The highest observed point is at 50 m elevation and is located in the southwestern part of the DEM area. A deep trough (Gräsörännan) runs in the north-south direction in the eastern part of the embayment, and the lowest point (-55 m elevation) is located in the northern part of this trough.

In the terrestrial areas, the DEM is based on aerial photographs taken from an altitude of 2,300 m. In the marine areas, the DEM is constructed using a combination of nautical charts, supplementary depth probing and marine geological surveys. The new DEM is an update of the previously developed DEM (Strömngren and Brydsten 2008), primarily based on supplementary ecosounding investigations in marine areas.



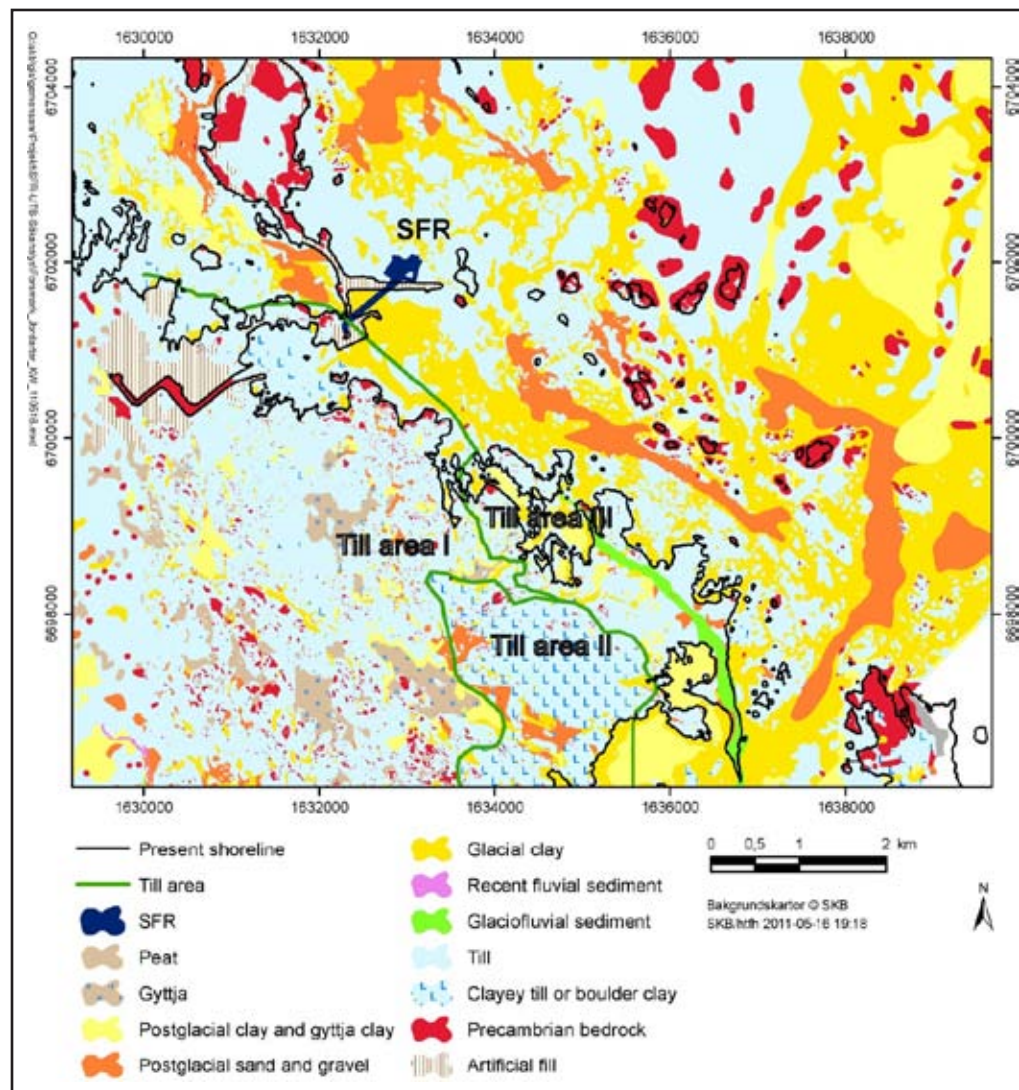
*Figure 4-1. DEM (digital elevation model) of the Forsmark area, including the bathymetry (bottom level) of lakes and the near-coastal sea. The map shows present lake shorelines, the present shoreline towards the sea and the location of the existing SFR facility.*

#### 4.1.2 Regolith

Regolith refers to unconsolidated deposits above the bedrock. The regolith in Forsmark was deposited during the Quaternary period and is therefore commonly denoted “Quaternary deposits” (QD). Soil is the upper part of the regolith in terrestrial areas that is affected by soil-forming processes in the form of e.g. frost action, weathering and bioturbation.

The descriptions of the spatial distribution of the QD and its properties are based on primary data obtained from extensive field mapping, investigations in the form of drilling, excavations and geophysics, and physical and chemical laboratory tests. For further details on the availability of primary data associated with the QD and soil and evaluations of such data, see Hedenström and Sohlenius (2008) and Lundin et al. (2004).

The surface distribution of the QD (Figure 4-2) is typical for areas located below the highest post-glacial coastline. Till is the dominant type of QD and occupies some 65% of the surface in terrestrial areas and 30% of the sea bottom outside Forsmark. Glaciofluvial sediments occur at the Börstilåsen esker. Clay occurs primarily in depressions on the sea bottom and below present lakes. Postglacial clay, including clay gyttja, is predominantly found in the deeper parts of the sea bottom. The sea bottom north of the SFR pier is dominated by till, whereas areas south of the pier are dominated by glacial clay.



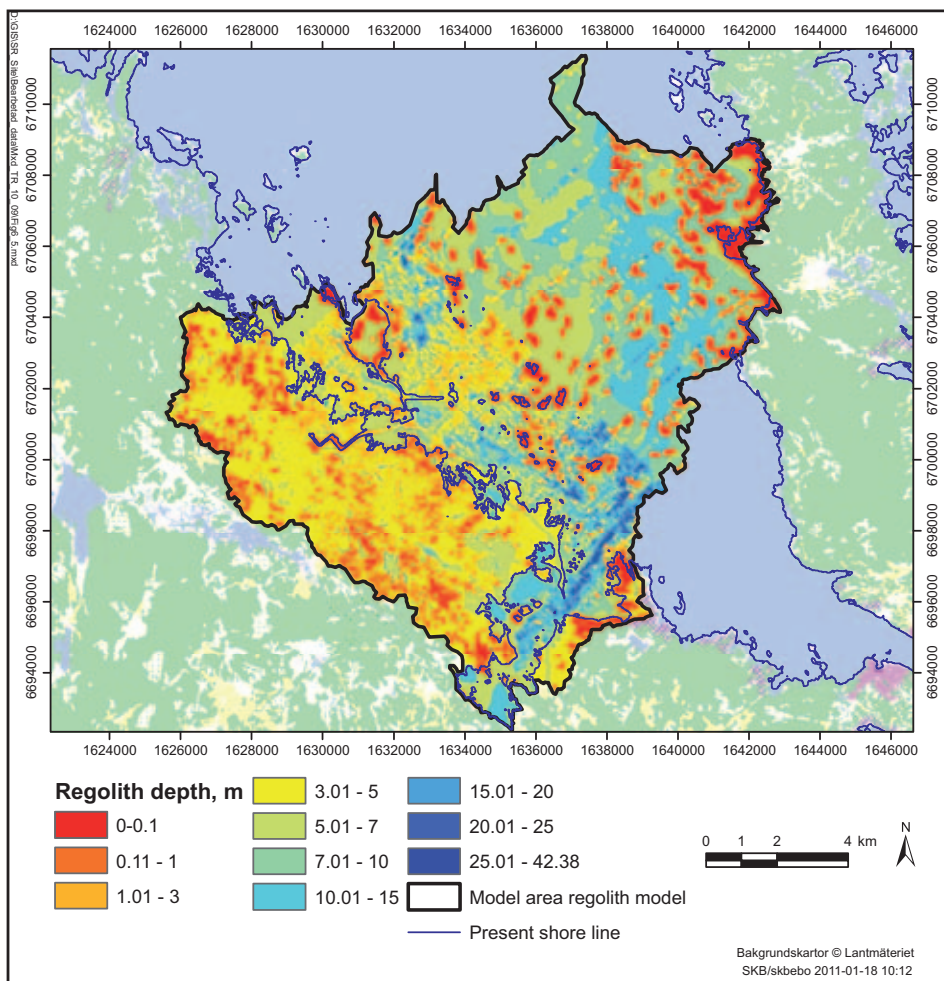
**Figure 4-2.** Surface distribution (at a depth of 0.5 m) of the QD and areas with exposed bedrock in the Forsmark area (modified from Figure 5-4 in SKB 2010). Note that lakes and the sea are shown without surface water. The map also shows the boundaries of the three local till domains (I – III) in terrestrial areas.

The description of the surface distribution of different soil types was obtained using the QD map (Figure 4-2) and background maps of vegetation type, land use and wetness index (a function of local contributing upslope area and slope). Soil type classifications were conducted in pits dug in each land use type. The dominating soil type found in terrestrial areas of Forsmark is Regosol, i.e. young soil characterised by poor soil profile development in areas without permafrost.

The till in the terrestrial areas of Forsmark is subdivided into three local domains (see Figure 4-2): (I) the largest domain, containing sandy and silty till, (II) clayey till and boulder clay, and (III) sandy till with a high boulder frequency (Hedenström and Sohlenius 2008). Till and glacial clay in Forsmark have a high content of calcium carbonate ( $\text{CaCO}_3$ ), which originates from Palaeozoic limestone that outcrops on the sea bottom north of the Forsmark area.

A regolith depth and stratigraphy model (RDM, Figure 4-3) has previously been developed to provide a geometric model of depths and layers at a landscape level (Hedenström et al. 2008). The RDM is based on the general top-down stratigraphy for the Forsmark area, consisting of peat, gyttja (present below lakes), clay gyttja-gyttja clay (present in coastal areas and below lakes), postglacial sand/gravel (present in marine areas), glacial clay, glaciofluvial sediments, and till.

In the RDM, the regolith (i.e. the QD) is subdivided into seven layers and three generalised lake sediment lenses. The total regolith depth in the RDM area varies between 0.1 and 42 m. As can be seen from Figure 4-3, the coastal zone and the islands (including the coastal zone of the island of Gräsö) are characterised by thin regolith and frequent bedrock outcrops. Generally, the regolith is deeper in the marine area (average depth c. 8 m), whereas the average depth in the terrestrial area is c. 4 m. The QD depth is up to 10 m north of the SFR pier and up to 20 m south of the pier.



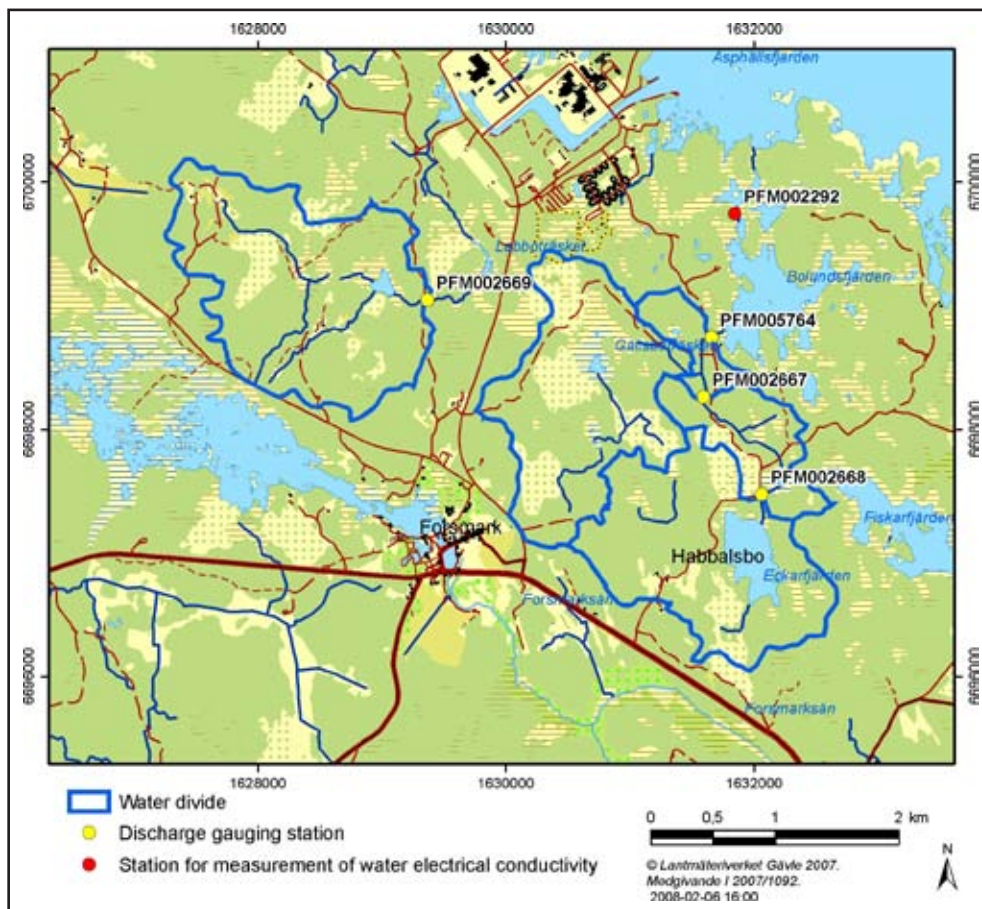
**Figure 4-3.** Modelled total regolith depth at Forsmark (Figure 5-5 in SKB 2010). A new RDM will be reported for SR-PSU.

A new RDM will be used in the safety assessment SR-PSU. Updates compared to the previous RDM (changes are not expected to be significant) are primarily based on supplementary marine geological surveys (Nyberg et al. 2011). Other supplementary information for the new RDM includes regolith depths and stratigraphy data obtained from probing and drilling in wetlands (Sohlenius and Hedenström 2009, Werner et al. 2009).

#### 4.1.3 Meteorology, hydrology and near-surface hydrogeology

Comprehensive field investigations and modelling activities have been conducted regarding meteorology, hydrology and near-surface hydrogeology at Forsmark. There is an ongoing long-term monitoring programme in the Forsmark area, including meteorological parameters, surface water levels, stream discharges and groundwater levels in the QD (SKB 2007). For further details on the availability of primary data and prior data evaluations, see Johansson (2008) and Johansson and Öhman (2008). Time series data collected subsequent to SDM-Site and evaluation of these data will be reported for SR-PSU.

In all, 25 lake-centred catchment and sub-catchment areas (sizes 0.03–8.67 km<sup>2</sup>) have been delineated within the Forsmark area (Brunberg et al. 2004). Wetlands are frequent and cover more than 25% of some sub-catchments (Johansson 2008). The largest lakes are the lakes Fiskarfjärden, Bolundsfjärden, Eckarfjärden and Gällsboträsket (see Figure 4-4). Even the largest lakes are smaller in size than 1 km<sup>2</sup> and they are also quite shallow (average depths less than 1 m). Seawater intrusion occasionally takes place into the lakes located close to the sea (Norra Bassängen, Puttan, Bolundsfjärden, Lillfjärden and Fiskarfjärden) during periods with very high sea level. The streams in Forsmark are small and long stream sections are dry during summer. However, the stream sections located downstream from Lake Gunnarsboträsket, Lake Eckarfjärden and Lake Gällsboträsket carry water for most of the year.



**Figure 4-4.** Overview map showing the four largest lakes in the Forsmark area (Fiskarfjärden, Bolundsfjärden, Eckarfjärden and Gällsboträsket). The map also shows the locations of streams, discharge gauging stations and associated catchment areas (Figure 2-5 in Johansson 2008). SKB's meteorological station is located near the shoreline, south of the cooling water channel for the Forsmark power plant.



The mean annual air temperature at Forsmark is approximately +7°C and the vegetation period (mean air temperature above +5°C) lasts approximately from May to September. The dominating wind direction is from the southwest. For the four-year period of June 2003–May 2007, the locally measured (and corrected for e.g. wind losses) mean annual precipitation was 563 mm (the estimated long-term mean annual precipitation is 559 mm), whereas the mean annual calculated potential evapotranspiration was 526 mm. Some 25–30% of the annual precipitation falls in the form of snow.

Based on the meteorological and hydrological monitoring programme (also including data from surrounding stations operated by SMHI, the Swedish Meteorological and Hydrological Institute), the long-term water balance of the Forsmark area can be estimated as precipitation = 560 mm·y<sup>-1</sup>, actual evapotranspiration = 400–410 mm·y<sup>-1</sup>, and runoff = 150–160 mm·y<sup>-1</sup>. The estimated long-term runoff in the Forsmark area is slightly lower than the long-term average at the SMHI discharge station at Vattholma (located further inland), due to less precipitation closer to the coast (Johansson et al. 2005).

The infiltration capacity of the QD generally exceeds rainfall and snowmelt intensities, and groundwater recharge is dominated by precipitation and snowmelt. Generally, the lakes are recipients of groundwater discharge during most of the year. However, intense evapotranspiration during summer lowers groundwater levels, and some lakes may periodically switch to becoming recharge areas.

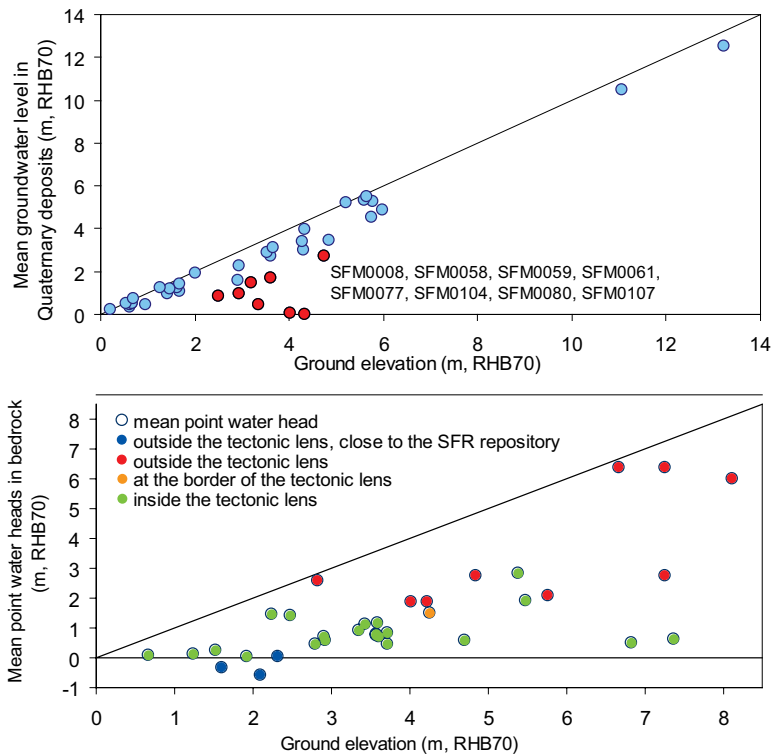
The horizontal hydraulic conductivity of the till that dominates the area decreases from more than 10<sup>-5</sup> m·s<sup>-1</sup> near the ground surface to c. 10<sup>-6</sup> and 10<sup>-7</sup> m·s<sup>-1</sup> at the depths for coarse and fine-grained till, respectively. Slug test data indicate a higher hydraulic conductivity at the bedrock-QD interface than in the till itself. Moreover, comparisons between field and laboratory data indicate that the till is anisotropic, with the horizontal hydraulic conductivity being on the order of 30 times greater than the vertical conductivity.

The groundwater table in the QD is generally shallow (within 1 m of the ground surface) and follows the ground surface topography (see the upper plot of Figure 4-5). Hence, surface water divides and groundwater divides in the QD can be assumed to coincide. The small-scale topography results in shallow, local groundwater flow systems in the QD that overlie larger-scale flow systems in the bedrock. Within the tectonic lens at Forsmark, measured groundwater levels in the bedrock are slightly above the current sea level and considerably lower than those in the QD (lower plot of Figure 4-5). The lens is hence characterised by a weak coupling between groundwater levels in the upper part of the bedrock and the ground surface elevation, in contrast to conditions outside the tectonic lens. As shown in Figure 4-5, groundwater levels measured in the bedrock close to the SFR facility are at or below the current sea level.

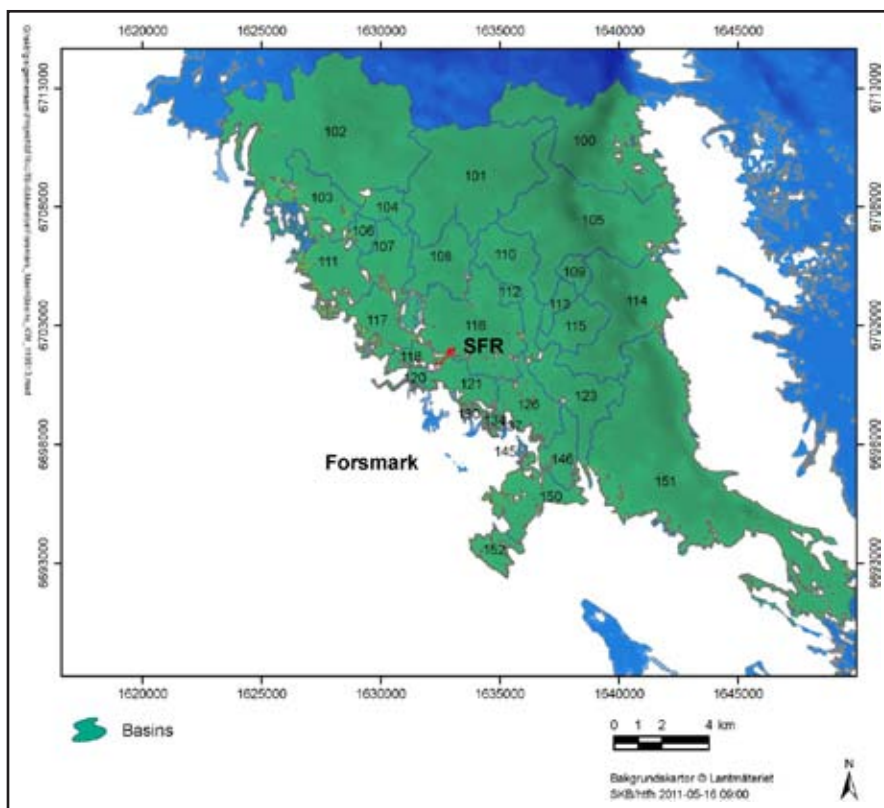
Comprehensive modelling activities concerning the hydrology and near-surface hydrogeology of the Forsmark area have been carried out using the modelling tool MIKE SHE. These modelling activities have focused on present (Bosson et al. 2008) as well as future conditions, including the construction and operating phases of a spent fuel repository and an extension of the SFR facility (Mårtensson and Gustafsson 2010, Mårtensson et al. 2010) and long-term landscape development (Bosson et al. 2010). An updated MIKE SHE model of the Forsmark area will be available for SR-PSU. The updated model will include the new DEM, the new RDM, as well as monitoring data collected subsequent to SDM-Site.

#### **4.1.4 Coastal oceanography**

The marine area at Forsmark consists of the open-ended embayment Öregrundsgrepen, with a wide and deep boundary towards the north and a narrow and shallower strait towards the south. Based on the sea bathymetry according to the previous DEM (Strömberg and Brydsten 2008), the marine area was divided into 28 sub-basins (Figure 4-6) with a total area of 246 km<sup>2</sup>. The sub-basin delineation will be updated based on the new DEM (Figure 4-1) and be available for SR-PSU. Most of this coastal area is shallow (sea depth less than 10 m), except for the previously mentioned Gräsörännan trough with sea depths exceeding 40 m. Salinity stratification in Öregrundsgrepen is generally weak. Local freshwater runoff produces slightly lower salinity compared to the Gulf of Bothnia (Aquilonius 2010). The direction of the flow through Öregrundsgrepen varies with time, but on an annual basis there is a net flow directed from north to south (Karlsson et al. 2010).



**Figure 4-5.** Cross plots of groundwater levels in QD (upper plot, red dots represent outliers) and bedrock (lower plot) versus ground surface elevations (Figures 3-41 and 3-47 in Johansson 2008). Groundwater levels in the bedrock are denoted “point water heads” due to differences in salinity (and thereby in density) with depth.



**Figure 4-6.** Coastal sub-basins (based on the previous DEM) projected on the bathymetry map of Forsmark (Figure 5-8 in SKB 2010). The SDM-PSU regional model area comprises the sub-basins denoted 116, 118 and 121. The inlet to the cooling water channel for the Forsmark power plant is visible in sub-basin 120, and the location of the SFR facility is indicated on the map. The sub-basin delineation will be updated based on the new DEM and available for SR-PSU.

According to the sub-basin delineation based on the previous DEM, the water retention time in the 28 sub-basins was calculated to vary between 13 and 34 days (22 on average) (Karlsson et al. 2010). Water turnover is more rapid in the deeper areas close to the open Bothnian Sea, whereas turnover is slower in the partly isolated shallow sub-basins 117 and 118 (see Figure 4-6). The water retention calculations will be updated when sub-basin delineations based on the new DEM are available. Most of the sea bottom consists of shallow and exposed hard bottoms (boulders or bedrock), interspersed by deeper valleys with soft-bottom communities. A few near-coastal bays (e.g. Kallrigafjärden in sub-basins 146, 150, 152) are more or less secluded and host soft-bottom communities.

#### 4.1.5 Hydrogeochemistry

The hydrogeochemistry (chemistry of surface water, groundwater, QD and sediments) of the surface system at Forsmark has been the subject of various site investigation and modelling activities, including studies of the hydrochemistry of limnic and marine systems (Andersson 2010, Aquilonius 2010, Qvarfordt et al. 2010, Sonesten 2005), the chemistry of terrestrial systems including geochemistry of QD and sediments (Hedenström and Sohlenius 2008, Löfgren 2010), and synthesis reports concerning the chemistry of the surface system (Tröjbom and Grolander 2010, Tröjbom and Nordén 2010, Tröjbom and Söderbäck 2006, Tröjbom et al. 2007). A recent study was also conducted to learn more about dissolved carbon pools in mires of Forsmark (Löfgren 2011). There is an ongoing long-term hydrochemical monitoring programme at the site, including surface waters and groundwater from QD and bedrock (SKB 2007).

The high content of calcium carbonate in the QD and the recent emergence of the area above sea level affect the chemistry of the surface water and shallow groundwater. Specifically, the surface water and shallow groundwater in Forsmark are generally slightly alkaline (pH 7.8) and have high contents of major constituents, caused by marine and glacial remnants deposited during the latest glaciation. The calcite has had a strong influence on the development of terrestrial and limnic ecosystems at the site. For instance, secondary calcite precipitation and co-precipitation of phosphate contribute to the development of the nutrient-poor oligotrophic hardwater lakes that are characteristic of the Forsmark area.

An important contribution of the hydrochemical data evaluation concerns interpretation of water flow systems in the Forsmark area, focusing on evidence for deep groundwater discharge. These issues are discussed further in Section 4.4.2.

## 4.2 Ecosystems

### 4.2.1 Terrestrial ecosystems

The terrestrial vegetation is strongly affected by topography, QD characteristics and human land use. Some three quarters of the land area in Forsmark is covered by forests, dominated by Scots pine (*Pinus sylvestris*) and Norway spruce (*Picea abies*) (Löfgren 2010). Due to the calcareous QD, the field layer is characterised by herbs, broad-leaved grasses and many orchid species. The area has a long history of forestry, with a large percentage of younger and older clear-cuts in different succession stages. As mentioned previously, wetlands are frequent and cover more than 25% of some sub-catchments. Most wetlands are coniferous forest swamps or open mires. Less mature wetlands consist of rich fens due to the high calcareous content of the QD. Agricultural land (arable land and grassland) covers only a minor portion of the land area of Forsmark.

The most common larger mammal species in the Forsmark area are roe deer (*Capreolus capreolus*) and moose (*Alces alces*). Altogether, 96 bird species have been found in the Forsmark area. The most common species in Forsmark are, as in the rest of Sweden, chaffinch (*Fringilla coelebs*) and willow warbler (*Phylloscopus trochilus*) (Löfgren 2010). It can be concluded that Forsmark is a very valuable area from a nature conservation point of view. The highest natural values are associated with wetlands and forests containing red-listed and/or legally protected species (Hamrén and Collinder 2010), such as the rare species fen orchid (*Liparis loeselii*) and pool frog (*Rana lessonae*).

Modelling of the carbon dynamics for two conifer forests (i.e. the dominant vegetation type in Forsmark) and one forested wetland show that the largest carbon flux in terrestrial ecosystems is the uptake of carbon by primary producers, and that the vegetation at all the investigated localities acts as a carbon sink (Löfgren 2010). This net primary production sets an upper limit on the potential uptake of different elements into biomass, which in turn limits the extent of further propagation up the food web. Eventually, biomass reaches the soil compartment as litter, where it is mineralised. The balance between litter production and heterotrophic respiration determines to what extent organic material (and incorporated elements) can be accumulated in the soil.

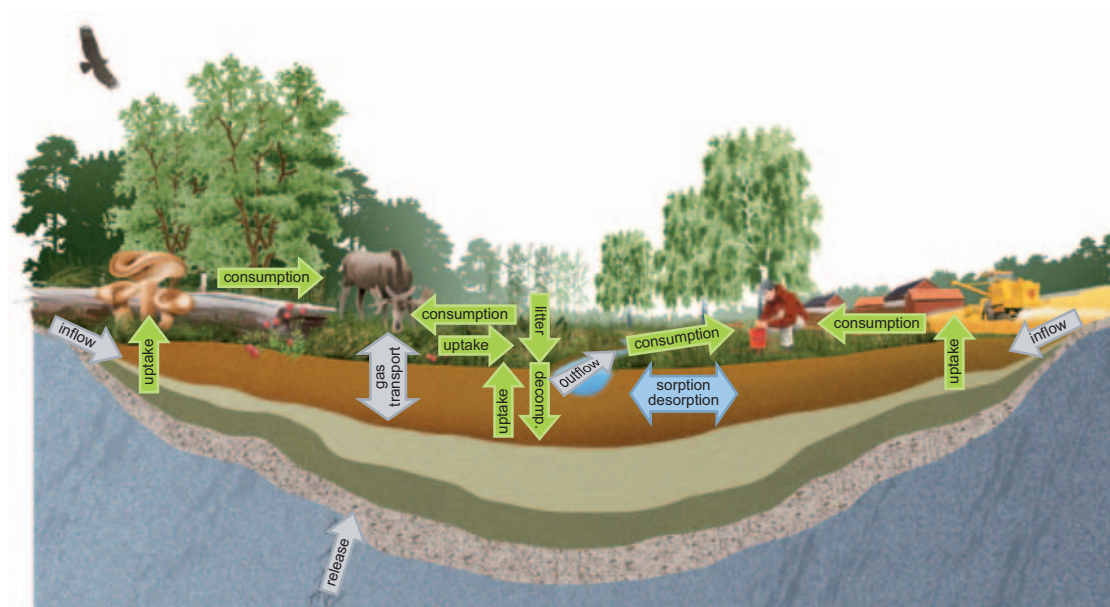
Dynamic vegetation modelling shows that also other vegetation types (e.g. deciduous trees, meadows and arable land) are carbon sinks, with the exception of clear-cut forests that act as carbon sources. Figure 4-7 illustrates a compilation of important processes for a mire ecosystem. Further details on the availability of primary data associated with terrestrial ecosystems and evaluations of such data are provided in Löfgren (2010).

#### 4.2.2 Limnic ecosystems

The lakes in the Forsmark area are small and shallow. They are characterised as oligotrophic hard-water lakes, with high levels of calcium and low nutrient levels (Andersson 2010). This lake type is common along the coast of northern Uppland, but rare in the rest of Sweden (Brunberg et al. 2002, Hamrén and Collinder 2010).

Shallow depths and moderate water colour permit photosynthesis in the entire benthic habitat, and the lake bottoms are covered by dense stands of macroalgae and a thick layer of microphytobenthos (microscopic algae and cyanobacteria). These two types of primary producers dominate the biomass and primary production, making phytoplankton biomass and production less important.

All lakes are surrounded by reed belts, which are extensive especially around the smaller lakes. The fish community in the lakes of Forsmark is dominated by perch (*Perca fluviatilis*), roach (*Rutilus rutilus*), tench (*Tinca tinca*) and crucian carp (*Carassius carassius*), of which the two latter species are resistant to low oxygen concentrations during winter.

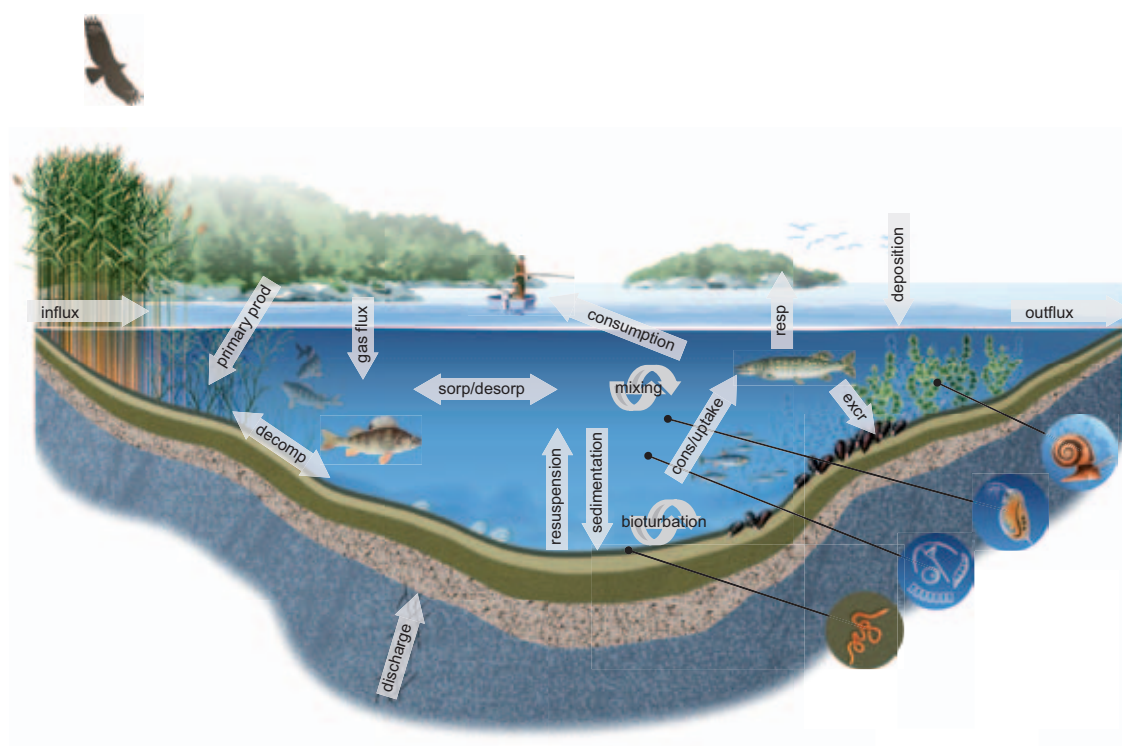


**Figure 4-7.** Conceptual model of important fluxes affecting transport and accumulation of elements in a wetland ecosystem and arable land on a drained part of a mire (Löfgren 2010). Green arrows are fluxes mediated by biota (including water for drinking), grey arrows are water and gas fluxes, the blue arrow represents sorption/desorption processes. The mire was preceded by a lake stage and a marine stage, in which gyttja/clay and postglacial clay were deposited prior to the peat (Figure 5-11 in SKB 2010).

The streams in the Forsmark area are small and long stream stretches are dry during summer. However, some streams close to the coast carry water for most of the year and may function as passages for migrating spawning fish, and extensive spawning migration has been observed between the sea and Lake Bolundsfjärden. The two large streams Olandsån and Forsmarksån, located outside of the Forsmark area, carry water during the whole year and discharge into the sea bay of Kallrigafjärden. The abundance of vegetation in the streams is heterogeneously distributed, varying between 0 and 100% coverage of the stream bed but with some longer parts with intense growth (75–100% coverage) (Andersson et al. 2011).

Both abiotic and biotic processes influence transport and accumulation of elements in limnic ecosystems (Figure 4-8). Modelling of carbon dynamics in limnic ecosystems shows that, contrary to typical Swedish lakes, primary production exceeds respiration in many lakes in the Forsmark area (Andersson 2010). In some of the larger lakes in the area (e.g. Bolundsfjärden and Eckarfjärden), the primary production involves large amounts of carbon compared with the amounts that are transported from the surrounding catchment area. Consequently, there is a large potential for carbon entering the lakes to be incorporated in the lake food web via primary producers. However, much of the primary produced carbon is circulated within the microbial food web and transferred back to abiotic pools or sequestered in sediments.

In the larger lakes, there is a relatively large accumulation in sediments, which can be a permanent sink for radionuclides and other pollutants. In smaller lakes, the amounts of carbon involved in primary production are small compared with the amounts transported from the surrounding catchment area. According to the ecosystems modelling, these lake systems function more as through flows. The chemical properties of the elements, the size of the lake and its location in the catchment area determine the fate of elements entering lake systems in the Forsmark area. Further details on the availability of primary data associated with limnic ecosystems and evaluations of such data are provided in Andersson (2010).



**Figure 4-8.** Conceptual model of important fluxes affecting transport and accumulation of elements in aquatic (i.e. limnic and marine) ecosystems (Figure 5-13 in SKB 2010).

### 4.2.3 Marine ecosystems

Due to upwelling along the coast, the marine ecosystems of the Forsmark area are rather productive in a region of otherwise fairly low primary production (Aquilonius 2010). The salinity of the seawater is low due to a large freshwater supply. The low salinity strongly affects the marine environment, as few organisms are adapted to such brackish conditions. Therefore, the fauna consists of a mix of freshwater and saltwater species. The marine biota in the area is dominated by benthic organisms such as microalgae, vascular plants and benthic microalgae. Both hard and soft bottom substrates are dominated by detritivores: snails and mussels feeding on dead material. The fish community is dominated by the marine species herring (*Clupea harengus*) in the pelagic zone, whereas limnic species (especially Eurasian perch, *Perca fluviatilis*) dominate in near-coastal areas and in secluded bays. Supplementary investigations that will be available for SR-PSU include vegetation mapping on the sea floor and mapping of reeds in shallow bays (Aquilonius 2011, Strömgren and Lindgren 2011).

As for limnic ecosystems (cf. Figure 4-8), both abiotic and biotic processes influence transport and accumulation of elements. However, modelling of carbon budgets show that in marine ecosystems advective flux (water turnover) is often the dominating factor for transport and accumulation of elements (in particular in open and more offshore basins), and in comparison, biotic fluxes (i.e. transport from terrestrial areas) are less important.

The modelling of the 28 delineated marine sub-basins based on the previous DEM (Figure 4-6) shows that the whole marine area as an average has positive NEP (Net Ecosystem Production). Specifically, shallow areas near the coastline have positive NEP, whereas more offshore areas have negative NEP. Further details on the availability of primary data associated with marine ecosystems and evaluations of such data are provided in Aquilonius (2010).

## 4.3 Human utilisation and natural resources

The Forsmark SDM-Site regional model area (see Figure 2-8) is sparsely populated and there are no permanent residents in a 20 km<sup>2</sup> area along the coast (Miliander et al. 2004). Land use has previously been dominated by commercial forestry, and wood extraction has been the only significant anthropogenic outflow of biomass from the area. The only agricultural activity at present is situated at Storskäret. It is focused on meat production and the cattle graze outdoors during the vegetation period.

The Forsmark power plant is a large industrial activity in an otherwise relatively undisturbed area. Current water handling at the Forsmark power plant includes a cooling water channel from the sea, the use of Lake Bruksdammen (west of “Forsmark” in Figure 4-4) as a drinking water supply, and a groundwater drainage system at the power plant. The predominant leisure activity in the area is hunting. Forsmark is only occasionally used for leisure activities due to the small local population, the relative inaccessibility of the area and its distance from major urban areas.

## 4.4 Surface-bedrock interactions

This section describes some aspects of the surface system that are of importance for the bedrock modelling and for the integrated conceptual description of Forsmark. The following description focuses on the upper part of the bedrock, the bedrock-QD interface and the QD itself.

### 4.4.1 Hydrology and hydrogeology

Within the tectonic lens at Forsmark, the uppermost part of the bedrock recognised as a separate fracture domain (Olofsson et al. 2007) has a large influence on the overall groundwater flow (Follin 2008). Specifically, the upper bedrock within part of the tectonic lens contains a lattice of high-transmissive structures (extensive horizontal fractures/sheet joints). As mentioned in Section 4.1.3, groundwater levels measured in the QD and the bedrock indicate groundwater recharge to the

bedrock within the tectonic lens. In contrast, for most areas outside the tectonic lens, MIKE SHE flow modelling results (Bosson et al. 2010) indicate groundwater discharge, with groundwater flow from the bedrock to the QD.

Site investigation data indicate that the horizontal hydraulic conductivity of the till overlying the bedrock decreases with depth, and data also indicate that the till is anisotropic (the vertical hydraulic conductivity is lower than the horizontal). Moreover, there are indications that the bedrock-QD interface is rather permeable. According to pumping-test data, there is a limited hydraulic contact between Lake Bolundsfjärden and the underlying till Johansson (2008), most likely due to low-permeable lake sediments.

Groundwater levels in the QD are of potential interest for setting the upper boundary condition in hydrogeological models. As described in Section 4.1.3, the groundwater table in Forsmark is shallow and generally follows the topography of the ground surface. Pronounced outliers, with greater depths to the groundwater table and also close correlations to sea-level variations, are located below the ridge of the Börstilåsen glaciofluvial deposit (esker). The depth to the groundwater table in the pier at SFR, which is constructed from coarse materials (blast rock), is also probably great, the groundwater table being at or close to sea level.

As an alternative to groundwater levels in the regolith, flux can be used when setting the upper boundary condition in hydrogeological models. Water balances are basic inputs for assigning a flux boundary condition, and such balances are available based on both measurements and calculations (see Section 4.1.3 and Johansson 2008).

#### **4.4.2 Hydrogeochemistry and solute transport**

Hydrochemical data have been used explicitly for interpretation of surface-bedrock groundwater flow systems. The emphasis has been on conditions within potential groundwater discharge areas, focusing on evidence for deep groundwater discharge (Johansson 2008, Tröjbom et al. 2007). Specifically, principal component analysis (PCA) was used to separate groundwater types in the bedrock in terrestrial areas and for comparisons with hydrochemical signatures of surface waters and groundwater in the QD.

According to the analysis, most groundwaters from the QD are of meteoric origin. Groundwater sampled in till below lakes and the sea has high salinity (high chloride content). Groundwater below Lake Gällsboträsket (and in its topographical depression) and below Lake Bolundsfjärden have influence from relict marine water (Littorina). Groundwater below Lake Fiskarfjärden also has a hydrochemical signature clearly influenced by relict marine water, whereas groundwater below Lake Eckarfjärden shows a non-marine, meteoric signature.

The hydrochemical signatures of groundwater sampled below Bolundsfjärden, Gällsboträsket and Fiskarfjärden indicate that groundwater flow rates below these lakes are very low in relation to the total annual water balance of the Forsmark area. Integrated hydrogeological and hydrochemical data evaluations indicate that shallow groundwater-flow systems discharge around lakes and in their near-shore zones (Lindborg 2008).

There are alternative, continued flow paths for solutes entering the bedrock-QD interface from below: either vertically through the QD or horizontally along the permeable interface (Johansson 2008, Lindborg 2008). Hence, there are different possible flow paths and discharge points in different parts of the surface system for solutes originating from the bedrock.

In addition to the above-mentioned potential effects on advective transport, the surface system may also provide capacity for retention of solutes by e.g. sorption and precipitation. Retention parameters and modelling of solute transport in the surface system are presented in Grandia et al. (2007), Piqué et al. (2010) and Sheppard et al. (2009, 2011). An important input to the safety assessment SR-PSU is supplementary QD and sediment sampling and analyses of solute transport properties (Sheppard et al. 2009, 2011). The results show that it is possible to relate  $K_d$  values (QD and sediment solid/liquid partition ratios) to environmental conditions, such as pH and clay and organic carbon content, in a statistically significant manner. Modelling results (Grandia et al. 2007, Piqué et al. 2010) demonstrate that the QD may provide significant solute retention, but also that predictions of its retention capacity can be highly sensitive to assumptions made in the development of process models.

## 4.5 Confidence and uncertainties

The DEM (digital elevation model) has a high resolution and elevation uncertainties are generally considered to be small. However, it is difficult to evaluate errors in the DEM for currently submerged areas. The reliability of the map of the surface distribution of QD varies considerably within the model area. The quality of the map is considered to be high in marine areas, in particular in near-shore areas mapped using regular marine geological methods. The quality of the RDM (regolith depth and stratigraphy model) also varies spatially depending on the density of direct observations of the bedrock. The quality is judged to be high in shallow parts of the marine area, even though the model is based almost exclusively of geophysical data in these areas.

It is judged that the general description of the hydrological and near-surface hydrogeological driving forces and the overall flow pattern and interactions (including surface-bedrock interactions) are well understood. The largest uncertainties in the hydrochemical modelling are those related to the use of combinations of hydrochemical data, water-flow data and spatial data on land uses and vegetation types. This is particularly the case for estimations of trace-element transport, due to the use of scale factors that relate trace-element transport to transport of major elements. The descriptions of terrestrial, limnic and marine ecosystems are generally based on large amounts of site-specific data. Quantifications of many different ecosystem processes such as respiration and consumption are based on site data on a very restricted temporal scale. Extensive comparisons with data from other studies in similar regions have ensured that the short-term studies are put in a larger temporal and spatial context.

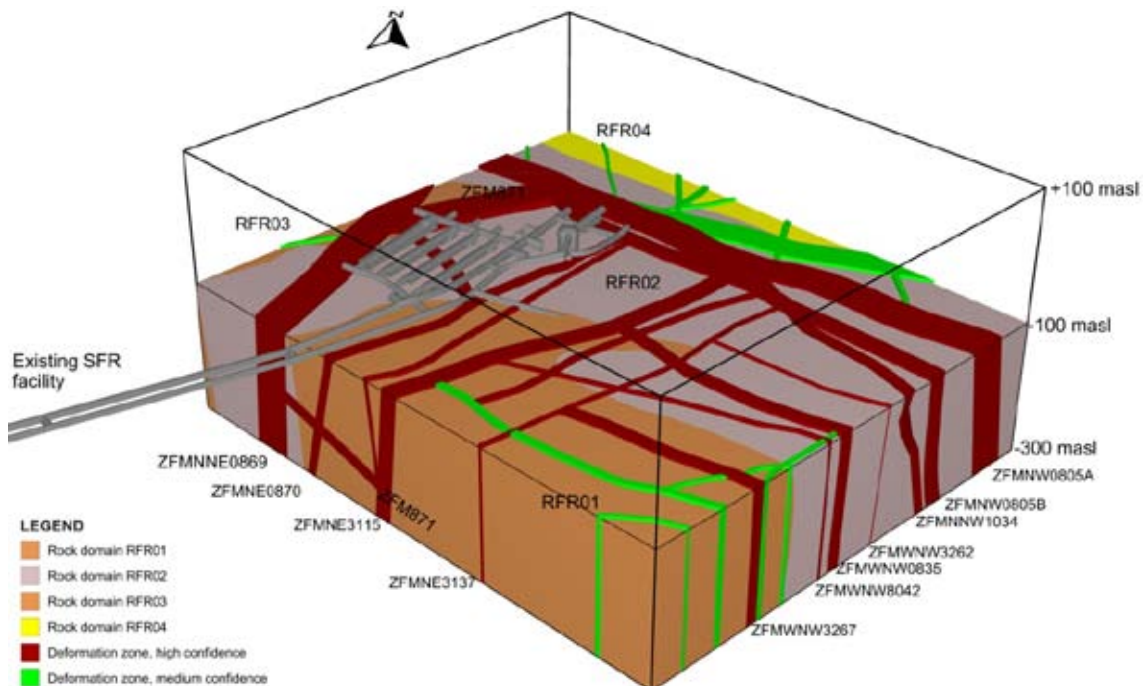


## 5 Bedrock geology

### 5.1 Overview

This chapter concerns the SFR version 1.0 geological model, previously described in Curtis et al. (2011), which includes both rock domain and deformation zone sub-models. The final geological model forms a basis for the modelling work by other disciplines, including rock mechanics, hydrogeology and hydrogeochemistry. The resulting multidisciplinary integrated model (Chapter 9) provides input for a site engineering evaluation in preparation for final repository design and long-term safety assessment. A site engineering assessment was not included under the umbrella of the geological modelling work in the SFR-PSU project work.

The geological modelling work incorporated in version 1.0 follows SKB's established methodology using the Rock Visualisation System (RVS). The contrasting needs of different users of the geological models – for example, hydrogeology, repository design and safety assessment – underscored the need to present both regional and more detailed local 3-D geological models. An important modelling prerequisite has been that the resolution of the modelled objects should be the same throughout the model volume, on any given modelling scale (Munier et al. 2003). The rock domain model produced in SFR model version 1.0 comprises the local model volume (Figure 5-1), whereas separate local and regional deformation zone models have been produced in SFR model version 1.0, using distinct resolution criteria for the different model volumes. The local model contains zones with a minimum size of 300 m, whereas the regional model has structures that have a minimum size constraint of 1,000 m trace length at the ground surface. The selection of these size limits is related to the maximum depth of the model volume (local model –300 m and regional model –1,000 m elevation) and the applied methodology, which requires the same model resolution throughout the defined model volume. To assist hydrogeological modelling work, an updated combined model, including all structures from both the regional and local models, has also been delivered.



*Figure 5-1. Rock domains and deformation zones included in the SFR local model, version 1.0. The relationship to the existing SFR underground facility is illustrated by a horizontal section at –100 m elevation, viewed to the north. Note that parts of the silo and the lower construction tunnel (NBT) are beneath that level.*

The deformation zone model, version 1.0, is a further development of the previous version 0.1 (Curtis et al. 2009). Whereas the main input to deformation zone model version 0.1 was older geological data from the construction of SFR, including drawings of the geological tunnel mapping and eleven drill cores remapped according to the Boremap system, input to version 1.0 of the rock domain and deformation zone models has included the results from eight new cored boreholes as well as a fuller integration of the Forsmark site investigation data, a more extensive review of the drill cores from an additional 32 boreholes associated with the construction of the existing SFR facility and an updated mapping of the lower construction tunnel. The current modelling work has also reviewed the older SFR data and models. Although details concerning the earlier zones lying in immediate contact with the existing SFR facility have been changed, the previous overall position, orientation and number of these deformation zones is maintained. A significant difference concerns their thickness due to the contrasting methodologies used during the different campaigns.

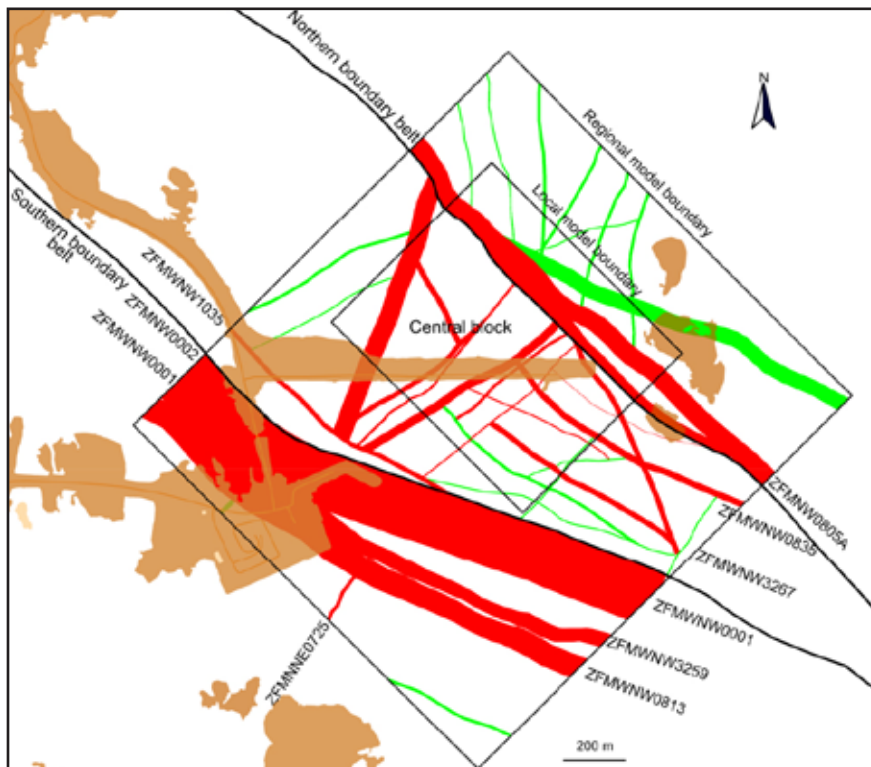
Four rock domains have been recognised in the local SFR model volume, mainly on the basis of rock composition and degree of heterogeneity. High resolution magnetic total field data, in combination with fixed points along drill cores, have made a significant contribution to the definition of boundaries between domains. Rock domain RFM021 in SDM-Site Forsmark has been divided into three separate rock domains in the SFR model on account of the higher level of resolution. A fourth domain corresponds to RFM033 in SDM-Site Forsmark. The existing SFR facility and the rock volume directly to the southeast, which is proposed for the extension, is situated within two rock domains, RFR01 in the southwest and RFR02 in the northeast (Figure 5-1). Both are part of RFM021 in SDM-Site Forsmark. Rock domain RFR01 is modelled as a major fold structure characterised by a relatively high degree of homogeneity and dominated by pegmatitic granite and pegmatite (101061) with a poorly-developed ductile deformational fabric, whereas rock domain RFR02 is far more heterogeneous and dominated by fine- to finely medium-grained metagranodiorite (to granite) (101057), often with a well-developed planar ductile deformational fabric.

The existing SFR facility and the rock volume proposed for the extension lie within a tectonic block that is bounded to the northeast and southwest by two broad belts: the Northern boundary belt and the Southern boundary belt, respectively, of concentrated ductile and brittle deformation (Figure 5-2). The Central block is less affected by deformation than the bounding belts. Within the Central block, in the rock volume for the planned extension, a series of WNW-NW-trending deformation zones are included in the local model. These are much smaller than the bounding belts and were initiated at a later stage in a brittle regime. Even smaller zones with the same general strike and character, below the current model resolution, are inferred to permeate the entire rock volume. A NE-to-ENE-striking set of brittle deformation zones is also present. Compared with the WNW-NW set they are generally thinner and shorter, due to termination against the broad WNW-NW-trending deformation belts.

The existence of gently dipping deformation zones was a particular focus of the project due to their previously identified engineering significance during the construction of SFR. No new significant gently dipping deformation zone was identified in the rock volume for the extension. However, there is a relatively high frequency of sub-horizontal open fractures in the upper part of the rock volume (above c. -200 m elevation), which are inferred to have formed or to have been opened in connection with stress release processes during unloading, due to deglaciation and/or exhumation, and also by strike-slip movements along the bounding steeply dipping zones. These sub-horizontal to gently dipping structures make a more significant contribution to the pattern of local groundwater flow in the upper part of the bedrock than the steeply dipping deformation zones (see Chapter 7).

The models described in this chapter follow the earlier established conceptual understanding of the geological evolution in the Forsmark area. At the end of development of model version 1.0, the overall confidence level concerning the regional deformation history and the broad tectonic framework of the region is judged to be high. However, the overall confidence level in the rock volume of specific interest to the SFR project, lying between deformation zones ZFMWNW0001 and ZFMNW0805A, is inevitably somewhat lower due to scale-related issues and the distribution of available data as discussed in this chapter. While certain details concerning particular deformation zones have been modified, there is nothing resulting from the current modelling work that has any significant impact on the earlier reported results for the Forsmark project for the final repository for spent nuclear fuel.

For the rock mass between the deformation zones, global fracture orientation sets, along with fracture type and frequency mean values, have been calculated (Curtis et al. 2011). However, no systematic evaluation of the fracture statistics (DFN) for the rock mass between the deformation zones has been carried out. This task was not included in the SDM-PSU project work.



**Figure 5-2.** Intersection at the current ground surface of deformation zone traces of all sizes inside the regional model area, i.e. a combined model version. The regional deformation zones ZFMWNNW0001 and ZFMWNNW0805A, along with their major splays, form the general southern and northern boundaries of the central SFR tectonic block. Confidence in existence: high = red, medium = green.

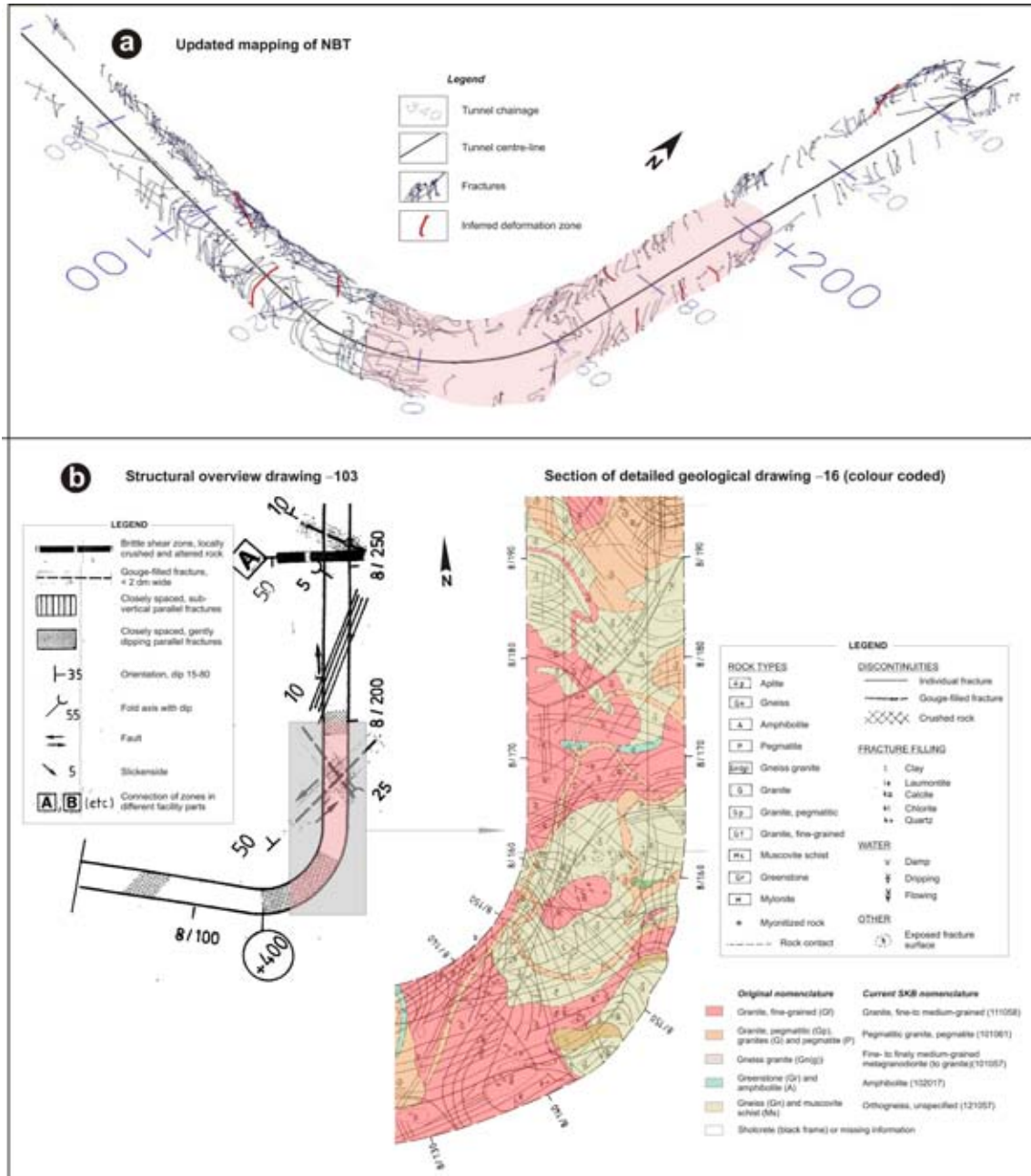
## 5.2 Evaluation of primary data

### 5.2.1 Geological tunnel data from SFR

The geological data from the underground openings of SFR comprise (1) geological maps generated during the construction of SFR (Christiansson and Bolvede 1987) and (2) an updated geological mapping of the lower construction tunnel (NBT) performed by Berglund (2008) during the current site investigation. The geological maps of Christiansson and Bolvede (1987) provide information on rock type, fractures, other tectonic structures and water seepage on a scale of 1:200. In addition, there are general drawings on a scale of 1:1,000 for rock types and 1:2,000 for tectonic structures (Figure 2-4) and water seepage. The tunnel mapping from the excavation phase is an important source of information and consequently considered a key document in the modelling work. However, the older tunnel data do not correspond to current SKB formats and quality standards. It has therefore been of importance to obtain updated geological information from SFR for the purpose of calibration. The facility has been re-inspected, and the NBT was selected for updated mapping as performed by Berglund (2008).

An important outcome of the updated mapping and modelling is that many of the structures marked in the overview structural drawing of Christiansson and Bolvede (1987) are identified as minor features without the necessary continuity for deterministic modelling demanded by the scale of resolution in the current modelling work. Another conclusion is that some of the minor structures in the drawing do not qualify as possible deformation zones in terms of the criteria currently applied by SKB. The primary criteria for defining the structures in the drawings have clearly been an increase in the frequency of open fractures (incohesive structures) and visual assessments of hydraulic conductivity, i.e. following traditional construction industry practice rather than current SKB criteria focusing also on long-term safety. Thus, the drawings from the construction phase have been used to define the position, orientation and basic character of a modelled deformation zone (fracture zone), whereas details concerning zone thickness, fracture frequencies, mineralogy, etc. are provided by borehole intercepts.

All the features in the general structural drawing of Christiansson and Bolvede (1987) have been noted as ‘possible tunnel deformation zones’ (tDZs) in order to follow a systemisation approximately equivalent to the possible deformation zones (PDZs) identified during the borehole single-hole interpretation process. The tDZs and tunnel intercept positions corresponding to all the deformation zones are documented in Appendix 2 in Curtis et al. (2011) and, when linked to a deterministically modelled zone in the local model in this study, are included in the property tables in Appendix 4.



**Figure 5-3.** Compilation showing the available geological information for a section of the lower construction tunnel (NBT), with an approximate chainage at 0+130 to 0+195. a) Three-dimensional view of the brittle structures registered during the updated geological mapping by Berglund (2008). b) Sections of the structural overview mapping and the rock type colour coded detailed geological mapping side by side. Both from Christiansson and Bolvede (1987). The section of the detailed drawing is marked in pink in a) and in the overview map in b). The legends in b) are translations of the original of Christiansson and Bolvede (1987) in Swedish. Note the two distinct fracture zones oriented  $230^{\circ}/50^{\circ}$  and  $310^{\circ}/80^{\circ}$  at approximately 8/180 in b) and 0+180 in a); none of them were of sufficient size for inclusion as deterministic structures in the model.

As mentioned in Chapter 2, a further integration of earlier SFR tunnel mapping results has been completed by (1) translation of the different rock types defined by Christiansson and Bolvede (1987) into the bedrock nomenclature introduced during the Forsmark site investigation (cf. Stephens et al. 2003), and by (2) colour coding of the rock types in all detailed drawings at the scale 1:200 according to SKB standards. A compilation showing an example of the available geological data for a section of the NBT is presented in Figure 5-3 and an overview of the whole SFR in Figure 5-5.

Ductile structures are treated very briefly, often in relation to brittle tectonics, in the original documentation from the construction of SFR. The tunnel drawings of Christiansson and Bolvede (1987) reveal scattered measurements of fold axes, but no other ductile structural data.

### **5.2.2 Rock units and possible deformation zones in boreholes**

The geological single-hole interpretation (SHI), which is an interpretation based on an integrated synthesis of geological and geophysical borehole information, provides a key link between the primary borehole data and the modelling work. The procedure includes 1) merging of sections with similar rock types or where one rock type is very dominant into rock units and 2) identification of possible deformation zones. A description of the procedures adopted during the SHI work is provided in Section 4.2.3 in Curtis et al. (2011), and includes primarily consideration of fracture frequency, rock alteration and focused resistivity.

In contrast to the SHI concept applied by SKB, the earlier definitions generally focused on open fractures and considered only the core or simply the groundwater-bearing part of a zone (cf. Carlsson et al. 1985, 1986). The geological SHI analysis of fracture frequencies is not restricted to open fractures, but also includes sealed fractures, sealed fracture networks, open and partly open fractures, and crush zones. In addition, current SHI practice gives equal weight to the presence and character of ductile deformation structures when defining deformation zones, in contrast to earlier judgements where such structures were to a certain extent ignored. The significant differences in the methodologies for defining the existence and boundaries of possible deformation zones mean that current SKB methodology generally leads to more zones with thicknesses that are usually significantly larger. Consequently, while a particular deformation zone's existence and overall geometry may be based on a mixture of older and newer data, the thickness and character of the zone is based first and foremost on SHI data.

The general principles of the SHI procedure were applied to all boreholes both from the newly completed Forsmark and SFR site investigations and from the 43 older SFR boreholes. However, deficiencies in the available geological data, not least the absence of fracture mapping for several boreholes, necessitated serious deviations from the established geological SHI methodology to define rock units and to identify possible deformation zones along the older SFR boreholes. A summary of the data included in the work and deviations from the established methodology is presented in Tables 4-2 and 4-3 in Curtis et al. (2011).

### **5.2.3 Major groups and types of rocks – properties, alteration and volumetric proportions**

#### ***Bedrock character***

The general properties and nomenclature of the rock types in the SFR area were initially established during the Forsmark site investigation (see SKB 2005). Additional geological and geophysical data generated from the SFR extension investigations conform well to the established rock type nomenclature and do not warrant changes. However, the generally more intense ductile overprinting and much more heterogeneous bedrock in the SFR area, compared with the Forsmark lens and its surroundings, lead to a revision of some of the rock type characteristics.

Four major groups of rock types (A to D) were distinguished in the Forsmark site investigation area on the basis of their relative age, whereas individual rock types were distinguished on the basis of their modal composition, grain-size and relative age (Stephens et al. 2007). The character of these rock groups and individual rock types in the SFR model volumes is summarised in Table 5-1.

**Table 5-1. Major rock groups and the character of individual rock types in the SFR model volume.**

Rock groups	Rock types SKB code	Composition, grain-size and occurrence
All rocks are affected by brittle deformation. The fractures generally intersect the contacts between different rock types, although the ductile structural character exerts a strong influence on the fracture pattern in certain rocks.		
Group D	Majority affected by deformation and metamorphism.	
	111058	Fine- to medium-grained granite, with a general low content of ferromagnesian minerals (< 5 vol.%). A spatial association with pegmatitic granite (101061) is noted locally. Typically there is a weakly developed linear mineral fabric, and locally a planar mineral fabric. However, there are occurrences that are strongly discordant to the structural trend in their older host rocks.
	101061	Pegmatite and pegmatitic granite, generally highly variable grain size. The rocks occur as segregation veins or pods, irregular bodies and dykes, with a highly variable relationship to the ductile deformation. Some occurrences are tightly folded and concordant to the structural trend in their older host rocks, whereas others are distinctly discordant. Most exposed bodies of pegmatitic granite have been affected at least to some degree by ductile deformation.
Group C	Affected by penetrative ductile deformation under lower amphibolite-facies metamorphism.	
	101051	Fine- to medium-grained granodiorite, tonalite and subordinate granite. Scarce in the model volumes. Intruded after some ductile deformation in the older rock groups.
Group B	Affected by penetrative ductile deformation under amphibolite-facies metamorphism.	
	102017	Amphibolite, forming irregular shaped occurrences as well as dyke-like bodies that are elongate following the the structural trend of the host rocks. The majority are fine-grained and the rock type includes virtually all mafic rocks in the SFR area, regardless of their structural and textural character. Minor occurrences and the margins of larger bodies display a distinct mineral fabric, whereas the more central parts of larger bodies are typically massive.
	101057	Fine- to medium-grained metagranodiorite (to granite) with a moderately to strongly developed planar, and to some extent linear, mineral fabric. Characterised by a texture of stretched, monomineralic domains and a content of ferromagnesian minerals ranging up to 10 vol.%.
Group A	Affected by penetrative ductile deformation under amphibolite-facies metamorphism.	
	103076	Felsic to intermediate metavolcanic rock, locally with a compositional banding. Since the rock is affected by intense ductile deformation and recrystallization, it is distinguished from the spatially associated metagranodiorite (to granite) (101057) by the grain size, higher content of ferromagnesian minerals and banding, rather than by volcanic structures or textures.

The SFR model volumes are situated within a broad deformation belt northeast of the Forsmark lens, where older rocks belonging to groups A and B generally consist of a heterogeneous package of mainly felsic-to-intermediate metavolcanic rocks (103076) intercalated with biotite-bearing metagranodiorite (to granite) (101057). They exhibit a penetrative foliation and are, in part, also lineated or banded, forming heterogeneous banded, foliated and lineated (BSL) tectonites. Due to the intense strain and recrystallization, these rocks are generally difficult to separate. Other subordinate rock types in this suite are amphibolite (102017) and aplitic metagranite (101058). Lithological contacts between these rocks are generally aligned parallel to the ductile tectonic foliation.

The group C rocks are rather scarce in the SFR model volumes. They consist of granitoids with primarily granodioritic to tonalitic composition, which intruded the older rocks after the most intense deformational phase under lower amphibolite-facies conditions. The youngest igneous suite, denoted group D, comprises granite (111058), pegmatitic granite and pegmatite (101061), which intruded during the waning stages of Svecokarelian orogenic activity. In proximity to and on the scale of the SFR underground facility, they constitute a substantial volume of the rock mass. In contrast to the Forsmark tectonic lens, where these rocks are only partly affected by the ductile deformation and metamorphism, a majority display a conspicuous stretching lineation and, locally, even a planar tectonic fabric in the SFR area. The grain size is highly variable in the rocks of this suite and may range from fine- to coarse-grained and pegmatitic in a single occurrence.

### **Properties**

The assessment of rock type was based on visual inspection, due to the lack of modal analyses from the SFR model volumes. The decision not to complete modal analyses during the present site investigation was based on experiences from the preceding Forsmark site investigation, where visual inspection generally turned out to be an adequate method for the distinction of the various rock types (Pettersson et al. 2004).

There are relatively few petrophysical laboratory data from the SFR area, and the physical properties of the major rock types have therefore been documented by using data from geophysical logging of the cored boreholes from the current SFR drilling campaign. This compilation integrates borehole measurements of density, magnetic susceptibility and natural gamma radiation with a selection of Boremap data for major rock types and alteration types with degree of intensity (see Appendix 4 in Curtis et al. 2011). Gamma spectrometry measurements to obtain the distribution of K, U and Th do not exist. A summary of the geological and physical properties of the major rock types in the local SFR model area is presented in Table 4-4 in Curtis et al. (2011). Other less frequently occurring rock types have not been included due to limitations in the data.

### **Alteration**

Alteration can affect both the thermal and the mechanical properties of rock and therefore needs to be assessed. Furthermore, the relationship between alteration and deformation zones needs to be evaluated since rock alteration is one of the primary data sets by which possible deformation zones are identified during the geological SHI. An assessment has been made by investigating the proportion of the bedrock affected by each type of alteration, both inside and outside modelled deformation zones (ZFM). The results are presented both as borehole lengths and as proportions of the borehole lengths in Tables 4-6 and 4-7 in Curtis et al. (2011).

Hematite dissemination, which is mapped and referred to as oxidation in Sicada, is by far the most abundant type of alteration within the boreholes. The second most frequent alteration type is muscovitization, which is mapped and referred to as sericitization in Sicada. All alteration types, except sericitization and albitization, show an association with the modelled deformation zones.

Quartz dissolution is one of the more spectacular alteration phenomena in the SFR boreholes. The most extensive occurrences are found in KFR27 and KFR102A, where the total affected borehole length amounts to 20.8 and 11.5 m, respectively. This alteration type was also recognised in some of the cored boreholes drilled during the Forsmark site investigation, where the most extensive of these occurrences was the focus of a special study by Möller et al. (2003). The vast majority of these occurrences have been included within possible deformation zones in the single-hole interpretation. However, there is no simple correlation between the occurrence of quartz dissolution and deformation zone orientation.

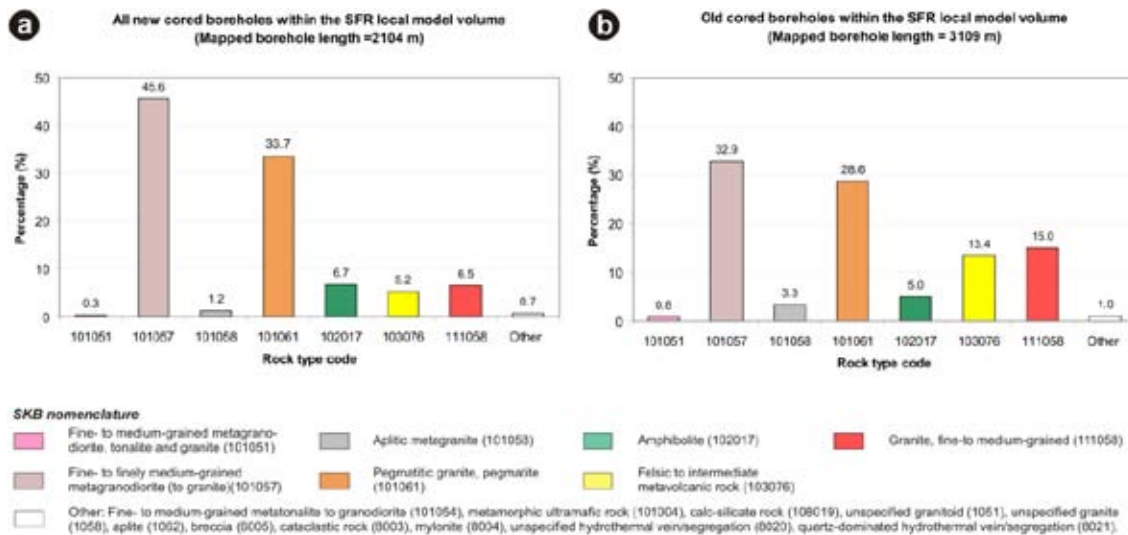
### **Volumetric proportions**

The proportions of the different rock types in the local SFR model volume, as well as KFR106 and HFR106 data outside this volume, have been estimated on a borehole by borehole basis by merging the data sets for rock type (> 1 m in borehole length) and rock occurrence (< 1 m in borehole length) in the Sicada database. The results of the analysis are summarised in Table 4-5 in Curtis et al. (2011) and separate histograms for the new cored boreholes and the cored boreholes from the construction of SFR are presented in Figure 5-4.

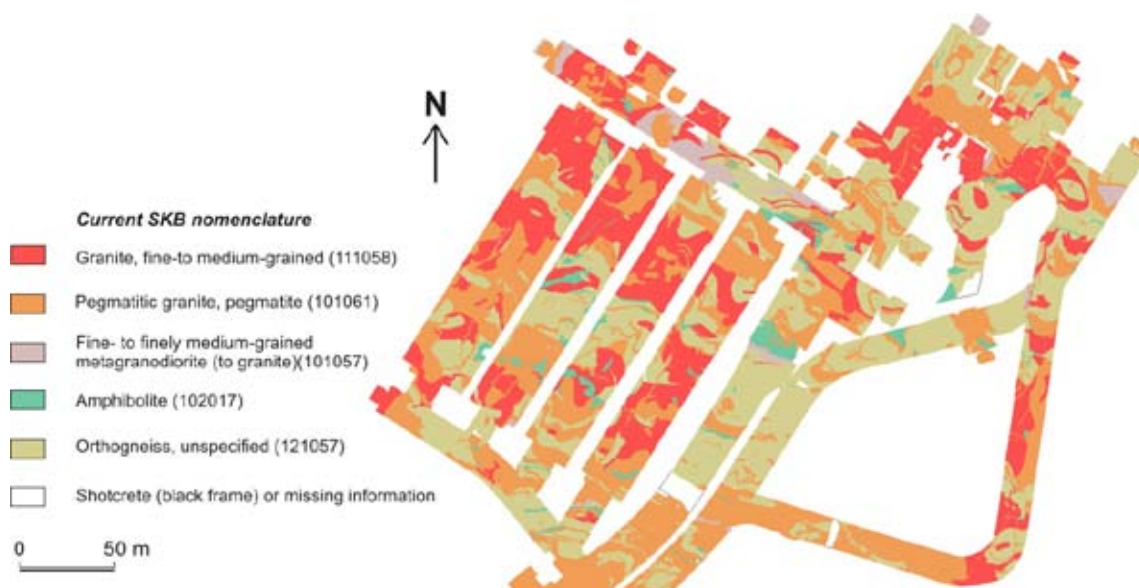
Compared with the Forsmark tectonic lens further south, the SFR area is highly variable and heterogeneous in terms of the distribution of different rock types. This heterogeneity is evident in the rock type colour-coded drawings of Christiansson and Bolvede (1987) (Figure 5-5) and is supported by the borehole results.

#### **5.2.4 Ductile deformation**

From the compilation of the ductile structural data obtained from a few well-exposed islets in the high-strain belt where SFR is situated (see Stephens and Forssberg 2006), a well-defined WNW-ESE to NW-SE structural trend is evident with both fold axes and mineral-stretching lineations consistently plunging towards the southeast. The structural trend is further supported by a few measurements of the anisotropy of magnetic susceptibility (AMS). Poles to the tectonic foliation/banding north-west of SFR tend to plot along a great circle with a pole at 124°/64°, and consequently reveal the existence of major folding.



**Figure 5-4.** Histograms showing the proportions of the major rock types in a) the cored boreholes from the recent SFR drilling campaign and b) old cored boreholes from the construction of SFR. Only data from the local SFR model volume as well as KFR106 outside this volume are included.



**Figure 5-5.** Rock type colour-coded drawings from Christiansson and Bolvede (1987), illustrating the lithological heterogeneity of the SFR underground facility. The term “orthogneiss, unspecified” (121057) includes both felsic-to-intermediate metavolcanic rock (103076) and metagranodiorite (to granite) (101057). Note that the tunnel walls are unfolded and presented horizontally along with the roof.

Structural variability characterises the ductile structural data from the SFR underground facility, although in general terms the planar structures – which primarily comprise foliation, but locally also tectonic banding and gneissosity – are steeply to vertically dipping, except north of and in close proximity to the silo, where they become more moderately dipping (60–70°) towards the southwest, and locally down to 15° under the silo (cf. Christiansson and Bolvede 1987, Berglund 2008). From the entrance of the access tunnels, through the Singö deformation belt and towards the SFR depositional area with the rock vaults, the strike of the foliation shifts from 135–150° to 145–160°. Within the deposition area, on the other hand, it ranges between 120 and 140°. The fold axes are typically oriented parallel or, more rarely, perpendicular to the foliation with gentle to moderate plunges towards the southeast or northeast (Christiansson and Bolvede 1987, Berglund 2008). Measurements of mineral-stretching lineation are lacking.



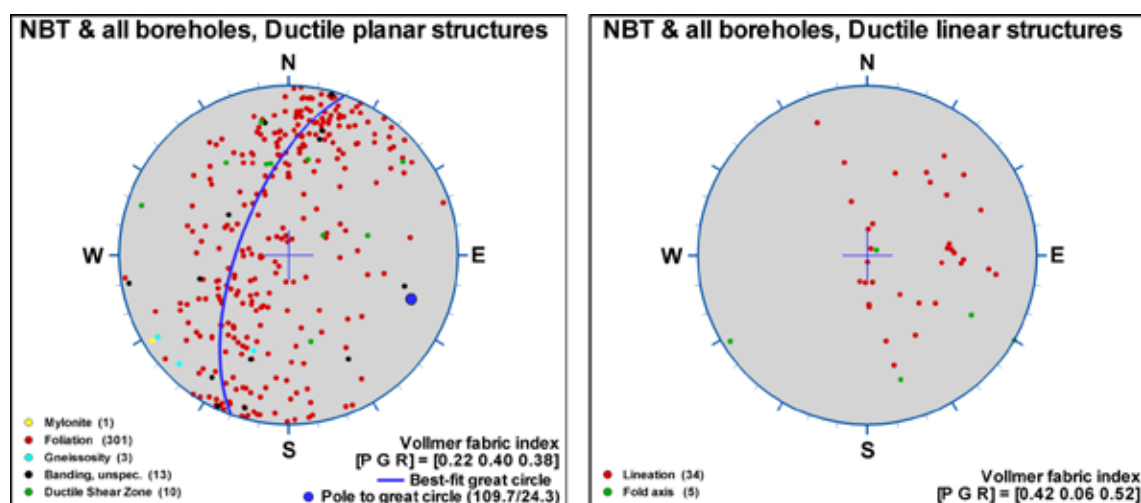
The ductile structures registered during the geological mapping of the boreholes comprise tectonic foliation and mineral-stretching lineation, as well as ductile and brittle-ductile shear zones and mylonite. The general pattern of NBT and all boreholes, as shown in Figure 5-6, is that the tectonic foliation has a WNW–ESE strike and a highly variable dip, whereas the mineral lineation data are rather few and indicate variable orientation, but mostly moderately plunging towards north-east to south-east. A crude, but yet distinguishable girdle pattern, with a best-fit pole of  $110^{\circ}/24^{\circ}$ , could support the existence of regional folding. Local deviations are considerable and this uncertainty in the structural statistics has implications for their use in the modelling work.

The folding has primarily affected the older rocks that belong to groups A and B, but also older members of group D, such as most of the pegmatitic granites (101061). It deforms the tectonic foliation, but evidence for folding of the mineral-stretching lineation is lacking in the Forsmark area. Consequently, it is inferred that the linear fabric was established prior to, but continued to develop during, the folding phase. It has been suggested that the folding developed initially with a normal cylindrical shape and was progressively drawn out, to a variable extent, in the stretching direction into sheath folds, so that the orientation of the folds follows the stretching lineation (Stephens et al. 2009).

To some extent, the scatter in the structural data may be the result of rheological differences between the heterogeneously distributed rock types in the SFR area. The vast majority of the registered measurements of ductile structures are for the foliated metagranodiorite (to granite) (101057), even in volumes dominated by pegmatitic granite (101061). In the latter case, the metagranodiorite (to granite) (101057) forms less competent occurrences or “islands” within the pegmatitic granite (101061).

### 5.2.5 Brittle deformation

Due to the lack of suitable outcrops in the SFR regional model area, no detailed mapping of fractures has been performed at the ground surface. Detailed fracture mapping data are mainly from the new boreholes with BIPS data and, to some extent, from the NBT, since most other underground openings in the SFR facility are lined with shotcrete, especially in highly fractured tunnel sections. An analysis of the orientation of fractures has been undertaken for each of the possible deformation zones identified in the borehole SHI procedure. Data from the drill core sections that help to define individual modelled deformation zones, so-called target intercepts (see Section 5.3), are presented in the zone property tables in Appendix 4. Fractures that are not visible in BIPS have been excluded from the analysis. Orientation data for open and partly open fractures are distinguished from data for



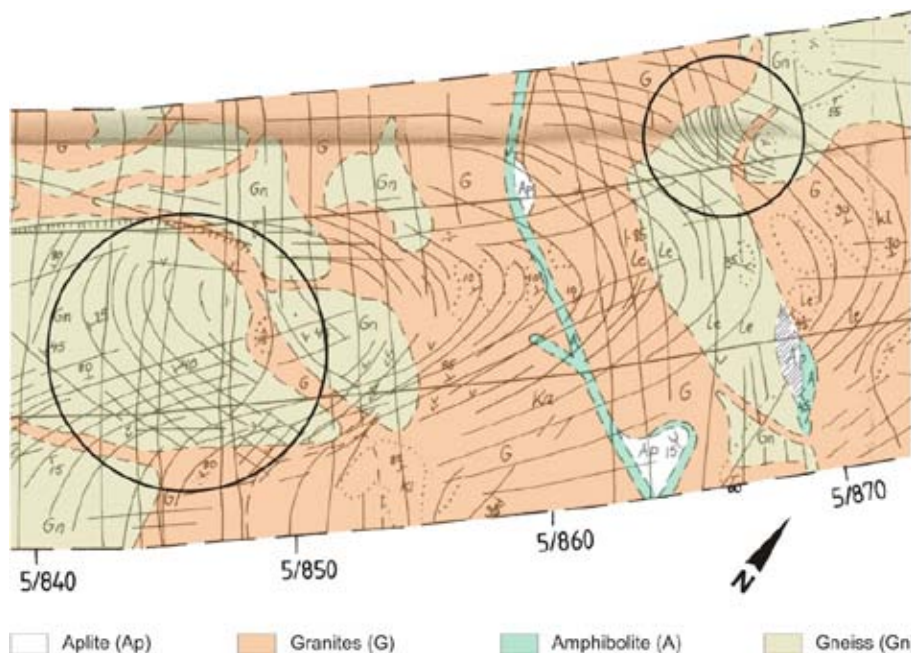
**Figure 5-6.** Orientation of ductile structures from the updated geological mapping of NBT and in all cored boreholes from the latest SFR drilling campaign (i.e. KFR27, KFR101, KFR102A, KFR102B, KFR103, KFR104, KFR105 and KFR106). Linear data and poles to planar structures have been plotted on the lower hemisphere of equal-area stereographic projections.

sealed fractures. In addition to the interpreted individual deformation zone/borehole intercepts, summary plots have also been collated for each modelled deformation zone and for each deformation zone orientation group. Data concerning fracture orientation, more generally inside and outside of deformation zones within the SFR regional model volume, are presented below.

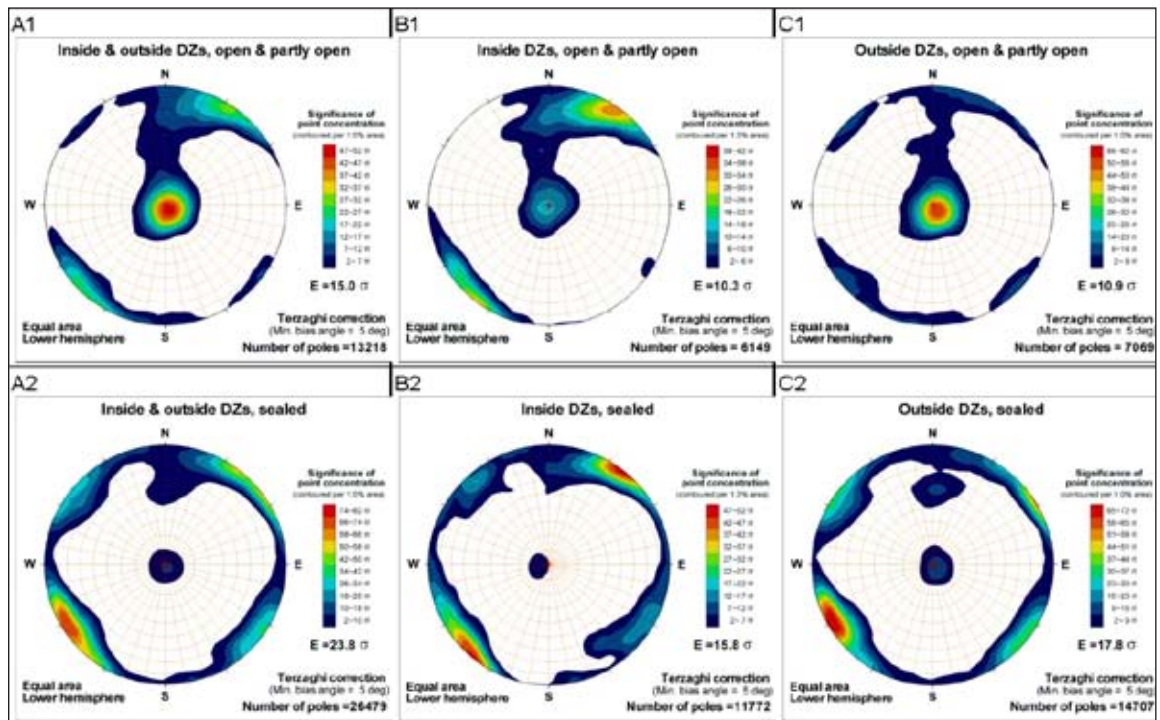
The orientation patterns are largely similar in the borehole and NBT tunnel data, and it is evident that some sets are more intensely developed in certain sections. Although no detailed correlation between rock type and fracture pattern has been performed, it is evident from the renewed mapping of NBT and tunnel drawings of Christiansson and Bolvede (1987) that there are lithologically related differences, as illustrated in Figure 5-7. The often well-developed fracture set, parallel to the foliation, in the metagranodiorite (to granite) (101057) and the metavolcanic rock (103076) locally ends or changes character as it meets rock types with a less pronounced ductile fabric, such as the pegmatitic granite (101061).

In addition, there is a clear difference in the intensity of the orientation patterns between open and sealed fractures. Taking the rock mass as a whole (A1–A2 in Figure 5-8), the horizontal orientation group dominates the open fractures, whereas sealed fractures are predominantly sub-vertical to steeply dipping and strike WNW-ESE to NW-SE or NE-SW. If the rock mass lying within the modelled deformation zones is considered in isolation (B1–B2 in Figure 5-8), it is the steep WNW-ESE to NW-SE set that dominates the open fractures. In the case of sealed fractures, a comparison of the pattern for the rock mass as a whole with that inside and outside of the modelled deformation zones is more stable and shows no great contrasts (A2–C2 in Figure 5-8). The sealed fractures are predominantly steep and strike NW-SE but there is also a clear steep NE-SW set, along with a weaker sub-horizontal set. There is also a strongly subordinate, moderately dipping set with an E-W strike that is seen most clearly outside the deformation zones (C2 in Figure 5-8).

It has been inferred that the different sets of fractures are genetically related and formed close in time during geologically ancient tectonic events (Stephens et al. 2007). However, some of the shallower, open, horizontal fractures possibly opened in connection with unloading, for example during a deglaciation, and general stress release. Thus, the current stress regime ( $\sigma_1 = \sigma_H$  at a bearing of  $145^\circ$ , and  $\sigma_3 = \sigma_v$  (SKB 2008b) would tend to open horizontal fractures at shallow depths, maintain the openness of steep fractures with WNW-ESE to NW-SE strike and close steep fractures with a NE-SW strike.



**Figure 5-7.** Rock type colour-coded sections of the construction tunnels (BT) from drawing -09 of Christiansson and Bolvede (1987), illustrating the fact that probable foliation parallel fractures in the unspecified orthogneiss (comprising metagranodiorite (to granite), 101057, and felsic-to-intermediate metavolcanic rock, 103076) locally end or change character in the contact towards the granites (equivalent to pegmatitic granite, 101061) (marked by open circles). For legend to the brittle structures see Figure 5-3.



**Figure 5-8.** Fracture orientation clustering inside and outside target intercepts for modelled deformation zones based on data from KFM11A and the cored boreholes KFR27, KFR101, KFR102A, KFR102B, KFR103, KFR104, KFR105 and KFR106.

Vertical trends in the intensity of open fractures in the rock mass lying outside the deformation zones have been investigated for open, sealed, steeply to moderately dipping and gently dipping fractures (Figure 5-9). Only data originating outside of deterministic structures (ZFM) are included.

Gaps in borehole coverage complicate the determination of, or significance of, depth trends in fracture frequency. Borehole coverage has an irregular pattern with elevation, partly caused by the exclusion of borehole sections classified as deterministic structures (ZFM). This causes an uncertainty related to the declining sample size with elevation: do observed trends relate to depth, or to local heterogeneity? For example, the lower half of the elevation range, below  $z = -308$  m elevation, is only covered by two boreholes KFR27 and KFR102A. In addition there are two issues concerning the confidence of the vertical borehole KFR27 data: firstly the unfavourable sampling bias of vertical fractures, which are primarily sealed fractures, and secondly the borehole is interpreted as lying within or bounding a deformation zone (ZFMWNW0835).

Nevertheless, visual inspection suggests a slight decline in frequency with depth, both for sealed fractures and open fractures. Linear regression (Figure 5-9) suggests that the decline in Terzaghi-compensated frequency, expressed as  $[m^{-1}]$  per 100 m depth, is: 1.81 for sealed fractures (if fractures inside networks are included), 0.15 for sealed fractures (if fractures inside networks are excluded), and 0.57 for open fractures + crush.

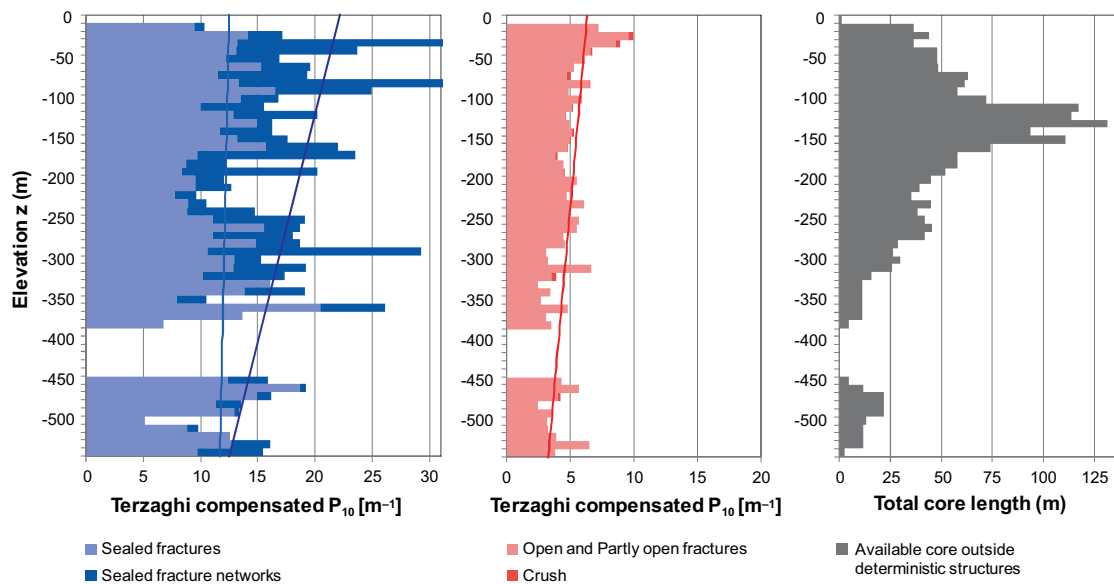
Terzaghi-weighted fracture frequency plots have been created for each of the deformation zone target intercepts identified in the boreholes. Open fractures, sealed fractures, sealed networks and crush are treated separately and in combination. Rock quality designation (RQD) numbers and frequencies for the different types of fractures are included in the property tables for deformation zones (see Appendix 4) as extremely simplistic indicators of rock quality within the zone.

Detailed studies of fracture mineralogy, involving the identification of different families of minerals, i.e. mineral parageneses, and the establishment of the relative age relationship between them, were conducted in connection with the Forsmark site investigation (Sandström et al. 2008b, 2009). The basic findings are expected to be applicable to the SFR regional model volume, since all the modelled Forsmark fracture domains (Olofsson et al. 2007), except for FFM02 domain (near-surface

realm), have essentially the same fracture mineralogy (Sandström et al. 2008b). In fracture domain FFM02, younger generations of minerals are more conspicuous relative to the other domains, especially along gently dipping to sub-horizontal fractures (SKB 2008b). A limited fracture mineralogy study performed as part of the SFR extension project (Sandström and Tullborg 2011) confirms this picture (see also Chapter 8).

The main sequence of fracture mineralisation, as presented by Sandström et al. (2008b, 2009), comprises four generations. The oldest high-temperature generation, which includes epidote, quartz and chlorite, occurs in all fracture sets, but especially in sub-horizontal and gently dipping fractures or in steep fractures that strike WNW-ESE to NW-SE. Generation 2 consists of a sequence of fracture minerals dominated by adularia, albite, prehnite, laumontite, calcite, chlorite and hematite, which are particularly common along steep fractures that strike ENE-WSW to NNE-SSW and NNW-SSE. A red staining (oxidation) of the wall rock due to hydrothermal alteration, as described in Section 5.2.3 (alteration), is associated with generation 1 and 2 minerals.

Generation 3 consists of calcite, quartz, pyrite, corrensite (clay) and asphaltite, and the fracture orientation generally suggests precipitation during reactivation of fractures with generation 1 and 2 minerals. Generation 4 is dominated by chlorite/clay minerals and thin precipitates of calcite in predominantly hydraulically conductive fractures and fracture zones. These minerals are prominent along sub-horizontal and gently dipping fractures. It has been inferred that the hydraulically conductive fractures are ancient structures and that precipitation of generation 4 minerals most likely occurred during reactivation (after the Palaeozoic). However, some of the near-surface, sub-horizontal to gently dipping fractures, which include sheet joints formed in connection with stress release, may be Quaternary in age. In addition, a very small proportion of fractures lacks visible mineral filling and wall rock alteration. A study of similar non-mineralised fractures from the Forsmark lens by Claesson Liljedahl et al. (2011) has revealed that the vast majority of these fractures actually are coated with microscopic amounts of minerals. The fracture minerals identified include hydroxyapophyllite, corrensite, quartz, calcite, barite and pyrite.



**Figure 5-9.** Fracture frequency depth trends. Fracture data and borehole coverage are binned per 10 m elevation. Values for elevation bins reflect the mid elevation of the bin. That is: the “-50 bin” covers data between 45 m and -55 m elevation. Borehole length inside casing is excluded (as well as inside ZFMs). Terzaghi-weighting uses 15° minimum bias angle, which corresponds to a maximum weight of 3.84. Data without orientation are assigned an average  $T_w$  set to 2, and are randomly assigned to the steeply or gently dipping population. Intensity of sealed networks and crushes calculated as 1000/piece\_length mm (i.e. not Terzaghi-compensated).

### 5.2.6 Identification, character and geological significance of lineaments

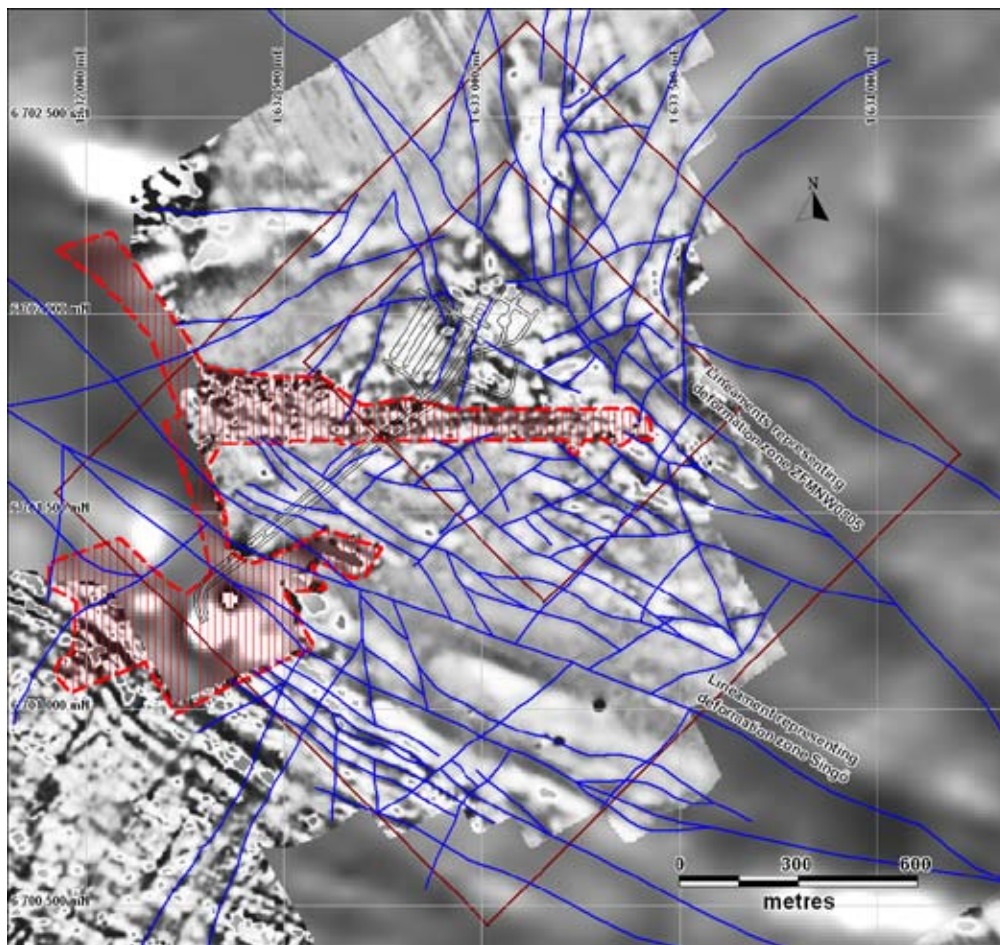
The identification of lineaments for modelling of steeply dipping deformation zones has followed the previously established SKB modelling methodology (see Isaksson 2003, Isaksson et al. 2004, 2006a, b, 2007, Isaksson and Keisu 2005) and has been based on magnetic minima in the high-resolution magnetic total field available from the ground survey in the SFR area. In addition, a helicopter-borne survey provided information on the magnetic total field, but with lower spatial resolution. The coverage of these and other geophysical surveys in the SFR area is shown in Figure 2-3.

Compared with the site investigation for Forsmark, sea coverage and lithological variability in the area have made the identification process more difficult, at the same time as the demand for detail is higher inside the current model area. In addition, there are several anthropogenic disturbances to the magnetic field, which include high frequency noise from scrap metal in the pier construction and long wave anomalies from iron objects in the underground SFR facility itself. The area close to the Fenno-Skan HVDC cable also shows an artificial banding along the magnetic survey lines. The density of lineaments in the most severely disturbed areas is consequently lower due to the high noise level.

A revision of stage 2.3 lineaments from the Forsmark site investigation reported by Isaksson et al. (2007) has been the basis in the identification process. The revision, on a more detailed scale in comparison with earlier work, has resulted in changes to some of the lineaments, as well as the addition of entirely new lineaments. An explicit aim of the revision work has been to maintain consistency across the boundary between the areas inside and outside the SFR regional model area. Hence, lineaments from the Forsmark site investigation entering the SFR regional model area have generally been maintained without any changes outside the SFR regional model area, whereas inside the SFR regional model area, changes in length, path or position were allowed. To a limited degree, low velocity zones from the refraction seismic profiles and depressions in the bedrock surface have also provided input to the revision process. Attributes for each lineament included in Figure 5-10 are presented in Appendix 5 in Curtis et al. (2009). Furthermore, many of the magnetic anomalies associated with the lineaments have been forward modelled in 3D using the programme package EncomModelVision Pro version 8.0. Geometrical information about the inferred sources of the identified lineaments is also provided by 3D inversion modelling. The results of all this modelling work are presented in Appendix 6 in Curtis et al. (2011).

Excavation work and drilling activities inside the Forsmark tectonic lens to investigate the nature of lineaments defined by discordant magnetic minima have led to the conclusion that they primarily represent fracture zones but could also represent dykes of granite and pegmatite (Stephens et al. 2007). Minima connections are related primarily to lithological contrasts that are aligned parallel to the ductile foliation in the bedrock, but the occurrence of minor fracture zones along the tectonic foliation cannot be excluded as a contributory factor to these lineaments (Stephens et al. 2007).

These conclusions are principally applicable inside the Forsmark tectonic lens. However, it is considered reasonable to assume that the character of concordant minima connections inside the ductile high-strain belts outside the lens, including a large part of the SFR regional model area, is similar. Some of these lineaments are known to be, and many have been modelled as, regionally significant deformation zones (Stephens et al. 2007). Based on these considerations, a pragmatic interpretation is that lineaments represented by features with high values of the length/width ratio in the magnetic total field data could primarily represent deformed rock. The lineaments are a key input in the deformation zone modelling, but they may be removed or modified during this procedure depending on other available data. The relationship between the lineaments and the deformation zone traces on the ground surface are described in the individual deformation zone property tables.



**Figure 5-10.** Map of the first vertical derivative of the magnetic total field from measurements on land, at sea, and from helicopter, showing the 127 lineaments that have been identified (blue lines). Only lineaments that are partly or entirely within the SFR regional and local model areas (boxes outlined in brown) are shown. Prominent low magnetic features in the southern and northeastern parts of the SFR regional model area correspond to the Singö deformation zone (ZFMWNW001) and zone ZFMNW0805A. The area containing severe disturbances of the magnetic total field caused by civil installations is outlined in red dashes.

### 5.2.7 Character and geological significance of seismic data

No new seismic refraction or reflection surveys have been carried out in connection with the current project. However, reprocessing and review of earlier produced surface or near-surface based seismic reflection data from two profiles covering the SFR regional model area (Figure 2-3) has been performed (Juhlin and Zhang 2010), with a focus on the shallow depth relevant to the SFR facility level. Two new reflectors that intersect the SFR model volumes were identified in connection with the reprocessing and re-interpretation of the earlier data: reflector B10 ( $025^{\circ}/35^{\circ}$ , confidence class 2 – medium) and reflector A13 ( $090^{\circ}/45^{\circ}$ , confidence class 3 – low). Neither corresponds to a lineament; however, their fairly gentle dips might exclude correlation with features represented by lineaments. Although a new seismic reflection survey would have been a useful tool to identify gently dipping structures, existing seismic profiles and evidence supplied by the rock conditions seen in the underground SFR facility, particularly in the silo (extending from c.  $-60$  to  $-140$  m elevation), were sufficient to justify not performing such a survey.

Seismic refraction surveys were carried out in 1981 to support the design work for the original SFR facility (Hagkonsult 1982) (Figure 2-3). An evaluation by Isaksson (2007) showed that there is only a moderate correlation between low-velocity anomalies and interpreted low-magnetic lineaments or modelled deformation zones. The main reason for this is probably the difficulty of resolving individual narrow low-velocity sections in data for longer sections composed of both intact and lower

quality bedrock. Thus, both survey methodology and geological conditions need to be considered in the assessment of the relatively poor correlation. Based on the narrow width of low velocity sections inferred to be associated with shorter lineaments in the area, as well as the possible masking of local occurrences of very compact till (cf. Carlsson and Christiansson 2007), the outcome of a new seismic refraction survey was considered to be of minor significance. Qualitative interpretation of ground magnetic data and correlation with geological features.

The detailed ground magnetic data covering the SFR area have been processed and filtered to better enhance geological structural patterns in the data, as well as reduce the response from man-made magnetic sources (cf. Section 4.6.4 in Curtis et al. 2011). This work included a qualitative interpretation, which in turn comprised identification and segmentation of the magnetic pattern into “banded” and “irregular” patterns. The former usually constitute supracrustal rock units and/or bedrock that is strongly deformed, whereas the latter commonly constitute more massive intrusive rocks. The magnetic pattern is then accordingly divided into low, moderate, high and very high intensity areas. Magnetic connections, or magnetic bands, further enhance the structural pattern and discordant magnetic lineaments, which usually indicate a deformation zone or a break in the bedrock units, are also identified and included.

In order to make use of the magnetic total field data for lithological modelling, it was necessary to evaluate the significance of the possible correlation between rock type and magnetic intensity. A compilation of the magnetic susceptibility of each of the major rock types in the area was conducted from the geophysical borehole loggings to enable this correlation to be made. Based on this, the following can be concluded regarding the correlation between rock type in the SFR area and magnetic susceptibility.

- Pegmatitic granite and pegmatite (101061) tend to have the lowest magnetic susceptibility of the major rock types existing in the SFR area.
- Susceptibility values in excess of  $1,500 \cdot 10^{-5}$  SI are generally restricted to amphibolite (102017) and felsic-to-intermediate metavolcanic rock (103076).
- All major rock types in the SFR area are well-represented in the intermediate susceptibility range, including pegmatitic granite and pegmatite (101061).

When assessing the relationship between these conclusions for magnetic susceptibility and patterns in the magnetic total field, it is essential to also consider the geometric context and other supporting data. The magnetic susceptibility of a rock can be strongly reduced by hydrothermal alteration, where magnetite is converted to hematite. This is a common feature along brittle deformation zones in the area, and consequently the low intensity in the magnetic total field can either be related to oxidation associated with brittle deformation or volumes dominated by rock types with low magnetic susceptibility (e.g. pegmatitic granite, pegmatite, 101061).

### **5.2.8 Inversion modelling of ground magnetic data**

Inversion modelling of the detailed ground magnetic data has been carried out to provide information on the 3D distribution of magnetic susceptibility in the bedrock as support to the modelling of rock domains and deformation zones. The primary use has been in the verification of deformation zones and inconsistency evaluation of rock domain elements. It has also been used for noise reduction along the pier at SFR.

The inversion methodology uses a mathematical technique in which high frequency anomalies are related to susceptibility variations in the uppermost part of the rock volume and lower frequencies to deeper parts. The magnetic inversion model used is isotropic, includes topography and is based on processed data adjusted to avoid magnetic sources outside and below the actual model. Moreover, it is made up of volumetric box elements, so-called voxels, that cover the SFR local model volume with dimensions of 1,200×1,200 m horizontally and 500 m vertically. The voxel resolution is 10 m in all directions, except for the uppermost 50 m which has a higher vertical resolution of 5 m.

Inversion modelling has resulted in the delineation of low susceptibility areas towards depth with a corresponding impact on the bedrock and deformation zone models. There is generally good agreement between the outcomes of inversion modelling and forward modelling by EncomModelVision Pro version 8.0, as described in Section 5.2.6.

## 5.3 Rock domain model

The term rock domain is used here according to the general guidelines in Munier et al. (2003). More specifically, individual domains have been defined primarily on the basis of an integration of information on the composition and heterogeneity in various rock units. The importance of ductile deformational data, which comprises the backbone of the Forsmark rock domain model, has been secondary in the current model, due to the pronounced heterogeneity in the SFR area that practically precludes detailed structural analysis. It should be noted that the degree of fracturing has not influenced the subdivision into rock domains.

The key inputs for the establishment of the rock domain model are 1) SHI rock units in the boreholes, 2) tunnel mapping of the SFR underground facility and 3) processing and interpretations based on the high-resolution magnetic total field data, including the 3D inversion model.

### 5.3.1 Conceptual understanding of the rock domains

#### *Heterogeneity and folding*

Folding on different scales has clearly affected most rock types in the SFR area, including a majority of the pegmatitic granites (101061) and younger granites (111058) belonging to rock group D. However, there are group D rocks, such as some pegmatite dykes, that evidently post-date the ductile deformation in the area. Data from different parts of the model volume reveal a rather irregular structural pattern, with a general orientation of mineral-stretching lineation and fold axes towards the southeast, or locally towards the northeast, with varying plunge. The data are generally consistent with a process where the linear fabric was established prior to, but continued to develop during, folding.

Within the local model volume with considerable volumes of pegmatitic granites (101061) and younger granites (111058), it is thus evident that the rheological heterogeneity of the rock mass prior to the folding has resulted in irregular folding on all scales. A structural concept with the development of major sheath folds, similar to that of the Forsmark tectonic lens, is therefore not fully applicable in the SFR area. Due to this structural uncertainty, it has not been possible to fully rely on the available structural data in the modelling work.

#### *Geological significance of areas with contrasting magnetic intensity*

The central part of the local SFR model area consists of a NW-SE-trending belt with high but variable magnetic intensity that extends from the SFR underground facility to an islet south of Grisselgrundet, just outside the local model area. This feature is related to lithology and the variability in the magnetic intensity conforms to the lithological heterogeneity in the SFR underground openings and boreholes that penetrate the volume.

This belt is surrounded by conspicuous areas with a low magnetic signature. Where sub-surface lithological data exist they reveal that the volumes beneath these areas are dominated by pegmatitic granite and pegmatite (101061) with low magnetic susceptibility. A WSW-ENE-trending belt of low magnetic intensity northwest of the SFR is associated with a broad ridge of high magnetic intensity. The magnetic low also coincides with several lineaments defined by magnetic minima and is, at least locally, accentuated by several steeply dipping deformation zones, including the high-confidence zones ZFMNNE0869 and ZFMNNW1209. The anomaly is, therefore, regarded as a composite result of oxidation related to minor brittle structures and larger volumes dominated by pegmatitic granite and pegmatite (101061). The broad ridge of high magnetic intensity coincides with a weakly defined seismic reflector (A13) if it is projected to the ground surface. Both the magnetic belt and the reflector can be related to lithological changes rather than to a deformation zone, although the exact nature is unclear.



### 5.3.2 Methodology and assumptions

An explicit aim has been, wherever possible, to maintain consistency between the current model and the rock domain model from the Forsmark site investigation (SKB 2008b), so as to simplify future studies of the interaction between the two models. However, it is important to consider that there is a much higher degree of resolution in the current model and, as a consequence, one of the domains in the Forsmark regional rock domain model has been divided into three separate domains in the current model.

Since the bedrock is very poorly exposed at the ground surface, the extent of the rock domains at this surface was largely determined by using the available high resolution magnetic total field data in the area. This information, together with available SHI rock units and SFR tunnel mapping, was used in the projection of the rock domains down to the base of the local model volume. Furthermore, projected surfaces were compared with the magnetic inversion model and, if necessary, adjusted to avoid conflicts. Although none of the domain boundaries are inferred to be strictly related to deformation zones, a comparison with the geometrical deformation zone model was also made.

The following assumptions have been adopted in the geometric modelling procedure.

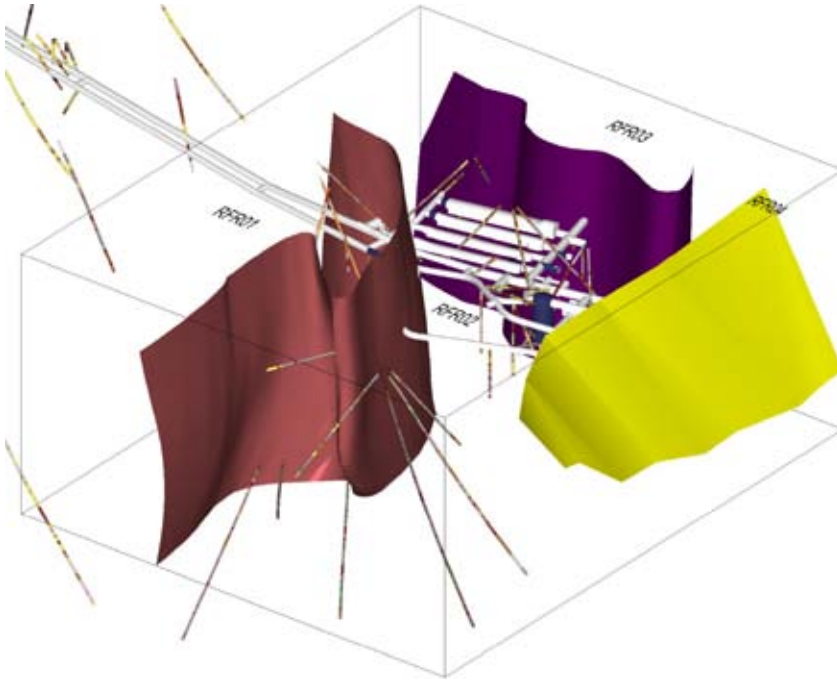
- An initial structural conceptual model where large-scale folding has affected the rocks that belong to groups A and B, as well as most of the pegmatitic granite (101061) that belongs to group D. The fold axes are assumed to plunge downwards in approximately the direction of the mineral-stretching lineation. However, the structural heterogeneity is far too great to permit modelling on a purely structural conceptual basis.
- All inferred rock domains are major geological features. Based on available geological and geophysical data, the domain boundaries are assumed to be steeply dipping and to extend downwards, at least to the base of the local model volume.

### 5.3.3 Geometric model and property assignment

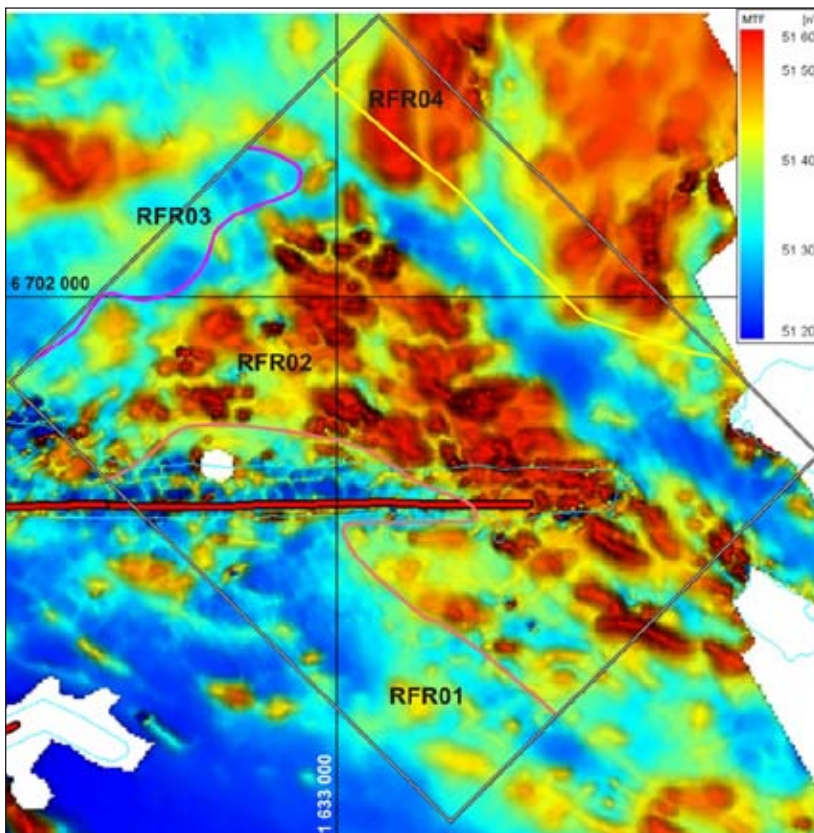
Four rock domains (RFR01–RFR04) have been recognised in the local SFR model volume (Figure 5-11). At the surface, domains RFR01 and RFR03 are recognised by their low intensity in the magnetic total field (Figure 5-12). A concept of irregular folding, due to the heterogeneity of the rock mass, is the basis for the modelling of these two marginal domains. The boundary between RFR02 and RFR04 is identical to the contact between RFM021 and RFM033, as defined in the deterministic rock domain model version 2.2 from the preceding Forsmark site investigation (Stephens et al. 2007). The criteria used to distinguish the four rock domains are summarised in Table 5-2 and the inferred occurrences in boreholes and tunnels are presented in Appendices 7 and 13 in Curtis et al. (2011).

**Table 5-2. Summary of criteria used to distinguish the four rock domains in the SFR local model volume.**

Rock domain	Borehole data	Tunnel data	Magnetic total field	Comment
RFR01	Rock units dominated by pegmatite, pegmatitic granite (101061).	Sections dominated by pegmatite, pegmatitic granite (101061).	Continuous area of low magnetic intensity.	–
RFR02	Rock units of varying composition, but with a dominance of meta-granodiorite (to granite) (101057) and metavolcanic rock (103076).	Heterogeneous sections dominated by bedrock coded as 'unspecified orthogneiss' (121057).	Continuous area of high, but variable magnetic intensity.	–
RFR03	–	–	Continuous area of low magnetic intensity.	Modelled to avoid borehole and tunnel intersections.
RFR04	–	–	Continuous area of moderate magnetic intensity.	Structural trend inferred from magnetic intensity differs from that of RFR02.



**Figure 5-11.** Three dimensional model view from east showing the boundaries between the four rock domains within the local SFR model volume relative to the borehole geology and the geometry of the SFR underground facility. The colour choice is only for legibility, where boundary RFR01–RFR02 is pinkish brown, RFR02–RFR03 violet and RFR02–RFR04 yellow.



**Figure 5-12.** Map of the magnetic total field after low-pass filtering and subtraction of the contribution from the SFR silo and caverns. The surface trace lines corresponding to the three rock domain boundaries within the local model area are also shown. The colours of the boundaries are identical to those in Figure 5-11. The red line along the pier represents a road.

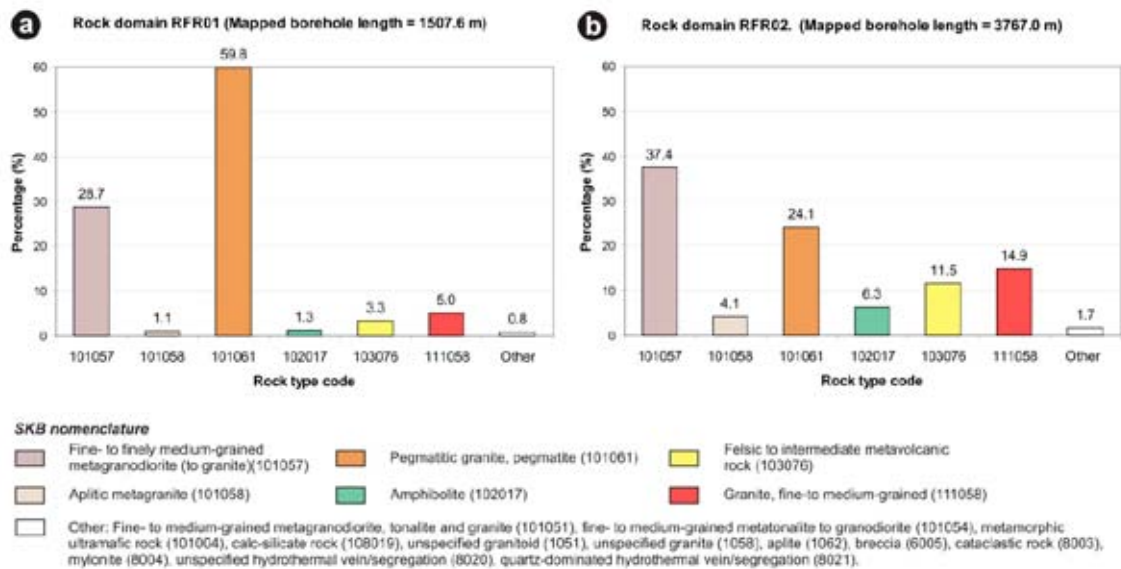
### 5.3.4 Character of rock domains

The geological borehole and SFR tunnel information is limited to rock domains RFR01 and RFR02, whereas data from the other two domains, RFR03 and RFR04, are lacking. More than 70% (3,767 m) of the mapped borehole length data are from RFR02, which also hosts most of the SFR underground facility. For this reason, property tables have only been constructed for RFR01 and RFR02 (Appendix 14 in Curtis et al. 2011). Key attributes include the proportions of major rock types, the degree of heterogeneity and the nature of ductile deformation, as well as textural, structural and petrophysical properties of the dominant rock type. In addition, judgements concerning the confidence of existence of a rock domain are provided for each domain. A quantitative estimate of the proportion of different rock types in both these domains is presented in Figure 5-13.

As stated earlier, no fracture domain modelling or statistical analysis of fractures outside the segments of rock domains between deterministically modelled deformation zones was done during the SFR extension project. However, a simple comparison of the mean fracture frequency obtained from borehole data outside modelled deformation zones in RFR01 and RFR02 shows no obvious differences between the two domains, with 3.6 open and 13.2 sealed fractures per metre inside RFR01 and 3.8 open and 13.5 sealed fractures per metre inside RFR02 (Table 5-3). Nevertheless, there are indications of correlations between lithology and the brittle deformation style. Table 5-3 reveals that a majority of the sealed fractures in RFR01, a domain dominated by pegmatitic granite (101061), comprise fracture networks, whereas most sealed fractures in RFR02 are registered as ‘individual’ fractures.

**Table 5-3. Summary of mean fracture frequencies per metre of mapped drill core for rock domains RFR01 and RFR02 outside modelled deformation zones (Terzaghi corrected values).**

Rock domain	Open	Partly open	Crush equivalent	Total open	Sealed	Sealed network	Total sealed
RFR01	3.32	0.24	0.01	3.57	5.75	7.43	13.18
RFR02	3.44	0.33	0.05	3.82	10.14	3.35	13.50



**Figure 5-13. Quantitative estimates in volume % of the proportion of different rock types in rock domains a) RFR01 and b) RFR02.**

### **Rock domain RFR01**

The boundary between RFR01 and RFR02 is defined by four fixed points from three boreholes and five from underground openings in SFR distributed between -71 and -205 m elevation in the model volume. Rock domain RFR01 is modelled as a major fold structure dominated by pegmatitic granite and pegmatite (101061) (Figure 5-13a). Another important constituent is fine- to finely medium-grained metagranodiorite (to granite) (101057), which occupies approximately 30% of the mapped borehole length within RFR01 (Figure 5-13a). The domain is characterised by a relatively high degree of homogeneity compared with domain RFR02 and other, subordinate rock types occupy approximately 10% of the mapped borehole length (Figure 5-13a). All major rock types within this domain are essentially fresh.

The predominant pegmatitic granite (101061) is generally massive, locally with a faint to weakly ductile fabric, and is consequently rather isotropic. Ductile structural data obtained mainly from subordinate rock types (i.e. the metagranodiorite (to granite), 101061, and the felsic-to-intermediate metavolcanic rock, 103076) scatter significantly. However, in agreement with the concept of large-scale folding, a very rough girdle distribution pattern is defined by poles to the planar structures in a stereographic projection (see Appendix 14 in Curtis et al. 2011). Whereas these data define a sub-horizontal fold axis, the ductile mineral lineation is moderately dipping and fold axis orientations of approximately  $090^{\circ}/70^{\circ}$  have been used to project the domain boundary to the model base. Due to the subordinate amounts of older rocks with well-developed planar fabric, it is evident that the foliation-parallel fracture set outside the modelled deformation zones is less important in RFR01 than in RFR02 (see Figure 5-7).

### **Rock domain RFR02**

Rock domain RFR02 is defined by the belt of high but variable magnetic intensity that extends with a NW-SE trend across the local model area. It was modelled to include all sub-surface geological data in the local SFR model volume that do not occur in RFR01. It is far more heterogeneous relative to rock domain RFR01 (Figure 5-13). The dominant rock type is the fine- to finely medium-grained metagranodiorite (to granite) (101057), which is commonly indistinguishable from the felsic-to-intermediate metavolcanic rock (103076) (Figure 5-13b). In consequence, it needs to be emphasised that there is a considerable uncertainty in the exact estimate of the two rock types.

Other volumetrically important rock types (Figure 5-13b) are pegmatitic granite and pegmatite (24%), younger granite (15%), amphibolite (6%) and aplitic metagranite (4%). A large-scale heterogeneity of this domain is reflected in the fact that the proportions among the subordinate rock types also differ between the southern and northern parts of the domain, especially for the younger granites, which occupy 18% of the boreholes in the northern part and 7% in the southern part.

The domain is characterised by both compositional heterogeneity and structural anisotropy, due to the volumes of rock types with moderately to strongly developed planar fabric. This is also reflected in the proportion of foliation-parallel fractures (cf. Section 5.2.5). As presented in Appendix 14 in Curtis et al. (2011), ductile planar structural data from RFR02 define a rough girdle distribution pattern in a stereographic projection, where steeply dipping structures with a WNW-ESE strike predominate. Mineral lineation data from the domain show a mean orientation of  $151^{\circ}/84^{\circ}$ , with a Fisher  $\kappa$  value of 12.

### **Rock domain RFR03**

Geological data from RFR03 are completely lacking and there is no information available other than the magnetic total field for modelling of the boundary between RFR02 and RFR03. The low magnetic belt that forms the surface expression of RFR03 has been treated as a composite result of oxidation related to brittle structures and volumes dominated by pegmatitic granite and pegmatite (101061). The parts of the low magnetic belt that lie directly above the SFR facility are, for example, inferred to be due to minor fractures zones rather than to differences in lithology.

The character of the boundary between rock domains RFR02 and RFR03 is unknown, but the magnetic signature resembles that of RFR01. For this reason, it was modelled so as to define the core of a major fold structure. Based on 1) the fact that no parts of the SFR underground facility

merit inclusion within RFR03 and 2) the magnetic inversion model, the boundary is inferred to be rather steeply dipping and a rough approximation used in the modelling work is the mean orientation of the mineral lineation data from RFR02. The geometrical extension of this domain towards the east and southeast remains uncertain in the absence of geological data. A connection with rock domain RFR01, outside the local model volume and beneath the pier, cannot be excluded according to the magnetic total field.

#### **Rock domain RFR04**

Geological data from RFR04 are completely lacking and there is no information available other than the magnetic total field for the location and orientation of the boundary between RFR02 and RFR04. For this reason, and in order to simplify future interactions with both the SFR local model and the regional rock domain model for Forsmark stage 2.2 (Stephens et al. 2007), it was decided to follow the contact between RFM021 and RFM033 as the boundary between RFR02 and RFR04. On the basis of the magnetic total field data, the boundary is tectonic, at least in its northwestern part. The close resemblance of the general magnetic signatures of RFR04 and RFR02 suggests that the bedrock character of RFR04 is similar to that of RFR02.

## **5.4 Deformation zone model**

Separate local and regional deformation zone models have also been created in model version 1.0. The local model contains all modelled deformation zones that have a size corresponding to a trace length on the ground surface of  $\geq 300$  m. The regional model contains only local major and larger zones, i.e. zones with a trace length on the ground surface of  $\geq 1,000$  m. This section summarises the overall character of the zones belonging to different orientation groups. Details concerning the individual deformation zones in the local model volume, including their physical character, geometries and terminations, are provided in Appendix 4.

The orientation of each zone is defined by a numerical strike and dip using the right-hand-rule method. However, the letters WNW, NW, NNW, NS, NNE, NE and ENE in the deformation zone name provide a general indication of the strike and they do not follow the right-hand-rule rule procedure. The zones in the different sets (e.g. NE) may dip in both directions (e.g. NW and SE) and can also be described as sub-vertical.

The key input for the establishment of the deformation zone model is 1) the SHI possible deformation zones (PDZs) in the boreholes, 2) tunnel mapping of the SFR underground facility, 3) lineaments identified by assessment of magnetic minima in the magnetic total field from surveys in the SFR area, 4) reprocessing and evaluation of existing reflection seismic data, and 5) processing and interpretations of the high-resolution magnetic total field data by forward magnetic modelling (Curtis et al. 2011).

### **5.4.1 Conceptual understanding of the deformation zone model**

The integrated site descriptive model for Forsmark (SKB 2008b) presents a concept for deformation in the brittle regime, where the primary attributes are the strong influence of the anisotropy in the ductile regime and the identification of four orientation sets of deformation zones. No information or interpretation work in the current study has come to light that contradicts the previously presented conceptual understanding, so the subdivision of zones has been maintained in the current report. However, it should be noted that no kinematic studies have been included in the current project.

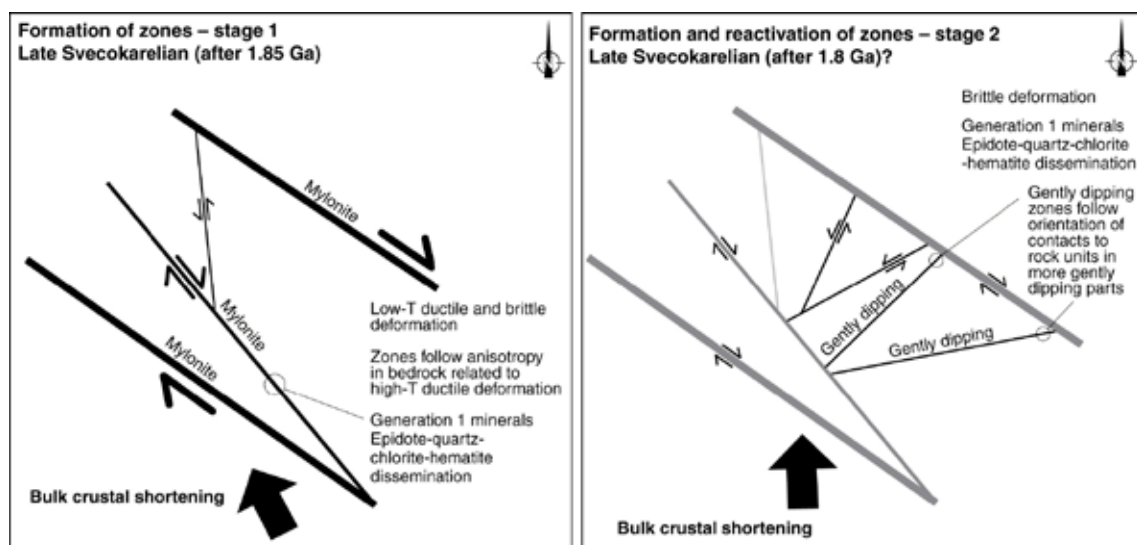
The oldest discrete structures in the area are the steeply dipping WNW-ENE and NW-SE zones (e.g. the Singö deformation zone), generally referred to as the WNW to NW set. These zones initiated their development in the ductile regime and continued to be active as faults in the brittle regime. Together with the broader structural belts with the same orientation, which developed earlier under higher-grade metamorphic conditions, they account for a pronounced structural anisotropy in the bedrock. In addition to the conspicuous WNW to NW zones, there are three distinctive sets of brittle deformation zones (fracture zones) in the area.

- Vertical to steeply dipping fracture zones that strike ENE-WSW (NE-SW) and NNE-SSW, generally referred to as the ENE to NNE set including ENE(NE) and NNE sub-sets.
- Vertical and steeply dipping fracture zones that strike NNW-SSE, generally referred to as the NNW set.
- Gently dipping ( $\leq 45^\circ$ ) fracture zones that, relative to all the other sets, contain a higher frequency of open fractures and non-cohesive fault rocks.

A concept where the four different sets of deformation zones formed initially in response to compressive tectonic regimes during the later part of the Svecokarelian orogeny was presented in the final geological model for Forsmark (Stephens et al. 2007, SKB 2008b) and supported by the interpretation of all kinematic data in Saintot et al. (2011). This concept involved dextral strike-slip displacement in low-temperature ductile and subsequently brittle regimes along the steeply dipping WNW to NW set and possibly even some sinistral displacement along the steeply dipping NNW set (Figure 5-14). This was followed by continued dextral strike-slip displacement along the WNW to NW set of zones in the brittle regime, in combination with sinistral strike-slip displacement along the steeply dipping ENE(NE) and NNE sub-sets (Figure 5-14). Bulk crustal shortening in a NW–SE to N–S direction during the later part of the Svecokarelian orogeny, involving clockwise stress deviation inside the Forsmark tectonic lens (Saintot et al. 2011), was inferred (Figure 5-14). It is inferred that reactivation along the WNW or NW belts continued in the brittle regime and that some of the smaller zones with WNW or NW strike could have formed more or less simultaneously with zones that show ENE, NE or NNE strike.

The modelled truncation of the gently dipping zones is based on the conceptual hypothesis that these structures formed after the steeply dipping set of WNW to NW regional zones, and more or less at the same time as the steeply dipping ENE(NE) sub-set, NNE sub-set and at least some of the steeply dipping NNW set in the brittle regime (Figure 5-14). For this reason, the gently dipping zones were extended in space as far as to the nearest steeply dipping zone, but are not necessarily truncated towards the steeply dipping ENE(NE) sub-set and the NNE sub-set.

All the four sets of deformation zones underwent reactivation in the brittle regime during the subsequent geological evolution, especially during the Sveconorwegian orogeny around 1.1–1.0 Ga (Stephens et al. 2007, Saintot et al. 2011). Furthermore, reactivation due to the effects of loading and unloading cycles during the latter part of the Proterozoic and Phanerozoic time periods has been recognised (Stephens et al. 2007). This type of reactivation in the form of extensional failure and the development of dilatational joints is most conspicuous along the gently dipping zones and in the near-surface realm.



**Figure 5-14.** Two-dimensional graphic illustrating the regional-scale geodynamics during the initial development of the steeply dipping WNW-ESE and NW-SE zones and the subordinate sets of brittle deformation zones in response to late stage Svecokarelian tectonic activity. After SKB (2008b).

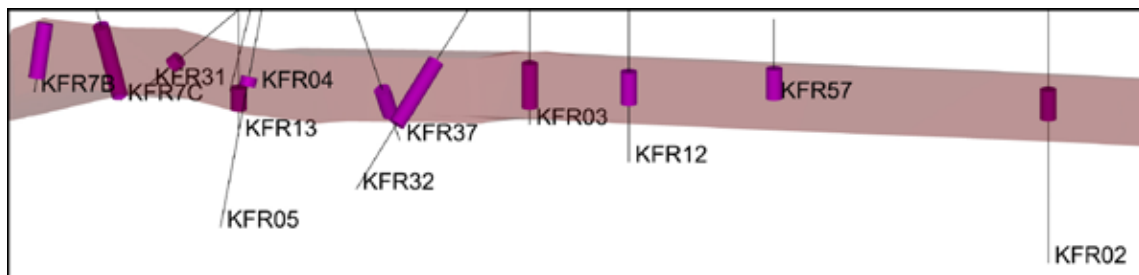
## 5.4.2 Methodology and assumptions

The current SKB definition of a deformation zone differs considerably from that applied in the previous structural models of SFR, where brittle deformation zones (fracture zones) were generally identified on the basis of the frequency of open fractures and hydrogeological information (cf. Carlsson et al. 1985, 1986). Zone thicknesses are currently estimated on the basis of the SHI borehole intercepts that take into account other features such as the frequency of sealed fractures and hydrothermal rock alteration. In general, this geological methodology generates much larger estimates of zone thickness compared with the earlier construction/engineering geological methodology. The geological methodology used here is in accordance with that used in the Forsmark site investigation (see especially Section 5.2.1 in Stephens et al. 2007). It should also be noted that deformation zone geometries are often complex, discontinuous and asymmetric.

Zone thickness is estimated primarily from SHI PDZ borehole data. Where multiple borehole intercepts are involved, the thickness of the modelled zone is generally taken to equal the thickest inferred PDZ intercept, as shown in Figure 5-15. The modelled thickness aims to contain at least the majority of the core(s) and damage zone(s) of each deformation zone. It is this envelope thickness that defines the deformation zone in the 3D RVS deterministic deformation zone model along with a generally centrally located middle plane with zero thickness.

The following basic assumptions underlie the current deformation zone modelling.

- Deformation zones can be interpreted from direct geological data. The confidence in geological character and possible extent (length and thickness) of deformation zones inferred from such data is higher than that for deformation zones identified from indirect observations (see bullets 2 and 3 below).
- Deformation zones can be interpreted from indirect sources of data such as topography and geophysics.
- Magnetic lineaments provide information about the location and trace length at the ground surface of possible deformation zones.
- Different sources of data can complement each other and increase the confidence in the interpreted deformation zone.
- Interpreted deformation zones can be interpolated between points of observation, if there are reasonable data to suggest the validity of such interpolation.
- Deformation zones are variable in their thickness and although they may in reality have a very complex architecture they can be modelled using an inferred generalised thickness.
- Within the limits of the regional or local model volumes, deformation zones interpreted at the ground surface can be extended downwards to a depth equal to the interpreted length of the mapped surface trace. This means, for example, that deformation zones longer than 1,000 m at the ground surface are extended to the base of the regional model volume (-1,100 m). Simplified zone length-depth classes have been applied in the modelling work.
- Each interpreted deformation zone has been ranked according to the confidence in its existence as being high, medium or low. Deformation zones that have high confidence ratings are based on direct data sources from boreholes and tunnels, complemented by indirect data sources mostly in the form of magnetic lineament indications. In addition to this simplistic classification, it is important that the reader considers the spread of the supporting evidence, details of which are provided in a property table for each zone.
- Deformation zones ranked with medium confidence are based solely on indirect information that has a relatively clear signal and geometry such as a magnetic lineament.
- Interpreted deformation zones with assigned low confidence are only supported by indirect sources of information with weaker associations to deformation such as deeper lying seismic reflectors.



**Figure 5-15.** Section view of ZFM871 looking down dip to the south (modelled thickness of 20 m). SHI PDZ sections shown in violet and the pink box shows the modelled zone thickness (based on the maximum SHI indicated thickness from KFR7C and KFR37).

The lineament map used in SFR model version 1.0, modified after the model stage 2.3 version in the Forsmark site investigation (Isaksson et al. 2007), forms the starting point for the surface interpretation of steeply dipping deformation zones. During the deformation zone modelling work, the lineaments, particularly their overall continuity, have been continually reviewed and the background data re-examined. Alternative alignments and extents for individual lineaments have been considered, often driven by geological information from boreholes or tunnel mapping and some have been implemented after a joint review by both the geologists and geophysicists.

The strike of the deformation zone is assumed to be the same as the trend of the matching lineament, whereas the dip is inferred by matching the lineament to the borehole intercept(s) and is documented as the average dip angle of the deformation zone along its entire extent. The matching process is largely geometrical, though previous experience from the Forsmark site investigation has shown that certain attributes can be used to further support SHI borehole PDZ and lineament correlation, for example the orientation of the most significant set of fractures. Deformation zones interpreted on the basis of magnetic lineament data alone are assumed to be vertical.

The steeply dipping deformation zones are assumed to terminate as indicated by the lineament map and in accordance with the conceptual understanding (see Section 5.4.1). Thus, the length of such zones at the ground surface is generally represented by the length of the corresponding lineament. For gently dipping deformation zones, the SFR version 1.0 modelling work has followed the concept in Stephens et al. (2007), where the modelled extent of such zones is constrained on the basis of the lateral extent of the supporting investigation evidence and the subsequent termination against the nearest steeply dipping zone outside the volume where this evidence exists.

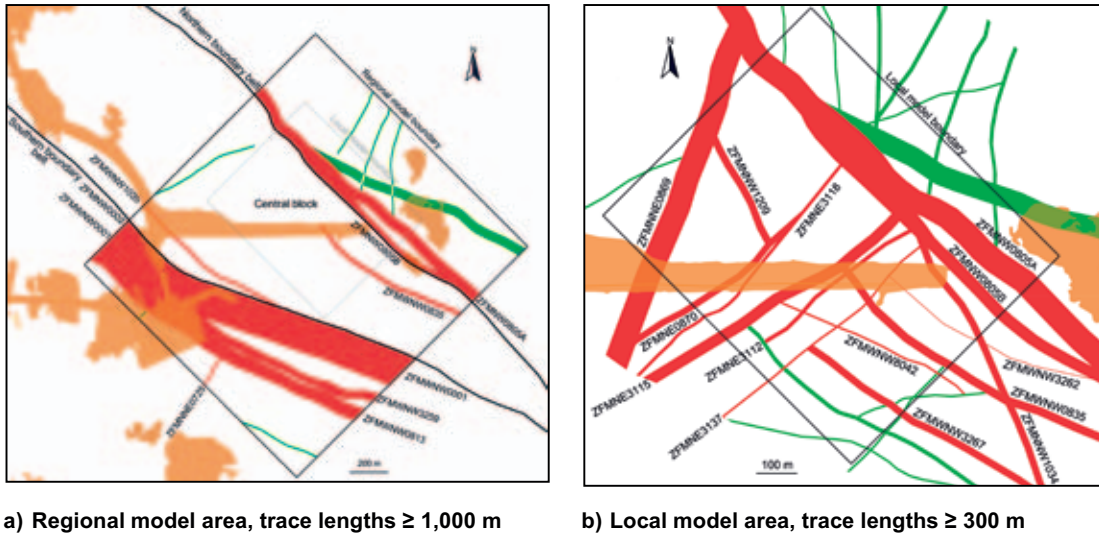
Since no statistically reliable thickness-length correlation has been obtained for the SFR deformation zones, a simple classification has been applied to estimate thicknesses of inferred zones that lack supporting borehole or tunnel data. In this classification, the thickness is estimated to be 1% of the associated lineament length, rounded off to the nearest 5 m to reflect it is a coarse and simplistic estimation.

The general principle that a deformation zone should be modelled to a depth equal to the length of the zone's surface trace has been applied. This principle, in combination with the selected modelling scales and model volume lower boundaries, entails in practice that any steeply dipping zone included in the local model terminates at the base of the local model volume, and in the case of the regional model constraints, any steeply dipping zone included terminates at the base of the regional model volume. A general classification grouping as defined in Curtis et al. (2011) has been applied for the combined regional and local deformation zone model.

### 5.4.3 Geometric models and property assignment

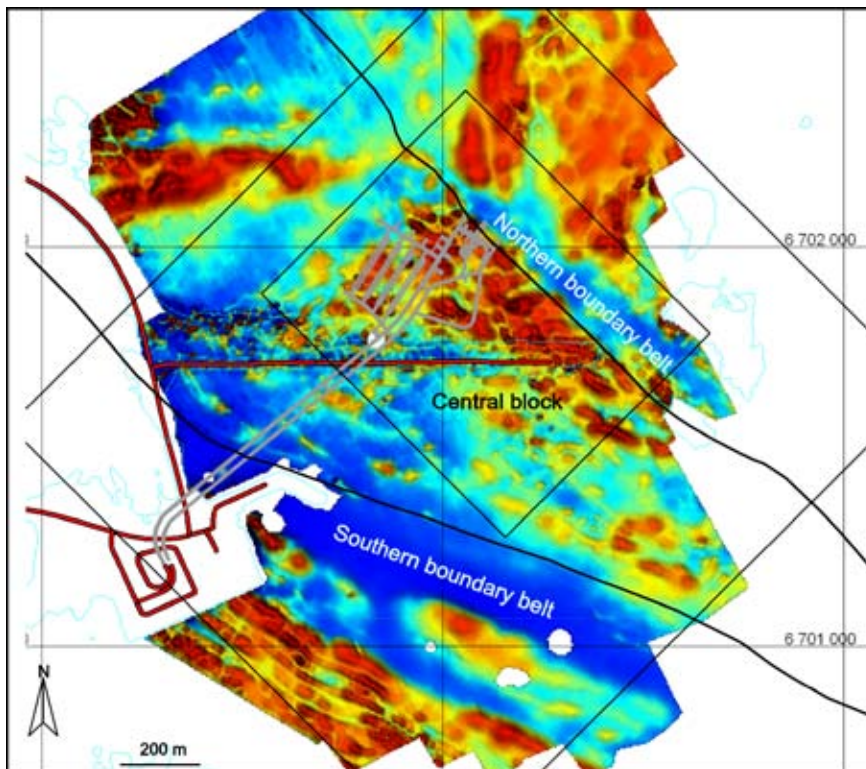
Forty deformation zones, of which 21 have been assigned a high confidence of existence, are included in the regional and local models (Figure 5-16 and Table 5-4). Twenty-eight zones occur inside the local model volume. The inferred occurrences of these zones in boreholes and tunnels are presented in Appendices 7, 8 and 9 in Curtis et al. (2011). Except for three gently dipping zones, they are all vertical or steeply dipping, and follow the orientation sets identified by their geological character in the earlier model for deformation zones at Forsmark (Stephens et al. 2007, SKB 2008b).





**Figure 5-16.** Intersection at the current ground surface of deformation zone traces within a) the regional model and b) the local model. The different colours refer to confidence in existence: high = red, medium = green.

The most prominent deformation zones in the region belong to the WNW to NW trending set, which mainly occur in two broad belts that delimit a tectonic wedge, denoted the ‘Central block’, and containing the existing SFR facility and the rock volume proposed for the new facility extension (Figure 5-17).



**Figure 5-17.** The central SFR block containing the existing SFR disposal facility, the Northern boundary belt (dominated by ZFMNW0805A) and the Southern boundary belt (dominated by ZFMW0001), along with the magnetic total field.

**Table 5-4. Table showing geometry of deformation zones present inside the regional and local model volumes.**

DZ Name	Confidence level	Present in regional model	Present in local model	Strike (°)	Dip (°)	Thickness (m)	Length (m) at ground surface	Lower cut off depth(-masl)	Comment
<b>Gently dipping DZs</b>									
ZFM871	H		x	074	19	20	-	-	No surface intersection. Irrespective of its limited modelled extent, it is recommended that this zone should be included in both local and regional modelling studies
ZFMA1	M	x		082	45	40	-	1,100	No surface intersection
ZFMB10	L	x		025	35	10	-	1,100	No surface intersection
<b>Steeply dipping DZs</b>									
<i>NNE to ENE set</i>									
ZFMNNE0725	H	x		201	84	12	1,763	1,100	
ZFMNNE0869	H		x	201	86	60	898	1,100	Depth class increased from 750 m since longer/deeper zones terminate against it
ZFMNNE2308	M	x		214	80	15	1,250	1,100	
ZFMNNE3130	M	x		030	90	5	411	750	Depth class increased from 500 m since longer/deeper zones terminate against it. Only included in the combined model version as a termination surface. It lies outside the local model volume and has a length of < 1000 m
ZFMNNE3264	M	x	x	031	90	10	1,128	1,100	
ZFMNNE3265	M	x	x	032	90	10	1,103	1,100	
ZFMNNE3266	M	x	x	034	90	10	1,015	1,100	
ZFMNE0870	H		x	232	76	16	559	750	
ZFMNE3112	H		x	233	89	10	474	500	
ZFMNE3118	H		x	044	84	8	743	750	
ZFMNE3134	M		x	041	90	5	370	500	
ZFMNE3137	H		x	230	90	5	672	750	
ZFMENE3115	H		x	236	84	28	793	1,100	Depth class increased from 750 m since longer/deeper zones terminate against it
ZFMENE3135	M		x	081	90	5	368	750	Depth class increased from 500 m since longer/deeper zones terminate against it
ZFMENE3151	M		x	074	90	5	421	500	
ZFMENE8031	M		x	063	90	5	537	750	
ZFMENE8034	M	x		067	90	10	1,203	1,100	
<i>WNW to NW set</i>									
ZFMWNNW0001	H	x		120	90	185	30,000	1,100	
ZFMWNNW0813	H	x		115	90	75	2,715	1,100	
ZFMWNNW0835	H	x	x	118	88	21	1,044	1,100	
ZFMWNNW0836	M	x	x	117	90	50	4,868	1,100	
ZFMWNNW1035	H	x		120	80	15	1,622	1,100	
ZFMWNNW1056	M	x		110	90	10	2,758	1,100	
ZFMWNNW3259	H	x		117	90	50	2,174	1,100	
ZFMWNNW3262	H		x	116	86	2	610	750	
ZFMWNNW3267	H		x	122	90	18	698	750	
ZFMWNNW3268	M		x	109	90	5	861	750	
ZFMWNNW8042	H		x	116	89	5	524	750	
ZFMWNNW8043	M		x	124	90	10	775	750	
ZFMNNW0002	H	x		310	90	50	18,000	1,100	
ZFMNNW0805A	H	x	x	312	82	60	3,643	1,100	
ZFMNNW0805B	H	x	x	315	75	30	1,181	1,100	
<i>NNW to NS set</i>									
ZFMNNW0999	M		x	170	90	5	692	750	
ZFMNNW1034	H		x	337	78	17	883	750	
ZFMNNW1209	H		x	151	83	18	341	500	
ZFMNNW3113	M		x	173	90	5	376	500	
ZFMNS3154	M		x	180	90	10	757	750	

The Central block is less affected by deformation than the bounding belts. South-east of the existing SFR facility, a series of WNW to NW trending deformation zones are included in the model. These are much smaller than the bounding belts and were initiated at a later stage in a brittle regime. A NE to ENE striking set of brittle deformation zones is also present. Compared with the WNW-NW set, they are thinner and shorter, due to termination against the broad WNW to NW trending deformation belts. In addition, there are a few N-S to NNW trending deformation zones in the model. However, on the basis of their low frequency of occurrence, this orientation set is judged to be of lower significance relative to the other sets at Forsmark (see also Stephens et al. (2007)).

None of the gently dipping zones is interpreted to intercept the ground surface. ZFM871 (old SFR zone H2) is the only of the three gently dipping zones that intersects the local model volume and has been assigned a high confidence. No gently dipping deformation zone was identified in the rock volume for the planned extension of SFR. However, there is a relatively high frequency of sub-horizontal open fractures in the upper part of the rock volume (above c. -200 m elevation), which are inferred to have formed or to have been reactivated in connection with stress release processes during unloading.

The geological and hydrogeological properties of the deformation zones inside the local model volume are compiled in Appendix 4. The geological properties of all the deterministically modelled deformation zones are presented in Appendix 11 in Curtis et al. (2011). A generalised summary of the character of each set or sub-set, based on these detailed property tables, is presented below and by representative drill core photographs in Figure 5-18.

#### **5.4.4 Character of different sets of zones**

##### ***Vertical to steeply dipping WNW to NW set***

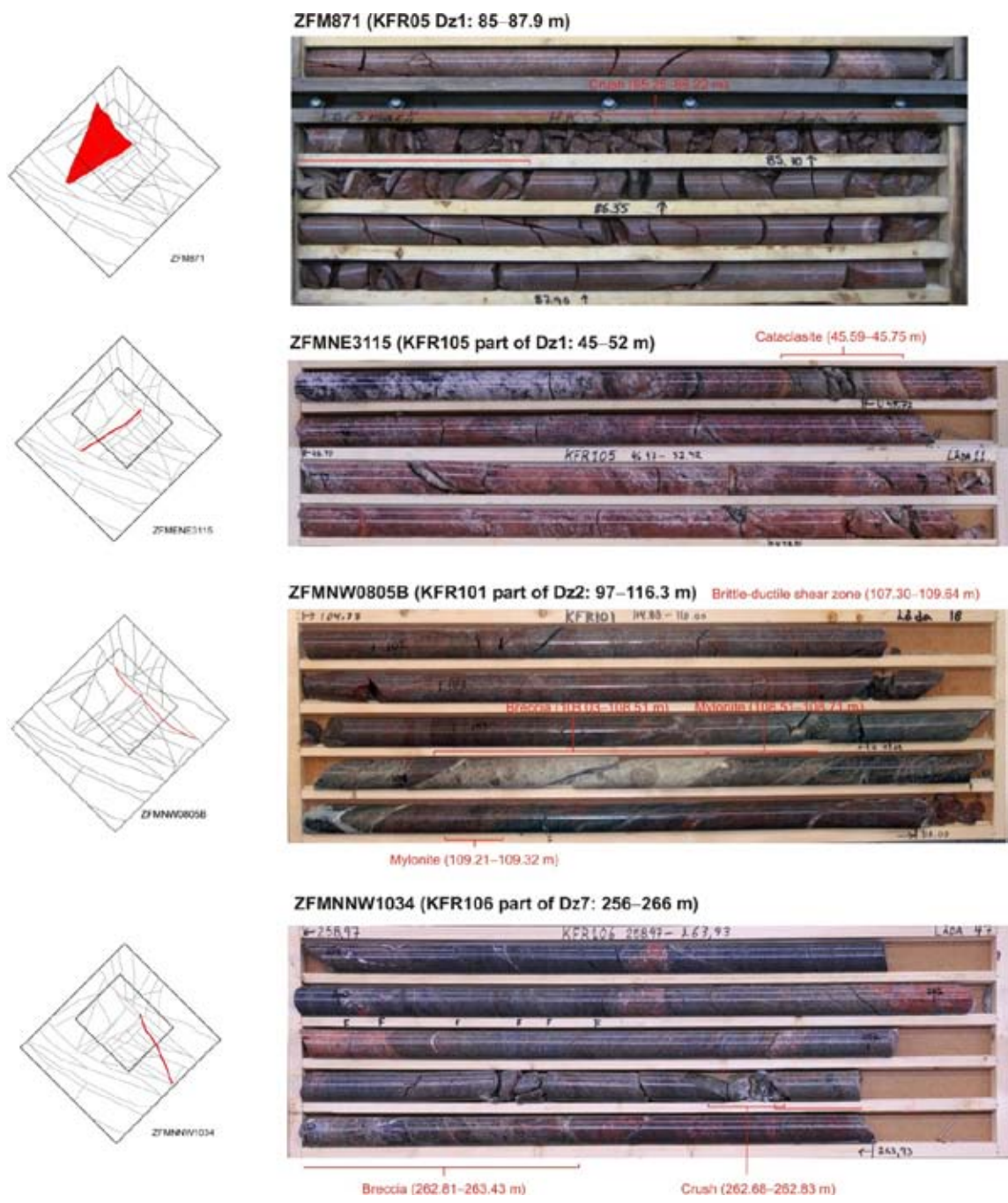
Members of this set of zones fall within the local minor to regional deformation zone size ranges, according to the terminology of Andersson et al. (2000). The set includes the dominant regional deformation zones that can be said to define the Northern and Southern boundaries of the Central block (Figure 5-17).

The zones in the vertical to steeply dipping WNW to NW set are generally composite features, characterised by an initial development in the ductile regime followed by brittle reactivation. It is the only set that exhibits ductile deformation. The majority of the fractures are sealed and mylonites, cataclasites and cohesive breccias occur locally, especially in the most prominent zones in the set (cf. Figure 5-18), i.e. ZFMWNW0001 (Singö deformation zone) and ZFMNW0805A/B (zone 8 in the older SFR nomenclature). The bedrock within these zones is typically affected by a varying degree of hematite dissemination. Two of the five deformation zones with occurrences of quartz dissolution (vuggy granite) belong to the WNW to NW set: ZFMNW0805A and ZFMWNW0835.

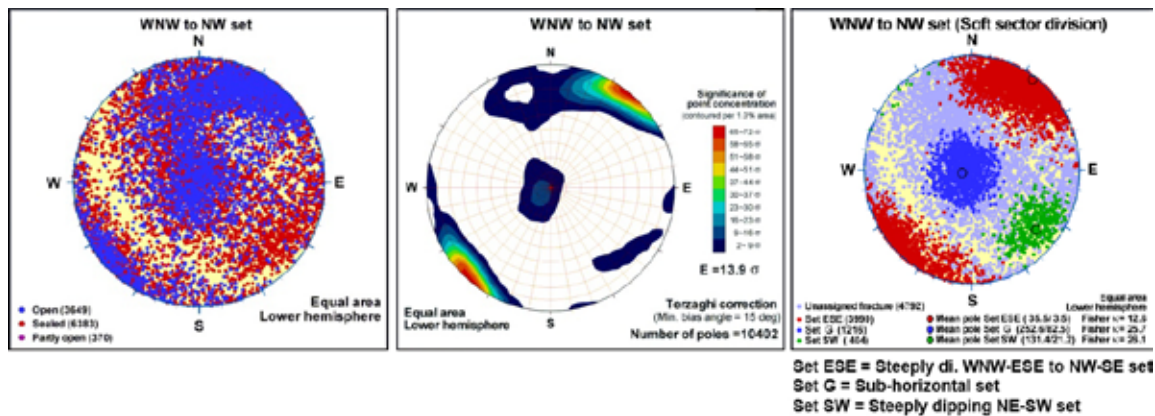
Besides the more common minerals calcite and chlorite, epidote, quartz, adularia, laumontite and clay minerals dominate the mineral fillings and coatings along the fractures in these zones. They represent examples of minerals from the oldest generation 1 and the younger mineral generations (Sandström et al. 2008b, 2009) and the zones have been reactivated repeatedly since they formed around and after 1.8 Ga

The zones of this group contain a dominant cluster of steeply dipping fractures that strike WNW-ESE (Figure 5-19). While the majority of these fracture are sealed, a significant proportion (37%) are also open. There is also a cluster of fractures that are almost exclusively sealed and strike NE-SW with steep dips to the northwest, and a sub-horizontal cluster of mixed open (40%), partly open (6%) and sealed (54%) fractures. The inferred oldest set, with a steep WNW-ESE strike, has been subject to the most reactivation cycles.

There are six zones that belong to the WNW to NW set of structures in the Central block, four with high confidence and two with medium confidence in existence. They are relatively short or at least their traceability is restricted with lengths ranging from 524 to 1,044 m. None of these zones have been modelled to intersect the existing SFR facility. They occur in the south-eastern part of the model volume, but are modelled to terminate against various ENE-to-NE-trending structures. Inspection of the map of interpreted lineaments (Figure 5-10) indicates what appears to be a change in character in the rock mass in the general area along zone ZFMENE3115.



**Figure 5-18.** Character of deformation zones in the four orientations in the SFR area, illustrated by drill core photographs of representative zone intersections. The position of each zone relative to the other modelled deformation zones and the SFR model boundaries are also included. ZFM871 (074°/19°): High frequency of open fractures and a crushed interval of almost 1 m length. ZFMNE3115 (236°/84°): Increased frequency of especially sealed fractures and sealed fracture networks, along with cataclasite. Frequent minerals in sealed fractures are calcite and laumontite. ZFMNW0805B (315°/75°): High frequency of both open and sealed fractures and a section of intense brittle-ductile deformation, which includes one interval with breccia and two intervals of mylonitization. ZFMNNW1034 (337°/78°): Increased frequency of sealed and locally open fractures, one crushed interval and one with breccia.



**Figure 5-19.** Fracture clustering within the WNW to NW oriented deformation zones. All plots utilise a lower-hemisphere, equal-area projection, with the Kamb contouring method applied to Terzaghi corrected pole plots.

To the north-west of this area, above the existing SFR facility, there are virtually no WNW-to-NW-trending lineaments lying within the Central block. However, the magnetic anomaly pattern is disrupted by both the man-made pier and changes in the dominant rock types when approaching from the south-east of the pier area. In addition, the mapping by Christiansson and Bolvede (1987) and Berglund (2008) indicates a general lack of WNW-NW-striking deformation zones and none that penetrate the full width of the central deposition area, comprising the four rock caverns and tunnels, and continue in a south-easterly direction into the rock volume intended for the disposal facility extension. There are four possible candidates in the old tunnel mapping that were considered for extrapolation and correlation with the modelled structures further to the southeast (Curtis et al. 2011). However, an assessment of all the available data reveals that such extrapolation and correlation was not possible.

It is possible that the extents of the minor WNW-NW structures may have been underestimated in the SFR mapping, since they were of reasonable rock engineering quality and were not judged at the time to be very significant for the excavation. An alternative interpretation is that the continuity of the steep structures with WNW strike in the local model volume to the southeast of the existing facility is over-emphasised in the current model and that the modelled structures are discontinuous and more like chains with missing links rather than the continuous features included in the model. This is considered possible due to the previously described problems regarding disruption of the magnetic lineament pattern.

### **Vertical to steeply dipping NNE to ENE set**

Compared with the WNW-to-NW set, the steep NNE-to-ENE zones penetrating the regional model area are much shorter, with lengths in the range of 368 to 1,763 m, falling within the local minor to local major deformation zone size ranges according to the terminology of Andersson et al. (2000). Their lengths are strongly controlled by older tectonic structures, generally terminating against WNW-to-NW deformation zones (i.e. strong truncation effects). The ENE sub-set additionally shows terminations against the structures in the NNE sub-set and the N-S-to-NNW set. The steep NNE-to-ENE zones are generally narrow, with thicknesses of around 5 m to 15 m. Two zones are clear exceptions with much thicker modelled thicknesses: ZFMNNE0869 (zone 3 in the older SFR nomenclature) with 60 m and ZFMENE3115 with 28 m. But in both cases the modelled thickness represents more than one structure. They are both interpreted as consisting of a packet or swarm of sub-parallel closely spaced, narrower structures rather than a single discrete zone (see Appendix 11 in Curtis et al. 2011 for details).

The steep NNE to ENE zones formed in the brittle regime and are dominated by sealed fractures. Calcite, chlorite, hematite-stained adularia, laumontite and quartz are conspicuous along the fractures in these zones (mainly generation 2 mineral paragenesis (Sandström et al. 2008b, 2009)). Younger generation 3 and 4 minerals, for example pyrite and clay minerals, are also present. Three of the five deformation zones with occurrences of quartz dissolution (vuggy granite) belong to the NNE-to-ENE set: ZFMENE3115, ZFMNE3118 and ZFMNNE0725.

The steep NNE-to-ENE zones contain a dominant cluster of steeply dipping, generally sealed fractures that strike NE-SW and a secondary cluster of sealed fractures that are steep and strike NNW-SSE. In addition, more commonly open fracture clusters with sub-horizontal and gentle dips to the south are also present (Figure 5-20).

The ENE sub-set consists of five zones within the Central block, only one of which, ZFMENE3115, has been identified with high confidence. The NE sub-set consists of five zones within the Central block. Four of these zones (ZFMNE0870 or zone 9 in the older SFR nomenclature, ZFMNE3112, ZFMNE3118 and ZFMNE3137) have been identified with high confidence. The zones are relatively thin (5–16 m) and short (370–743 m).

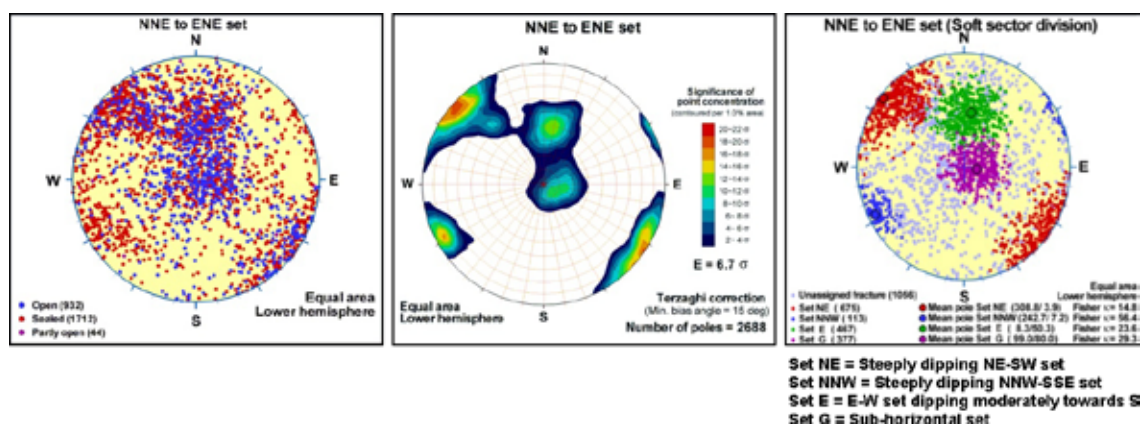
The NNE sub-set consists of seven zones, two of which are high confidence and only one of which, ZFMNNE0869, lies within the Central Block. Lengths range from 411 to 1,763 m, although the longer values are associated with zones at the edge of the regional model area, north of zone ZFMNW0805A. The two high-confidence zones, ZFMNNE0725 and ZFMNNE0869, have modelled thicknesses of 12 and 60 m, respectively. However, the modelled thickness of ZFMNNE0869 represents a group of thinner, sub-parallel fracture zones, including crushes and alteration, that diverge and converge in a complex pattern rather than a single well-defined zone (see conceptual model in Figure 5-1 in Stephens et al. 2007).

### Vertical to steeply dipping N-S-to-NNW set

There are five zones in this group, although only two of them, ZFMNNW1209 and ZFMNNW1034, lie within the Central block and have been identified with high confidence. The other three are medium-confidence zones that lie to the north of zone ZFMNW0805A. The members of this group have terminations against all three of the other steeply dipping deformation zone sets.

All the zones in this group that intersect the regional model volume are local minor in size according to the terminology of Andersson et al. (2000). The two high-confidence zones have similar modelled thicknesses of 17 m and 18 m. However, although the 18 m modelled thickness of ZFMNNW1209 is based on SHI data, evidence for the zone seen in the rock caverns indicates that the zone is composed of a group of parallel thin discontinuous structures rather than a single thick discrete zone with a central core.

These zones are dominated by sealed fractures. High-confidence zones in this group are brittle with minor cohesive breccias, fine-grained hematite dissemination and calcite, chlorite, epidote, adularia and laumontite (generation 1 and 2 mineral parageneses (Sandström et al. 2008b, 2009)). However, younger generation 3 and 4 minerals, for example pyrite and clay minerals, also occur. A subordinate brittle-ductile component is also locally present in ZFMNNW1034.



**Figure 5-20.** Fracture clustering within the NNE to ENE oriented deformation zones. All plots utilise a lower-hemisphere, equal-area projection, with the Kamb contouring method applied to Terzaghi corrected pole plots.

These zones contain a dominant cluster of steeply dipping, generally sealed fractures with NNW-SSE strike, along with a clear steeply dipping cluster of predominantly sealed fractures that strike E-W. There is also a more weakly developed cluster of sealed fractures that strike E-W and dip gently to moderately to the south and a cluster of sub-horizontal, predominantly open fractures (Figure 5-21).

**Gently dipping zones**

Three zones are present within this orientation group: ZFMA1 of medium confidence, located on the southern side of ZFMWNW0001, ZFMB10 of low confidence, located at significant depth beneath the local model volume, and ZFM871 (old SFR zone H2) of high confidence, located within the local model volume (Figure 5-22).

ZFMA1 was identified during the Forsmark site investigation and reported in /Stephens et al. 2007/. The inferred zone corresponds to the A1 seismic reflector with an orientation of 082°/45°. ZFMB10 also corresponds to a seismic reflector, B10, which was identified during re-processing and reinterpretation of existing seismic data in connection with the current project (Juhlin and Zhang 2010). The inferred low confidence zone has an orientation of 025°/35°. Alternative interpretations of A1 and B10 are that one or both of the reflectors are related, wholly or partly, to compositional variations in the bedrock.

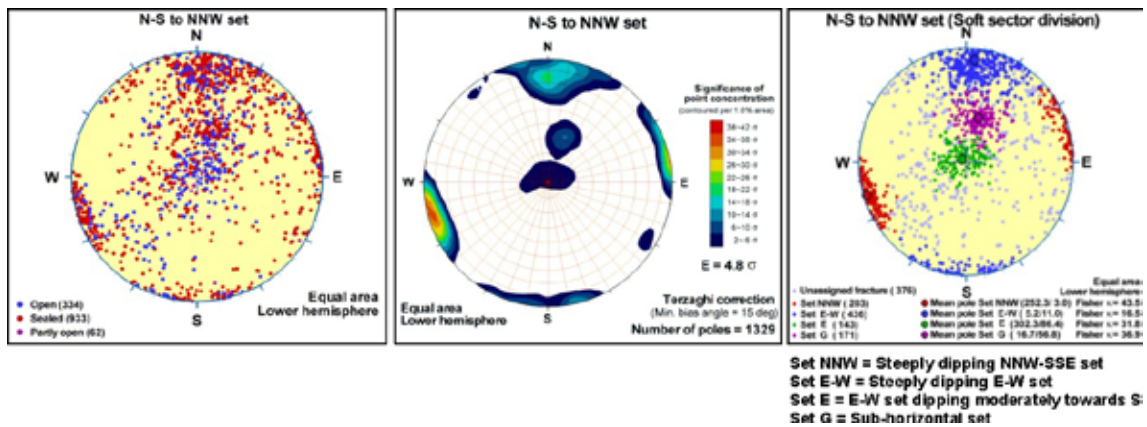


Figure 5-21. Fracture clustering within the N-S to NNW oriented deformation zones. All plots utilise a lower-hemisphere, equal-area projection, with a Terzaghi correction of the Kamb-plots.

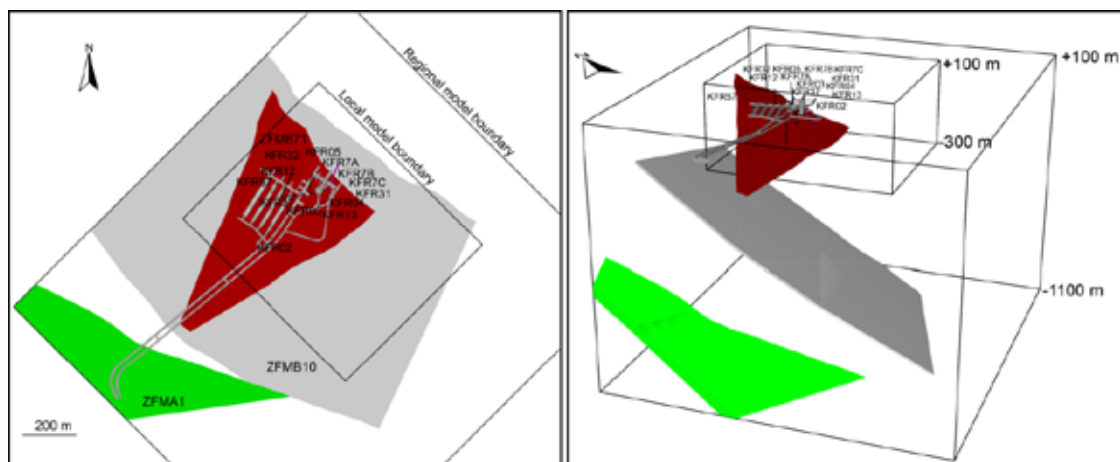


Figure 5-22. Gently dipping zones penetrating the SFR regional model volume. ZFM871 (red, high confidence), ZFMA1 (green, medium confidence), ZFMB10 (grey, low confidence).

ZFM871, formerly called H2 during the SFR construction phase (Christiansson and Bolvede 1987), has an orientation of 074°/19°. Its general character corresponds to the description of the other gently dipping fracture zones identified during the Forsmark site investigation as reported in Stephens et al. (2007). These zones are interpreted as having formed in the brittle regime and, relative to all the other sets, contain a higher frequency of open fractures and incoherent crush material. Chlorite, calcite and clay minerals are conspicuous along the fractures in these zones.

Zone ZFM871 has been modelled to terminate against zones ZFMENE3115, ZFMNNE0869, ZFMNW0805A, ZFMNW0805B and ZFMWNW1035. Its terminations against the surrounding steeply dipping zones and the resulting limited extent of the zone mean that it no longer has an intersection with the sea bottom and no coincidence with a lineament.

Due to the open and water-bearing character of ZFM871 identified during the earlier excavation phase and the number of gently dipping zones identified during the Forsmark site investigation, efforts have been made to identify the existence of similar gently dipping structures in the SFR model volumes. Any potential deformation zone with gentle to moderate dip to the southeast would generate intercepts in existing boreholes but, more importantly, in the existing tunnels, caverns and silo as well. Whilst sub-horizontal to gently dipping fractures are common in the SFR excavation, no evidence for a corresponding gently dipping zone has been found.

### ***Structures not included in the deterministic deformation zone model***

#### **Possible deformation zones (PDZs) in the single-hole interpretation (SHI)**

A total of 31 PDZs identified during the simplified and standard SHI could not be included in the deterministic deformation zone model. Details of these PDZs are included in Table 5-5. The position of these PDZs relative to the modelled deformation zones and the existing SFR facility are shown in Figure 5-23. Approximately 70% of them are defined as low- or medium-confidence by SHI.

There are distinct differences between the 17 PDZs in the old data set in the vicinity of SFR and the 14 PDZs in the new data set (Figure 5-23). Note that four PDZs inferred from the new data set (HFR106\_DZ1, KFR101\_DZ3, KFR103\_DZ1 and KFR106\_DZ6) are PDZs included in the hydrogeological definitions of deterministic SBA-structures (see Chapter 7).

The 17 PDZs are from older boreholes lacking BIPS orientation data. Only five of these PDZs were judged to be high-confidence during SHI. It has not been possible to estimate any orientation or true thickness for these structures, and further hydrogeological modelling work identifies no, or only weak, hydrological support (Öhman et al. 2012 and Figure 5-22). The lack of apparent correlation between nearby boreholes and the lack of significant deformation zones in the surrounding existing tunnels, in particular the nearby silo, suggests that most of these structures are minor features, with a size smaller than the resolution level for the deterministic modelling work adopted in version 1.0. In some cases these PDZs may be minor splays to some of the deterministic structures. In addition, Christiansson and Bolvede (1987) report that the silo has only minor tunnel water inflow, and consequently the PDZs around the silo are assumed to be hydraulically insignificant. Further study and hydrogeological assessment of all of these structures is described in Chapter 7.

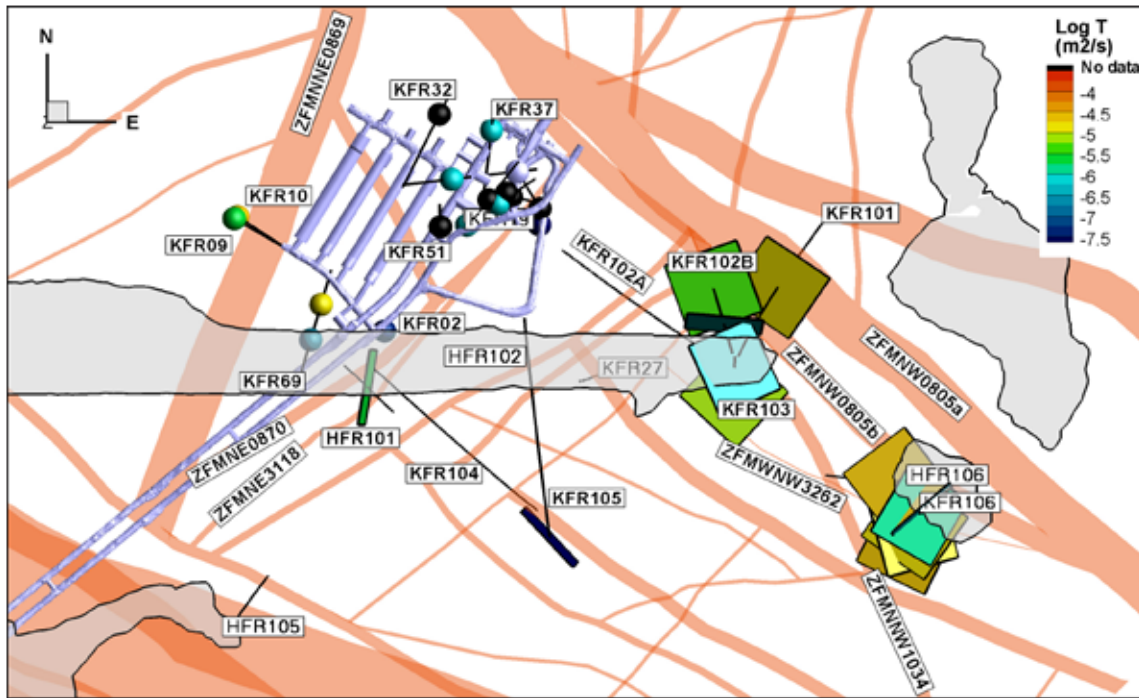
Of the 14 PDZs in the new cored boreholes, the existence of eight is judged to be of high confidence. Low-confidence estimates of the orientation and true thickness of nine of these isolated PDZs, using the orientation of fractures, have been calculated in order to assist other modelling disciplines. These geological interpretations have been integrated with the results of hydrological logging and testing in an attempt to better characterize these structures.

PDZs in the new boreholes have distinct hydraulic signatures with predominantly subhorizontal, high-transmissive ( $T > 10^{-6} \text{ m}^2/\text{s}$ ) PFL-f data. These PDZs are found down to c. -160 m elevation and seem laterally concentrated to a wedge defined by the Northern boundary belt (ZFMNW0805A/B) and ZFMNNW1034 (Figure 5-23). Their hydraulic character and further interpretation are reported in Öhman et al. (2012) and Section 7.3.2. It should be noted that KFR104, KFR102A and KFR105, which dominate the central block to the west of ZFMNNW1034 contain no significant PDZs that have not been included in the deterministic model (Figure 5-23).



**Table 5-5. Summary of SHI possible deformation zones (PDZs) not linked to deterministic deformation zones. SHI confidence level: 1 = low, 2 = medium, 3 = high confidence. (Table A12-1 in Appendix 12 in Curtis et al. 2011.)**

BH	SHIPDZ	BH length Sec_up (m)	BH length Sec_low (m)	SHI Conf. Level	Estimated orientation (alt. est)	Apparent thickness (m)	Estimated true thickness (m) (alt. est)	Comment
HFR101	DZ2	101	115	1	–	14	–	Too much scatter in the data to enable estimation of orientation.
HFR106	DZ1	38	40	1	–	2	–	Limited data set and too much scatter to enable estimation of orientation.
KFR02	DZ2	99.2	100.2	1	–	1	–	No orientation data. Possible association with ZFM871?
KFR03	DZ1	6	12	2	–	6	–	No orientation data. Possible splay of ZFMNE0870?
KFR04	DZ1	0	3	1	–	3	–	No orientation data.
KFR09	DZ2	69	74.3	3	–	5.3	–	No orientation data. Possible association with ZFMNNE0869?
KFR10	DZ2	95.65	107.28	3	–	11.63	–	No orientation data. Possible association with ZFM871?
KFR13	DZ1	20	30	3	–	10	–	No orientation data. Possible association with ZFMNE3118?
KFR13	DZ2	36	41	1	–	5	–	No orientation data. Possible association with ZFMNE3118?
KFR19	DZ1	38.53	49.32	2	–	10.79	–	No orientation data. Meeting point of long fractures?
KFR20	DZ1	48.50	52.00	1	–	3.50	–	No orientation data.
KFR31	DZ1	82.05	91.70	2	–	9.65	–	No orientation data.
KFR32	DZ1	155.70	159.00	3	–	3.3	–	No orientation data. Possible association with ZFM871?
KFR37	DZ1	36.60	45.60	2	–	9.00	–	No orientation data. Possible association with ZFMNW0805B?
KFR51	DZ1	9.84	11.15	1	–	1.31	–	No orientation data.
KFR52	DZ1	19.85	22.40	2	–	2.55	–	No orientation data.
KFR55	DZ1	0	3.3	2	–	3.3	–	No orientation data.
KFR69	DZ1	52.38	79.00	2	–	26.62	–	No orientation data.
KFR69	DZ2	121.60	146.10	3	–	24.5	–	No orientation data. ( $T \approx 10^{-5} \text{ m}^2/\text{s}$ . Possible correlation with major grout takes during construction inferred to be associated with horizontal fractures above the tunnel roof. (Öhman et al. 2012, Appendices A and D, Christiansson and Bolvede 1987)
KFR101	DZ3	179	186	3	–	7	–	Too much scatter in the data to enable estimation of orientation.
KFR101	DZ4	197	213	2	120/90	16	10.5	Interpreted as a short splay between ZFMNW0805A and ZFMNW0805B.
KFR102B	DZ1	67	70	3	098/81	3	2	
KFR102B	DZ3	149.5	150.5	2	229/08	1	< 1	
KFR103	DZ1	24.5	26.5	3	–	2	–	Too much scatter in the data to enable estimation of orientation.
KFR103	DZ2	84	91	3	298/86 (343/12)	7	4 (6)	
KFR105	DZ5	293.6	304	2	319/88	10.4	6	
KFR106	DZ1	15	20	3	216/90	5	< 1	
KFR106	DZ2	36.5	52	2	–	15.5	–	Too much scatter in the data to enable estimation of orientation.
KFR106	DZ4	84.5	86	3	181/14	1.5	1.5	
KFR106	DZ5	100.5	101	3	012/12	0.5	< 1	
KFR106	DZ6	153	157	3	098/19	4	3	SBA5 (see Chapter 7)



**Figure 5-23.** PDZs not included in the deterministic model compared to deterministic structures. PDZs lacking modelled orientation are shown as spheres (old borehole data, in the vicinity of SFR), while oriented PDZs shown as planes, interpreted from a combination of PFL and fracture data (new borehole data, south-east of SFR). Most of the PDZs of the new data set are spatially coupled to the Northern boundary belt (ZFMNW0805A/B) or ZFMNNW1034 (Öhman et al. 2012).

### Sub-horizontal stress release structures

The planned depth of the facility,  $-50$  to  $-200$  m elevation (see Section 2.9.2), is of particular importance in relation to the overall character of the rock volume. The SFR extension will lie wholly within the same depth range as the so-called shallow bedrock aquifer domain (SBA) as described by Follin (2008) and in Section 7.4.3. In this relatively shallow rock volume, stress release associated with loading and unloading cycles has resulted in the development of a high frequency of sub-horizontal open fractures (Stephens et al. 2007, Fox et al. 2007). These fractures, rather than the steeply dipping deformation zones, dominate the pattern of groundwater flow. In accordance with the conceptual thinking (Stephens et al. 2007), this pattern is likely to be reversed at greater depths, with the brittle deformation zones dominating the flow. A detailed discussion of such patterns is available in Öhman et al. (2012).

The existence of such horizontal structures, but with a limited lateral extent, lying above the existing silo was proposed by Carlsson et al. (1985). These particular structures, addressed in Curtis et al. (2009, 2011) are horizontal, located at an elevation of c.  $-25$  m, and are similarly interpreted as stress release features rather than deformation zones related to regional-scale tectonic activity. Modelled geometries (Curtis et al. 2009, 2011) have not been included in the deformation zone model but have provided input to hydrogeological modelling (Table 5-6). Such features are considered to be ubiquitous in the uppermost part of the bedrock in the Forsmark region (Stephens et al. 2007, SKB 2008b). Sub-horizontal so-called sheet joints or SBAs (Follin 2008) have been interpreted at lower elevations and have been included as deterministic features in the hydrogeological model (see Section 7.4.3).

**Table 5-6. Borehole intercepts for potential sub-horizontal stress release structures (Table A12-2 in Appendix 12 in Curtis et al. 2011.)**

ID	BH	Control point (BH length m)	Intercept defined by /Carlsson et al. 1985/ (BH length m)		Intercept defined by geological SHI (BH length m)			Comment
			Sec_up	Sec_low	PDZ	Sec_up	Sec_low	
H1	KFR21	29.5	26	33	–	–	–	
H1	KFR22	39	39	39	–	–	–	
H1	KFR23	23	23	23	–	–	–	
H1	KFR24	35	35	35	–	–	–	
H1	KFR25	48.5	42	55	–	–	–	
H1	KFR37	33	31	35	DZ1	36.60	45.60	
H1	KFR38	40	39	41	–	–	–	
H3	KFR31	60	56	64	–	–	–	
H3	KFR32	62.5	60	65	–	–	–	
H3	KFR33	57.5	55	60	–	–	–	
H3	KFR35	40	39	41	–	–	–	Carlsson's intercept lie within the much more extensive SHI DZ1 (32.70–70 m), as being ZFMNNW1209.
H5	HFR105	133	–	–	DZ3	119	147	
H5	HFR106	179.5	–	–	DZ3	177	182	
H5	KFR27	114	–	–	DZ1	108	120	
H5	KFR101	182.5	–	–	DZ3	179	186	
H5	KFR102A	155	–	–	DZ1	149	161	
H5	KFR102B	176.5	–	–	DZ4	173	180	
H5	KFR103	181.25	–	–	DZ3	180	182.5	
H5	KFR104	127.5	–	–	–	–	–	Increased frequency of open sub-horizontal fractures in the interval 120–135 m.
H5	KFR105	–	–	–	–	–	–	Radar reflector no 8 has a sub-parallel leg at ~195–220 m, at a distance of 15–20 m from the BH.
H5	KFR106	155	–	–	DZ6	153	157	
H6	KFR27	114	–	–	DZ1	108	120	
H6	KFR102B	150	–	–	DZ3	149.5	150.5	

## 5.5 Confidence and remaining uncertainties

### 5.5.1 Deterministic model for rock domains

The geometries of the rock domain model rely on the accuracy of the SFR tunnel mapping and the positioning of boreholes at depth. Data from the construction of SFR lack much of the quality assurance that marks current SKB methodology, not least regarding positioning. It is impossible to quantify these uncertainties, but they need to be considered when using the model. Calculated uncertainties for the spatial position of boreholes from the Forsmark site investigation and the latest drilling campaign in the area are judged to be minor in character, considered in the context of the uncertainties in the position of older data from the construction of SFR. However, there are uncertainties related to the geological mapping that affect the general uncertainty in the rock domains.

Specific uncertainties of importance for the rock domains include the following.

- Deviation measurements were not available in the SKB database Sicada for any of the boreholes from the construction of SFR.
- Geometries of all SFR underground openings in the drawings of Christiansson and Bolvede (1987) are theoretical rather than 'as built' and involve deliberate mapping generalisations as a result of the unfolding. Laser-defined tunnel centre-lines were used for positioning of the drawings in the model volume.
- Translation of the bedrock mapping from Christiansson and Bolvede (1987) into the rock type nomenclature introduced during the Forsmark site investigation.
- Orientation of linear structures in boreholes, especially percussion-drilled boreholes.
- The separation of the fine- to finely medium-grained metagranodiorite (to granite) (101057) and the felsic-to-intermediate metavolcanic rock (103076) by visual inspection. However, the overlap in the petrophysical and structural properties suggests similar mechanical properties.
- The character of the rock described as fine- to finely medium-grained metagranodiorite (to granite) (101057), especially in terms of modal composition and origin.
- The physical properties of the rocks in the SFR area are based on density and magnetic measurements on a fairly small number of samples from drill core. There are few surface-related petrophysical data and gamma spectrometry measurements on outcrops or in boreholes.
- The extreme bedrock heterogeneity on the tunnel scale, as a contributing factor to the difficulty of defining rock domains.

With four fixed points from boreholes and five from underground openings in SFR, distributed between -71 and -205 m elevation in the model volume, the uncertainty in the geometry of the boundary between RFR01 and RFR02 is judged to be low. The use of the high-resolution magnetic total field has refined the modelling of the boundary at levels where direct geological information is lacking. Sufficient data are available to estimate quantitatively the proportions of different rock types in RFR01 and RFR02, and associated uncertainties are judged to be low to moderate.

The geometry of the domain boundary between RFR02 and RFR03 is defined by geological information from RFR02 and the high-resolution magnetic total field, with no fixed points. Uncertainties in the geometry are consequently considered to be moderate to high.

The domain boundary between RFR02 and RFR04 is identical to the contact between RFM021 and RFM033 in the stage 2.2 regional rock domain model for Forsmark, which was in turn defined by geological information outside the local SFR model volume and without the use of the high-resolution ground magnetic data currently available inside this volume. Therefore, uncertainties in the geometry are considered to be moderate to high.

Geological data are lacking for both RFR03 and RFR04 and uncertainties in the properties are considered to be high. However, since the rock domains are peripheral to the volume of interest for extension of SFR, this lack of data is not judged to be of any major significance.

### **5.5.2 Deterministic model for deformation zones**

The overall confidence level regarding the deformation history and the broad tectonic framework of the region is judged high, based on the detailed work associated with the Forsmark site investigation and the associated modelling work as reported in Stephens et al. (2007) and elsewhere.

The confidence level in the existence of each of the deformation zones included in the local model volume is indicated in Table 5-4. As noted earlier, it is important for the reader to consider the nature and spread of supporting evidence for any deformation zone classed with a high confidence of existence. The classification system means that a zone based on a single borehole intercept has the same confidence level as a zone based on multiple borehole and tunnel intercepts. Similarly, the spread of evidence needs to be considered; a high confidence zone, coloured red in the model, is shown to have high confidence over its entire length even though supporting borehole evidence may be extremely local.

The overall confidence in the position, character and extent of the Southern and Northern bounding tectonic belts, dominated by ZFMWNW0001 and ZFMNW0805A, respectively, is high. Similarly, confidence is high in the steep to sub-vertical nature of the vast majority of the deformation zones in the SFR area as well as in the surrounding Forsmark area, inferred from the underlying conceptual model presented by Stephens et al. (2007). This concept has gained independent support from the results of inversion modelling and, in particular, forward modelling of magnetic data carried out as part of the current study (Curtis et al. 2011). In addition to the extremely local evidence from boreholes, it is these two geophysical modelling techniques that have provided indications, albeit general in character, of the overall dip of larger volumes of rock associated with the structures in the rock mass.

The overall confidence level in the deterministic modelling of the rock volume lying between zones ZFMWNW0001 and ZFMNW0805A is naturally scale-related. Confidence is high with regard to local major zones, but the confidence level drops as increasingly smaller structures are considered. As well as being scale-related, the confidence levels in the central SFR block are generally lower away from the existing tunnels than within the Forsmark local model area. The reason for this is that the initial basis for much of the modelling of steeply dipping deformation zones at both Forsmark and SFR is the identification and inferred extent of lineaments defined by magnetic minima.

When compared with the Forsmark model area, the SFR regional and particularly the local model areas have a natural magnetic field that is strongly disrupted. The identification of linear low-magnetic anomalies, possibly associated with deformation zones, around SFR is made difficult by masking and interference due to the overlying seawater and sediment, the man-made pier and buried scrap metal, the existing tunnels and cavern excavations, the deposited waste and its metal containers and the general disturbing influence of the nearby submarine electric cable, in combination with a heterogeneous lithology. Due to these effects, as well as the focus on the detection of smaller-scale structures, confidence levels are inevitably lower. As discussed in Section 5.4.4, a specific uncertainty remains concerning the continuity and length of the smaller zones in the steeply dipping WNW to NW set located within the Central block. However, even allowing for these disturbing factors, the assessment is that no local major structure of significant length has been missed.

The site investigations and modelling work have focused on locating local major gently dipping deformation zones in the local model volume. In this regard, key evidence is furnished by the rock conditions found in the existing underground SFR facility and, in particular, in the silo, extending from c. -60 to -140 m elevation, where no significant gently dipping structures were identified (note that zone ZFM871 lies beneath the silo). Due to this evidence, in combination with the borehole data, confidence is high that no previously unknown local major gently dipping zone exists in the investigated rock volume. The southeast corner of the local model volume is poorly covered by investigation data and has an accordingly higher level of uncertainty.

Uncertainty remains concerning the lateral extent of zone ZFM871, previously referred to as zone H2. In version 1.0, the zone is modelled as terminating against ZFMNW0805B (boundary to the NE), ZFMNNE0869 (boundary to the NW) and ZFMENE3115 (boundary to the SE). This interpretation suggests a smaller extent of the zone than that suggested by Axelsson and Mærsk Hansen (1997) and it is closer to the earlier interpretation by Carlsson et al. (1985). Clearly, alternative interpretations are possible. Due to the stepped and undulating character of the zone, if it does extend further to the northwest and even intercept the sea bottom, the prediction of the outcrop position is uncertain, and it is considered unlikely that such a structure would generate a clear lineament. A reasonable alternative is that the zone extends at least beyond ZFMNW0805B to ZFMNW0805A in a northeast direction. Particular focus was placed on identifying the possible greater extent of the zone to the southeast, beyond ZFMENE3115, using the new borehole information. However, no geological evidence in support of a further extent in this direction was found. The uncertainty of the extent of ZFM871 will be further investigated during hydrological modelling in SR-PSU (see Section 9.9.2).

A remaining key uncertainty is the existence, frequency and position of gently dipping deformation zones that are smaller than the resolution level for the deterministic modelling work in this study, which may be of less significance from a geological viewpoint but highly significant from an engineering viewpoint, due to their open, water-bearing character and their interaction with similarly open, sub-horizontal, stress release fractures. Experience from the SFR excavations, including the investigation of zone ZFM871, has shown that there are difficulties in identifying such small,

gently dipping structures. Christiansson (1986) reports that zone ZFM871 has a very heterogeneous character with two to three gently dipping fracture sets, individually recorded zone thicknesses of up to 10 m and a hydraulic thickness varying from 2 to 20 m. The hydraulic thickness of a zone may be thicker than the geological zone thickness since water is not used to define a zone or its boundaries in the geological SHI even though it may be closely associated with a zone. For example, a vertical zone may be water-bearing with steeply dipping transmissive open fractures associated with the zone itself; the surrounding background fracture system outside the zone also has open fractures, many subhorizontal, which are in contact with the open water-bearing fractures of the zone. Water is determined to be laterally near the zone by the existence of chokes and channelling etc. This means that when approaching a zone with an advancing tunnel you may meet inflows of water (associated with the zone but also located outside the damaged zone) before you meet the zone itself. In this case the zone itself has a certain geological thickness, but its hydraulic thickness is greater. The gently dipping fractures, in combination with an increased frequency of steeply dipping fractures, gives rise to a stepped structure consisting of highly fractured, flat-lying lenses that are hydraulically interconnected. All of these conclusions, with minor adjustments, are supported by the current modelling work, and the correlation of smaller zones between boreholes with similar heterogeneous geological characteristics is clearly not straightforward. The existence and frequency of such structures is best established by hydrogeological investigations and modelling.

The importance of stress-release structures rather than zones formed in response to tectonic shear stresses has been proposed in the Forsmark site investigation (Stephens et al. 2007). There is high confidence that minor sub-horizontal structures do exist but with equivalent trace lengths of a couple of hundred metres or less, down to the single fracture scale. These features are interpreted as occurring at least in the upper 200 m of the rock mass. At very shallow depths, < 15 m, these features are clearly related to stress release with wide apertures filled with sediment and rock fragments (Carlsson 1979, Leijon 2005, Carlsson and Christiansson 2007). With increasing depth, the apertures become smaller and more standard mineral infillings and clay occur rather than sediment. The special character of the fracturing in the upper part of the bedrock at Forsmark was addressed in the Forsmark site investigation (Olofsson et al. 2007, Fox et al. 2007, Stephens et al. 2007), and in practical terms, the frequency and persistence of sub-horizontal structures was noted in the roof during the SFR tunnel excavations. These fractures are open and in some cases hydraulically interconnected with high transmissivities and have been identified down to elevations of c. -200 m (see Section 0).

Finally, there is still some uncertainty associated with the PDZs from the SHI not included in the model. Details of these zones are included in Appendix 12 in Curtis et al. (2011). However, the length of the borehole intersections suggests that most of these structures are minor features, with a size smaller than the resolution level for the deterministic modelling work adopted in version 1.0.

## 6 Rock mechanics

This chapter presents a rock mechanics site descriptive model of the SFR area. Note that no new data were acquired during the current SFR extension project. The description is based partly on data collected during planning and construction of the existing SFR facility and partly on data collected in the Forsmark site investigation. First the deformation and strength properties of intact rock are described for the four main rock types in the SFR area (Section 6.1), followed by rough estimates of the normal and shear stiffnesses of single fractures (Section 6.2). This part of the description differs from the description given in SDM-Site Forsmark (SKB 2008b), since the depth of the planned SFR extension is relatively shallow (approximately –60 to –200 m elevation) compared with the depth of the planned repository for spent nuclear fuel (c. –500 m elevation).

Section 6.3 concerns the engineering quality indices that are often used to describe the general suitability of the rock from a construction point of view. The description is based on the experience gained during the construction of the existing SFR and on the work done in the Forsmark site investigation. Empirical indices are also used to make rough estimates of large scale rock mass deformation and strength properties.

Section 6.4 concerns the *in situ* state of stress and predicts the magnitudes and orientations of the stresses at SFR, taking into account the difference in spatial location and depth compared with SDM-Site Forsmark. Finally, a short section concerning the confidence and uncertainties of each part of the model concludes the rock mechanics chapter (Section 6.5).

### 6.1 Intact rock properties

The deformation and strength properties of the intact rock are described for the different major groups and types of rocks, following the methodology employed in the Forsmark site investigation. As described in Section 5.2.3, there are five rock types that together comprise at least about 95% of the bedrock volume. For these five rock types, five different parameters are modelled (uniaxial strength, crack initiation strength, tensile strength, Young's modulus and Poisson's ratio).

Table 6-1 shows the available data from SFR that were not included in the database for SDM-Site Forsmark. The values are taken from the Sicada database. The rock mechanics descriptive model in SDM-Site Forsmark constitutes an important basis for the description for the SFR area as well, since the modelled rock volumes are very close and the rock types occurring are the same. The number of samples tested of each rock type is listed in Table 6-2, including the test samples from domain FFM01 in the Forsmark site investigation, but the details of the Forsmark data are not presented here and the reader is referred to SKB (2008b). The data from domain FFM01 at Forsmark is used because the number of sampled data is large from this domain (no data were acquired from the near-surface realm rock domain FFM02). Data from the earlier SFR investigation and construction phases are summarised in SKB (2004).

#### 6.1.1 Compressive strength

During the construction of the existing SFR facility, a number of uniaxial compressive strength (UCS) tests were performed on samples collected in cored boreholes in the SFR area (Table 6-1). The quality and documentation of the UCS tests are expected to be lower than for the testing performed later during the Forsmark site investigation, which followed the current SKB test procedures. However, since these older test samples were collected from boreholes in the actual area to be described, these data are analysed and still constitute an important basis for the description. Furthermore, a larger number of point-load tests were conducted.

**Table 6-1. Rock mechanics intact rock data available in Sicada from the SFR model volume. The values indicate the number of test results available. The location of the boreholes is shown in Figure 2-7.**

Borehole	Uniaxial compressive test – UCS	Uniaxial compressive test – E, v	Point load test At site	Point load test In lab
KFR19	2	2	–	3
KFR20	3	2	–	2
KFR21	11	6	38	14
KFR22	10	5	24	15
KFR23	8	4	24	10
KFR24	4	2	26	5
KFR25	–	–	50	–
KFR31	12	6	–	12
KFR32	12	6	–	12
KFR35	8	4	–	8
KFR37	16	8	–	16
Total	86	45	162	97

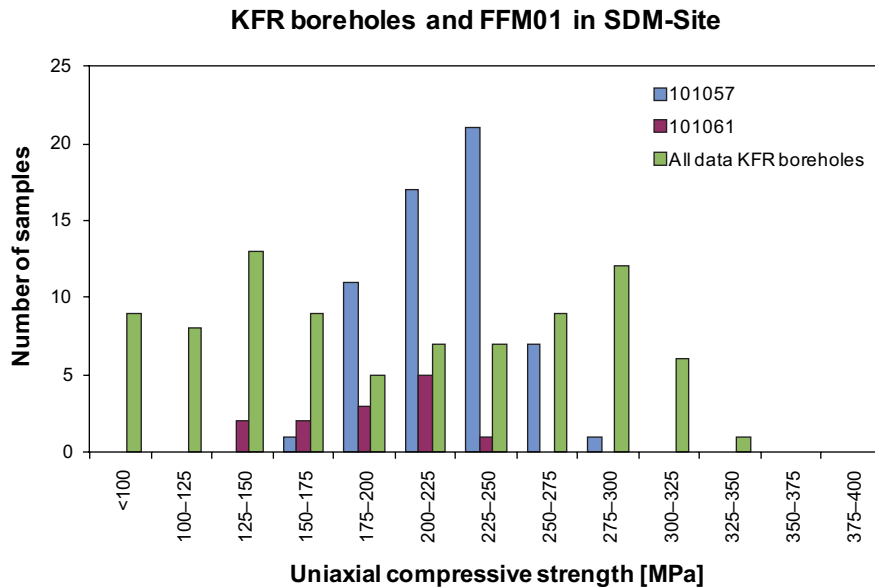
**Table 6-2. Rock mechanics intact rock data available in Sicada, sorted by rock types occurring in the SFR model volume.**

Rock Code	Rock type (reclassified)	Expected volume occurrence in RFR02 (Figure 5-13)	Uniaxial compressive tests – SFR boreholes UCS (E,v)	Point load test At site (SFR)	Point load test In lab (SFR)	SDM-Site Forsmark UCS (Table 7-3, FFM01, SKB 2008b and Glamheden et al. 2008)
101057	Metagranite to granodiorite	37%	60 (32)	102	58	47
101061	Pegmatite, pegmatitic granite	24%	10 (5)	19	18	13
111058	Fine to medium-grained granite	15%	–	–	–	1
103076	Felsic to intermediate metavolcanic rock	12%	4 (2)	30	21	–
102717	Amphibolite	6%	11 (6)	–	–	–
Total		94%	85 (43)	151	97	61

Figure 6-1 shows histograms of the UCS for the two most common rock types in domain FFM01 in Forsmark, together with all the USC test results from the KFR boreholes in SFR. (FFM01 is the main fracture domain described in SDM-Site). It can be concluded that the SFR data cover the entire range of possible expected strength, and that only a separation into rock types would make for a more useful description. The bimodal distribution also indicates that significant differences in strength can be expected in the SFR area. The old data were therefore sorted, here based simply on the original nomenclature used as available in Sicada. Where rock type information was missing, the coding was inferred from other tests performed on samples in nearby sections of the drill core. Based on previous rock coding work on SFR drill cores, presented in Petersson et al. (2011), the following translations from original names to rock codes were used: “Gneiss” = 101057; “Gneissic granite” = 101057; “Granitic gneiss” = 101057; “Pegmatite” = 101061; “Gneiss, pegmatite” = 101061; “Metavolcanic rock” (all varieties) = 103076; “Greenstone” = 102017; “Amphibolite” = 102017 (cf. section ). Note that this means that originally differently named rock types were put into the same rock type code (101057). The samples themselves, or photographs, were not utilised for the classification into rock types.

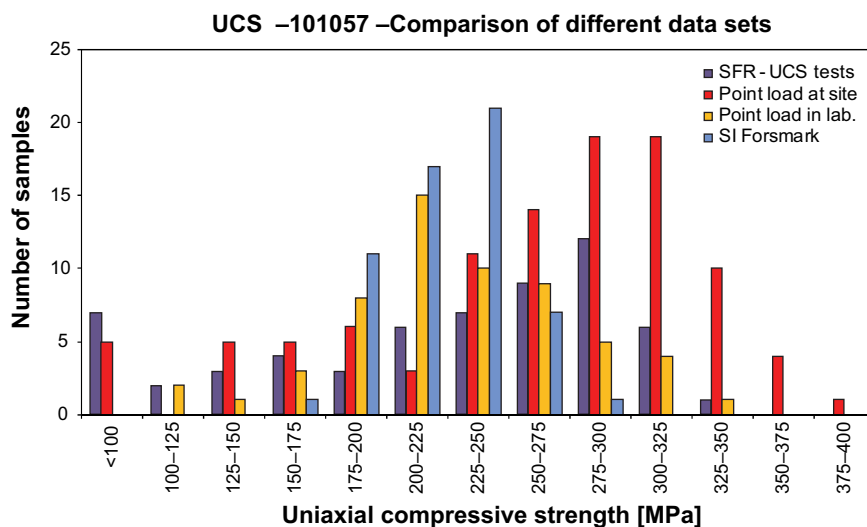
Data compilation for the two main rock types are presented in the form of histograms in Figure 6-2 and Figure 6-3. Each diagram presents four different sets of test results together, namely: 1) the ordinary uniaxial strength tests performed in the laboratory on samples taken from KFR boreholes at SFR; 2) uniaxial strength estimated from point load tests performed at the site *in situ*; 3) point load tests performed in the laboratory and 4) the data from fracture domain FFM01 in the Forsmark site investigation. (See also Table 6-3).





**Figure 6-1.** Uniaxial compressive strength (UCS) from laboratory tests (point load tests are not included). Comparison between older existing data from SFR, irrespective of rock type, and data from the Forsmark site investigation, including only granite to granodiorite (101057) and pegmatite (101062). Modified from SKB (2008b).

For the metagranite to granodiorite (101057), Figure 6-2, the number of tests is fairly satisfactory. However, there are differences between the data sets that still make the choice of values for the UCS model problematic. Rather than simply lumping the data together, it is considered more appropriate to make a choice based on the following reasoning: The standard uniaxial test in the laboratory, on samples from KFR boreholes, gives a median result closer to the Forsmark data but still somewhat higher, while the point loads performed in the laboratory have a mean value fairly similar to the Forsmark results. The point load tests done at the site are believed to be the least reliable in terms of absolute value and are therefore not used for estimation of that value, but the results indicate that there is a normal distribution in UCS. However, there is one advantage in the point load data sets over the uniaxial test set sets, which is that the samples are better spatially distributed along the boreholes. One sample is taken per ten metres of drill core. The standard samples are taken from a few core boxes of the available boreholes.

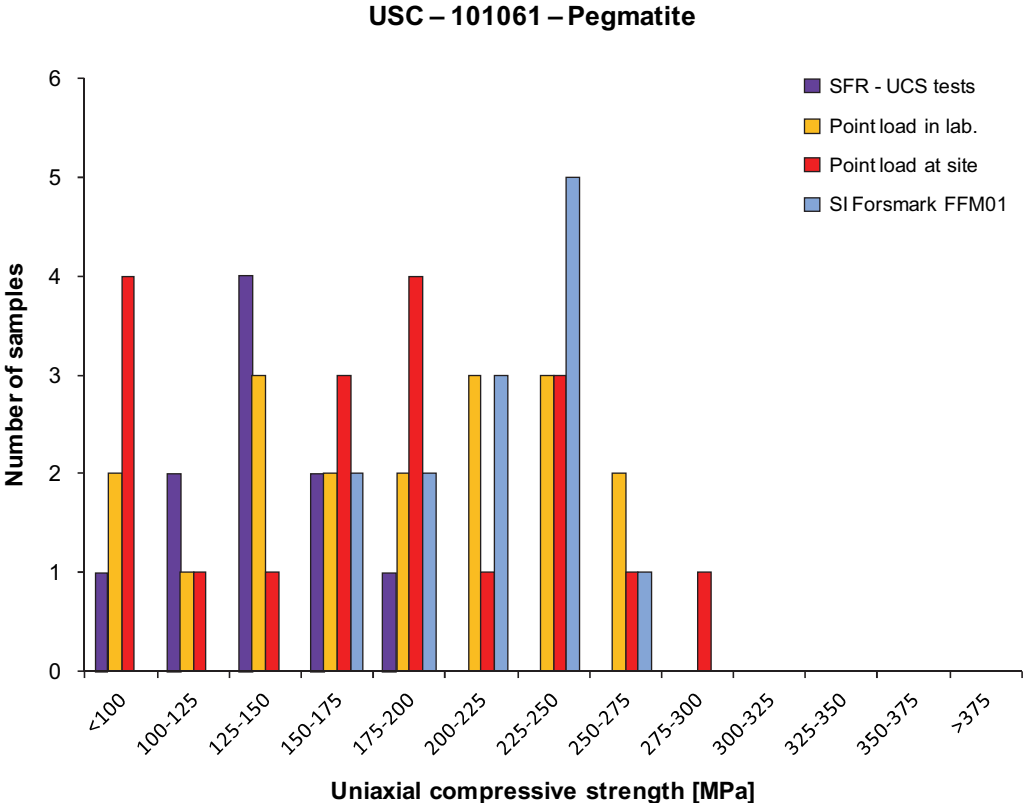


**Figure 6-2.** Histograms of uniaxial compressive strength (UCS) from uniaxial and point load tests (cf. Table 6-2). Comparison of different data sets for the same rock type (101057 – Metagranite to granodiorite). For explanation of the differences see legend and text. Sampled boreholes in SFR are presented in Table 6-1. Data taken from Sicada.

The model mean values chosen for metagranite to granodiorite (101057) (see Table 6-3) are the same as in the Forsmark site investigation, since confidence in the more recent test methodology was given greater weight. The spread in the model is greater than in the Forsmark model, since it is expected that the rock types are slightly more heterogeneous in SFR, and there are differences in terms of grain size, mineralogy and degree of foliation (Section 5.2.3). The SFR data also supports a larger spread. The maximum and minimum truncation values are selected as corresponding to two standard deviations from the mean. All models for the intact rock property parameters are truncated normal distributions. If only one single most likely model parameter value is desired, the mean value of the model distribution should be used.

For pegmatite (101061) (Figure 6-3), the different underlying data for the modelling are also scattered, and the number of test samples is less, making the comparison of sets questionable. The considerable spread in resulting values does however suggest that this rock type has a large variation in properties, which is perhaps not surprising considering the character of the rock type. Pegmatite, falls under the same rock code classification as pegmatitic granite, exhibits a wide variation in grain size with some very large grains, of the same order of magnitude as the tested samples themselves. The geometry of the grains in the samples will therefore determine the strength result. To ensure a good representation of the *in situ* behaviour of the rock type, the samples should preferably be larger than in the standard UCS test. For the model description of pegmatite (101061), the mean value selected is the mean value of all uniaxial compressive tests, both from Forsmark and from KFR boreholes.

As far as data coverage is concerned, there are two factors worthy of note. Firstly, only one test is done for the fine- to medium-grained granite (111058) reported in Glamheden et al. (2008), and no data are available from SFR for this rock type. This is not fully satisfactory, since this is the third largest (15%) rock type expected to occur in rock domain RFR02, in which the extended SFR facility is planned to be built (see Figure 5-13). The descriptive model for (111058), which obviously has a high uncertainty, is based on the single test value with a mean value of 245 MPa and an expected spread of the distribution chosen similar to the other rock types.



**Figure 6-3.** Histograms of uniaxial compressive strength. Comparison between different data sets for the same rock type (101061 – Pegmatite). For explanation of the differences see legend and text. Sampled boreholes in SFR are presented in Table 6-1.

**Table 6-3. Rock mechanics descriptive model parameters for intact rock in SFR model volume.**

Rock Code*Mean/StDev Min-Max**	101057	101061	111058	103076	102017
Uniaxial compressive strength (MPa)	226/50 126–326	183/45 90–270	280/45 210–350	139/45 100–200	142/45 60–230
Crack initiation stress (MPa)	116/26 64–168	114/22 64–166	148/22 104–192	–	–
Indirect tensile strength (MPa)	13/2 10–18	12/3 8–16	16/2 12–20	9/2 5–13	9/2 5–13
Young's modulus (GPa)	75/3 69–81	74/4 66–82	74/2.5 70–79	99***/3 93–105	81/4 73–89
Poisson's ratio	0.23/0.04 0.14–0.30	0.30/0.03 0.26–0.35	0.28/0.03 0.22–0.32	0.35***/0.03 0.29–0.41	0.22/0.04

\* 101057 – Granite to granodiorite, 101061 – Pegmatite, pegmatitic granite, 111058 – Fine to medium-grained granite, 103076 – Felsic to intermediate metavolcanic rock, 102017 – Amphibolite.

\*\* Parameters are described as normal distribution with truncations at the given Min-Max values. The most likely parameter value is the mean value.

\*\*\* Only 2 tested samples.

Secondly, there are no more recent tests performed on amphibolite (102017) within the Forsmark site investigation, and in Glamheden et al. (2008), i.e. Forsmark version 2.3, the description was also based on the available data from SFR (11 tests). The limited number of samples makes the description uncertain, but the samples are from three different boreholes, namely KFR21, KFR23 and KFR37 located in the northeastern part of SFR. Amphibolite is the weakest rock type in the region, according to available UCS results, so some extra attention to the description of this rock type may be justified. However, amphibolites often occur in dykes (see Section 5.2.3), and the influence of amphibolites on the repository design will be dependent on the thickness and abundance of such occurrences. The current geological model predicts that only around 6% of the volume is occupied by amphibolites in rock domain RFR02 (Figure 5-13).

### 6.1.2 Tensile strength

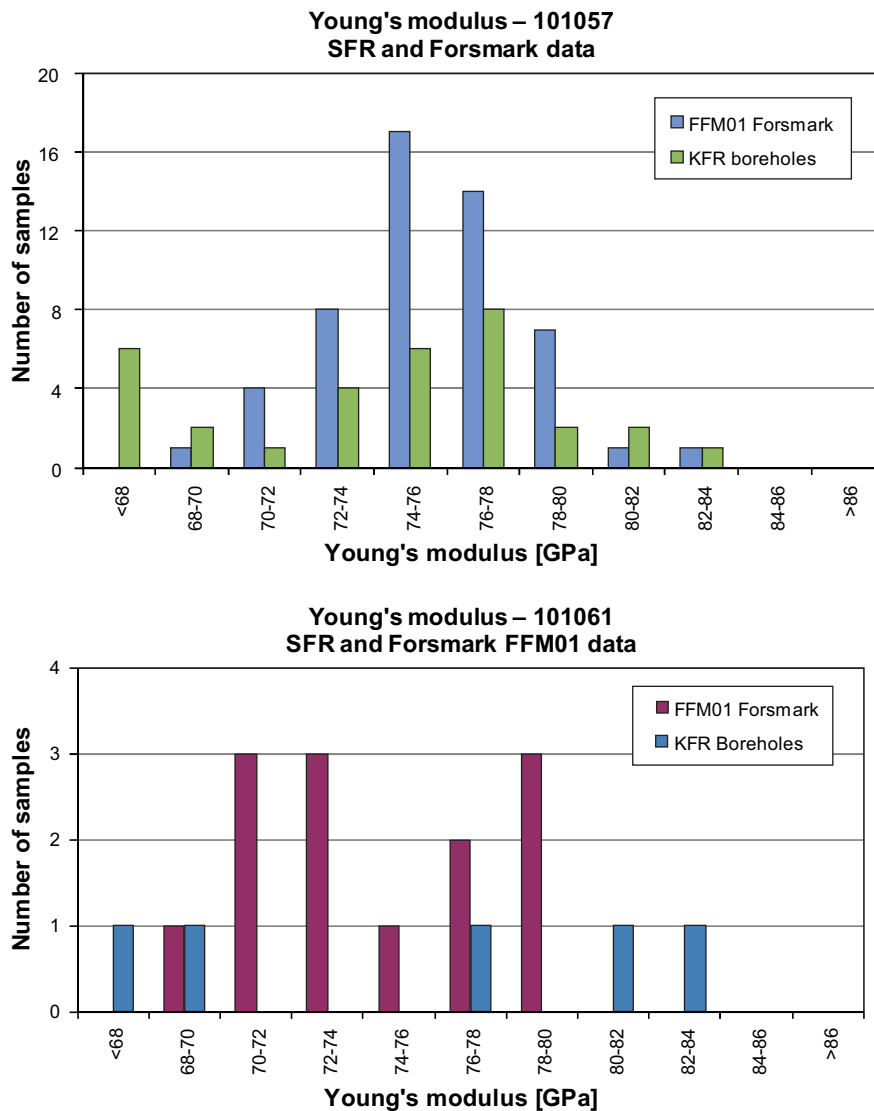
There are no SFR site-specific data in Sicada concerning tensile strength ( $\sigma_t$ ). However, the comprehensive indirect tensile testing (Brazilien test) performed during the site investigations at Forsmark, Simpevarp and Laxemar has provided evidence that the ratio between tensile strength and compressive strength has a total range of 0.056–0.089, i.e. the tensile strength is approximately 10–20 times lower than the compressive strength.

Results are available from the Forsmark site investigations for the two main rock types, metagranite to granodiorite (101057) and pegmatite (101061). The Forsmark model's (SKB 2008b) mean value is also used for the SFR model, see Table 6-3. No test data are available for rock type 111058, however, and the estimated mean values are based on a  $\sigma_t$ /UCS ratio of 0.057, because this is the ratio for the other high strength SFR rock type 101057. The  $\sigma_t$ /UCS ratio for rock type 101061 was used for rock types 103076 and 102017. In the same way, standard deviations are selected based on the UCS model, using the same ratio, and the truncation values are chosen as two standard deviations from the mean value.

It may be noted that the tensile-to-UCS ratio is fairly low in this description compared with the values found for rock types in Simpevarp and Laxemar. The  $\sigma_t$ /UCS ratio there was in the range 0.067–0.089, depending on rock types. Tensile strength could therefore be slightly underestimated in the SFR model, and the uncertainty in the model is considerable.

### 6.1.3 Deformation properties

The available data for modelling of the deformation properties of the intact rock are listed in Table 6-2. The data for granite to granodiorite (101057) and pegmatite (101061) are shown as histograms in Figure 6-4. As for the uniaxial and tensile strength, there is a lack of supporting data, in particular for three of the rock types described. Expert estimates of the parameters could still be made, however, and these are included in Table 6-3, based on general knowledge of the rock type.



**Figure 6-4.** Histogram of Young's modulus determined from uniaxial compressive test performed on samples from Forsmark and SFR. a) 101057 = Metagranite to granodiorite and b) 101061 = Pegmatite, pegmatitic granite). The results are from samples collected in domain FFM01 in Forsmark. There are no data available for domain FFM02, which is located closer to the SFR model volume.

The model shows that all occurring intact fresh rock types at SFR have very high stiffness (6,884 GPa). Due to the lack of data, the uncertainty regarding the mean is fairly large, but the importance of the stiffness of the intact rock is undoubtedly limited for the design and safety assessments. The stiffness or compliance of the rock on a larger scale would be more important. The stiffness of the materials in the deformation zones will make a greater contribution to the rock mass properties on a larger scale. These properties are discussed in section 6.2.

## 6.2 Single fracture properties

There are very few site-specific laboratory data from single fractures at SFR, but 11 shear tests were performed in connection with the construction of the existing SFR facility (Stille et al. 1985). The results of the shear tests are presented below in Table 6-4 for each of the five joint sets, as defined by Stille et al. (1985). The results of the shear tests are presented for each of the five joint sets, as defined in their report.

**Table 6-4. Results of shear tests performed on fractures from SFR by Stille et al. (1985). Samples were collected from boreholes KFR22 and KFR24, at depths varying from 18 to 141 m. The total number of tests is 11.**

Fracture Set	Normal stiffness [MPa/mm] for stress range		Friction angle 1 [°] for stress range 0 0.5 MPa	Friction angle 2 [°] for stress range 0.5 1.5 MPa	Apparent cohesion for stress range 0.5 1.5 MPa	
	0.04	0.9 MPa				
Set EW	37	4.8	48	35	0.2	
Set NW	29	4.4	51	37	0.4	
Set NE	31	2.8	48	29	0.4	
Set NS	24	2.7	48	30	0.3	
Set SH	24	8.3	66	32	0.4	
Random	25	10.4	54	35	0.5	

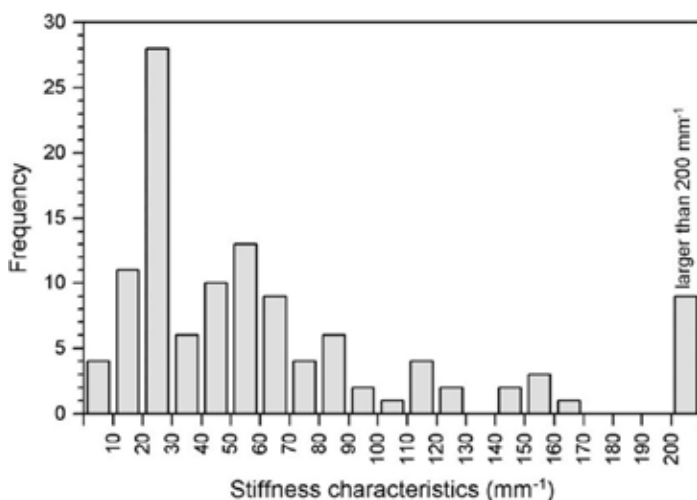
All values are available in Sicada. In addition to these data, results are available from 57 tests in the Forsmark site investigation reported in Glamheden et al. (2007).

The following parameters describing the mechanics properties of single fractures will be presented in the following sections: normal stiffness, hydraulic normal stiffness, shear stiffness, friction angle and cohesion. A descriptive model with quantitative estimates for each parameter is shown in Table 6-6 at the end of this section.

### 6.2.1 Normal and shear stiffness

Since the stiffness of rock fractures is strongly dependent on the normal stress acting on the fracture plane, it is not meaningful to discuss stiffness without considering the actual stress level. To enable data from tests at different stress conditions to be compared, the normalised parameter “stiffness characteristics” has been used, which is the stiffness divided by the normal stress (Zangerl et al. 2008), see Figure 6-5. It can be concluded from their results that even when normalised, the spread in stiffness for fractures is large. This is not surprising considering that the geological history of fractures may vary considerably, resulting in large differences in fracture surface matedness (i.e. how well the two surfaces match each other, which determines contact areas and aperture distribution) as well as also major differences in surface coatings and fillings.

According to the estimations performed by Bono et al. (2010), the deformation modulus for rock mass in the uppermost shallow rock at Forsmark is in the range 8–30 GPa for four test sites, while the normal stiffness for two single sub-horizontal fractures is 2 and 1.5 MPa/mm. The characteristic stiffness for these two fractures was determined to be 6.7 and 17.0 mm<sup>-1</sup>.



**Figure 6-5. Histogram of characteristic stiffness (normal stiffness/normal stress) of rock fractures. From Zangerl et al. (2008).**

**Table 6-5. Estimations of normal stiffness used in analyses of Bono et al. (2010).**

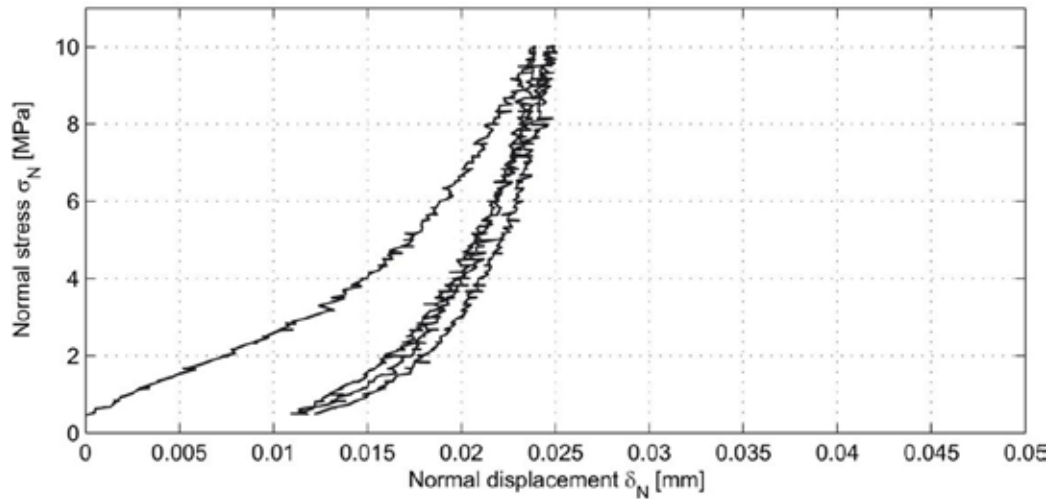
Depth	Effective normal stress in sub-horizontal fractures (MPa)	Normal stiffness (MPa/mm)
20	0.34	2–6
100	1.7	10–29

Following the results and line of reasoning in Bono et al. (2010), the descriptive model chosen for normal stiffness of single sub-horizontal fractures at SFR is a function of depth, which corresponds to an estimated constant characteristic stiffness property of 10. It is important to note that this value is only valid for the relative shallow parts of the rock. At deeper levels the stiffness is higher.

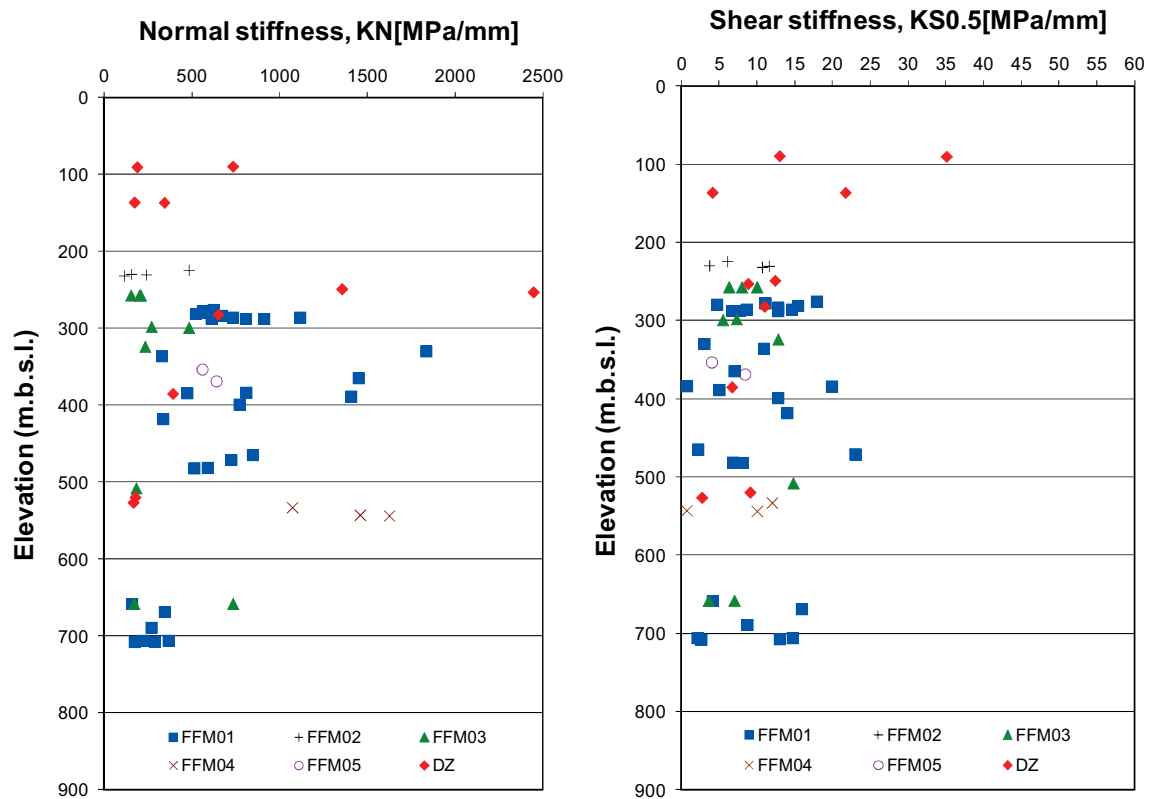
The above estimate can be compared with the knowledge gained from the Forsmark site investigation, where small-scale samples from 100–700 m depth were tested in the laboratory. The normal stiffness of these samples was in the order of 160 MPa/mm or higher. This is not regarded as inconsistent, since the stiffness of the type of fracture considered here can be expected to be much less for three reasons: 1) the normal stiffness determined from the laboratory tests was calculated for higher normal stress (from 0.5–5 MPa, see typical result curve in Figure 6-6), and the normal stiffness is highly non-linearly stress-dependent, 2) the type of fractures tested were not the same as the sheet joints in the shallow SFR rocks (see Figure 6-7) and 3) any correction for the actual fracture scale compared to laboratory tests is always towards lower stiffness ( e.g. Rutqvist 1995, Pinto da Cunha 1990).

To further support the description of fracture properties, a source of information apart from the core samples is to study the characters of the fractures as they appear in the borehole walls. At SFR this is possible to a limited extent, but Figure 6-8 shows geophysical logging results from borehole KFR103, where both optical and acoustic televiewer logging was performed. This borehole has an inclination of  $-54^\circ$  and an azimuth of  $180^\circ$ , i.e. directed towards south. This makes horizontal fractures show up in the logs with an intersection angle of about  $36^\circ$ . (This angle should be considered when the aperture is studied in the images. The aperture is best interpreted and estimated from the inflexion point of the curves.) The televiewer logging images are presented here to illustrate the difference in character between different type of fractures and to support the description above concerning the low stiffness of the sub-horizontal fracture at shallow depth. All the shown fractures correspond to PFL fractures in this borehole. That is, they are all among the interpreted water-bearing fractures that are transmissive enough to be measured with the Posiva Flow Log (see results described in Chapter 7). The PFL fractures are visible in the televiewer log, whereas many other open fractures are visible in the drill core and observed in BIPS but not visible in the televiewer log. When fractures in points a) to d), located down to 26 m depth, are compared with fractures in e) to g), the former are sub-horizontal and have a clearly larger aperture. The appearances of the fractures in the logs are clearly different. The fracture in c) shows how the different sides of the fracture match well; the aperture seems to have been created by simply opening rather than by a shear movement. This is the character one would expect from a tensional sheet joint. The low stiffness and high conductivity of such open fractures are easy to envisage. However, these *in situ* properties would not be possible to test on small-scale laboratory samples where the stress and aperture conditions would not be the same.

The samples tested in the Forsmark site investigation (Figure 6-6 and Figure 6-7) are not of the character of a PFL fracture, which is, as previously mentioned, why those results may not be used to describe all fractures at the SFR site.

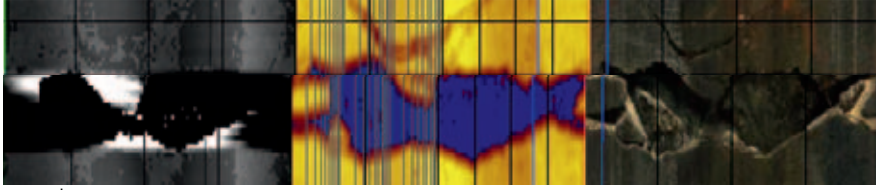


**Figure 6-6.** Example of typical result curves from normal stiffness tests on small-scale ( $25 \text{ cm}^3$ ) fracture samples in the Forsmark site investigations. The records start at 0.5 MPa normal stress and the load increases up to 10 MPa in two cycles. The stress-displacement curve is highly non-linear. The stiffness values in Figure 6-7 are determined as the stiffness between 0.5 and 10 MPa for the second loading cycle. From Jacobsson and Flansbjer (2005).

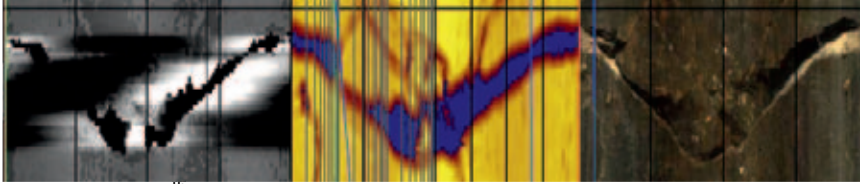


**Figure 6-7.** Results from stiffness testing on small scale fractures samples within Forsmark site investigation. (Glamheden et al. 2007).

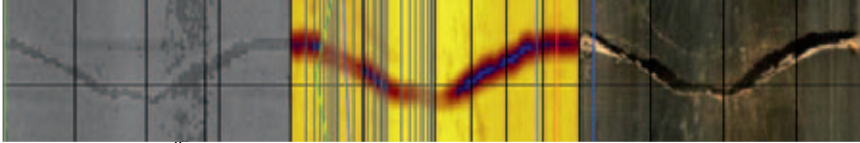
a) 1<sup>st</sup> red point



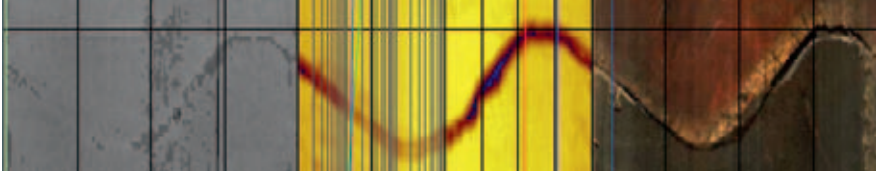
b) 2<sup>nd</sup> red point



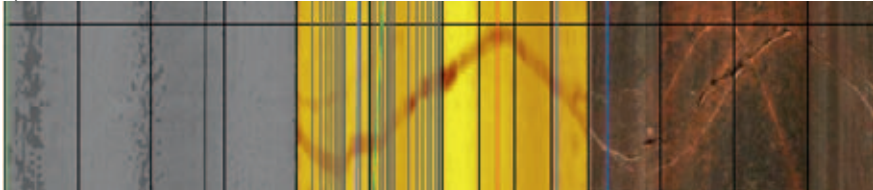
c) At 20.4 m, 4<sup>th</sup> red point



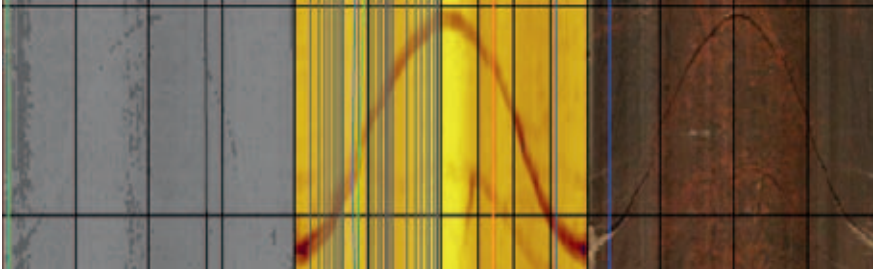
d) At 26.3 m, 5<sup>th</sup> yellow point



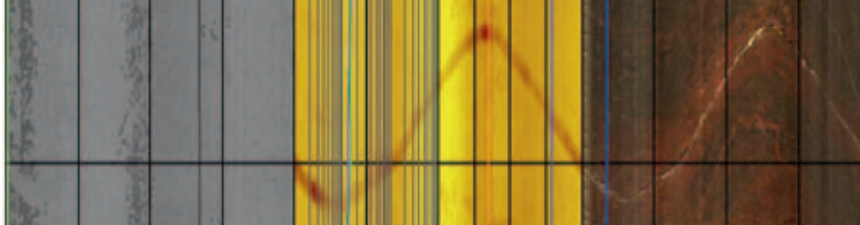
e) At 38.6 m, blue



f) At 42.15 m, steeply dipping, green



g) At 43.1 m, steeply dipping, green



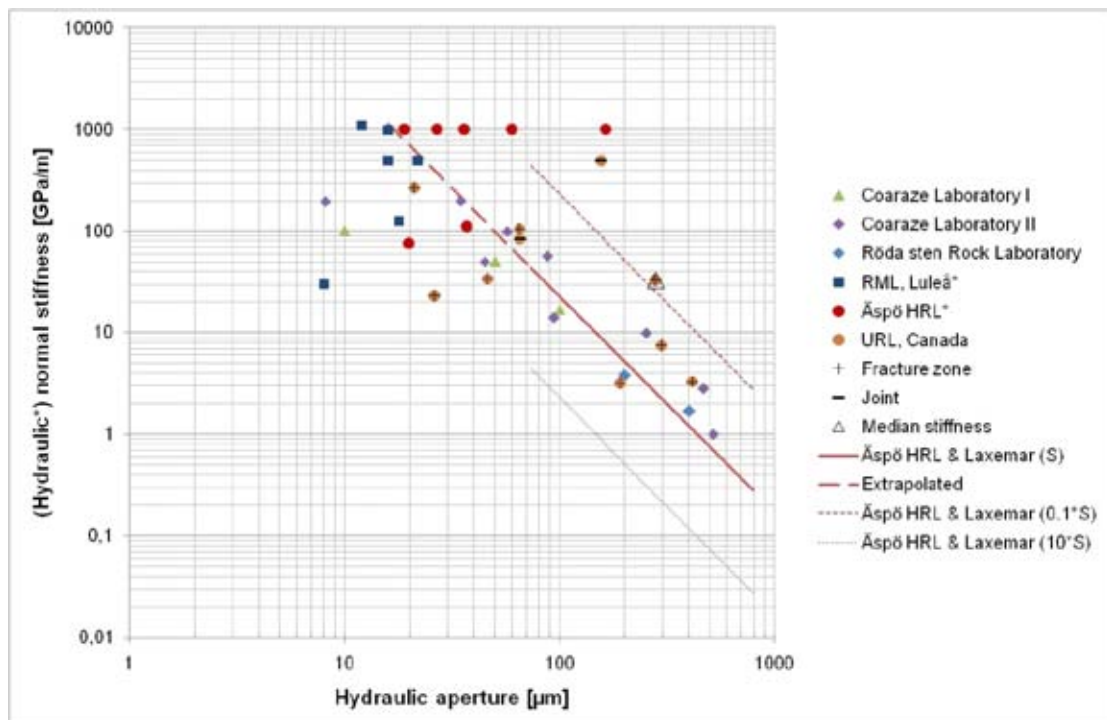
**Figure 6-8.** Examples of geophysical logging results from borehole KFR103 at SFR. The image to the right is the optical (BIPS) log, the middle image shows the amplitudes from the acoustic televiewer log and the left image shows the radii from the acoustic televiewer log. a) to g) are log sections at PFL fractures in the borehole (see text). From Nielsen and Ringgaard (2009). The length of the borehole sections shown is 0.10–0.15 m. The corresponding transmissivities for these fractures are presented in Figure E-11 of Öhman et al. (2012).



## 6.2.2 Hydraulic normal stiffness

In considering hydraulic property changes due to normal stress changes it may be useful to characterise the “hydraulic normal stiffness” of the single fracture, instead of the normal stiffness. The “hydraulic stiffness” is the parameter correlating change in stress to change in hydraulic aperture. This stiffness may be different from the ordinary normal stiffness parameter since the hydraulic aperture will not be exactly the same as the mechanical aperture when the mechanical aperture changes over the surfaces and there are also contact points between the fracture surfaces hindering a straight flow. A compilation of literature data on hydraulic normal stiffness was made by Fransson (2009), see Figure 6-9. The area where we expect to find the subhorizontal open fractures in the shallow rock is marked on top of this figure. For an expected aperture between 0.2 mm and 1 mm, the normal stiffness should, according to the compiled data, be in the order of 1–10 GPa/m (= MPa/mm), and this magnitude agrees with what was estimated above based on mechanical tests. Among the cases compiled by Fransson (2009), the data set from Röda Sten Rock Laboratory is the one that is judged closest to the SFR situation, since the depth of the fractures is only 70 m and the fractures are sub-horizontal. The hydraulic normal stiffness for this case is determined to be 2–4 MPa/mm.

Further, the logarithmic axis of this chart indicates how fast the aperture stiffness is expected to increase for fractures with smaller apertures. From being practically stress-insensitive at depth where stiffness is high, the open tensional fractures are expected to be strongly stress-sensitive close to ground surface. But this is not to say that fractures with large apertures cannot exist at greater depth, even if they are clearly fewer (see Chapter 7 about the occurrence of water-bearing fractures and the hydraulic model and Chapter 9 for a tentative explanation model of the decreasing flow rate to the existing SFR facility). Such fractures, which are shear fractures, will also be stress-insensitive and have a high stiffness but with unmated surfaces.



**Figure 6-9.** Compilation of (equivalent) hydraulic aperture and normal stiffness (or hydraulic normal stiffness, identified by \*). The symbols +; – and unfilled triangle are related to URL. From Fransson (2009). The red ellipse is added in this report to indicate the area where shallow sub-horizontal fractures are predicted in SFR.

### 6.2.3 Single fracture strength parameters

Fractures are often described using the Coulomb slip model, which assumes that the strength is linearly dependent on the normal stress over the fracture surface. In this case we do not have many measurement data on these fracture parameters, but the data in Table 6-4 are utilised to select reasonable estimates, although the number of data is very low. Some at least qualitatively reliable observations can be made from Table 6-4: The friction angle is higher for the very low normal stress situation and there is no obvious difference between the different fractures depending on their orientation. These strength results were also compared with results from the Forsmark site investigation, but for the reason already discussed the friction and cohesion values were not based on these results, even though the laboratory tests are judged to be of better quality, since the stress levels of the tests were too high. The dilation values are, however, estimated based on the results for the 0.5 MPa normal stress case in the direct shear tests for the Forsmark site investigations (Glamheden et al. 2007). Selected descriptive model values are presented in the following section.

### 6.2.4 Single fracture property model

In Table 6-6, the properties are described differently for two groups of fractures, the sub-horizontal to gently dipping shallow fractures down to –60 m elevation and all other fractures, irrespective of orientation. Given values are estimated most likely values, and the variation between fractures is expected to be great. Note that these properties are only predicted for the rock volume of the SFR extension (0–150 m depth) and should not be used for fractures at depth where normal stresses are high.

## 6.3. Rock mass mechanics properties

### 6.3.1 Rock domains

Based on the data sets that were collected at the time, two studies (Hagkonsult 1982, Stille et al. 1985) have empirically characterised the rock mass at the existing SFR facility. The first study (Hagkonsult 1982) (based on analysis of boreholes KFR21, KFR22, KFR23, KFR24, KFR25, KFR27) quantified the RMR79 (Bieniawski 1979) between 69 and 83 (RMR classes: 60–80 = “good” to 80–100 = “very good” rock). The second study by Stille et al. (1985) (which added data from borehole KFR19 and KFR20) resulted in slightly lower values of RMR79 (60–72) and Q (5–10) (Barton 2002). This result compared well with the first study, because the additional boreholes had a higher fracture frequency.

This description compares well with the description for the different fracture domains and also the deformation zones in the Forsmark site investigation. However, except for the shallow lying fracture domain FFM02, the rock in SFR should not be directly compared with the estimates

**Table 6-6. Rock mechanics single fracture property estimates. The uncertainty in the estimates is quite high and the variation between single fractures is also expected to be great.**

Parameter	Sub-horizontal (Dip 0–20°) fractures with a depth (z) 0–50 m	All other fractures depth 0–150 m and subhorizontal > 50 m
Effective normal stress, $\sigma_n'$ [MPa]	$\sigma_n' = \rho gh - u$	
Normal stiffness, $K_n$ [MPa/mm]	$K_n = 10 \times \sigma_n'$	$K_n = 10 \times \sigma_n'$
Shear stiffness, $K_s$ [MPa/mm]	$K_s = K_n / 3$	$K_s = K_n / 20$
Friction angle, $\varphi_1$ [°] for normal stress range 0–0.5 MPa	66°	48°
Friction angle, $\varphi_2$ [°] for normal stress range 0.5–1.5 MPa	32°	35°
Apparent cohesion for normal stress range 0.5–1.5 MPa	0.4	0.4
Dilatancy	15°	15°

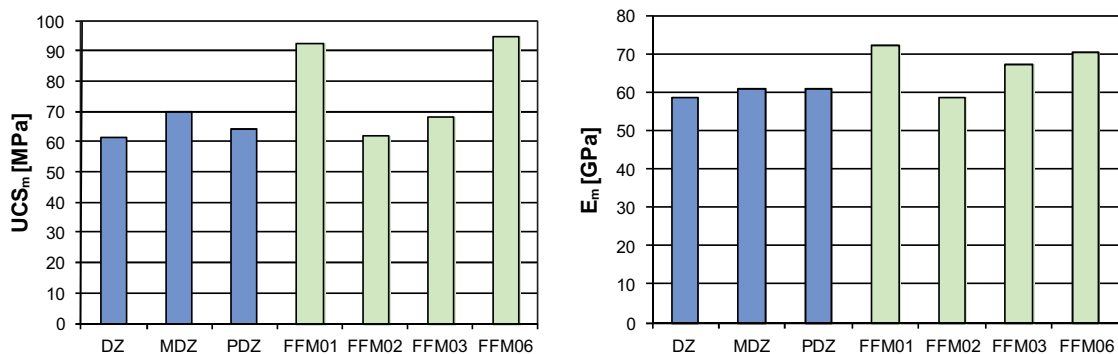
for the Forsmark domains because of the depth difference. It may also be noted that rock mass parameters in SDM-Site were defined to correspond to high stress levels, and not the stress levels we expect at SFR. Both UCS and deformation modulus decrease slightly with stress, but for the sake of simplicity, and since we do not have a basis for a more elaborate description, the rock mass properties will be described as a single value for 20–150 m depth conditions, which would correspond to a model for rock masses at about 0.5–4 MPa confining stress.

As described in the section about single fracture properties, the rock mass in the most shallow rock, down to –60 m elevation, could be a special case due to the occurrences of sheet joints (see also the hydrogeological model Section 7.2.5). These fractures may create special rock engineering conditions due to high water transmissivities, which is important to be aware of, but this is not believed to dramatically change the purely mechanical properties of the rock mass. Generally, the experience from previous excavations at SFR also confirms the picture of good to very good rock conditions from a stability point of view (Carlsson and Christiansson 2007). The exception to this is the conditions inside the major deformation zones, where the rock quality is much more variable and can be poor in short sections. The mechanical properties of deformation zones are therefore roughly estimated separately in the next section.

In the Forsmark site investigation, an empirical classification was made along the investigation boreholes and the empirical indices were used to estimate the uniaxial compressive strength for the rock mass (on a 25 m scale) as well as the deformation modulus. These two parameters were – along with the Poisson’s ratio, friction angle, and cohesion – estimated within SDM-Site for the rock mass in different “fracture domains” (domains with similar fracturing characteristics) and within the deformation zones. Examples of these results are given in Figure 6-10. From the uniaxial strengths predicted, which are shown in Figure 6-10, it may be concluded that strength is quite good for all categories, including the three different categories of deformation zones. This result is believed to be attributable to the way deformation zone sections in boreholes were defined (quite wide on each side of the core) and averaging effects. Note also that the rock mass between deformation zones in fracture domain FFM02 has properties which are lower than those of the rock mass in the other fracture domains. FFM02 is the domain that includes the more shallow, and more fractured, rock at Forsmark (SKB 2008b).

Some surface mapping and Q classification at the surfaces was done by Barton in 2003 and is summarised in SKB (2004). However, since these classifications were performed on outcrops and not on underground input data located on the southwest side of the Singö deformation zone, the relevance of these Q values for the SFR underground excavations was judged to be low compared with other data, and they were not used as a basis for the description.

There are some more recent empirical estimates available in Sicada from inside the SFR regional model volume. These are empirical estimates from borehole KFM11A performed as a part of the Forsmark site investigations. These results are presented in Table 6-7. It can be noted from these results that the deformation modulus is estimated lower, probably because of the depth and stress difference. Further, it can be noted that, as seen also in Figure 6-10, there is no dramatic variability in the parameters, even though this borehole intersects a major regional deformation zone.



**Figure 6-10.** Results from determination of uniaxial compressive strength (left) and the deformation modulus (right) for the rock mass in the Forsmark site investigations. (SKB 2008b).

The UCS of Table 6-7 is defined as the apparent Mohr-Coulomb uniaxial strength for stress levels 5–20 MPa and should therefore not be compared with the UCS for a Hoek-Brown material model in Figure 6-10.

The rock mass properties can also be estimated based on a “theoretical approach”, i.e. analysing the large-scale rock mass behaviour based on a knowledge of intact rock and fracture network properties. Such an attempt is made in Glamheden et al. (2007).

Based on a combination of the above-presented sources of information, estimates were made of the mechanical properties of the rock mass at the depth of the planned extended SFR facility. The values are shown in Table 6-8.

### 6.3.2 Deformation zones

Empirical classifications (Q and RMR) of the rock quality in the rock mass were made during the construction of the existing SFR facility (Hagkonsult 1982, Stille 1985). However, these studies focus on the silo areas and Q and RMR classification were not used in the access tunnels (Carlsson and Christiansson 2007). The deformation zones and their quality are described only in general terms in Hagkonsult (1982).

In the larger deformation zones, the rock mass properties will vary over the cross-section through the zone. The mechanical properties are obviously not the same in the transition zone and the core, and the thickness of the different zones will vary from deformation zone to deformation zone. In some cases a zone may also have multiple cores. In Glamheden et al. (2007), numerical modelling was used to simulate the mechanical behaviour of the rock mass in a large zone (the Singö deformation zone, part of the southern boundary belt) and the simulations resulted in estimates of the properties. Since the properties can vary so strongly across a zone, a property description must be done separately for the core and the rock mass in the transition zone. In the case of the SFR model, the choice was made to conform to use the estimates made by Glamheden et al. (2007), but to select values corresponding to the lower confining stress. The parameter values are shown in Table 6-9. The certainty of these estimates is low.

**Table 6-7. Result from empirical classifications in 5 m section along cored borehole KFM11A, performed within the Forsmark site investigation. The location of this borehole is to the west in the regional model volume. The inclination of KFM11A is  $-60^\circ$  towards the northeast (Figure 2-7a). KFM11A is interpreted as intersecting the Singö deformation zone from borehole length 498–824, according to Curtis et al. (2011). Data in table from Sicada.**

Secup-Seclow (along bh)	Section length	Q Most frequent	RMR Most frequent	Em_Q (most freq. Q)	Em_RMR	USC
220–245	25	19	78	36	51	125
245–355	110	40	74	38	41	138
355–375	20	33	73	36	37	158
375–410	35	30	72	37	36	157
410–585	175	22	71	33	34	143
585–660	75	17	73	35	38	287
660–700	40	37	73	38	37	138
700–725	25	36	78	44	52	222
725–785	60	37	73	41	40	173
785–825	40	27	74	41	41	272
825–845	20	132	78	66	49	214

**Table 6-8. Estimates of mechanical properties of the rock mass.**

20–150 m depth	RMR	Q	USC <sub>m</sub> (H-B) [MPa]	Friction angle, M-C	Cohesion, M-C [0–5 MPa]	Em [GPa]	Poisson's ratio
All rock domains, only outside deformation zones	74	20–40	62	50°–60°	13 MPa	50 GPa	0.34

**Table 6-9. Rock mechanics property estimates for the rock mass inside deformation zones.**

Rock domain 20–150 m depth at about 0.5 MPa confining stress	Friction angle, M-C [0.5–5 MPa]	Cohesion, M-C [0.5–5 MPa]	Em [GPa]	Poisson's ratio
Transition zone to major regional deformation zone	51	2	13	0.35
Core of major regional deformation zone	37	2	2.6	0.46

## 6.4 *In situ* state of stress

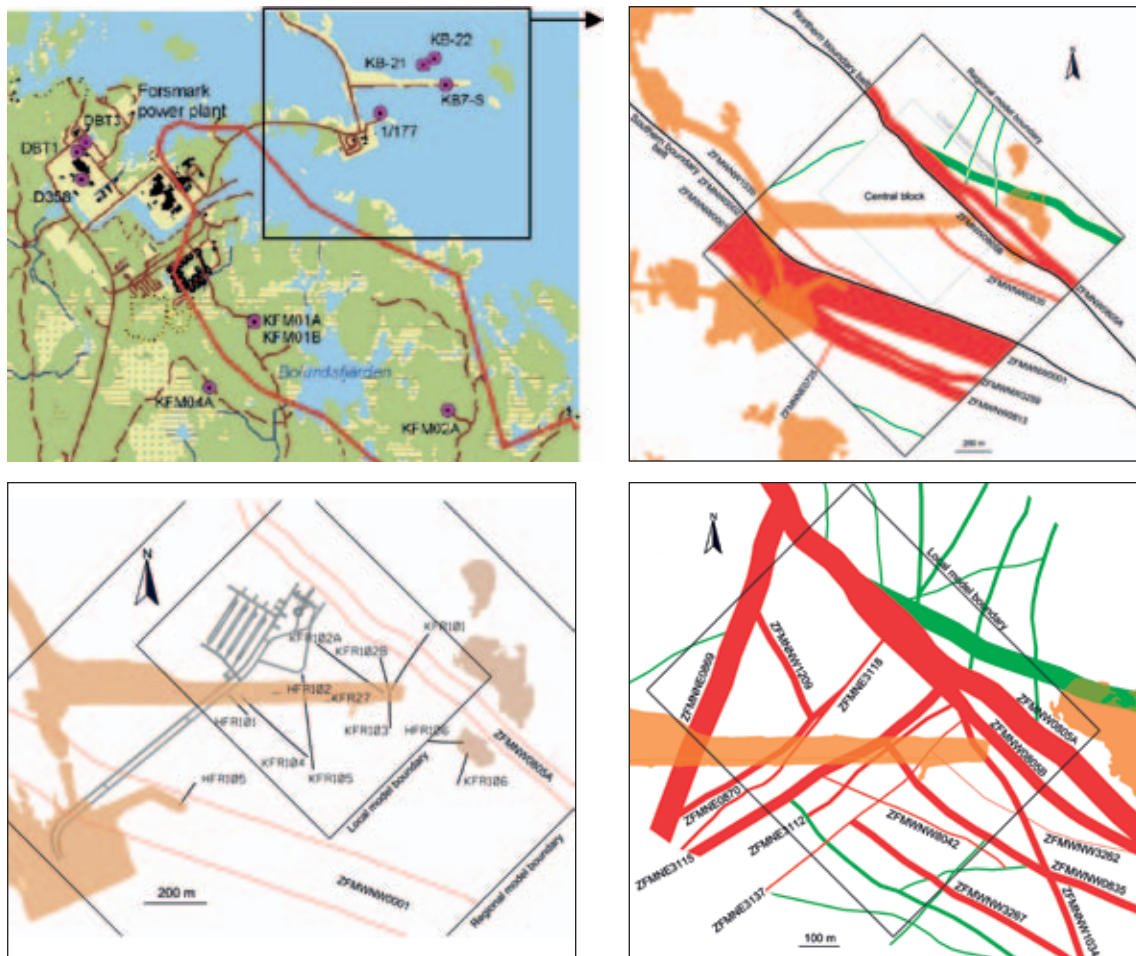
### 6.4.1 Primary data

A fairly large effort was made to measure *in situ* stresses in the Forsmark site investigation. The stress situation in the region and at Forsmark has also been analysed and discussed in several reports e.g. Glamheden et al. (2007), Sjöberg et al. (2005), Martin (2007) and is not repeated here. The main aim in this section is to identify any condition that is different or particularly relevant for the SFR area, and to arrive at a description of the *in situ* stresses in the SFR local model volume.

The direct measurement data available from SFR and the Forsmark nuclear power plant are presented in Table 6-10. The locations of these measurement boreholes are shown in Figure 6-11. These measurements were performed in connection with the construction of the nuclear power plant and later the existing SFR facility. It is particularly noteworthy from Figure 6-11 and the relative locations of measurements and deformation zones that four of the old boreholes are located on the northeastern side of the southern boundary belt, including the Singö deformation zone, whereas the other data, including the Forsmark site data, are from the southwestern side of this major regional structure. Generally speaking, large deformation zones may divide a rock mass into domains with different stress conditions, which was a reason to study the northeastern data in comparison with the measurement data from the southwestern side.

**Table 6-10. Stress measurement data available in Sicada from the SFR and Forsmark power plant areas.**

Borehole ID	Old name	Method	Reference
KFK041	D358	Overcoring	SSPB 1982, Hiltcher and Strindell 1976
TFKB12	Discharge tunnel, 4 short holes	Overcoring, Doorstopper	SSPB 1982, Martna et al. 1983
KFR89	BH SFR 1/177	Overcoring	Ljunggren and Persson 1995
KFR51	KB-21	Overcoring	Ljunggren and Persson 1995
KFR52	KB-22	Overcoring	Ljunggren and Persson 1995
KFR27	KB7-S	Overcoring	Ljunggren and Persson 1995
KFK001	DBT-1	Overcoring	Perman och Sjöberg 2003
KFK001	DBT-1	Hydraulic fracturing	Stephansson and Ångman 1984
KFK003	DBT-3	Overcoring	Perman och Sjöberg 2003

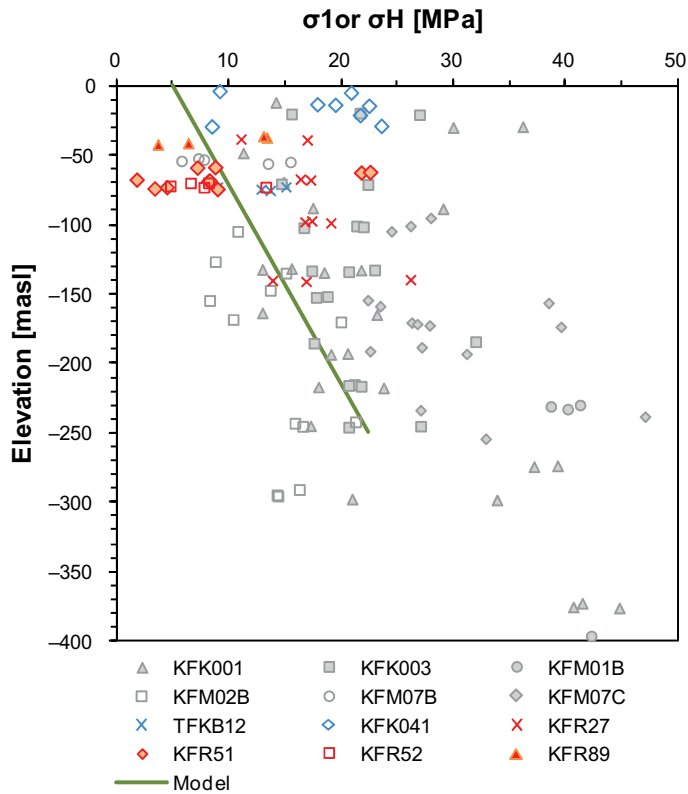


**Figure 6-11.** a) Locations of boreholes for stress measurements (cf. Table 6-10, b): the Singö deformation zone (i.e.ZFMWNW0001) runs between the Forsmark power plant and SFR, dividing the stress measurement data; c) KFR27 is located inside the planned volume for the SFR extension (see Figure 2-7 for all boreholes); d)dDeformation zone model on a more detailed scale of the local model area (cf. Figure 5-16b). Most stress measurements at SFR could be influenced by the presence or proximity of deformation zones.

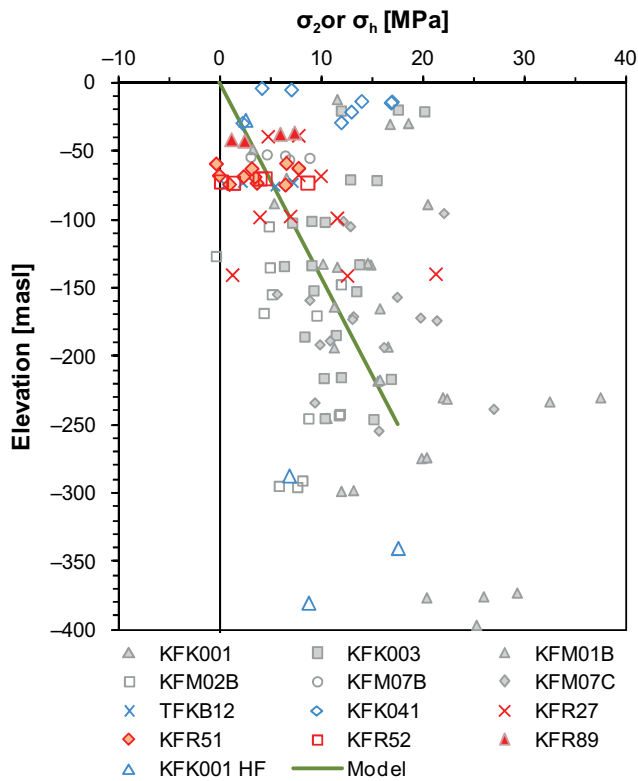
## 6.4.2 Rock stress magnitude

The results of the measurements in terms of the magnitudes are presented in the diagrams in Figure 6-12, Figure 6-13 and Figure 6-14. The red marks are from the SFR boreholes. Looking at the horizontal stresses the following conclusions can be drawn:

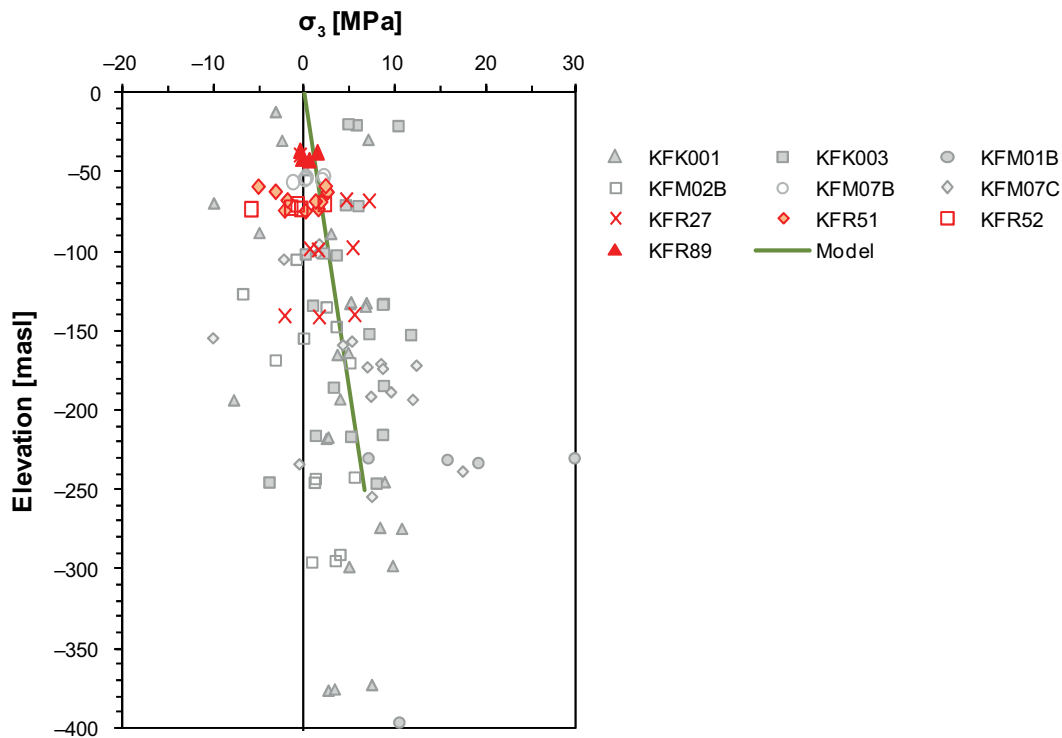
1. There is considerable spread in the individual overcoring measurements, both the older and the more recent sets of data. For further discussion of the measurement methods and the interpretation challenges, the reader is referred to e.g. Sjöberg et al. (2005) or Martin (2007).
2. There is a clear increase in stress with depth, as expected, even though the spread in the data makes the gradient difficult to determine with certainty.
3. The data from SFR (red) seem so be on average of lower magnitude compared with the other data.



**Figure 6-12.** Major principal stress (or major horizontal stress) from measurements. Red symbols indicate data points in SFR local model volume. Grey and blue symbols indicate data on the south-western side of the southern boundary belt. The line indicates the descriptive model for  $\sigma_1$  at SFR (see text and Table 6-11).



**Figure 6-13.** Intermediate principal stress (or minor horizontal stress) from measurements. Red symbols indicate data points in SFR local model volume. Grey and blue symbols indicate data on the western side of the southern boundary belt. The line indicates the descriptive model for  $\sigma_1$  at SFR (see text and Table 6-11).



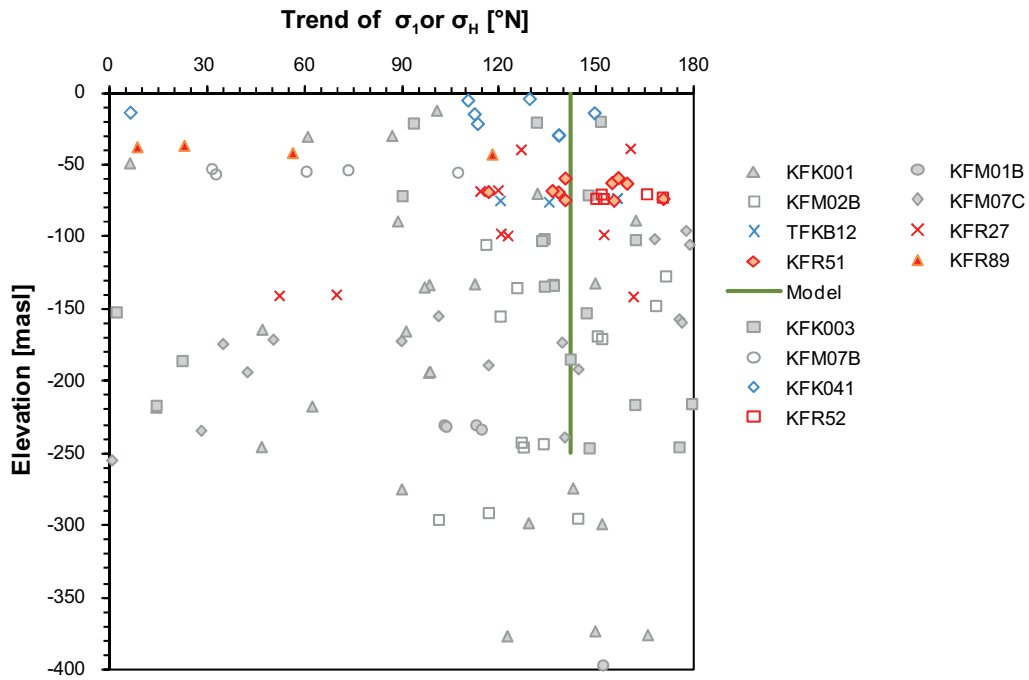
**Figure 6-14.** Minor principal stress (or vertical stress) from measurements. Red symbols indicate data points in SFR local model volume. Grey and blue symbols indicate data on the western side of the southern boundary belt. The line indicates the weight of overburden,  $\rho gh$ , used as the model.

### 6.4.3 Rock stress orientation

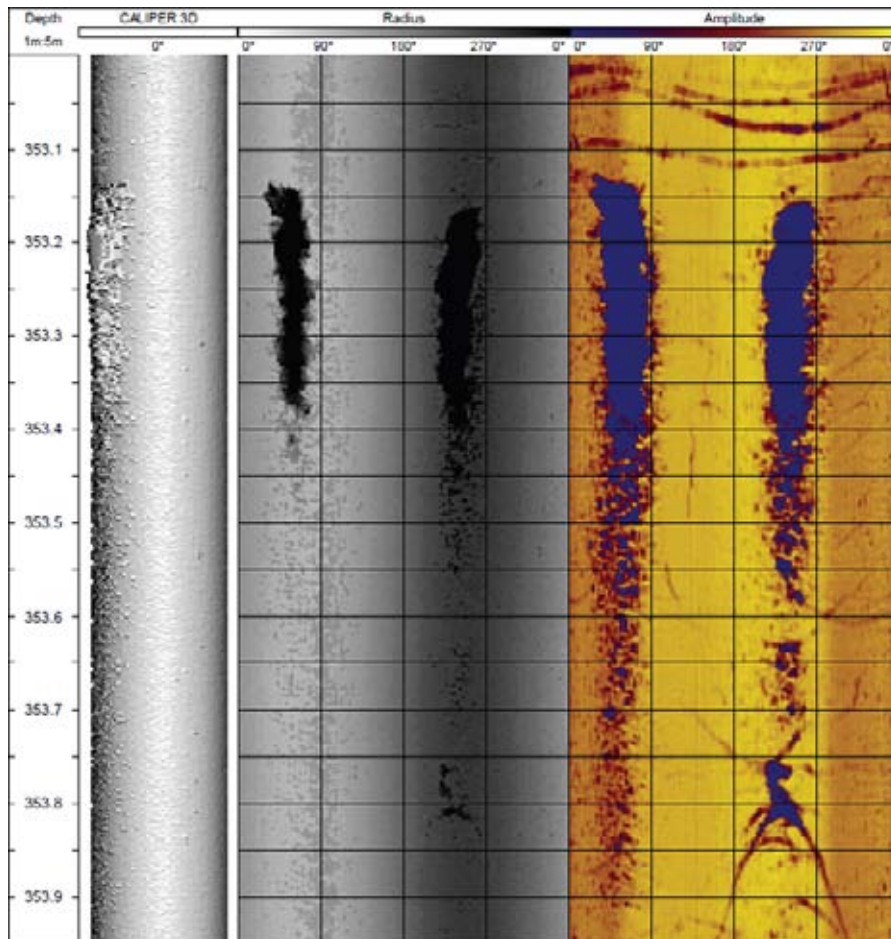
The *in situ* stress orientation of the region is known with fairly high certainty from the previous testing within the Forsmark site investigation. The major horizontal stress is expected to be oriented in a NW-SE direction ( $145^\circ \pm 15^\circ$ ) (SKB 2008b). In the case of the SFR model volume it is still of interest to compare this with the data available from the SFR local model area. The orientations of the SFR boreholes whose magnitudes are presented in Figure 6-12 are shown in Figure 6-15. It can be concluded that the single measurement points have a large spread but that there is a strong tendency towards NW-SE orientation. Some overcoring data do not indicate that the principal stress is nearly horizontal, which may be a sign of either measurement error or a reorientation of the general stress field at that point. It should be borne in mind that these SFR data are older measurements and there has been no reassessment of raw data here, see further (Sjöberg et al. 2005). Regardless of the reason for the spread it seems reasonable to select the median value for all measurements in the four SFR boreholes as an estimate of the mean stress direction at SFR. This value is  $140^\circ$  from north.

Apart from the direct stress measurement using overcoring methods, another way to determine the stress orientation is to study breakouts, or microfallouts, in the borehole walls (for an explanation of the equipment and procedures see e.g. Ringgaard 2007). This method has been used also in the Forsmark site investigation and is judged to be a robust way of determining orientation and a good complement to the overcoring results as it is a completely different approach. At SFR there is only one vertical borehole where televiwer logging has been performed, and this is borehole KFR27. Although this borehole is interpreted to be located inside or close to a deformation zone, it is located inside the volume that is planned for the SFR extension, and thus relevant as a base for the local prediction. Breakouts will occur mainly if the stresses are fairly high or the rock is locally weaker, so no breakouts are found in the upper part of the borehole where stresses are lower. Fortunately, one clear breakout section was found at about 353 m depth, see Figure 6-16. This breakout indicates a major horizontal stress direction of  $144^\circ$  from north. This compares well with both the overcoring in SFR and with the Forsmark site investigation data. The model numbers selected to describe the stress conditions in the local model volume are presented in Table 6-11.





**Figure 6-15.** Orientation of the maximum principal stress or the major horizontal stress from the overcoring measurements at SFR (in red). Corresponding data from boreholes on the western side of the southern boundary belt are also shown for comparison (grey or blue). Only data down to 400 m depth are shown. All available data points are shown as single data points. The location of boreholes is shown in Figure 6-11.



**Figure 6-16.** Televiwer login results from a section in borehole KFR27 where there is a breakout. The centreline on each side is indicated by the red dashed lines at 54° and 234° (180° separation), which indicates a major horizontal stress direction of 144° from north.

#### 6.4.4 Rock stress model for SFR

Based on the results from overcoring in boreholes at SFR, a linear function with depth was roughly fitted to the SFR data (see green line in Figure 6-12 to Figure 6-14), which assumes a slightly lower stress at SFR compared with the southwestern side of the southern boundary belt. The stress model for SFR is presented as a function of depth in Table 6-11. *In situ* rock stress estimates are restricted to the rock in the SFR local model volume, from the ground surface down to 250 m depth. The gradient for horizontal stresses is 0.07 MPa per depth metre and may therefore not be used for very deep predictions.

**Table 6-11. *In situ* rock stress estimates for the rock in the SFR local model volume, from the ground surface down to 250 m depth.**

All rock domains	Major horizontal stress. Depth z = 0–250 m	Minor horizontal stress. Depth z = 0–250 m	Vertical stress Depth z = 0–250 m
Magnitude [MPa]	$5 + 0.07z$	$0.07z$	$0.027z$
Orientation [Trend from north]	142°	55°	vertical

### 6.5 Confidence and remaining uncertainties

#### 6.5.1 Intact rock mechanics properties

At shallow depth the stresses across sub-horizontal fractures is low and the non-linearity of the fracture properties must be considered. Laboratory test results on large-scale, low stress, highly conductive fractures are not available, and such a test is almost impossible to perform. Confidence in the absolute values for the single-fracture parameters is therefore low. However, the model description presented includes an uncertainty range that is meant to reflect this condition. A model for stiffness and strength properties that differentiates between the most shallow sub-horizontal fractures (sheet joints) and the other fractures is provided. This division takes into consideration the differences in stress and geological origin between different types of fractures. The main importance of the rock mechanics single-fracture description is to enhance an integrated conceptual understanding and to clarify hydromechanical issues, such as in the prediction of future groundwater flow conditions (see Chapter 9). However, single-fracture mechanical parameters are not indispensable in dealing with anticipated engineering design issues.

#### 6.5.2 Single fractures mechanics properties

At shallow depth the stresses over sub-horizontal fractures is low and the non-linearity of the fracture properties must be considered. Laboratory test results on large scale, low stress, highly conductive fractures is not available, and such test is almost impossible to perform, and thus the confidence in the absolute values for the single fracture parameters is fairly low. However, the model description presented includes an uncertainty span that is meant to reflect this condition. A model for stiffness and strength properties is provided that differentiate between the most shallow sub-horizontal fractures (sheet joints) and the other fractures, considering the importance of differences in stress and geological origin between different types of fractures. The main importance of the rock mechanics single fracture description is for the integrated conceptual understanding and hydro-mechanical issues, such as in the prediction of future ground water flow conditions. However, single fracture mechanics parameters are not indispensable to solve foreseen engineering design issues.

#### 6.5.3 Rock mass mechanics properties

Confidence in rock mechanics parameter values for the rock mass is moderately high between deformation zones and low inside deformation zones. However, since engineering experience exists from the existing SFR facility there is high confidence in predicting how the rock mass in the planned area will behave. Experience suggests that the rock mass is of good quality outside the deformation zones. The existing SFR tunnels intersect different quality rock masses, from weak in

the Singö deformation zone up to the very good rock, from an excavation stability point of view, in the SFR silo area. The main uncertainty of significant importance for the design work for the SFR extension concerns the occurrence and the uncertainty in geometrical positions of the deformation zones of different magnitudes.

#### **6.5.4 *In situ* stress conditions**

In the absence of direct stress measurements inside the Central Block planned for the SFR extension, confidence in the stress magnitudes must be considered moderate. A higher variability in stress in the shallowest parts of the bedrock is often observed in measurement data and can therefore be expected. Accordingly, the uncertainty range in the description of rock stresses is fairly great, expressed as a percentage of the most probable value. Still, since the stress levels are relatively low at these limited depths, the stress levels as such are not expected to be a major concern for the stability of the planned excavations. Confidence in the orientation of the stresses is quite high, however, since the indications in the data from the region are so consistent.

## 7 Bedrock hydrogeology

### 7.1 Overview of hydrogeological modelling

This chapter provides a summary of the hydrogeological model for bedrock version 1.0 presented in Öhman et al. (2012, 2013). Version 1.0 is based on a comprehensive compilation, analysis and interpretation of all available hydrogeological data in the bedrock with regard to geological model version 1.0 by Curtis et al. (2011) presented in Chapter 5.

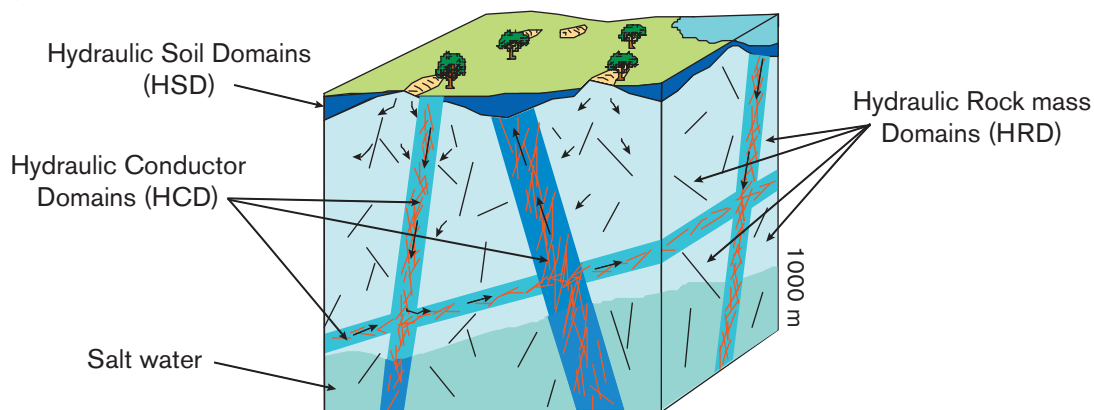
The conceptual hydrogeological modelling of the bedrock has been carried out in three stages, referred to as model versions 0.1, 0.2 and 1.0, which successively incorporated historic and recent data from the SFR extension investigation as well as feedback from the other modelling disciplines. The work has followed SKB's established methodology for hydrogeological modelling (Rhén et al. 2003). In essence, this methodology entails that the subsurface is divided into three hydraulic domains as illustrated in Figure 7-1, where:

- the Hydraulic Conductor Domain (HCD) represents deterministically modelled deformation zones,
- the Hydraulic Rock mass Domain (HRD) represents the less fractured rock mass volumes (fracture domains) in between (outside) the deformation zones, and
- the Hydraulic Soil Domain (HSD) represents the regolith, i.e. unconsolidated material on top of the bedrock, e.g. Quaternary deposits, fill, and weathered bedrock.

The division into hydraulic domains constitutes the basis for the conceptual modelling and the subsequent groundwater flow modelling. Depending on the spatial variability of the geometric-hydraulic properties of flowing fractures, the hydraulic properties of the HCDs and the HRDs are conceived to be more or less heterogeneous and anisotropic. This is handled by multiple realisations of the groundwater flow model, where the geometric-hydraulic properties are generated stochastically. In SKB's systems approach, the generation of stochastic properties of the HRD uses a discrete fracture network (DFN) model, which consists of probabilistic fracture parameter distributions.

A cornerstone in the hydrogeological modelling of the bedrock is the geological delineation of borehole intervals with deformation-zone-type properties, known as possible deformation zones (PDZs). These are identified by the geological single-hole interpretation (SHI), see Chapter 5 for details. During the course of the geological modelling, the majority of the identified PDZ intercepts are modelled deterministically as deformation zones in 3D, which implies that they have been tied to other sources of information, e.g. lineaments on the ground. The remaining PDZ intercepts are here referred to as unresolved PDZs. It is noted that the geological and hydraulic properties of the unresolved PDZs vary significantly from one PDZ to the next. For both geological and hydraulic reasons they should be analysed individually and not treated as a random sample from a parent population of PDZs.

#### Hydrogeological description



**Figure 7-1.** Illustration showing the division of the crystalline bedrock and the regolith (Quaternary deposits mainly) into three hydraulic domains, HCD, HRD and HSD (Rhén et al. 2003).

The bedrock hydrogeological model version 0.1 (Öhman and Follin 2010a) is based on a review of the existing hydraulic data acquired in the boreholes drilled in the vicinity of the existing SFR (the old data set). The review was made with regard to the bedrock geological model version 0.1, previously described in Curtis et al. (2009). The associated groundwater flow modelling is described in Öhman (2010).

During the course of the SFR extension investigation, it was decided to omit the bedrock geological model version 0.2 and focus on final bedrock geological model version 1.0. Pending delivery of this model, Öhman and Follin (2010b) developed a preliminary hydrogeological model version 0.2 based on the hydraulic data acquired in the boreholes drilled in the area of the planned extension (the new data set). The bedrock hydrogeological model version 0.2 is a hydrogeological DFN model of the SFR local model area with parameter distributions for three depth-related HRDs<sup>1</sup> based on geometric-hydraulic data acquired in boreholes outside the delineated PDZs. The derivation of the hydrogeological DFN model version 0.2 resembles the approach used in SDM-Site Forsmark (Follin et al. 2007b).

Section 5.4.3 describes the geometry and assigns the geological properties to the 40 deformation zones contained in bedrock geological model version 1.0 reported in Curtis et al. (2011). The general character of each of the four sets of deformation zones is described in Section 5.4.4. A key feature is the demarcation of a tectonic unit, the so-called Central block, sandwiched between the Southern and Northern boundary belts (Figure 5-2 and Figure 5-17). Bedrock geological model version 1.0 provides a different conceptual framework for the analysis of available hydrogeological data compared with the previous bedrock geological model version 0.1. Among other things, the following features should be noted.

1. Borehole KFR27, which is located in the centre of the Central block, is not drilled in a rock mass volume between deformation zones. According to bedrock geological model version 1.0, KFR27 is drilled within and alongside the steeply dipping deformation zone ZFMWNW0835 (Figure 7-2).
2. Out of a total of 95 PDZs, 31 are not included in bedrock geological model version 1.0 (Figure 7-2), which means that they are interpreted as geological structures smaller than the scale of resolution used for the deterministic geological modelling work. Seventeen of the 31 unresolved PDZs occur in the vicinity of the existing SFR (the old data set). The other 14 unresolved PDZs occur in the area of the planned extension (the new data set).
3. Boreholes KFR106 and HFR106, which are drilled outside the local model domain, provide essential information about the hydraulic contact between the Northern boundary belt and the eastern part of the Central block where the steeply dipping deformation zone ZFMNNW1034 is located (Figure 7-2). The hydraulic data in these boreholes fit the possible deformation zones listed in Table 5-5. In conclusion, ZFMNNW1034 reduces the size of the tectonic wedge between the Northern and Southern boundary belts towards east, hence the size of the Central block and, presumably, the degree of freedom of the target volume available for the SFR extension.

The first of the two reports describing the hydrogeological model for bedrock version 1.0 (Öhman et al. 2012) is primarily conceptual and presents both primary hydraulic data gathered at the site and the suggested hydrogeological modelling of:

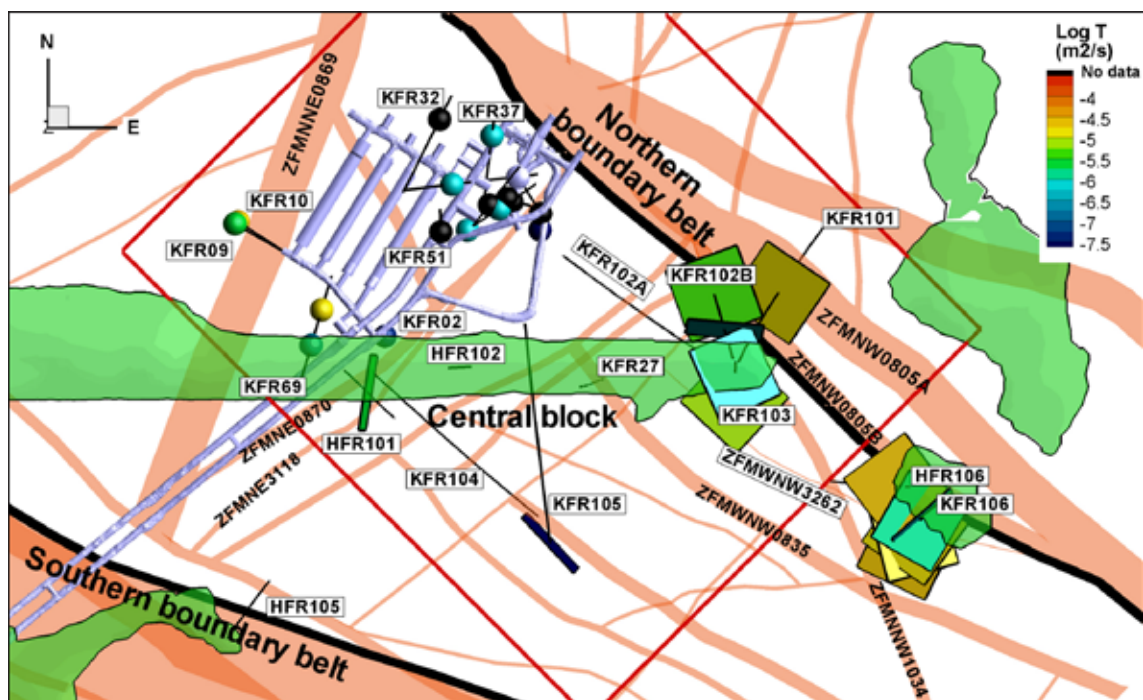
- 40 deformation zones, 28 of which are encompassed by the local model domain. Equivalent to the 40 deformation zones listed in Table 5-4. These were all handled as HCDs.
- 31 unresolved possible deformation zones (PDZs). Equivalent to the 31 PDZs listed in Table 5-5, see Chapter 5 for details. Most of these structures have been inferred to be minor geological features, with a size smaller than the resolution level for the deterministic geological modelling work adapted in version 1.0 (300 m). *Seventeen unresolved PDZs were removed from the hydrogeological modelling, five unresolved PDZs were handled deterministically as part of SBAs and seven unresolved PDZs were modelled stochastically as conditioned random features.*

---

<sup>1</sup> There is little or no evidence to support a division of the bedrock into lateral HRDs based on the rock domains delineated in the geological modelling of the bedrock, see Section 4.2.2 in /Öhman et al. 2012/ for details.

- Eight so-called shallow bedrock aquifer structures<sup>2</sup> (SBA1-8), see Appendix B and Appendix H in Öhman et al. (2012) for details. These were handled deterministically and include five unresolved PDZs and the stress release structure H1–H3 identified in Chapter 5.
- Three hydraulic rock mass domains (HRDs); the Shallow (bedrock) HRD, the Repository level HRD and the Deep bedrock HRD, see Öhman and Follin (2010b) and Appendix F in Öhman et al. (2012) for details. The three HRDs are equivalent to depth slices through the bedrock between the deformation zones, independent of rock domains, but based on fracture frequency statistics. *This concerns the stochastic modelling of a residual HRD data set after removal of data from the unresolved PDZs and the SBAs.*

The HCDs and SBAs are modelled as deterministic features. By contrast, the HRDs are modelled as discrete fracture network (DFN) realisations, with stochastic geometrical and hydraulic properties derived from the fracture mapping and single-hole hydraulic tests carried out in the new boreholes; see Appendix 5 for DFN property tables.



**Figure 7-2.** Location of the 31 unresolved PDZ intercepts coloured according to transmissivity. These occur between 0 and –160 m elevation, i.e. in the rock mass corresponding to the two upper hydraulic rock mass domains. The deformation zone model is shown as pinkish traces of various lengths and thicknesses, and the red rectangle is the SFR local model area. The existing SFR facility is shown in pale lilac and the thin black lines represent boreholes. 17 unresolved PDZs lack orientation data and are shown as spheres. These occur in the old boreholes drilled in the vicinity of the existing SFR. Fourteen PDZs have orientation data and are shown as planes. These occur in the new boreholes drilled southeast of the existing SFR facility. Most of the unresolved PDZs in the new data set are horizontal to gently dipping and occur close to the Northern boundary belt and the steeply dipping deformation zone ZFMNNW1034 (cf. Figure 5-2 and Figure 5-17). Borehole KFR27 is located in the centre of the Central block and is drilled within and alongside the steeply dipping deformation zone ZFMWNNW0835.

<sup>2</sup> The SBA concept is adopted from SDM-Site. There the uppermost 150 m of bedrock was inferred to host extensive and highly transmissive horizontal to gently dipping sheet joints, see /Follin et al. 2007a, c, Follin 2008/ for details. The SBA-structures in SDM-PSU are less extensive and less transmissive. Yet, they form an important part of the flow system with regard to the planned extension, see Section 7.2.5 for structural details and Section 7.4.3 for hydraulic parameterisation.

The 31 unresolved PDZs were studied hydraulically and divided into four groups<sup>3</sup>:

1. Extension or splay to an HCD (2;0).
2. Deterministic SBA-structure (1;4).
3. Database for stochastic realisations of unresolved PDZs (0;7).
4. Excluded from further modelling (deleted) (14;3).

The derivation of the hydrogeological DFN model in version 1.0 takes into account the delineation of the 40 deformation zones, the handling of the 31 unresolved PDZs, and the definition of the eight SBA-structures. Further, the HSD model developed for SR-Site (Bosson et al. 2010) is adopted without modifications in SDM-PSU, but it will be updated in due time for SR-PSU.

The second report describing the hydrogeological model for bedrock version 1.0, (Öhman et al. 2013) deals with groundwater flow modelling and uses the conceptual hydrogeological model for the bedrock described in Öhman et al. (2012) together with DarcyTools (Svensson et al. 2010) and FracMan (Dershowitz et al. 1998). The results from the groundwater flow simulations are compared with present-day inflow data and head field information. The first part of Öhman et al. (2013) examines the sensitivity of the implemented flow model to a series of parameter perturbations including a demonstration of the hydrogeological DFN model. The second part focuses on two hydraulic interference tests carried out at the site.

## 7.2 Evaluation of primary data

Three different data sources are used in this study see Figure 2-1.

1. Old data from the site investigation and the construction of the existing SFR facility (1980 to 1986).
2. Data from the nearby Forsmark site investigation (2002 to 2007).
3. New data from the SFR extension investigation (2008 to 2009).

It is not straightforward how these three data sources should be combined; they are of different quality and cover different parts of the SFR model area. In the recent SFR extension investigation, only one borehole was drilled underground from the existing SFR facility (KFR105; see Figure 7-2) due to safety regulations that restrict its accessibility, see Nilsson G (2009) for details.

Essential weaknesses of the old data set are the lack of oriented fracture data as well as the limited confidence in data quality. The benefit of the old data set is that it provides additional information about the near-field of the existing SFR facility not covered by the new data set. The old data set is primarily used for conceptual understanding and hydraulic parameterisation of deformation zones (HCD) in proximity to the existing SFR facility. The old data set cannot be used for hydrogeological DFN modelling of rock mass volumes (HRDs) between deformation zones (HCDs).

The SFR model area is located in the centre of the Forsmark regional model area, see Figure 2-1. Hence, the conceptual understanding of the bedrock hydrogeology within the SFR model area is intimately linked with the conceptual understanding of the bedrock hydrogeology of the Forsmark model area. In all, 25 cored boreholes and 38 percussion boreholes were drilled into the bedrock during the Forsmark site investigation. The boreholes KFM11A, HFM34, and HFM35 are of particular relevance for the hydrogeological modelling of the SFR area, as their location in the Southern boundary belt provides hydrogeological data useful for conceptual modelling and hydraulic parameterisation of the associated HCDs, see Figure 2-1. However, the data acquired in these boreholes are not representative for the characterisation of HRDs.

In contrast to the old data set, the new data set provided by the SFR extension investigation conforms to SKB's current quality standards and requirements in terms of traceability. In addition, this more recent data set includes orientations of sealed, open and partly open fractures as well as flowing fractures detected by the Posiva Flow Log (PFL), known as PFL-f data. The combination

---

<sup>3</sup> The two numbers between parantheses refer to the number in each data set, old and new, respectively.

of geometric and hydraulic fracture properties forms the basis for the established methodology for describing the HRD by means of hydrogeological DFN modelling, see Follin et al. (2007b) for details. Thus, the new data set is judged to be considerably more useful and trustworthy than the old data set for the parameterisation of site-specific properties inside the SFR model area.

In summary, the primary data forming the basis of the hydrogeological bedrock model version 1.0 are the following.

- Observations from the existing SFR facility (tunnel fracture trace maps, tunnel inflow measurements, and monitored heads in boreholes).
- Interference test responses (intentional cross-hole tests, as well as monitored head disturbances during drilling and other borehole activities). Comparison of response indices.
- Hydrogeochemical data gathered in the existing SFR facility and in monitored borehole sections (electric conductivity and chemical composition of water samples).
- Orientation and frequency of open fractures.
- Single-hole hydraulic test data (various kinds of old types of double packer test data, impeller flow logging (HTHB) data and difference flow logging (PFL-f) data).

The listed data are thoroughly described, cross-compared, and put into context of bedrock geological model version 1.0, see Öhman et al. (2012) for details.

### 7.2.1 Observations from the existing SFR facility

It is noted in Chapter 5 that there is a clear difference in the intensity of the orientation patterns between open and sealed fractures. Taking the rock mass as a whole (A1–A2 in Figure 5-8), the horizontal orientation group dominates the open fractures, whereas sealed fractures are predominantly sub-vertical to steeply dipping and strike WNW-ESE to NW-SE or NE-SW. If the rock mass lying outside the modelled deformation zones is considered in isolation (C1–C2 in Figure 5-8), it is the horizontal to gently dipping fractures that dominate the open fractures.

The occurrence of horizontal to gently dipping open fractures in the rock mass between the steeply dipping deformation zones in the Forsmark area was recognised already during the construction of the nuclear power plants (Carlsson 1979), see Figure 7-3 for an example. These were inferred by Stephens et al. (2007) to be sheet joints, formed by release of stress during exhumation of the crystalline bedrock in connection with unloading, rather than regional tectonic processes. Their heterogeneous hydraulic character with locally very high transmissivities was not realised before SDM-Site. The term Shallow Bedrock Aquifer (SBA) was introduced in Follin et al. (2007c) to denote their hydraulic importance.



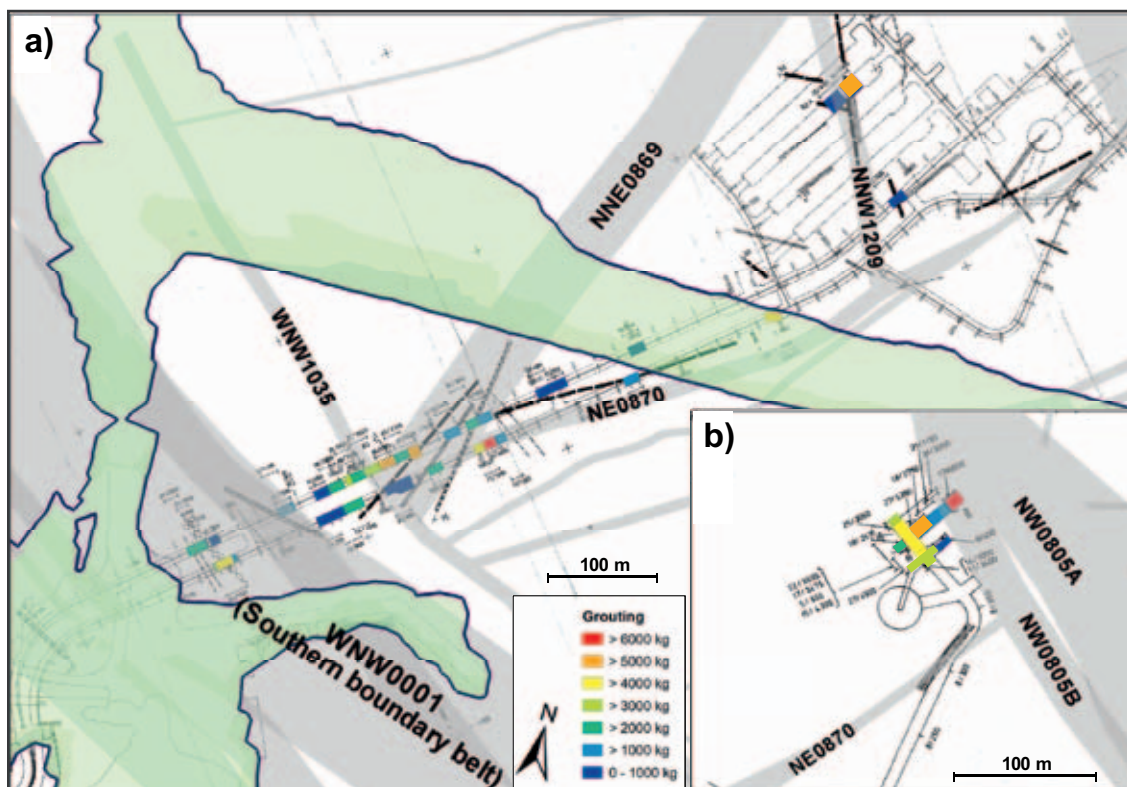
**Figure 7-3.** The channel between the nuclear power reactors and the Baltic Sea exposing extensive undulating sheet joints. Photograph by G Hansson. Reproduced from Carlsson and Christiansson (2007).



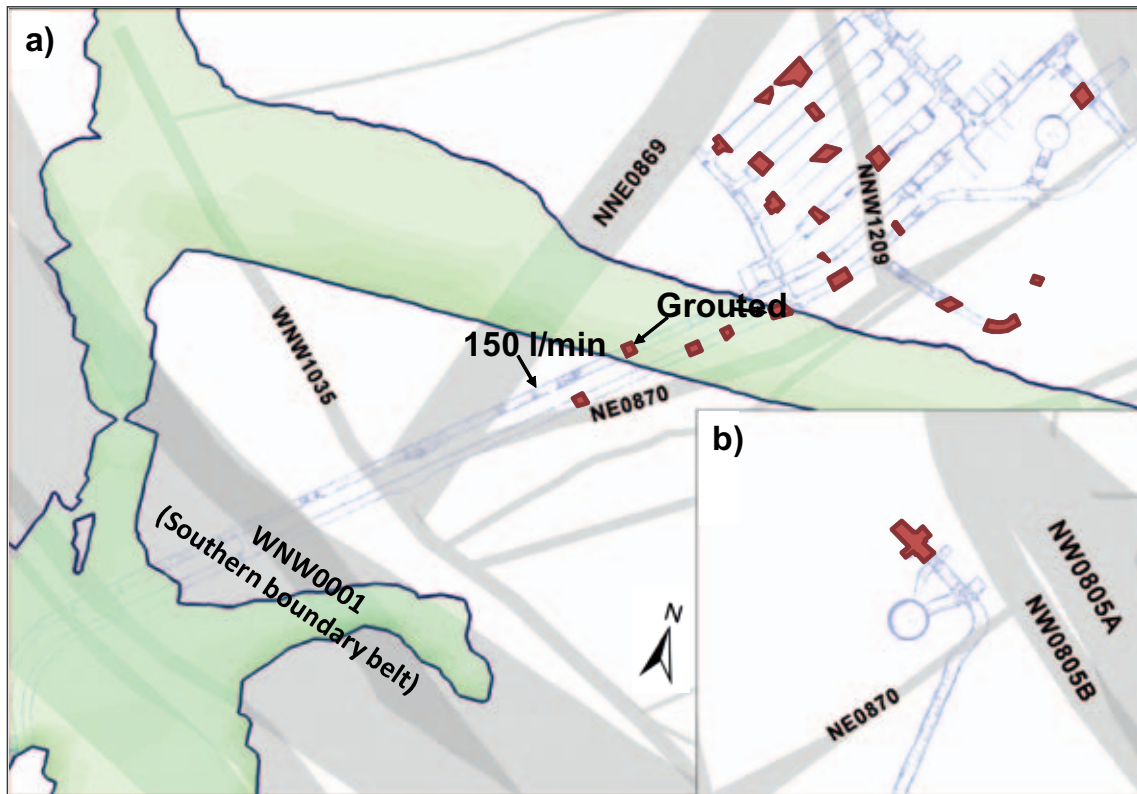
The water-bearing traces mapped during the construction of the existing SFR facility have been described as “locally flowing” inside deformation zones, and as “moisture” or “dripping” outside zones (Christiansson and Bolvede 1987). Except for two examples, grouting was primarily associated with steeply dipping fractures, see Figure 7-4. The locations of the two exceptions with sub-horizontal fractures are shown in Figure 7-5. They had the following characteristics:

- The first exception required substantial grouting. The fracture trace on the tunnel wall can be correlated to one of the unresolved PDZ intercepts located in the nearby borehole KFR69 ( $T \approx 10^{-5} \text{ m}^2/\text{s}$ ; see Figure 7-2). For this reason, the orientation and size of this unresolved PDZ intercept are modelled deterministically as a shallow bedrock aquifer feature (SBA8) in hydrogeological model version 1.0.
- The second exception had the single largest noted inflow (150 L/min) in the entire SFR facility. This occurred in a bolt hole drilled in the ceiling at chainage 1/600 (c. -50 m elevation; see Figure 7-5). The water was judged to originate from a sub-horizontal structure running above the tunnel (Christiansson and Bolvede 1987). This observation means that there are unknown sub-horizontal fractures.

Today, the two main discrete sinks are judged to be: 1) the intersection of the access tunnels BT and DT with the southern boundary belt, ZFMWNW1035 and ZFMNNE0869, and 2) the intersection of NDB/NBT with ZFM871. There is also a long diffuse line-sink along the intersection between tunnel BT and ZFMNE0870 (Figure 7-5).



**Figure 7-4.** Grouted tunnel sections in the existing SFR facility. For readability, the original drawing –104 by Christiansson and Bolvede (1987) has been coloured by injected cement and placed in the context of the ground traces of the deformation zones of the SFR geological model v. 1.0. The inset b) illustrates the lower-level SFR tunnels intersecting the gently dipping ZFM871, which is located beneath the existing SFR facility and is hence not visible in the image.



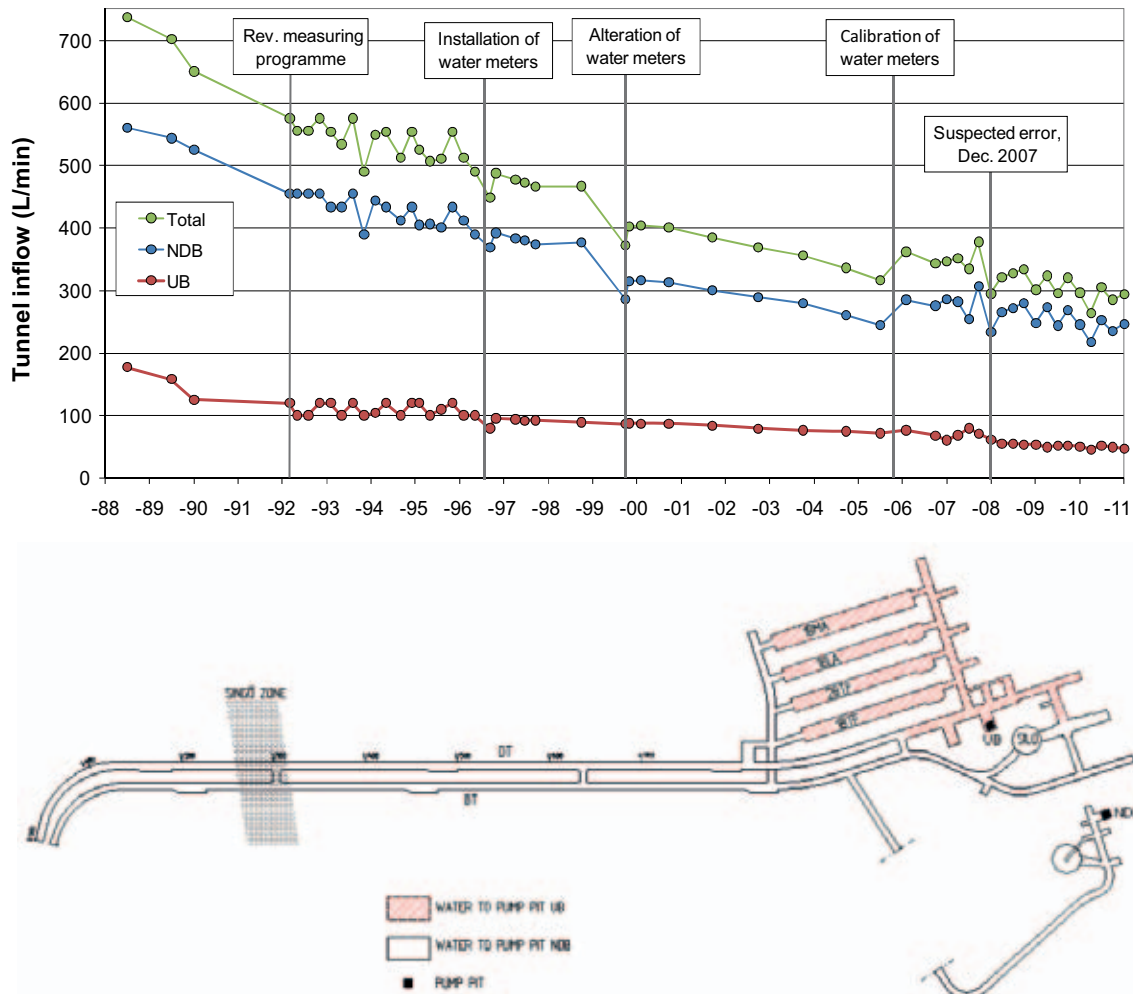
**Figure 7-5.** a) Illustration showing structures consisting of closely spaced, sub-horizontal parallel fractures (dip < 15°) digitised from sketch 103 in Christiansson and Bolvede (1987). Only two of these structures required grouting; b) Illustration showing the lower level of the NDB tunnel, which intersects the gently dipping deformation zone below ZFM871 (located beneath the existing SFR facility and hence not visible in the image). This intersection required 67.5 m<sup>3</sup> of grout.

Measurements of the inflow to the SFR facility have been carried out regularly since January 1988 (Carlsson and Christiansson 2007). The total inflow in 1988 was about 720 L/min. Since then there has been a decreasing trend of inflow that has been relatively steady for the last 15 years (Figure 7-6). The total inflow has decreased to about 285 L/min (average value for 2010), which corresponds to a 61% decrease compared with the 1986 value. Since no grouting has occurred since the completion of the existing SFR facility, the decreasing inflow trend is due to other mechanisms. Gustafson (2009) suggests the following processes as plausible explanations for the decreasing trend:

- increasing effective normal stress,
- two-phase flow, and
- chemical precipitation.

An analysis of the importance of the first process requires a combination of geological, hydrogeological and rock mechanics data, whereas the other two processes require a combination of geological, hydrogeological and hydrogeochemical data. An assessment is presented in Chapter 9.

There are few measurements of the groundwater level (head) conditions prior to the excavation of the existing SFR facility. These indicate discharge conditions, but the measurements are of a poor quality and the interpretations made are considered unreliable from a technical standpoint (Carlsson et al. 1986, p. 55).

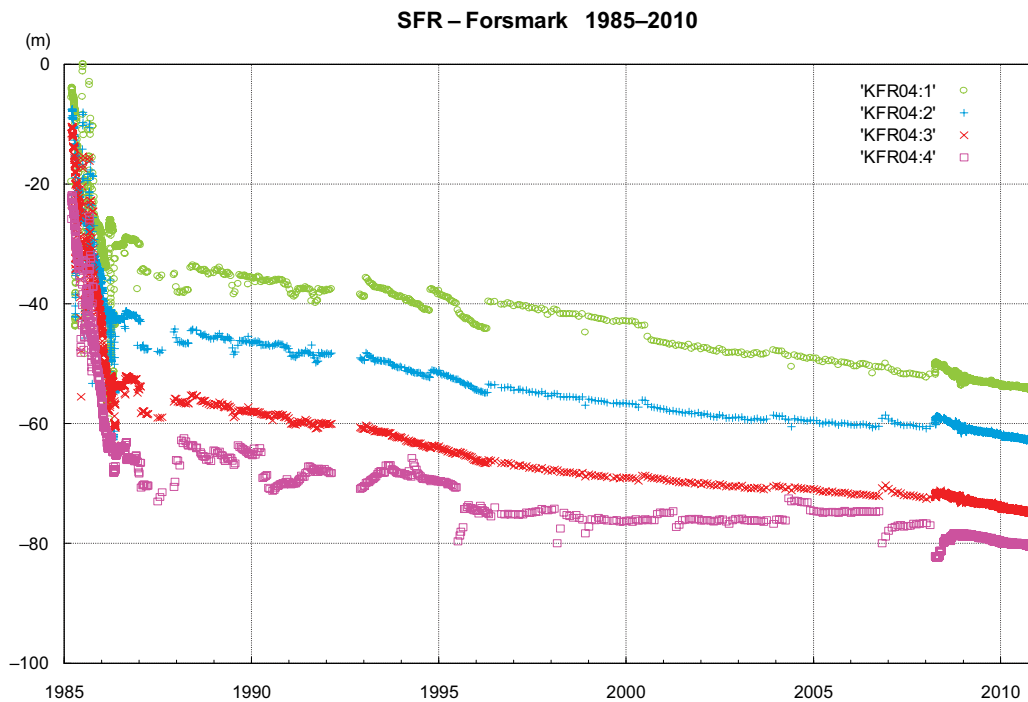


**Figure 7-6.** Inflow of groundwater to the existing SFR facility between 1988 and 2011. Curves marked UB and NDB refer to drainage of the pumping pits in the operational area and in the lower construction tunnel, see the location map.

Today, the entire head field is more or less affected by the ongoing drainage, but the drawdowns (head changes) indicate quite heterogeneous hydraulic conditions. In total, there are 38 sections in 12 boreholes in the vicinity of the existing SFR that are monitored. The results are reported on a yearly basis, see e.g. SKBdoc 1233647. In general, the head field dropped rapidly during the construction period and at the first time of measurement thereafter. However, the head stabilised quickly in the largest zones ZFMWNW0001 (part of the Southern boundary belt) and ZFMNW0805A/B (part of the Northern boundary belt). In the tectonic unit between these two boundaries, the Central block, there has been a slow, relatively constant decreasing head trend in most borehole sections since 1987–1988, see Figure 7-7 for an example.

The head drop has been most pronounced in the vicinity of the Silo, associated with zones ZFMNE0870 and the gently dipping ZFM871. In these boreholes, the head decrease was about  $-0.5$  to  $-1$  m/yr during year 2009 and the total drawdown exceeded tens of metres. In contrast, KFR09, which is located inside ZFMNNE0869 (also referred to as zone 3), shows only a small total drawdown ( $-1.9$  m) after approximately 25 years of operation, in spite of its location close to a non-grouted tunnel wall.

The head trends in the borehole sections that penetrate the gently dipping zone ZFM871 vary in space, but with various rates of decrease in KFR02, KFR03, KFR04, KFR05, KFR13, and KFR7B. This indicates that ZFM871 is hydraulically heterogeneous and/or geometrically discontinuous.



**Figure 7-7.** Examples of time series showing the trend in hydraulic head in borehole KFR04. The monitored borehole sections in KFM04 are located at distances between 16 and 42 m from the SFR facility.

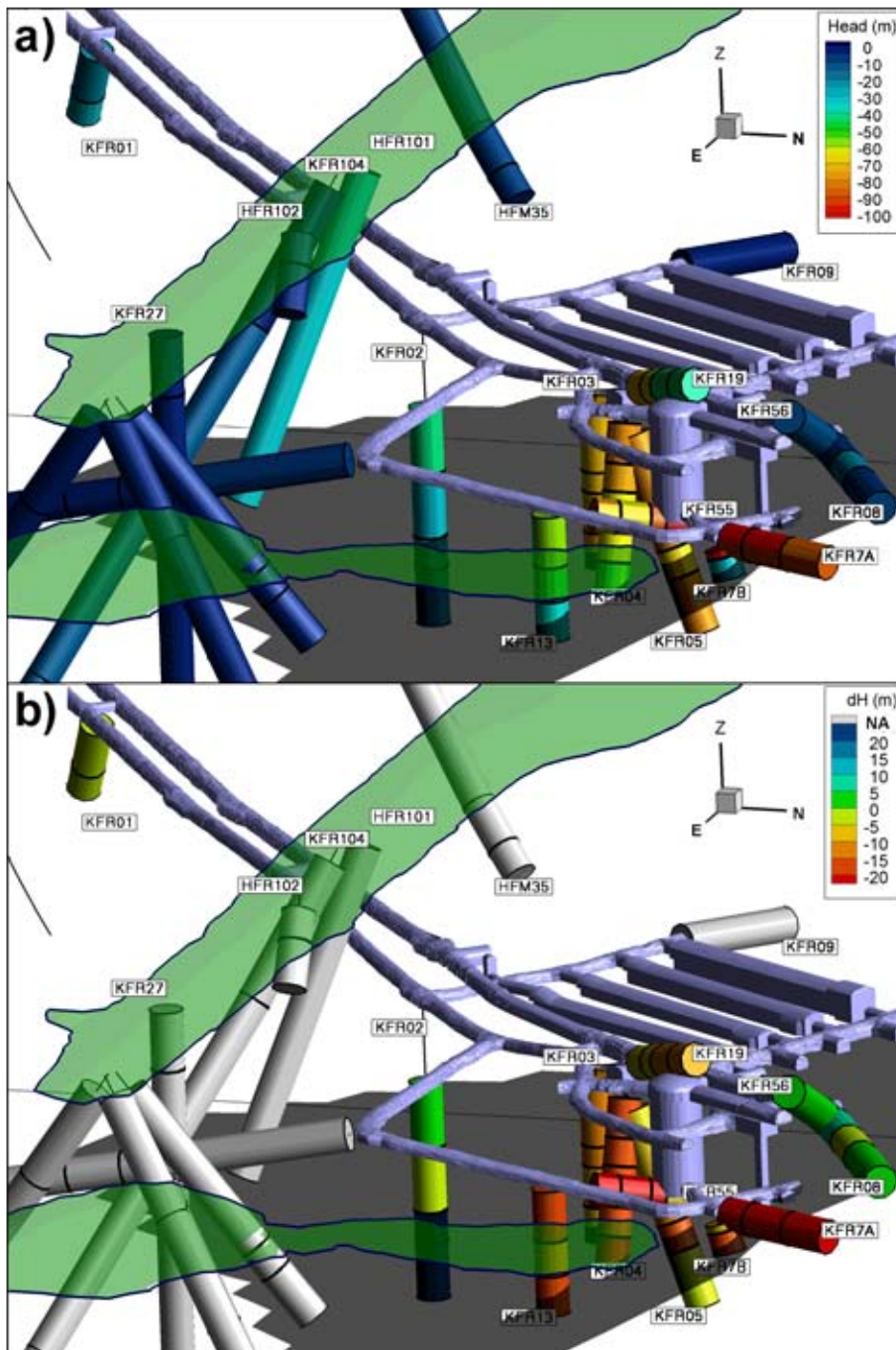
Most striking in the old data set is the “unintentional interference test” in KFR80 (penetration of ZFM871 during grouting), which was tentatively interpreted to cause drawdown in KFR01, at a distance of 870 m (Axelsson and Mærsk Hansen 1997). The interference data, as well as single-hole transmissivity data, support the notion that KFR09\_DZ2 can be interpreted as a splay of ZFMNNE0869, and KFR10\_DZ2 as an extension of ZFM871 (see Chapter 5).

KFR7A is located inside ZFMNW0805A/B, but exhibits a clearly different head and transient trend from the other monitored borehole sections inside this zone, KFR08 and KFR56, see Figure 7-8. KFR7A is modelled to also intercept ZFM871 in bedrock geological model version 1.0. It may possibly be affected by the heavy grouting at the tunnel intersection with ZFM871, see illustration b) in Figure 7-4. KFR7A and KFR08 are in good structural contact according to the geological model, but their water chemistry differs significantly with more Baltic Sea water in KFR08 and more Littorina Sea water in KFR07, see Chapter 8 for details. Further, KFR7A showed the highest drawdown as well as the largest decrease during year 2009 ( $-2$  m/yr).

## 7.2.2 Measured heads in 2010

Figure 7-9 shows the measured groundwater levels (heads) in all monitored borehole sections in 2010, i.e. including the new boreholes<sup>4</sup>. Öhman et al. (2012) provide a detailed analysis of the observed heads with regard to bedrock geological model version 1.0. HFR101 and the mid-section of KFR104 have the largest drawdowns among the new boreholes. HFR101 is partially unsaturated with a groundwater level at  $-31.0$  m. This indicates that HFR101 is indirectly connected to the existing SFR facility. It also indicates that it is poorly connected to the sea, even at shallow depth (the casing ends at  $-4.65$  m), possibly constrained by low-permeable regolith.

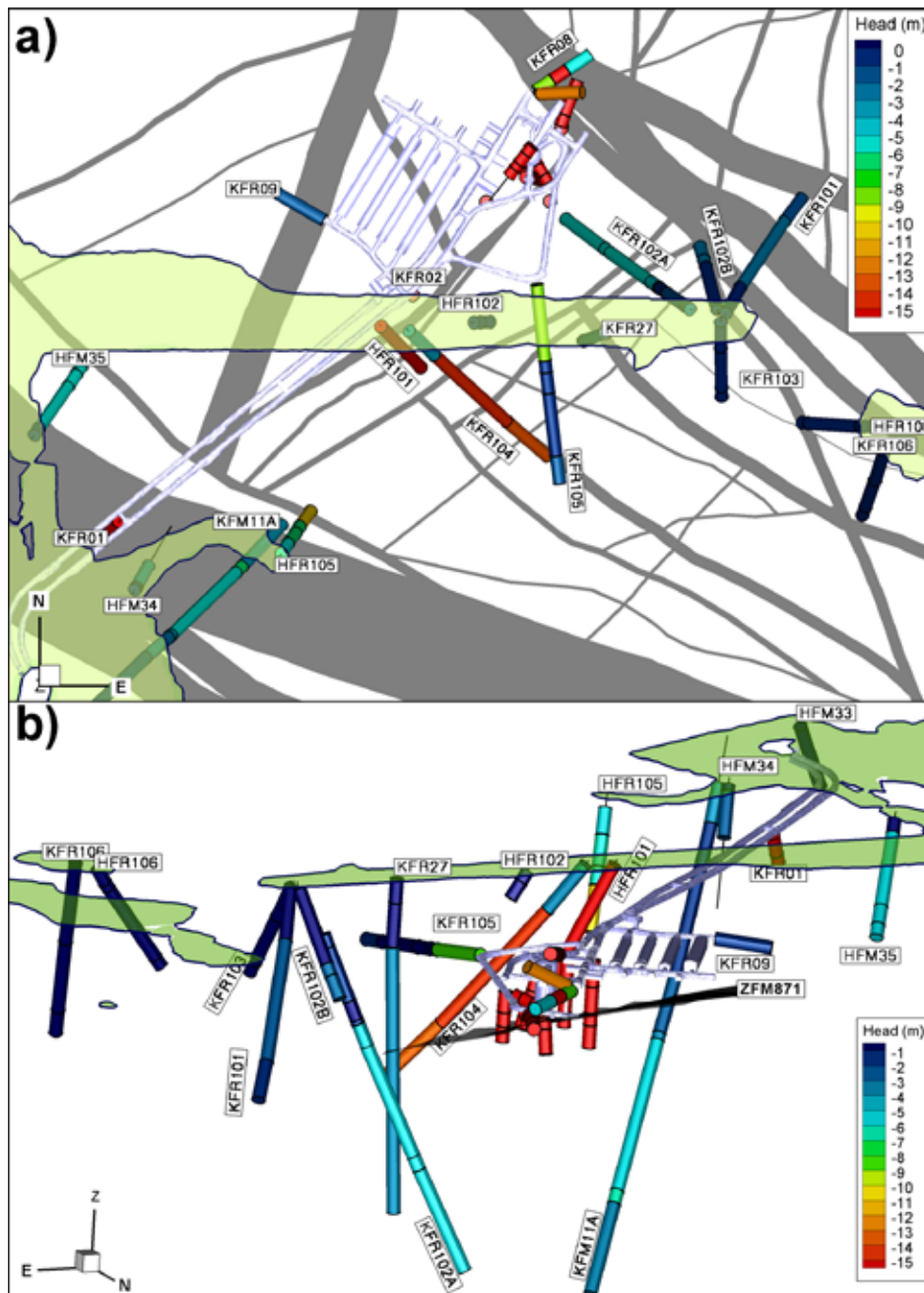
<sup>4</sup> Groundwater levels measured underground in boreholes drilled from the existing SFR (the old boreholes mainly) are reported as freshwater heads (FWH), whereas groundwater levels measured in surface boreholes (the new boreholes mainly) are reported as point water heads (PWH). As the density contrasts are small and the depths are shallow, this measurement difference is considered to be insignificant for the hydrogeological modelling of the SFR area reported here. Unless specially noted, measurements at different locations are regarded as comparable, including sea level. To simplify the discussion, all groundwater levels are called heads in the hydrogeological modelling.



**Figure 7-8.** Heads in SFR tunnel boreholes (coloured cylinders); a) 2010 and b) change in head between 1988 and 2010. The reference year 1988 was chosen because the decreasing head trends in most borehole sections have been relatively constant since this year. The greyish surface below the existing SFR is the gently dipping ZFM871 as modelled in geological model version 1.0. The heads in this deformation zone are monitored by several borehole sections.

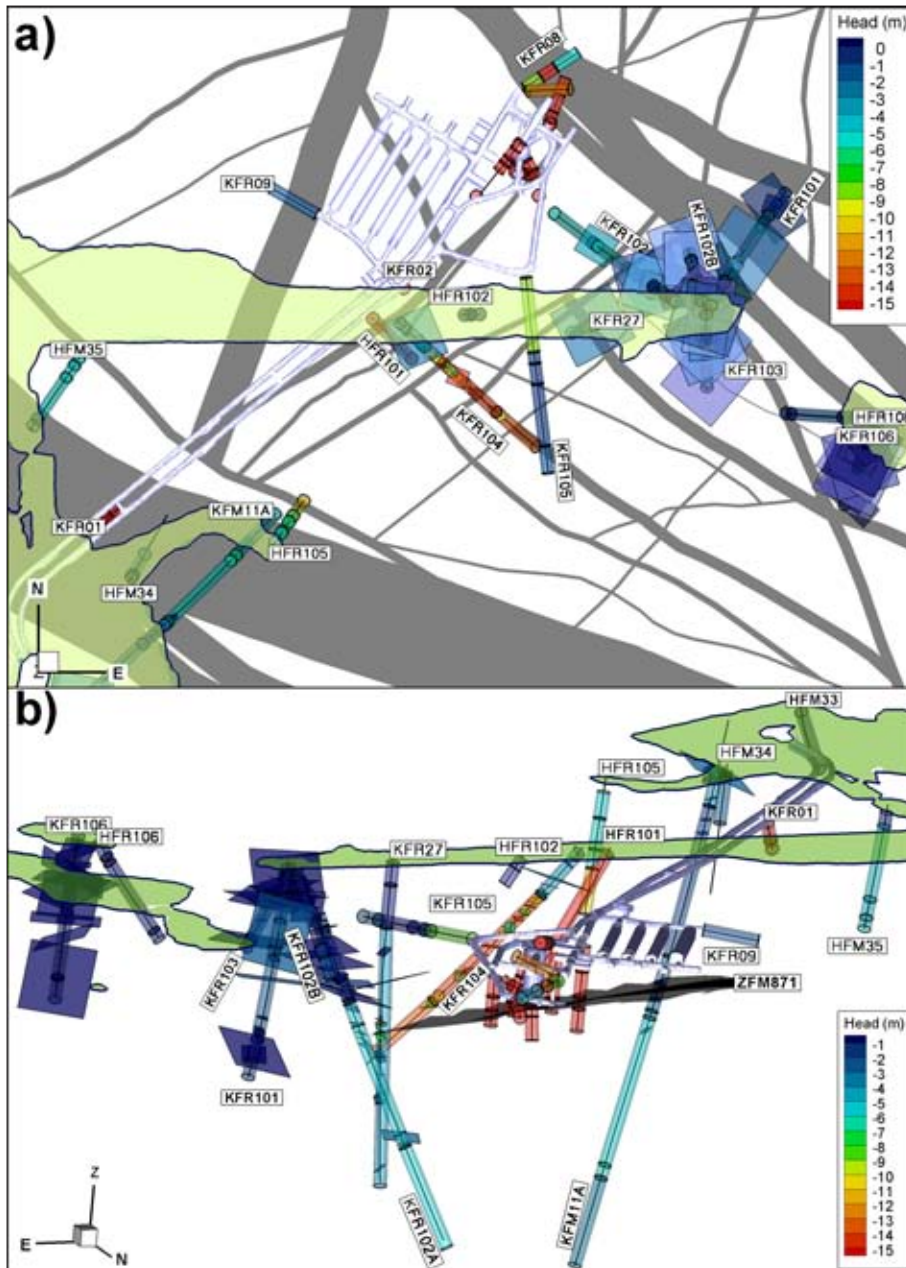
Figure 7-9 indicates that the lateral extent of drawdown appears to propagate mainly along the gently dipping ZFM871 and the Northern boundary belt. The disturbances seen in the Southern boundary belt are probably due to leakage into the two access tunnels as they cross the Singö deformation zone.

In general, the head in a majority of the observation sections shows a strong correlation with sea-level fluctuations. The ongoing transient change in head and inflow indicates a disturbed system with a complex hydraulic contact with the Baltic Sea. The best correlations with the sea-level fluctuations occur inside the deformation zones located in the proximity of the Northern boundary belt, including the gently dipping zone ZFM871.



**Figure 7-9.** Measured heads in monitored sections 2010; a) top view and b) side view along the dip of ZFM871. The heads in the old data set that are below  $-15$  m are resolved in Figure 7-8.

The calculation of apparent fracture transmissivities from PFL-f data involves a calculation of *in situ* heads. In general, the *in situ* heads are consistent with the monitored heads, but they give a more detailed picture of drawdown heterogeneity associated with the PFL-f data, see Figure 7-10. For instance, KFR27 is an old borehole that is located in the centre of the SFR model area. The length of the borehole was extended from  $-140$  m to  $-470$  m during the SFR extension investigation. The extended drilling of KFR27 caused not only interferences in ZFM871, but also within the Northern boundary belt.



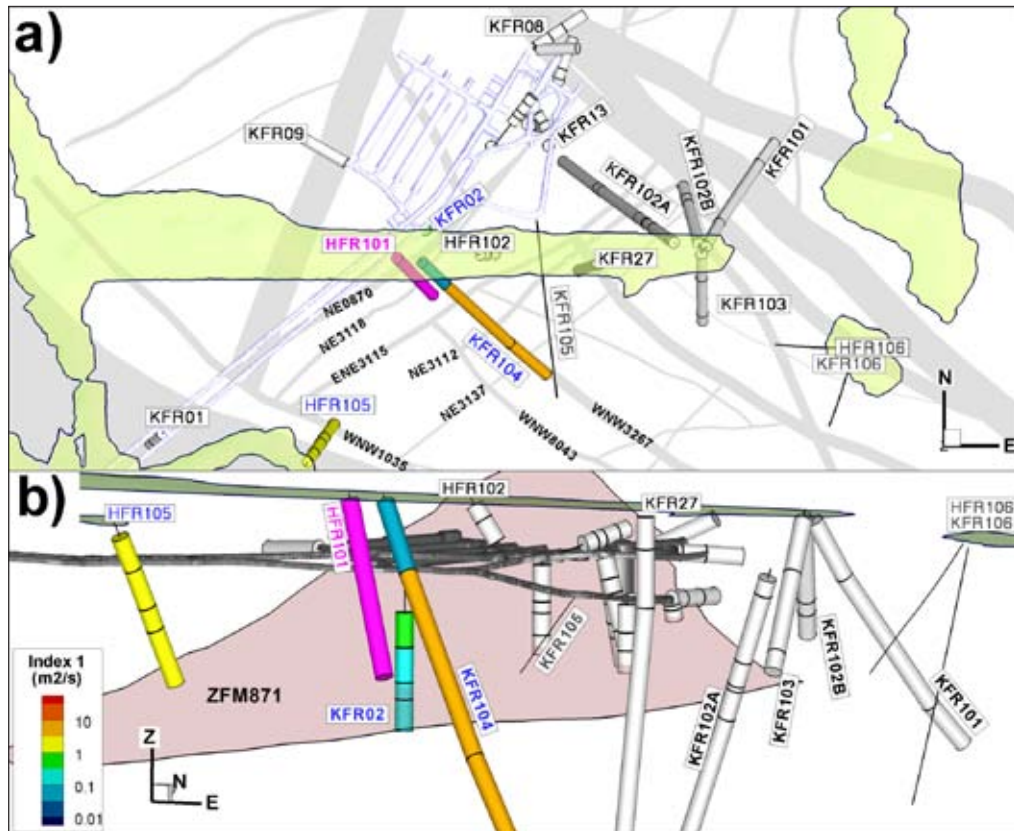
**Figure 7-10.** Evaluated heads from PFL-f data plotted as square fractures of different sizes according to the hydrogeological DFN model derived by Öhman and Follin (2010b); a) top view and b) side view along the dip of ZFM871. Monitored heads are shown as transparent cylinders. The heads in the old data set that are below  $-15$  m are resolved in Figure 7-8.

### 7.2.3 Interference tests and hydraulic responses during drilling

Evaluation of hydraulic interferences had a key role in interpreting and describing the superficial bedrock in the nearby region described in SDM-Site Forsmark, confirming the existence and hydraulic significance of sheet joints in the near-surface realm. One of the key issues in the SFR extension investigation was to determine if similar structures also exist within the SFR regional model area. Both similarities and differences between the two sites have been demonstrated in the evaluation of primary data. A common characteristic is that the highest transmissivities in the shallow rock mass outside deterministically modelled deformation zones are horizontal to gently dipping. A difference is that the maximum transmissivities measured in the SFR local model area are at least two orders of magnitude lower than reported in SDM-Site Forsmark.

The old underground interference tests performed between 1985 and 1987 provide insight into the connectivity between zones surrounding the existing SFR facility. The general impression from the old data set is that ZFM871 has a central role in the hydraulic connectivity around the existing SFR facility. Disturbances in ZFM871 are monitored in all steeply dipping deformation zones (ZFMNE0870, ZFMNW0805A/B, and ZFMNNE0869), and vice-versa, disturbances in steeply dipping deformation zones are generally monitored in ZFM871. However, there also exists evidence of a lack of internal connectivity inside ZFM871, i.e. monitored sections in ZFM871 fail to respond to a disturbance created within ZFM871, as well as no or indirect responses between ZFM871 and surrounding steeply dipping zones. The hydraulic contact between ZFM871 and the Northern boundary belt zones ZFMNW0805A and B is of particular interest. ZFM871 is better connected to ZFMNW0805A than it is to ZFMNW0805B, which is somewhat surprising, considering that ZFMNW0805A is located northeast of ZFMNW0805B. Based on single-hole hydraulic tests, ZFMNW0805A is judged to be more transmissive than ZFMNW0805B. Hence, ZFM871 is interpreted as conductive but heterogeneous/discontinuous.

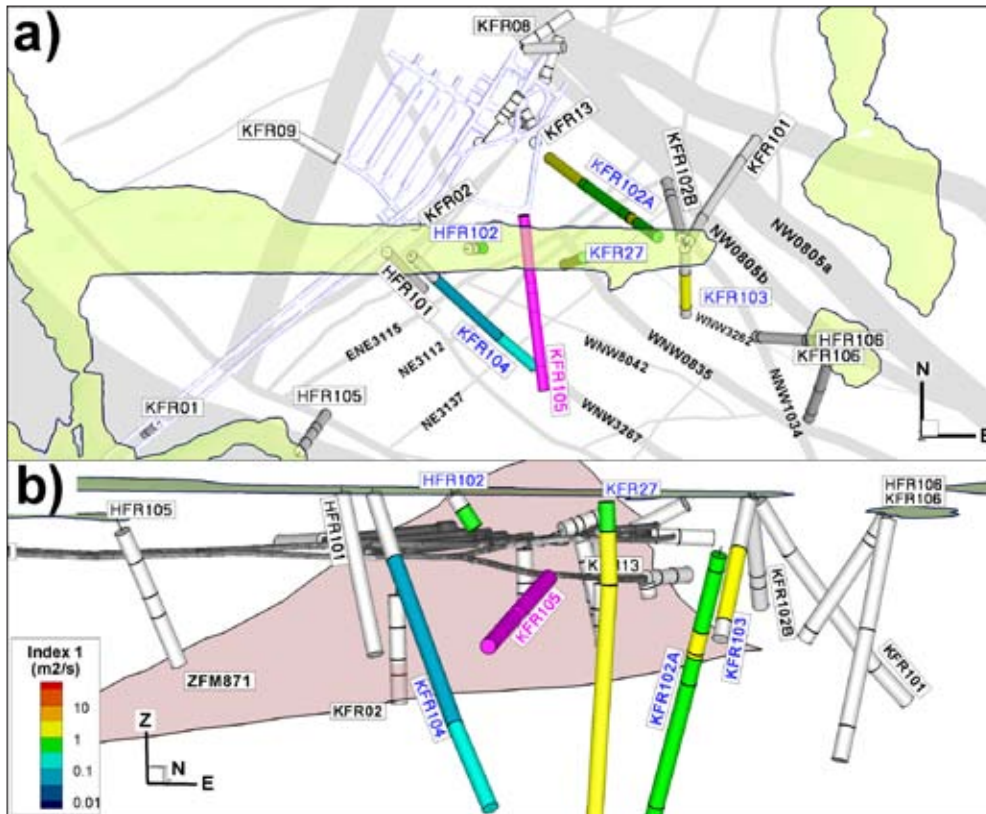
Two planned interference tests were conducted during the SFR extension investigation: a pumping test in HFR101 and the opening of the underground borehole KFR105. The two interference tests have been evaluated in terms of the response index  $r_s^2/dt_L$ , which is a common first-order approximation for hydraulic diffusivity<sup>5</sup>. Figure 7-11 and Figure 7-12 depict the response index values deduced from the two interference tests.



**Figure 7-11.** Hydraulic responses during interference test conducted in HFR101 (purple); a) top view and b) side-view looking towards the north-west. Index 1 stands for  $r_s^2/dt_L$ , which is the ratio between the square of the “observation distance”,  $r_s^2$ , and the elapsed time until interference,  $dt_L$ .

<sup>5</sup> Hydraulic diffusivity is defined as ratio between hydraulic conductivity and specific storage ( $K/S_s$ ). The response index is simply the ratio between the square of the “observation distance”,  $r_s^2$ , and the elapsed time until the interference is observed,  $dt_L$ . The response index has the same units as the hydraulic diffusivity ( $m^2/s$ ).





**Figure 7-12.** Hydraulic responses during the interference test conducted in KFR105 (purple): a) top view and b) side-view looking towards the north-west. Index 1 stands for  $r_s^2/dt_L$ , which is the ratio between the square of the “observation distance”,  $r_s^2$ , and the elapsed time until interference,  $dt_L$ .

Figure 7-11 depicts the three-day long interference test conducted in HFR101 in April 2009. Clear responses were observed in 11 out of a total of 68 monitoring sections. The maximum observed radius of influence (spherical distance) was c. 360 m.

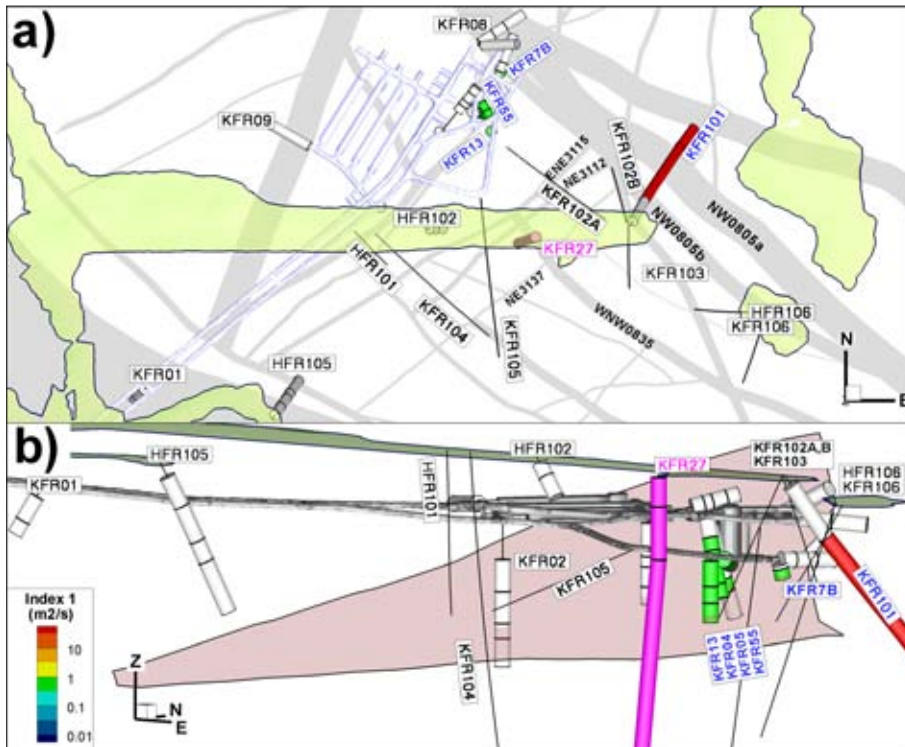
Figure 7-12 depicts the one-day long interference test conducted in KFR105 in March 2010. Clear responses were observed in 15 out of a total of 76 monitoring sections. The maximum observed radius of influence (spherical distance) was c. 400 m.

In addition to the two interference tests, the hydraulic responses from five different types of borehole activities such as drilling and nitrogen flushing have been analysed and evaluated. The evaluations have comprised a qualitative classification of the responses at different drilling depths and a quantitative estimation of the apparent hydraulic diffusivity between the drilled borehole and the observation section. Similarly, Figure 7-13 through Figure 7-17 depict the response index values deduced from the five borehole activities, respectively

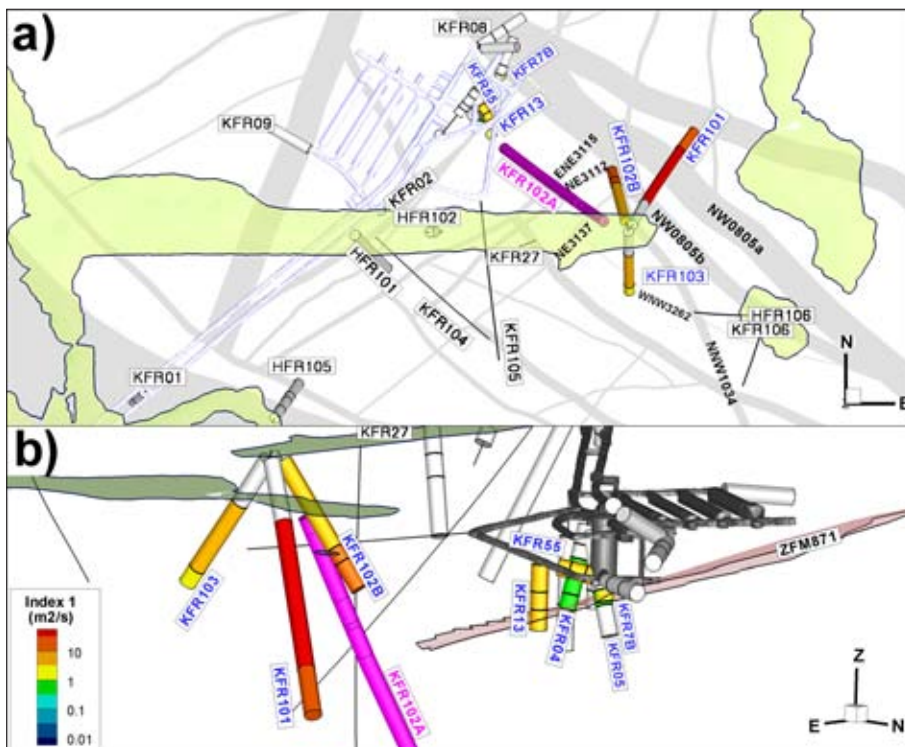
Figure 7-13 depicts hydraulic responses during the drilling (extension) of KFR27 in October 2008. Clear responses were observed in 12 out of a total of 48 monitoring sections. The maximum observed radius of influence (spherical distance) was c. 340 m.

Figure 7-14 depicts the hydraulic responses during the drilling of KFR102A in November–December 2008. Clear responses were observed in 17 out of a total of 54 monitoring sections. The maximum observed radius of influence (spherical distance) was c. 290 m.

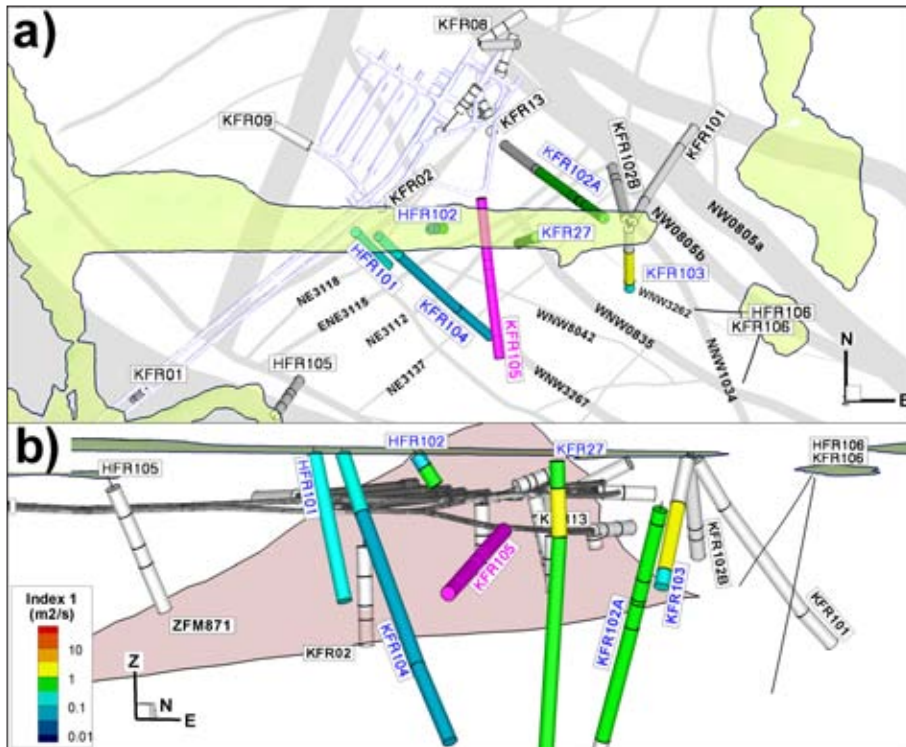
Figure 7-15 depicts the hydraulic responses during the drilling of KFR105 in April–June 2009. Clear responses were observed in 14 out of a total of 69 monitoring sections. The maximum observed radius of influence (spherical distance) was c. 270 m.



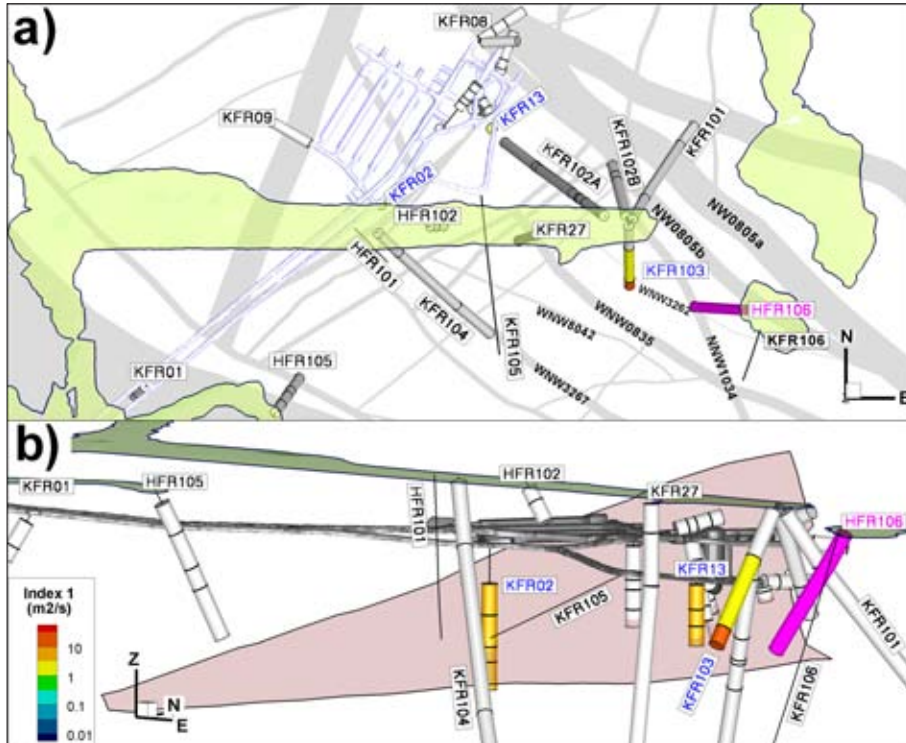
**Figure 7-13.** Hydraulic responses during the drilling (extension) of KFR27 (purple); a) top view and b) side view looking towards the northwest. Index 1 stands for  $r_s^2/dt_L$ , which is the ratio between the square of the “observation distance”,  $r_s^2$ , and the elapsed time until interference,  $dt_L$ .



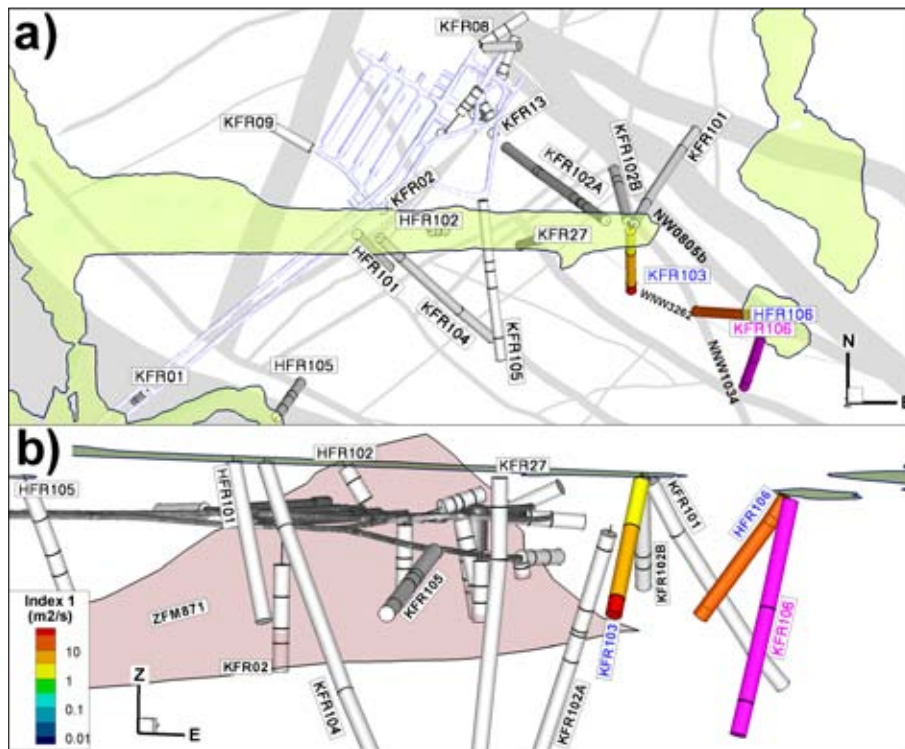
**Figure 7-14.** Hydraulic responses during the drilling of KFR102A (purple): a) top view and b) side view looking towards the southwest. Index 1 stands for  $r_s^2/dt_L$ , which is the ratio between the square of the “observation distance”,  $r_s^2$ , and the elapsed time until interference,  $dt_L$ .



**Figure 7-15.** Hydraulic responses during the drilling of KFR105 (purple) (cf. Figure 7-12): a) top view and b) side view looking towards the northwest. Index 1 stands for  $r_s^2/dt_L$ , which is the ratio between the square of the “observation distance”,  $r_s^2$ , and the elapsed time until interference,  $dt_L$ .



**Figure 7-16.** Hydraulic responses during the drilling of HFR106 (purple): a) top view and b) side view looking towards the northwest. Index 1 stands for  $r_s^2/dt_L$ , which is the ratio between the square of the “observation distance”,  $r_s^2$ , and the elapsed time until interference,  $dt_L$ .



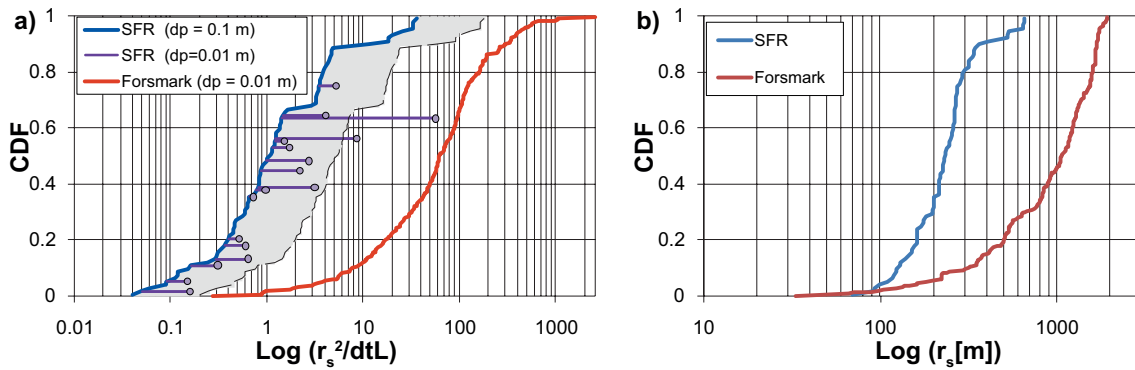
**Figure 7-17.** Hydraulic responses during the drilling of KFR106 (purple): a) top view and b) side view looking towards the northwest. Index 1 stands for  $r_s^2/dt_L$ , which is the ratio between the square of the “observation distance”,  $r_s^2$ , and the elapsed time until interference,  $dt_L$ .

Figure 7-16 depicts the hydraulic responses during the drilling of HFR106 in June–July 2009. Clear responses were observed in 9 out of a total of 69 monitoring sections. The maximum observed radius of influence (spherical distance) was c. 650 m

Figure 7-17 depicts the hydraulic responses during the drilling of KFR106 in August–September 2009 (X). Clear responses were observed in 5 out of a total of 76 monitoring sections. The maximum observed radius of influence (spherical distance) was c. 340 m.

Sea level fluctuations cause a high data noise level in the head measurements in the SFR extension investigation. To mitigate interpretation uncertainties, a head change criterion ( $dp$ ) of 0.1 m is used in SDM-PSU. This value is ten times larger than the value used in onshore investigations at Forsmark for SDM-Site,  $dp = 0.01$  m. There, sea level fluctuations were not an issue and a finer detection criterion was possible. However, the difference in head change criterion implies that the time required for a certain response to be detected ( $dt_L$ ) is longer in SDM-PSU than in SDM-Site. Since  $dt_L$  affects the determination of the response index  $r_s^2/dt_L$ , 17 interference test responses in SDM-PSU were evaluated for  $dp = 0.01$  m as well. Figure 7-18a shows the results. Without accounting for the difference in response criteria, the value of  $r_s^2/dt_L$  is on the average a factor of 46 higher onshore, i.e. within the tectonic lens at Forsmark (percentile-to-percentile matched; a). The grey shading in a) represents a uniform translation of the blue curve ( $dp = 0.1$  m) by a factor of five. Whether this estimation is sufficiently biased is unclear, but judging by eye, the responses in the SFR area are about one order of magnitude less rapid than those inside the tectonic lens at Forsmark.

This result suggests that imposed short-term hydraulic transients are less distinct (more diffuse) in the SFR area than within the tectonic lens at Forsmark. Plausible reasons for this difference are less transmissive fractures and a higher frequency of open connected fractures in the SFR area (which is assumed to increase the storativity). Figure 7-18b reveals a significantly greater median “response distance” within the tectonic lens at Forsmark. The median value of all response distances is approximately four times greater at Forsmark than in the SFR extension investigation, i.e. 1 km versus 225 m.



**Figure 7-18.** Comparison of values of hydraulic diffusivity ( $\approx r_s^2/dt_L$ ), and response distance ( $r_s$ ) between the SFR extension investigation and SDM-Site Forsmark: a) cumulative distribution of  $r_s^2/dt_L$  and b) cumulative distribution of response distances.

The number of available monitoring sections has grown as the SFR extension investigation has progressed. Some of the responses are of particular interest for the location of the planned repository extension, e.g.:

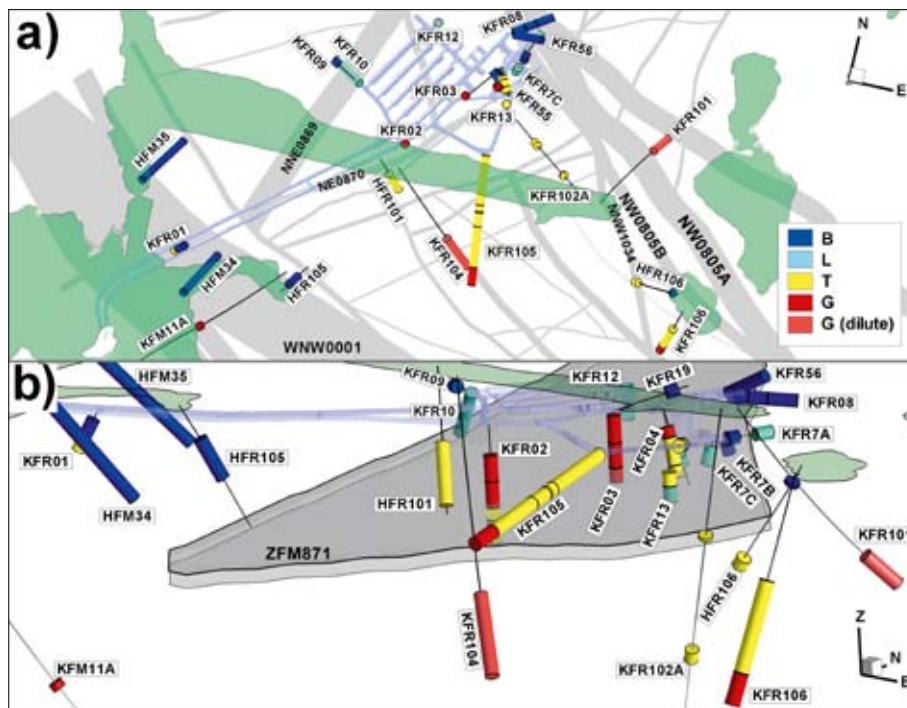
- The types of interference caused by the drilling activities in KFR27 and KFR102A are very similar. Responses were found both in ZFM871 and close to the Northern boundary belt (cf. Figure 7-13 and Figure 7-14).
- The drilling of HFR106 and KFR106, which are located outside the SFR local model area close to the Northern boundary belt, caused interference at depth in KFR103 (Figure 7-16 and Figure 7-17). Note that HFR106 also caused remote interferences (c. 650 m) in some of the monitored sections inside ZFM871 (KFR02 and KFR13), whereas no responses could be observed in KFR27 and KFR102A (Figure 7-16).
- The response index values deduced from the interference test conducted in KFR105 are greater towards the Northern boundary belt than towards the centre of the Central block.

## 7.2.4 Integration with geology and hydrogeochemistry

The hydrogeochemical sampling during the SFR extension investigation has resulted in data from a total of twelve borehole sections in four cored boreholes and one percussion borehole, see Chapter 8 for details. There are also data from two open percussion boreholes. Furthermore, the database contains data from two open percussion boreholes in the Forsmark site investigation and from a total of 45 borehole sections in 18 older cored boreholes drilled from the existing SFR facility tunnels (Nilsson et al. 2011).

The distribution of the different water types presented in Chapter 8 shows that the major steeply dipping deformation zones have served, and still serve, as important conduits between the superficial and deeper water in the bedrock over long periods of geological time, whereas the fracture networks in the rock volumes outside these zones (and in the gently dipping ZFM871) generally contain older and more isolated non-marine water of the brackish glacial groundwater type. Today, the general picture from the hydrogeochemical interpretations presented in Chapter 8 is that water flows vertically from the Baltic Sea to the existing SFR facility via the steeply dipping ZFMWNW0001, ZFMNNE0869, and ZFMNW0805A deformation zones and then laterally via horizontal to gently dipping structures and fractures towards the existing SFR facility (Figure 7-19).

Due to groundwater/rock interaction, the Baltic Sea water composition is changed and the resulting groundwater in the bedrock is referred to as Local Baltic Sea type groundwater, see Chapter 8 for details. However, the existing SFR facility seems to have a channelised hydraulic contact with ZFMNW0805A and B (Northern boundary belt) and poor contact with ZFMNNE0869, since groundwater with a considerable fraction of older marine water, referred to as Littorina groundwater type (which includes also a glacial melt-water component), is still present in the gently dipping ZFM871 at its connection with the vertical ZFMNW0805A and ZFMNNE0869 zones. Generally, all borehole intersections representing zone ZFM871 have a larger marine component and are more saline compared with the brackish-glacial groundwaters present above and below the zone.

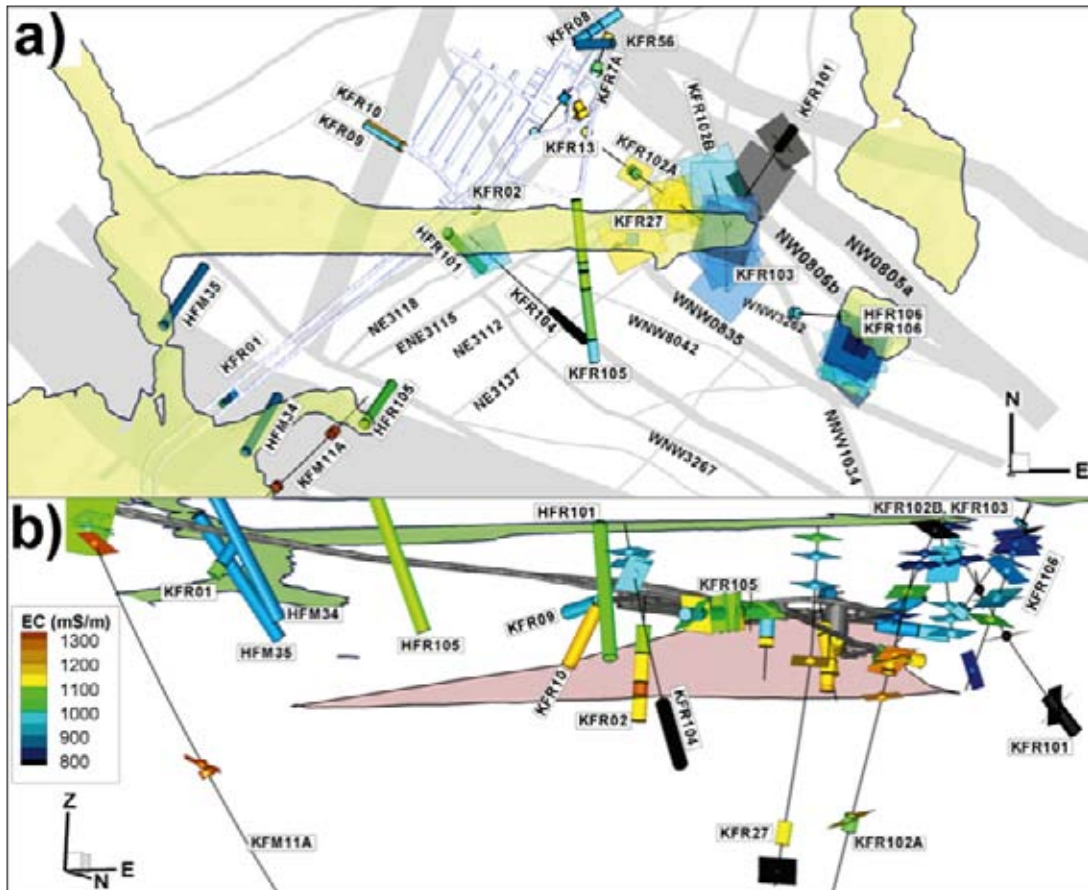


**Figure 7-19.** Present water types (cf. Chapter 8 for definitions); a) top view and b) side view towards the northwest. The reference water types are Local Baltic (B; blue), Littorina (L; cyan), Brackish glacial (G; red), and Mixed transition (T; yellow).

This may possibly be linked to the heterogeneous character of ZFM871, as well as to grouting. The remnants of older water types in the bedrock, despite tunnel inflow, suggest either poor fracture connectivity to the sea and/or compartmentalised fracture systems.

It is noted that a large number of samples that could not be definitively assigned to one of the above three water types were assigned to a fourth groundwater type called mixed transition type groundwater. This is not a specific water type; rather, it reflects water significantly influenced by mixing of glacial and brackish marine waters of different ages. The mixed transition type waters are present at depths from about  $-60$  to  $-400$  m and have become more frequent over the last two decades as indicated by the long-time-series data. This is probably a result of the changing hydrogeological conditions in the SFR area influenced by drawdown inflow to the tunnels (Figure 7-19). In conclusion, the description of the spatial distribution of different water types is not readily generalised, since there a strong influence appears to be exerted by the spatial variability of the structural-hydraulic properties.

Besides individual chemical constituents, the hydrogeochemical programme also measures the electrical conductivity of the groundwater. During the entire observation period (1988–2010), the observed electrical conductivity (EC) values in the monitored older boreholes have been in the range  $600$ – $1,600$  mS/m (Figure 7-20), which corresponds to a chloride concentration range of approximately  $1,500$ – $5,500$  mg/L. (By comparison, Baltic Sea water has a salinity of about  $2,800$  mg/L of Cl, or an EC value of c.  $890$  mS/m.) With few exceptions, most shallow data (above  $-100$  m) have EC values that are within the range  $900$  to  $1,000$  mS/m (Figure 7-20). The EC values in the boreholes that intersect the sub-horizontal zone ZFM871 below the existing SFR facility are in the range  $1,100$  to  $1,300$  mS/m and are related to a varying contribution of Littorina Sea water, resulting in the Littorina type or the mixed transition type of groundwater (close to the Northern boundary belt or ZFMNNE0869 and at distance from the Northern boundary belt, respectively). Remarkably, less saline water has been found below more saline water in several boreholes, KFR02, KFR101, KFR102A, KFR104, KFR106, and KFR27 (Figure 7-20), and at the bottom of boreholes KFR101 and KFR104, the salinity was even lower than in the Baltic Sea. This is an unusual observation since salinity normally increases with depth. Hence, there is a strong indication of the preservation of isolated non-saline palaeoclimatic water types in parts of the bedrock outside deformation zones. This reinforces the conceptual structural-hydraulic interpretation of a predominantly horizontal to gently dipping flowing fracture network with limited vertical fracture connectivity outside the vertical zones.



**Figure 7-20.** Electrical conductivity (EC) measurements; a top view and b) side view looking towards the north-west. EC from PFL flow logging shown as planes and EC from monitored borehole sections represented as cylinders. (A deep PFL-f-logged interval in KFR27 (409.6 to 435.6 m borehole length) is also represented by a cylinder).

Since 1988, the ongoing control programme for the existing SFR facility analyses the chemical composition of the drainage water that is pumped from the UB and NDB pumping pits shown in Figure 7-6. Water samples are analysed four times per year. Although the control programme is not as elaborated as the investigation programme for SDM-PSU, the results from the two pumping pits confirm the general picture described above, i.e. a slowly decreasing presence of water of Littorina groundwater type and a slowly increasing presence of a Local Baltic Sea groundwater type.

### 7.2.5 Orientation and intensity of open fractures

The existing SFR facility and the rock volume directly to the southeast, which is proposed for the extension, is situated within two rock domains, RFR01 in the southwest and RFR02 in the northeast. A central question is whether the rock domain model justifies lateral subdivision of the rock mass into separate HRDs. In terms of frequency of different fracture types, the difference between RFR01 and RFR02 is deemed to be minor, see Table 7-1 and Section 4.2.2 in Öhman et al. (2012) for details.

**Table 7-1. Mean fracture frequency of mapped drill core outside deformation zones per rock domain. Modified from Table 4-9 in Curtis et al. (2011).**

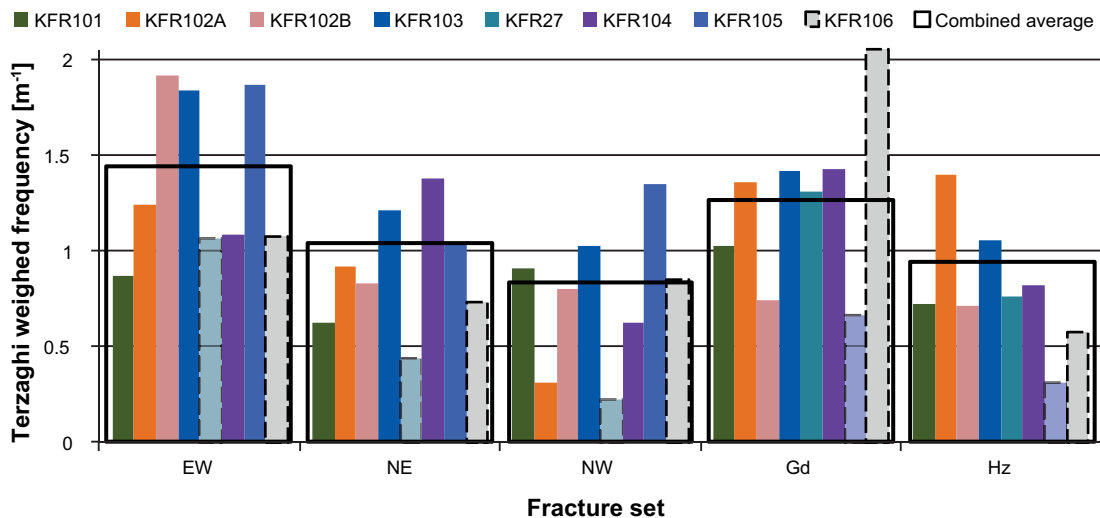
Rock domain	A. Open fractures (m <sup>-1</sup> )	B. Partly open fractures (m <sup>-1</sup> )	C. Crush equivalent (m <sup>-1</sup> )	Total A–C (m <sup>-1</sup> )	D. Sealed fractures (m <sup>-1</sup> )	E. Sealed network (m <sup>-1</sup> )	Total D–E (m <sup>-1</sup> )
RFR01	3.32	0.24	0.01	3.57	5.75	7.43	13.18
RFR02	3.44	0.33	0.05	3.82	10.14	3.35	13.50

The stereonet shown in Figure 5-8 reveal a clear difference in orientation patterns between open and partly open fractures versus sealed fractures: sub-horizontal to gently dipping fractures are predominantly open and partly open, whereas steeply dipping fractures are predominantly sealed. There are several explanations for this, related to the anisotropic stress regime, fracture genesis and age, see Chapter 5, Glamheden et al. (2007) and Martin and Follin (2011) for details.

Figure 5-9 reveals weak vertical trends in the fracture frequency of all fractures in the rock masses lying outside the deformation zones. Gaps in borehole coverage complicate inferences regarding the determination or significance of depth trends in fracture frequency. For example, the lower half of the elevation range shown in Figure 5-9 (below  $z = -308$  m elevation) is only covered by two boreholes KFR27 and KFR102A. In addition, there are two issues concerning the confidence of the vertical borehole KFR27 data: firstly, the unfavourable sampling bias of vertical fractures, which are primarily sealed, and secondly, the borehole is interpreted as lying within or bounding a deformation zone ZFMWNW0835. Similarly, there is an unfavourable sampling bias of sub-horizontal fractures in the sub-horizontal borehole KFR105.

In summary, the stereonet shown in Figure 5-8 suggest that horizontal to gently dipping fractures within the local model domain occur both inside and outside the deterministically modelled steeply dipping deformation zones. Secondly, the vertical trend in open fracture frequency shown in Figure 5-9 is weak. Thirdly, the benefit of a lateral division of the open fractures is judged to be minor.

In the final hydrogeological model of the bedrock version 1.0, open fractures are divided into five sets referred to as EW, NE, NW, GD (gently dipping), and HZ (sub-horizontal). Further, the weak vertical trend is differentiated into three depth intervals according to intensity: the Shallow bedrock HRD (above  $-60$  m), the Repository level HRD ( $-60$  to  $-200$  m), and the Deep bedrock HRD (below  $-200$  m), see Appendix 5 for details. The intensity of open fractures inside the three HRDs decreases weakly with depth (cf. Figure 5-9). Since the Repository level HRD has the best total borehole coverage, this domain provides the best basis for detailed intensity calculations. In this interval, the intensity of open fractures was calculated for each fracture set and for each borehole, see Figure 7-21. The sets have similar intensities at repository level, approximately  $1 \text{ m}^2/\text{m}^3$  for each set (cf. Figure 5-9).



**Figure 7-21.** Set-wise open fracture intensity in the interval  $-60$  m to  $-245$  m. A combined average was calculated for each set weighted by borehole length. To mitigate structural biases, boreholes/data parallel to the fracture sets were excluded. The boreholes excluded in each set-average calculation are shown by dashed lines. For instance, KFR106 was excluded for all sets as it is affected by its proximity to the Northern boundary belt; steeply dipping data in KFR27 were excluded for the steeply dipping fracture sets as KFR27 is drilled within/alongside a steeply dipping deformation zone; and the gently dipping data in KFR105 was excluded for the gently dipping fracture sets as the borehole is gently dipping.



Open fractures exhibit local heterogeneity, but spatial trends in open fractures inside the local model domain are not judged to be significant in relation to gaps in borehole coverage, see Appendix F in Öhman et al. (2012) for details. The decrease in intensity of open fractures with depth is small and the set-wise intensity varies only slightly between boreholes, although this may well be an artefact of local heterogeneity and gaps in borehole coverage. The cored borehole data acquired outside the local model area, i.e. in boreholes KFM11A and KFR106, are not judged to be representative of the HRDs in the SFR regional model area, since they are influenced by the Southern and Northern boundary belts, respectively.

The SFR model domain has high open fracture intensity in HRDs, relative to the observations made in SDM-Site Forsmark (Table 7-2). In SDM-Site Forsmark, a significant contrast was found between the intensively fractured uppermost c. 200 m (FFM02) and the sparsely fractured tectonic lens below (FFM01). No such stark contrast is observed at SFR; rather, the decline in open fracture intensity with depth is small. It should be noted that fracture domain FFM02 at SDM-Site Forsmark is mainly covered by borehole data below –100 m RHB70. Thus, for the uppermost part of the bedrock ( $z \geq -200$  m RHB70), the difference between the two sites may be smaller in actuality than is indicated by Table 7-2. In order to ensure consistency in the comparison between the two sites, the intensities are both Terzaghi-compensated with a maximum weight of 7 (i.e. a minimum bias angle of 8.2°). Furthermore, no steeply dipping, NS-striking set has been defined at SFR; for comparative purposes it may be considered as part of the NE and NW sets at SFR.

Note that the total intensities in Table 7-1 are different from those reported in Table 7-2. There are three reasons for this:

- the values in Table 7-1 are only Terzaghi-compensated with a maximum weight of 3.8 (or a minimum bias angle of 15°),
- borehole sections falling outside RFR01 and RFR02 are excluded in Table 7-1, and
- the geometrically biased sets were excluded in Table 7-2 (cf. “combined average” in Figure 7-21).

## 7.2.6 Single-hole hydraulic tests

Three different sources of single-hole test data have been used in version 1.0 of the hydrogeological model (Figure 2-1):

1. Hydraulic data acquired in the old boreholes drilled in the vicinity of the existing SFR facility (various types of short-term, classic hydraulic double-packer tests conducted between 1980 and 1986).
2. Hydraulic data acquired in boreholes drilled in the vicinity of the Singö deformation zone (impeller flow logging (HTHB) and difference flow logging (PFL-f) tests conducted in 2006 and 2007).
3. Hydraulic data acquired in the new boreholes drilled in the area of the planned extension of the existing SFR facility (impeller flow logging (HTHB) and difference flow logging (PFL-f) tests conducted 2008 and 2009).

**Table 7-2. Comparison of open fracture intensity in HRDs with SDM-Site Forsmark.**

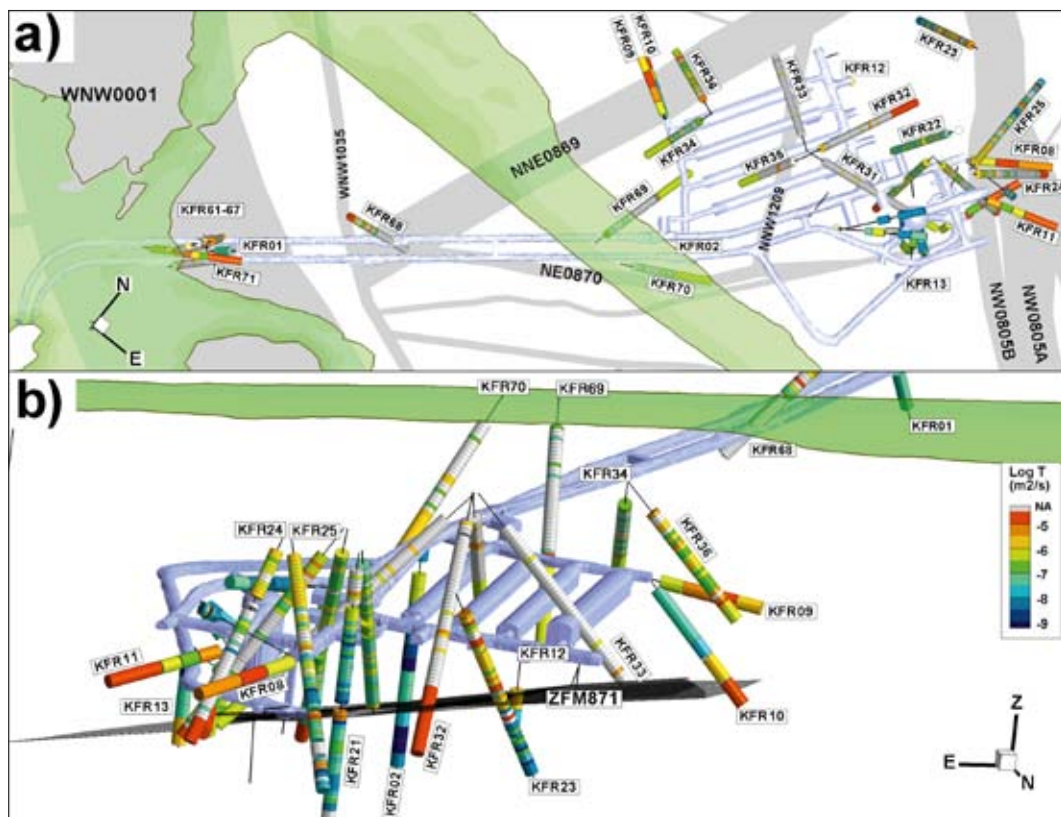
Set	Upper bedrock, $z \geq -200$ m (RHB70)		Deeper bedrock, $z < -200$ m (RHB70)	
	SDM-Site Forsmark (FFM02)	SFR extension (all core data)	SDM-Site Forsmark (FFM01)	SFR extension (all core data)
NS	0.34	NA	0.07	NA
EW	0.16	1.58	0.09	1.07
NE	0.75	1.06	0.32	1.03
NW	0.34	0.84	0.11	0.67
HZ (+ Gd)	1.58	2.29	0.54	2.24
Total	3.2	5.8	1.1	5.0

It is noted that the different types of single-hole test data differ in quality and cover different parts of the SFR model domain. Fundamental weaknesses of the old hydraulic data set are the lack of fracture orientations and the poorer (higher) hydraulic measurement threshold. Hence, the old data set is primarily used for conceptual understanding and as a complementary data set for deformation zone parameterisation, particularly in the near field of the existing SFR facility, see Figure 7-22. The following zones are associated with hydraulic data from the old data set: ZFMNW0805A and –B, ZFMNE0869, ZFM871, and ZFMNNW1209.

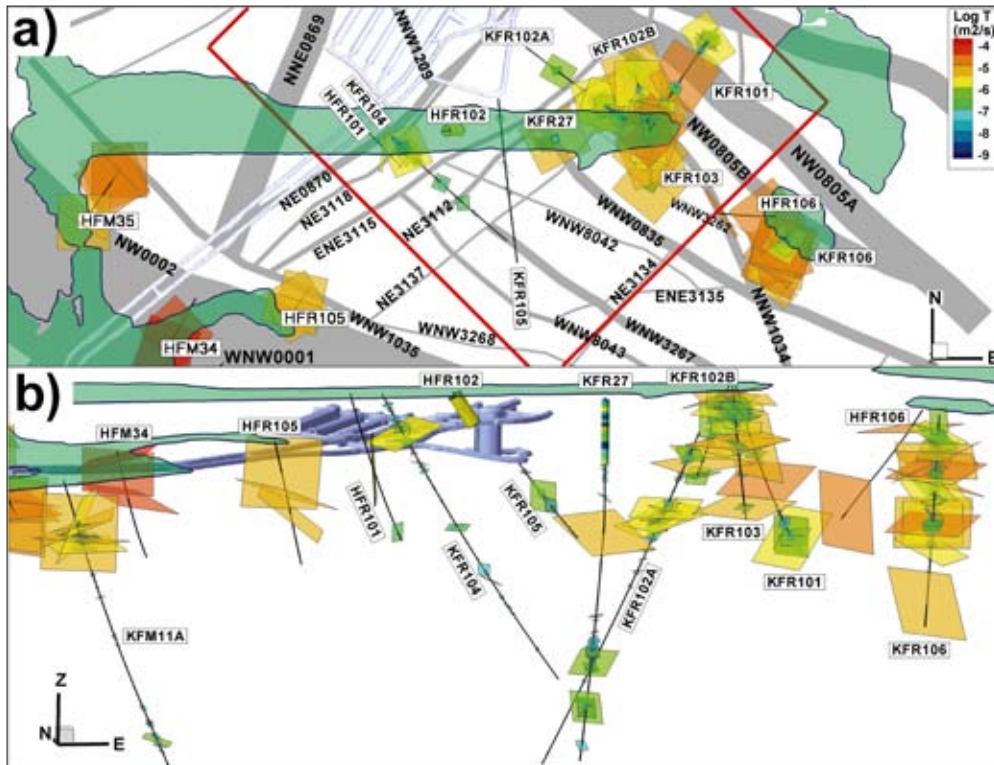
By contrast, the new hydraulic data set conforms to SKB’s current quality standards and requirements in terms of traceability. Furthermore, it provides orientations of flowing fractures (PFL-f). This information is a cornerstone for the assignment of hydraulic properties to the HRDs by means of hydrogeological DFN modelling. Thus, the recent data set is judged to be considerably more useful for the parameterisation of site-specific properties inside the SFR model volume.

A large-scale, lateral pattern in PFL-f data seems to exist that is related to the Southern and Northern boundary belts (Figure 7-23). Transmissivities greater than  $10^{-6}$  m<sup>2</sup>/s are only found close to these geologically defined borders. High transmissivities are absent in the data acquired with the Central block – at least below –60 m.

The data interpretation must account for borehole locations and their representativeness of the domain. Four of the cored boreholes originate from the same starting point at the tip of the pier, KFR101, KFR102A, KFR102B, and KFR103; these boreholes are all close to the Northern boundary belt. Similarly, KFR106 and HFR106 drilled from the islet southeast of the Pier are also close to the Northern boundary belt. The Central block, which is the target area for the SFR extension, has considerably less borehole coverage, particularly in terms of the evaluation of horizontal to gently dipping PFL-f data. In particular, there are no data in the southern corner of the SFR local model area (Figure 2-10).



**Figure 7-22.** Single-hole hydraulic data from the old data set in the vicinity of the existing SFR facility: a) top view with the traces of modelled deformation zones and b) side view towards the south, along the dip of ZFM871. Note that ZFMNE0870 dips towards the NW and intersects the construction tunnel (BT; Bygg Tunnel), more or less, over its entire length.



**Figure 7-23.** Transmissivity data from the SFR extension investigation: a) top view and b) side view looking north. Injection test data in HFR102 and 5 m sequential PFL data in KFR27 are shown as cylinders. PFL-f data (KFR-boreholes) and HTHB data (HFR boreholes) are shown as fracture planes sized according to the transmissivity-size relationships estimated in Öhman et al. (2012). Note that estimated orientations for HTHB data are uncertain. The SFR local model domain is shown by red lines.

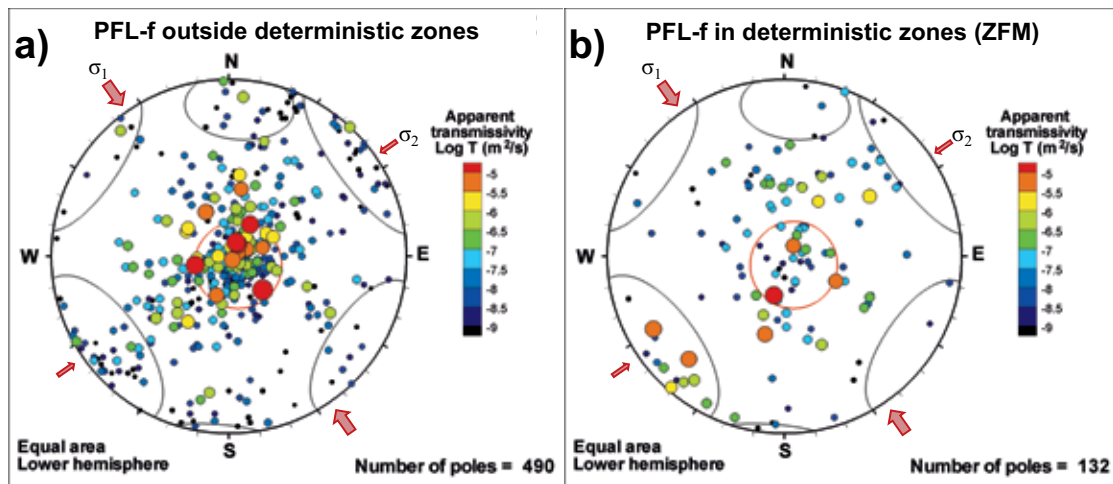
The properties of the Central block are mainly studied via KFR104, and with some deficiencies KFR105, KFR27 and HFR101. KFR105 is sub-horizontal, entailing a sampling bias for the important sub-horizontal hydraulic features. No core is available in the upper 148.5 m of KFR27, and the borehole is located more or less within/alongside the steeply dipping ZFMWNW0835. HFR101 only has two HTHB records and is not useful for hydrogeological DFN parameterisation.

Flowing fractures detected by the PFL-f method are assigned hydraulic properties and divided into the same fracture sets as those defined for the open fractures (Figure 7-21). The pattern of flowing fractures inside the ZFMs (HCDs) is similar to that outside the ZFMs (Figure 7-24). That is, the hydraulically active fractures in the steeply dipping deformation zones are primarily horizontal to gently dipping, followed by the steeply dipping NW-SE striking fractures. The pattern is seen outside the ZFMs.

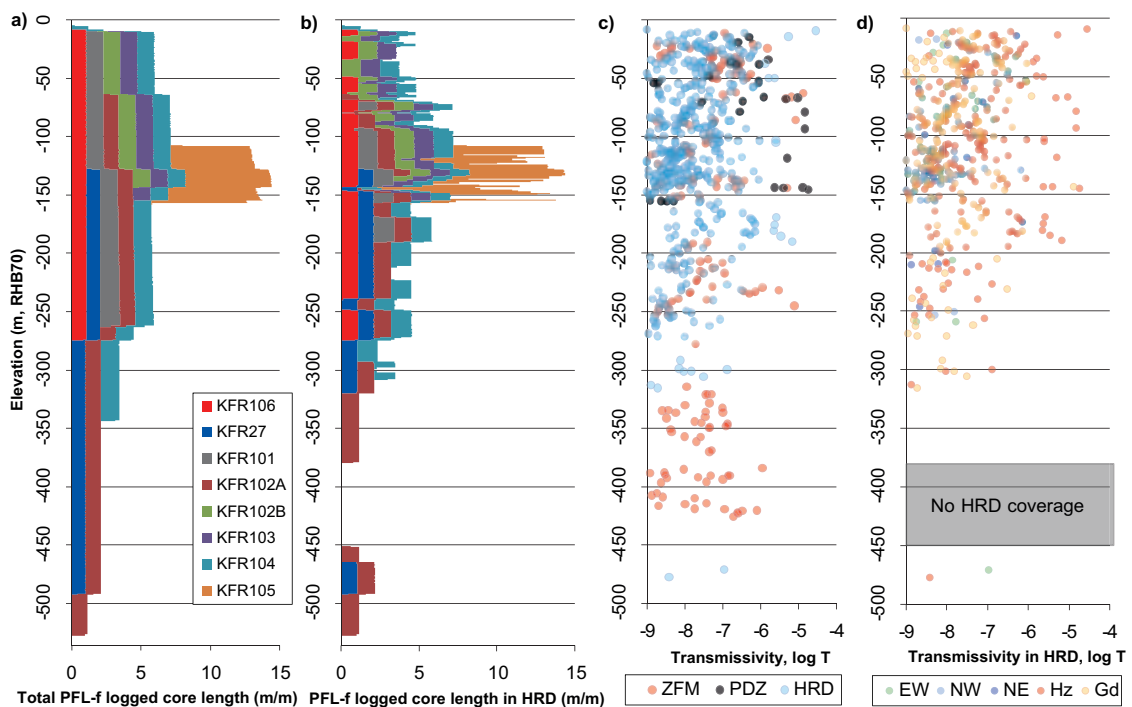
The majority of the flowing fractures detected by the PFL method above  $-200$  m elevation, particularly the largest transmissivities ( $T > 10^{-6}$  m<sup>2</sup>/s), are sub-horizontal to gently dipping (Figure 7-25d). Outside the deterministic zones, the most transmissive features within this interval are associated with horizontal to gently dipping unresolved PDZs (Figure 7-25c and d)<sup>6</sup>. According to Section 5.2.5, this is consistent with the conceptual understanding of the geological processes active at the site in connection with the formation of horizontal to gently dipping fractures.

The differences in transmissivity between the gently and steeply dipping fractures in the PFL-f data appear to be correlated to the rock stress model presented in Chapter 6 (Table 6-11). The maximum horizontal stress at Forsmark is trending at approximately  $145^\circ$  and the magnitude of the maximum horizontal stress is approximately 1.5 times the minimum horizontal stress. Hence, steeply dipping fractures could be subjected to significantly different normal stresses depending on their orientation.

<sup>6</sup> The depth interval  $> -200$  m is the same as that of the shallow bedrock aquifer (SBA) modelled in SDM-Site Forsmark. However, the most transmissive horizontal sheet joints contained in the SBA in SDM-Site Forsmark are about 50–100 times more transmissive than the most transmissive unresolved PDZs observed within the SFR extension investigation.



**Figure 7-24.** Orientations of fractures detected by PFL method with respect to stress-field; a) outside deterministic deformation zones and b) inside deterministic deformation zones (ZFM). The horizontal principal stress orientations ( $\sigma_1$  and  $\sigma_2$ ) shown by red arrows (cf. Table 6-11). Hard sectors representing fracture set clusters included for reference.



**Figure 7-25.** Borehole coverage and PFL-f transmissivity with depth: a) total core length of PFL-f logging binned by elevation and borehole, b) core length of PFL-f logging outside deterministically modelled deformation zones (ZFM) binned by elevation and borehole, c) PFL-f data divided by ZFM, unresolved PDZ and HRD, and d) PFL-f data outside ZFM divided by fracture set. Note that the sub-horizontal underground borehole KFR105 makes a large contribution to PFL-f logged core length in the interval  $-105$  to  $-157$  m RHB 70 (orange bars).

The rock stress model shown in Table 6-11 suggests that the maximum horizontal stress varies approximately between 5 and 33 MPa in the uppermost 0–400 m of the bedrock, whereas the vertical stress varies approximately between 0 and 11 MPa. According to Indraratna et al. (1999), little or no decrease in transmissivity occurs when the confining stress on laboratory samples exceeds 10 MPa. Hence, because of the 10–33 MPa stress range for the steeply dipping NW-SE striking deformation

zones, the transmissivity values may not exhibit any relationship with the normal stress below approximately –100 m elevation (Figure 7-25b). However, the majority of the horizontal to gently dipping fractures and deformation zones are subjected to normal stresses ranging from 1 to 11 MPa, which according to Indraratna et al. (1999) is the range in which the normal stress should have a significant impact (Figure 7-25d).

### **7.3 Hydrogeological model for the bedrock – conceptualisation and modelling methodology**

The evaluation of primary data presented in Section 7.2 creates notions and hypotheses about the hydrogeological system in the SFR local model domain. The essence of the conceptual hydrogeological model of the bedrock version 1.0 is summarised below.

#### **7.3.1 Inflow and groundwater levels**

The SFR model area is predominantly submerged, i.e. located below the Baltic Sea. In principle, this would result in very low natural hydraulic gradients in the bedrock. However, due to the drainage of the existing SFR facility, which was taken into operation in 1987, hydraulic gradients have developed towards the depressurised tunnel system. The deepest parts of the existing SFR facility reach approximately –140 m elevation, and all monitored borehole sections in the bedrock reveal disturbed groundwater levels (heads), i.e. they are more or less affected by the drainage of the existing SFR facility, although some drawdowns are difficult to distinguish due to sea level fluctuations. The distance to the most remote borehole within the investigation area is approximately 700 m.

The existing SFR facility is located in the Central block but closer to the wedge between the Northern boundary belt and the Southern boundary belt. In general, drawdown decreases with distance from the existing SFR facility (both laterally and vertically). The lateral extension of the drawdown appears to propagate mainly along the gently dipping ZFM871 and the Northern boundary belt. The drawdowns seen in the Southern boundary belt are probably mainly due to inflow into the access tunnels where they cross the Singö deformation zone at a shallow depth. However, at greater depth, the conceptual model is more uncertain as the drawdown in KFM11A is very large. In addition to a disturbance from the crossing of the Singö deformation zone by the access tunnels, the possibility of an influence on the inflow to the existing SFR facility due to a larger size of ZFM871 than modelled cannot be excluded.

The decreasing trends in both inflow and heads are indicative of ongoing sealing processes. However, since no grouting has occurred after the completion of the existing SFR facility, the decreasing trend of inflow is due to other mechanisms, see Section 7.2.1. The site investigation did not investigate the listed processes in particular, but it is imagined that the key explanation is a compartmentalised fracture network with predominantly horizontal to gently dipping features together with an increase in effective normal stress as the pore pressures decrease due to drainage. Two-phase flow and chemical precipitation probably contribute, but these processes are assumed to occur predominantly in the proximity of the tunnel interface where atmospheric conditions prevail.

#### **7.3.2 Transmissivity in the bedrock along HCDs**

The geological model of the bedrock in the SFR area version 1.0 (Curtis et al. 2011) is a refinement of the regional SDM-Site Forsmark geological model (Stephens et al. 2007). The conceptual hydrogeological model version 1.0 for the bedrock contained inside the local SFR model domain encompasses:

- The three major tectonic units defined in the bedrock geological model version 1.0: the Northern boundary belt, the Southern boundary belt and the Central block.
- Twenty-seven steeply dipping hydraulic conductor domains (HCD). These coincide with deterministically modelled deformation zones (ZFM).
- One hydraulic gently dipping conductor domain (HCD) coinciding with a deterministically modelled deformation zone (ZFM871).

In SDM-Site, an exponential model was formulated for the depth dependency in HCD transmissivity (Follin et al. 2007b):

$$T(z) = T_0 10^{-z/k} \quad (7-1)$$

where  $T(z)$  is the transmissivity at elevation  $z$ ,  $T_0$  is the expected transmissivity at zero elevation, and  $k$  is a depth trend parameter that defines the depth interval over which the transmissivity decreases by one order of magnitude. The value of  $T_0 = T(0)$  can be calculated by inserting a measured value  $T(z')$  at the intercept elevation  $z'$ :

$$T_0 = T(z') 10^{-z'/k} \quad (7-2)$$

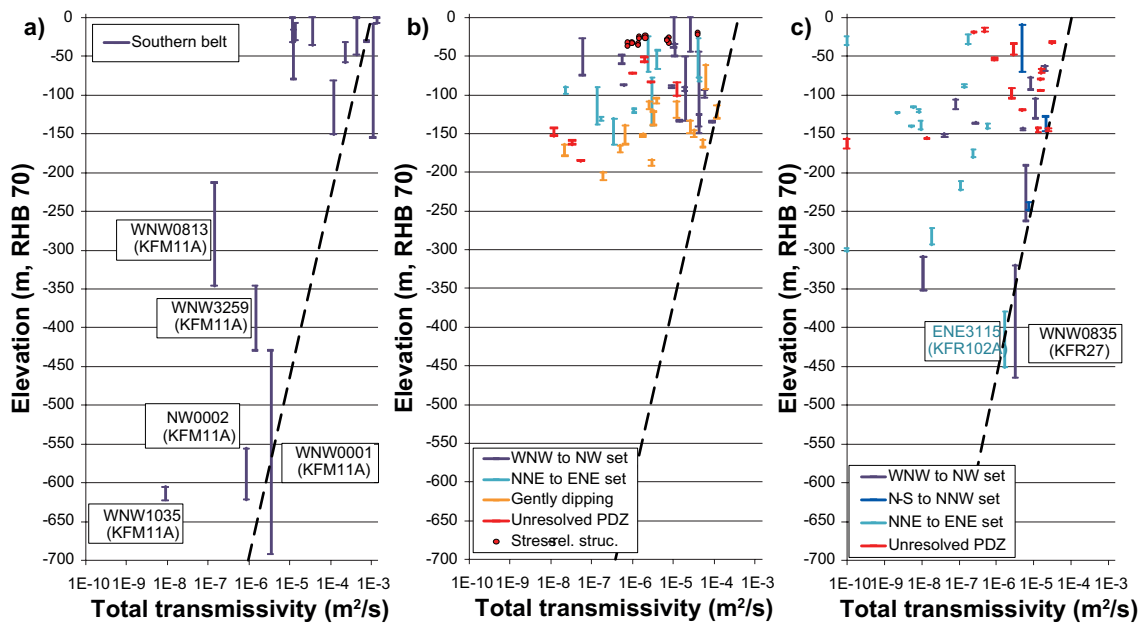
HCD transmissivity at zero elevation,  $T_0$ , is calculated for each intercept elevation. A geometric mean  $T_{\text{eff}}(0)$  and a log-normal standard deviation are calculated for each HCD in cases where several intercepts exist. Using the same approach, a global geometric mean and a standard deviation of all intercepts for all HCDs can be calculated for each HCD set. In SDM-Site, a common value of the depth trend parameter was used for all sets and the lateral heterogeneity around the deterministic depth trend model was simulated by adding a log-normal random deviate to the exponent in Equation (7-1):

$$T(x, y, z) = T_{\text{eff}}(0) 10^{z/k + N(0, \log(T))} \quad (7-3)$$

Equation (7-3) can be used for modelling heterogeneity within the HCDs, but requires that  $k$  is known. In SDM-Site, the value of the depth interval parameter was determined to be 232.5 m and the value of the log-normal standard deviation was determined to be 0.635. In order to account for structural differences when comparing the data acquired in the SFR extension investigation with the depth-dependency trend model at Forsmark, data were divided into three sub-groups:

- the Southern boundary belt data set (Figure 7-26a),
- the old hydraulic data set acquired near the existing SFR facility (Figure 7-26b), and
- the new hydraulic data set acquired to the southeast of the existing SFR facility (Figure 7-26c).

Data for the Southern boundary belt HCD intercepts (Figure 7-26a) were obtained from SDM-Site Forsmark (boreholes HFM34, HFM35, and KFM11A) as well as older data from the construction of the existing SFR facility (boreholes KFR61, KFR62, KFR64, KFR65, KFR67, KFR68, and KFR71).



**Figure 7-26.** The sum of the transmissivity values inside the bounds of each HCD intercept is plotted here for the interval 0 to –700 m elevation: a) Southern boundary belt intercepts, b) old data, and c) new data set. The depth trend model from SDM-Site Forsmark (black dashed line in all diagrams),  $k = 232.5$  m, Equation (7-1), has been fitted to the maximum values of each data set. Transmissivity below the detection limit is shown as  $10^{-10}$  m<sup>2</sup>/s.

The shallow HCD transmissivities in Figure 7-26a are incomplete, since the borehole intercepts penetrate only a part of the modelled zone thickness. Nevertheless, the shallow intercept transmissivities are extremely high ( $T_{\text{HCD}} > 10^{-4} \text{ m}^2/\text{s}$ ). These shallow values may reflect sheet joints of the same type that were found in SDM-Site Forsmark. However, such extremely high transmissivity values at shallow depths have not been found north of the Southern boundary belt within the SFR regional model area (Figure 7-26b and Figure 7-26c). At depth in the Southern boundary belt, the available transmissivity data are also incomplete due to partial penetration. The only exception is the 579 m long PDZ interval referred to as KMF11A\_DZ1 in the geological single-hole interpretation. The information in this interval is complex and the intersection with ZFMWNW0001 is affected by splays of other zones occurring within the Southern boundary belt.

North of the Southern boundary belt, the largest transmissivities in the old data set (Figure 7-26b) are found among the WNW-to-NW-striking HCDs forming the Northern boundary belt, ZFMNNE0869, and the gently dipping structures forming the gently dipping ZFM871. However, the vertical span of the old data set, 0 to -200 m, is insufficient for determining depth dependency.

The data from the SFR extension investigation has somewhat larger vertical data coverage (Figure 7-26c). The largest transmissivities are found among the WNW-to-NW-striking HCDs forming the Northern boundary belt, and ambient deformation zones, i.e. ZFMNNW1034 and ZFMWNW3262, as well as among the more or less horizontal to gently dipping unresolved PDZs.

In conclusion, the gently dipping structures, along with the WNW-striking HCD set, are in general more transmissive than the NNE-to-ENE-striking HCD set. This observation agrees well with the observations previously reported for SDM-Site Forsmark (Follin 2008).

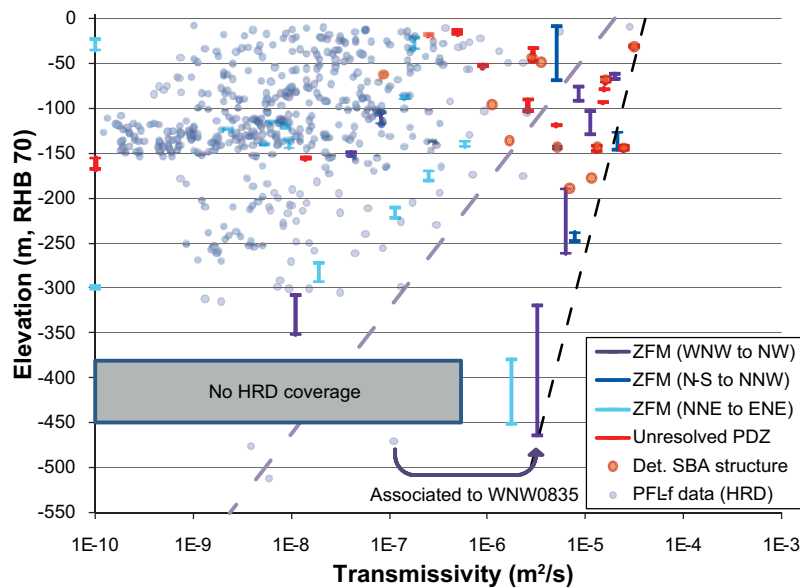
It will be recalled that the value of the depth trend parameter,  $k = 232.5 \text{ m}$ , derived in SDM-Site Forsmark (Follin et al. 2007b), represents the depth trend of the maximum transmissivities observed at each elevation regardless of HCD set, i.e. it does not represent a statistical regression of the transmissivity data acquired within each HCD set. According to Figure 7-26a, b and c, a similar value of the depth trend parameter also appears to be applicable to the most transmissive HCD data at each elevation within the SFR local model area. However, the determination of the lateral variability around this depth trend model is uncertain. The key uncertainties in this respect concern the modelling of the NNE-to-ENE-striking HCD set and the gently dipping deformation zone ZFM871, both of which appear to be quite heterogeneous.

An alternative to using a common depth trend parameter for all HCD sets is to use set-specific depth trend models for each HCD set. For instance, both the NNE to ENE striking HCD (Figure 7-26c) set and the gently dipping ZFM871 (Figure 7-26b) appear to show stronger depth dependencies.

### 7.3.3 Transmissivity of fractures in the bedrock outside HCDs

The maximum borehole coverage outside HCDs in the new data set is found in the depth interval -100 m to -150 m, with approximately 13 m of PFL-f logged core length per vertical metre (Figure 7-25b), with the sub-horizontal KFR105 contributing the most. Below -300 m, the average borehole coverage outside HCDs is only 1.0 m PFL-logged core per vertical metre. In the interval -380 to -450 m, there is no data coverage at all outside HCDs, since both KFR27 and KFR102A intercept deformation zones (ZFMWNW0835 and ZFMENE3115, respectively; Figure 7-26c) in this interval. The PFL-f data from different boreholes are treated here as a homogenous population. Hence, there is a risk that gaps in borehole coverage with depth, in combination with local heterogeneity and lateral trends, have erroneously been interpreted as a depth trend.

The most transmissive PFL-f data in Figure 7-27 are from horizontal to gently dipping fractures (dip angle less than  $40^\circ$ ) and seem to have a depth trend parameter similar to that of the NNE-to-ENE-striking HCD set; the grey line represents a depth trend parameter of  $k = 140 \text{ m}$  for the largest PFL-f transmissivities outside deformation zones, which is the same value as was fitted to the old data set in hydrogeological model version 0.1, previously reported in Öhman and Follin (2010a).



**Figure 7-27.** Transmissivity of various geological features by elevation, HCDs and outside HCDs, i.e. unresolved PDZs, SBA-structures and HRD. The depth trend model from Forsmark, Equation (7-1) with  $k = 232.5$  m, is represented by a black line, and the HRD depth trend model from Öhman and Follin (2010a) is shown with a grey line. Both trend lines are evaluated for the maximum values in each data set by elevation. The Silo and the four rock caverns (black silhouettes) are included for vertical reference only. Only PFL-f data from the recent data set are shown in this plot.

#### Recognition of the HRD data sets – Unresolved PDZs, SBAs and residual HRDs

Figure 7-28 shows a preliminary layout of the SFR extension relative to the existing facility and the local model area, together with the Forsmark site investigation boreholes and the boreholes from the SFR extension drilling campaign. In Figure 7-29 and Figure 7-30, boreholes HFR101, KFR104 and KFR105 are referred to as Group 1 and boreholes HFR106, KFR101, 102A, 102B, 103, and 106 are referred to as Group 2. Borehole HFR102 is excluded because it is short (55 m) and no impeller flow logging was performed. Borehole KFR27 is excluded because of data uncertainties since it is partially drilled within and partially outside an inferred steeply dipping deformation zone, ZFMWNW0835.

The lateral contrasts in transmissivity between the Central block data set (Group 1) and the data set closest to ZFMNNW1034 and the Northern boundary belt (Group 2) are compared in Figure 7-29. The difference between the two data sets is striking and clearly more pronounced than the contrast between HCD transmissivity and HRD transmissivity for each tectonic unit alone. As shown in Figure 7-30, the suggested modelling of SBA-structures and unresolved PDZs along ZFMNNW1034 and the Northern boundary belt have a profound impact on the data set intended for HRD modelling.

Figure 7-31a shows the Terzaghi-weighted flowing fracture intensity distribution outside deterministically modelled deformation zones (HCDs) in the depth interval  $-60$  to  $-200$  m RHB 70. Figure 7-31b shows the practical detection limit for the transmissivity measurements in each borehole. Since only PFL-f data are used for stochastic HRD modelling, Figure 7-32a and Figure 7-32b are compiled to show the effect of excluding all transmissivity data associated with percussion-drilled boreholes and all PFL-f transmissivity data associated with conditioned unresolved PDZs and SBA-structures. Among other things, this caused all PFL-f data in KFR106 to be excluded from Group 2 HRD. The data sets from the other boreholes containing PFL-f data associated with unresolved PDZs were only partially modified. In summary, Figure 7-31a and Figure 7-32a reveal that the transmissivity data in the two groups representing HRD data alone do not need to be distinguished from one another. Once all PFL-f data associated with unresolved PDZs are excluded, the PFL-f data in the two groups could be assumed to be statistically homogeneous.

In conclusion, unresolved PDZs, SBAs and the remaining flowing fractures have been treated as different compartments of the bedrock outside the HCDs. It is noted that the PDZs and SBAs are neither parts of the HRD concept nor the HCD concept shown in Figure 7-1 but treated separately. In the following, the hydrogeological conceptualisation and modelling of the three compartments are elaborated.



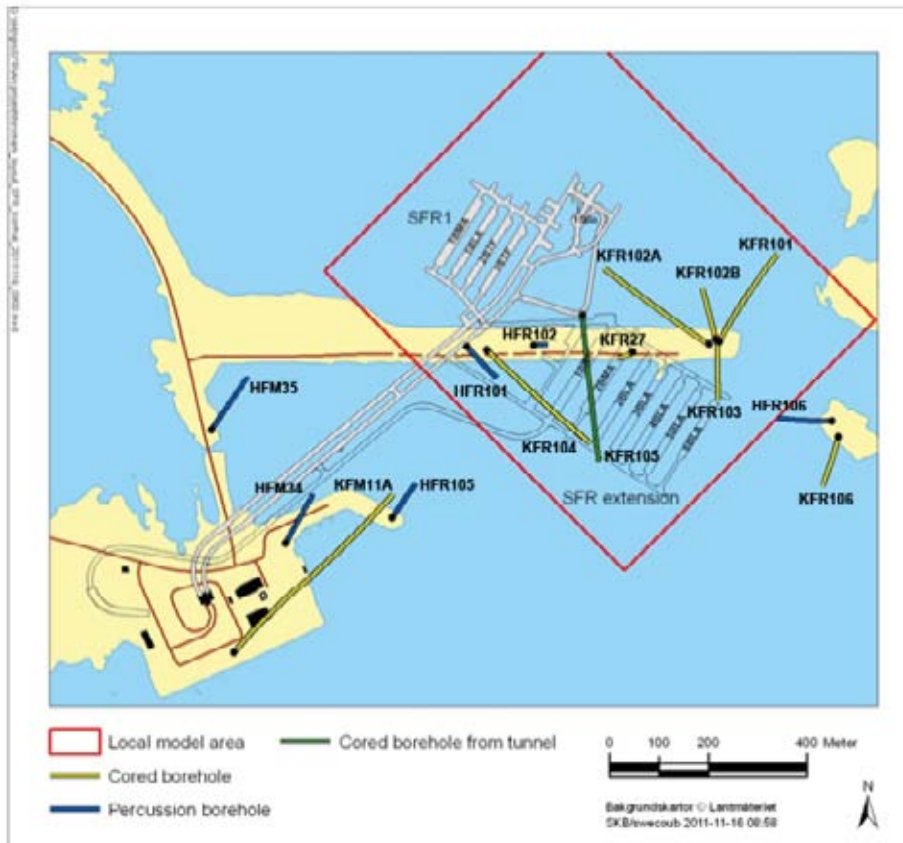


Figure 7-28. Preliminary layout of the SFR extension relative to the existing SFR 1 and the local model area together with the Forsmark site investigation boreholes and the boreholes from the SFR extension drilling campaign.

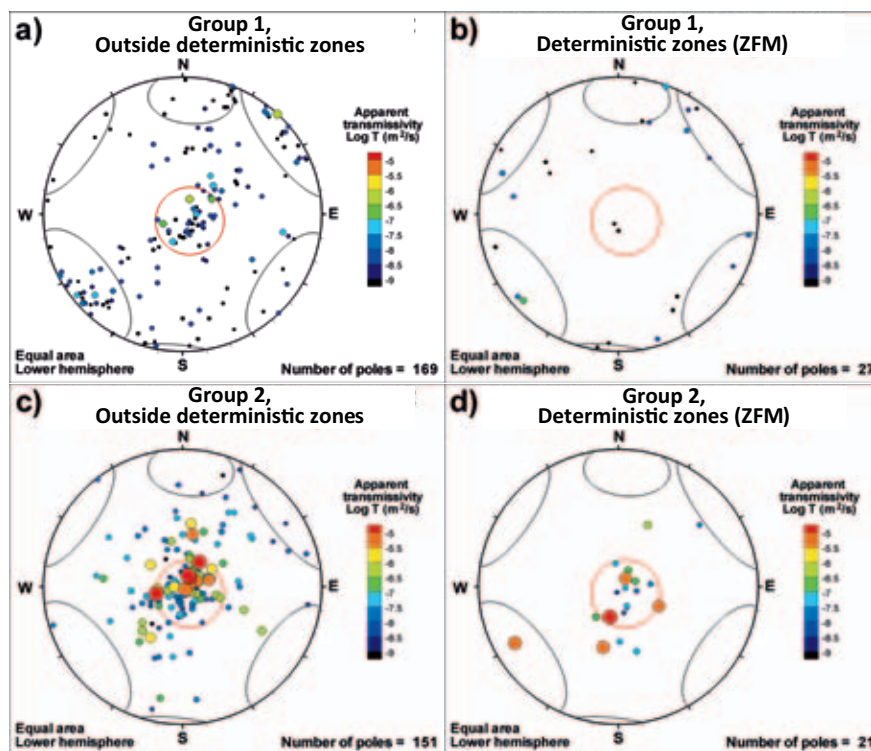
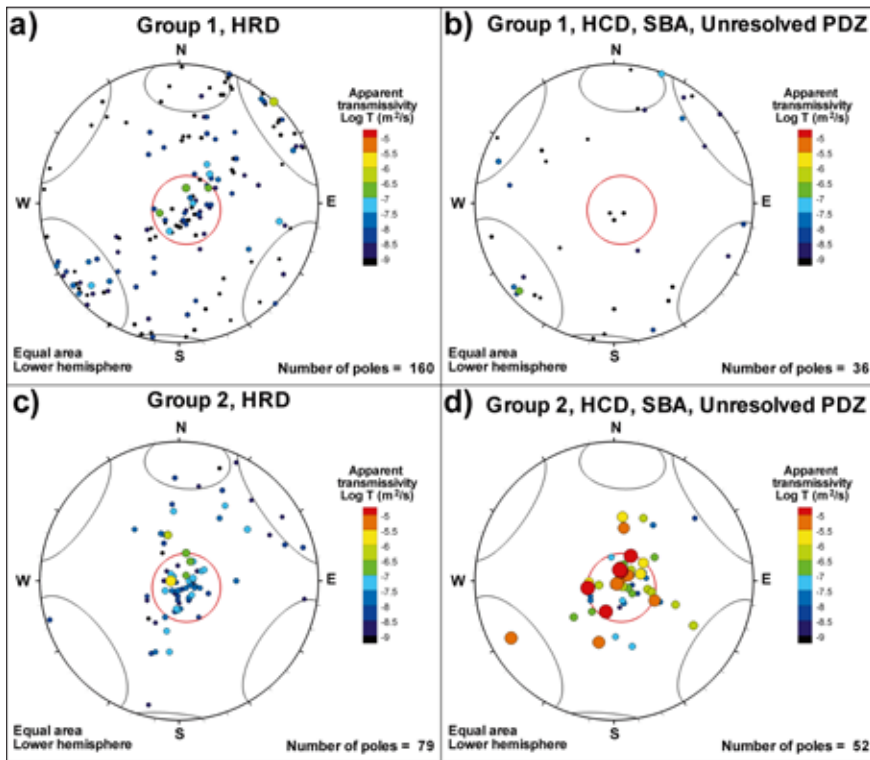
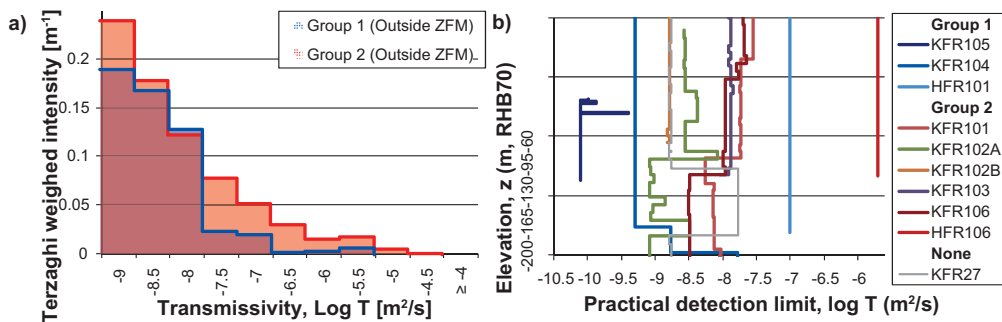


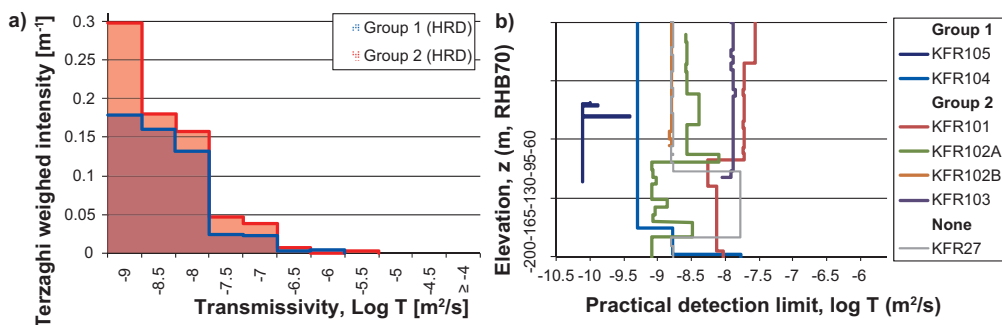
Figure 7-29. Comparison of PFL-f orientations at the Repository level HRD (-60 to -200 m) between Group 1 (KFR104 and KFR105) and Group 2 (KFR101, -102A, -102B, -103, and -106). Poles are coloured and scaled according to PFL-f transmissivity.



**Figure 7-30.** Comparison of PFL-f orientations at the Repository level HRD (-60 to -200 m) between a modified Groups 1 and Group 2, i.e. the data used for modelling of SBA-structures and conditioned unresolved PDZs are separated from the HRD data and plotted together with the HCD data. Poles are coloured and scaled according to PFL-f transmissivity.



**Figure 7-31.** Terzaghi-weighted flowing fracture intensity distribution outside deterministically modelled deformation zones (ZFM, i.e. HCDs) in the depth interval -60 to -200 m RHB 70: a) comparison between Groups 1 and 2, and b) practical detection limit.



**Figure 7-32.** Terzaghi-weighted flowing fracture intensity distribution in HRD (PFL-f data only) in the depth interval -60 to -200 m RHB 70: a) comparison between modified Groups 1 and 2, i.e. all data used for modelling of SBA-structures and conditioned unresolved PDZs are separated from the HRD and b) practical detection limit.

### **Modelling of unresolved PDZs**

The handling of the 31 unresolved possible deformations and the delineation of the so-called SBA-structures are cornerstones in the conceptual hydrogeological modelling of the bedrock. For this reason, available geological and hydraulic information of each of the 31 unresolved PDZs has been scrutinised in detail and the results are reported in Appendix A in Öhman et al. (2012). In summary, the following characteristics apply to the 17 unresolved PDZs associated with the old (historic) data set:

- They all lack interpreted orientations and true thicknesses, which complicate modelling.
- Only five out of 17 have a high SHI confidence level of existence.
- Many have poor or no hydraulic data (black spheres in Figure 7-2 indicate missing hydraulic data). Three out of the five with a high SHI confidence level are also transmissive (yellow to green spheres in Figure 7-2).
- Many are observed close to the tunnel walls of the existing SFR facility, but there is little or no geological evidence on the tunnel walls to support their modelling in 3D. The lack of tunnel intercepts suggests that they are minor structures.
- The three most confident unresolved PDZs, with high both geological and hydraulic confidence, have been assigned hypothesised deterministic interpretations in the hydrogeological model in SDM-PSU:
  - KFR10\_DZ2 is assumed to be a potential extension of ZFM871.
  - KFR09\_DZ2 is considered to be a possible splay of ZFMNNE0869.
  - KFR69\_DZ2 is possible to link to a tunnel fracture trace and is hence modelled deterministically. It is conceived as a shallow bedrock aquifer feature, SBA8, and assigned a transmissivity of  $1.1 \cdot 10^{-5} \text{ m}^2/\text{s}$ .

The following characteristics apply to the 14 unresolved PDZs in the new (recent) data set:

- Generally high SHI confidence level of existence (except for two unresolved PDZs occurring in percussion boreholes HFR101 and HFR106).
- Distinct hydraulic and geometrical signatures compared with the surrounding rock: high PFL-f transmissivity and predominantly horizontal to gently dipping fracture intercepts. Exceptions are in KFR105\_DZ4 and KFR102B\_DZ1, which are steeply dipping and considerably less transmissive, and KFR101\_DZ4, where the transmissivity value is below the detection limit of the PFL method.
- Five of the 14 unresolved PDZs lack geologically interpreted orientations, i.e. KFR103\_DZ1, KFR106\_DZ2, HFR106\_DZ1, KFR101\_DZ3 and HFR101\_DZ2. In the hydrogeological model of the bedrock, four have been assigned gently dipping orientations and one a steep NNE orientation based on the orientation data of the associated PFL-f transmissivity data or BIPS images, see Table 7-3 in this report and Appendix A in Öhman et al. (2012) for details.
- The four most prominent unresolved PDZs in the new data set have hypothesised deterministic interpretations based on geometrical and/or hydraulic interferences with other boreholes. They are conceived as SBA-structures with the following transmissivities:
  - KFR103\_DZ2 (SBA2 and SBA3) is assigned a transmissivity of  $1.6 \cdot 10^{-5} \text{ m}^2/\text{s}$ .
  - KFR106\_DZ6 (SBA5) is assigned a transmissivity of  $2.4 \cdot 10^{-5} \text{ m}^2/\text{s}$ .
  - HFR106\_DZ1 (SBA3) is assigned a transmissivity of  $3.1 \cdot 10^{-5} \text{ m}^2/\text{s}$ .
  - KFR101\_DZ3 (SBA6) is assigned a transmissivity of  $1.3 \cdot 10^{-5} \text{ m}^2/\text{s}$ .
- The three most uncertain unresolved PDZs in the new data set are excluded due to low geometrical confidence and/or low transmissivity ( $< 10^{-8} \text{ m}^2/\text{s}$ ), i.e. KFR101\_DZ4, KFR105\_DZ5 and HFR101\_DZ2.
- The properties of the remaining seven (= 14–4–3) unresolved PDZs in the new data set are treated as input to stochastic realizations of random PDZs. They are spatially constrained to intercept the structural wedge between the Northern boundary belt and deformation zone ZFMNNW1034, as well as the Southern boundary belt.

Bearing in mind the data quality and model confidence, the majority of the 17 unresolved PDZs in the old data set are interpreted as being less hydraulically significant. Furthermore, it is noted that SBA1–6 are based on the new data set, whereas SBA7–8 are based on the old data set. Since SBA8 is grouted, it was excluded from the groundwater flow modelling carried out by Öhman et al. (2013). However, SBA7 is included.

Finally, it is emphasised that boreholes KFR106 and HFR106 disclose essential information on high-transmissive horizontal to gently dipping features in contact with the Northern boundary belt. The information gained from cross-hole hydraulic interferences with these boreholes is used for modelling of SBA3–5 and four of the seven aforementioned unresolved PDZs. Because of their proximity to the Northern boundary belt and ZFMNNW1034, data in KFR106 and HFR106 are not representative for HRD (hydrogeological DFN) modelling of the target area for the SFR extension.

Some complementary information is provided below for the sake of clarity regarding the 14 unresolved PDZs that occur in the new data set (Figure 7-2) and the delineation of the eight SBA-structures.

The unresolved PDZs in the recent data set have a very distinct hydraulic signature, characterised by one or a few high-transmissive PFL-f data with values around  $10^{-5}$  m<sup>2</sup>/s. The PFL-f data associated with unresolved PDZs reveal predominantly horizontal to gently dipping zones (Figure 7-30d) with orientations similar to geologically modelled PDZ orientations, where these have been determined (see Table 7-3). These PDZs are found down to c. –160 m elevation and are commonly laterally concentrated to the wedge between the Northern boundary belt and ZFMNNW1034 (Figure 7-2). Three exceptions can be identified: HFR101\_DZ2, KFR105\_DZ5 and KFR101\_DZ4; these are considered to be of lesser confidence/ significance in the hydrogeological model, see Öhman et al. (2012) for details.

**Table 7-3. Unresolved PDZs in the new data set.**

	Borehole length (m)		Elevation (m, RHB 70)		SHI conf. <sup>4)</sup>	Orientation (Strike/Dip)		Dominant PFL-f	
	From	To	From	To		Geological	PFL-f <sup>5)</sup>	Log T	Set
<b>11 PDZs included in the stochastic (7) or deterministic (4) modelling</b>									
KFR102B_DZ1	67	70	–51.9	–54.3	3	(098/81)	(95/79)	–6.1	EW
KFR102B_DZ3	149.5	150.5	–118.4	–119.2	2	(229/08)	(160/4)	–5.3	Hz
KFR103_DZ1	24.5	26.5	–17.5	–19.1	3	–	(336/29)	–6.6	Gd
KFR103_DZ2 <sup>3)</sup>	84	91	–65.6	–71.2	3	(343/12)	(223/2)	–5.0	Hz
KFR106_DZ1	15	20	–13.1	–17.8	3	(216/90)	(49/83)	–6.3	NE
KFR106_DZ2	36.5	52	–33.2	–47.8	2	–	(30/23)	–5.8	Hz
KFR106_DZ4	84.5	86	–78.3	–79.7	3	(181/14)	(125/7)	–4.8	Hz
KFR106_DZ5	100.5	101	–93.3	–93.7	3	(012/12)	(344/16)	–4.8	Hz
KFR106_DZ6 <sup>3)</sup>	153	157	–142.4	–146.1	3	(098/19)	(116/7)	–4.7	Hz
HFR106_DZ1 <sup>3)</sup>	38	40	–30.9	–32.6	1	–	(233/7) <sup>1)</sup>	–4.5 <sup>2)</sup>	Hz
KFR101_DZ3 <sup>3)</sup>	179	186	–142.0	–147.5	3	–	(124/18)	–4.9	Hz
<b>3 PDZs excluded from the stochastic or deterministic modelling</b>									
KFR101_DZ4	197	213	–156.0	–168.2	2	(120/90)	–	< –8	–
KFR105_DZ5	293.6	304	–154.7	–156.2	2	(319/88)	(317/85)	–8.3	NW
HFR101_DZ2	101	115	–90.9	–103.6	1	–	(9/86) <sup>1)</sup>	–5.6 <sup>2)</sup>	–

<sup>1)</sup> Orientation has low confidence, estimated from BIPS inspection of percussion borehole.

<sup>2)</sup> HTBH data.

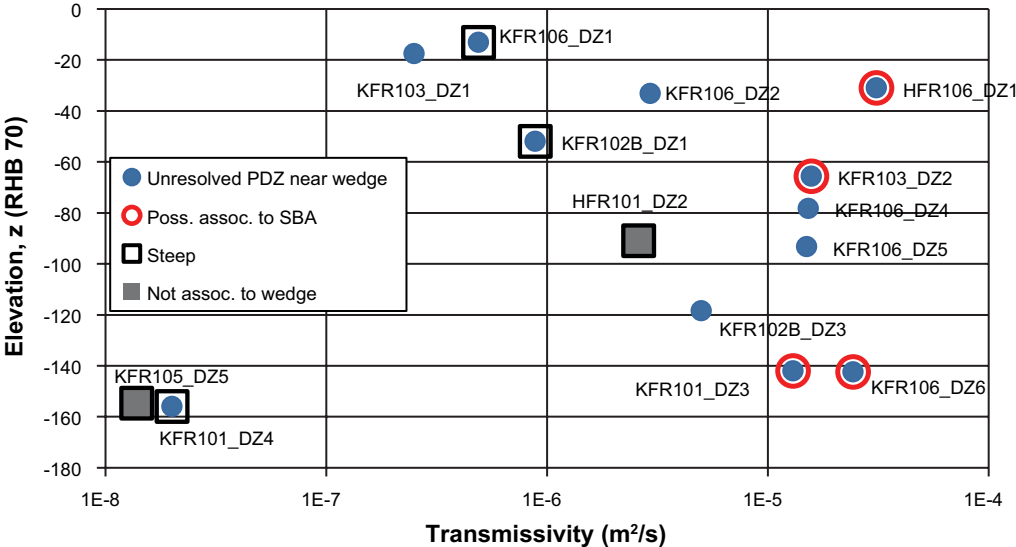
<sup>3)</sup> Alternatively, part of deterministic SBA-structure, see Figure 7-33.

<sup>4)</sup> SHI confidence level: 1 = low, 2 = medium, 3 = high.

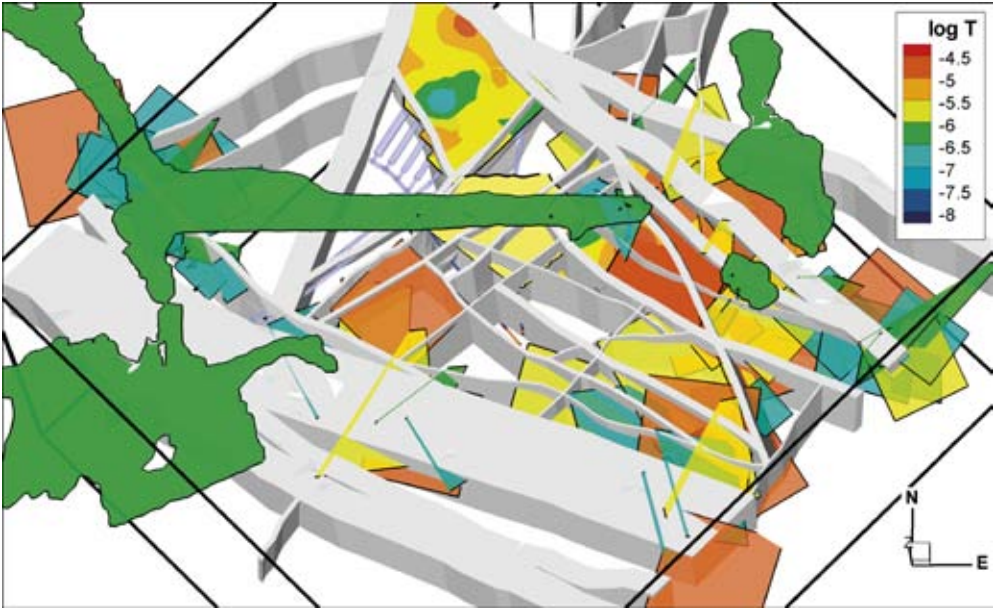
<sup>5)</sup> Orientation estimated from PFL-f data.

The 14 unresolved PDZs that occur in the new data set (Figure 7-2) are also shown in Figure 7-33. Several of these are horizontal to gently dipping and have high transmissivities (Figure 7-30d). Four of the 14 unresolved PDZs have been included in the bedrock hydrogeological model version 1.0 as so-called SBA-structures. SBA stands for shallow bedrock aquifer and was suggested by Follin et al. (2007a) as a means to model the significant impact of shallow sheet joints on groundwater flow in SDM-Site.

In conclusion, the properties of the remaining seven unresolved PDZs in the new data set (= 14–(3 excluded)–(4 SBA)) are treated as input for stochastic realisations of random PDZs (Figure 7-34). The PDZ realisations are spatially constrained to intercept the structural wedge between the Northern boundary belt and deformation zone ZFMNNW1034, as well as to the Southern boundary belt, see Öhman et al. (2012) for details.



**Figure 7-33.** Transmissivity of unresolved PDZs plotted by elevation. Only the 14 data from the new boreholes are shown. Most of these PDZs are horizontal to gently dipping and located close to the Northern boundary belt (ZFMNNW1034 and ZFMNNW0805a,b). The four unresolved PDZs associated with deterministically modelled SBA-structures are shown with red circles. Steeply dipping unresolved PDZs are indicated by squares and unresolved PDZs located far from the Northern boundary belt are shown in grey.



**Figure 7-34.** An example of a conditioned stochastic PDZ realisation.

Put into practice, each PDZ realisation consists of seven loops, i.e. one loop for each of the seven unresolved PDZs. The seven loops are run in sequence and any loop ends once a generated feature is intersected by any of the cored boreholes from the recent SFR investigation. Then the next loop starts etc. The random PDZs features are generated as square planes with a side length randomly ranging from 1 m to 300 m. The size distribution was probabilistically estimated from complex geometrical aspects, involving intercept location in relation to the structural wedge, PDZ orientation, surrounding borehole information, and ground surface intercept. A random component  $\pm 10^\circ$  (uniform distribution) was added to both the strike and dip of the estimated orientations from PFL-f data (Table 7-3). In order to reduce numerical artefacts of the simplistic geometrical representation, the planes are generated with an arbitrary orientation around its pole (i.e. its normal to the fracture plane). The location of features is only partly conditioned at its borehole intercept (i.e. the borehole length specified in Table 7-3), i.e. the intercept is allowed to occur anywhere within its fracture plane and therefore the exact location in 3D space includes a stochastic component. A fuller description is provided in Appendix A of Öhman et al. (2012).

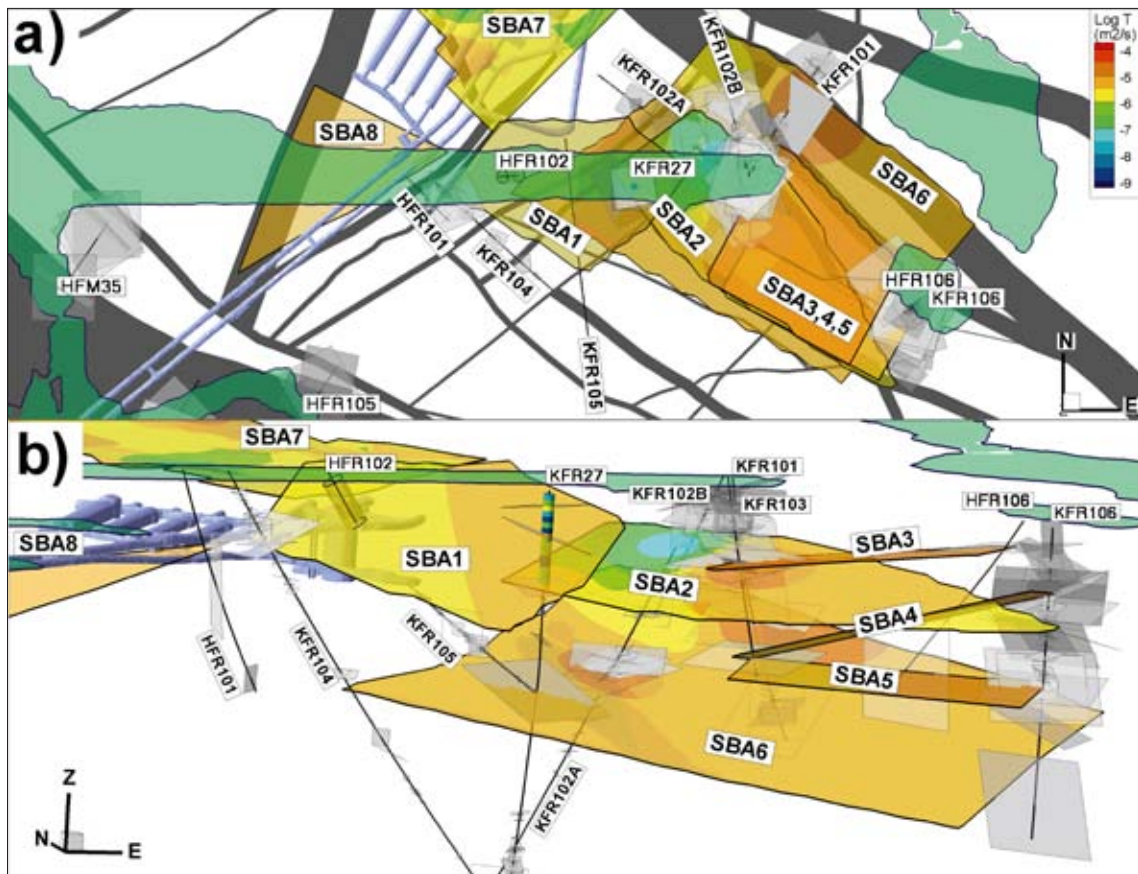
### **Modelling of SBA-structures**

A conclusion from the presented hydrogeological data is that the upper c. 200 m of the bedrock is hydraulically dominated by a system of interconnected sub-horizontal to gently dipping transmissive fractures. An alternative way to a stochastic modelling is to introduce a number of deterministic discrete hydraulic structures to represent some of the more dominant hydraulic fractures. A primary idea with this representation in the hydrogeological model is to allow for a discussion about their potential importance for safety assessment since current data suggest that transmissive, sub-horizontal to gently dipping structures may intersect the rock volume of the planned extension of the existing SFR facility depending on the decided location. The postulated modelling of the SBA-structures by Öhman et al. (2012) is based on an integrated judgement of single-hole observations and cross-hole hydraulic test interferences in several boreholes (see Section 4.4.2 and Appendix H in Öhman et al. (2012)). The borehole intercepts were constrained by coupling the most prominent observed interferences above  $-200$  m elevation to oriented PFL-f transmissivity (or HTHB data for percussion-drilled boreholes) with anomalous character. The selected PFL-f data came from sub-horizontal features and were, with one exception, high-transmissive ( $T \geq 10^{-6}$  m<sup>2</sup>/s). The selection of borehole intercepts was supported by hydraulic head data, meaning that boreholes intersecting the same feature show similar drawdown. In several cases, the location and orientation of the intercepts are supported by oriented radar reflectors and other geophysical data (Table 7-4). The features were terminated against deterministically modelled deformation zones and/or borehole intercepts that lacked hydraulic responses. The six resulting SBA-structures SBA1–6 are shown in Figure 7-35.

**Table 7-4. Summary of modelled borehole intercepts for six of the deterministic shallow bedrock aquifer structures SBA1–6.**

Feature	Borehole	Intercept (length m)	Supporting data (in addition to interferences and PWH)
SBA1	KFR27	55	5 m PFL, radar reflector, geophysics
SBA1	HFR102	eoh <sup>1)</sup>	Interference only
SBA2	KFR27	98	5 m PFL, geophysics
SBA2	KFR102A	72	PFL-f (concealed behind installed steel pipe)
SBA2	KFR103	86	PFL-f, Unresolved PDZ
SBA3	KFR103	86	PFL-f, Unresolved PDZ
SBA3	HFR106	39	HTHB, radar reflector, Unresolved PDZ
SBA4	KFR103	182	PFL-f (alternative to ZFMWNW3262)
SBA4	KFR106	71	PFL-f, radar reflector, (alternative to ZFMWNW3262)
SBA5	KFR103	182	PFL-f (alternative to ZFMWNW3262)
SBA5	KFR106	155	PFL-f, radar reflector, Unresolved PDZ
SBA6	KFR27	193	PFL-f, radar reflector
SBA6	KFR101	181	PFL-f, radar reflector, Unresolved PDZ
SBA6	KFR102A	206	PFL-f, radar reflector
SBA6	KFR102B	172	PFL-f (rim of ZFMENE3112)

1) eoh = end of borehole.



**Figure 7-35.** There are in all eight SBA-structures included in the hydrogeological model version 1.0; six are based on the new data set (SBA1–6), and two are based on the old data set (SBA7–8): a) top view, b) side view looking towards the north-east. The structures are coloured by transmissivity interpolated from the transmissivity of the borehole intercepts. Although modelled as single features in the hydrogeological model it is emphasised that each SBA-structure is probably more of a “stairway of interconnected sub-horizontal and steeply dipping fractures” than a single fracture.

A possible sub-horizontal stress-release structure was also defined by Curtis et al. (2011), based on the original interpretation of zones H1 and H3 by Carlsson et al. (1985). This seventh structure is referred to as SBA7 (Figure 7-35). Another structure, referred to as SBA8, is extrapolated between tunnel mapping and a nearby transmissivity anomaly (Figure 7-35), although this extrapolation is considerably more uncertain, with less support from hydrogeological data.

Although modelled as single features it is emphasised that each SBA-structure is believed to represent a “stairway of interconnected sub-horizontal and steeply dipping fractures” rather than a single fracture. It is also noted that the certainty regarding the postulated extension of each SBA-structure varies. In some cases the interpreted sizes are primarily based on similarities in geometrical and hydraulic data in individual boreholes and in other cases additional data are available such as cross-hole hydraulic interferences (see Appendix H in Öhman et al. 2012 for details). Additional boreholes and hydraulic testing together with a geological discrete fracture network (DFN) model could possibly have improved the structural-hydraulic modelling in this regard.

In conclusion, the lateral hydraulic connectivity and hydraulic responses identified within the Repository level HRD are conceptually modelled as eight potential SBA-structures. SBA1–6 are connected to the Northern boundary belt. SBA7 and SBA8 occur in the area of the existing SFR facility, which demonstrates that the shallow bedrock aquifer phenomenon is not constrained to occur solely in the area of the planned extension. SBA7 corresponds to zones H1 and H3, as discussed in Appendix 12 in Curtis et al. (2011). SBA8 intercepts KFR69 and the existing SFR facility (Figure 7-35) and its transmissivity required substantial grouting (Figure 7-5). (It is noted that the mapped gently dipping structures found in SFR could not be modelled to cross-cut several tunnels or caverns except for SBA8.)

Inside the Central block, the SBA-structures appear to override the hydraulic signature of the less conductive steeply dipping ENE-striking and WNW-striking deformation zones. However, there is high uncertainty in the modelled spatial extent of the SBA-structures in the southern parts of the Central block owing to insufficient borehole coverage (Figure 7-28). Nevertheless, it is quite possible that one or more of the modelled SBA-structures, SBA1–6, or other similar structures, also occupy the bedrock in the southern part of the SFR local model domain. Different strategies to compensate for this are suggested by Öhman et al. (2012).

The spacing between SBA-structures, if present, probably varies within the SFR local model domain. The spacing between SBA-structures can be estimated in different ways, e.g.:

1. Between –32 m (SBA3 in HFR106) and –194 m (SBA6 in KFR102A) elevation there are in all 13 observations used to model six SBA-structures (SBA1–6). Six SBA-structures over a distance of approximately 160 m suggest a mean spacing of approximately 32 m between the SBA-structures. However, since the SBA-structures are not infinite in size, this spacing is probably not representative for the Central block, but perhaps more valid near the Northern boundary belt and zone ZFMNNW1034.
2. The spacing between SBA-structures in the Central block is unknown, since there are few observations in this part of the model domain, but if the total vertical borehole coverage of 1,600 m between 0 and –200 m elevation is divided by 13 SBA-structures, a mean spacing of approximately 124 m is obtained.

### ***Stochastic modelling of residual HRD data set***

#### **Open fractures**

The hydrogeological model of the residual HRD data set employs the stochastic discrete fracture network (DFN) approach (Dershowitz et al. 1998). This divides the open fractures into sets with regard to orientation (strike and dip). Each fracture set is assigned a fracture intensity value (fracture surface area per unit volume of rock) and series of parameter values describing its statistical properties with regard to fracture size, fracture location and fracture transmissivity. The properties are inferred from measurements at SFR and SDM-Site Forsmark (Öhman et al. 2012).

The five fracture sets inferred for the HRDs inside the local SFR model domain are denoted EW, NE, NW, GD (gently dipping), and HZ (horizontal) (Figure 7-21). The weak vertical trend is differentiated into three depth intervals/HRDs according to fracture intensity:

- Shallow bedrock HRD (above –60 m),
- Repository level HRD (–60 to –200 m), and
- Deep bedrock HRD (below –200 m).

The intensity of open fractures inside the three HRDs decreases weakly with depth (cf. Figure 5-9). The Repository level HRD has the best total borehole coverage and hence provides the best basis for detailed intensity calculations. In this interval, the intensity of open fractures was calculated for each fracture set and for each borehole. The sets have similar intensities at repository level, approximately 1 m<sup>2</sup>/m<sup>3</sup> for each set (cf. Figure 5-9 and Figure 7-21).

Open fractures exhibit local heterogeneity, but spatial trends in open fracture intensity inside the local model domain are not judged significant in relation to gaps in borehole coverage, see Appendix F in Öhman et al. (2012) for details. The decrease in intensity of open fractures with depth is small and the set-wise intensity varies only somewhat between boreholes, although this may well be an artefact of local heterogeneity and gaps in borehole coverage. The cored borehole data acquired outside the local model area, i.e. in boreholes KFM11A and KFR106, are not judged to be representative of the HRDs in the SFR regional model area, since they are influenced by the Southern and Northern boundary belts, respectively.



## Flowing fractures

Flowing fractures detected by the PFL-f method are assigned transmissivities and divided into the same fracture sets as those defined for the open fractures (Figure 7-21). The pattern of flowing fractures inside the ZFMs (HCDs) is similar to that outside the ZFMs (Figure 7-24). That is, the hydraulically active fractures in the steeply dipping deformation zones are primarily horizontal to gently dipping, followed by the steeply dipping NW-SE-striking fractures. The same pattern is seen also outside the ZFMs. This is consistent with the conceptual understanding of the geological processes active at the site in connection with the formation of horizontal to gently dipping fractures.

Figure 7-24, in combination with Figure 7-25b, -c and -d, reveals that the majority of the largest PFL-f transmissivities ( $T > 10^{-6} \text{ m}^2/\text{s}$ ) above  $-200 \text{ m}$  elevation are found outside the deterministic deformation zones. In addition, the most transmissive features above  $-200 \text{ m}$  elevation are horizontal to gently dipping and occur in borehole intervals with unresolved PDZ-type properties in the geological model (Figure 7-25c and d). Borehole KFR106 is special in this regard and it is important to note that it is located east of the area intended for the SFR extension in close proximity to the deformation zone ZFMNNW1034. This zone cuts through the wedge between the Northern and Southern boundary belts. The derivation of the parameter values suggested for DFN modelling at SFR is presented in detail in Öhman et al. (2012) and tabulated in Appendix 5 in this report.

### 7.3.4 Summary

The conceptual hydrogeological model, version 1.0, for the bedrock contained inside the local model domain is sketched in 3D in Figure 7-36. In summary, this domain encompasses:

- Three major tectonic units defined in bedrock geological model version 1.0: the Northern boundary belt, the Southern boundary belt and the Central block.
- Twenty-seven steeply dipping hydraulic conductor domains (HCDs) coinciding with deterministically modelled deformation zones (ZFMs).
- One hydraulic gently dipping conductor domain (HCD) coinciding with a deterministically modelled deformation zone (ZFM871).
- Eight deterministically modelled shallow bedrock aquifer structures (SBA1–8).
- Stochastic PDZ realisations that are spatially constrained to occur along the structural wedge between the Northern boundary belt and deformation zone ZFMNNW1034 as well as along the Southern boundary belt. The simulated positions, orientations and transmissivities of the generated features are based on the seven unresolved PDZs contained in the new data set.
- Three hydraulic rock mass domains (HRDs: Shallow bedrock HRD, Repository level HRD and Deep bedrock HRD), each with stochastic discrete fracture network (DFN) properties.

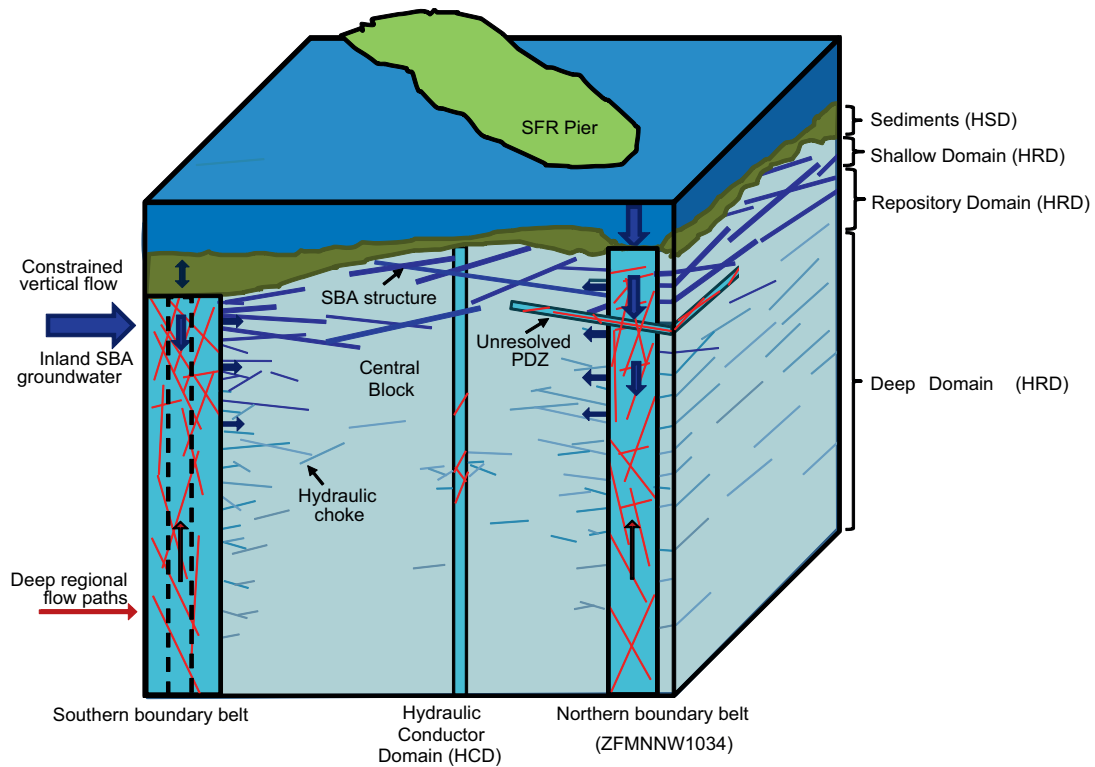
All of the listed features reveal parameter heterogeneity, and the observed depth trends and lateral variations in transmissivity are implemented in the model.

## 7.4 Parameterisation of hydraulic domains

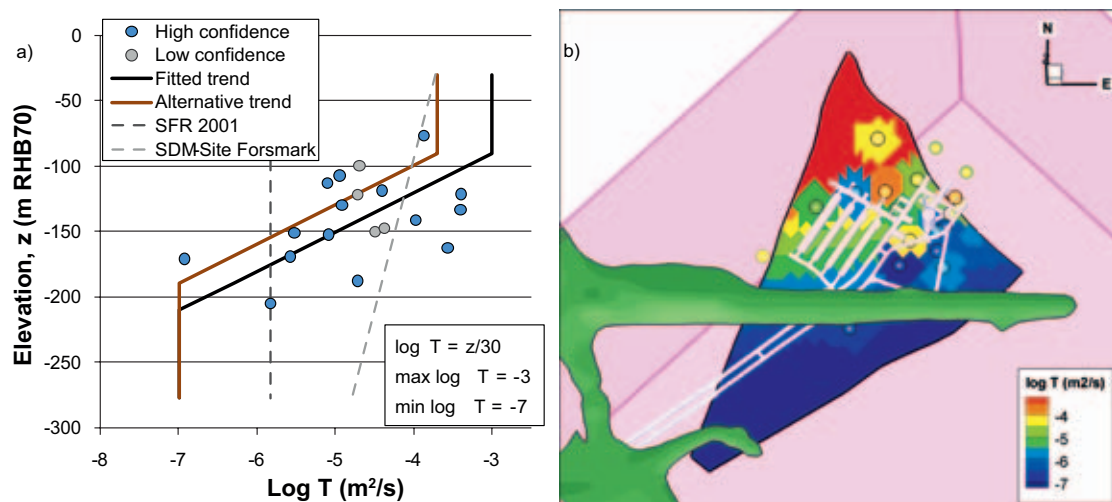
### 7.4.1 Hydraulic conductor domains

The parameter values of HCD model version 1.0 are shown in Appendix 4. Except for the gently dipping ZFM871, the assignment of transmissivity data to all HCDs is based on Equation (7-1) with  $k = 232.5 \text{ m}$  and  $T_0$  values and hydraulic thicknesses as specified in Appendix 4. A truncated exponential depth trend model is suggested for ZFM871 with  $k = 30 \text{ m}$ . The  $T_0 = 1 \text{ m}^2/\text{s}$  value is recommended on the basis of the 19 transmissivity determinations shown in Figure 7-37. Appendix 4 also provides the data needed for conditional simulation of each zone.

Alternatively, transmissivity data can be assigned to the HCDs based on Equation (7-3). Öhman et al. (2010b) provided values of the geometric mean  $T_{\text{eff}}(0)$  and a log-normal standard deviation for each HCD set.



**Figure 7-36.** Side view facing east showing the conceptual model of hydraulic units, the interconnected flowing fracture network, and potential flow paths towards the Central block due to inflow to the existing SFR facility or borehole pumping during the SFR site investigation. The vertical deformation zones (HCDs) contained in the Northern and Southern boundary belts connect the Baltic Sea to the bedrock and may thus act as potential positive hydraulic boundaries for inflow to the planned SFR extension. However, flow from the bounding belts towards the Central block is partly constrained by hydraulic chokes. The horizontal and vertical dimensions of this illustration are approximately 1.5 km and 1.1 km, respectively.



**Figure 7-37.** Fitted trend model for assigning transmissivity data to the gently dipping ZFM871.

#### 7.4.2 Hydraulic rock mass domains

The parameter values of hydrogeological DFN model version 1.0 are shown in Appendix 5. The depth trend in flowing fracture characteristics is numerically represented by dividing the SFR model domain into three depth intervals: the Shallow, Repository, and Deep domains. Five fracture sets are parameterised in each of these depth domains. Three steeply dipping fracture sets are referred

to by strike: East-West (EW), Northwest (NW), and Northeast (NE). Two fracture sets are referred to by dip: gently dipping (Gd) and subhorizontal (Hz). The orientation model for the fracture sets is defined by mean poles and the spread around the mean pole.

### 7.4.3 Shallow bedrock aquifer structures

The hydraulic data available for parameterising the deterministically modelled SBA-structures SBA1–8 are shown in Table 7-5 to Table 7-7. A parameterisation for SBA1–7 is achieved by interpolation across each feature, e.g. using the inverse-distance weighted interpolation method. There is only one value recorded for SBA8, though Figure 7-35 shows an example of visualisation.

Finally, SBA6 is the most certain of the six SBA-structures, and the data shown in Figure 7-38 and Figure 7-39 reveal that the transmissivities of SBA6 are of the same magnitude as the transmissivities of ZFM871 at comparable depths.

**Table 7-5. Summed transmissivity and its mean elevation for all intercepts between boreholes and the deterministically modelled shallow bedrock aquifer structures SBA1 to SBA6. An empty cell shows that there is no intercept. The four PDZs associated with deterministically modelled SBA-structures are highlighted.**

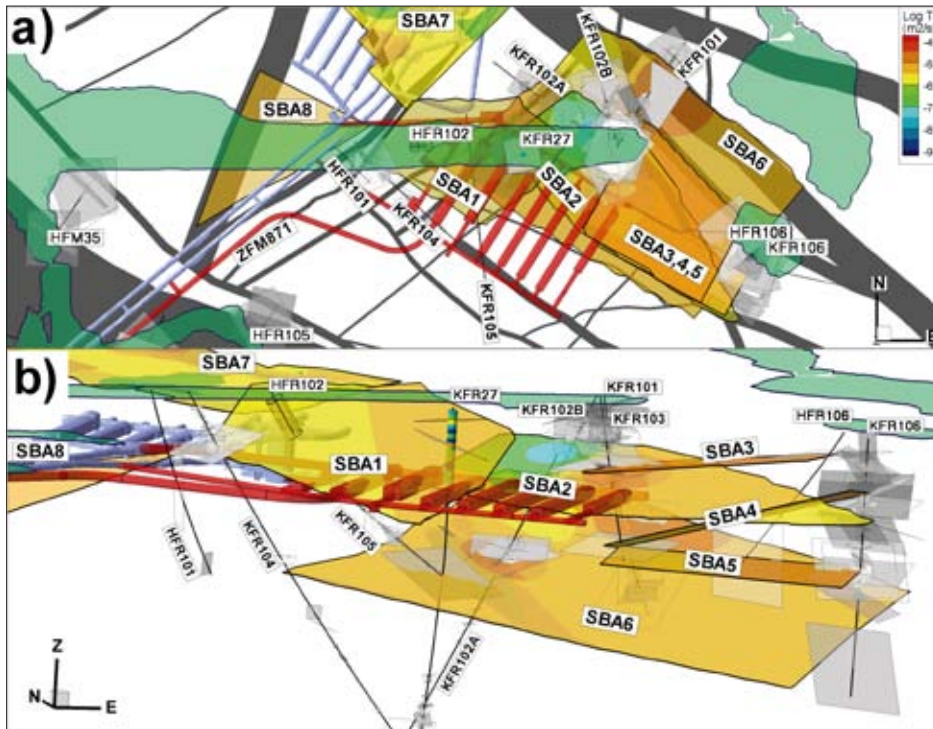
SBA#	Transmissivity (m <sup>2</sup> /s)							
	HFR102	HFR106	KFR101	KFR102A	KFR102B	KFR103	KFR106	KFR27
SBA1	2.8·10 <sup>-6</sup> (-44 m)							3.5·10 <sup>-6</sup> (-49 m)
SBA2				8.6·10 <sup>-8</sup> (-63 m)		1.6·10 <sup>-5</sup> (-69 m)		1.1·10 <sup>-6</sup> (-96 m)
SBA3		3.1·10 <sup>-5</sup> (-32 m)				1.6·10 <sup>-5</sup> (-68 m)		
SBA4						5.1·10 <sup>-6</sup> (-143 m)	2.4·10 <sup>-5</sup> (-65 m)	
SBA5						5.1·10 <sup>-6</sup> (-143 m)	2.4·10 <sup>-5</sup> (-144 m)	
SBA6			1.3·10 <sup>-5</sup> (-144 m)	1.1·10 <sup>-5</sup> (-194 m)	1.7·10 <sup>-6</sup> (-173 m)			6.8·10 <sup>-6</sup> (-192 m)

**Table 7-6. Summed transmissivity and its mean elevation for all intercepts between boreholes and the deterministically modelled shallow bedrock aquifer structure SBA7. (SBA7 corresponds to H1–H3, as discussed in Appendix 1 in Curtis et al. 2011.)**

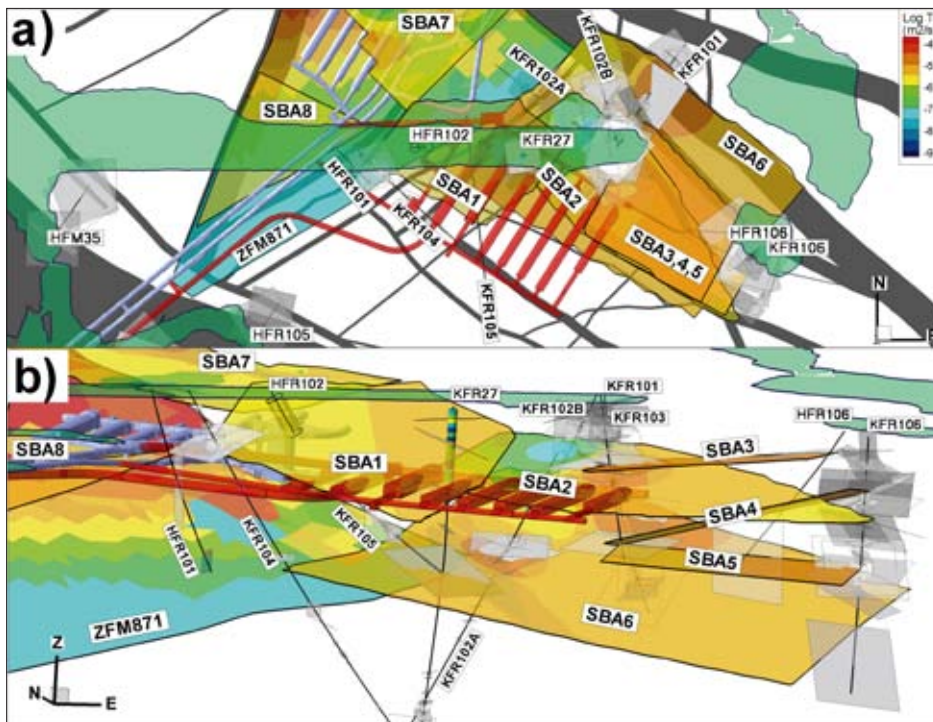
SBA#	Transmissivity (m <sup>2</sup> /s)							
	KFR21	KFR22	KFR23	KFR31	KFR33	KFR35	KFR37	KFR38
SBA7	7.7·10 <sup>-6</sup> (-29 m)	9.9·10 <sup>-7</sup> (-33 m)	3.9·10 <sup>-5</sup> (-21 m)	1.4·10 <sup>-6</sup> (-35 m)	7.8·10 <sup>-7</sup> (-35 m)	1.5·10 <sup>-6</sup> (-26 m)	2.1·10 <sup>-6</sup> (-24 m)	6.9·10 <sup>-6</sup> (-29 m)

**Table 7-7. Summed transmissivity and its mean elevation for the intercept between borehole KFR69 and the deterministically modelled shallow bedrock aquifer structure SBA8.**

SBA#	Transmissivity (m <sup>2</sup> /s) KFR69
SBA8	1.1·10 <sup>-5</sup> (-93 m)



**Figure 7-38.** Visualisation of the eight SBA-structures in the hydrogeological model version 1.0 with regard to a preliminary layout of the extended SFR: a) top view, b) side view looking towards the north-east. The SBA-structures are coloured according to transmissivity interpolated from the transmissivity of the borehole intercepts.



**Figure 7-39.** The same image as in Figure 7-38, but with the addition of ZFM871.

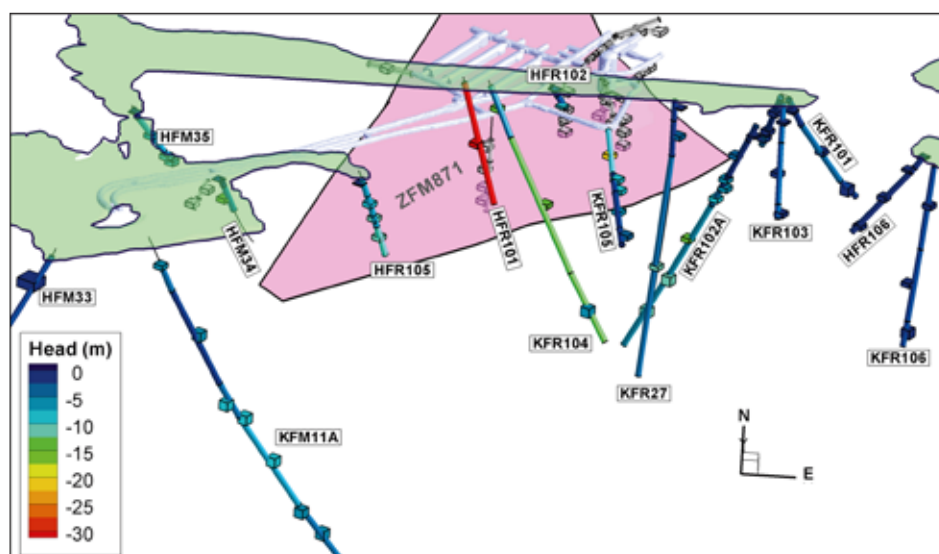
## 7.5 Groundwater flow modelling

The report by Öhman et al. (2013) deals with groundwater flow modelling and explores the conceptual hydrogeological model for the bedrock by Öhman et al. (2012) along with DarcyTools (Svensson et al. 2010) and FracMan (Dershowitz et al. 1998). The results from the groundwater flow simulations are compared with present-day inflow data and head field information.

The first part of Öhman et al. (2013) uses DarcyTools to examine the capability of eight steady-state groundwater flow model exercises, M0–M7, to match present-day tunnel inflow rates and borehole section heads, where M0 had the simplest setup and M7 the most complex. The main conclusion drawn from this “sensitivity test” is that even the simplest flow model exercise, M0, can be reasonably calibrated against the measured inflow rates, but at the cost of excessive drawdowns. To mitigate this effect, parameter heterogeneity and anisotropy must be incorporated into the flow model. This is demonstrated by flow model exercise M7, which to a greater extent takes into account the structural geology and the hydrogeological interpretation of the site. However, it is noted that perfect head matches are doubtful for any equivalent continuum model, since the flow medium is in actuality discrete (fractured) and the head measurements represent long borehole sections (Figure 7-40). In conclusion, the parameter uncertainties at hand are best handled by multiple realisations driven by a discrete fracture network approach and upscaled to an equivalent continuous porous medium.

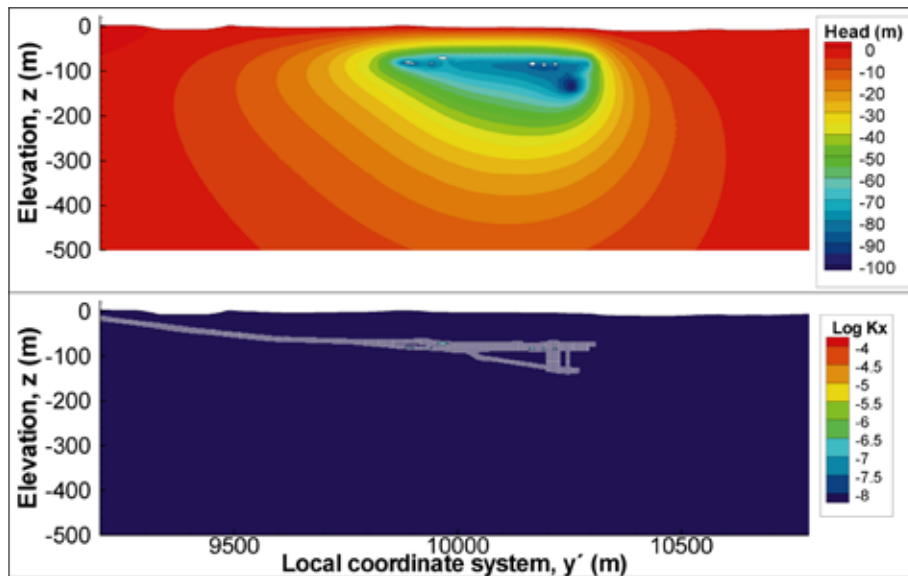
Öhman et al. (2013) provide a thorough description of the setup of an implementation in DarcyTools of each model exercise M0–M7, as well as a discussion of the simulation results. A few visualisations from model exercise M0 are shown in Figure 7-41, Figure 7-42 and Figure 7-43 for the sake of clarity.

The second part of Öhman et al. (2013) focuses on the short-term hydraulic interference tests carried out at the site. The experience from SDM-Site is that hydraulic interference tests provided key evidence for the characterisation of the uppermost 150 m of bedrock at Forsmark, in particular the existence and character of horizontal to gently dipping sheet joints. The interference tests are carried out under quite different boundary conditions in the SFR area than at Forsmark, since the SFR area is located below the Baltic Sea, close to an open underground facility. That is, at a given monitoring point, the measured drawdown can be interpreted as an indication of its hydraulic connection to the SFR area relative to its hydraulic connection to the Baltic Sea. In other words, a large drawdown far away from the existing SFR facility implies relatively poor connection to the overlying sea, whereas a small drawdown close to the facility indicates poor connection to the facility. While keeping this in mind, it is also recalled that many monitored groundwater levels (heads) are continuously decreasing in spite of the decreasing inflow rate.

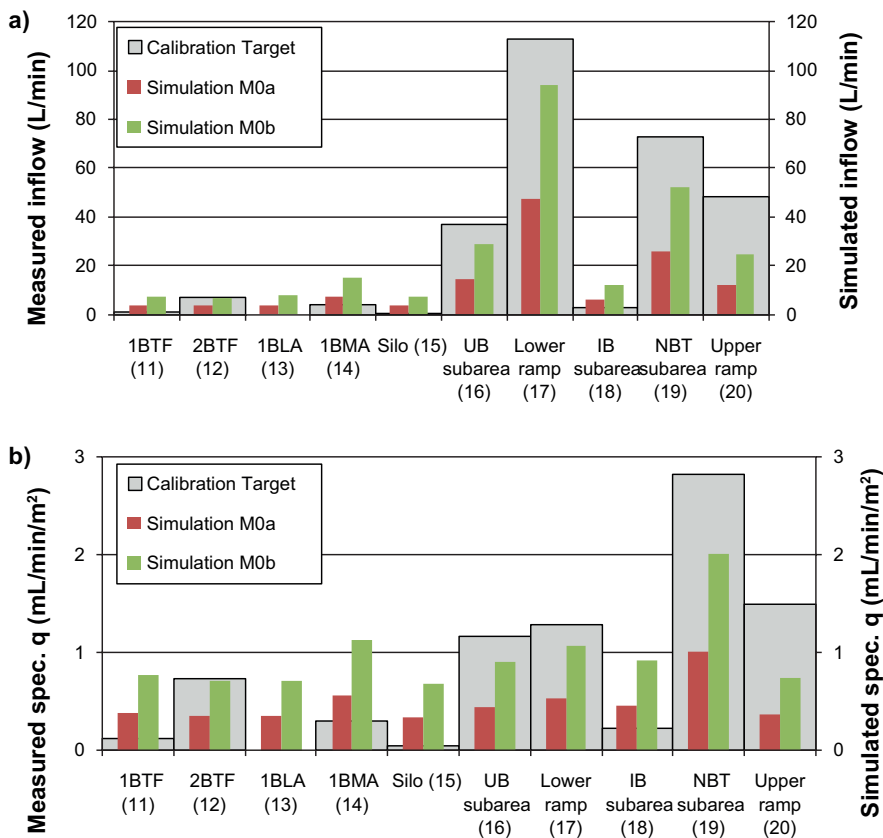


**Figure 7-40.** Sample visualisation showing the difference in resolution between measured heads in borehole sections (shown as coloured cylinders) and simulated heads in DarcyTools (shown as coloured grid cells). The existing SFR and the extension are shown as transparent grey shades.

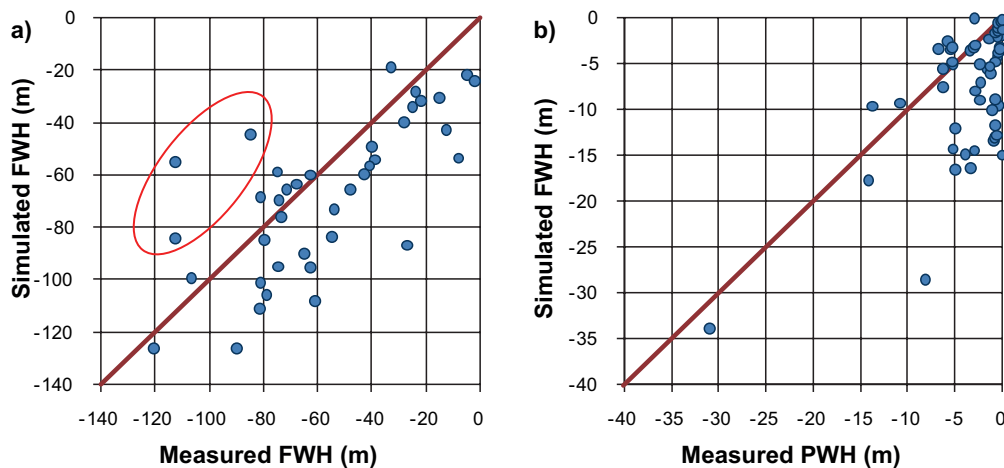
A summary of the premises for modelling short-term hydraulic interference tests in the SFR area is given below along with a description of the chosen modelling methodology by Öhman et al. (2013). The main conclusions drawn from the modelling of the short-term interference tests are also presented.



**Figure 7-41.** In model exercise M0, the entire model domain is homogeneous and isotropic: a) head field; b) hydraulic conductivity field. In variant M0a,  $K_{HRD} = 6.5 \cdot 10^{-9}$  m/s (same as in Holmén and Stigsson 2001). In variant M0b,  $K_{HRD}$  is doubled,  $1.3 \cdot 10^{-8}$  m/s. In effect, the inflows differ by a factor of two, but the resulting head fields are the same since the boundary conditions are unchanged.



**Figure 7-42.** Results from model exercise M0, variants M0a and M0b. Simulated inflows assuming steady-state flow compared to measured inflows: a) inflow,  $Q$ , and b) specific inflow,  $q$  ( $Q$  normalised per cross-sectional area). As  $K_{HRD}$  is doubled in M0b, the total simulated inflow is also doubled.



**Figure 7-43.** Simulated heads at steady-state compared with measured heads for variant M0: a) SFR tunnel boreholes and b) recent boreholes. The simulated heads are generally too low. The heads are the same for exercise M0b as the flow medium is homogeneous and the specified boundary conditions are unchanged. The outliers inside the red ellipse are found in KFR7A (cf. Figure 7-7).

The interference tests studied in detail by Öhman et al. (2013) are listed in Table 7-8. HFR101 is an open, percussion-drilled borehole with a free groundwater level at c. –30 m RHB 70. HFR101 was drilled from the surface and was pumped for three days in April 2009. KFR105 is an underground cored borehole, drilled from the NBT tunnel in the existing SFR facility at approximately –107 m RHB 70. The interference test in KFR105 was performed in March 2010 by releasing the shut-in pressure of five borehole packers and letting the water flow freely (apart from tubing resistance) into the SFR tunnel for one day. HFR101 has an inclination of about 65 degrees, whereas KFR105 is sub-horizontal (9° inclination), hence the two boreholes are likely to intersect different types of structures due to orientation bias.

**Table 7-8. Interference tests performed in the SFR extension investigation.**

Borehole	Interval	Date	Duration t (hrs)	Flow Q (L/min)	$s_{\max}$ (m)	$Q/s_{\max}$ (m <sup>2</sup> /s)	Type
HFR101	8.04–209.3	2009-04-06	73.2	10.0	16	$1 \cdot 10^{-5}$	Pumping
KFR105	0–306.81	2010-03-03	23.6	11.4	~90	$2 \cdot 10^{-6}$	Free flow

The following site conditions have an impact on the modelling of the interference tests:

- The ongoing changes in heads and inflow rates in the SFR area indicate a disturbed flow system with a complex hydraulic contact with the Baltic Sea. For example, the majority of the observation sections show good correlation of head with sea level fluctuations. The head correlations are difficult to interpret without more data, since they could be indicative of changes in mechanical loading rather than changes in the hydraulic head at the sea bottom, depending on the hydraulic conductivity of the regolith and the bedrock. In addition, these disturbances make the head recordings noisy and affect the quality of the information gathered. For instance, the interference test in KFR105 is considerably more affected than the test in HFR101. Due to the noise caused by sea level fluctuation, it was decided to use a drawdown criterion (dp) of 0.1 m in the test response interpretations, see Walger et al. (2011) for details.
- The best head correlations with sea level fluctuations occur inside the deformation zones located near the Northern boundary belt and in the gently dipping zone ZFM871 below the existing SFR facility.

- The relatively short durations of the interference tests necessitate transient model simulations, which requires an assumption about the highly uncertain fracture storativity (S). Here, the empirical relationship suggested by Rhén et al. (1997) was tentatively used to estimate storativity from transmissivity (T):

$$S = 0.0007 \sqrt{T}$$

- Not all boreholes were drilled and/or properly monitored at the time of the interference test in HFR101.
- Some of the responding observation sections lack intercepts with deterministically modelled features.
- The effect of grouting adjacent to the existing SFR facility is unknown.

The limited information that could be gained from two short-term interference tests together with the significant *in situ* disturbances at the upstream and downstream boundaries impose considerable constraints on what could be achieved in terms of flow model calibration for SDM-PSU. Bearing this in mind, the modelling methodology used by Öhman et al. (2013) can be summarised as follows:

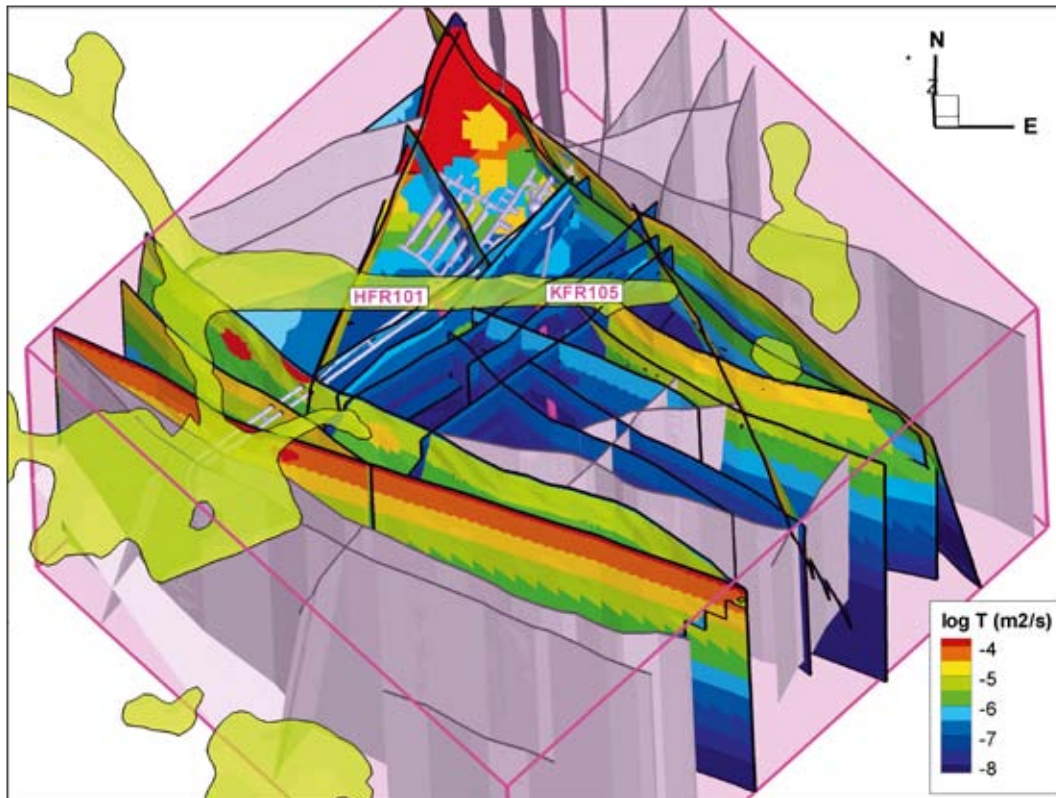
- 1) Based on the experience gained from the eight groundwater flow model exercises, M0–M7, a discrete (fractured) medium modelling tool was chosen (FracMan). This to allow for detailed comparisons without increasing the computational constraints.
- 2) The model setup focused on the deterministically modelled HCDs and SBA-structures considered to be the most important features for groundwater flow in the region of interest. In other words, the HRDs and unresolved PDZs<sup>7</sup> were excluded. Figure 7-44 and Figure 7-45 depict the modelled HCDs and SBA-structures, respectively.
- 3) The *in situ* head field around the existing SFR facility was first simulated by a steady-state solution, where the overlying sea and the SFR tunnel were assigned constant prescribed-head boundary conditions. Figure 7-46 depicts the measured *in situ* and simulated head fields and Figure 7-47 show cross-plots of the same data.
- 4) With the steady-state solution as a starting point, the transient interference tests were simulated, beginning with a pumping phase followed by a recovery phase. Figure 7-48 shows the measured field responses from the interference test in HFR101 and Figure 7-49 shows the simulated responses.
- 5) The simulated responses were compared with the field observations, drawdown and response time reported in Walger et al. (2011).
- 6) The model setup was modified in order to explore the general agreement of the simulation results versus data observations. Figure 7-50 shows the simulated responses from the original model setup of the interference test in HFR101 and Figure 7-51 shows the simulated responses for a model modification.

The expected constraints of the modelling methodology used in the short-term interference tests are:

- Since a discrete modelling tool is used and the HRDs and unresolved PDZs are excluded, groundwater flow outside modelled deformation zones and SBA-structures is not possible. Hence, field responses observed in borehole sections lacking intercepts with the modelled structures could not be addressed.
- The homogeneous hydraulic parameterisation of the modelled structures (with the exception of imposed depth trends and local borehole conditioning) potentially exaggerates the hydraulic continuity. As a result, some borehole sections will have unjustified responses.

<sup>7</sup> The HRDs and unresolved PDZs are modelled by hydrogeological discrete fracture network (DFN) models, which are based on a statistical analysis of fracture data and hydraulic tests in boreholes. The statistical basis entails uncertainty and introduces a stochastic component in the groundwater flow model, which is best handled by carrying out multiple realisations.





**Figure 7-44.** Deformation zones included in the model setup coloured by transmissivity parameterisation. Excluded deformation zones are shown grey-shaded. Boreholes where interference tests were performed are shown as pink cylinders. Ground surface is shown as transparent green shade.

In conclusion, the main objective of the flow modelling of the two interference tests is to study the hydraulic importance of the deterministically modelled features in the area of interest, not to establish a fine-tuned parameterisation of a particular build of the conceptual hydrogeological model of the bedrock.

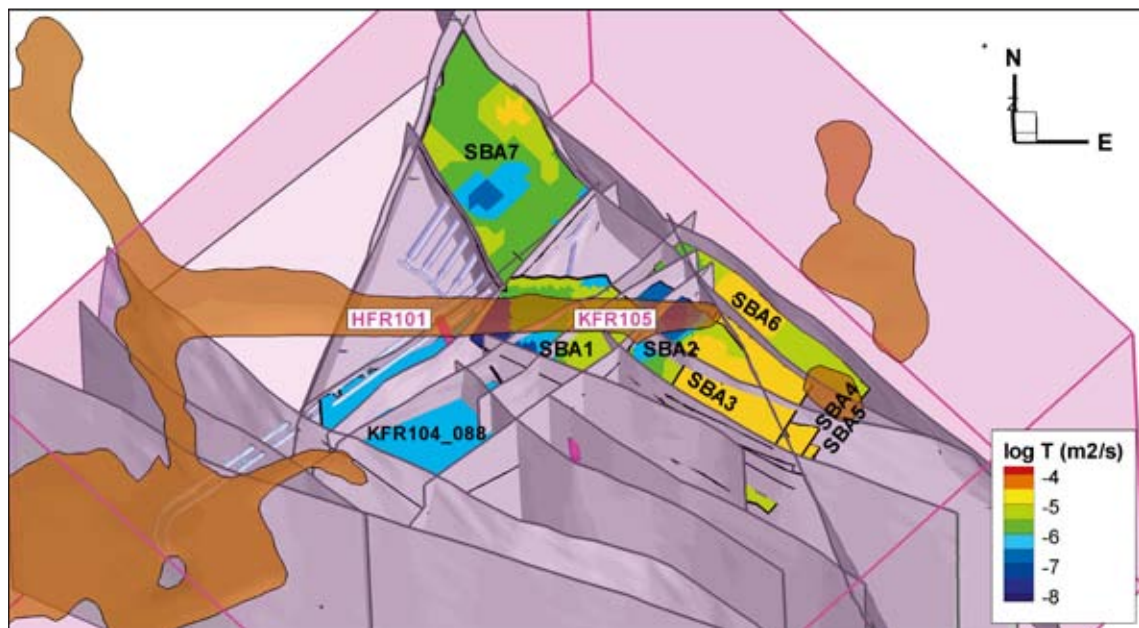
Öhman et al. (2013) provide thorough descriptions of the model setup and implementation in FracMan of the two interference tests, as well as a discussion of the simulation results. The main conclusions drawn from the modelling of the short-term interference tests are:

- In the light of the simplified model setup, the pattern of the simulations bears a reasonable resemblance to field observations. In general, responses exceeding the drawdown criterion  $dp = 0.1$  m are simulated in borehole sections interpreted as “responding” by Walger et al. (2011), and a lack of response has been simulated in borehole sections interpreted as “non-responding”. However, discrepancies can be noted at the more detailed level, in terms of both response magnitudes and response times. In addition, a number of unjustified responses are simulated as well.
- It is noteworthy that delayed drawdown, i.e. a drawdown trend continuing after the shut-in of the interference test, is observed in the observation borehole sections both in data and in simulations (although not for the same sections). This phenomenon is interpreted here as a combined effect of geometry and heterogeneous hydraulic properties that may, for example, occur in compartmentalised dead-end structures. In a porous medium, discrepancy in response time is expected to be related to the storage coefficient or storativity, which is not readily comparable for a discrete (fractured) medium since the storativity of individual fractures is generally small.

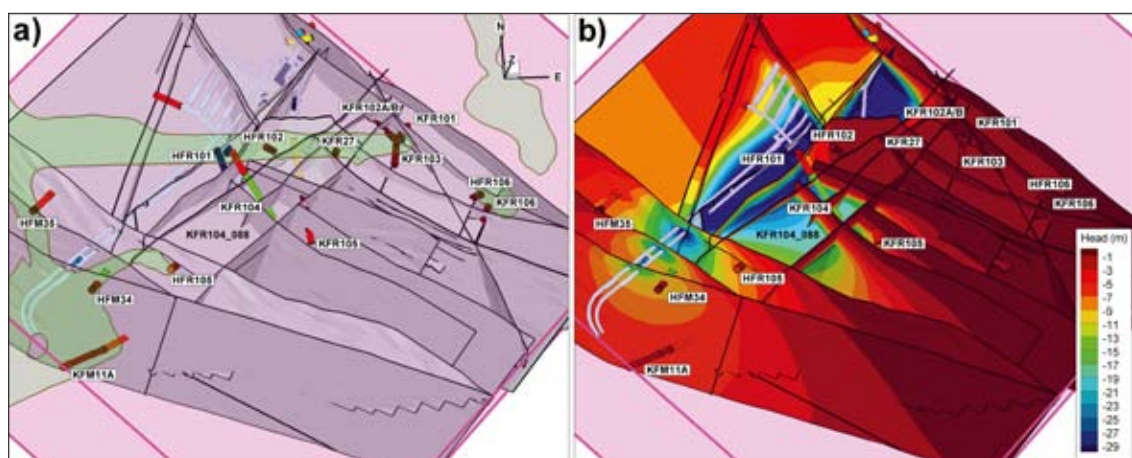
In addition to the overall conclusions, the following detailed observations are noted:

- Changes in the hydraulic properties alone were in general useful for model calibration. A few geometrical changes were required, however. One of the required changes is introducing a large-scale horizontal connectivity close to the Southern boundary belt (represented as feature KFR104\_88 in Figure 7-44), see Öhman et al. (2013) for details.

- During the course of model calibration, storativity was confirmed to be an important model parameter. To simplify the calibration procedure, the aforementioned empirical relationship for estimating storativity from transmissivity was multiplied by two different factors, one factor for all HCDs ( $f_{HCD}$ ) and one for all SBA-structures ( $f_{SBA}$ ). In general, it was found that  $f_{HCD}$  should be greater than  $f_{SBA}$ , implying a greater “storage effect” in the HCDs. However, the actual combination of values of  $f_{HCD}$  and  $f_{SBA}$  was found to be important for maximising the number of “target responses” versus minimising the number of “unjustified responses”. The following combinations illustrate the level of sensitivity:
  - The combination  $f_{HCD} = 8$  and  $f_{SBA} = 1/8$  rendered few “unjustified responses” but at the cost of too few “target responses”.
  - The combination  $f_{HCD} = 7$  and  $f_{SBA} = 2$  rendered a good match of the number of “target responses”, but at the cost of too many “unjustified responses”.



**Figure 7-45.** Sub-horizontal structures (SBA1–SBA7) included in the model setup coloured by transmissivity parameterisation. A single PFL-f record (KFR104, no. 88) is also included as a deterministic structure. Deformation zones are shown grey-shaded. Boreholes where interference tests were performed are shown as pink cylinders. Ground surface is shown as transparent brown shade.



**Figure 7-46.** Simulated initial-state drawdown; a) monitored borehole sections and b) simulated head in modelled structures. Drawdown exceeding 30 m is shown as dark blue (unresolved by the colour scale). Ground surface is shown as transparent green shade.

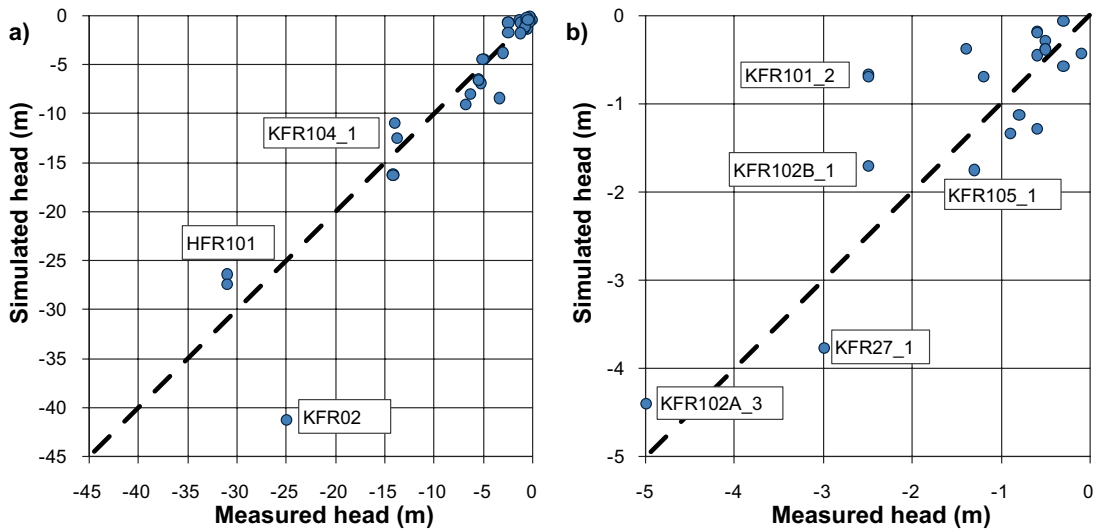


Figure 7-47. Cross plot between in situ measurements and initial-state simulations; a) all recently installed monitored borehole sections (and KFR02) and b) close up for monitored sections with low drawdown.

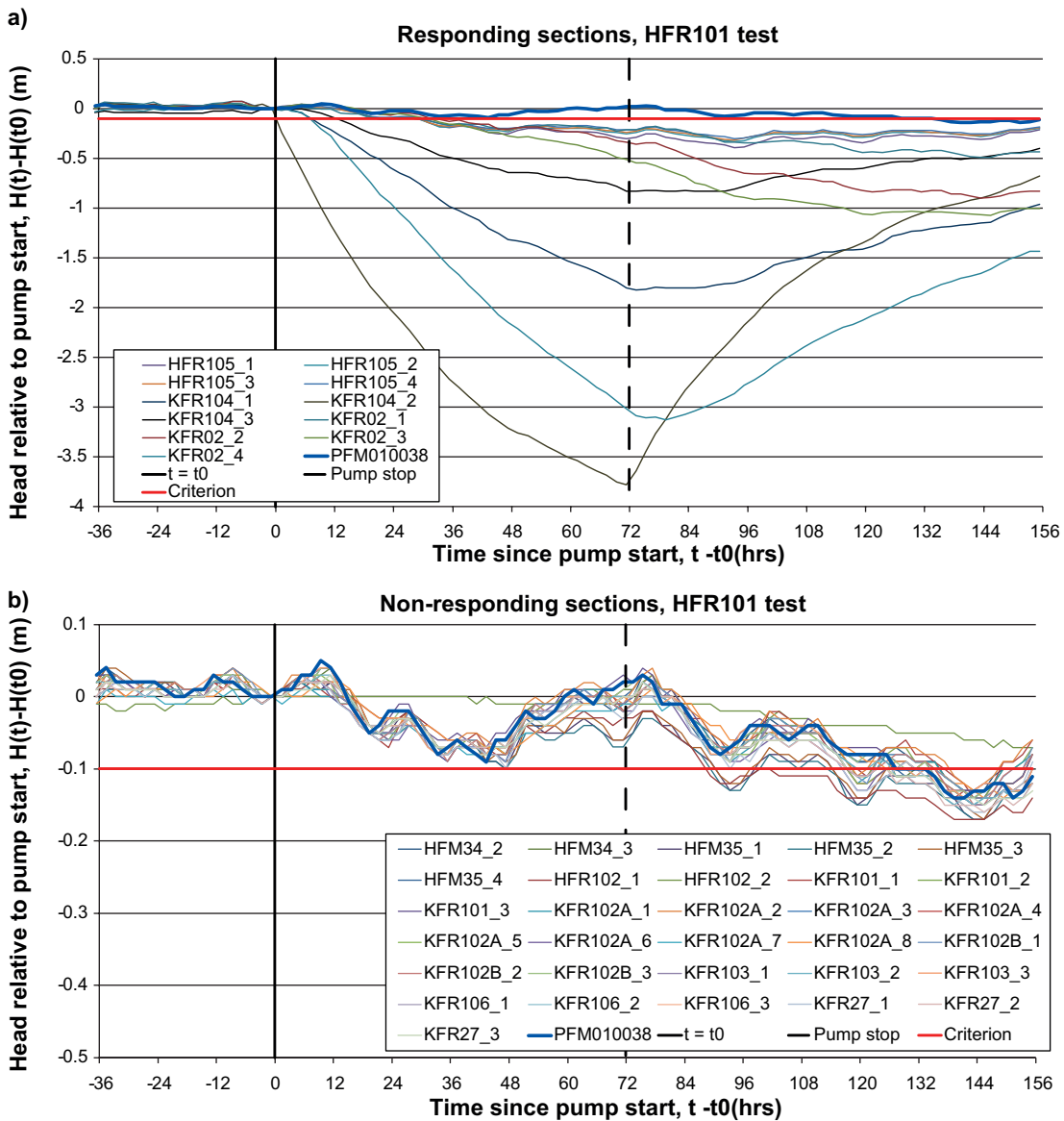
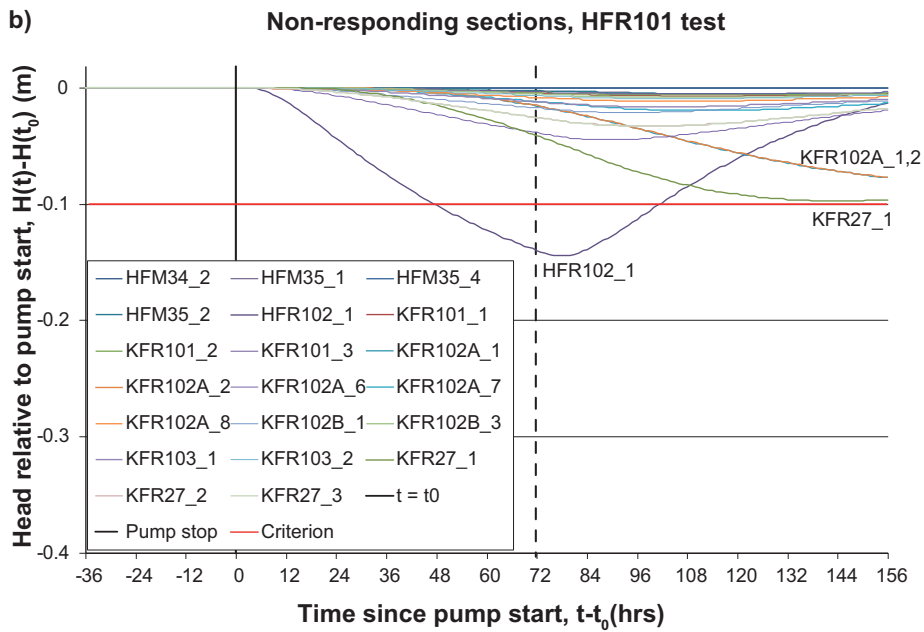
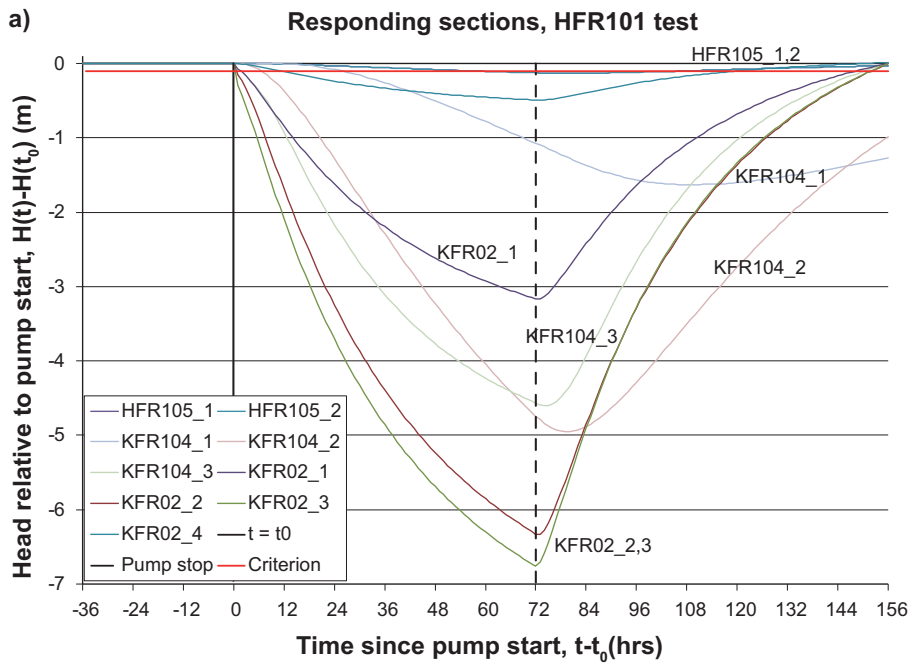
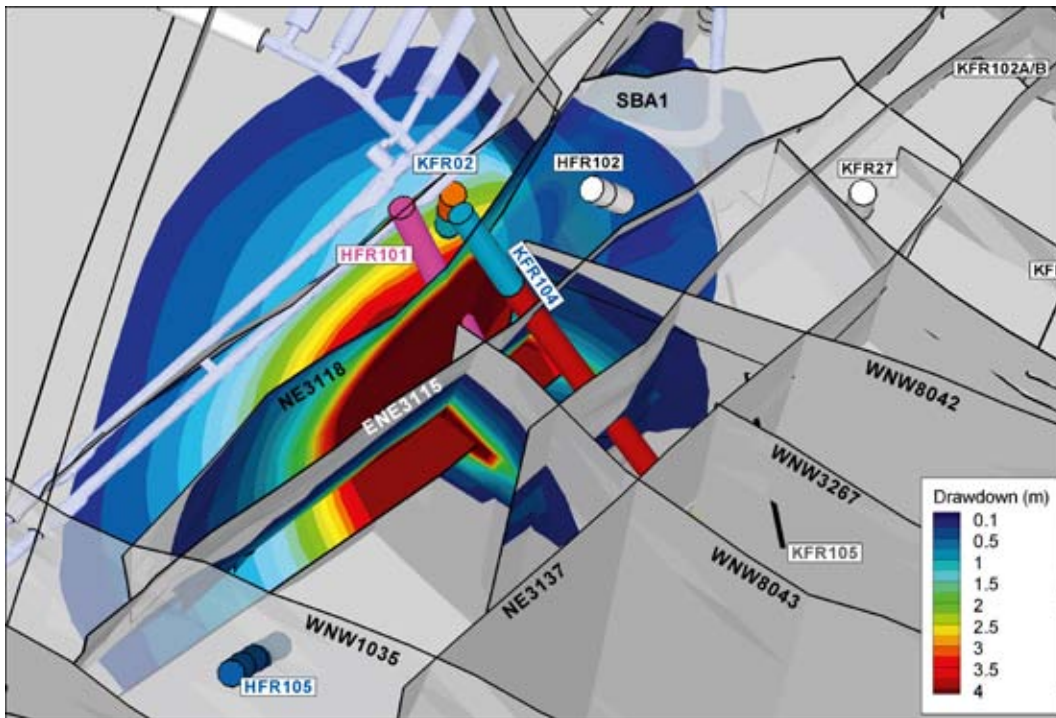


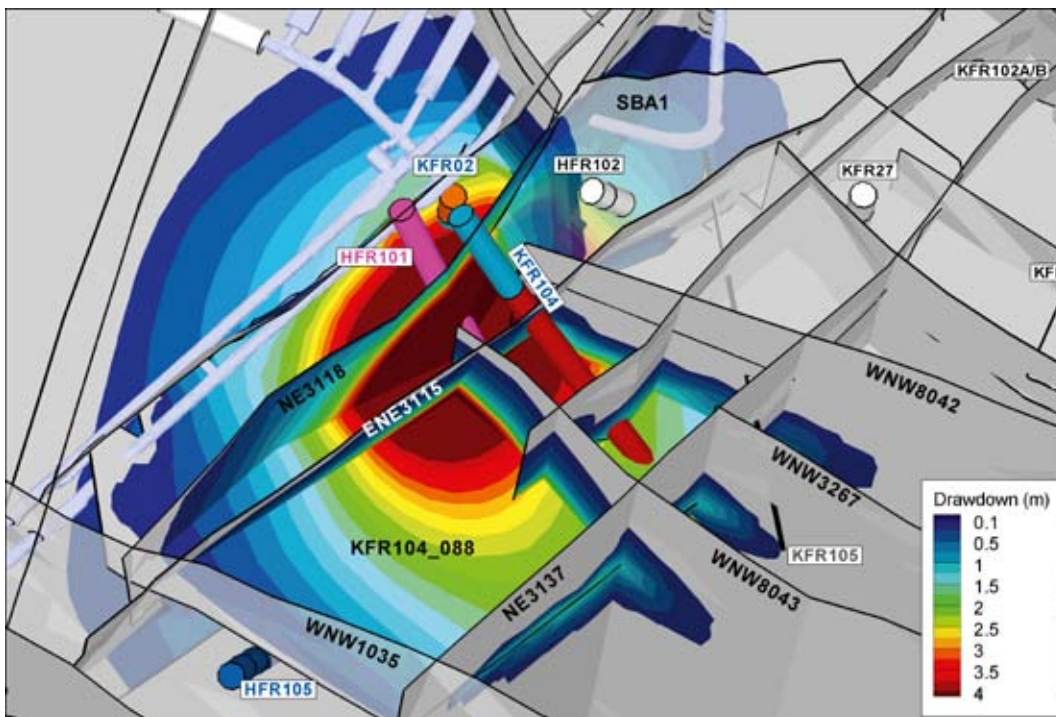
Figure 7-48. Monitored head relative to pump start in the HFR101 interference test; a) Responding sections, and b) non-responding sections. Sea level indicated by blue line (PFM010038).



**Figure 7-49.** Simulated responses to the HFR101 test in borehole sections classified as; a) “responding” and b) “non-responding”.



**Figure 7-50.** Simulated drawdown after 72 hrs of pumping in HFR101 with the original model setup. The responses observed in KFR104 and HFR105 are not reproduced. Only drawdown exceeding response criterion  $dp = 0.1$  m shown.



**Figure 7-51.** Simulated drawdown after 72 hrs of pumping in HFR101 for a modified model setup that mimicked the responses observed in KFR02, KFR104, and HFR105. Only drawdown exceeding response criterion  $dp = 0.1$  m is shown.

## **7.6 Confidence and remaining uncertainties**

### **7.6.1 Integration with geology and hydrogeochemistry**

The hydrogeological model for the bedrock incorporates components of the geological model and the hydrogeochemistry model; hence, identified uncertainties in Section 5.5 and Section 8.6 propagate into parameterisation uncertainty and model performance uncertainty. The regolith potentially has an important role in controlling the contact between the sea (positive flow boundary) and the underlying bedrock. The regolith layers of the SDM-Site Forsmark model have been assigned effective hydraulic conductivity values by means of model calibration to surface hydrological data in the Forsmark inland (Bosson et al. 2010). Although it has not been explicitly confirmed, these effective parameters are assumed to be valid for offshore marine sediments at SFR as well. It is possible that the hydraulic conductivity on land is somewhat enhanced due to frost heave, worm holes, tree roots, etc. Uncertainties in the regolith model and the possible need for new rock mechanics data will be handled in the SR-PSU safety assessment project.

Although confidence in the occurrence of steeply dipping deterministic deformation zones in the target volume intended for the SFR extension facility is high and the occurrence of undetected steeply dipping deformation zones longer than 300 m is judged unlikely, the sub-horizontal to gently dipping structures above –200 m elevation, including minor zones and discrete fractures, make a much more significant contribution to the pattern of local groundwater flow in the upper part of the bedrock than the steeply dipping deformation zones.

The hydrogeochemical database in the SFR area reveals complex mixing patterns arising from different evolutionary stages of the Baltic Sea as well as from the presence of the existing SFR facility. The general picture from hydrogeochemical interpretations is that water flows from the Baltic Sea to the existing SFR via a few steeply dipping deformation zones and then via sub-horizontal to gently dipping structures towards the existing SFR facility. However, considerable portions of older, pre-existing waters are still present close to the existing SFR facility, which suggests a heterogeneous and/or compartmentalised horizontal to gently dipping fracture system. Otherwise, the content would have been flushed out during approximately 25 years of operation.

The principal remaining uncertainty in SDM-PSU concerns the occurrence, size, nature and transmissivity of sub-horizontal to gently dipping structures in the uppermost part of the bedrock. Additional boreholes and hydraulic testing together with a geological discrete fracture network (DFN) model could possibly have improved the structural-hydraulic modelling in this regard. In SDM-PSU, the issue was handled in the hydrogeological modelling work by including a shallow bedrock aquifer (SBA) concept for some of the unresolved possible deformation zones together with a conditional hydrogeological DFN model for the remaining unresolved possible deformation zones, similar to that used in SDM-Site Forsmark. This setup is recommended as a hydrogeological base case for the SR-PSU safety analysis project, and it is suggested that the uncertainties involved be studied by means of alternative models, see Section 9.9.

Eight so-called SBA-structures have been inferred from the acquired structural and/or hydraulic data. In the context of data support and interpreted spatial extent in 3D space, the confidence in existence of the deterministically modelled SBA-structures varies (see Appendix H in Öhman et al. 2012 for details). A primary idea with their present interpretation in the hydrogeological model is to allow for a discussion about their potential importance for safety assessment since current data suggest that transmissive, sub-horizontal to gently dipping structures may intersect the rock vaults of the planned extension of the existing SFR facility depending on the decided location.

### **7.6.2 Discipline-specific issues**

Concerning the discipline-specific objectives of the modelling work, all collected hydrogeological data have been analysed and the interpretations, together with knowledge from previous modelling work, provide the basis for the hydrogeological model of the SFR area in SDM-PSU. There are various kinds of uncertainties in the collected data that should be noted. The most important of these are listed below. Öhman et al. (2012, 2013) describe their implications and handling in detail.

- All data have been collected in a disturbed hydrogeological setting; it is difficult to differentiate the characteristics of the natural fracture system from locally/temporarily affected properties.
- The historic and recent data are of different quality and test types/entities, and reflect different stages of the SFR disturbance. This complicates the use of a single hydrogeological model for the different sub-domains of SFR model volume.
- The PFL-f data indicate notably lower transmissivity inside the Central block compared with the surrounding rock mass closer to the Southern and Northern boundary belts. It is unclear to what extent this observation reflects an actual lateral trend in fracture-scale properties or a scaling effect, i.e. whether it reflects effective properties related to flow path length; see discussions on the role of PFL data subject to hydraulic chokes in Follin (2008), Follin et al. (2011) and Öhman and Follin (2010b).
- The PFL-f data has a key role in parameterisation of the hydrogeological DFN model for the less fractured rock mass outside deformation zones. The key uncertainties of the DFN parameterisation are related to the conceptual methodology where fracture size is coupled to measured transmissivity (i.e. apparent transmissivity). The DFN parameterisation was primarily calibrated to the transmissivity range of highest confidence, c.  $10^{-9}$  to  $10^{-6}$  m<sup>2</sup>/s (where data are abundant). Thus, the greatest uncertainties are found in the upper and lower tails of size/transmissivity distributions. More precisely, censoring of the practical detection limit in the PFL-f logging causes uncertainty in the intensity of low-transmissive features; this is perhaps of lesser significance in flow simulations, but due to the nature of power-law scaling, it causes a large uncertainty in the total intensity of the DFN. Power-law scaling also leads to particular uncertainty in the maximum size/transmissivity, which is related to available borehole length. In the DFN model, the upper tails of size/transmissivity are extrapolated beyond the largest measured transmissivity. This is related to the fact that the most transmissive fracture inside the model domain has not necessarily been captured in the available data sample; on the other hand, the existence of extrapolated high-transmissive features is not supported by the available data.
- The sample size of borehole data declines with depth. Scarce data at depth lead to uncertainty in depth trend analyses. Also, a depth trend fitted to maximum transmissivity may be artificially exaggerated, as a smaller sample size reduces the probability of finding large values (particularly in such highly skewed distributions as log-normal or power law). Nevertheless, the hydraulic data at SFR suggest the existence of a depth trend. Due to data limitations, the HCD depth trend for SDM-Site Forsmark (Follin 2008) was accepted as valid for the hydrogeological model for SFR. The HRD depth trend is numerically represented by defining three depth domains; the parameterisation of the Shallow and Deep domains is particularly uncertain due to little borehole coverage.
- There are several possible reasons for the decreasing trend in inflow, but more important is that probably all of them are reversible, meaning that the disturbed conditions seen today will not prevail at future times assessed by safety assessment. Since flow model calibration against present-day inflow rates represent disturbed conditions, interference tests conducted in the target area for the SFR extension are considered more useful for flow model calibration. Data from two interference tests are currently available. Unfortunately, these tests are of very short duration (3 days and 1 day) and the interpretations are complicated by sea level fluctuation and proximity to the existing SFR (potentially acting as a negative hydraulic flow boundary). The short duration of the tests necessitates that consideration be given to storativity in model calibration, introducing an additional source of uncertainty. Further, longer-duration interference tests, on the order of three weeks or more, could provide more robust data for model calibration purposes.
- The air ventilation system causes uncertainty in measured inflow data due to temperature and moisture differences between the SFR facility and the surrounding open air. The total contribution to flow measurements is expected to range from +30 L/min (condensing moisture during summer) to about -30 L/min (evaporation during dry winter months) (Öhman et al. 2012). The uncertainties in inflow measurements for subareas of the SFR control programme are estimated and discussed in Carlsson and Christiansson (2007). For example, it is unclear whether all the water from tributary areas passes the measuring point.

## 8 Bedrock hydrochemistry

### 8.1 Overview

Chapter 8 is based on the SFR hydrogeochemical site description version 1.0 (Nilsson et al. 2011). Both the geological and the hydrogeological model versions 1.0 underpin the hydrogeochemical modelling work which mainly follows SKB's established methodology (Smellie et al. 2002) (cf. Section 8.2). The location of the sampled boreholes and the midpoint of each sampled borehole section are shown in Figure 8-1.

#### 8.1.1 Palaeohydrochemistry

Like other sites studied by SKB, and especially that at Forsmark, the palaeohydrochemistry at SFR reveals the introduction and mixing of waters with different origins and varying salinity, mainly dating back to last deglaciation and Holocene times (cf. Figure 8-2). Prior to the last deglaciation, the groundwaters at the SFR are considered to have comprised non-marine types changing from brackish to saline with increasing depth and with components of an old meteoric water and maybe also old glacial meltwaters present at shallow and intermediate depths. During the last deglaciation (about 13,000 to 8800 BC), dilute glacial meltwaters under high hydraulic gradients penetrated to the maximum depths investigated at SFR (~400 m elevation) and probably to even greater depths, in agreement with observations at Forsmark. These waters mixed with the resident non-marine brackish to saline and old meteoric groundwaters, resulting in a range of brackish-glacial mixtures. Subsequently, during the Holocene, following the Ancylus Lake (8800/7500 BC), the Littorina Sea transgression (starting about 7500 BC with its maximum around 4500 to 3000 BC) resulted in a density-driven infiltration of saline waters into the bedrock along many of the same transmissive flow paths that previously channelled the glacial meltwaters. This produced varying degrees of mixing, whereas sometimes in less hydraulic conductive fractures or less transmissive rock mass between the major deformation zones, the glacial meltwaters appear to have been preserved. This is indicated by the occurrence of brackish-glacial groundwaters resident at higher levels in the bedrock than the later Littorina type groundwaters found at some locations.

However, unlike Forsmark, following the Littorina stage (and the subsequent transition to Baltic Sea conditions), the SFR area continued to be submerged, and slow moving, deep regional discharge flow paths within the highly transmissive deformation zones once again became established. This was the likely hydrogeological situation prior to commencement of the SFR investigation phase in 1985.

#### 8.1.2 Investigation prerequisites

Subsequent hydrogeochemical investigations at SFR contrasted with previous SKB site investigations in several important aspects.

- The present day hydrochemistry at SFR is influenced by anthropogenic mixing of the existing palaeo-groundwater types due to hydraulic drawdown (and some upconing) effects resulting from the excavation, construction and finally the operational phases of the SFR.
- Younger local Baltic-type waters have been introduced which, based on their tritium contents, are relatively recent and reflect drawdown effects since the SFR construction.
- The SFR site represents a shallow to intermediate groundwater environment (~400 m elevation) with most data from above -250 m elevation.
- The focus of investigations at other SKB sites was at greater depths (400/700 m) where the hydraulic systems are less dynamic and anthropogenic disturbance (i.e. contamination and mixing) is a more minor problem.
- Most of the available data from the SFR are concentrated around the disposal facility with the result that the hydrochemistry both laterally and vertically outside the facility is less well characterised, and the full extent of the drawdown/upconing mixing effects is still uncertain.
- Long-term series data (1986–2010) collected at different occasions are available from boreholes in the area of the SFR repository, whereas groundwater sampling campaigns in new boreholes (i.e. collection of a time series during continuous discharge) have generally been performed just once in each selected borehole section.



### 8.1.3 Interpretation and modelling

Groundwater samples collected from the early boreholes in the SFR repository (1986 to 2010), as well as from boreholes drilled within the recent SFR extension project (2007 to 2010), reveal complex mixing patterns arising from the different evolutionary stages of the Baltic Sea as well as from the presence of the SFR facility. The hydrochemical indicators Cl, Mg and  $\delta^{18}\text{O}$  indicate a large variation linked to the origin and residence time of the groundwaters despite the relatively small variation in salinity. The subdivision into groundwater types used for the Forsmark site was therefore modified for application to the SFR data. Based on the variation of Cl, Mg and  $\delta^{18}\text{O}$ , together with the palaeoclimatic history described above, a subdivision of the groundwaters into three major types was made: 1) local Baltic Sea groundwater type, 2) Littorina type groundwater with a glacial component, and 3) brackish-glacial type groundwater. Large numbers of samples that could not be allocated with certainty to any of the three groups above were assigned to a fourth group termed mixed transition type groundwater. This is not a specific water type since it reflects groundwater significantly influenced by mixing of glacial and brackish marine waters of different ages. These mixed transition type groundwaters, present at depths from about 60 to 400 m, have become more frequent over the last two decades as indicated from groundwater monitoring. This is probably a result of changing hydrogeological conditions in the SFR area caused by drawdown inflow to the tunnels. Principal Component Analysis using Cl,  $\delta^{18}\text{O}$ ,  $\delta^2\text{H}$  and  $\text{SO}_4$  supported the discrimination of groundwater types based on expert judgment described above.

These defined groundwater types are central to the explorative analyses performed in order to evaluate the variations in groundwater chemistry as well as for further detailed evaluation using different modelling approaches such as mixing modelling, geochemical equilibrium modelling and redox modelling. Some important findings and results can be summarised as follows.

- Most of the SFR groundwaters seem to be in equilibrium or slightly oversaturated with respect to calcite. The latter condition may either represent a real situation or be a result of  $\text{CO}_2$  outgassing during pH measurements. Although some calcite dissolution may occur during infiltration of Baltic Sea waters, the intensity of this process must be low due to the high alkalinity content and near neutral pH of sea waters. Thus, the alkalinity buffer capacity of the system does not appear to be reduced by the input of Baltic Sea waters.
- The main source of sulphur in the SFR groundwaters is the intrusion of past (Littorina) and present (Baltic) sea waters, which have mixed with the earlier resident groundwaters. According to the available isotopic data ( $\delta^{34}\text{S}$ ), sulphate-reducing microbial activity seems to have played a minor role in determining dissolved sulphate concentrations, except in some of the Brackish-glacial type groundwaters with low sulphate content and high  $\delta^{34}\text{S}$  values. Also, some of the groundwaters with large fractions of present-day Baltic Sea waters exhibit  $\text{SO}_4/\text{Cl}$  ratios that suggest the existence of active sulphate-reducing processes, although the effect is small. Like the Forsmark groundwaters, all the SFR groundwaters are undersaturated with respect to gypsum and celestite and in equilibrium with respect to barite. However, none of these minerals appear to have appreciably affected the dissolved sulphate contents. The fact that the waters are saturated with respect to barite suggests that not only barium concentrations, but also radium concentrations, are related to the sulphate concentrations in the groundwaters (Gimeno et al. 2011).
- The potentiometric Eh measurements in the SFR groundwaters provide both positive and negative values. Reducing conditions (Eh values between  $-140$  and  $-190$  mV) are in line with those measured in the Forsmark groundwaters and are apparently caused by the occurrence of an iron phase with an intermediate crystallinity and/or by ferrous clay minerals, both of which have been identified. Oxidising conditions in groundwaters (represented by Eh values between  $+30$  and  $+110$  mV) appear to be controlled by amorphous Fe(III) oxyhydroxides and should indicate the existence of present-day or recent oxic environments, since these phases quickly recrystallise (e.g. months) to less soluble and more stable phases under reducing conditions.
- The redox capacity provided by the fracture minerals in the hydraulically conductive fractures is mainly found in Fe (+II) present in chlorite and clay minerals and to some extent in the less abundant sulphides (mainly pyrite).
- M3 modelling did not resolve perfect mixing proportions of the end-member waters that have contributed to the chemical composition of the SFR groundwaters. The results reveal the expected limitations in the M3 modelling of a dataset reflecting mixing of waters with different ages and origins but with small differences in chemical composition (e.g. Baltic versus Littorina). M3 helped to recognise these difficulties which correspond closely to the present conceptual understanding of the site.

### 8.1.4 Integration with geology and hydrogeology

The division into different groundwater types has also facilitated interaction and integration with the geological and hydrogeological models, making it possible to construct a hydrogeochemical site descriptive model (SDM) for the SFR site. The distribution of the different groundwater types shows that the major deformation zones appear to have served as groundwater flow pathways over long periods of geological time, whereas single discrete fractures in rock volumes between these major zones generally contain older and more isolated groundwaters. The steeply dipping structures in particular have facilitated the drawdown of modern Baltic Sea water which has been observed since the excavation and construction of the SFR commenced some twenty five years ago.

The evolution of the groundwater system over time, i.e. since the last glaciation and more recently since excavation and construction of the SFR repository, shows that: 1) present-day hydraulic conditions have preserved groundwater patterns which replicate to a large extent what will occur during the next deglaciation (long-term perspective), and 2) some indication of the future impact of extended excavations and underground construction on groundwater chemistry is suggested from previous and present-day observations at the SFR site (short-term perspective). There are several examples of observations and conclusions associated with bedrock features and hydrogeology (Öhman et al. 2012).

- Several major zones are heterogeneous with respect to hydraulic properties as well as to groundwater composition. Furthermore, the hydraulic transmissivity data above –200 m elevation were not found to be higher inside or close to deformation zone intercepts if no distinction is made regarding types of deformation zones. The few transmissivity data below –200 m elevation appear more correlated to deformation zones.
- There are several examples of borehole sections with less saline groundwater located below sections with more saline water in the same borehole. The most extreme examples are boreholes KFR101 and KFR104, where the chloride concentrations in the groundwater at the bottom of both boreholes are significantly lower than in the Baltic Sea. These conditions, which are not usually observed (but probably do occur) in groundwater environments below land, provide strong indications of preserved isolated groundwaters in parts of the less transmissive bedrock between and within compartments in the major deformation zones.
- There is a significant change in the groundwater composition towards increased Littorina infiltration in several boreholes at their intercepts with zone ZFM871 (formerly zone H2). It is obvious that this plane is, at least in part, substantially more transmissive than the bedrock volumes above and below and thereby acts as an important groundwater flow pathway. However, at a distance from zone ZFMNW0805A, B, infiltration is less pronounced and has resulted in a mixed transition type groundwater.
- Different sediment thicknesses may have also played a role in the presence of local Baltic type groundwaters. For example, time-series hydrochemical data indicate that whilst the Northern boundary belt and zone ZFMNNE0869 (formerly zone 3) (associated with thin sedimentary cover and rapid intrusion of local Baltic type water) strictly follows a mixing line between Littorina and local Baltic type groundwaters, the Southern boundary belt (associated with thick sedimentary cover which impedes rapid intrusion of local Baltic type water) shows a less marine signature.
- An additional water source may include the discharge of shallow inland groundwater from Forsmark via the upper conductive shallow sheet joints constituting the hydraulic cage feature, later referred to as the Shallow Bedrock Aquifer (SBA) (Öhman et al. 2012). Potentially, this may supply a groundwater mixture of young meteoric and Littorina origin to this depth interval within the Southern boundary belt. However, it is not clear at the moment whether this mixture could progress further to the northeast beyond the Southern boundary belt to the SFR site. This transport may also cause or contribute to the less marine signature of the groundwater in the Southern compared with the Northern boundary belt.

## 8.2 Methodology

The SFR investigations differ from those at Forsmark and Laxemar (Laaksoharju et al. 2008, 2009) in that the bulk of the data have been accumulated over a period of about 25 years, with the result that only the most recent data representing the SFR extension studies have benefited from the Forsmark and Laxemar experience. For this reason, not all of the methodology guidelines for the Forsmark and Laxemar hydrogeochemical programmes as set out in Smellie et al. (2002) could be applied to the SFR studies.

The investigation programme within the SFR extension project was carried out in 2008 and 2009 with some supplementary studies conducted in October 2010 and June 2011. The geoscientific investigations entailed the drilling of four percussion boreholes and seven cored boreholes (Figure 8-1). All the cored boreholes are of the conventional type (SKB 2008a), apart from one telescopic-type borehole (KFR102A) (SKB 2001) similar to those frequently used during the Forsmark site investigations. Furthermore, all percussion boreholes and six of the cored boreholes are drilled from the surface (from the pier and from the little islet close to the pier) and one cored borehole is drilled from the construction tunnel in the present SFR facility (cf. Figure 8-1). Time-saving considerations and the exposed location under rough weather conditions on the pier were the conclusive arguments for the choice of conventional boreholes. For the same time-saving reasons, groundwater sampling in preinstalled fixed borehole sections was preferred over the more advanced downhole equipment previously used in the site investigations at Forsmark (Laaksoharju et al. 2008) and capable of sampling and measuring variable section depths and section lengths.

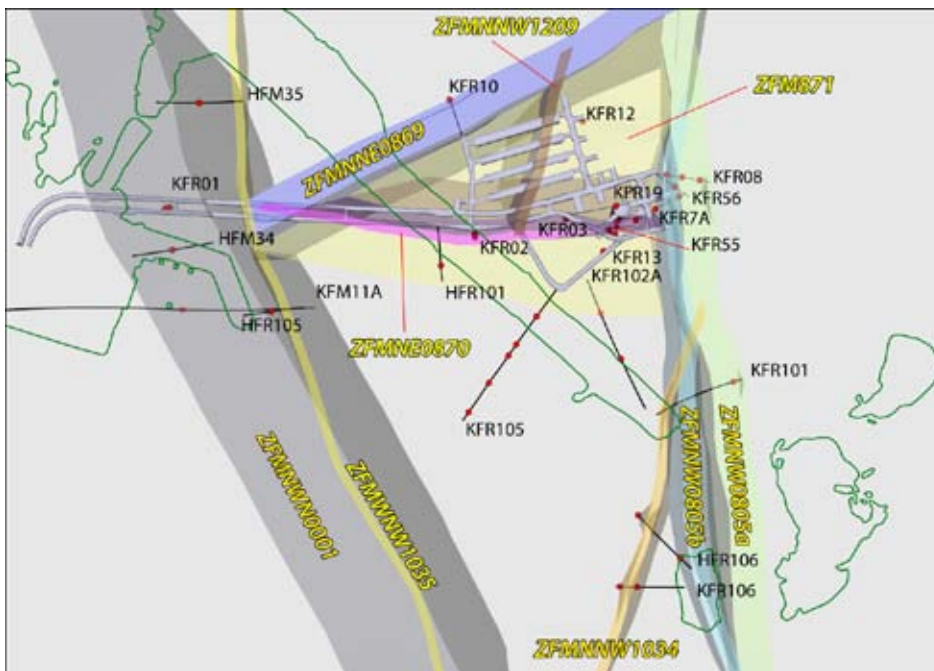
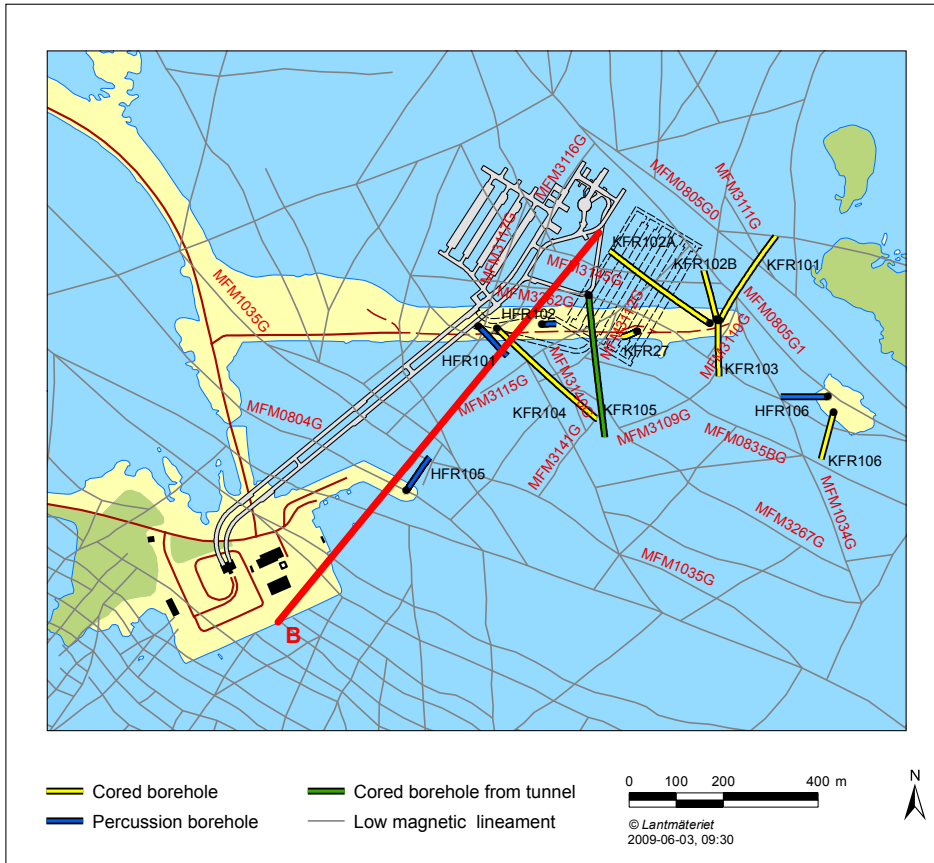
Information from BIPS logging (Borehole Image Processing System) and Differential Flow Logging (Posiva Flow Log) was essential for locating the optimum borehole sections for groundwater sampling and pressure monitoring.

The methodology used to evaluate the hydrogeochemical data for the SFR site resembles generally that used in the Forsmark site investigations (cf. Laaksoharju et al. 2008). In contrast, the modelling work was performed in three steps, resulting in three model versions/reports (0.1, 0.2 and 1.0). The strategies employed, and the stepwise progress and reporting occasions, are outlined below.

- Initially, a systematic data evaluation and retrospective QA was performed. This included the early SFR boreholes drilled in the 1980s and hydrochemical data obtained during the period 1984 to 2007.
- Compilation of the hydrochemistry data table version 0.1 including groundwater data from early boreholes drilled from the present SFR repository and representing the time period 1984 to 2007.
- A first visualisation in 3D of chloride, magnesium and  $\delta^{18}\text{O}$  values in relation to major deformation zones (geological site descriptive model, version 0) resulted in a better understanding of the importance of the deformation zones, or rather the differences in hydraulic transmissivity, in explaining the variation in groundwater composition in different geological environments. It was observed, in common with the Forsmark site and even more clearly, that a younger groundwater with a marine signature was present within or close to the deformation zones, whereas older non-marine groundwaters occurred mainly in the less transmissive bedrock.

This work was reported in hydrochemical site description version 0.1 presented in Nilsson A-C (2009). The main purpose was to become acquainted with the dataset and groundwater variability, as well as to report inconsistencies and outliers among the data. This data quality evaluation provided the basis for the following interpretation steps listed below.

- Adaption of a conceptual palaeohydrogeochemical model to the SFR site, based on the recent conceptual model for the Forsmark site.
- Evaluation of additional hydrochemistry data. Sample quality assessment and compilation of the hydrochemistry data table version 0.2, including the recent data from boreholes drilled within the SFR extension project and the period from 1984 to 2009.
- Identification/definition of four different groundwater types based on the palaeohydrogeochemical conceptual model. Groundwater-type classification of the samples in hydrochemistry data table version 0.2 was based on the procedure used at Forsmark (Laaksoharju et al. 2008). Chloride, magnesium and  $\delta^{18}\text{O}$  data were used to further refine the different groundwater types.
- Explorative data evaluation using traditional geochemical approaches, such as x-y scatter plots, to describe depth variations and provide an initial understanding of the origin and evolution of the groundwaters and to check correlations related to groundwater types.



**Figure 8-1.** Top: Locations of recent boreholes drilled within the SFR extension project, where the red line B represents the vertical cross-section outlined in Figure 8-9. Bottom: Location of sampled borehole sections in relation to major deformation zones, top view. Three Forsmark boreholes (HFM34, HFM35 and KFM11A) are added to the figure. The centre of each section is shown as a solid red circle and the zones are labelled according to present terminology. The green contour represents the coast line.

This work was presented in hydrochemical site description version 0.2 (Nilsson et al. 2010), which focussed on water-type classification, explorative analyses and construction of a preliminary conceptual model. The identified groundwater types were depicted in 3D and in relation to major deformation zones (based on the geological site descriptive model, version 0.1). The next stage included the following components.

- Evaluation of additional hydrochemistry data from 2010. Sample quality assessment and compilation of hydrochemistry data table version 1.0 including data from the period from 1984 to 2010. The additional complementary data from 2010 included fracture mineral studies and redox measurements.
- Water type classification of additional samples from the supplementary investigations in 2010. The water type classification of the entire data set was supported by Principal Component Analyses (PCA).
- Mixing modelling, geochemical equilibrium modelling and redox modelling.

The geochemical modelling of the major groundwater/mineral systems was performed using all available data of acceptable quality, which provided input to determine the main geochemical processes influencing the behaviour of variables such as pH and Eh and, in general, all the parameters influenced by microbial or water-rock interaction processes. These include: carbonate, sulphate, silica, fluoride and the redox-sensitive elements (Fe(II), S(-II), Mn, N(III, V, -III)), as well as the gases CH<sub>4</sub> and H<sub>2</sub>. The approach involved:

- Hydrogeochemical modelling was performed with the PHREEQC code (Parkhurst and Appelo 1999) and using the WATEQ4F thermodynamic database (Ball and Nordstrom 2001), with the modifications reported in Gimeno et al. (2008, 2009).
- As a first step, modelling was focussed on speciation-solubility calculations related to the carbonate, sulphate, silica and fluoride systems.
- The second step was modelling of the redox systems including evaluation of the potentiometric Eh measurements, redox pair calculations and speciation-solubility calculations for the main redox mineral phases. These results were integrated with the mineralogical and microbiological (when applicable) data.
- In all the cases, a substantial effort was made to integrate existing information concerning hydrochemistry, mineralogy and microbiology (when applicable).

A special effort was made to analyse the uncertainties associated with the measurement, modelling and interpretation of:

- groundwater origin and water type definition,
- temporal and spatial variability,
- the present-day inflow of Baltic sea waters into the bedrock, as the main anthropogenic effect influencing the SFR system,
- data uncertainties.

Finally, all available results were integrated to construct an overall conceptual model for the SFR area. The final version 1.0 is reported in Nilsson et al. (2011).

## **8.3 Groundwater type categorisation and groundwater origins**

### **8.3.1 Present conceptual model**

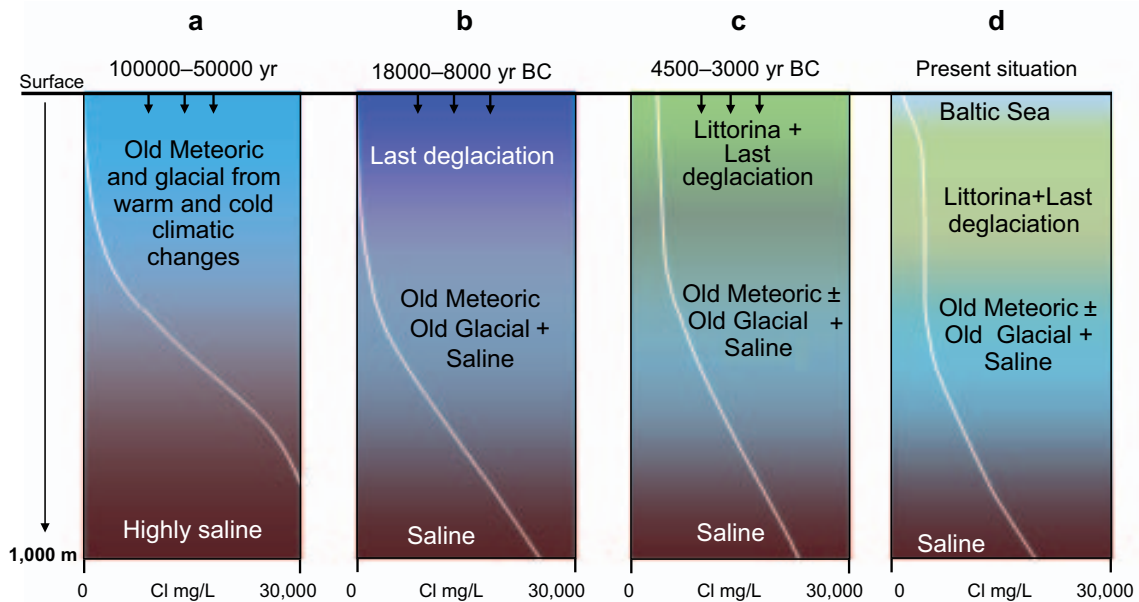
During the Phanerozoic when the Forsmark region, like most of Sweden, was covered with sediments overlying the present bedrock surface (cf. Figure 3-2), the groundwater was probably very saline (around 20 wt% consisting mainly of Ca-Cl fluids (Sandström et al. 2008 a, b). It is therefore

reasonable to assume that the Precambrian Shield area of southeast Sweden was saturated with brine solutions during this period, and the present-day deep non-marine saline groundwater may still contain components of this original brine water.

Of much greater importance for the present-day groundwater chemistry at SFR is, however, the evolution during Weichselian and Holocene times. Figure 8-2a shows a tentative distribution of groundwater types and salinity gradients in the SFR area before the intrusion of meltwater from the last deglaciation just prior to the Holocene. Based on an understanding of the climatic changes that have occurred since the last deglaciation, it is assumed that old meteoric waters containing components derived from both temperate and cold climate events were present at that time. Assuming favourable gradients, old meteoric waters could have been partially mixed with deeper, more saline groundwaters, but the high density contrast would have prevented further mixing. What can be said with confidence is that the residual old brackish waters in the Forsmark/SFR region do not have a marine signature. In the SFR model volume, the old non-marine water has been mixed with glacial water from the last deglaciation (Figure 8-2b), and the largest components of glacial waters are found between -100 and -300 m elevation.

During the subsequent Littorina Sea stage (Figure 8-2c), the SFR area was covered by brackish marine water with an assumed salinity of 6,500 mg/L Cl (Pitkänen et al. 1999, 2004). This maximum salinity (twice the present salinity of the Baltic Sea) lasted at least between 4500 and 3000 BC. Due to the unstable density situation caused by the introduction of higher-density Littorina Sea water above previously infiltrated meltwater of lower density from the last deglaciation, the Littorina Sea water entered the deformation zones and fractures and mixed with or displaced the previously resident fresh water of glacial and old meteoric character.

The present-day situation is shown in Figure 8-2d, which illustrates the intrusion of present Baltic Sea water in some fractures down to about -100 m elevation. This intrusion is probably driven to a large extent by the hydraulic gradient created by the existing SFR storage facility.



**Figure 8-2.** Sketch showing tentative salinities and groundwater type distributions versus depth down to 1,000 m depth for the transmissive deformation zones at the SFR (modified after Laaksoharju et al. 2008). From left to right: a) situation prior to the last deglaciation, b) last deglaciation and intrusion of Late Weichselian meltwater, c) Littorina Sea water penetration caused by density intrusion, and d) the present-day situation with possible penetration of local Baltic Sea water. The white line shows chloride concentration versus depth.

### 8.3.2 Groundwater types

The dataset of the SFR groundwaters shows some characteristic features:

1. The range in chloride concentration of the SFR groundwaters is small (1,500 to 5,500 mg/L Cl) compared with the Forsmark site investigation area (50 to 16,000 mg/L Cl), but the  $\delta^{18}\text{O}$  values show similar variation ( $-15.5$  to  $-7.5\%$  V-SMOW) as at Forsmark ( $-16$  to  $-8\%$  V-SMOW).
2. The SFR data set covers depths down to about  $-250$  m with two sampling locations at approximately  $-300$  and  $-400$  m elevation.
3. Fresh meteoric water components of present-day precipitation type are assumed to be minor at all depths.
4. Marine indicators, such as Mg/Cl, K/Cl and Br/Cl ratios, show relatively large variations, especially considering the limited salinity range and the shallow depth of sampling, and it can be suspected that components of both the more saline Littorina Sea water and the more diluted present-day Baltic Sea water are present.

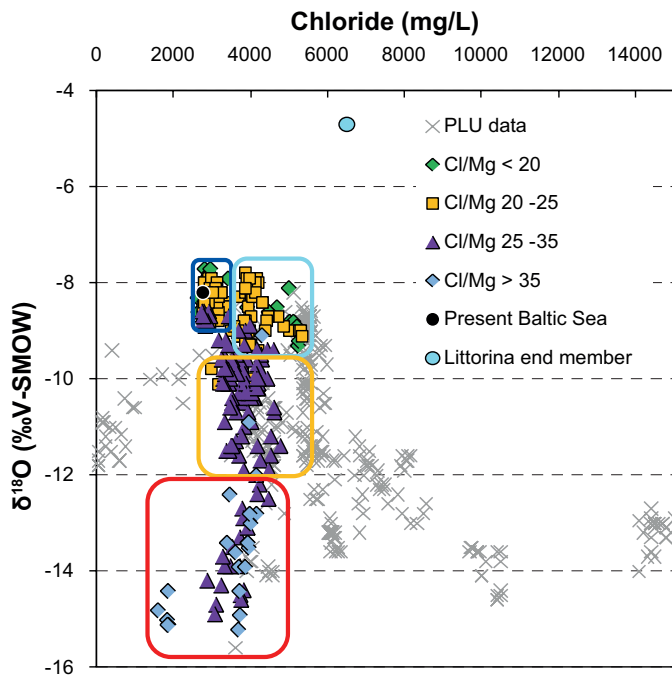
Based on chloride, magnesium and  $\delta^{18}\text{O}$  data and the palaeoclimatic evolution outlined above, and considering the need to separate groundwaters of different origins and residence times in the bedrock, a modified subdivision of the groundwaters was necessary compared with the one used during the Forsmark site investigation. In contrast to the situation at Forsmark, where the aim of the hydrogeochemical programme was to provide a description of undisturbed conditions in the bedrock, the SFR samples cover a time span from 1986 to 2010 during which the entire SFR facility was constructed and put into operation. The present-day groundwater chemistry is influenced by drawdown to the tunnel, which will be important in some of the sampled sections where inflow of Baltic Sea water can be expected. In other borehole sections, altered hydraulic conditions have led to a significant mixing of different groundwaters, whereas other borehole sections have remained unaffected and show stable groundwater chemistry throughout the operational phase of the SFR.

It is evident that the SFR samples, like the Forsmark samples, show great variation in Mg for groundwaters with similar Cl contents. However, almost all of the SFR samples are somewhat depleted in magnesium compared with the initial marine Mg/Cl ratio. Sulphate is another marine indicator that shows the same major trends as Mg when plotted versus Cl. However, in the early analyses there was unfortunately a greater uncertainty in the  $\text{SO}_4$  measurements, so the Mg/Cl ratio has been preferred as a marine indicator. Figure 8-3 shows all the groundwater samples suitable for modelling (1986–2010), coded according to their Cl/Mg ratio and plotted in a Cl versus  $\delta^{18}\text{O}$  diagram. The plot also shows the Cl and  $\delta^{18}\text{O}$  values for the different groundwater types: Local Baltic, Littorina with a glacial component, brackish-glacial and the brackish water of the mixed transition type (cf. Table 8-1 for description).

The present-day method of subdividing the SFR groundwaters into different types for a better understanding has been broadly successful and has also been tested using principal component analysis with Cl,  $\text{SO}_4$ ,  $\delta^2\text{H}$  and  $\delta^{18}\text{O}$  as input compositional variables (Nilsson et al. 2011), which lent further support to the subdivision.

### 8.3.3 Groundwater residence time

A key factor in validating the suggested past and present groundwater evolution in the SFR model volume is to constrain the average residence time for each of the defined groundwater types. Tritium ( $^3\text{H}$ ) and carbon-14 (as percentage modern carbon, pmC) can suggest different times of isolation from the atmosphere. However, in defining the different groundwater types, the ratio of the stable oxygen isotopes (expressed as  $\text{d}^{18}\text{O}$ ) has been used also to distinguish groundwaters with cold climate components (glacial meltwater), which in turn provides relative information on residence time. A small number of chlorine-36 analyses are also available and have been interpreted together with previously analysed samples from the Forsmark, Laxemar/Simpevarp and Olkiluoto sites.



**Figure 8-3.** Plot of  $\delta^{18}\text{O}$  ‰ (V-SMOW) versus chloride concentration. The SFR data are from the period 1986–2010. PLU data include data from the Forsmark site only. The figure shows the groundwater samples categorised according to the Cl/Mg weight ratio, and the boxed areas signify different groundwater types (cf. Table 8-1). There is continuous mixing between the Baltic and the Littorina type groundwaters. The boundary between the two marine groundwater types is set at a chloride concentration equal to 3,500 mg/L.

**Table 8-1. Presentation of groundwater types used to categorise groundwater samples from the SFR site.**

**Local Baltic Sea type** ■

**Water type;** Brackish marine water with a Cl content of 2,500 to 3,500 mg/L and  $\delta^{18}\text{O}$  of  $-9$  to  $-7.5$ ‰ V-SMOW; Na-(Ca)-(Mg)-Cl-SO<sub>4</sub> in type. This is a brackish water with a Cl/Mg weight ratio  $< 27$  (with a few exceptions) indicating a marine origin, which is further supported by the concentrations of sulphate and potassium and the Br/Cl ratio. Some modification of this water has occurred due to ion exchange and microbial reactions, resulting in a lowering of Mg, K, Na and SO<sub>4</sub><sup>2-</sup> and enrichment of Ca and HCO<sub>3</sub><sup>-</sup> compared with the Baltic Sea. However, the Cl and  $\delta^{18}\text{O}$  ranges correspond to that of Baltic Sea water sampled off the coast at SFR. Some samples referred to as the Local Baltic Sea type also contain components of Littorina and glacial water types. The Local Baltic Sea waters are the youngest waters present at the SFR.

**Littorina type water with a glacial component** ■

**Water type:** Brackish marine water with a Cl content of 3,500 to 6,000 mg/L and  $\delta^{18}\text{O}$  of  $-9.5$  to  $-7.5$ ‰ V-SMOW; Na-Ca-(Mg)-Cl-SO<sub>4</sub> in type. This water type has a higher salinity than the present-day Baltic Sea and is commonly found in the Forsmark area to the west. The Cl/Mg ratio is generally  $< 27$ , but exceptions do occur. The sulphate concentration and Br/Cl ratio suggest a marine origin for the saline component. The potassium concentration is elevated but not as high as in the Local Baltic Sea type groundwater. The Na/Ca ratio is lower than the marine ratio. These changes are due to ion exchange but also to dilution by the contributing glacial meltwater. The Littorina type groundwater previously observed during the site investigations at Forsmark is often more saline and shows similar potassium concentrations to the Baltic Sea water. The depleted  $\delta^{18}\text{O}$  values compared with the Littorina end member ( $-5$ ‰ V-SMOW) indicate a significant component of glacial water probably from the last deglaciation. Some samples may also contain portions of Baltic Sea water.

**Mixed brackish water (transition type)** ■

**Water type:** Brackish groundwater with a Cl content of 2,500 to 6,000 mg/L and  $\delta^{18}\text{O}$  of  $-12.0$  to  $-9.5$ ‰ V-SMOW; Na-Ca-(Mg)-Cl-(SO<sub>4</sub>) in type. The waters in this group result from mixing of the above three groundwater types (mixing may be either natural or artificial due to the drawdown caused by the SFR repository or during the drilling and sampling procedures). Most of these waters contain components of brackish marine waters (maybe of different ages but mostly Littorina in type) + glacial waters (from the last deglaciation or older) ± weakly brackish waters.

**Brackish-glacial type** ■

**Water type:** Brackish-glacial: Na-Ca-Cl groundwater with a Cl content of 1,500 to 5,000 mg/L and  $\delta^{18}\text{O}$   $< -12.0$ ‰ V-SMOW; Na-Ca-Cl in type. This water type has a low Mg (Cl/Mg ratio  $> 32$ ) and K, higher Br/Cl ratios than marine waters, and is usually relatively low in SO<sub>4</sub> and HCO<sub>3</sub>. It is a mixture of glacial (last deglaciation or older) + brackish non-marine water ± Littorina. The marine signature is generally weak and the Br/Cl ratio deviates from that of marine waters. The brackish-glacial waters are the oldest present at the SFR and the amounts of post-glacial components are small.



It is important to bear in mind that the groundwater samples are usually influenced by mixing. This is especially true of the SFR samples, as the present SFR tunnels have altered the hydrogeological conditions resulting in an increased drawdown of young Baltic Sea water along some fracture zones, and in others resulting in the mixing of groundwater types of different age and origin. The oldest groundwater in the SFR area contains significant portions of glacial meltwater identified by depleted  $\delta^{18}\text{O}$ . The waters with the most depleted  $\delta^{18}\text{O}$  also show the lowest  $^{14}\text{C}$  and tritium below the detection limit, indicating that the contribution of postglacial (Littorina) water has been small and that the contribution of present Baltic Sea water is negligible.

The chlorine-36 analyses of four groundwater samples from SFR (two waters of brackish-glacial type, one Littorina type and one present Baltic type) showed patterns similar to the Forsmark samples, although the Littorina type sample (which showed a fairly low Cl concentration of about 3,700 mg/L) indicated a significant portion of Baltic Sea water. The two brackish glacial samples supported the presence of non-marine brackish water mixed with the glacial component.

In the larger fracture zones, and especially at shallow depth, the groundwater was probably very dilute following the deglaciation and during the following period of fresh water accumulation on the sediment/bedrock surface (the Ancylus Lake). When the Littorina Sea transgressed it intruded into the bedrock driven by density differences. The combined isotope information supports the presence of marine water with higher salinity and longer residence times than the present Baltic Sea groundwater type. This brackish marine water subsequently mixed with dilute water with depleted  $\delta^{18}\text{O}$ . It is also clear that the Littorina water has not penetrated the less transmissive fractured bedrock between the more highly transmissive fracture zones to the same extent as the glacial meltwater.

The fact that all samples from the SFR model volume contain groundwaters with bicarbonate concentrations higher than 30 mg/L, and the fact that all carbon isotope analyses show the presence of radiocarbon (5 to 65 pmC), indicate that the major input to the carbon system has occurred after the last deglaciation.

The last water type to intrude is the present Baltic Sea. Based on its tritium content, which is similar in many of the SFR sampling sections, this intrusion is relatively late and has been accelerated by the drawdown caused by the SFR facility. The origin of the groundwaters and the sequence of events are summarised in Table 8-2.

## 8.4 Groundwater composition and reactions

### 8.4.1 Major ion trends and behaviour

The hydrogeochemical data included in SFR version 1.0 represent the depth range -20 to -400 m elevation (mostly above 250 m depth) and plots of selected major groundwater ions and pH are shown in Figure 8-4a to f (relative to elevation), Figure 8-5a to f (relative to chloride), and Figure 8-6a and b (pH relative to elevation and chloride), respectively. The colour codes refer to the major groundwater types characterising the SFR.

Chloride (Figure 8-4a) is one of the main components in the SFR groundwaters, ranging at most between about 1,600 to 5,500 mg/L; most plot between 2,700 to 4,500 mg/L. The most saline groundwater is generally found at intermediate depths (100-200 m) and is of the brackish marine Littorina type. The more dilute brackish water found at shallow depths (~ 100 m) is of local Baltic type, and the most dilute waters (1,600 mg/L Cl) are of brackish-glacial type at about 240 m depth.

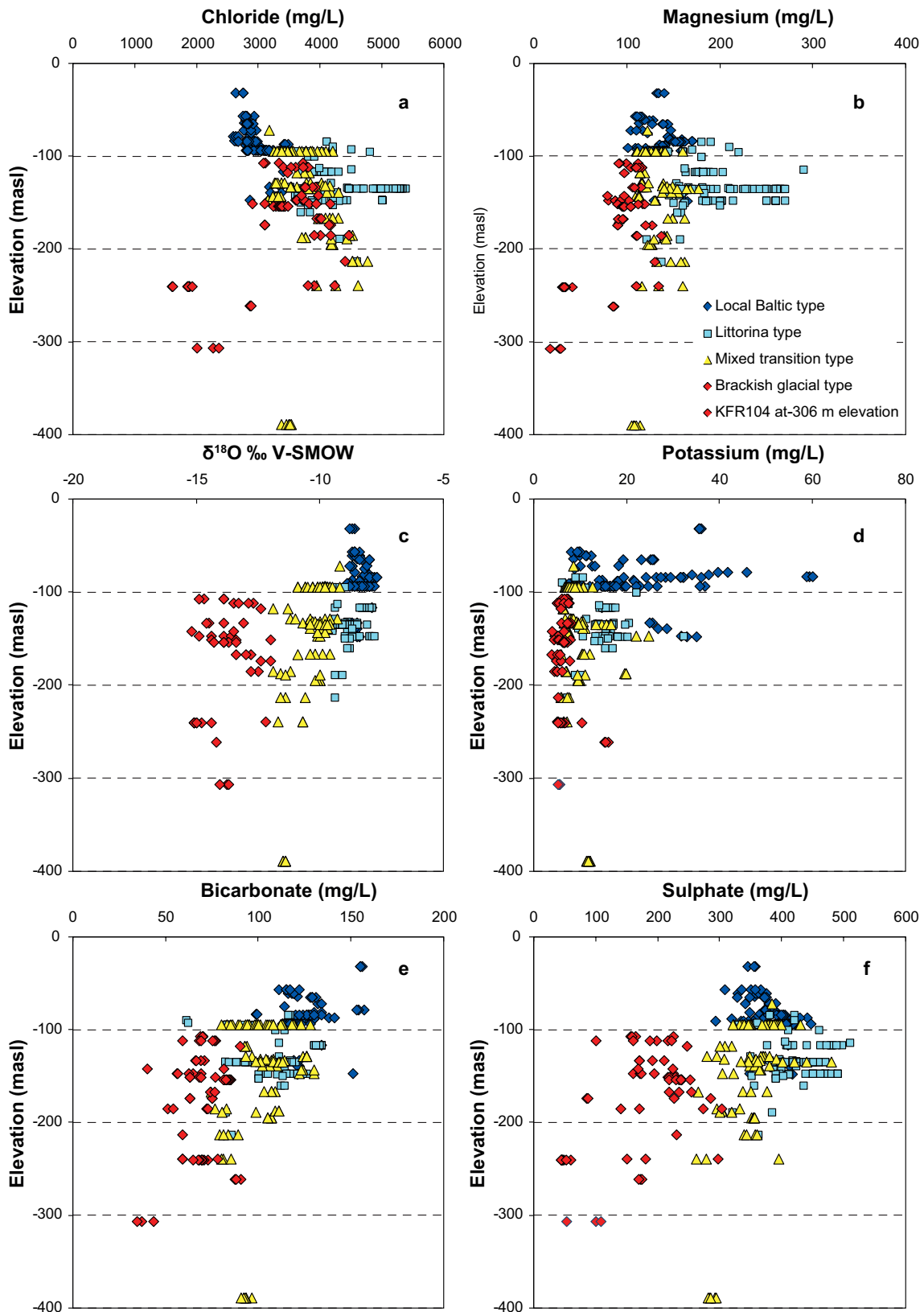
The magnesium concentration (Figure 8-4b) shows the marine influence in most groundwaters within the SFR model volume and varies between 30 and 300 mg/L. The younger marine groundwaters of the local Baltic type generally show magnesium concentrations between 90 and 150 mg/L and are found down to depths of about 100 m, whereas the older marine groundwaters of the Littorina groundwater type show magnesium concentrations between 150 and 280 mg/L and are found at depths between 100 and 200 m. The magnesium concentrations in groundwaters of the two mainly non-marine water types are still relatively high, although the Mg/Cl ratio is reduced. Magnesium (Figure 8-5a) is susceptible to ion-exchange reactions, and consequently the brackish marine groundwaters do not strictly follow the mixing line between pure end members. However, despite the effect of reactions, the Mg content in the brackish marine groundwaters is still useful as a distinct marine indicator.

**Table 8-2. Origin of groundwaters and sequence of events influencing their chemistry at SFR.**

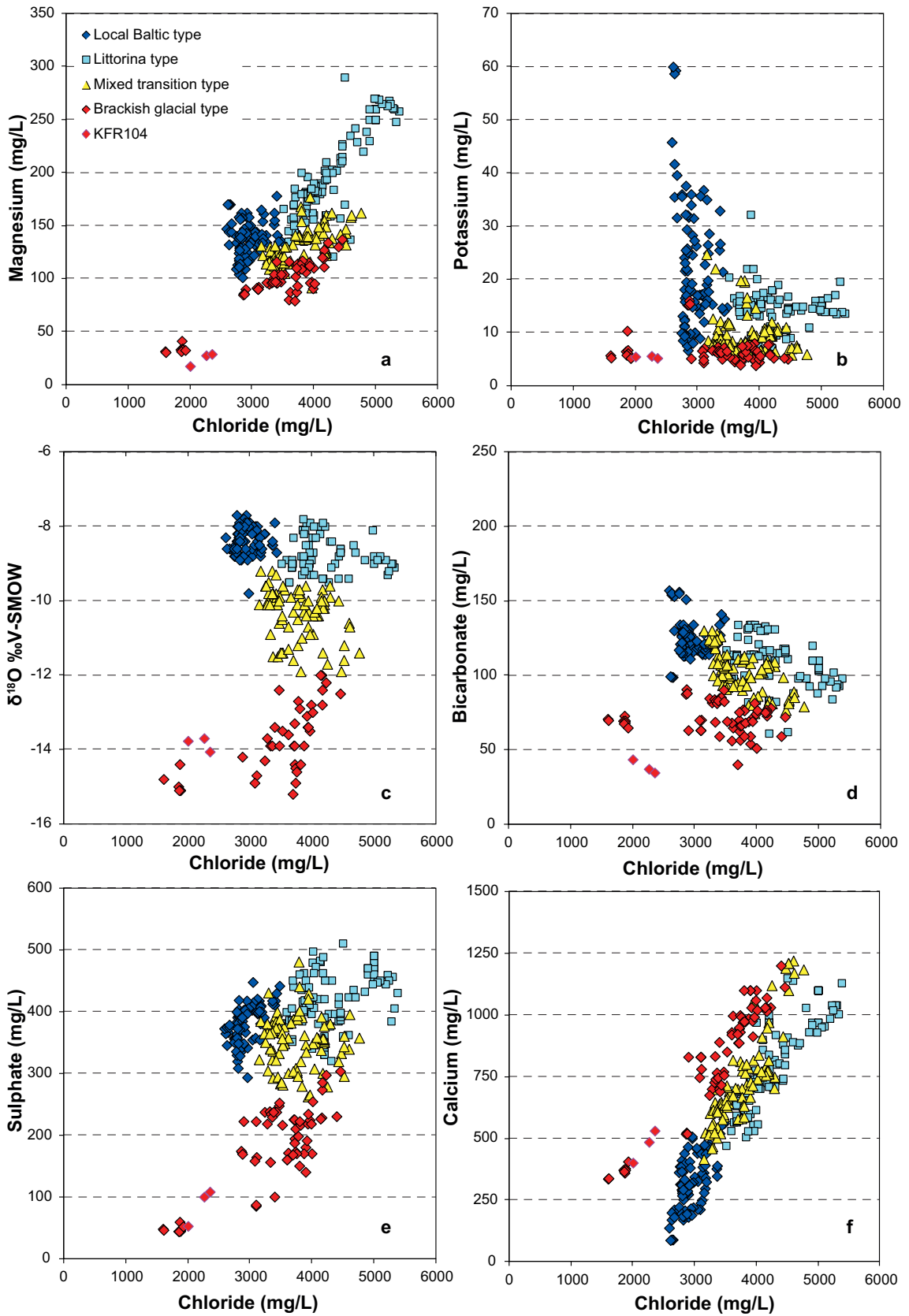
Origin of ground-water	Approximate residence time	Depth	Type of structures	Comment
<b>Present Baltic Sea water</b>	Modern water from the last 50 years based on tritium.	Down to 100 m depth.	Steeply dipping fracture zones with surface contact.	It is unclear whether Baltic Sea water was present in the fracture zones before construction of the SFR tunnels.
<b>Littorina Sea water</b>	The Littorina maximum occurred between 4500 and 3000 BC.	80 to 220 m depth.	Most common in the larger fracture zones, especially the vertical zones ZFMNE0870A and B and ZFMNNE0869 (zones 8 and 3) at the connection with the sub-horizontal zone ZFM871 (zone H2).	The Littorina Sea water is mixed with pre-existing glacial meltwaters in the fracture zones, becoming more dilute (lower Cl) and with a significantly more depleted $^{18}\text{O}$ .
<b>Glacial meltwater</b>	This water is most probably from the last deglaciation that occurred at Forsmark c. 11,000 years ago.	The waters with the most depleted $^{18}\text{O}$ values (indicative of glacial meltwater) are found at depths between 100 to 250 m.	Usually confined to single discrete fractures in the less transmissive parts of the bedrock.	The glacial meltwater has mixed with the pre-existing brackish non-marine water producing some of the lowest Cl contents (1,600 mg/L Cl in KFR101: -240 m elevation).
<b>Non-marine brackish water</b>	Older than the last deglaciation (>15,000 years).	This water is only found in relatively small fractions mixed with the glacial meltwater and with the brackish marine water of Littorina type.	Usually confined to the less transmissive parts of the bedrock.	The origin of the brackish non-marine water is unclear, but probably includes components of old meteoric water and may also contain older glacial water, together with non-marine water of unknown age.
<b>Saline water</b>	Older than the last glaciation with components probably much older (hundreds of thousands years).	This water is not identified in the present-day SFR dataset but is assumed to be present at depths below ~ 700 metres, based on experience from the Forsmark site.	Resides at great depth and as pockets in low-transmissive rocks.	The origin of the deep saline water is unclear. It may contain old marine as well as non-marine components and the chemistry of the water was subsequently modified by long-term water/rock interaction processes.

Data on  $\delta^{18}\text{O}$  ratios are sparsely available before 1995. With respect to  $^{18}\text{O}$  (Figure 8-4c), three ranges are distinguished: a) enriched values ranging from  $\delta^{18}\text{O} = -9.5$  to  $-7.5\text{‰}$  V-SMOW, b) values in the intermediate range between  $\delta^{18}\text{O} = -12$  and  $-9.5\text{‰}$  V-SMOW, and finally c) depleted values of  $\delta^{18}\text{O} = -16$  to  $-12\text{‰}$  V-SMOW with a significant glacial component giving a low  $\delta^{18}\text{O}$  signature. The enriched values are found at shallow (local Baltic type) and intermediate depths (Littorina type) and in association with deformation zones, whereas the most depleted values are found above and below zone ZFM871 (formerly Zone H2) and also relatively deep in zone ZFMNW0805 (formerly zone 8; KFR101). Figure 8-5c displays the narrow chloride concentration range and at the same time a wide variation in  $\delta^{18}\text{O}$ .

Figure 8-4d, e and f show the variation of potassium, bicarbonate and sulphate with elevation. By comparing the brackish marine and the brackish non-marine groundwaters at similar depths (i.e. in this case with Cl), the marine groundwaters generally show higher potassium and sulphate concentrations than the non-marine groundwaters. This is more or less also true of bicarbonate (Figure 8-5e). The potassium concentration is higher in both types of brackish marine groundwaters, which is demonstrated for the local Baltic type of groundwater by the peak in Figure 8-5b at chloride concentrations close to 3,000 mg/L. The Littorina type of groundwater has potassium peak values at a higher chloride concentration range (above 5,500 mg/L) that is not included in the SFR dataset (cf. Nilsson et al. 2011). The bicarbonate concentrations (Figure 8-5d) are related to the microbial breakdown of organic material and are, as expected, highest in the shallow brackish marine groundwaters of the local Baltic type (usually higher than the original 70–90 mg/L found in the Baltic Sea water at the surface). In addition, the mixed transition and the brackish-glacial groundwaters have concentrations well above 50 mg/L. It is clear from Figure 8-5e that the major source of sulphate in the SFR groundwaters is of marine origin, and correspondingly high sulphate contents are associated with both the local Baltic and Littorina type groundwaters.



*Figure 8-4a-f.* Distribution of chloride, potassium, magnesium, sulphate,  $\delta^{18}O$  and bicarbonate with depth (1986–2010) related to the different groundwater types defined for the SFR site in Section 8.3. Recent samples from borehole KFR104 (June 2011) are included.



**Figure 8-5a-f.** Plots of magnesium, potassium,  $\delta^{18}\text{O}$ , bicarbonate, sulphate and calcium versus chloride concentration (1986–2010). The groundwater samples are colour coded according to the different groundwater types defined for the SFR site in Section 8.3. Recent samples from borehole KFR104 (June 2011) are included.

The lowest calcium concentrations (and highest Na/Ca ratios) in the SFR groundwaters are associated with Local Baltic type groundwaters. Some of these groundwaters show calcium contents only slightly higher than the present Baltic Sea (around 75–80 mg/L), which can be attributed to their dominant Baltic signature, slightly modified by water-rock interaction processes (mainly calcite dissolution). However, most of the Baltic type groundwaters show calcium concentrations (mostly between 200 and 600 mg/L) clearly higher than the Baltic Sea waters and with a rough positive correlation with chloride contents (Figure 8-5f). Thus, although modified by heterogeneous reactions (e.g. calcite dissolution-precipitation, cation exchange), a mixing influence still seems to be noticeable. Some noteworthy observations are listed below.

- There are no systematic hydrochemical depth trends; any trends reflect more the consequences of groundwater type (i.e. heterogeneous density variability) and association with different deformation zones.
- There is no clear pH trend with depth (cf. Figure 8-5f), which may reflect the lateral heterogeneity of the groundwater system. The pH trend with chloride concentration (cf. Figure 8-6b) indicates generally somewhat higher pHs at low chloride concentrations, but the trend is unclear here as well.
- Despite the fact that it is possible to discriminate different groundwater types and the evidence of intruding modern Baltic Sea water during the excavation and operation of the SFR, the hydrochemical environment has been rather stable and the variation in terms of pH, Eh and calcite saturation is very limited. The overall effect is a minor decrease in the chloride concentrations.
- The Littorina and Baltic Seas are the main sources of sulphur; isotopic data ( $\delta^{34}\text{S}$ ) indicate that sulphate-reducing microbial activity seems to have had a minor influence on dissolved sulphate concentrations.

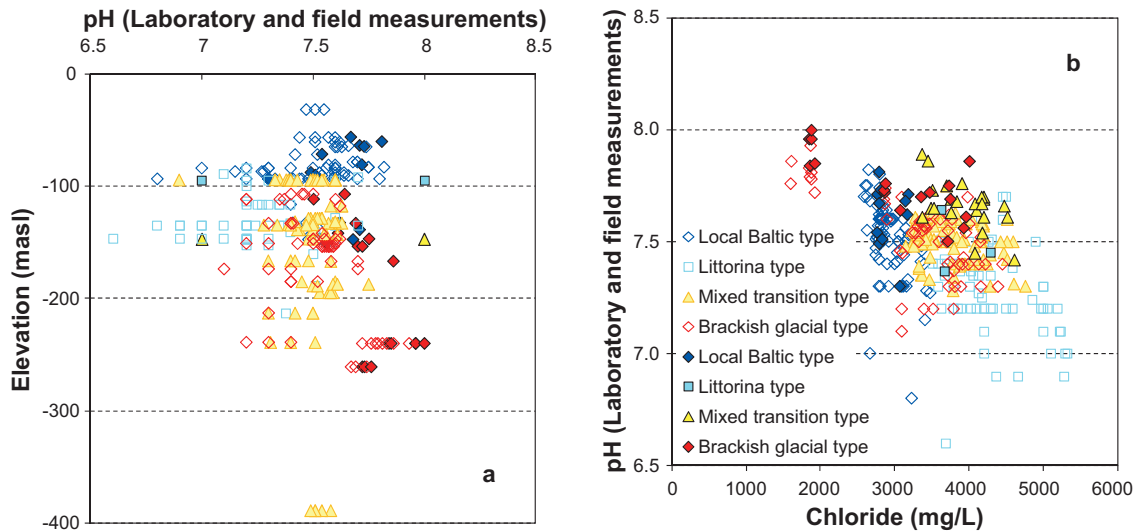
#### 8.4.2 Redox geochemical systems and redox-buffering capacity

The potentiometric Eh data (12 measurement sequences) representing the SFR groundwaters provided oxidising (6 logs) and reducing (6 logs) values. Reducing values (from –140 to –190 mV) are in line with those measured in the Forsmark groundwaters. The measured positive Eh values in the SFR groundwaters (from +30 to +110 mV) appear to be caused by amorphous Fe(III)-oxyhydroxides (Gimeno et al. 2011). These indicate the existence of present-day or recent oxic environments, since these phases quickly recrystallise (in the course of months) to less soluble and more stable phases under reducing conditions. Chemical parameters (e.g. pH and Eh values) for these groundwaters are very similar to those observed in the Äspö Hard Rock Laboratory (Banwart 1999) when reducing groundwaters were introduced in contact with the oxygen-rich atmosphere of the tunnel, and microbes were observed to catalyse the formation of amorphous Fe(III)-oxyhydroxides.

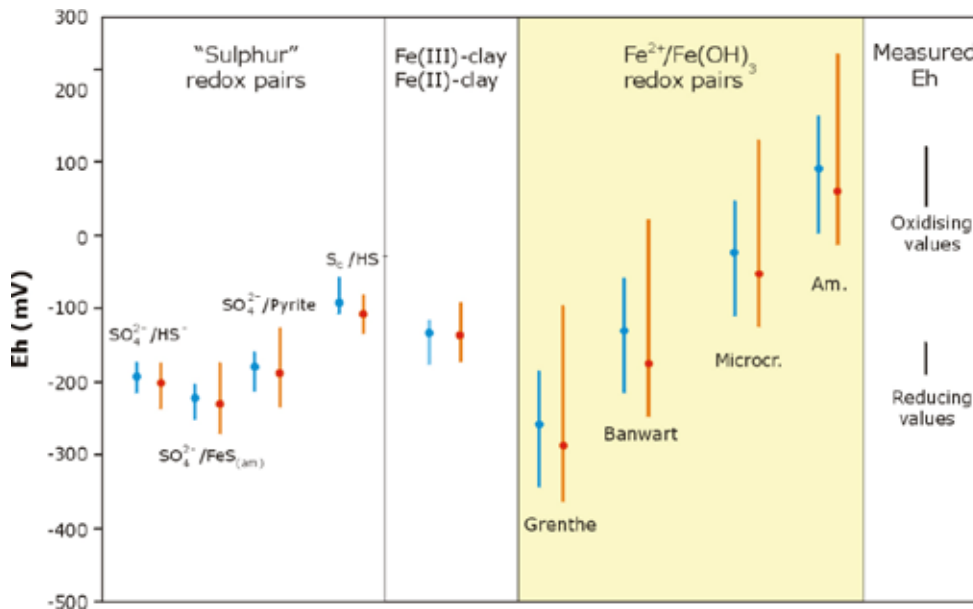
Thus, the oxidising conditions, similar to the ones at the Äspö Hard Rock Laboratory, are representative of the groundwater situation close to the oxic environment in the tunnels, changing towards more reducing conditions in the case of outflow/discharge. The gradual removal of the groundwater from the borehole section being measured and the subsequent progressive input of pristine formation water may have caused a disequilibrium, and consequently long stabilisation periods towards reducing conditions were observed (cf. Gimeno et al. 2011).

Mineralogical studies in the fracture fillings at the SFR indicate that mixed layer clays (poorly ordered smectite-illite) are the most abundant minerals in the fracture fillings from water-conducting fractures. The presence of hematite and other unclassified iron oxyhydroxides has also been identified at almost all examined depths (Sandström and Tullborg 2011), which supports the results obtained with the  $\text{Fe}^{2+}/\text{Fe}(\text{OH})_3$  and the  $\text{Fe}^{3+}\text{-clay}/\text{Fe}^{2+}\text{-clay}$  redox pairs.

In Figure 8-7, calculated Eh values for different redox couples of sulphur and iron (including the  $\text{Fe}^{3+}\text{-clay}/\text{Fe}^{2+}\text{-clay}$  redox pair) are compared with the measured values from the SFR site. The calculations were performed with both the measured pH values and the ones calculated in equilibrium with calcite.



**Figure 8-6a, b.** Plots of pH versus elevation and chloride concentration (1986–2010). The groundwater samples are colour coded according to the different groundwater types defined for the SFR site in Section 8.3. Laboratory measurements are shown as open symbols, whereas field measurements are shown as solid black symbols.



**Figure 8-7.** Eh values calculated from different redox couples for the complete suitable set of SFR groundwaters, compared with the potentiometrically measured Eh values. Red lines represent the range of values obtained with the measured pH and blue lines the range of Eh values obtained with the calculated pH (calcite equilibrium). Solid circles represent the mean value for each case (Gimeno et al. 2011).

The mineralogical redox buffer capacity of fracture minerals and the host rock minerals is dominated by ferrous iron in fracture minerals and the rock matrix and Fe(II)-bearing minerals (Tullborg et al. 2008, Drake et al. 2009, Sidborn et al. 2010). At the SFR these minerals mainly comprise chlorite, clay minerals and pyrite ( $FeS_2$ ); pyrite also contains  $S^{2-}$ , and is therefore a strong reductant. Based on data from quantitative mapping of fracture minerals during the Forsmark site investigation (Eklund and Mattson 2009, Löfgren and Sidborn 2010) and from geochemical data on fracture-filling minerals (Sandström et al. 2008a, b), the amount of Fe(II) available in the fracture system at the Forsmark site investigation area was calculated and presented in Sidborn et al. (2010). As mentioned above, no quantitative mapping has been carried out on the SFR drill cores, but they are expected to be broadly similar to the Forsmark data (cf. Table 8-3). No analyses of the Fe(II)/Fe(total) in fracture fillings have been carried out so far during the SFR site investigation, and the amount of available Fe(II) in the clay minerals is not known; this will be addressed in future investigations.

**Table 8-3. Fe(II) content in bulk fracture fillings on fracture surfaces from the Forsmark site investigation area, E(x) = expected value or mean. Parameters  $\mu$  and  $\sigma$  are the mean and the standard deviation of the natural logarithm of the content obtained from the lognormal distribution. Data from Sidborn et al. (2010).**

E(Fe(II) <sub>mean</sub> )	3.7 wt%
$\mu$ of ln(Fe(II) <sub>mean</sub> )	0.84
$\sigma$ of ln(Fe(II) <sub>mean</sub> )	0.97
E(Fe(II))	23 g/m <sup>2</sup>
$\mu$ of ln(Fe(II)/m <sup>2</sup> )	2.10
$\sigma$ of ln(Fe(II)/m <sup>2</sup> )	1.44

### 8.4.3 Uranium, radium and radon

The uranium concentrations in the groundwaters in the early SFR boreholes, as well as in the new SFR extension boreholes, show large variations from a few  $\mu\text{g/L}$  up to 140  $\mu\text{g/L}$ , but most concentrations are higher than 10  $\mu\text{g/L}$ . These elevated concentrations seem to have no connection to any specific groundwater type at the SFR, however. The highest values ( $> 100 \mu\text{g/L}$ ) are found in groundwaters with a large component of Baltic Sea water, but other samples of the same groundwater type show values  $< 10 \mu\text{g/L}$ . Furthermore, the plot does not indicate any clear depth dependence. It can also be concluded that all the groundwaters analysed from the SFR show bicarbonate contents  $> 50 \text{ mg/L}$ , and the redox potential in the seven sections measured all show Eh values  $\geq -190 \text{ mV}$ . Higher amounts of dissolved uranium can exist in groundwaters under mildly reducing conditions if stabilised by carbonate complexation. This was demonstrated by the results from investigations at Forsmark, where elevated uranium concentrations ( $> 10 \mu\text{g/L}$ ) were found in several borehole sections at depths down to 600 metres. These were generally associated with groundwaters that were not oxidising but had Eh values  $> -190 \text{ mV}$  and bicarbonate contents  $> 30 \text{ mg/L}$ . Solubility calculations showed that a stable U(VI) carbonate complex is probably responsible for the higher concentrations observed in these groundwaters (Gimeno et al. 2008).

The study of fracture fillings from some of the sampled sections at SFR made it possible to identify uranium phases from some of the water-conducting fractures, and the bulk chemistry of the fracture-filling material suggests a remobilisation of U ( $\text{Th/U} > 2$ ) at some time in the past. Current efforts are focussed on locating and describing the solid uranium phases.

A few samples were analysed for radium and radon activities. No obvious correlation between radium, radon and other parameters was observed. It can be concluded that no extreme values were found and the measured values are within the interval measured at Forsmark.

## 8.5 Hydrogeochemical site description and visualisation

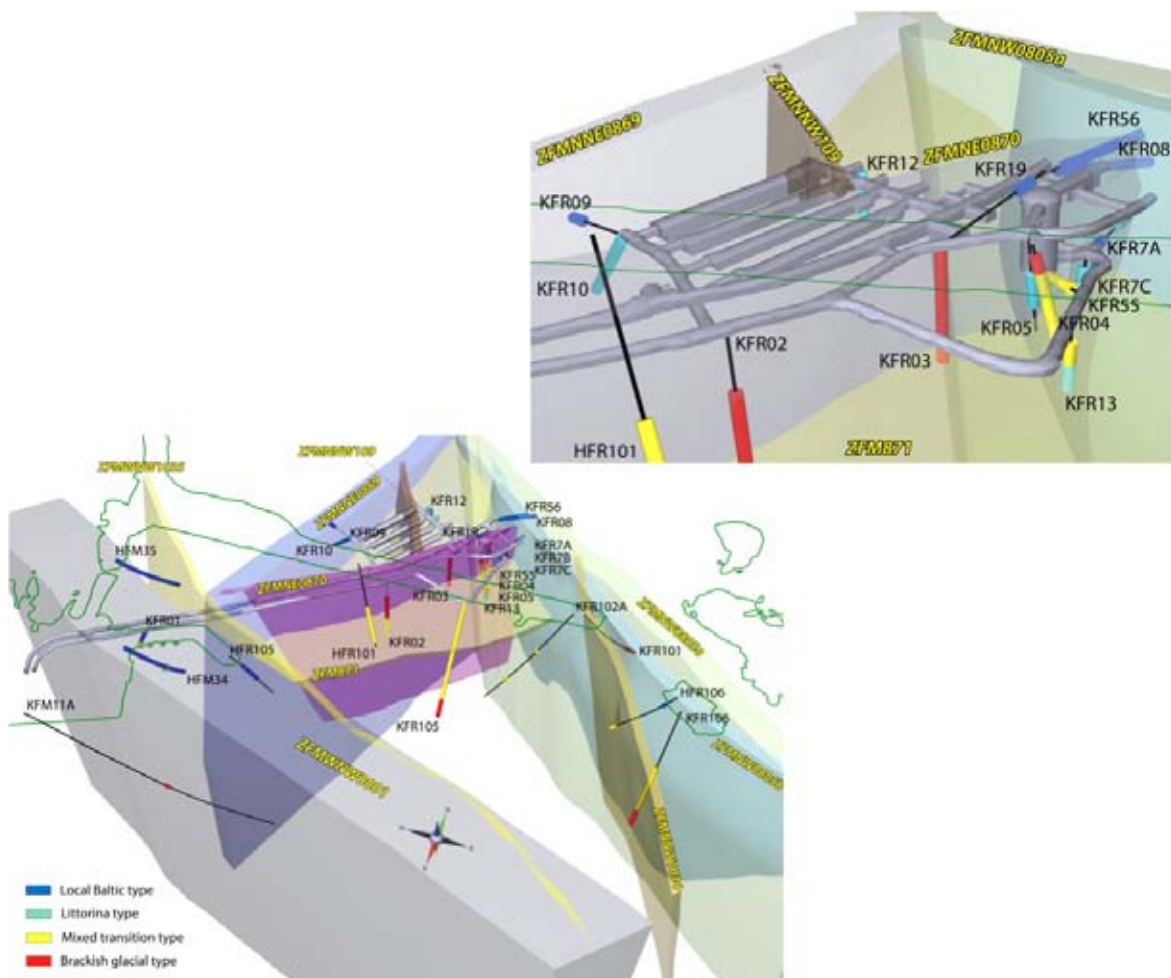
In the same way that hydrology is dependent on the geological model, the hydrogeochemical model is closely dependent on the integrated hydrogeological model. The close relationship of the SFR site hydrogeochemical interpretation to geology and hydrogeology is exemplified by the use of 3D (cf. Figure 8-8 as well as Figure 7-19) and 2D visualisations taken directly from the geological model and modified to accommodate and discuss the hydrochemistry (cf. Figure 8-9). Furthermore, the conceptual hydrogeological model of the SFR site has been modified to visualise and discuss the distribution and chemistry of the different groundwater types (cf. Figure 8-3).

### 8.5.1 Structural and hydrochemical considerations

The SFR site is delimited by the Northern and Southern boundary belts, i.e. two vertical to steeply dipping deformation zones, ZFMWNW0001 (Singö) to the southwest and ZFMNW0805A and B (formerly Zone 8a and b) to the northeast (Figure 8-8). Together with the other steeply dipping zones – ZFMNE0870A and B (formerly zone 9a and b), ZFMNNW1209 (formerly zone 6) and ZFMNNE0869 (formerly zone 3) inside the Central block – they have served as important groundwater flow paths over long periods of geological time. Some of these vertical zones (e.g. ZFMNNE0869, ZFMNW0805A, B and ZFMNE0870) may have hydraulic contact with the gently dipping deformation zone ZFM871 (formerly zone H2), which is located just beneath the silo at SFR and covers most of the local model area.

Prior to the construction of the SFR waste storage facility, the groundwater flow was considered regional, slow moving and discharging upwards along the important flow paths. With the commencement of the SFR excavation and construction phases, these paths have facilitated the dynamic drawdown of near-surface waters (e.g. Baltic Sea) and possibly of mixtures of Littorina and young meteoric water types. In addition, these SFR inflow paths appear to bypass much of the bedrock, suggesting that the flow system is compartmentalised and very discrete. Furthermore, groundwater sampling and/or hydraulic testing in boreholes on groundwater mixing may have had some local effects, but these can be considered unimportant compared to the large volumes of drawdown groundwaters which are circulating in the major hydraulically connected fracture systems.

The two vertical 2D sections (one of which is illustrated in Figure 8-9) provide simplified visualisations of the SFR area where the actual intersections of the structural zones are indicated and the boreholes, when not aligned along the section, are extrapolated onto the same 2D plane. The figure shows schematically the division at about -200 m elevation between the shallow bedrock aquifer (light beige colour), with a high frequency of interconnected transmissive fractures, and the underlying bedrock (darker beige colour), characterised by a decrease of interconnected fracture frequency with depth and therefore a lower transmissivity. As commented on above, and discussed in detail below, the hydrostructural properties of the SFR site have determined the distribution and degree of mixing of the different groundwater types, most of which have been introduced since the last deglaciation. These groundwater types (Local Baltic Sea, Littorina with a glacial component, Brackish-glacial and Mixed transition brackish water) residing at shallow to intermediate depths (maximum elevation depth studied is about -400 m) are indicated in Figure 8-9.



**Figure 8-8.** 3D presentation, viewed from above and from the southeast, of the groundwater type distribution in relation to major zones in the regional model volume; see also Figure 7-19. The SFR boreholes are enlarged in the inset. The green outline at the surface demarcates the coastline with the pier and small islets. Note the decrease in colour intensity along the boreholes when viewed through a penetrated rock/deformation zone volume.

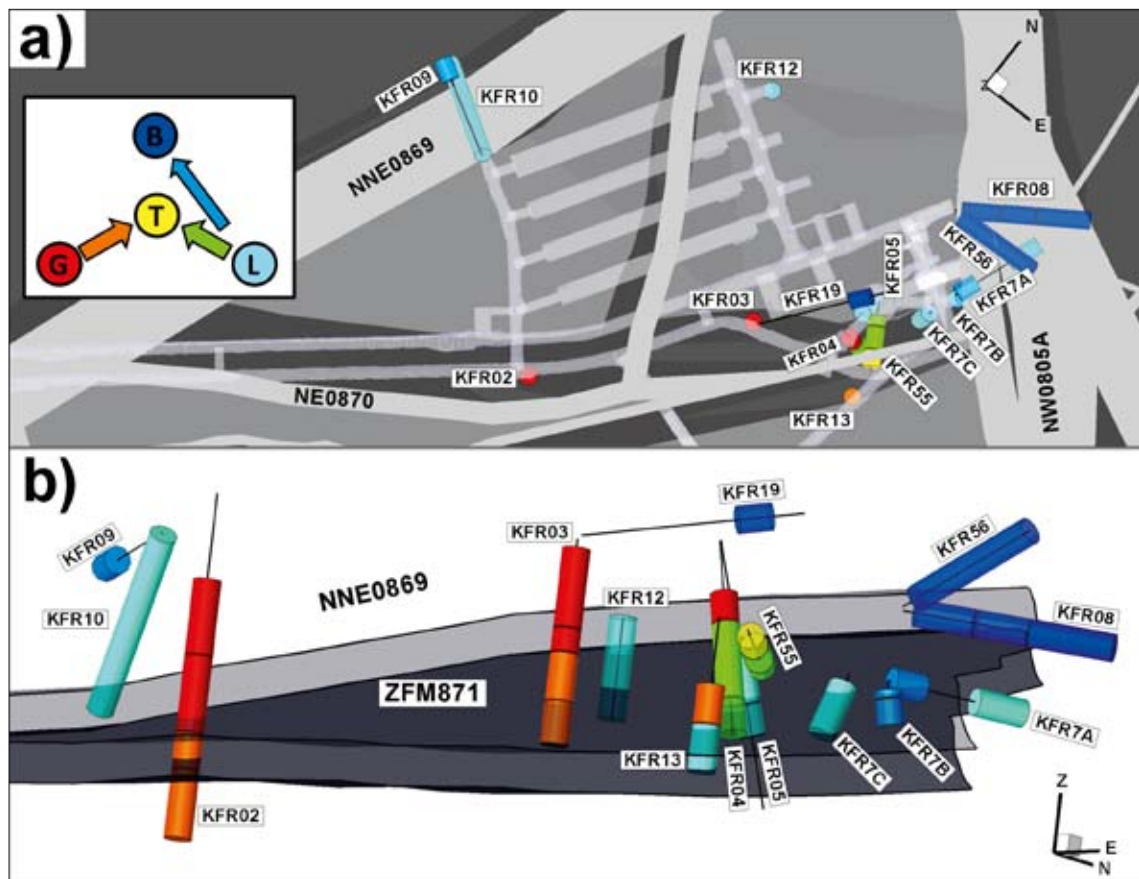




### 8.5.3 The influence of the SFR on groundwater chemistry

The impact of changes in flow paths and groundwater drawdown effects during and following construction of the SFR tunnel system has influenced the groundwater composition in the investigated boreholes. In the early drilled SFR boreholes, which penetrated several major transmissive fracture zones, the effects of changes in groundwater inflow rates (cf. Figure 7-6) and groundwater compositions (cf. Figure 8-10) are observed from long-term trends measured over periods of years (1988–2011 and 1986–2010), the latter indicating generally slow but systematic alterations in chemistry (Laaksoharju and Gurban 2003, Nilsson A-C 2009).

Changes in water composition can be observed at several sampling locations since the first samples were collected in 1986/87. Where and how the changes occur provides valuable information about the hydraulic conditions at the site and especially in the different major deformation zones. However, it is possible that some changes were sufficiently rapid and had already occurred before the first sampling occasion, which could explain, for example, the occurrence of the Baltic type of groundwater in boreholes KFR19, KFR08 and KFR56 already from the first sampling occasions in 1989–95 (the sampling started later in these boreholes). An attempt to visualise the changes in water types with time is presented in Figure 8-10.



**Figure 8-10.** Change of groundwater types between 1986 and 2010: a) top view, and b) side view towards the northwest. The defined groundwater types are Local Baltic (B; blue), Littorina (L; cyan), Brackish-glacial (G; red), and Mixed transition (T; yellow). Note that the transient changes are indicated by the colours of the arrows in the inset figure (Figure 8-10a). Incomplete ongoing changes are not resolved. Sections with poor coverage of the chosen time interval are shown as translucent. Deformation zones are shown in grey. The grey plane in Figure 8-10b represents the gently dipping zone ZFM871 (formerly zone H2).

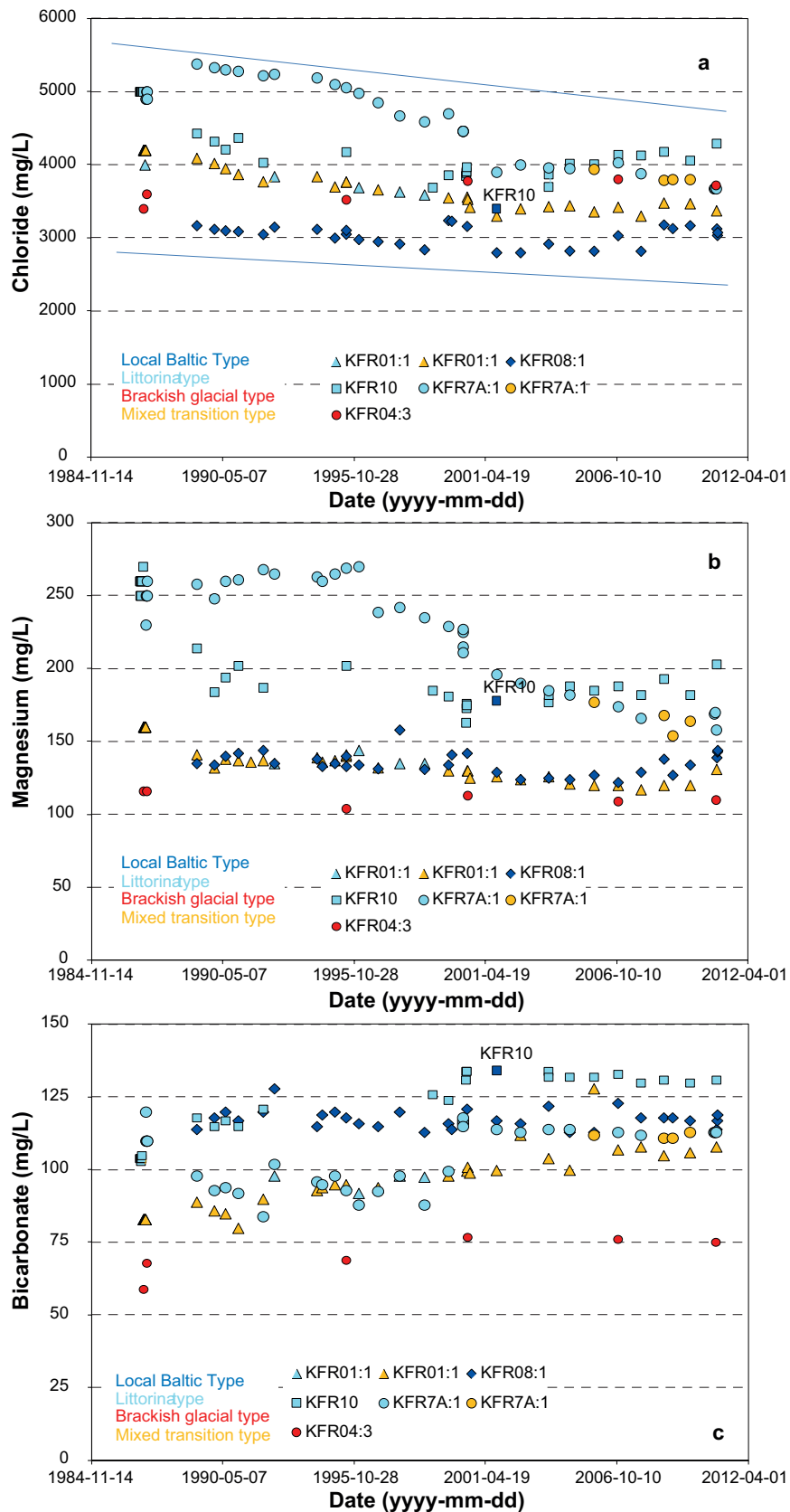
Observed changes and comments to Figure 8-10 can be summarised as follows.

- Changes from the Littorina type to local Baltic type groundwaters occur in or close to the shallow parts of the major vertical zones, i.e. in the Northern boundary belt and zone ZFMNNE0869 (formerly zone 3), as well as in the Southern boundary belt (not included in Figure 8-10).
- Changes from Brackish-glacial type to the Mixed transition type occur to the west at some distance from the Northern boundary belt at the intercept with zone ZFM871 (formerly zone H2; boreholes KFR02 and KFR03) and above the intercept (KFR04) in one case.
- Changes from the Littorina type to the Mixed transition type occur at or close to the intercept with zone ZFM871 in two boreholes (KFR04 and KFR55) at an intermediate distance from the Northern boundary belt.

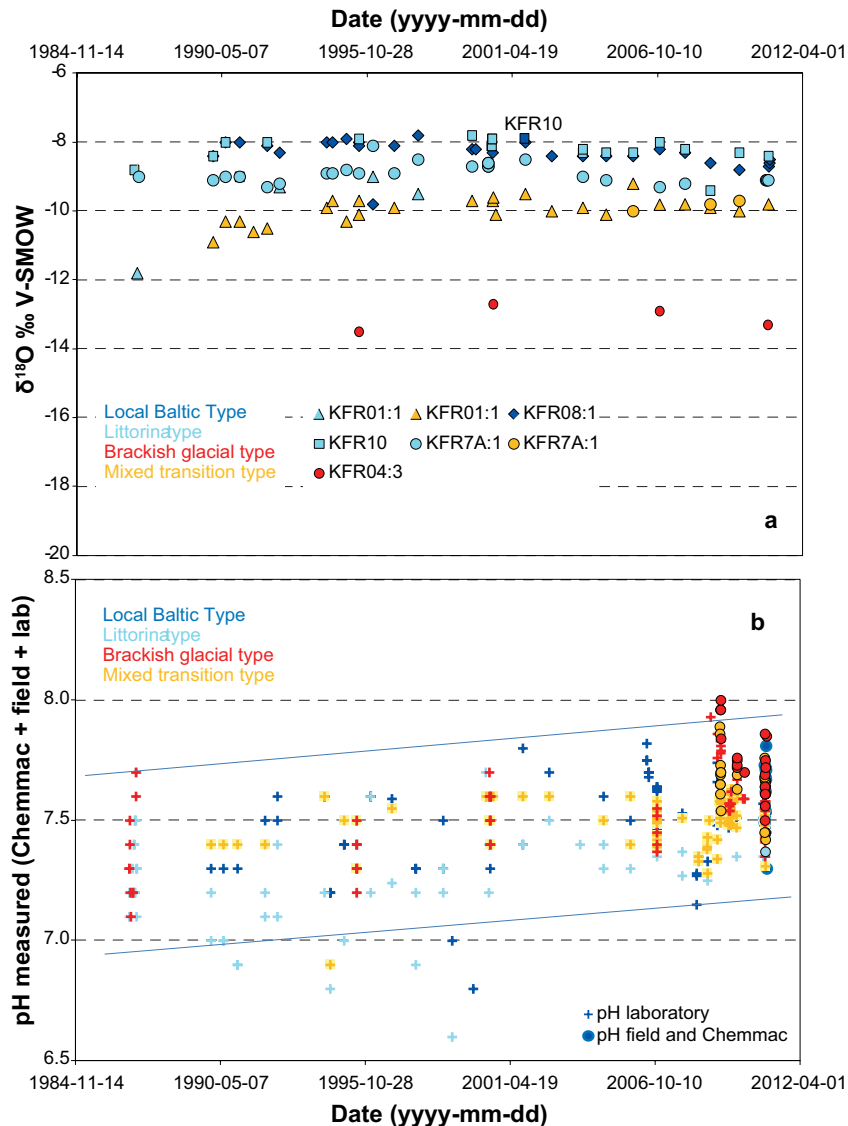
Most of the changes showed a slightly decreasing chloride concentration between 1986 and 2000 followed by a nearly stable period until 2010. As expected, the greatest changes in groundwater pressure and inflow to the boreholes and the tunnel system occurred soon after construction.

Measurements of the inflow to the SFR facility have been carried out on a regular basis since January 1988 (cf. Section 7.2.1). The total inflow directly after the completion of excavations has decreased from 720 L/min (1986) to 285 L/min (2010). No grouting has been carried out since completion of the existing SFR and the decreasing trend of inflow is therefore due to other processes, such as clogging caused by chemical precipitation and material transport as listed in Section 7.2.1). Unfortunately no studies of possible clogging were done in the site investigation and therefore no information is available to support or otherwise this possibility. There are, however, no strong indications of changes in groundwater chemistry that could be definitively attributed to clogging processes.

Conditions have slowly stabilised to reach a near-equilibrium situation around year 2000. This naturally also affects the groundwater composition. The slightly decreasing or near-stable chloride and magnesium trends as well as the minor increase in bicarbonate concentration between 1986 and 2010 (associated with the different groundwater types) are displayed in Figure 8-11. The  $\delta^{18}\text{O}$  as well as the pH trends are shown in Figure 8-12. Figure 8-11a, b and c and Figure 8-12a include the annually sampled boreholes KFR01, KFR08, KFR10 and KFR7A as well as a selected typical borehole section (KFR04:3 at 28.0 to 33.0 m borehole length) showing the Brackish-glacial groundwater type. This latter borehole section was sampled more seldom. Figure 8-12b shows all pH values (irrespective of borehole section) from the period 1986 to 2010. The slight increase in bicarbonate content is accompanied by a weaker trend in pH, possibly due to the greater uncertainties in the measurements and the fact that only laboratory measurements are available for most of the period.



**Figure 8-11a-c.** Chloride, magnesium and bicarbonate concentrations plotted versus sampling date; groundwaters from annually sampled borehole sections (bottom sections) in KFR01, KFR08, KFR10 and KFR7A as well as from KFR04 at 28.0 to 43.0 m borehole length. Note that KFR10 had packers installed (section 87.0–107.28 m borehole length) probably until year 1987, and after that the entire borehole was sampled. The single Baltic type groundwater sample from KFR10, collected in 2001, is probably due to an erroneously low chloride value. Furthermore, this borehole lacks data for a period during the 1990s.

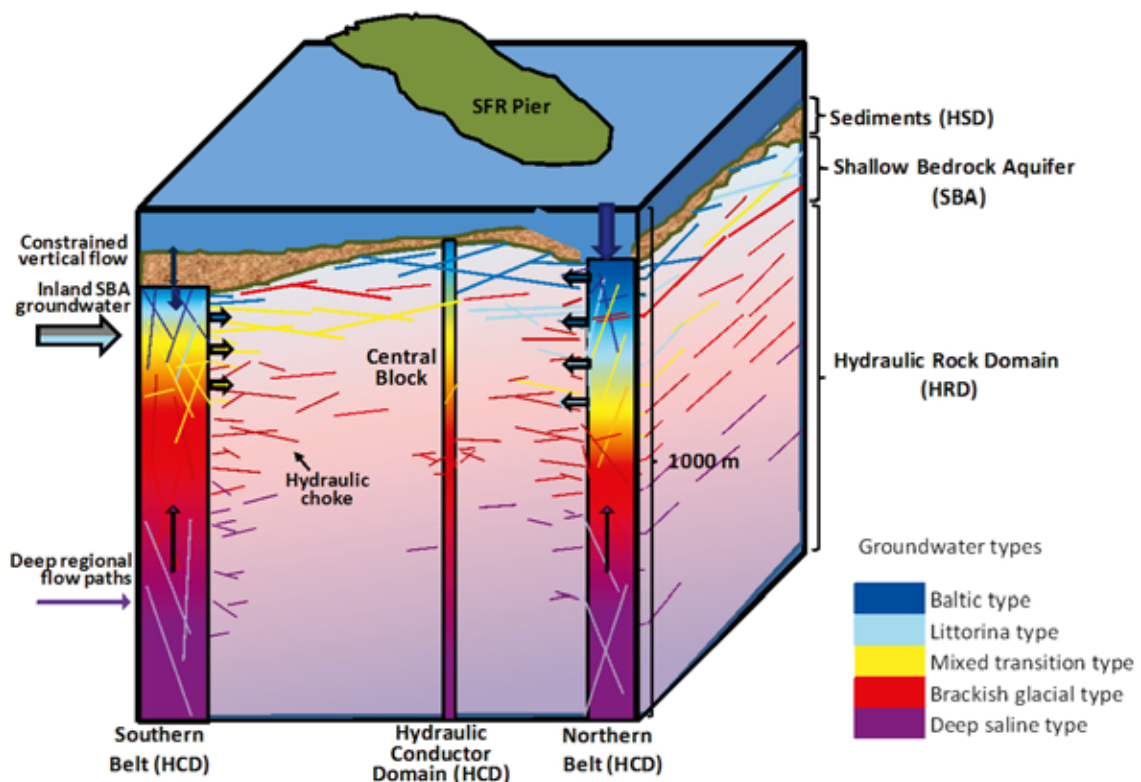


**Figure 8-12a–b.**  $\delta^{18}O$  value a) plotted versus sampling date; groundwaters from annually sampled bore-hole sections (bottom sections) in KFR01, KFR08, KFR10 and KFR7A and from KFR04 at 28.0 to 43.0 m borehole length. Note that KFR10 had packers installed (section 87.0–107.28 m borehole length) probably until 1987, and after that the entire borehole was sampled. The single Baltic groundwater type sample from KFR10, collected in 2001, is probably due to an erroneously low chloride value. Furthermore, this borehole lacks data for a period during the 1990s. The pH trends b) include all pH values irrespective of borehole and borehole section.

#### 8.5.4 Hydrogeochemical conceptual model

A visualisation integrating the major hydrogeological and hydrogeochemical features of the investigated SFR rock volume (Figure 8-13) is presented based on the hydrogeological 01,000 m depth conceptual model illustrated in Figure 7-36 and described in Öhman et al. (2012). Modifications to this model to satisfy hydrochemical considerations include colour coding of the main groundwater types in the three major flow path structures and in less transmissive discrete fractures that characterise the general SFR rock volume between these structures. The conceptual block model illustrated in Figure 8-13 is described as follows.

- A saline non-marine groundwater type (deep saline) is ascribed to the deepest part of the bedrock (deep lilac colour). This is an assumption based on Forsmark data because no data below –400 m elevation are available from the SFR. The groundwater type is associated with the two highly transmissive deformation areas (the Southern and Northern boundary belts) and the Central block (Hydraulic Conductor Domain (HCD)); a weak upward regional flow direction is indicated by the upward pointing black arrows. A more subdued lilac colour increasing in intensity with depth represents the less transmissive rock volume between these structures characterised by few discrete fractures of low conductivity. These discrete fractures (and possibly also the rock matrix pore waters) probably represent similar salinities to the deepest groundwaters in the major conducting structures (i.e. deeper than about 700 m based on the Forsmark investigations).
- The introduction of glacial meltwaters particularly along the highly transmissive deformation zones and mixing with the older non-marine saline to brackish groundwaters (and components of old meteoric water) has given rise to the Brackish-glacial groundwater types (bright red colour).
- This was followed by infiltration and mixing of the Littorina Sea water with different portions of glacial meltwater, giving rise to the Littorina-type groundwater (turquoise colour). The Littorina Sea water entered preferentially along the more highly conductive fracture zones, i.e. the same zones that facilitated the glacial meltwaters.
- Mixing of these Littorina type waters with the earlier brackish-glacial groundwaters has occurred to different degrees, producing the Mixed transition brackish type groundwaters (yellow colour).
- Modern Baltic Sea water (dark blue colour) is most probably a recent component that has intruded via the highly transmissive deformation zones comprising the Northern and Southern boundary belts due to the drawdown effect from the SFR facility during the excavation/ construction/operation phases.



**Figure 8-13.** Conceptual block model (0–1,000 m depth) integrating the major hydrogeological and hydrogeochemical features of the investigated SFR rock volume. The different groundwater types are indicated by the colour scheme displayed on the right hand side. The deep saline groundwater which is indicated by lilac is not present as a dominant groundwater type in the SFR rock volume. See text for explanation to the different arrow types. (Modified after Öhman et al. 2011a).

There are locations where mixing has not occurred and where the brackish-glacial groundwaters have remained at shallower levels in the bedrock (“pockets”) shielded from the passage of the later Littorina-type groundwaters. This is schematically shown as solid red fractures at higher levels than the maximum depths achieved by the Littorina-type groundwaters. Moreover, Littorina-type groundwaters have been preserved at higher levels (indicated by the turquoise colour of some of the near-surface discrete fractures) because horizontal hydraulic gradients, typical in this area beneath the sea, are very weak and unable to displace the dense Littorina waters.

Sea-bottom sedimentation has been much greater (i.e. thicker) above the Southern boundary belt compared with the Northern one, allowing a greater volume of Baltic Sea-type water to preferentially infiltrate into the latter (indicated by the larger and thicker downward pointing blue arrow in Figure 8-13). As indicated by the concentration of short thick horizontal arrows from the upper approximately 400 m parts of the Northern and Southern boundary belts, SFR drawdown has gradually pulled in groundwaters along conducive fracture zones into the Central block area and towards the SFR site. These groundwaters, already the product of natural mixing processes affecting Brackish-glacial and Littorina-type waters, have therefore undergone additional anthropogenic mixing involving a Baltic Sea input, and this has been compounded by the increased flow resulting from drawdown effects.

The input flow sources to the Central block area of mixed groundwaters of Littorina and Baltic type are visualised to show close to the surface in the Northern boundary belt the dark blue of the Baltic Sea and lower down a dominant Littorina component. In contrast, the Southern boundary belt is considered to be less transmissive because of the thick sediment cover which has inhibited initially the amount of Littorina Sea and later the Baltic Sea waters infiltrating into the deformation zones from mixing with the resident Brackish-glacial-type groundwaters. This explains the restricted vertical extent of the Mixed transient groundwater types. Compare the vertical extent of the yellow colouring between the two belts and note the less dominant Littorina and Baltic components in the Southern boundary belt. The conceptual model also shows a lateral flow direction to the Southern boundary belt from the near-surface Shallow Bedrock Aquifer (SBA), which may have transported mixtures of modern meteoric water with some residual Littorina-type water from inland, i.e. from the northeastern part of the Forsmark area. However, this is based on too few data and may simply reflect the hydrogeological and hydrogeochemical heterogeneity of the bedrock system.

## **8.6 Confidence and uncertainty in the hydrogeochemical model**

### **8.6.1 Measured and modelled uncertainties**

The case with an existing repository in operation in or close to the investigated site introduces conditions not previously encountered in SKB’s site investigations, for example, significant changes in groundwater flow and associated mixing of different groundwater types. But these conditions also offer certain advantages, including the possibility to follow changes in groundwater composition during the last twenty years. This can be of importance for future predictions of open and more dynamic hydraulic conditions associated with repository construction for the disposal of radioactive waste. However, describing such a dynamic groundwater system also involves an additional degree of difficulty and uncertainty in the interpretation work.

#### ***Data uncertainty***

Compared with studies relating to a spent fuel repository, the fact that undisturbed groundwater samples from boreholes do not exist is even more relevant in the SFR case, where most of the studied groundwaters originate from the upper approximately 250 m of bedrock. A number of different conditions can therefore impact directly on the integrity of the sampled groundwaters, the most important of which result from drawdown effects and altered flow paths in the vicinity of the tunnel system. These latter factors comprise part of the model to be developed. Furthermore, data uncertainties have changed with time due to the use of data collected over the last twenty years. For example, during this time the collected data have been archived using different methods and levels of documentation and most probably reflect different quality standards of sampling performance and analyses.

Analytical uncertainties are addressed in Nilsson A-C (2009) and Nilsson et al. (2010) where general uncertainties reported for the different methods and components are given. The different possible impacts on sampling and sampling conditions are identified and discussed in Nilsson et al. (2011). This report also includes quality assessment of the samples contained in the SFR dataset for model version 1.0. The approach is similar to the one used in the Forsmark site investigation and accounts for impacts from sampling conditions as well as from analytical performance. However, at SFR it had to be adapted to a 25-year long sample time series with all the associated uncertainties outlined above. In general, rather few of the samples can be considered of the highest quality, but most of the data were nevertheless judged to be of acceptable quality for interpretation purposes. Some of the samples that did not conform to the previously accepted standards used in the Forsmark site investigation were nevertheless used in order to include as much data as possible to cover the period from 1986 to 2010. Samples with questionable analytical confidence for single components are evident from some of the plots shown in Figure 8-4 and Figure 8-5 where they occur as outliers. Such samples are easily recognisable, and the uncertain values can be discarded if necessary, although they are too few in number to mask the general chemical trends.

### ***Temporal and spatial variability***

Temporal hydrogeochemical variability is largely dependent on the hydraulic conditions in the vicinity of the SFR repository as well as on the hydraulic properties of the boreholes. The variability of different components on a 20-year scale illustrates minor changes in, for example, chloride, bicarbonate, pH and tritium. This variability is manifest as more or less stable trends with a certain degree of predictability. Occasional local variations in groundwater composition may occur due to heavy pumping or discharge of large volumes of groundwater from the sampled borehole or boreholes in its vicinity, as well as other temporary conditions that affect groundwater mixing patterns or flow paths. Repeated regular sampling from each sampling location can verify hydrogeochemical stability or regular trends. However, all the recent SFR boreholes, except borehole KFR101, have been sampled as campaigns (collection of a sample series of three to four samples) on one occasion only, so some uncertainty exists regarding their stability.

The most obvious cause of uncertainties in spatial variability is low and/or irregular data coverage. The SFR dataset is undoubtedly dominated by samples from closely located early boreholes in the present-day SFR facility, whereas few borehole data are available from the area of interest for the repository extension. Moreover, most of the data are associated with deformation zones at, or close to, both the Northern and Southern boundary belts, whereupon the Central block is less well covered. Additional boreholes, i.e. more available borehole sections for groundwater sampling in the Central block would improve the hydrogeochemical model of the target area for the SFR extension.

The spatial variability of the groundwater types reflects the hydrogeology of the shallow bedrock, which is considered to be anisotropic with limited contact with the overlying Baltic Sea. The hydraulically conductive fracture system is dominated by subhorizontal fractures, although steep deformation zones are expected to play an essential role in any vertical hydraulic connection with the sea. The zones are judged to be heterogeneous, discontinuous in character, and there is abundant evidence of isolated, compartmentalised rock volumes. The spatial variability of the groundwater types would therefore be expected to be high and this is generally the case, and more so when the impact of the SFR construction is considered. The discrete fractures characterising the lower transmissive bedrock between the major deformation zones are less well known, as is the spatial variability of groundwater types associated with them.

### ***Other model uncertainties***

Other uncertainties may include conceptual uncertainties, degree of confidence in the selected model, and bias in predictions etc. These include:

- Conceptual uncertainties exist in the sense that even though the important hydraulic features have been identified around the existing facility, the exact connections and pathways are not well understood to the south.
- Pore water data from the upper bedrock might provide useful additional Holocene palaeo-hydrogeological information that could be of interest both for SFR (submerged environment) and Forsmark (emerged environment), where there is a general lack of data.



- Compared with more frequent data points from the Forsmark site investigation, only a small amount of microbe and gas data were available from SFR for comparison. To make a significant impact on the hydrogeochemical understanding of the SFR site, significant amounts of additional data are needed.
- Uncertainties and problems regarding mixing calculations, equilibrium calculations and measured as well as calculated Eh data are thoroughly discussed in Gimeno et al. (2011), and uncertainties in fracture mineral frequency and fracture mineral composition are discussed in detail in Sandström and Tullborg (2011).

The hydrogeochemical site visualisation (cf. Section 8.5) is based on a systematic, step-wise approach to determining depth trends and hydrochemical groupings of the groundwaters. Understanding of the system therefore reflects the interpretation of hydrochemical data that has undergone a rigorous quality check and categorisation; in other words, it is associated with a good degree of confidence. Coupled with the results of quality-assured hydrogeological measurements and modelling, in turn based on geological models of a high standard, the input properties to the hydrogeochemical visualisation represent the best quality available at this time. Uncertainties undoubtedly remain, perhaps stemming from inadequacies (insufficient data in places) in the geological model which may impact on the hydrogeological interpretation and possibly therefore on the integrity of the hydrogeochemical model and visualisation.

### 8.6.2 General confidence level

The following aspects of the hydrogeochemical model are associated with the highest confidence.

- The major outlines regarding the development and flow paths of the defined groundwater types before and after the construction of the SFR repository.
- The origin of the most recent end members (Baltic and Littorina Sea water, glacial meltwater) and the major processes (qualitative control concerning Eh and pH buffer capacity and major reactions) affecting the present groundwater composition at the sampled locations. These compositions are expected to be similar to those shown in Figure 8-12 based on the geological and hydrogeological analogy (same rock domain, no major sub-vertical HCDs).
- Predictability of expected groundwater composition in the sense that no extreme groundwater compositions, other than those already encountered, are likely to be discovered during the excavation phase at the depth ranges considered.
- The conceptual models, which are based on close agreement between all three disciplines (geology, hydrogeology and hydrogeochemistry).

The following aspects of the hydrogeochemical model are associated with the lowest confidence.

- The natural hydrogeochemical conditions prior to the construction of the SFR facility are not known since there are no groundwater chemistry data from the first drilling stage prior to the commencement of the excavation phase.
- The groundwater type distribution in the southwestern part of the Central block as well as outside the deformation zones in the model volume is largely unknown due to the locations of the boreholes.
- Certain groundwater aspects (pore water, microbes, gas) are treated briefly due to lack of data or very few data from the actual SFR site.
- In common with the hydrogeological model, uncertainties exist at the detailed level regarding flow paths at connections between major vertical zones ZFMNW0805A,B and ZFMNNE0869 and the gently dipping zone ZFM871 (formerly zone H2).

## 9 Current understanding of the site

### 9.1 Introduction

This chapter provides an executive summary of the integrated model of present-day conditions in the bedrock at completion of the SFR extension site investigation, PSU. The analysis and modelling of the acquired data for geology, hydrogeology and hydrogeochemistry are presented in detail in Curtis et al. (2011), Öhman et al. (2012, 2013), Nilsson et al. (2011) and summarised in Chapters 5, 7 and 8 of the present report.

Evolutionary aspects and a description of the surface system are also included in the report (Chapters 3 and 4). However, these are by and large excerpts of the information presented in Söderbäck (2008) and Lindborg (2008) supporting the site descriptive model for a final repository for spent fuel at Forsmark, SDM-Site (SKB 2008b). New data for the modelling of the surface system will be available after the completion of SDM-PSU.

For reasons of quality, data acquired during the SFR extension site investigation and the Forsmark site investigation have generally been given precedence over older data collected during the planning and construction of the existing SFR facility. However, some older data, such as the geological tunnel mapping, have been considered of particular value in the modelling work reported here (Chapter 5). As far as rock mechanics is concerned, a compilation of older data collected during the planning and construction of the existing SFR facility and recent data collected during the Forsmark site investigation was considered sufficient for SDM-PSU (SKB 2008a). This compilation is presented in Chapter 6.

In summary, SDM-PSU for repository engineering (RE) and safety assessment (SA) has delivered:

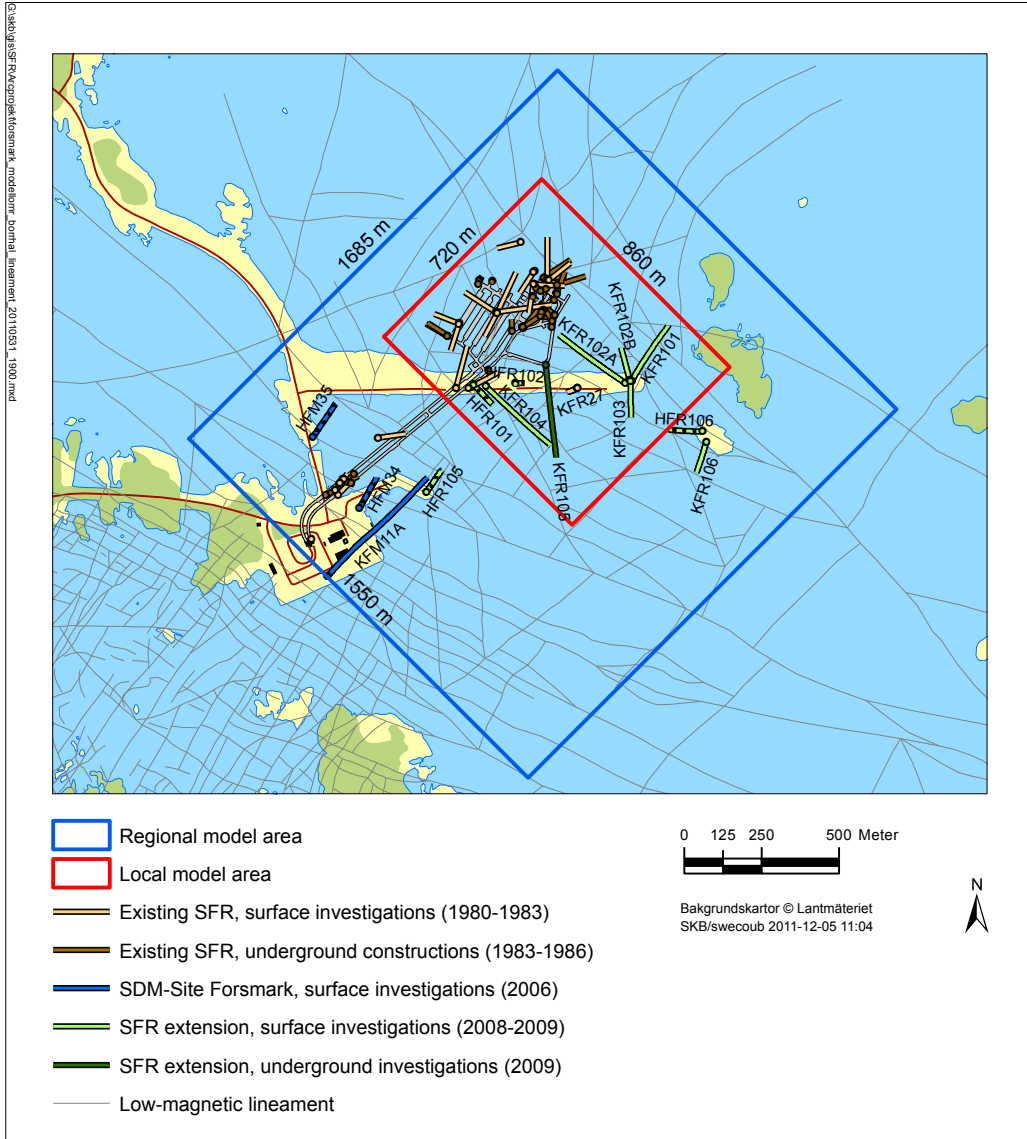
- a local 3D model of the rock domains (RE),
- deterministic deformation zones on local and regional scales (RE),
- a conceptual model of bedrock hydrogeology with hydraulic properties of the hydraulic conductor domains and hydraulic rock mass domains (RE, SA), and
- a conceptual model of hydrogeochemistry that describes, in general terms, the present-day chemical composition, origin, reactions and processes, and residence times of the groundwater (SA).

Figure 9-1 shows a map of the older boreholes drilled during the planning and construction of the existing SFR facility and the recent boreholes drilled during the SFR extension site investigation. Two of the new boreholes, HFR106 and KFR106, were drilled outside the local model area, i.e. east of the area intended for the planned extension. The boreholes located to the southwest within the SFR regional model area were drilled as part of the Forsmark site investigation, SDM-Site (SKB 2008b).

### 9.2 Surface system

The description of the surface system is in itself multi-disciplinary in that it relies on an integrated understanding of meteorology, hydrology, oceanography, hydrochemistry, Quaternary geology and ecosystems in the Forsmark area. A brief summary of the regolith model used for groundwater flow modelling in SDM-PSU is provided here, since the stratification and hydraulic parameterisation of the regolith affects the inflow to the existing SFR facility and hence the calibration of the groundwater flow model, see Öhman et al. (2013) for details. The hydraulic parameterisation of the regolith model is denoted by HSD in SKB's systems approach for hydrogeological modelling (cf. Figure 7-1).

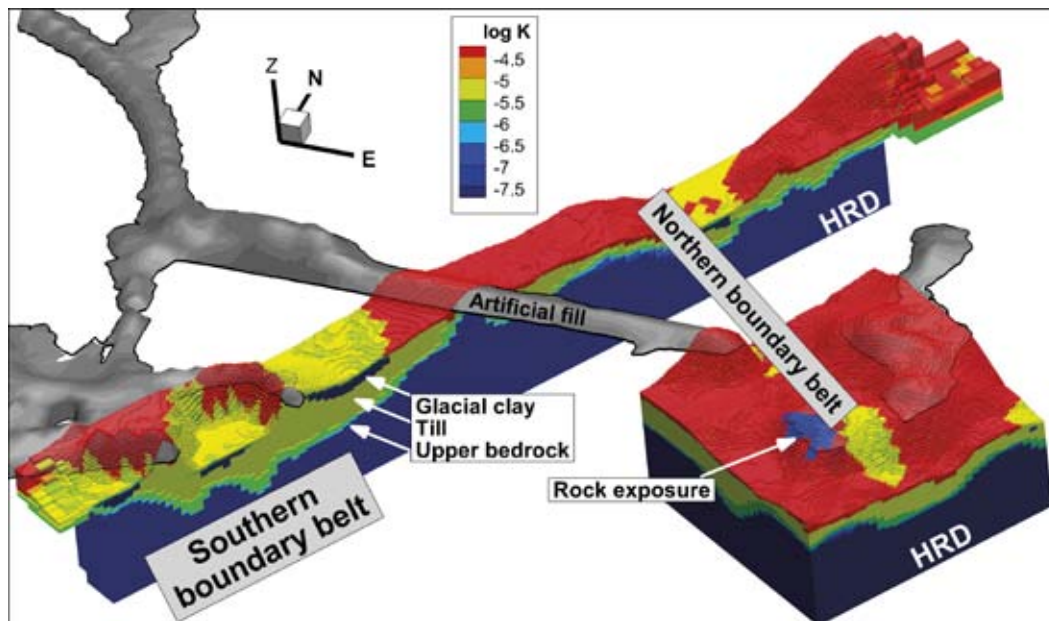
In SDM-Site, a conceptual model of the spatial distribution and stratification of Quaternary deposits inside the flow model area was developed during the site investigation at Forsmark (Hedenström et al. 2008). The conceptual model is deterministic and consists of nine layers, but not all layers exist everywhere. The total thickness of the Quaternary deposits varies from zero to tens of metres.



**Figure 9-1.** Map visualising the low magnetic lineaments and the borehole coverage within the model area showing the horizontal component of inclined boreholes. Boreholes are colour-coded by investigation project/period. Cored boreholes (KFRXX) are shown with solid colour and percussion boreholes (HFRXX) have black dots. Boreholes belonging to the Forsmark site investigation programme are shown with blue colour.

In SDM-Site, effective conductivity values were calibrated for each layer by means of surface hydrological modelling based on conditions measured in the terrestrial part of the flow model domain inside the Forsmark tectonic lens (Bosson et al. 2008). This calibration was updated slightly in SR-Site (Bosson et al. 2010).

Figure 9-2 shows an excerpt of the HSD implementation for SDM-PSU, which is identical to that used in SR-Site (Bosson et al. 2010). It is noted that the hydraulic properties above and below the current sea level were assumed to be identical in both SDM-Site and SR-Site. It could be asserted, however, that the present-day hydraulic properties of the regolith below the current sea level are probably less permeable than those in the regolith above the current sea level. Examples of processes affecting the hydraulic conductivity of the regolith in connection with shoreline displacement include erosion (shoreline wave erosion and topographical surface runoff), biological activity (e.g. wormholes and root threads), freezing and frost heave. In order to analyse the sensitivity of the groundwater flow model to this uncertainty, different parameter combinations could be attempted. However, *in situ* measurements of the hydraulic properties of the regolith below the current sea level are needed in order to constrain the range of uncertainty. These data are currently lacking.



**Figure 9-2.** Visualisation of the HSD parameterisation for SDM-PSU using data from SR-Site (Bosson et al. 2010) together with DarcyTools (Öhman et al. 2013). Except for Glacial clay ( $K_z = 2 \cdot 10^{-8}$  m/s), the conductivity of HSD is considerably higher than that of the underlying bedrock ( $K_{HRD} = 6.5 \cdot 10^{-9}$  m/s). HCD properties associated with the Southern and Northern boundary belts are not included in this figure. The vertical resolution is exaggerated ten times relative to the horizontal in this image.

### 9.3 Rock domain model and general fracture characteristics

Four rock domains (RFR01–RFR04) have been recognised in the SFR local model volume (Figure 9-3). The key information for their establishment is:

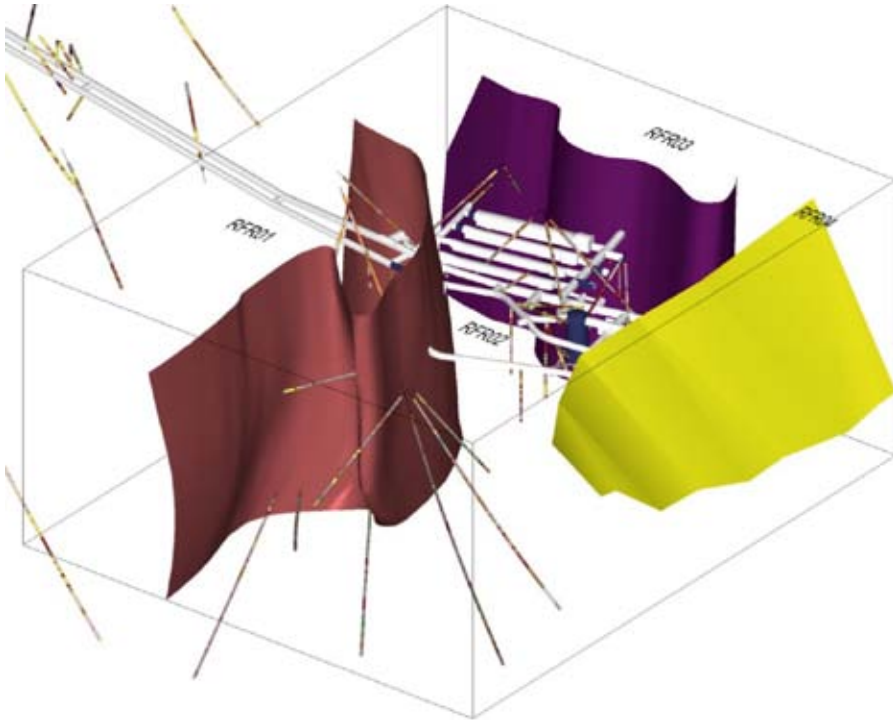
- the lithological composition and heterogeneity in various rock units, and
- interpretations based on high resolution magnetic total field data in combination with fixed points along drill cores, including a 3D inversion model (Figure 9-4).

The importance of ductile deformation data, which formed the backbone of the Forsmark deformation zone model, has been secondary due to the scarcity of reliable data bearing on linear ductile fabrics as well as the pronounced heterogeneity of the data available in the SFR area. Both these features preclude a detailed structural analysis.

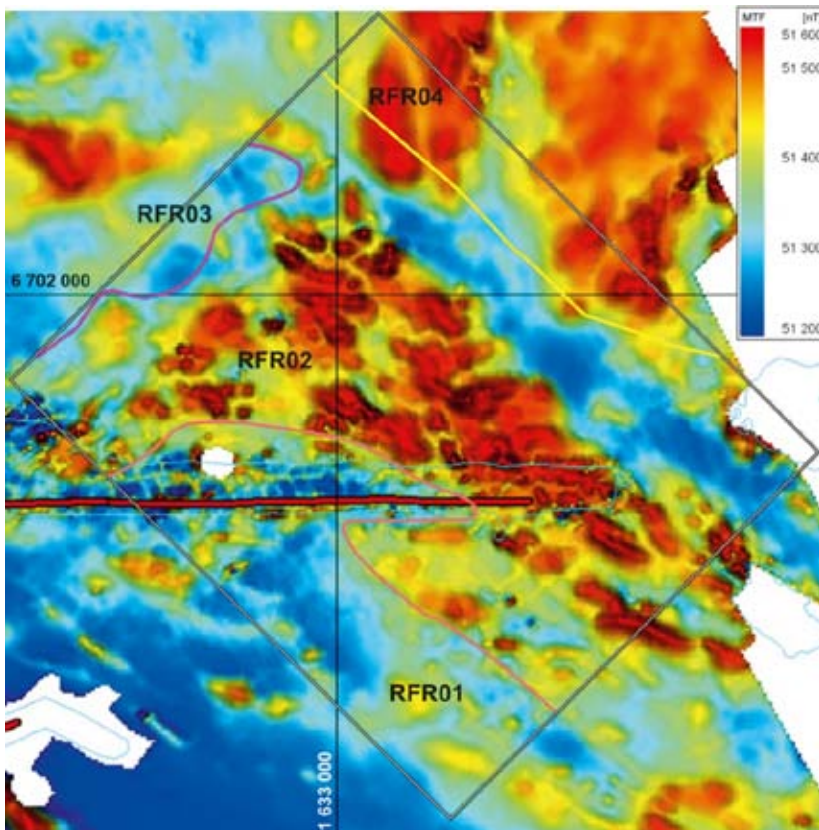
The existing SFR facility and the rock volume directly to the southeast proposed for the extension are situated within two rock domains, RFR01 in the southwest and RFR02 in the northeast. Geological borehole and SFR tunnel information is limited to rock domains RFR01 and RFR02. More than 70% (3,767 m) of the mapped borehole length data are from RFR02, which also hosts most of the existing SFR underground facility.

Rock domain RFR01 is modelled as a major fold structure characterised by a relatively high degree of homogeneity and dominated by pegmatitic granite and pegmatite with a poorly-developed ductile deformational fabric, whereas rock domain RFR02 is far more heterogeneous and dominated by fine- to finely medium-grained metagranodiorite (to granite), often with a well-developed planar ductile deformation fabric.

No fracture domain modelling and no statistical analysis of sealed and open fractures within the segments of rock domains outside deterministically modelled deformation zones was planned or carried out during the SFR extension project. However, a simple comparison of the mean fracture frequency obtained from borehole data outside modelled deformation zones in RFR01 and RFR02 shows no obvious differences between the two domains, with 3.6 open and 13.2 sealed fractures per metre inside RFR01 and 3.8 open and 13.5 sealed fractures per metre inside RFR02 (Table 9-1).



**Figure 9-3.** Three dimensional model view from east showing the boundaries between the four rock domains within the local SFR model volume relative to the borehole geology and the geometry of the SFR underground facility. The colour choice is only for legibility, where boundary RFR01–RFR02 is pinkish brown, RFR02–RFR03 violet and RFR03–RFR04 yellow.



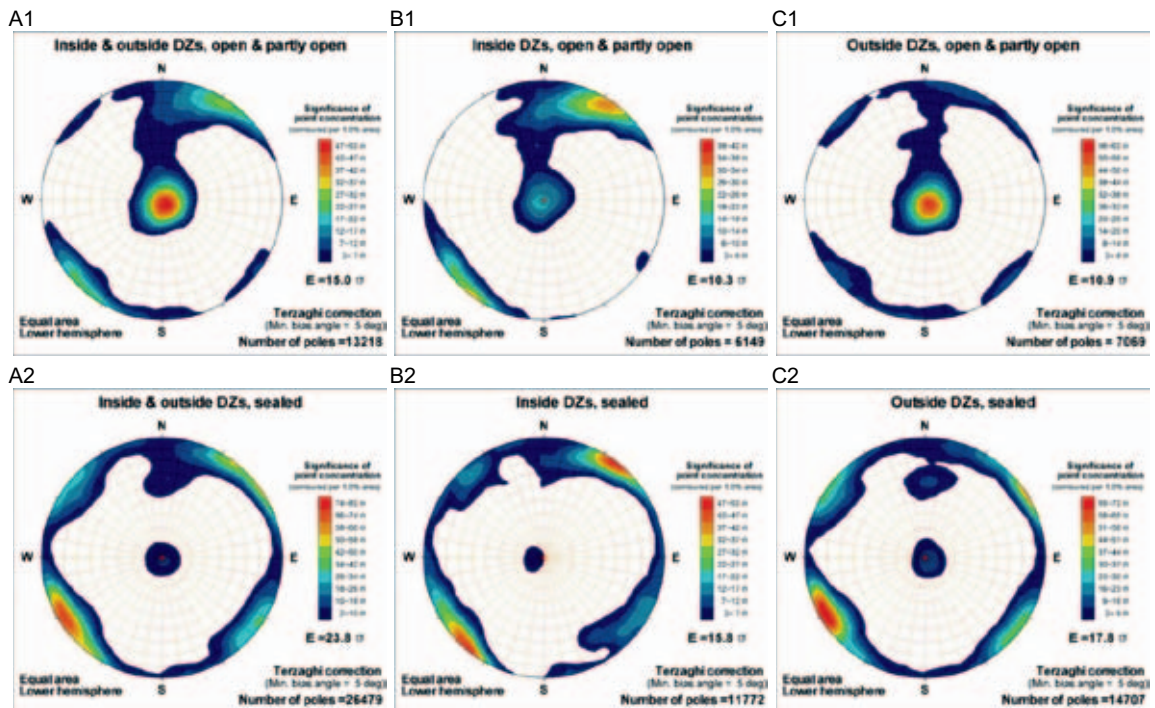
**Figure 9-4.** Map of the magnetic total field after low-pass filtering and subtraction of the contribution of the SFR silo and caverns. The surface trace lines corresponding to the three rock domain boundaries within the local model area are also shown. The colours of the boundaries are identical to those in Figure 9-3. The red line along the pier represents a road.

Nevertheless, there are indications of correlations between lithology and the brittle deformation style. Table 9-1 reveals that a majority of the sealed fractures in RFR01, a domain dominated by pegmatitic granite, form fracture networks, whereas most sealed fractures in RFR02 are registered as “individual” fractures.

A central question for bedrock hydrogeology is whether the rock domain model warrants lateral subdivision of the rock mass into separate HRDs. The difference between RFR01 and RFR02 is judged to be minor in terms of frequency of different fracture types (Table 9-1). However, there is a clear difference in intensity of the orientation patterns between open and sealed fractures. Taking the rock mass as a whole (A1–A2 in Figure 9-5), the *horizontal orientation group dominates the open fractures*, whereas sealed fractures are predominantly sub-vertical to steeply dipping and strike WNW-ESE to NW-SE or NE-SW. If the rock mass lying within the modelled deformation zones is considered in isolation (B1–B2 in Figure 9-5), it is the steep WNW-ESE to NW-SE set that dominates the open fractures. The dominance of sub-horizontal, open fractures in the rock mass outside the target intercepts in boreholes for modelled deformation zones is visible in C1 in Figure 9-5. For sealed fractures, a comparison of the pattern for the rock mass as a whole with the pattern inside and outside of the modelled deformation zones is more stable and shows no great contrasts (A2–C2 in Figure 9-5). The sealed fractures are predominantly steep and strike NW-SE but there is also a clear steep NE-SW set, along with a weaker sub-horizontal set. There is also a strongly subordinate, moderately dipping set with an E-W strike that is seen most clearly outside the deformation zones (C2 in Figure 9-5).

**Table 9-1. Mean fracture frequencies per metre of mapped drill core for rock domains RFR01 and RFR02 outside modelled deformation zones (Terzaghi corrected values).**

Rock domain	Open	Partly open	Crush equivalent	Total open	Sealed	Sealed network	Total sealed
RFR01	3.32	0.24	0.01	3.57	5.75	7.43	13.18
RFR02	3.44	0.33	0.05	3.82	10.14	3.35	13.50



**Figure 9-5. Fracture orientation clustering inside and outside target intercepts for modelled deformation zones based on data from KFM11A and the cored boreholes KFR27, KFR101, KFR102A, KFR102B, KFR103, KFR104, KFR105 and KFR106.**

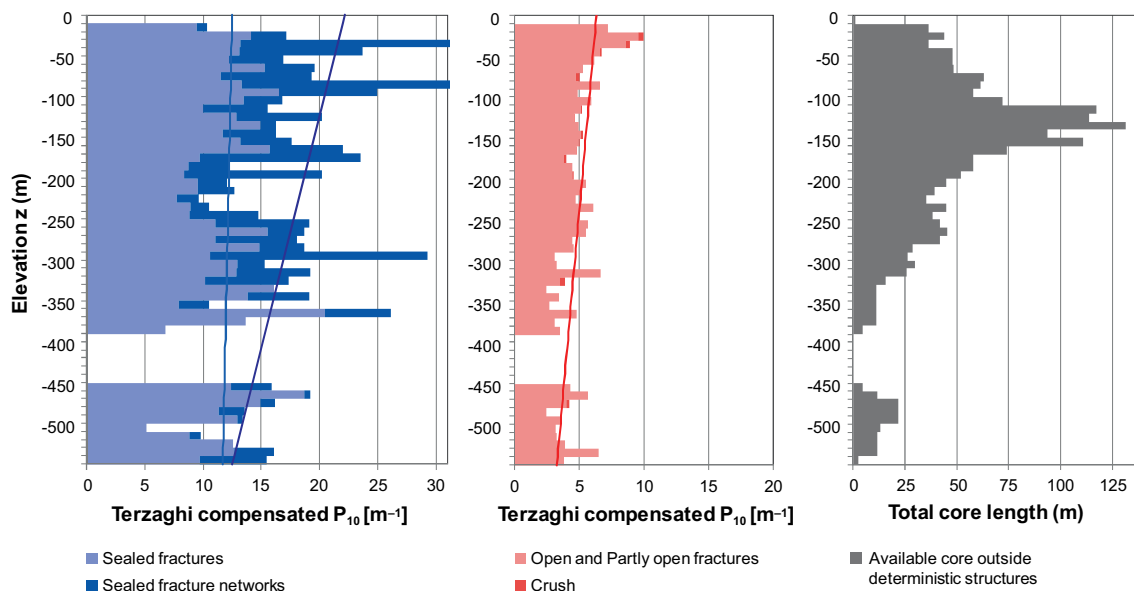
Vertical trends in the intensity of open fractures in the rock mass lying outside the deformation zones have been investigated for open, sealed, steeply to moderately dipping and gently dipping fractures (Figure 9-6). Only data originating outside of deterministic deformation zones (ZFM) are included.

Gaps in borehole coverage complicate the determination or significance of depth trends in fracture frequency. However, visual inspection suggests a slight decline in frequency with depth, both for sealed fractures and open fractures. Linear regression (Figure 9-6) suggests that the decline in Terzaghi-compensated frequency, expressed as  $[m^{-1}]$  per 100 m depth, is: 1.81 for sealed fractures (if fractures inside networks are included), 0.15 for sealed fractures (if fractures inside networks are excluded), and 0.57 for open fractures + crush.

The SFR local model domain has a high open fracture intensity compared with the observations made in the target volume in SDM-Site Forsmark (Table 9-2). It should be noted, however, that fracture domain FFM02 at SDM-Site Forsmark is mainly covered by borehole data below  $-100$  m RHB 70. Thus, for the uppermost part of the bedrock ( $z \geq -200$  m), the difference between the two sites may be smaller in reality, than that indicated by Table 9-2. Furthermore, in SDM-Site Forsmark, a significant contrast was found between the intensively fractured uppermost c. 200 m (FFM02) and the sparsely fractured tectonic lens below (FFM01). No such prominent contrast is observed at SFR; instead, the decline in open fracture intensity with depth is small (cf. Figure 9-6).

**Table 9-2. Comparison of Terzaghi-compensated open fracture frequency ( $P_{100,corr}$ ) in the SFR local model domain with SDM-Site Forsmark. In order to ensure consistency in the comparison between the two sites, the intensities are both Terzaghi-compensated with a maximum weight of 7 (i.e. a minimum bias angle of  $8.2^\circ$ ). Note that the total intensities in Table 9-1 are different since a different weight was used for the Terzaghi-compensation.**

	Upper bedrock, $z \geq -200$ m		Deeper bedrock, $z < -200$ m	
	SDM-Site Forsmark (FFM02)	SFR extension boreholes	SDM-Site Forsmark (FFM01)	SFR extension boreholes
$P_{100,corr}$	3.2	5.8	1.1	5.0



**Figure 9-6. Fracture frequency depth trends.** Fracture data and borehole coverage are binned per 10 m elevation. Values for elevation bins reflect the median elevation of the bin. In other words: the “ $-50$  bin” covers data between 45 m and  $-55$  m elevation. Borehole length inside casing is excluded (as well as inside ZFM). A Terzaghi weighting ( $T_w$ ) of  $15^\circ$  minimum bias angle is used here, which corresponds to a maximum weight of 3.84. Data without orientation are assigned an average  $T_w$  set of 2 and are randomly assigned to the steep or gently dipping population. Intensity of sealed networks and crushes is calculated as  $1000/piece\_length$  mm (i.e. not Terzaghi-compensated).

## 9.4 Current stress field

Based on the results of overcoring in boreholes at SFR, a linear function with depth was roughly fitted to the SFR data (see green line in Figure 6-12 to Figure 6-14). The stress model for SFR is presented as a function of depth in Table 9-3. The gradient for horizontal stresses is 0.07 MPa per depth metre and may therefore not be used for very deep predictions. For the sake of comparison, Table 9-3 also shows the recommended horizontal and vertical stress magnitudes for the Forsmark target area.

**Table 9-3. *In situ* rock stress estimates for the rock in the SFR local model volume, from the ground surface down to 250 m depth (cf. Table 6-11), and in the target area at Forsmark down to –150 m elevation (Glamheden et al. 2007).**

Site d = vertical depth (m)	Major horizontal stress, $\sigma_H$ (MPa)	Trend (°)	Minor horizontal stress, $s_h$ (MPa)	Trend (°)	Vertical stress, $s_v$ (MPa)
SFR, d = 0–250 m	$5 + 0.07d$	142	$0.07d$	055	$0.027d$
Forsmark, d = 0–150 m	$19 + 0.008d \pm 20\%$	$145 \pm 20$	$11 + 0.006d \pm 25\%$	055	$0.027d \pm 2\%$

Based on Table 9-3 it is concluded that the current stress field at SFR would tend to keep horizontal fractures at shallow depths open, maintain the openness of steep fractures with a WNW-ESE to NW-SE strike and close steep fractures with a NE-SW strike. This agrees with the fact that the horizontal orientation group dominates the open fractures (Figure 9-5).

## 9.5 Deformation zones and their transmissivity

### 9.5.1 Geological data and modelling

The key input for the establishment of the deformation zone model is 1) the single-hole interpretation in the boreholes (SHI) of intervals with possible deformation zone type properties (PDZ), 2) tunnel mapping of the SFR underground facility, 3) lineaments identified by assessment of magnetic minima in the magnetic total field from surveys in the SFR area, 4) reprocessing and evaluation of existing reflection seismic data, and 5) processing and interpretations of the high resolution magnetic total field data by forward magnetic modelling (Curtis et al. 2011).

It is noted that the current SKB definition of a deformation zone differs considerably from that applied in the previous structural models of SFR, where brittle deformation zones (fracture zones) were generally identified on the basis of the frequency of open fractures and hydrogeological information (cf. Carlsson et al. 1985, 1986). Zone thicknesses have currently been estimated on the basis of geophysical data and interpretation of lineaments and reflectors and the SHI borehole intercepts that take into account other features such as the frequency of sealed fractures and hydrothermal rock alteration. The geological methodology used here conforms to that used in the Forsmark site investigation (see especially Section 5.2.1 in Stephens et al. 2007). It should also be noted that deformation zone geometries are often complex, discontinuous and asymmetric.

Concerning the single-hole interpretation, 64 out of a total of 95 borehole intervals with possible deformation zone type properties have been used to establish the deterministic deformation zone model. Hence, 31 PDZ intervals remain unresolved in the geological model. Seventeen of the 31 unresolved PDZ intervals occur in the vicinity of the existing SFR facility (the old data set). The other 14 unresolved PDZ intervals occur in the area of the planned extension (the new data set). In addition, six of the 14 unresolved PDZ intervals in the new data set occur in boreholes HFR106 and KFR106, which are both drilled outside the local model area, hence outside the area intended for the SFR extension (Figure 9-1). It is noted that:

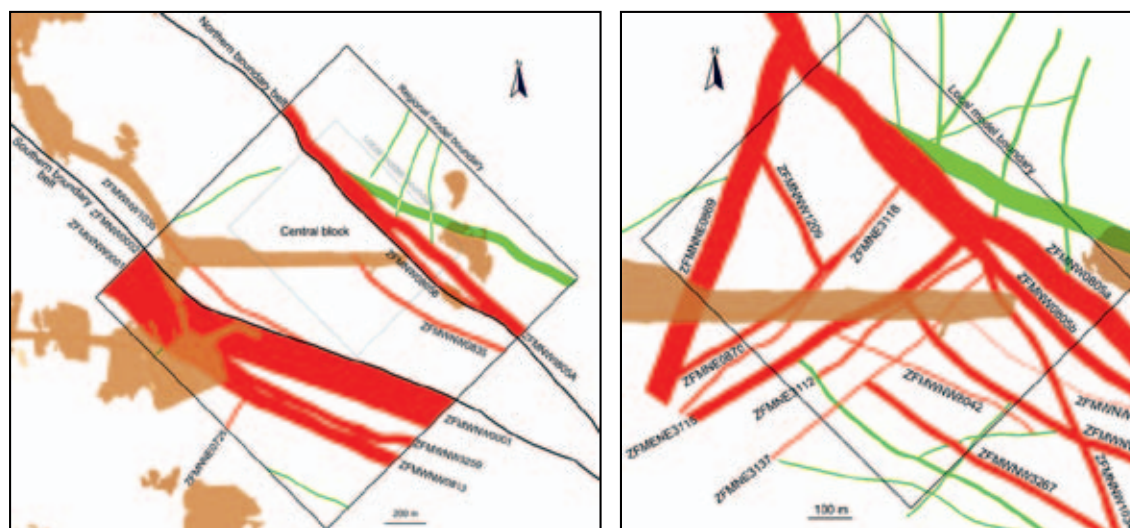
1. The 31 unresolved PDZs are inferred to be predominantly minor geological structures with a size outside the scale of resolution adopted for the geological modelling work (300 m).
2. 17 PDZs are ignored in the hydrogeological modelling work, mainly because of low confidence in identification issues and/or little hydraulic significance.



3. The remaining 14 PDZs are significant from the hydraulic viewpoint and are predominantly inferred to be gently dipping or sub-horizontal structures.
4. 5 of the hydraulically significant PDZs are handled deterministically as part of SBAs (see below in Section 9.6.3), 7 are modelled stochastically (see Section 9.6.4 below) and 2 are modelled as extensions or splays of deterministically modelled deformation zones (see Section 7.3.3 above).

In summary, 40 deformation zones, 21 of which have been assigned a high confidence of existence, are included in the regional and local models (Curtis et al. 2011). Twenty-eight zones occur inside the local model volume. The regional model contains only local major and larger zones, i.e. zones with a trace length on the ground surface of  $\geq 1,000$  m, whereas the local model contains all modelled deformation zones that have a size corresponding to a trace length on the ground surface of  $\geq 300$  m (Figure 9-7). The selection of these size limits is related to the model volume's maximum depth (local model  $-300$  m and regional model  $-1,000$  m elevation) and the applied methodology that requires the same model resolution throughout the defined model volume /Munier et al 2003, Stephens et al. 2007/. However, to assist hydrogeological modelling work, an updated combined model, including all structures from both the regional and local models, has also been delivered (Figure 9-8).

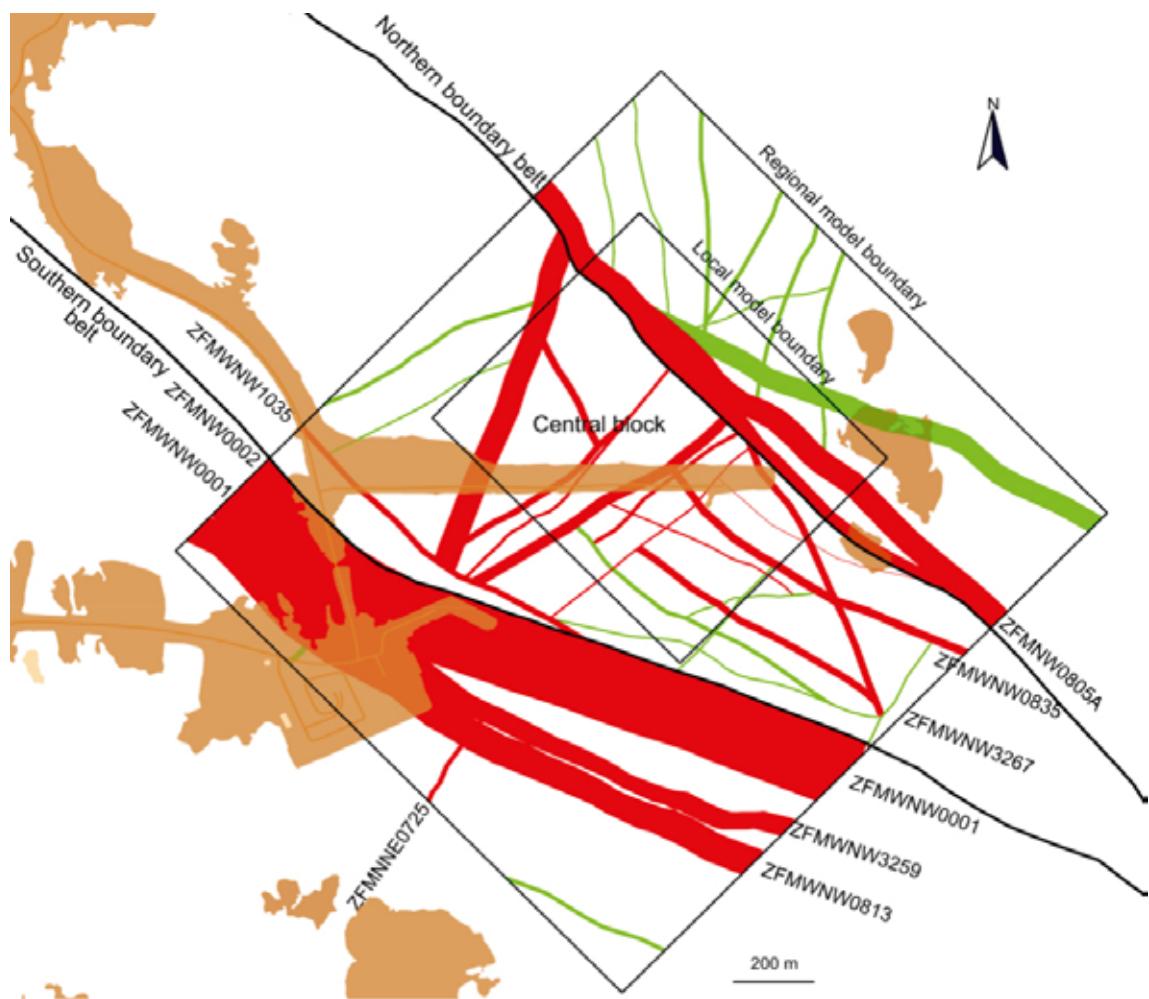
Three of the 40 zones in the regional model and one of the 28 zones in the local model are gently dipping. All other deterministic deformation zones are vertical or steeply dipping and follow the orientation sets identified by their geological character in the earlier model for deformation zones at Forsmark (Stephens et al. 2007, SKB 2008b). The most prominent deformation zones in the region belong to the WNW-to-NW-trending set and mainly occur in two broad belts that delimit a tectonic wedge, denoted the "Central block", containing the existing SFR facility and the rock volume proposed for the new facility extension (Figure 9-9). The Central block is less affected by deformation than the bounding belts, which are denoted the Northern boundary belt and the Southern boundary belt. The similarities to the volume studied in Forsmark SDM-Site are noted: the structural layout of "Southern boundary belt-Central block-Northern boundary belt" in a SW-to-NE direction in the SFR area bears similarities to the structural layout of "Southern boundary belt-Forsmark tectonic lens-Eckarfjärden deformation zone" in a NE to-SW direction in the Forsmark SDM-Site volume, see Stephens et al. (2007).



a. Regional model area, trace lengths  $\geq 1,000$  m

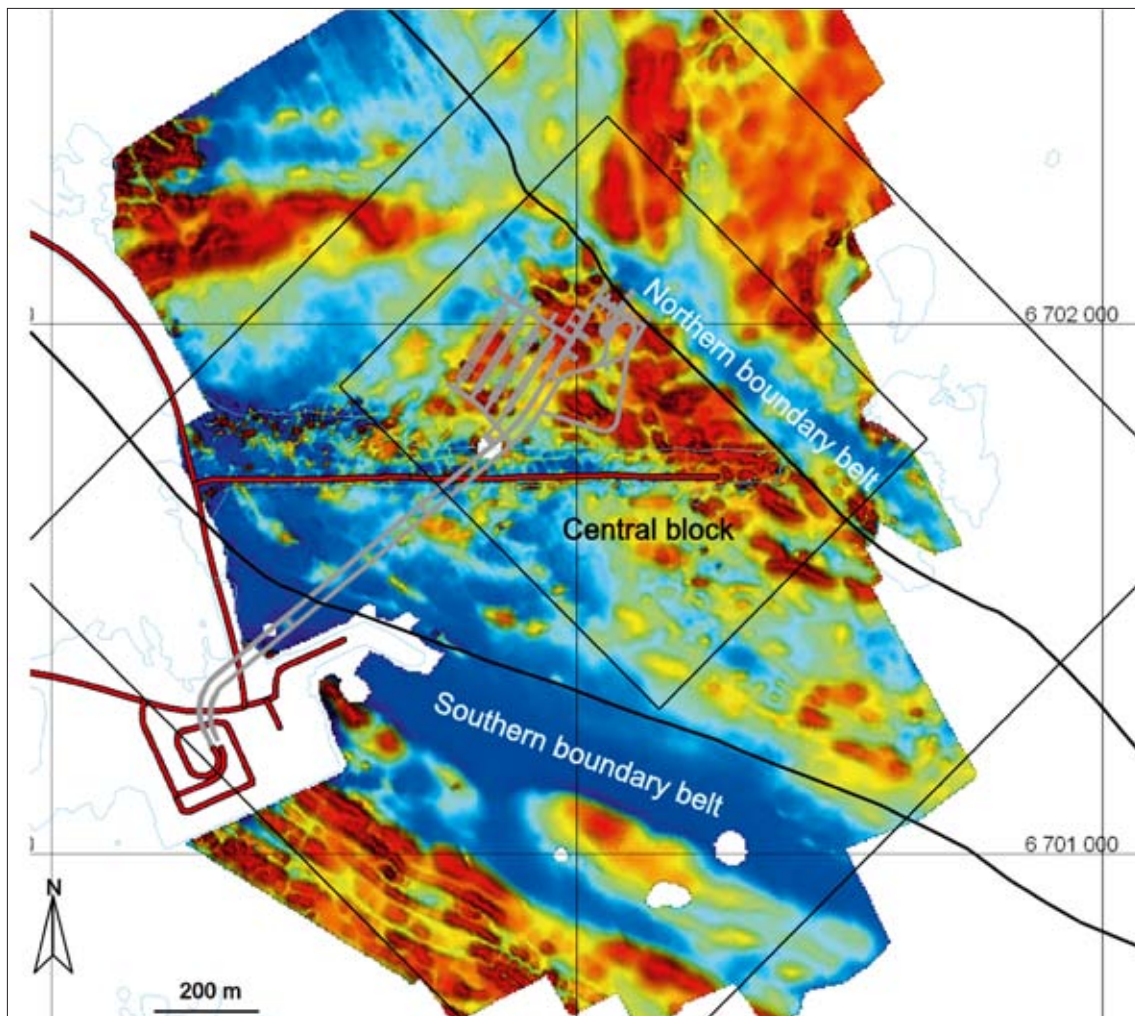
b. Local model area, trace lengths  $\geq 300$  m

**Figure 9-7.** Intersection at the current ground surface of deformation zone traces within a) the regional model and b) the local model. The different colours indicate confidence in existence: high = red, medium = green.



**Figure 9-8.** Intersection at the current ground surface of deformation zone traces of all sizes inside the regional model area, i.e. a combined model version. The regional deformation zones ZFMNNW0001 and ZFMNNW0805A, along with their major splays, form the general southern and northern boundaries of the central SFR tectonic block. Confidence in existence: high = red, medium = green.

Southeast of the existing SFR facility, a series of WNW-to-NW-trending deformation zones are included in the model. These are much smaller than the bounding belts, which contain composite ductile and brittle deformation zones and were initiated at a later stage in a brittle regime. A NNE-to-ENE-striking set of brittle deformation zones is also present. Compared with the WNW-NW set, they are thinner and shorter, due to termination against the broad WNW-to-NW-trending deformation belts. In addition, there are a few N-S-to-NNW-trending deformation zones in the model. However, on the basis of their low frequency of occurrence, this orientation set is judged to be of lower significance relative to the other sets at Forsmark (see also Stephens et al. 2007). However, it is noted that HFR106 and KFR106 are drilled in proximity to the deformation zone ZFMNNW1034.



**Figure 9-9.** The central SFR block containing the existing SFR storage facility, the Northern boundary belt (dominated by ZFMNW0805A) and the Southern boundary belt (dominated by ZFMWNW0001), along with the magnetic total field.

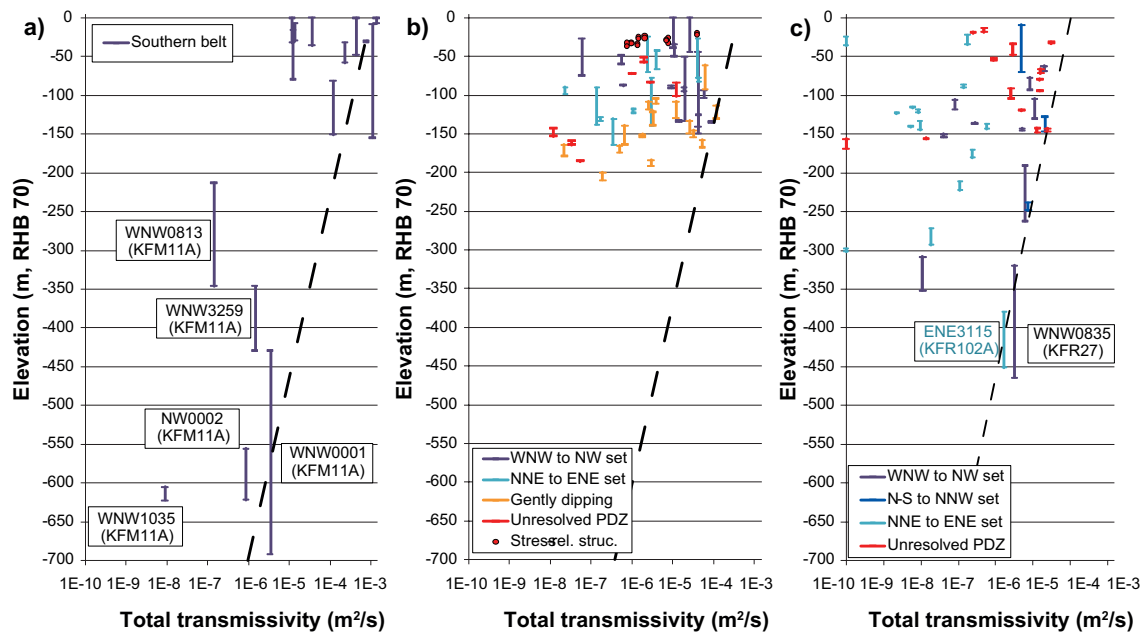
### 9.5.2 Hydraulic properties

The geological model of the bedrock version 1.0 (Curtis et al. 2011) is a refinement of the regional SDM-Site Forsmark structural model (Stephens et al. 2007). In SDM-Site, an exponential model was formulated for the depth dependency in HCD transmissivity (Follin et al. 2007b):

$$T(z) = T_0 10^{-z/k} \quad (9-1)$$

where  $T(z)$  is the transmissivity at elevation  $z$ ,  $T_0$  is the expected transmissivity at zero elevation, and  $k$  is a depth trend parameter which defines the depth interval over which the transmissivity decreases by one order of magnitude. In SDM-Site, the value of the depth interval parameter  $k$  was determined to be 232.5 m based on the trend of the maximum transmissivity with depth. In order to account for structural differences when comparing the data acquired in the SFR extension investigation with the depth-dependency trend model at Forsmark, data were divided into three sub-groups:

- the Southern boundary belt data set (Figure 9-10a),
- the old hydraulic data set acquired in the proximity of the existing SFR facility (Figure 9-10b), and
- the new hydraulic data set acquired in the area of the SFR extension site investigation (Figure 9-10c).



**Figure 9-10.** The sum of transmissivity values inside the bounds of each HCD intercepts are plotted here for the interval 0 to -700 m elevation: a) Southern boundary belt intercepts, b) old data, and c) new data set. The depth trend model from SDM-Site Forsmark (black dashed line in all diagrams),  $k = 232.5$  m, Equation (9-1), has been fitted to the maximum values of each data set. Transmissivity below the detection limit is shown as  $10^{-10}$  m<sup>2</sup>/s.

In the Southern boundary belt (Figure 9-10a), the shallow transmissivities are extremely high ( $T_{HCD} > 10^{-4}$  m<sup>2</sup>/s). Potentially, these reflect intercepts with sheet joints of the same type that were found in SDM-Site Forsmark. However, such extremely high transmissivity values at shallow depths have not been found north of the Southern boundary belt within the SFR regional model area (Figure 9-10b and Figure 9-10c). At depth in the Southern boundary belt, the available transmissivity data are incomplete because the zones are only partially penetrated by the boreholes.

North of the Southern boundary belt, the largest transmissivities in the old data set (Figure 9-10b) are found among the WNW-to-NW-striking deformation zones forming the northern boundary belt along ZFMNNE0869, and along the gently dipping structures forming the gently dipping ZFM871. However, the vertical range of the old data set, 0 to -200 m, is not sufficient to determine depth dependency.

The data from the SFR extension investigation has a slightly larger vertical data coverage (Figure 9-10c). The largest transmissivities are found among the WNW-to-NW-striking HCDs forming the Northern boundary belt and along ambient deformation zones, i.e. ZFMNNW1034 and ZFMWNW3262, as well as among a number of borehole intervals with unresolved PDZ type properties. The flowing fractures in these intervals are horizontal to gently dipping.

In conclusion, the gently dipping structures together with the WNW-striking HCD set are generally more transmissive than the NNE-to-ENE-striking HCD set. This observation is in good agreement with the observations previously reported for SDM-Site Forsmark (Follin 2008).

The value of the depth trend parameter,  $k = 232.5$  m, derived in SDM-Site Forsmark (Follin et al. 2007b) represents the depth trend of the maximum transmissivities observed at each elevation regardless of HCD set. It does not represent a statistical regression of the transmissivity data acquired within each HCD set. According to Figure 9-10a, b and c, a similar value of the depth trend parameter also appears to be applicable to the most transmissive HCD data at each elevation within the SFR local model area. However, the determination of the lateral variability around this depth trend model is uncertain. The key uncertainties in this respect concern the modelling of the NNE-to-ENE-striking HCD set and the gently dipping deformation zone ZFM871, both of which appear to be quite heterogeneous. From a hydraulic point of view it is necessary to account for deformation

zone heterogeneity, since not all deformation zones may be permeable. Equation (9-2) could be used for modelling parameter heterogeneity within the HCDs. Specific values of  $T_{eff}(0)$ ,  $k$  and  $s_{\log(T)}$  are provided for each deformation zone in Öhman et al. (2013).

$$T(x, y, z) = T_{eff}(0) 10^{z/k + N(0, s_{\log(T)})} \quad (9-2)$$

An alternative to using a common depth trend parameter for all HCD sets is to use set-specific depth trend models for each HCD set. For instance, both the NNE-to-ENE-striking HCD (Figure 9-10c) set and the gently dipping ZFM871 (Figure 9-10b) appear to show stronger depth dependencies.

## 9.6 Hydrogeological model of the rock mass between deformation zones

### 9.6.1 Open fractures

The hydrogeological model of the bedrock between deformation zones (hydraulic rock mass domain, HRD) divides the open fractures into five sets with regard to orientation (strike and dip). These are denoted by EW, NE, NW, GD (gently dipping), and HZ (horizontal). The weak vertical trend is differentiated into three depth intervals/HRDs according to intensity: the Shallow bedrock HRD (above -60 m), the Repository level HRD (-60 to -200 m), and the Deep bedrock HRD (below -200 m). The intensity of open fractures inside the three HRDs decreases weakly with depth (cf. Figure 9-6). The Repository level HRD has the best total borehole coverage and, as a consequence, provides the best basis for detailed intensity calculations. In this interval, the intensity of open fractures was calculated for each fracture set and for each borehole. The sets have similar intensities at repository level, approximately  $1 \text{ m}^2/\text{m}^3$  for each set (cf. Figure 9-6 and Figure 7-21).

Open fractures exhibit local heterogeneity, but spatial trends in open fracture intensity inside the local model domain are not deemed significant in relation to gaps in borehole coverage, see Appendix F in Öhman et al. (2012) for details. The decrease in intensity of open fractures with depth is small and the set-wise intensity varies only slightly between boreholes, although this may well be an artefact of local heterogeneity and gaps in borehole coverage. The cored borehole data acquired outside the local model area, i.e. in boreholes KFM11A and KFR106, are not judged to be representative of the HRD of the SFR regional model area, since they are influenced by the Southern and Northern boundary belts, respectively.

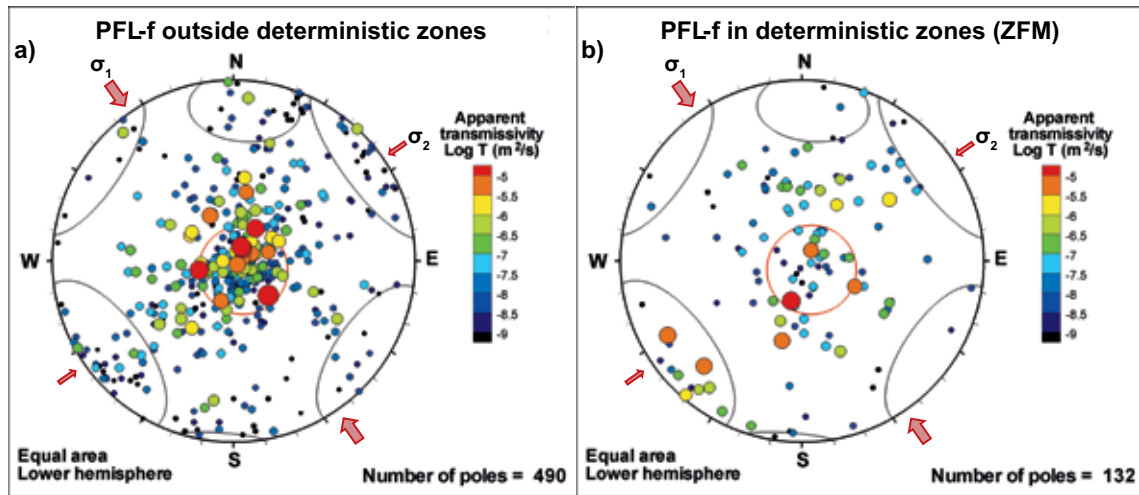
### 9.6.2 Flowing fractures

Flowing fractures detected by the PFL-f method are assigned transmissivities and divided into the same fracture sets as those defined for the open fractures (Figure 7-21). The pattern of flowing fractures outside the ZFMs (HCDs) is similar to that inside the ZFMs (Figure 9-11). That is, the hydraulically active fractures in the steeply dipping deformation zones are primarily horizontal to gently dipping, followed by the steeply dipping NW-SE striking fractures. This is consistent with the conceptual understanding of the geological processes active at the site in connection with the formation of sub-horizontal to gently dipping fractures, and not least their aperture.

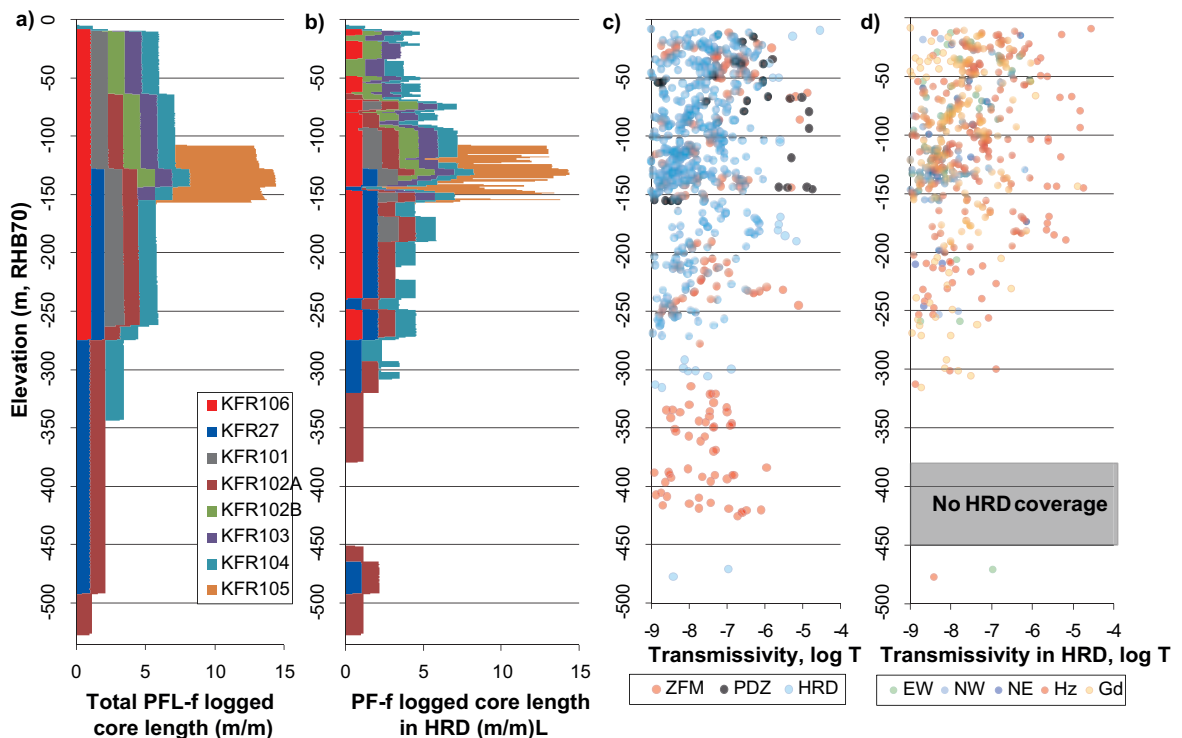
Figure 9-11 in combination with Figure 9-12b, -c and -d reveals that the majority of the largest PFL-f transmissivities ( $T > 10^{-6} \text{ m}^2/\text{s}$ ) above -200 m elevation are found outside the deterministic deformation zones. In addition, the most transmissive features above -200 m elevation are horizontal to gently dipping and occur in borehole intervals with unresolved PDZ-type properties in the geological model (Figure 9-12c and d). Borehole KFR106 is special in this regard and it is important to note that it is located east of the area intended for the SFR extension in close proximity to the deformation zone ZFMNNW1034. This zone cuts through the wedge between the Northern and Southern boundary belts.

The differences in PFL transmissivity between the horizontal and gently dipping fractures on the one hand and the steeply dipping fractures on the other conforms well to the rock stress model presented in Section 9.4. The rock stress model shown in Table 9-3 suggests that the maximum horizontal stress varies approximately between 5 and 33 MPa in the uppermost 0–400 m of the bedrock, whereas the vertical stress varies approximately between 0 and 11 MPa. According to Indraratna et al. (1999), little or no decrease in transmissivity occurs when the confining stress on

laboratory samples exceeds 10 MPa. Hence, because of the 10–33 MPa stress range for the steeply dipping NW-SE-striking deformation zones, the transmissivity values may not show any relationship to the normal stress below approximately –100 m elevation (Figure 9-12c). However, the majority of the horizontal to gently dipping fractures and deformation zones are subjected to normal stresses ranging from 1 to 11 MPa, which according to Indraratna et al. (1999) is the range in which the normal stress should have a significant impact (Figure 9-12d).



**Figure 9-11.** Orientations of PFL-f data with respect to stress-field; a) outside deterministic deformation zones and b) inside deterministic deformation zones (ZFM). The horizontal principal stress orientations ( $\sigma_1$  and  $\sigma_2$ ) are shown by red arrows (cf. Table 9-3). Hard sectors representing the five fracture sets are included for reference.

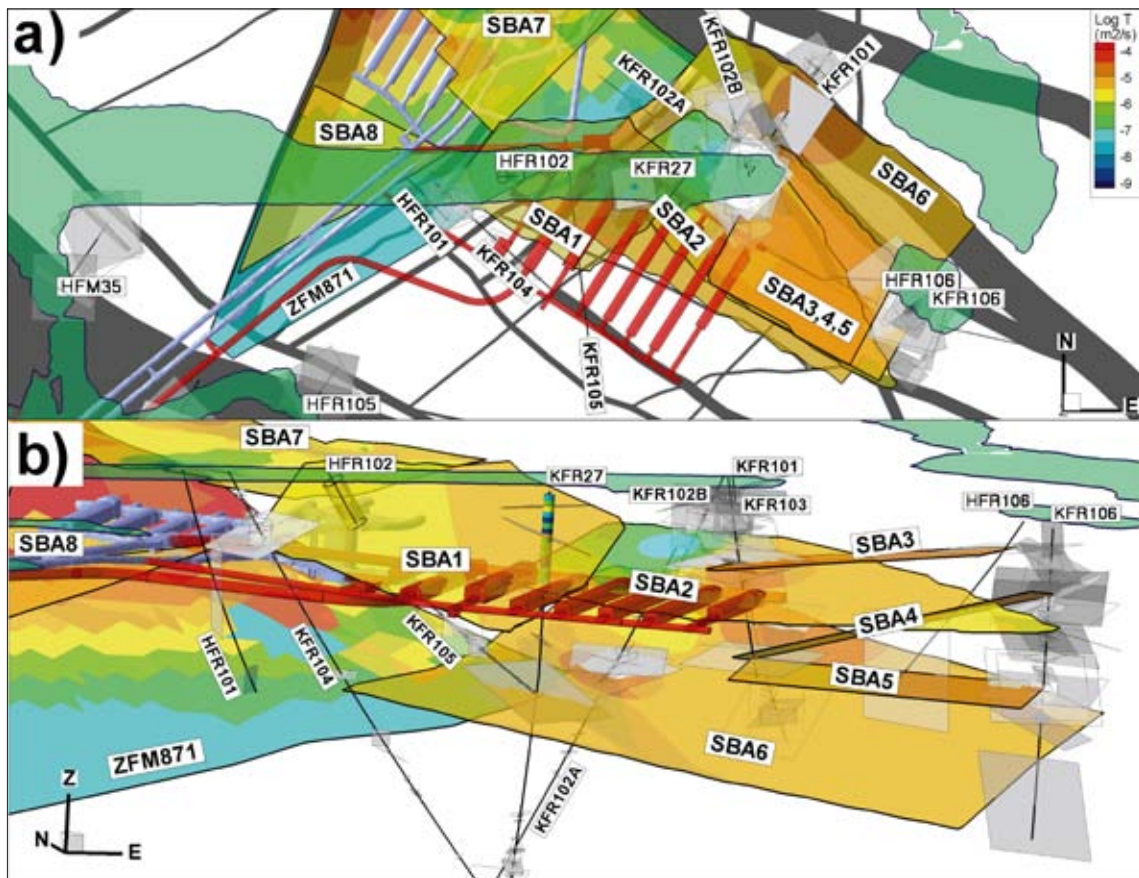


**Figure 9-12.** Borehole coverage and PFL-f transmissivity with depth; a) total core length of PFL-f logging binned by elevation and borehole, b) core length of PFL-f logging outside deterministically modelled deformation zones (ZFM) binned by elevation and borehole, c) PFL-f data divided by ZFM, unresolved PDZ and HRD, and d) PFL-f data outside ZFM divided by fracture set. Note that the sub-horizontal underground borehole KFR105 makes a large contribution to PFL-f logged core length in the interval –105 to –157 m RHB 70 (orange bars).

### 9.6.3 Shallow bedrock aquifer concept

In SKB's systems approach to bedrock hydrogeology (Figure 7-1), the rock mass volumes between deterministic deformation zones (HRDs) are assigned stochastic hydraulic properties using the discrete fracture network (DFN) approach (Rhén et al. 2003). In SDM-Site Forsmark, the possible deformation zones (PDZ) identified at depth in the geological single-hole interpretation work were treated as a model variant in the hydrogeological modelling and added to the deterministic deformation zones. In addition, a modified approach was used for the uppermost 150 m of bedrock because of the significant hydraulic responses observed in this interval. Three one-metre thick horizontal features were introduced at approximately 25 m, 75 m and 125 m depth and assigned heterogeneous hydraulic properties according to the data observed in single-hole as well as cross-hole (interference) hydraulic tests. Although the hypothesis for their genesis was not well established at the time of modelling, these features were assumed to be sheet joints (determined by borehole TV images and bedrock trenches). A commonly accepted causal mechanism for sheet joints, at least in the superficial bedrock, is the stress release associated with, for example, the unloading after the last deglaciation. In SDM-Site Forsmark, the term shallow bedrock aquifer (SBA) was introduced to avoid a deeper discussion about their genetic origin and focus on their hydraulic importance for the uppermost 150 m of bedrock, see Follin (2008) for a summary. A similar approach has been adopted for five of the unresolved borehole intervals with possible deformation-zone-type properties (PDZ) in the geological model developed for SDM-PSU. To highlight the conceptual similarity, the term "SBA-structure" is used in the hydrogeological modelling in SDM-PSU.

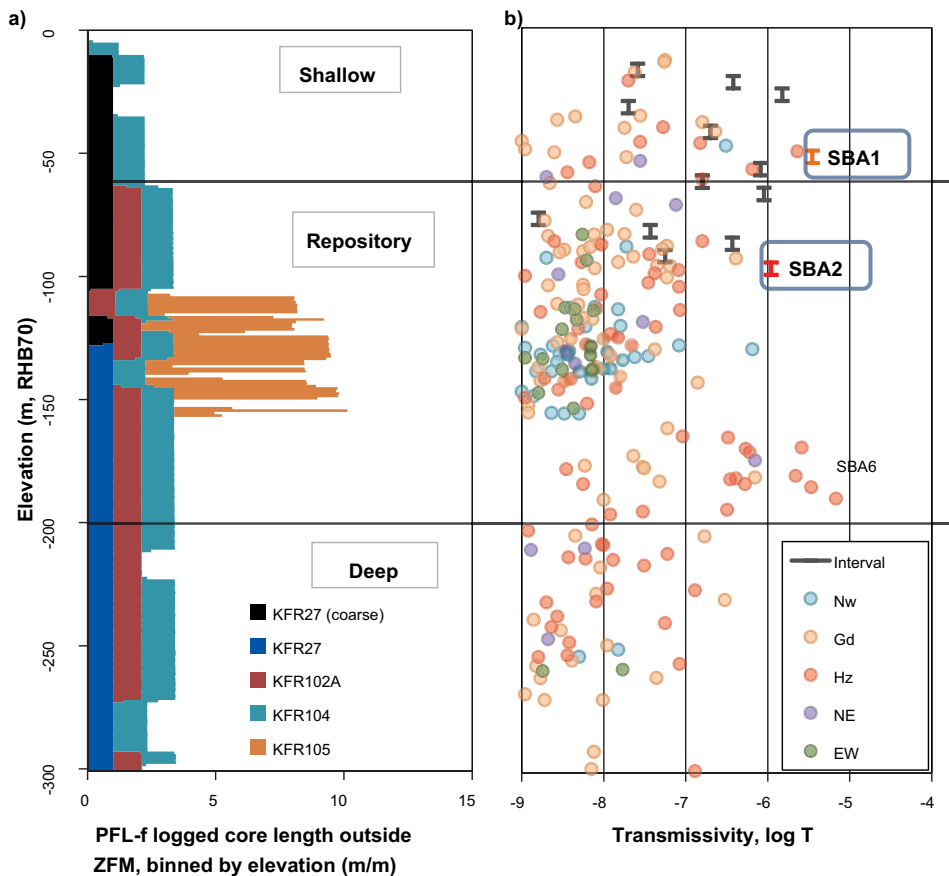
The lateral hydraulic connectivity and hydraulic responses identified within the Shallow and Repository level HRDs are conceptually modelled in terms of eight SBA-structures and shown here in Figure 9-13. SBA1–6 are connected to the Northern boundary belt and ZFMNNW1034, whereas



*Figure 9-13. Visualisation of the eight SBA-structures and deformation zone ZFM871 relative to a preliminary layout of the extended SFR facility: a) top view, b) side view looking towards the northeast. The structures are coloured according to transmissivity interpolated from the transmissivity of the borehole intercepts.*

SBA7 and SBA8 occur in the proximity of the existing SFR facility. The delineation of SBA7 and SBA8 was accomplished during the integrated modelling stage and demonstrates that the shallow bed-rock aquifer phenomenon is not constrained to occur solely in the area of the planned extension (see Section 7.3.3 above). Although modelled as single features it is emphasised that each SBA-structure is believed to represent a “stairway of interconnected sub-horizontal and steeply dipping fractures” rather than a single fracture. It is also noted that the certainty regarding the postulated extension of each SBA-structure varies. In some cases the interpreted sizes are primarily based on similarities in geometrical and hydraulic data in individual boreholes and in other cases additional data are available such as cross-hole hydraulic interferences (see Appendix H in Öhman et al. 2012 for details). Additional boreholes and hydraulic testing together with a geological discrete fracture network (DFN) model could possibly have improved the structural-hydraulic modelling in this regard.

In conclusion, the spacing between SBA-structures, where present, probably varies within the SFR local model domain. The spacing between SBA-structures can be estimated in different ways depending on how their supporting strands of evidence are handled. In Chapter 7, the minimum spacing is estimated to be approximately 30–40 m and the maximum spacing is estimated to be approximately 120–130 m. Figure 9-14 shows the hydraulic data acquired inside the Central block closest to the area of the planned extension. Figure 9-14 suggests that the interval between 100–150 m contains fewer high-transmissive fractures than the interval between 50–100 m. SBA6 is the most certain of the six SBA-structures, and the data shown in Figure 9-13 reveal that the transmissivities of SBA6 are of the same magnitude as the transmissivities of ZFM871 at comparable depths.



**Figure 9-14.** a) Borehole coverage (total core length) inside the Central block closest to the area of the planned extension, and b) PFL-f and PSS transmissivity data outside ZFM from the associated boreholes divided by fracture set. The interval between 100–150 m contains fewer high-transmissive fractures than the interval between 50–100 m.



It is emphasized that a primary idea with the interpretation of so called SBA-structures in the hydro-geological model is to allow for a discussion about their potential importance for safety assessment since current data suggest that transmissive, sub-horizontal to gently dipping structures may intersect the rock vaults of the planned extension of the existing SFR facility depending on the decided location.

#### 9.6.4 Delineation of discrete features for stochastic modelling

Flowing features not modelled as SBA-structures are displayed as grey features in Figure 9-13. Many of the grey features are:

- sub-horizontal to gently dipping,
- occur in boreholes HFR106 and KFR106 drilled outside the local model area in close proximity to the Northern boundary belt and ZFMNNW1034, and
- coincide with some of the unresolved borehole intervals with possible deformation-zone-type properties (PDZs) in the geological model (Table 7-3 and Figure 7-33).

Figure 9-15 reveals that the boreholes located in the Central block (Group 1: KFR104 and KFR105) are significantly less transmissive than the boreholes located closer to ZFMNNW1034 and the Northern boundary belt (Group 2: KFR101, 102A, 102B, 103, and 106). In addition, this lateral contrast in transmissivity is greater than the contrast between HCD and HRD transmissivity for each tectonic unit alone. This observation is vital for the bedrock hydrogeological modelling.

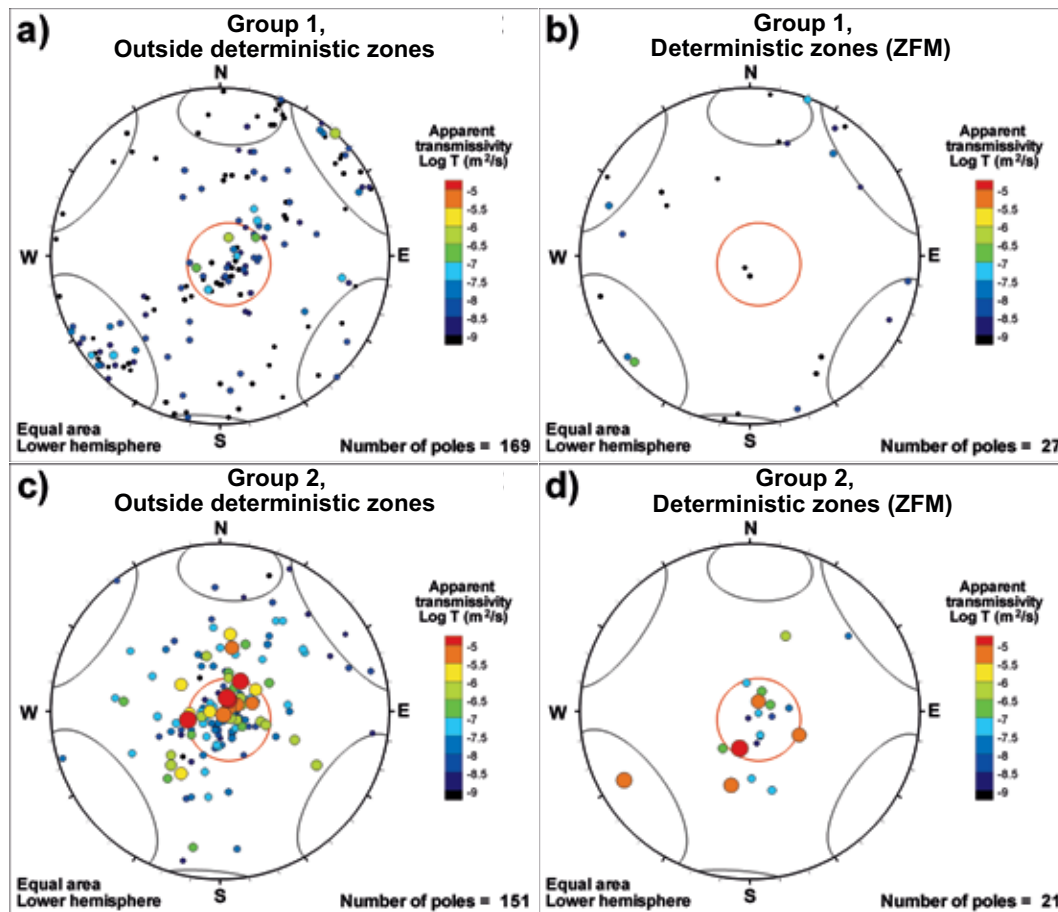
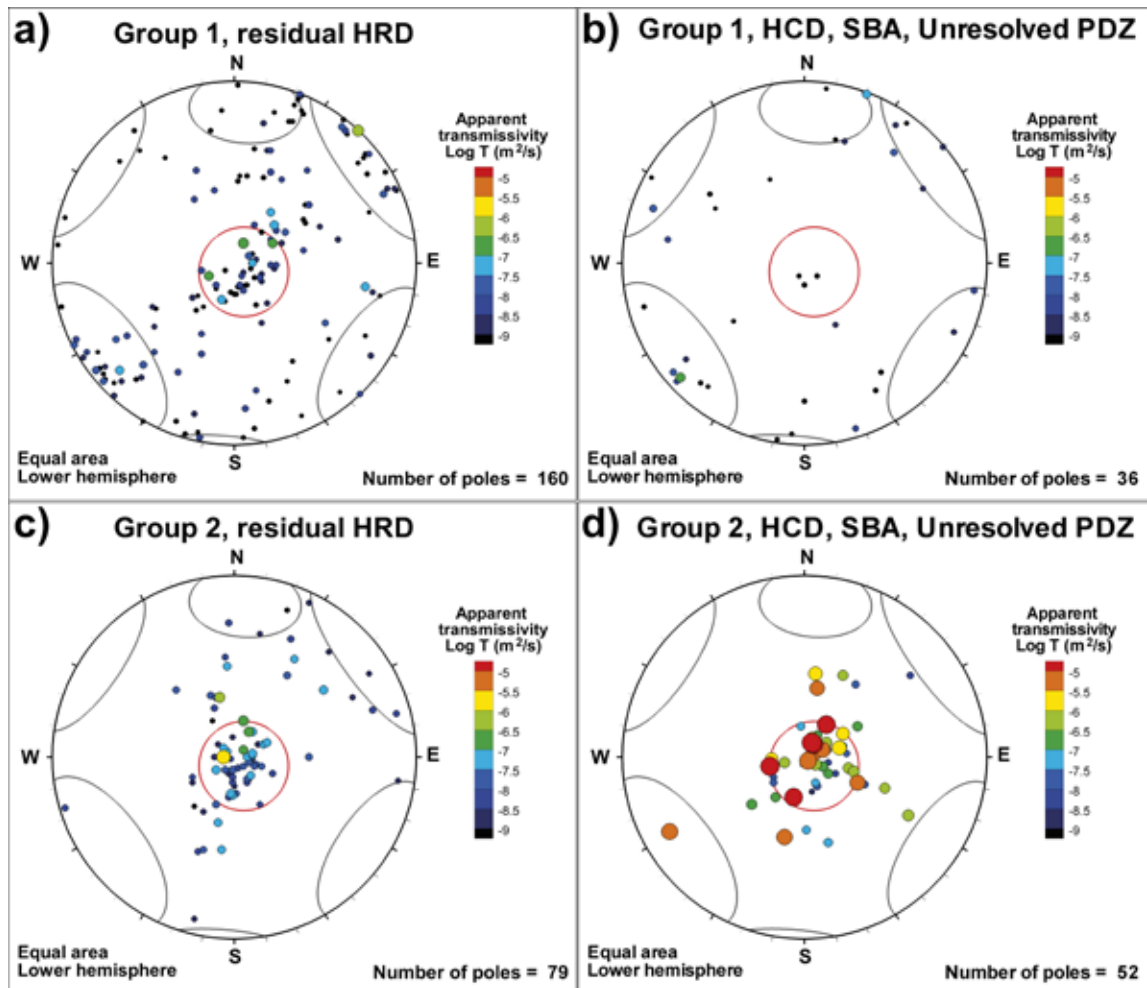


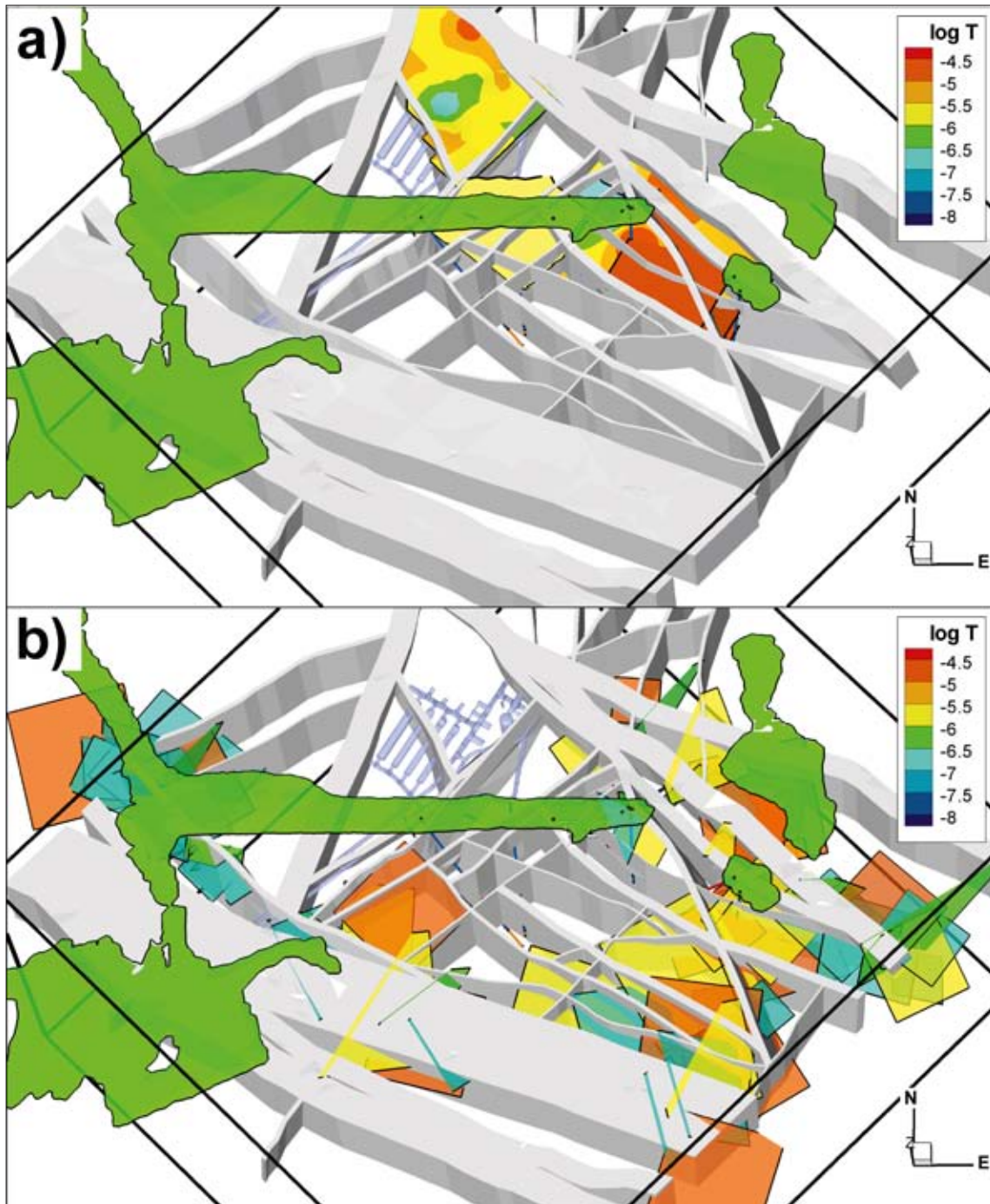
Figure 9-15. Comparison of PFL-f orientations at the Repository level HRD (-60 to -200 m) between Group 1 (KFR104 and KFR105) and Group 2 (KFR101, 102A, 102B, 103, and 106). The fracture poles are coloured and scaled according to PFL-f transmissivity.

The stereonet shown in Figure 9-16 suggest that the flowing features associated with SBA-structures and unresolved PDZs along the Northern boundary belt and ZFMNNW1034 will have a profound impact on the DFN data set intended for HRD modelling unless they are excluded and treated separately. In the current bedrock hydrogeological model, PFL-f data associated with observations of SBAs and unresolved PDZs have been excluded from the DFN data set intended for HRD modelling. The excluded unresolved PDZ data were either modelled as deterministic SBA-structures (Section 9.6.3) or used to condition stochastic realisations of random features of similar geometrical and hydraulic characteristics as the ones excluded, see Appendix A in Öhman et al. (2012) for details.

In conclusion, the proposed hypothesis posits a hydraulically connected fringe of SBA-structures and stochastic unresolved PDZs around the Central block, i.e. the target area for the SFR extension. The fringe has a key role in connecting the flowing fracture network inside the Central block to the Northern and Southern boundary belts, see Figure 9-17a and -b.



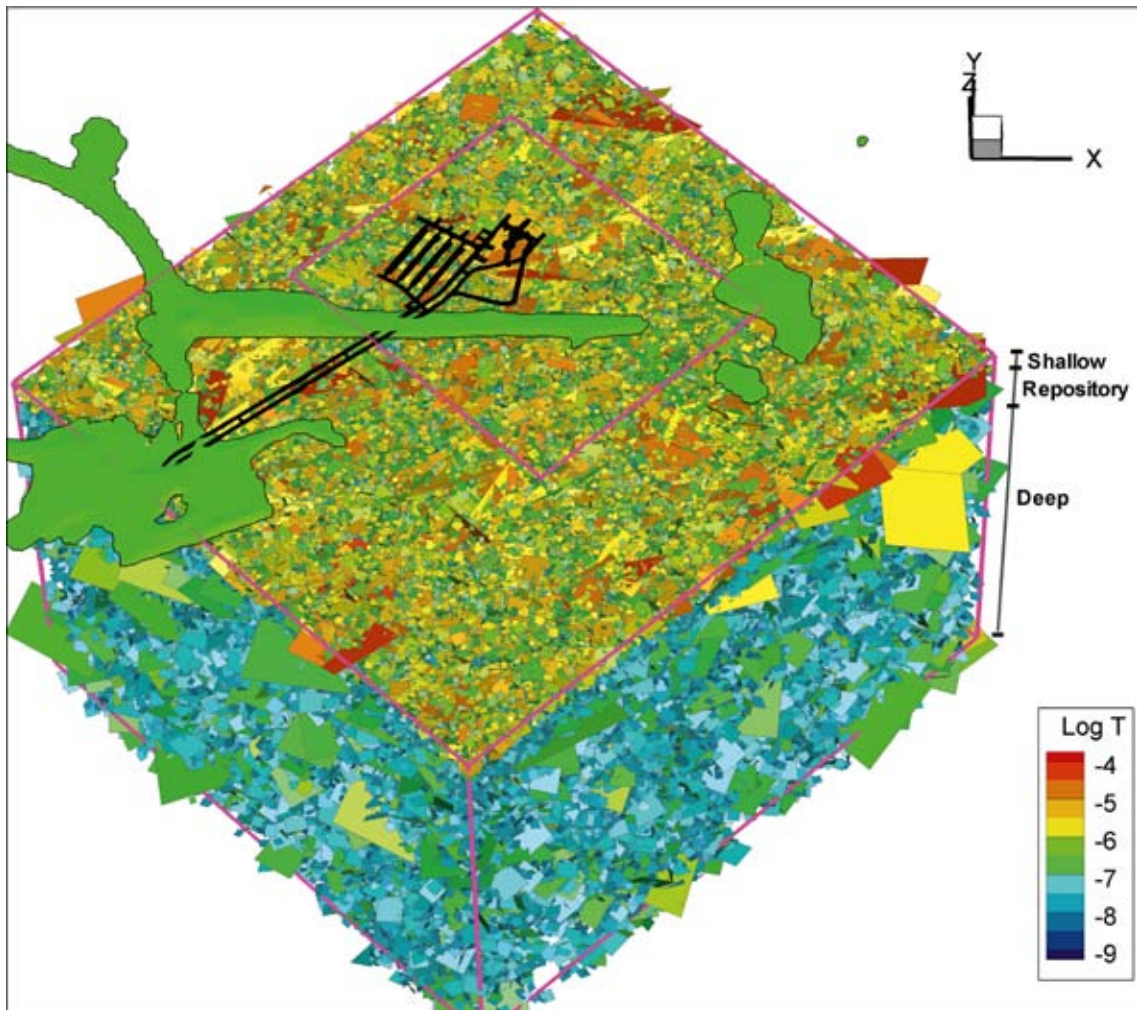
**Figure 9-16.** Comparison of PFL-f orientations at the Repository level HRD (-60 to -200 m) between modified Groups 1 and Group 2, i.e. the data used for modelling of SBA-structures and conditioned unresolved PDZs are separated from the residual HRD data and plotted together with the HCD data. The fracture poles are coloured and scaled according to PFL-f transmissivity.



**Figure 9-17.** Overview of the interpreted spatial pattern of the most hydraulically significant structures: a) deterministically modelled SBA-structures, and b) conditioned stochastic representation of the remaining unresolved PDZs.

### 9.6.5 Modelling of residual HRDs

The exclusion of fringe features, modelled either as SBA-structures (Section 9.6.3) or as conditioned stochastic realisations (Section 9.6.4), homogenises the data set intended for hydrogeological DFN modelling inside the Central block (cf. Figure 7-31 and Figure 7-32). The deduced DFN parameter values intended for use in the safety assessment project, SR-PSU, are shown in Appendix 5 and Figure 9-18 shows a stochastic realisation of connected open fractures ( $R_1$ ) based on these settings.

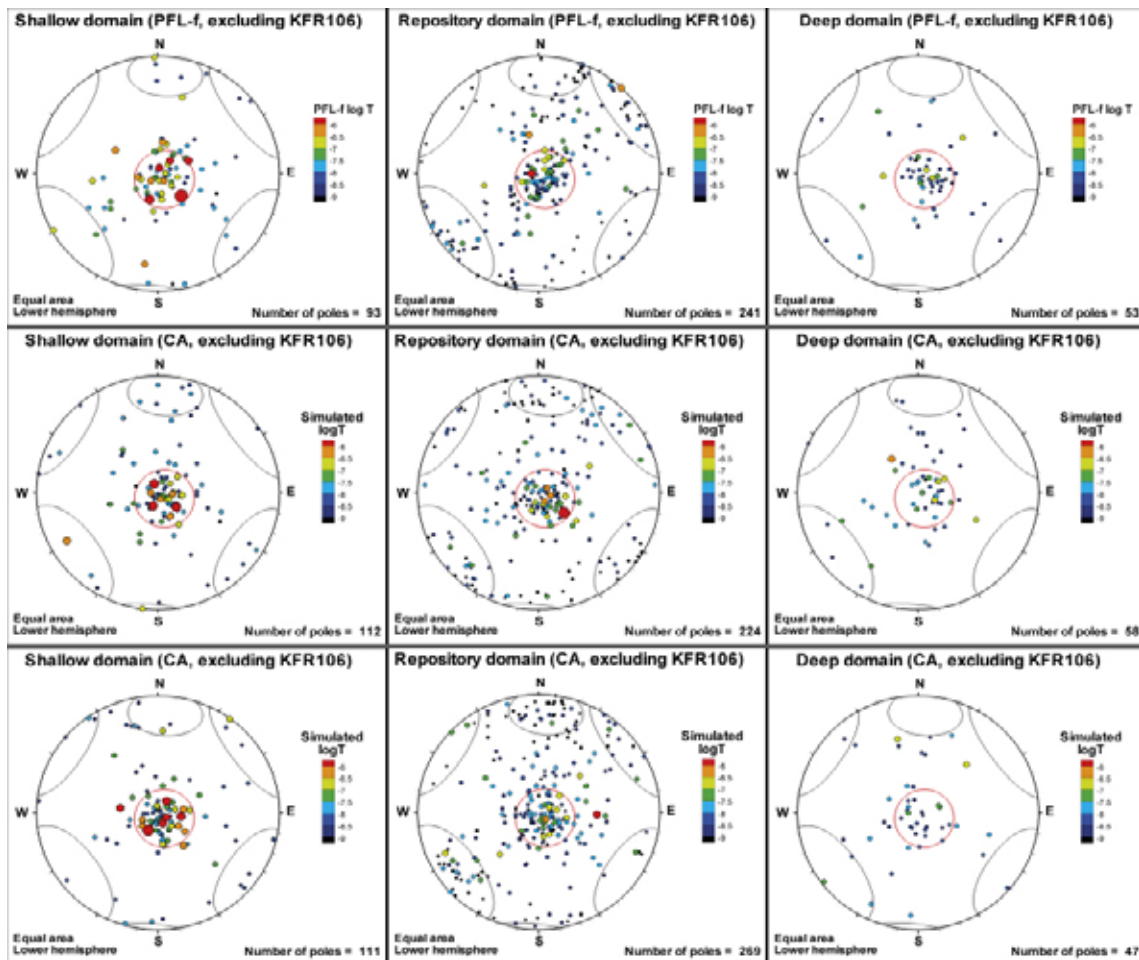


**Figure 9-18.** Example of a stochastic realisation ( $R_1$ ) of the hydrogeological DFN model delineated for the Central block using the parameters specified in Appendix 5.

By inserting scan lines with identical positions, trajectories and lengths into the generated 3D realisations ( $R_1, R_2, R_3, \dots, R_N$ ), qualitative and quantitative comparisons can be made with the *in situ* 1D observations in boreholes used to deduce the DFN parameter values. For instance, the stereonets shown in Figure 9-19 allow for comparisons between measured and sampled flowing features with regard to borehole fracture transmissivity, orientation, and frequency. In addition, these comparisons are made by HRD interval (Shallow, Repository and Deep).

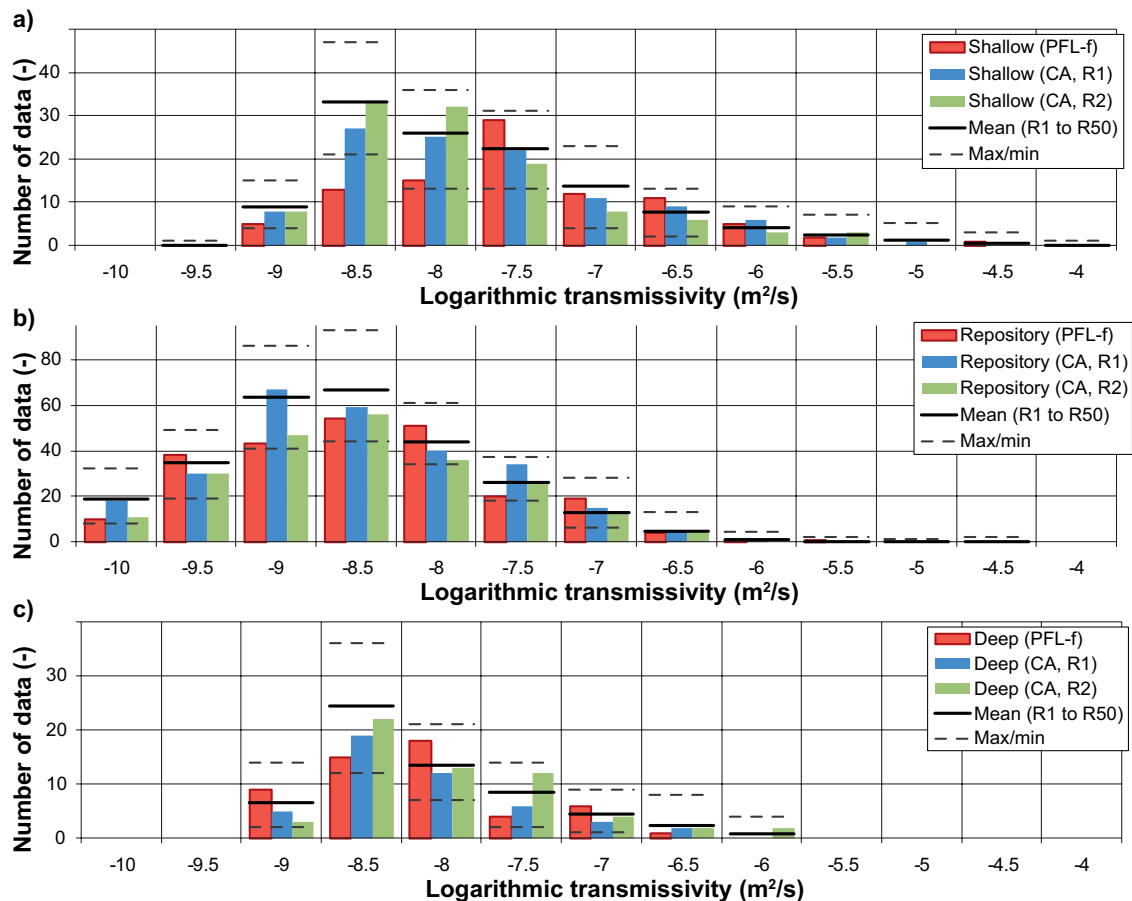
**Table 9-4. Compilation of the number of fracture counts in the stereonets shown in Figure 9-19.**

Data set	Shallow HRD	Repository HRD	Deep HRD
Measured	93	241	53
Realisation $R_1$	112	224	58
Realisation $R_2$	111	269	47



**Figure 9-19.** Stereonets of fractures poles coloured and scaled according to transmissivity: Measured PFL transmissivities (top row), sampled transmissivities in realisation  $R_1$  (middle row) and sampled transmissivities in realisation  $R_2$  (bottom row). The left column represents the Shallow bedrock HRD, the centre column represents the Repository level HRD and the right column represents the Deep bedrock HRD.

By the same token, the histograms shown in Figure 9-20 allow for comparisons between measured and sampled flowing features with regard to the distribution of borehole PFLf fracture transmissivity data. In addition to data for two realisations,  $R_1$  and  $R_2$ , the mean, maximum and minimum values of an ensemble of 50 realisations are also shown. Judging by eye, the two realisations,  $R_1$  and  $R_2$ , resemble the measured data, but the mean of 50 realisations suggests that on the average the DFN model inside the Central block is too permeable below approximately  $T = 1 \cdot 10^{-8} \text{ m}^2/\text{s}$ . A quick look at Appendix 5 reveals that this is equivalent to saying that there are too many steeply dipping features with a radius less than approximately 5 m and/or too many horizontal to gently dipping features with a radius less than approximately 1 m.



**Figure 9-20.** Measured PFL-f transmissivities (red), sampled transmissivities in realisation  $R_1$  (blue) and sampled transmissivities in realisation  $R_2$  (green) divided by HRD, where a) Shallow bedrock HRD, b) Repository level HRD and c) Deep bedrock HRD. The mean transmissivity in each bin of 50 realisations is shown as solid black lines with dashed lines above and below representing the maximum and minimum values in each bin, respectively.

## 9.7 Groundwater – composition and flow

### 9.7.1 Hydrogeochemical data and modelling

The hydrogeochemical sampling during the SFR extension investigation has resulted in data from a total of thirteen borehole sections in five cored boreholes and one percussion borehole. There are also data from two open percussion boreholes. Furthermore, the database contains data from two open percussion boreholes in the Forsmark site investigation and from a total of 45 borehole sections in 18 older cored boreholes drilled from the existing SFR tunnels (Nilsson et al. 2011).

The hydrogeochemical database in the SFR area covers a depth down to  $-250$  m with single sampling locations at  $-300$  m and  $-400$  m. The database represents a relatively limited salinity range (1,500 to 5,500 mg/L chloride). However, the  $\delta^{18}\text{O}$  values show a wide variation ( $-15.5$  to  $-7.5$  ‰ V-SMOW) similar to that reported from the Forsmark site investigations (Laaksoharju et al. 2008). The marine indicators such as Mg/Cl, K/Cl and Br/Cl also show relatively large variations considering the limited salinity range. Samples collected from the early boreholes in the existing SFR facility area (1986 to 2010), as well as from boreholes drilled within the recent SFR extension investigation (2007 to 2010), reveal complex mixing patterns arising from different evolutionary stages of the Baltic Sea as well as from the presence of the existing SFR facility.

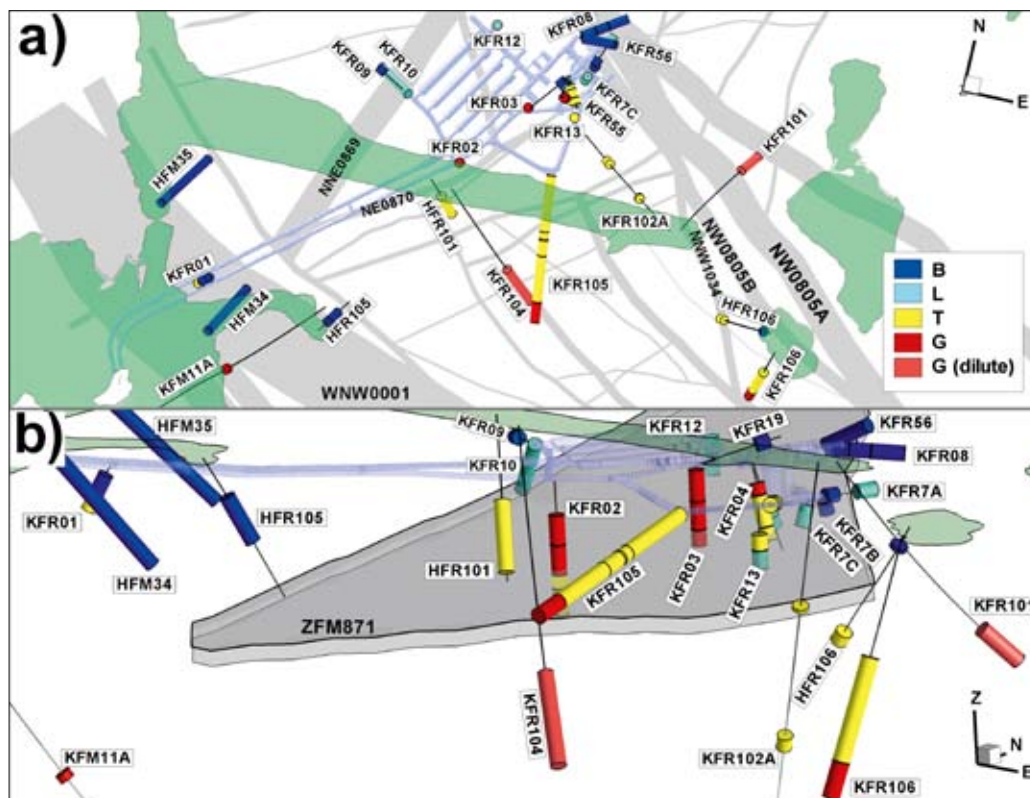
Based on the chemical variables Cl, Mg and  $\delta^{18}\text{O}$ , which indicate a large variation linked to the origin and residence time, a subdivision into *groundwater types* has been made. Taken into consideration the palaeoclimatic history of the Holocene epoch, the following groundwater types were distinguished:

1. *Local Baltic Sea groundwater type*: This is the youngest water type but still it is modified compared with Baltic Sea water due to ion exchange and microbial reactions in the bedrock. These reactions have resulted in lowering of Mg, K, Na and SO<sub>4</sub> and enrichment of Ca and HCO<sub>3</sub>.
2. *Littorina groundwater type*: This groundwater type has a higher salinity than the present-day Baltic Sea. However, compared to the original Littorina Sea water (with the highest salinity 5,000 to 6,000 years ago), it has been diluted and the δ<sup>18</sup>O values are depleted (lowered) by a contributing glacial component.
3. *Brackish-glacial groundwater type*: Groundwater belonging to this type is a mixture of mainly glacial (last deglaciation or older) and brackish non-marine waters.

A large number of samples that could not be definitively assigned to one of the above three groups were assigned to a fourth group called *Mixed transition type groundwaters*. This is not a specific groundwater type; rather, it reflects groundwater significantly influenced by mixing of glacial and brackish marine groundwaters of different ages. The Mixed transition type groundwaters are present at depths from about -60 to -400 m elevation and have become more frequent over the last two decades as indicated by the long-time-series data. This is probably a result of the changing hydrogeological conditions in the volume influenced by drawdown inflow to the existing SFR facility (Figure 9-21). Principal component analysis using Cl, δ<sup>18</sup>O, δ<sup>2</sup>H and SO<sub>4</sub> supported the discrimination of groundwater types based on expert judgement.

From measured Eh values, and in accordance with the chemistry of Fe, Mn, S and U, it is concluded that mildly reduced conditions (-140 to -190 mV) generally prevail in the investigated groundwaters and, importantly, for the youngest Baltic-Sea-type groundwaters as well. In terms of redox buffer capacity, the most important fracture minerals available are the Fe(II)-bearing minerals coating the water conductive fractures, which at SFR mainly comprise chlorite, clay minerals and pyrite.

Most of the groundwaters in the database seem to be in or close to equilibrium with respect to calcite. Although some calcite dissolution may occur during infiltration of Baltic Sea waters, the intensity of this process must be low due to the high alkalinity content and near-neutral pH of sea waters.

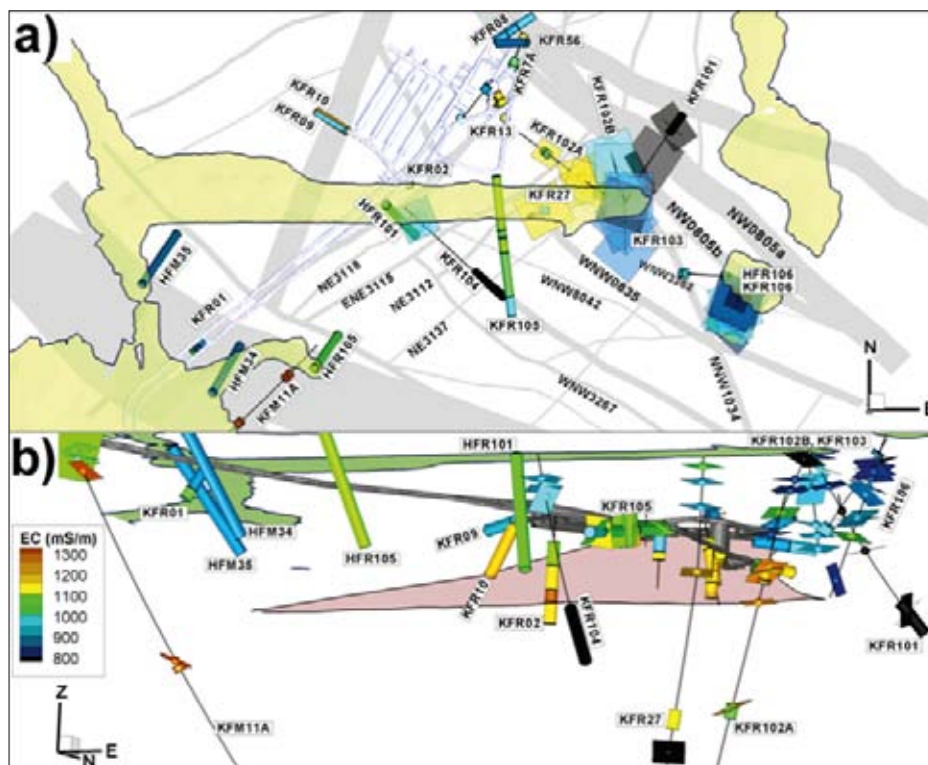


**Figure 9-21.** Present-day water types (cf. Chapter 8 for definitions); a) top view and b) side view towards the northwest. The reference water types are Local Baltic (B; blue), Littorina (L; cyan), Brackish glacial (G; red), and Mixed transition (T; yellow).

No major shift in bicarbonate content or pH over time can be seen, although a weak increase is indicated. Calcite coatings are frequent, which results in a rapid response to changes in pH by dissolution or precipitation and thereby provides an important buffering capacity against acidification.

The general picture from hydrogeochemical interpretations is that water flows from the Baltic Sea to the existing SFR via the steeply dipping zones ZFMWNW0001, ZFMNNE0869, and ZFMNW0805A and then via horizontal features towards the existing SFR facility (Figure 9-21). However, the existing SFR facility seems to have a channelised hydraulic contact with ZFMNW0805A and B (Northern boundary belt) and poor contact with ZFMNNE0869, since considerable portions of pre-existing water (Littorina-type groundwater including a glacial component) are still present close to and within the Northern boundary belt in contact with the gently dipping ZFM871. Otherwise, the content would have been flushed out during approximately 25 years of operation. By and large, all borehole intersections representing the zone ZFM871 have a larger marine component and are more saline compared to the Brackish-glacial groundwaters present above and below the zone. This can probably be linked to the generally heterogeneous characteristics of ZFM871, as well as the grouting. The remnants of the Littorina-type groundwater and even more so the older Brackish glacial waters (mainly present beneath and above zone ZFM871), despite tunnel inflow, suggest either poor connectivity with the sea and/or compartmentalised flow.

Besides individual chemical constituents, the hydrogeochemical programme also measures the electrical conductivity of the groundwater. During the entire observation period (1988–2010), the observed electrical conductivity (EC) values in the monitored older boreholes have been in the range 6001,600 mS/m (Figure 9-22), which corresponds to a chloride concentration range of approximately 1,5005,500 mg/L. (By comparison, Baltic Sea water has a salinity of about 2,800 mg/L of Cl, or an EC value of c. 890 mS/m.) With few exceptions, most shallow data (above –100 m) have EC values that are within the range 900 to 1,000 mS/m (Figure 9-22). The EC values in the boreholes that intersect the sub-horizontal zone ZFM871 beneath the existing SFR facility are in the range 1,100 to 1,300 mS/m and are related to a varying contribution of Littorina Sea water, resulting in the Littorina-type groundwater or the Mixed-transition-type groundwaters (close to the Northern boundary belt or ZFMNNE0869 and at a distance from the Northern boundary belt, respectively).



**Figure 9-22.** Electrical conductivity (EC) measurements; a top view and b) side view looking towards northwest. EC from PFL flow logging shown as planes and EC from monitored borehole sections represented as cylinders. (A deep PFL-logged interval in KFR27 (409.6 to 435.6 m borehole length) is also represented by a cylinder).



Remarkably, less saline water has been found below more saline water in several boreholes, KFR02, KFR101, KFR102A, KFR104, KFR106, and KFR27 (Figure 9-22) and at the bottom of boreholes KFR101 and KFR104, the salinity was even lower than in the Baltic Sea. This is an unusual observation since salinity normally increases with depth. Hence, there is a strong indication of the preservation of isolated non-marine and less saline palaeoclimatic water types in parts of the bedrock mainly outside deformation zones. This reinforces the conceptual structural-hydraulic interpretation of a predominantly horizontal to gently dipping flowing fracture network with limited vertical fracture connectivity outside the vertical zones.

### 9.7.2 Integrated conceptual model

Figure 9-23 combines the conceptual geological-hydrogeological block model illustrated in Figure 7-36 with the conceptual hydrogeological-hydrogeochemical block model illustrated in Figure 8-13. The colour coding in the latter model shows the main groundwater types that characterise the investigated SFR rock volume.

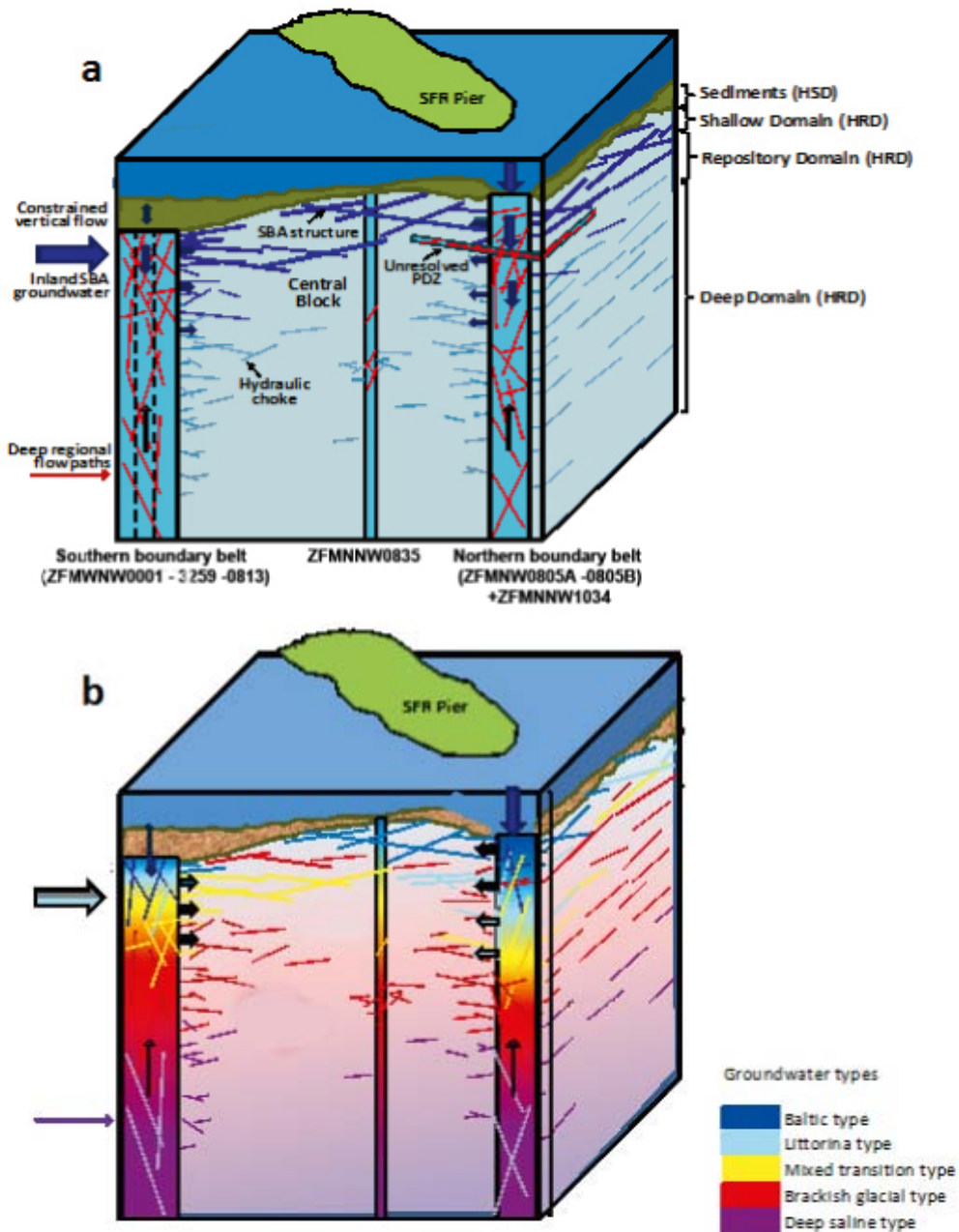
- A saline non-marine groundwater type (deep saline) is ascribed to the deepest part of the bedrock (deep lilac colour). This is an assumption based on Forsmark data because no data below -400 m elevation are available from the SFR.
- The introduction of glacial meltwaters, particularly along the transmissive Northern and Southern boundary belts, and mixing with the older non-marine saline to brackish groundwaters (and components of old meteoric water) has given rise to the Brackish-glacial groundwater types (bright red colour).
- This was followed by the infiltration and mixing of the Littorina Sea water with different portions of glacial meltwater, giving rise to the Littorina-type groundwater (turquoise colour). The Littorina Sea water entered preferentially along the more highly conductive deformation zones, i.e. the same zones that facilitated the glacial meltwaters.
- Mixing of these Littorina-type waters with the earlier brackish-glacial groundwaters has occurred to different degrees, producing the Mixed transition brackish water type groundwaters (yellow colour).
- Modern Baltic Sea water (dark blue colour) is most probably a recent component that has intruded via the highly transmissive deformation zones comprising the Northern and Southern boundary belts due to the drawdown effect from the SFR facility during the excavation/construction/operation phases.

There are locations where mixing has not occurred and where the brackish-glacial groundwaters have remained at shallower levels in the bedrock (“pockets”) shielded from the passage of the later Littorina-type groundwaters. This is schematically shown as solid red fractures at higher levels than the maximum depths achieved by the Littorina-type groundwaters. Moreover, Littorina-type groundwaters have been preserved at higher levels (indicated by the turquoise colour of some of the near-surface discrete fractures) because horizontal hydraulic gradients, typical in this area beneath the sea, are very weak and unable to displace the dense Littorina waters.

Sea-bottom sedimentation has been much greater (i.e. thicker) above the Southern boundary belt compared with the Northern one, allowing a greater volume of Baltic Sea type water to preferentially infiltrate into the latter (indicated by the larger and thicker downward pointing blue arrow). As indicated by the concentration of short thick horizontal arrows from the upper approximately 400 m parts of the Northern and Southern boundary belts, the SFR drawdown has gradually pulled in groundwaters along conductive fracture zones into the Central block area and towards the SFR site. These groundwaters, already the product of natural mixing processes affecting Brackish-glacial and Littorina-type waters, have therefore undergone additional anthropogenic mixing involving a Baltic Sea input, and this has been compounded by the increased flow resulting from drawdown effects.

The input flow sources to the Central block area of mixed groundwaters of Littorina and Baltic type are visualised to show close to the surface in the Northern boundary belt the dark blue of the Baltic Sea and lower down a dominant Littorina component. In contrast, the Southern boundary belt is considered to be less transmissive because of the thick sediment cover which has initially inhibited the amount of Littorina Sea and later the Baltic Sea waters infiltrating into the deformation zones from

mixing with the resident Brackish-glacial type groundwaters. This explains the restricted vertical extent of the Mixed transient groundwater types. Compare the vertical extent of the yellow colouring between the two belts and note the less dominant Littorina and Baltic components in the Southern boundary belt. The conceptual model also shows a lateral flow direction to the Southern boundary belt from the near-surface SBA-structures, which may have transported mixtures of modern meteoric water with some residual Littorina-type water from inland, i.e. from the northeastern part of the Forsmark area. However, this is based on too few data and may simply reflect the hydrogeological and hydrogeochemical heterogeneity of the bedrock system.



**Figure 9-23.** a) Conceptual block model incorporating the major geological and hydrogeological features of the investigated SFR rock volume. The horizontal and vertical dimensions of this model are approximately 1.5 km by 1.1 km. b) Conceptual block model incorporating the major hydrogeological and hydrogeochemical features of the investigated SFR rock volume. The different groundwater types are indicated by the colour scheme displayed on the right hand side. The deep saline groundwater, which is indicated by lilac, is not present as a dominant groundwater type in the SFR rock volume. See text for explanation of the different arrow types

### 9.7.3 Flow to the existing SFR facility

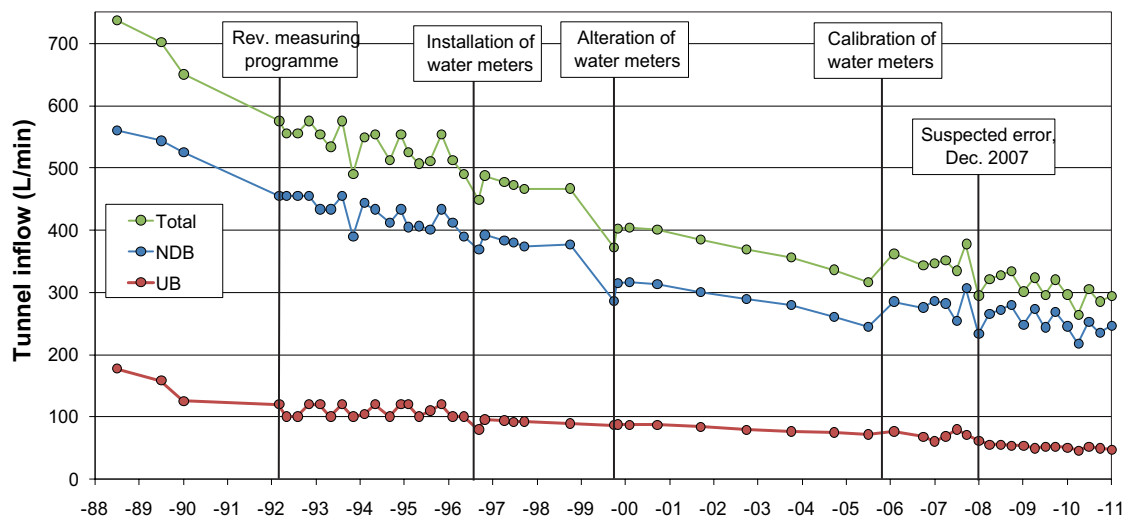
Measurements of the inflow to the SFR facility have been carried out regularly since January 1988 (Carlsson and Christiansson 2007). The total inflow in 1988 was about 720 L/min. Since then there has been a decreasing trend of inflow that has been relatively steady for the last 15 years (Figure 9-24). The total inflow has decreased to about 285 L/min (average value for 2010), which corresponds to a 61% decrease compared to the 1986 value. Today, the entire head field is affected by the ongoing drainage, but the drawdowns (head changes) indicate quite heterogeneous hydraulic conditions. Altogether, there are 38 sections in 12 boreholes in the vicinity of the existing SFR that are monitored. The results are reported on a yearly basis, see e.g. SKBdoc 1233647. In general, the head field dropped rapidly during the construction period and during the initial measurement period after that. However, the head stabilised quickly in the largest zones, ZFMWNW0001 (part of the Southern boundary belt) and ZFMNW0805A/B (part of the Northern boundary belt). In the tectonic unit between these two boundaries, the Central block, there has been a slow, relatively constant, decreasing head trend between  $-0.5$  and  $-2$  m/year in most borehole sections since 1987–1988, see Figure 9-25 for an example.

The head drop has been most pronounced in the vicinity of the Silo, associated with zones ZFMNE0870 and the gently dipping ZFM871. The head decrease in these boreholes in 2009 was about  $-0.5$  to  $-1$  m/yr and the total drawdown exceeded tens of metres. In contrast, KFR09, which is located inside ZFMNNE0869 (also referred to as zone 3), shows only a minor total drawdown ( $-1.9$  m) after approximately 25 years of operation, in spite of its location close to a non-grouted tunnel wall.

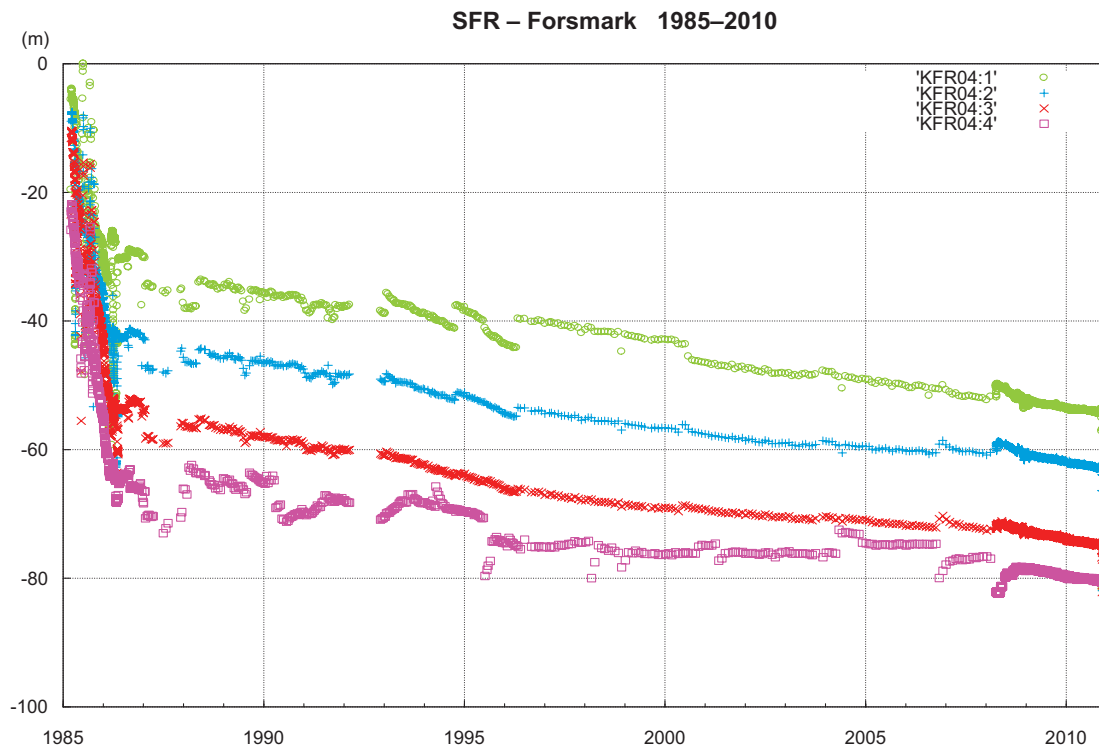
The head trends in the borehole sections that penetrate the gently dipping zone ZFM871 vary in space, but with various rates of decrease in KFR02, KFR03, KFR04, KFR05, KFR13, and KFR7B. This indicates that ZFM871 is hydraulically heterogeneous and/or geometrically discontinuous.

Since no grouting has occurred after the completion of the existing SFR facility, the decreasing inflow trend is due to other mechanisms. Gustafson (2009) points at the following processes as plausible explanations for the decreasing trend:

- increasing effective normal stress with drainage,
- two-phase flow, and
- fracture clogging caused by chemical precipitation.



**Figure 9-24.** Inflow of groundwater to the existing SFR facility between 1988 and 2011. Curves marked UB and NDB refer to drainage of the pumping pits in the operational area and in the lower construction tunnel, see Figure 7-6.



**Figure 9-25.** Examples of time series showing the trend in hydraulic head in borehole KFR04. The monitored borehole sections in KFR04 are located at distance of 16–42 m from the SFR facility.

In addition to these processes, flow compartmentalisation can be mentioned. Flow compartmentalisation is a phenomenon that occurs in isolated or poorly connected fracture networks. The existing SFR facility is located beneath the Baltic Sea, but since there is not much inflow, the network of flowing fractures around the existing SFR does not appear to be very well connected vertically. The interpretation that the network of connected flowing fractures is compartmentalised is supported by three independent observations.

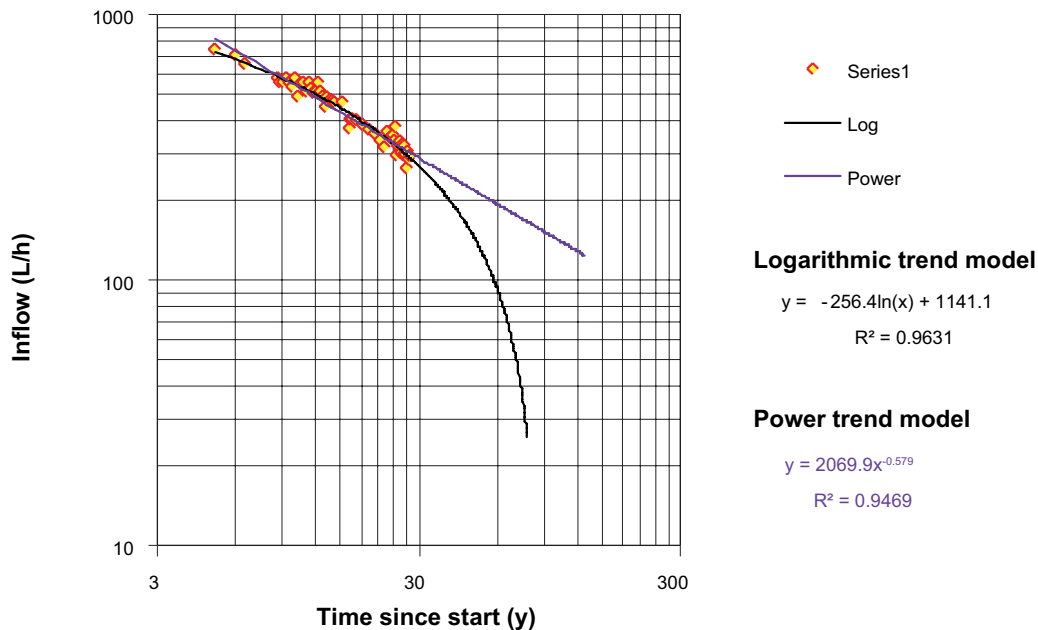
- **Structural-hydraulic anisotropy:** The geological model concludes that there is a relatively high frequency of horizontal to gently dipping open fractures in the upper part of the rock volume (above approximately –200 m elevation), which are inferred to have formed, or to have been opened, as a result of stress release processes in connection with unloading due to deglaciation and/or exhumation, as well as strike-slip movements along the bounding steeply dipping zones. The flowing fractures with the highest PFL-f transmissivities are predominantly horizontal to gently dipping fractures.
- **Hydrogeochemistry:** There is a strong indication of preservation of isolated marine, as well as non-marine, less saline palaeoclimatic water types in parts of the bedrock. The remnants of these waters, despite 25 years of tunnel inflow, suggest either poor connectivity to the sea and/or compartmentalised flow.
- **Flow regime:** The decrease in flow rate does not indicate a spherical or a cylindrical flow regime, but rather a linear, or sub-linear, flow regime, see Figure 9-26.

An increase in effective normal stress is another plausible explanation for the decreasing trend in inflow. Drawdown causes a drop in the pore pressure ( $p$ ) in the flowing fractures, and the effective normal stress ( $\sigma'$ ) increases accordingly:

$$\nabla\sigma' = -\nabla p \quad (9-3)$$

The increase in effective normal stress reduces the fracture aperture ( $e$ ) in proportion to the normal stiffness of the fracture ( $k_n$ ), i.e.:

$$\delta e = -\nabla\sigma'/k_n \quad (9-4)$$



**Figure 9-26.** Log-log plot of the total measured inflow of groundwater shown in Figure 9-24. Two hypothetical trend models are inserted for the sake of visualisation. The power trend model is commensurate with a linear flow regime, whereas the tentative logarithmic trend model suggests a sub-linear flow regime.

*In situ* tests at the Forsmark Power Plant by Bono et al. (2010) indicate that the fracture normal stiffness varies linearly with depth from 2–6 MPa/mm at 20 m depth to 1029 MPa/mm at 100 m depth (cf. Chapter 6 for details). Figure 9-27 suggests that the changes in hydraulic head (or pore pressure) between 1988 and 2010 could be seen as far as 100 m from the existing SFR facility. An average change in hydraulic head of approximately 10 m implies an increase in the effective normal stress of about 0.1 MPa.

Taken together, these data suggest a change in fracture aperture of 25  $\mu\text{m}$  at 20 m depth if the fracture normal stiffness is set to 4 MPa/mm, and 5  $\mu\text{m}$  at 100 m depth if the fracture normal stiffness is set to 20 MPa/mm. According to the cubic law:

$$e = \sqrt[3]{\frac{12\mu T_f}{\rho g}} \quad (9-5)$$

a fracture transmissivity ( $T_f$ ) of  $1 \cdot 10^{-6} \text{ m}^2/\text{s}$  corresponds to a fracture aperture of about 107  $\mu\text{m}$ . Using the values of the fracture normal stiffness discussed above, the average change in hydraulic head of 0.1 MPa reduces the fracture transmissivity by approximately 55% at 20 m depth and by approximately 13% at 100 m depth.

The processes listed in the last two bullets in the beginning of this section, two-phase flow and chemical precipitation, are closely related and generally considered to be important causes for decreasing trends of inflow to underground constructions, see e.g. Jarsjö and Destouni (2000), Laaksoharju et al. (2009), Gustafson (2009), Chasset et al. (2011). It is noted, however, that these processes occur predominantly in proximity to the tunnel wall (so called skin effect), which suggests that the hydraulic head at some distance from the tunnel wall should increase. As shown in Figure 9-27, this is not the case. On the contrary, the hydraulic heads away from the repository continue to decrease, which is exemplified in Figure 9-25 and Figure 9-28. The near-linear trends shown in the two time series plots suggest a compartmentalised flow system.

The ongoing monitoring programme for the existing SFR facility has analysed the chemical composition of the drainage water that is pumped from the UB and NDB pumping pits shown in Figure 9-24 since 1988. Water samples are analysed four times per year. Although the monitoring programme is not as elaborate as the investigation programme for SDM-PSU, the results from the two pumping pits confirm the general picture described above in Section 9.7.2; i.e. a slowly decreasing presence of water of the Littorina groundwater type and a slowly increasing presence of a Local Baltic Sea groundwater type.

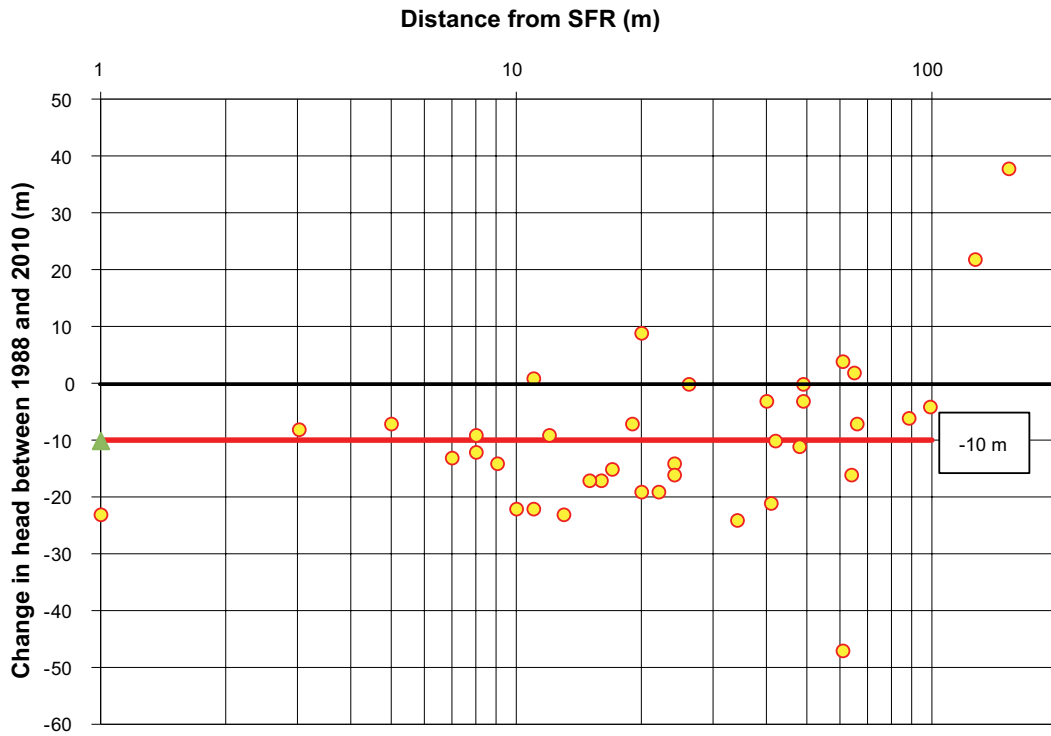


Figure 9-27. Change in head between 1988 and 2010 versus the distance from the exiting SFR facility.

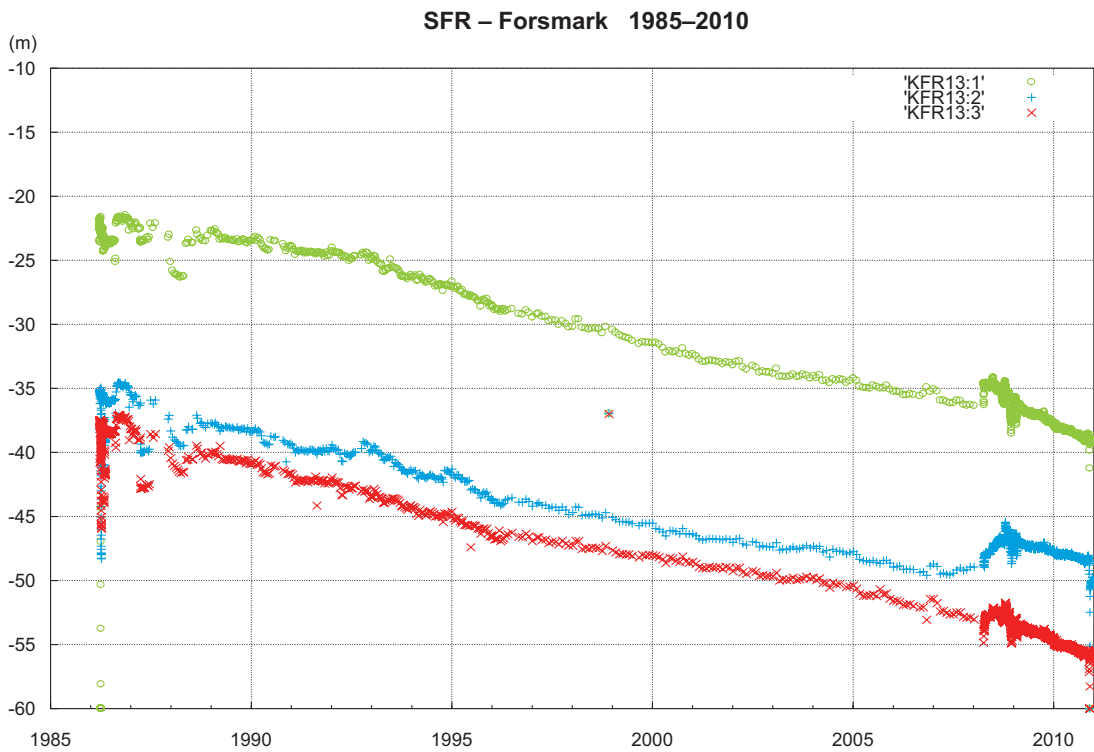


Figure 9-28. Examples of time series showing the trend in hydraulic head in borehole KFR13. The monitored borehole sections in KFR13 are located at distances of 1764 m.

## 9.8 Remaining key uncertainties

A key uncertainty in the hydrogeological characterisation of the site is the existence, position and frequency of gently dipping deformation zones that are smaller than the resolution level for the geological deterministic modelling work, i.e. 300 m, in the uppermost part of the bedrock. This uncertainty overlaps with the interpretation of the unresolved borehole intervals with possible deformation zone (PDZ) properties. Since it has not been possible to link the latter to low magnetic lineaments and since they commonly occur along short borehole intervals, it was judged that they are predominantly minor zones in the geological model and could not be modelled deterministically.

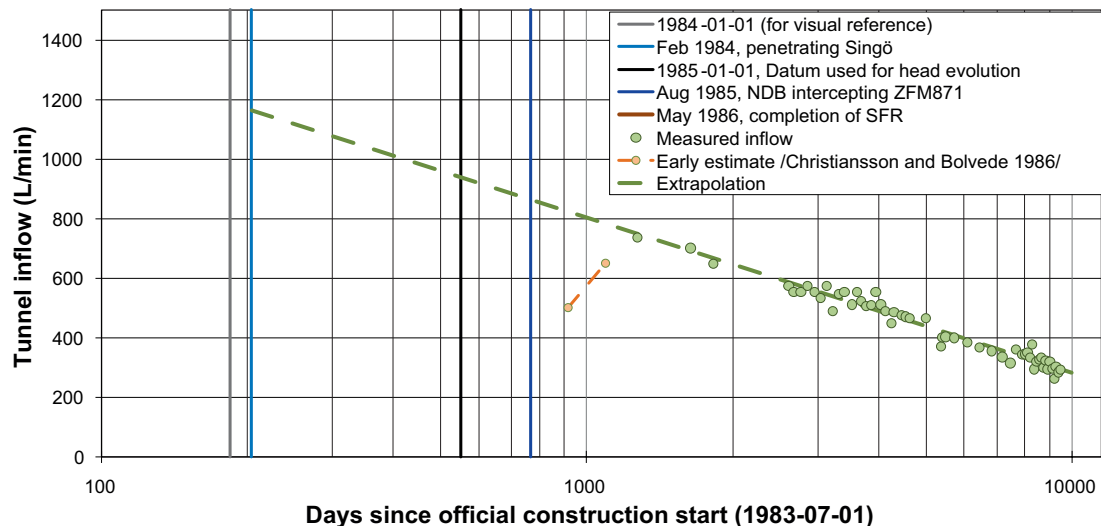
These structures may be of little significance from an engineering viewpoint but may be highly significant from a safety assessment viewpoint, due to their open, water-bearing character and their interaction with similarly open, sub-horizontal, stress release fractures. Experience from the SFR excavations, including the investigation of zone ZFM871, has shown that there are difficulties in identifying such small, sub-horizontal to gently dipping structures. For instance, Christiansson (1986) reports that zone ZFM871, which is considered to be the most prominent gently dipping deformation zone in the SFR area, has a very heterogeneous character with two to three gently dipping fracture sets, individually recorded zone thicknesses of up to 10 m and a hydraulic thickness varying from 2 to 20 m.

Most of the largest PFL-f transmissivities ( $T > 10^{-6} \text{ m}^2/\text{s}$ ) above  $-200 \text{ m}$  elevation are found outside the deterministic deformation zones. In addition, the most transmissive features above  $-200 \text{ m}$  elevation are sub-horizontal to gently dipping and occur in borehole intervals with unresolved PDZ-type properties in the geological model. These findings constitute a cornerstone in the conceptual hydrogeological-hydrogeochemical model for the bedrock in the area intended for the SFR extension. Borehole KFR106 is special in this regard, and it is important to note that it is located east of the area intended for the SFR extension in close proximity to deformation zone ZFMNNW1034. This zone cuts through the wedge between the Northern and Southern boundary belts. In effect, it is forecasted that the eastern part, and possibly also the southern part, of the area intended for the SFR extension is intersected by one or more horizontal to gently dipping structures of significant transmissivity ( $10^{-4} \text{ m}^2/\text{s} > T > 10^{-6} \text{ m}^2/\text{s}$ ). With regard to geometrical properties, i.e. size and spacing, one can only speculate since the borehole coverage is insufficient in these parts of the model domain. If no more boreholes are drilled and no more investigations carried out, this needs to be studied further by safety assessment by means of sensitivity tests.

Another important question for safety assessment is whether the phenomena that cause the observed significant decrease in inflow to the existing SFR facility are reversible (temporary) or irreversible (permanent). In concrete terms, what is the undisturbed inflow to the existing SFR facility if all processes causing the decrease in inflow are reversible? This is also an important question from a flow modelling point of view, since it affects the procedure for flow model calibration. It is considered to be conservative from a radiological point of view to assume that all processes are reversible, implying that the rock mass around the saturated tunnel will in future resume its original hydraulic properties, i.e. with high transmissivities in the sub-horizontal to gently dipping structures.

If a logarithmic function is fitted to the inflow data measured between 1988 and 2010 and extrapolated back in time, a rough estimate is obtained of an “undisturbed initial total inflow” of approximately 1,000 to 1,200 L/min (Figure 9-29). Inflow rates of this order of magnitude are reported in groundwater flow modelling conducted by Öhman et al. (2013).

In SDM-PSU, the issue with minor water-bearing structures in the uppermost part of the bedrock is handled in the hydrogeological modelling work by including a shallow bedrock aquifer (SBA) concept for some of the unresolved possible deformation zones, similar to that used in SDM-Site Forsmark, together with a conditional hydrogeological DFN model for the remaining unresolved possible deformation zones. In the context of data support and interpreted spatial extent in 3D space, the confidence in existence of the deterministically modelled SBA-structures varies.



**Figure 9-29.** Backward extrapolation of declining inflow over time in order to estimate an “undisturbed initial total inflow”. It is noted that tunnel construction was not instantaneous, but rather gradually introduced as a sink term to the hydrogeological system over a time span of c. three years. Two main hydraulic disturbances can be identified that are associated to large tunnel inflow: the penetration of the Singö deformation zone and the penetration of the gently dipping deformation zone below SFR, ZFM871.

## 9.9 Groundwater flow modelling in SR-PSU

### 9.9.1 Hydrogeological base case

The suggested hydrogeological base case model set-up for SR-PSU is as follows:

1. The deformation zone model developed by Curtis et al. (2011) is used for HCD modelling inside the SFR regional model domain. Outside this domain, the deformation zone model derived for SDM-Site Forsmark by Stephens et al. (2007) is used for HCDs throughout the remaining flow model domain shown in Figure 1-3. The deformation zones should be divided into smaller segments in order to allow for spatial variability in transmissivity (cf. Equation 7-3). Depending on the area of interest, input data for transmissivity assignment are provided in Appendix 4, Appendix 6, Appendix C in Follin et al. (2008) and in the model set-up for the temperate climate simulations in SR-Site, see Joyce et al. (2010) for details.
2. Eight SBA-structures, SBA1-8, are modelled as deterministic features according to the geometrical and hydraulic description provided in Appendix B in Öhman et al. (2012). Four of these SBA-structures include unresolved PDZs from the single hole interpretation.
3. Unresolved PDZs are modelled as stochastic features according to the modelling procedure and property assignment described in Appendix A in Öhman et al. (2012).
4. The generation of discrete fracture network realisations inside the SFR local model domain is based on the properties provided in Appendix 5. These properties are also used within the SFR regional model domain except in the area south of the Southern boundary belt, where SDM-Site properties are used, see Appendix C in Follin (2008). Outside the SFR regional model domain, the generation of discrete fracture network realisations is based on the model set-up of the extended heterogeneity case used for the temperate climate simulations in SR-Site, see Joyce et al. (2010) for details.
5. Pending the delivery of the ongoing work within the SFR extension project to develop an updated DEM, regolith model and HSD model, it is suggested that the data models used for SR-Site Forsmark be used for groundwater flow modelling, see Bosson et al. (2010) for details.



### 9.9.2 Model variants

Model variants should reflect geometrical and hydraulic uncertainties in the base case model setup listed in Section 7.6.2. With regard to the five items listed for the base case model setup, see Section 9.9.1, the uncertainties listed below could be addressed alone or two or more in combination.

1. Although confidence in the occurrence of steeply dipping deterministic deformation zones in the target volume intended for the SFR extension facility is high, the hydraulic properties of the steeply dipping deformation zones are less certain. It is suggested that different model variants are studied where e.g. the role of homogeneity versus heterogeneity, depth dependence versus no depth dependence, and conditioning versus no conditioning, is evaluated.
2. The confidence in the gently dipping deformation zone ZFM871 is high and the role of this zone is for groundwater flow in the vicinity of the existing SFR facility is recognised. However, there is an uncertainty as to whether the modelled size of ZFM871 is correct. It is suggested that at least one model variant should aim at evaluating the role of this uncertainty, e.g. by extending ZFM871.
3. In the area intended for the SFR extension facility, the high frequency of shallow, sub-horizontal to gently dipping structures makes a much more significant contribution to the pattern of local groundwater flow than the steeply dipping deformation zones. In SDM-PSU, the issue is handled by including a shallow bedrock aquifer (SBA) concept similar to that used in SDM-Site. It is noted that the sheet joints in the SFR local model area are probably both less transmissive and not as large as they are inside the tectonic lens at Forsmark. Notwithstanding, it is suggested that at least one model variant should aim at evaluating the hydraulic role of the SBA concept if the SFR extension facility is located at the same level as the existing SFR facility, i.e. c. -70 m elevation. If a deeper level is chosen this variant is not considered necessary.
4. The geometric and hydraulic uncertainty associated with unresolved PDZs and DFN invokes a stochastic modelling approach. It is suggested that a large number of PDZ and DFN realisations are generated and as a means to identify potential extremes.

## 10 Conclusions

Bearing in mind the overall objective of the site descriptive modelling work in the SFR area, it can be concluded that an integrated description of the site, based on available complete site investigation data, has been developed and documented. The description is supported by a large amount of data and the results of analyses and modelling that are mutually consistent. This demonstrates that a considerable understanding of the current state of conditions and the ongoing processes in the SFR area, from the sea bottom down to approximately –200 m elevation, has been achieved. In addition, the properties of the site can be explained in the context of an understanding of its past evolution through a long period of geological history.

Concerning the specific objectives of the site descriptive modelling work, it is concluded that all collected data have been analysed, and the results provide, together with knowledge from previous modelling work, the basis for the site-descriptive model of the SFR area. Models of the bedrock geology (Curtis et al. 2011), bedrock hydrogeology (Öhman et al. 2012, 2013) and hydrogeochemistry (Nilsson et al. 2011) have been documented separately and delivered to repository engineering and safety assessment. With regard to rock mechanics, a compilation of older data collected during the planning and construction of the existing SFR facility and recent data collected during the Forsmark site investigation was considered sufficient for SDM-PSU.

The final site descriptive model for SDM-PSU builds on a geological model for the bedrock in 3D into which the other discipline-specific models, i.e. bedrock hydrogeology and bedrock hydrogeochemistry, have been integrated. The existing model of the regolith developed in SR-Site was considered sufficient for SDM-PSU.

Although confidence in the occurrence of steeply dipping deterministic deformation zones in the target volume intended for the SFR extension facility is high and the occurrence of undetected steeply dipping deformation zones longer than 300 m is deemed unlikely, shallow sub-horizontal to gently dipping structures make a much more significant contribution to the pattern of local groundwater flow in the upper part of the bedrock than the steeply dipping deformation zones. In conclusion, the principal remaining uncertainty in SDM-PSU concerns the inclusion, size, nature and transmissivity of sub-horizontal to gently dipping structures in the uppermost part of the bedrock. Additional boreholes and hydraulic testing together with a geological discrete fracture network (DFN) model could possibly have improved the structural-hydraulic modelling in this regard. In SDM-PSU, the issue is handled by the hydrogeological model by including a shallow bedrock aquifer (SBA) concept similar to that used in SDM-Site Forsmark for some of the unresolved possible deformation zones together with a conditional hydrogeological DFN model for the remaining unresolved possible deformation zones. Eight so called SBA-structures have been inferred from the acquired structural and/or hydraulic data. Their certainty in terms of data support and interpreted spatial extent in 3D varies. A primary idea with their present interpretation in the hydrogeological model is to allow for a discussion about their potential importance for safety assessment since current data suggest that transmissive, sub-horizontal to gently dipping structures may intersect the rock vaults of the planned extension of the existing SFR facility depending on the decided location.

It is forecasted that the southern part of the area intended for the SFR extension may possibly be intersected by one or more horizontal to gently dipping structures of potentially significant transmissivity ( $10^{-4} \text{ m}^2/\text{s} > T > 10^{-6} \text{ m}^2/\text{s}$ ). With regard to geometrical properties, i.e. size and spacing, one can only speculate since the borehole coverage is insufficient in these parts of the model domain. If no more boreholes are drilled and no more investigations are carried out, this needs to be studied further in the safety assessment by means of sensitivity tests.

## References

SKB's (Svensk Kärnbränslehantering AB) publications can be found at [www.skb.se/publications](http://www.skb.se/publications).  
References to SKB's unpublished documents are listed separately at the end of the reference list.  
Unpublished documents will be submitted upon request to [document@skb.se](mailto:document@skb.se).

- Andersson E (ed), 2010.** The limnic ecosystems at Forsmark and Laxemar-Simpevarp. SKB TR-10-02, Svensk Kärnbränslehantering AB.
- Andersson E, Aquilonius K, Sivars Becker L, Borgiel M, 2011.** Site investigation SFR. Vegetation in streams in the Forsmark area. SKB P-11-18, Svensk Kärnbränslehantering AB.
- Andersson J, Ström A, Svemar C, Almén K-A, Ericsson L O, 2000.** What requirements does the KBS-3 repository make on the host rock? Geoscientific suitability indicators and criteria for siting and site evaluation. SKB TR-00-12, Svensk Kärnbränslehantering AB.
- Aquilonius K (ed), 2010.** The marine ecosystems at Forsmark and Laxemar-Simpevarp. SR-Site Biosphere. SKB TR-10-03, Svensk Kärnbränslehantering AB.
- Aquilonius K, Qvarfordt S, Borgiel M, 2011.** Validation of the marine vegetation model in Forsmark. SFR-Site Forsmark. SKB P-11-10, Svensk Kärnbränslehantering AB.
- Axelsson C-L, Mærsk Hansen L, 1997.** Update of structural models at SFR nuclear waste repository, Forsmark, Sweden. SKB R-98-05, Svensk Kärnbränslehantering AB.
- Axelsson C-L, Ekstav A, Lindblad Påsse A, 2002.** SFR – Utvärdering av hydrogeologi. SKB R-02-14, Svensk Kärnbränslehantering AB (in Swedish).
- Ball J W, Nordstrom D K, 2001.** User's manual for WATEQ4F, with revised thermodynamic data base and test cases for calculating speciation of major, trace, and redox elements in natural waters. Open File Report 91-183, U.S. Geological Survey, Denver, Colorado.
- Banwart S A, 1999.** Reduction of iron(III) minerals by natural organic matter in groundwater. *Geochimica et Cosmochimica Acta* 63, 2919–2928.
- Barton N, 2002.** Some new  $Q$ -value correlations to assist in site characterisation and tunnel design. *International Journal of Rock Mechanics and Mining Sciences* 39, 185–216.
- Berg J, Jansson U, Wästfelt A, 2006.** Landscape, history and people in a geographical perspective. Studies of land-use, settlement and livelihood in Oskarshamn and Forsmark. SKB R-06-37, Svensk Kärnbränslehantering AB.
- Berglund J, 2008.** Site investigation SFR. Geological mapping and laser scanning of the lower construction tunnel. SKB P-09-74, Svensk Kärnbränslehantering AB.
- Bieniawski Z T, 1979.** Engineering rock mass classifications: a complete manual for engineers and geologists in mining, civil and petroleum engineering. New York: Wiley.
- Bono N, Fredriksson A, Maersk Hansen L, 2010.** Sättningsanalys Forsmarks kärnkraftverk – aggregat 1. SKB P-10-48, Svensk Kärnbränslehantering AB.
- Bosson E, Gustafsson L-G, Sassner M, 2008.** Numerical modelling of surface hydrology and near-surface hydrogeology at Forsmark. Site descriptive modelling, SDM-Site Forsmark. SKB R-08-09, Svensk Kärnbränslehantering AB.
- Bosson E, Sassner M, Sabel U, Gustafsson L-G, 2010.** Modelling present and future hydrology and solute transport at Forsmark. SR-Site Biosphere. SKB R-10-02, Svensk Kärnbränslehantering AB.
- Brunberg A-K, Nilsson E, Blomqvist P, 2002.** Characteristics of oligotrophic hardwater lakes in a postglacial land-rise area in mid-Sweden. *Freshwater Biology* 47, 1451–1462.
- Brunberg A-K, Carlsson T, Blomqvist P, Brydsten L, Strömberg M, 2004.** Forsmark site investigation. Identification of catchments, lake-related drainage parameters and lake habitats. SKB P-04-25, Svensk Kärnbränslehantering AB.

- Bödvarsson R, Lund B, Roberts R, Slunga S, 2006.** Earthquake activity in Sweden. Study in connection with a proposed nuclear waste repository in Forsmark or Oskarshamn. SKB R-06-67, Svensk Kärnbränslehantering AB.
- Carlsson A, 1979.** Characteristic features of a superficial rock mass in Southern central Sweden: horizontal and sub-horizontal fractures and filling material. PhD thesis. Uppsala University, Sweden. (Striae 11)
- Carlsson A, Christiansson R, 2007.** Construction experiences from underground works at Forsmark. Compilation report. SKB R-07-10, Svensk Kärnbränslehantering AB.
- Carlsson L, Carlsten S, Sigurdsson T, Winberg A, 1985.** Hydraulic modeling of the final repository for reactor waste (SFR). Compilation and conceptualization of available geological and hydrogeological data. Edition 1. SKB SFR 85-06, Svensk Kärnbränslehantering AB.
- Carlsson L, Winberg A, Arnefors J, 1986.** Hydraulic modeling of the final repository for reactor waste (SFR). Compilation and conceptualization of available geological and hydrogeological data. SKB SFR 86-03, Svensk Kärnbränslehantering AB.
- Chasset C, Jarsjö J, Erlström M, Cvetkovic V, Destouni G, 2011.** Scenario simulations of CO<sub>2</sub> injection feasibility, plume migration and storage in a saline aquifer, Scania, Sweden. *International Journal of Greenhouse Gas Control* 5, 1303–1318.
- Christiansson R, 1986.** Geologisk beskrivning av zoner kring slutförvaret. SKB SFR 86-02, Svensk Kärnbränslehantering AB. (In Swedish.)
- Christiansson R, Bolvede P, 1987.** Byggnadsgeologisk uppföljning. Slutrapport. SKB SFR 87-03, Svensk Kärnbränslehantering AB. (In Swedish.)
- Claesson Liljedahl L, Munier R, Sandström B, Drake H, Tullborg E-L, 2011.** Assessment of fractures classified as non-mineralised in the SICADA database. SKB R-11-02, Svensk Kärnbränslehantering AB.
- Curtis P, Petersson J, Triumph C-A, Isaksson H, 2009.** Site investigation SFR. Deformation zone modelling. Model version 0.1. SKB P-09-48, Svensk Kärnbränslehantering AB.
- Curtis P, Markström I, Petersson J, Triumph C-A, Isaksson H, Mattsson H, 2011.** Site investigation SFR. Bedrock geology. SKB R-10-49, Svensk Kärnbränslehantering AB.
- Dershowitz W, Lee G, Geier J, Foxford T, La Pointe P, Thomas A, 1998.** FracMan. Interactive discrete feature data analysis, geometric modeling and exploration simulation. User documentation, version 2.6. Redmond, WA: Golder Associates Inc.
- Drake H, Tullborg E-L, MacKenzie A B, 2009.** Detecting the near-surface redox front in crystalline bedrock using fracture mineral distribution, geochemistry and U-series disequilibrium. *Applied Geochemistry* 24, pp 1023–1039.
- Eklund S, Mattson K-J, 2009.** Forsmark site investigation. Quantitative mapping of fracture minerals in Forsmark. SKB P-08-47, Svensk Kärnbränslehantering AB.
- Follin S, 2008.** Bedrock hydrogeology Forsmark. Site descriptive modelling, SDM-Site Forsmark. SKB R-08-95, Svensk Kärnbränslehantering AB.
- Follin S, Johansson P-O, Levén J, Hartley L, Holton D, McCarthy R, Roberts D, 2007a.** Updated strategy and test of new concepts for groundwater flow modelling in Forsmark in preparation of site descriptive modelling stage 2.2. SKB R-07-20, Svensk Kärnbränslehantering AB.
- Follin S, Levén J, Hartley L, Jackson P, Joyce S, Roberts D, Swift B, 2007b.** Hydrogeological characterisation and modelling of deformation zones and fracture domains, Forsmark modelling stage 2.2. SKB R-07-48, Svensk Kärnbränslehantering AB.
- Follin S, Johansson P-O, Hartley L, Jackson P, Roberts D, Marsic N, 2007c.** Conceptual model development and numerical modelling using CONNECTFLOW, Forsmark modelling stage 2.2, SKB R-07-49, Svensk Kärnbränslehantering AB.
- Follin S, Ludvigson J-E, Levén J, 2011.** A comparison between standard well test evaluation methods used in SKB's site investigations and the generalised radial flow concept. SKB P-06-54, Svensk Kärnbränslehantering AB.

- Fox A, La Pointe P, Hermanson J, Öhman J, 2007.** Statistical geological discrete fracture network model. Forsmark modelling stage 2.2. SKB R-07-46, Svensk Kärnbränslehantering AB.
- Fransson Å, 2009.** Literature survey: Relations between stress change deformation and transmissivity for fractures and deformation zones based on *in situ* investigations. SKB R-09-13, Svensk Kärnbränslehantering AB.
- Fredén C (ed), 2002.** Sveriges nationalatlas. Berg och jord. 3rd ed. Stockholm: SNA Förlag. (In Swedish.)
- Gimeno M J, Auqué L F, Gómez J B, Acero P, 2008.** Water-rock interaction modelling and uncertainties of mixing modelling. Site descriptive modelling, SDM-Site Forsmark. SKB R-08-86, Svensk Kärnbränslehantering AB.
- Gimeno M J, Auqué L F, Gómez J B, Acero P, 2009.** Water-rock interaction modelling and uncertainties of mixing modelling. Site descriptive modelling, SDM-Site Laxemar. SKB R-08-110, Svensk Kärnbränslehantering AB.
- Gimeno M J, Auqué L F, Gómez J B, Acero P, 2011.** Site investigation SFR. Water-rock interaction and mixing modelling in the SFR. SKB P-11-25, Svensk Kärnbränslehantering AB.
- Glamheden R, Fredriksson A, Röshoff K, Karlsson J, Hakami H, Christiansson R, 2007.** Rock mechanics Forsmark. Site descriptive modelling, Forsmark stage 2.2. SKB R-07-31, Svensk Kärnbränslehantering AB.
- Glamheden R, Lanaro F, Karlsson J, Lindberg U, Wrafter J, Hakami H, Johansson M, 2008.** Rock mechanics Forsmark. Modelling stage 2.3. Complementary analysis and verification of the rock mechanics model. SKB R-08-66, Svensk Kärnbränslehantering AB.
- Grandia F, Sena C, Arcos D, Molinero J, Duro L, Bruno J, 2007.** Quantitative assessment of radionuclide retention in the near-surface system at Forsmark. Development of a reactive transport model using Forsmark 1.2 data. SKB R-07-64, Svensk Kärnbränslehantering AB.
- Gustafsson B G, 2004a.** Millennial changes of the Baltic Sea salinity. Studies of the sensitivity of the salinity to climate change. SKB TR-04-12, Svensk Kärnbränslehantering AB.
- Gustafsson B G, 2004b.** Sensitivity of the Baltic Sea salinity to large perturbations in climate. *Climate Research* 27, 237–251.
- Gustafsson G, 2009.** Hydrogeologi för bergbyggare. Stockholm: Formas. (T / Forskningsrådet Formas 2009:2). (In Swedish.)
- Hagkonsult, 1982.** Geologiska undersökningar och utvärderingar för lokalisering av SFR till Forsmark. SKBF/KBS SFR 81-13, Svensk Kärnbränsleförsörjning AB. (In Swedish.)
- Hagkonsult, 1983.** Geologiska undersökningar och utvärderingar för förvarsutrymmen i berg. SKBF/KBS SFR 83-05, Svensk Kärnbränsleförsörjning AB. (In Swedish.)
- Hamrén U, Collinder P, 2010.** Vattenverksamhet i Forsmark: Ekologisk fältinventering och naturvärdesklassificering samt beskrivning av skogsproduktionsmark. SKB R-10-16, Svensk Kärnbränslehantering AB. (In Swedish, with summary in English.)
- Hedenström A, Risberg J, 2003.** Shore displacement in northern Uppland during the last 6500 calendar years. SKB TR-03-17, Svensk Kärnbränslehantering AB.
- Hedenström A, Sohlenius G, 2008.** Description of the regolith at Forsmark. Site descriptive modelling, SDM-Site. SKB R-08-04, Svensk Kärnbränslehantering AB.
- Hedenström A, Sohlenius G, Strömgren M, Brydsten L, Nyman H, 2008.** Depth and stratigraphy of regolith at Forsmark. Site descriptive modelling, SDM-Site Forsmark. SKB R-08-07, Svensk Kärnbränslehantering AB.
- Hiltscher R, Strindell L, 1976.** Bergspänningsmätning som underlag vid projektering av stora berggrum. In *Bergmekanikdag 1976*. Stockholm: Stiftelsen Bergteknisk Forskning, 151–157. (In Swedish.)
- Holmén J G, Stigsson M, 2001.** Modelling of future hydrogeological conditions at SFR. SKB R-01-02, Svensk Kärnbränslehantering AB.

- IAEA, 1995.** Reference and intercomparison materials for stable isotopes of light elements: Proceedings of a consultants meeting held in Vienna, 1-3 December 1993. IAEA-TECDOC-825, International Atomic Energy Agency.
- Indraratna B, Ranjith P G, Gale W, 1999.** Single phase water flow through rock fractures. *Geotechnical and Geological Engineering* 17, 211–240.
- Isaksson H, 2003.** Forsmark site investigation. Interpretation of topographic lineaments 2002. SKB P-03-40, Svensk Kärnbränslehantering AB.
- Isaksson H, 2007.** Correlation between refraction seismic data, low magnetic lineaments and deformation zones (model stage 2.2). In Stephens M B, Skagius K (eds). *Geology – Background complementary studies. Forsmark modelling stage 2.2.* SKB R-07-56, Svensk Kärnbränslehantering AB, 113–130.
- Isaksson H, Keisu M, 2005.** Forsmark site investigation. Interpretation of airborne geophysics and integration with topography. Stage 2 (2002–2004). An integration of bathymetry, topography, refraction seismics and airborne geophysics. SKB P-04-282, Svensk Kärnbränslehantering AB.
- Isaksson H, Thunehed H, Keisu M, 2004.** Forsmark site investigation. Interpretation of airborne geophysics and integration with topography. Stage 1 (2002). SKB P-04-29, Svensk Kärnbränslehantering AB.
- Isaksson H, Pitkänen T, Thunehed H, 2006a.** Forsmark site investigation. Ground magnetic survey and lineament interpretation in an area northwest of Bolundsfjärden. SKB P-06-85, Svensk Kärnbränslehantering AB.
- Isaksson H, Thunehed H, Pitkänen T, Keisu M, 2006b.** Forsmark site investigation. Detailed ground and marine magnetic survey and lineament interpretation in the Forsmark area – 2006. SKB P-06-261, Svensk Kärnbränslehantering AB.
- Isaksson H, Thunehed H, Pitkänen T, Keisu M, 2007.** Forsmark site investigation. Detailed ground and marine magnetic survey and lineament interpretation in the Forsmark area, 2006–2007. SKB R-07-62, Svensk Kärnbränslehantering AB.
- Jacobsson L, Flansbjer M, 2005.** Forsmark site investigation. Borehole KFM07A. Normal loading and shear tests on joints. SKB P-05-213, Svensk Kärnbränslehantering AB.
- Jarsjö J, Destouni G, 2000.** Degassing of deep groundwater in fractured rock around boreholes and drifts. *Water Resources Research* 36, 2477–2492.
- Johansson P-O, 2008.** Description of hydrology and near-surface hydrogeology at Forsmark. Site descriptive modelling, SDM-Site Forsmark. SKB R-08-08, Svensk Kärnbränslehantering AB.
- Johansson P-O, Öhman J, 2008.** Presentation of meteorological, hydrological and hydrogeological monitoring data from Forsmark. Site descriptive modelling, SDM-Site Forsmark. SKB R-08-10, Svensk Kärnbränslehantering AB.
- Johansson P-O, Werner K, Bosson E, Berglund S, Juston J, 2005.** Description of climate, surface hydrology, and near-surface hydrogeology. Preliminary site description Forsmark area – version 1.2. SKB R-05-06, Svensk Kärnbränslehantering AB.
- Joyce S, Simpson T, Hartley L, Applegate D, Hoek J, Jackson P, Swan D, Marsic N, Follin S, 2010.** Groundwater flow modelling of periods with temperate climate conditions – Forsmark. SKB R-09-20, Svensk Kärnbränslehantering AB.
- Juhlin C, Palm H, 2005.** Forsmark site investigation. Reflection seismic studies in the Forsmark area, 2004: Stage 2. SKB R-05-42, Svensk Kärnbränslehantering AB.
- Juhlin C, Zhang F, 2010.** Site investigation SFR. Reprocessing of reflection seismic profiles 5b and 8, Forsmark. SKB P-10-50, Svensk Kärnbränslehantering AB.
- Karlsson A, Eriksson C, Borell Lövstedt C, Liungman O, Engqvist A, 2010.** High-resolution hydrodynamic modelling of the marine environment at Forsmark between 6500 BC and 9000 AD. SKB R-10-09, Svensk Kärnbränslehantering AB.
- Kautsky U (ed), 2001.** The biosphere today and tomorrow in the SFR area. SKB R-01-27, Svensk Kärnbränslehantering AB.

- Keisu M, Isaksson H, 2004.** Forsmark site investigation. Acquisition of geological information from Forsmarksverket. Information from the Vattenfall archive, Räcksta. SKB P-04-81, Svensk Kärnbränslehantering AB.
- Koistinen T, Stephens M B, Bogatchev V, Nordgulen Ø, Wennerström M, Korhonen J V, 2001.** Geological map of the Fennoscandian Shield, scale 1:2 000 000. Espoo: Geological Survey of Finland, Trondheim: Geological Survey of Norway, Uppsala: Geological Survey of Sweden, Moscow: Ministry of Natural Resources of Russia.
- Laaksoharju M, Gurban I, 2003.** Groundwater chemical changes at SFR in Forsmark. SKB R-03-03, Svensk Kärnbränslehantering AB.
- Laaksoharju M, Smellie J, Tullborg E-L, Gimeno M, Hallbeck L, Molinero J, Waber N, 2008.** Bedrock hydrogeochemistry Forsmark. Site descriptive modeling, SDM-Site Forsmark. SKB R-08-47, Svensk Kärnbränslehantering AB.
- Laaksoharju M, Gimeno M, Auqué L F, Gómez, J B, Acero P, Pedersen K, 2009.** Hydrogeochemical and microbiological effects on fractures in the Excavation Damaged Zone (EDZ). SKB R-09-05, Svensk Kärnbränslehantering AB.
- Leijon B (ed), 2005.** Forsmark site investigation. Investigations of superficial fracturing and block displacements at drill site 5. SKB P-05-199, Svensk Kärnbränslehantering AB.
- Lindborg T (ed), 2008.** Surface system Forsmark. Site descriptive modelling, SDM-Site Forsmark. SKB R-08-11, Svensk Kärnbränslehantering AB.
- Ljunggren C, Persson M, 1995.** Beskrivning av databas – Bergspänningsmätningar i Sverige. SKB Djupförvar Projektrapport PR D-95-017, Svensk Kärnbränslehantering AB. (In Swedish.)
- Lundin L, Lode E, Stendahl J, Melkerud P-A, Björkvald L, Thorstensson A, 2004.** Soils and site types in the Forsmark area. SKB R-04-08, Svensk Kärnbränslehantering AB.
- Löfgren A (ed), 2010.** The terrestrial ecosystems at Forsmark and Laxemar-Simpevarp. SR-Site Biosphere. SKB TR-10-01, Svensk Kärnbränslehantering AB.
- Löfgren A, 2011.** Dissolved inorganic carbon and organic carbon in mires in the Forsmark area. A pilot study. SKB P-11-23, Svensk Kärnbränslehantering AB.
- Löfgren M, Sidborn M, 2010.** Statistical analysis of results from the quantitative mapping of fracture minerals in Forsmark. Site descriptive modelling – complementary studies. SKB R-09-30, Svensk Kärnbränslehantering AB.
- Martin C D, 2007.** Quantifying in situ stress magnitudes and orientations for Forsmark. Forsmark stage 2.2. SKB R-07-26, Svensk Kärnbränslehantering AB.
- Martin D, Follin S, 2011.** Review of possible correlations between in situ stress and PFL fracture transmissivity data at Forsmark. SKB R-08-69, Svensk Kärnbränslehantering AB.
- Martna J, Hiltcher R, Ingevald K, 1983.** Geology and rock stresses in deep boreholes at Forsmark in Sweden. In Proceedings of the 5th International Congress on Rock Mechanics, Melbourne, 10–15 April 1983. Vol 2. Rotterdam: Balkema, F 111 – F 116.
- Miliander S, Punakivi M, Kyläkorpi L, Rydgren B, 2004.** Human population and activities in Forsmark. Site description. SKB R-04-10, Svensk Kärnbränslehantering AB.
- Munier R, Stenberg L, Stanfors R, Milnes A G, Hermanson J, Triumf C-A, 2003.** Geological Site Descriptive Model. A strategy for the model development during site investigations. SKB R-03-07, Svensk Kärnbränslehantering AB.
- Mårtensson E, Gustafsson L-G, 2010.** Hydrological and hydrogeological effects of an open repository in Forsmark: Final MIKE SHE flow modelling results for the Environmental Impact Assessment. SKB R-10-18, Svensk Kärnbränslehantering AB.
- Mårtensson E, Gustafsson L-G, Gustafsson A-M, Aneljung M, Sabel U, 2010.** Hydrologiska och hydrogeologiska effekter på våtmarker och skogsområden av slutförvarsanläggningen i Forsmark: Resultat från modellering med MIKE SHE. SKB R-10-19, Svensk Kärnbränslehantering AB. (In Swedish, with summary in English.)

- Möller C, Snäll S, Stephens M B, 2003.** Forsmark site investigation. Dissolution of quartz, vug formation and new grain growth associated with post-metamorphic hydrothermal alteration in KFM02A. SKB P-03-77, Svensk Kärnbränslehantering AB.
- Nielsen U T, Ringgaard J, 2009.** Site investigation SFR. Geophysical borehole logging in the boreholes KFR27 (0–500 m), KFR102A, KFR102B, KFR103, KFR104 and HFM07. SKB P-09-16, Svensk Kärnbränslehantering AB.
- Nilsson A-C, 2009.** Site investigation SFR. Presentation and evaluation of hydrogeochemical data from SFR-boreholes, 1984–2007. SKB P-09-45, Svensk Kärnbränslehantering AB.
- Nilsson A-C, Tullborg E-L, Smellie J, 2010.** Preliminary hydrogeochemical site description SFR (version 0.2). SKB R-10-38, Svensk Kärnbränslehantering AB.
- Nilsson A-C, Tullborg E-L, Smellie J, Gimeno M J, Gómez J B, Auqué L F, Sandström B, Pedersen K, 2011.** SFR site investigation. Bedrock hydrogeochemistry. SKB R-11-06, Svensk Kärnbränslehantering AB.
- Nilsson G, 2009.** Site investigation SFR. Drilling of the cored borehole KFR105. SKB P-09-41, Svensk Kärnbränslehantering AB.
- Nyberg J, Elhammer A, Sohlenius G, Kjellin B, Nordgren P, 2011.** Results from marine geological investigations outside Forsmark. SKB P-11-39, Svensk Kärnbränslehantering AB.
- Odén M, 2009.** Site investigation SFR. Hydrogeological modelling at SFR using DarcyTools. Site description SFR version 0.0. SKB P-08-94, Svensk Kärnbränslehantering AB.
- Olofsson I, Simeonov A, Stephens M B, Follin S, Nilsson A-C, Röshoff K, Lindberg U, Lanaro F, Fredriksson A, Persson L, 2007.** Site descriptive modelling Forsmark, stage 2.2. A fracture domain concept as a basis for the statistical modelling of fractures and minor deformation zones, and interdisciplinary coordination. SKB R-07-15, Svensk Kärnbränslehantering AB.
- Parkhurst D L, Appelo C A J, 1999.** User's guide to PHREEQC (version 2): a computer program for speciation, batch-reaction, one-dimensional transport, and inverse geochemical calculations. Water-Resources Investigations Report 99-4259, U.S. Geological Survey, Denver, Colorado.
- Perman F, Sjöberg J, 2003.** Forsmark site investigation. Transient strain analysis of overcoring measurements in boreholes DBT-01 and DBT-03. SKB P-03-119, Svensk Kärnbränslehantering AB.
- Petersson J, Berglund J, Danielsson P, Wängnerud A, Tullborg E-L, Mattsson H, Thunehed H, Isaksson H, Lindroos H, 2004.** Forsmark site investigation. Petrography, geochemistry, petrophysics and fracture mineralogy of boreholes KFM01A, KFM02A and KFM03A+B. SKB P-04-103, Svensk Kärnbränslehantering AB.
- Petersson J, Curtis P, Bockgård N, Mattsson H, 2011.** Site investigation SFR. Rock type coding, overview geological mapping and identification of rock units and possible deformation zones in drill cores from the construction of SFR. SKB P-10-07, Svensk Kärnbränslehantering AB.
- Pinto da Cunha A (ed), 1990.** Scale effects in rock masses 93: proceedings of the Second International Workshop on Scale Effects in Rock Masses, Lisbon, Portugal, 25 June 1993. Rotterdam: Balkema.
- Piqué À, Grandia F, Sena C, Arcos D, Molinero J, Duro L, Bruno J, 2010.** Conceptual and numerical modelling of radionuclide transport in near-surface systems at Forsmark. SR-Site Biosphere. SKB R-10-30, Svensk Kärnbränslehantering AB.
- Pitkänen P, Luukkonen A, Ruotsalainen P, Leino-Forsman H, Vuorinen U, 1999.** Geochemical modelling of groundwater evolution and residence time at the Olkiluoto site. Posiva 98-10, Posiva Oy, Finland.
- Pitkänen P, Partamies S, Luukkonen A, 2004.** Hydrogeochemical interpretation of baseline groundwater conditions at the Olkiluoto site. Posiva 2003-07, Posiva Oy, Finland.
- Pässe T, 2001.** An empirical model of glacio-isostatic movements and shore-level displacement in Fennoscandia. SKB R-01-41, Svensk Kärnbränslehantering AB.



**Qvarfordt S, Borgiel M, Berg C, 2010.** Monitoring Forsmark. Hydrochemical investigations in four calciferous lakes in the Forsmark area. Results from complementary investigations in the Forsmark area, 2008–2009. SKB P-10-25, Svensk Kärnbränslehantering AB.

**Rhén I (ed), Gustafson G, Stanfors R, Wikberg P, 1997.** Äspö HRL – Geoscientific evaluation 1997/5. Models based on site characterization 1986–1995. SKB TR 97-06, Svensk Kärnbränslehantering AB.

**Rhén I, Follin S, Hermanson J, 2003.** Hydrogeological Site Descriptive Model – a strategy for its development during site investigations. SKB R-03-08, Svensk Kärnbränslehantering AB.

**Ringgaard J, 2007.** Mapping of borehole breakouts. Processing of acoustical televiewer data from KFM01A, KFM01B, KFM02A, KFM03A, KFM03B, KFM04A, KFM05A, KFM06A and KFM07C. SKB P-07-07, Svensk Kärnbränslehantering AB.

**Rutqvist J, 1995.** Coupled stress-flow properties of rock joints from hydraulic field testing. PhD thesis. Royal Institute of Technology, Stockholm.

**Saintot A, Stephens M B, Viola G, Nordgulen Ø, 2011.** Brittle tectonic evolution and paleostress field reconstruction in the south-western part of the Fennoscandian Shield, Forsmark, Sweden. *Tectonics* 30, TC4002. doi:10.1029/2010TC002781

**Sandström B, Tullborg E-L, 2011.** Site investigation SFR. Fracture mineralogy and geochemistry of borehole sections sampled for groundwater chemistry and Eh. Results from boreholes KFR01, KFR08, KFR10, KFR19, KFR7A and KFR105. SKB P-11-01, Svensk Kärnbränslehantering AB.

**Sandström B, Tullborg E-L, Smellie J, MacKenzie A B, Suksi J, 2008a.** Fracture mineralogy of the Forsmark site. Final report. SKB P-08-97, Svensk Kärnbränslehantering AB.

**Sandström B, Tullborg E-L, Smellie J, MacKenzie A, Suksi J, 2008b.** Fracture mineralogy of the Forsmark site. SDM-Site Forsmark. SKB R-08-102, Svensk Kärnbränslehantering AB.

**Sandström B, Tullborg E-L, Larson S Å, Page L, 2009.** Brittle tectonothermal evolution in the Forsmark area, central Fennoscandian shield, recorded by paragenesis, orientation and  $^{40}\text{Ar}/^{39}\text{Ar}$  geochronology of fracture minerals. *Tectonophysics* 478, 158–174.

**Sheppard S, Long J, Sanipelli B, Sohlenius G, 2009.** Solid/liquid partition coefficients ( $K_d$ ) for selected soils and sediments at Forsmark and Laxemar-Simpevarp. SKB R-09-27, Svensk Kärnbränslehantering AB.

**Sheppard S, Sohlenius G, Omberg L-G, Borgiel M, Grolander S, Nordén S, 2011.** Solid/liquid partition coefficients ( $K_d$ ) and plant/soil concentration ratios (CR) for selected soils, till and sediments at Forsmark. SKB R-11-24, Svensk Kärnbränslehantering AB.

**Sidborn M, Sandström B, Tullborg E-L, Salas J, Maia F, Delos A, Molinero J, Hallbeck L, Pedersen K, 2010.** SR-Site: Oxygen ingress in the rock at Forsmark during a glacial cycle. SKB TR-10-57, Svensk Kärnbränslehantering AB.

**Sjöberg J, Lindfors U, Perman F, Ask D, 2005.** Evaluation of the state of stress at the Forsmark site. Preliminary site investigation Forsmark area – version 1.2. SKB R-05-35, Svensk Kärnbränslehantering AB.

**SKB, 2001.** Site investigations. Investigations, methods and general execution programme. SKB TR-01-29, Svensk Kärnbränslehantering AB.

**SKB, 2004.** Preliminary site description Forsmark area – version 1.1. SKB R-04-15, Svensk Kärnbränslehantering AB.

**SKB, 2005.** Preliminary site description Forsmark area – version 1.2. SKB R-05-18, Svensk Kärnbränslehantering AB.

**SKB, 2007.** Forsmark site investigation. Programme for long-term observations of geosphere and biosphere after completed site investigations. SKB R-07-34, Svensk Kärnbränslehantering AB.

**SKB, 2008a.** Geovetenskapligt undersökningsprogram för utbyggnad av SFR. SKB R-08-67, Svensk Kärnbränslehantering AB. (In Swedish.)

- SKB, 2008b.** Site description of Forsmark at completion of the site investigation phase. SDM-Site Forsmark. SKB TR-08-05, Svensk Kärnbränslehantering AB.
- SKB, 2008c.** Safety analysis SFR. Long-term safety. SKB R-08-130, Svensk Kärnbränslehantering AB.
- SKB, 2009.** Site description of Laxemar at completion of the site investigation phase. SDM-Site Laxemar. SKB TR-09-01, Svensk Kärnbränslehantering AB.
- SKB, 2010.** Biosphere analyses for the safety assessment SR-Site – synthesis and summary of results. SKB TR-10-09, Svensk Kärnbränslehantering AB.
- Smellie J, Laaksoharju M, Tullborg E-L, 2002.** Hydrogeochemical site descriptive model – a strategy for the model development during site investigations. SKB R-02-49, Svensk Kärnbränslehantering AB.
- Smellie J, Tullborg E-L, Nilsson A-C, Sandström B, Waber N, Gimeno M, Gascoyne M, 2008.** Explorative analysis of major components and isotopes. SDM-Site Forsmark. SKB R-08-84, Svensk Kärnbränslehantering AB.
- Sohlenius G, Hedenström A, 2009.** Platsundersökning Forsmark. Stratigrafiska undersökningar i våtmarksobjekt. SKB P-09-18, Svensk Kärnbränslehantering AB. (In Swedish, with abstract in English.)
- Sonesten L, 2005.** Chemical characteristics of surface waters in the Forsmark area. Evaluation of data from lakes, streams, and coastal sites. SKB R-05-41, Svensk Kärnbränslehantering AB.
- SSPB, 1982.** Characterization of deep-seated rock masses by means of borehole investigations. In-situ rock stress measurements, hydraulic testing and core-logging. Final report. Research and Development Report 5:1, The Swedish State Power Board.
- Stephansson O, Ångman P, 1984.** Hydraulic fracturing stress measurements at Forsmark and Stidsvig, Sweden. Research Report TULEA 1984:30, Luleå University of Technology.
- Stephens M B, Forssberg O, 2006.** Rock types and ductile structures on a rock domain basis, and fracture orientation and mineralogy on a deformation zone basis. Preliminary site description. Forsmark area – version 1.2. SKB R-06-78, Svensk Kärnbränslehantering AB.
- Stephens M B, Lundqvist S, Bergman T, Andersson J, Ekström M, 2003.** Forsmark site investigation. Bedrock mapping. Rock types, their petrographic and geochemical characteristics, and a structural analysis of the bedrock based on Stage 1 (2002) surface data. SKB P-03-75, Svensk Kärnbränslehantering AB.
- Stephens M B, Lundqvist S, Bergman T, Ekström M, 2005.** Forsmark site investigation. Bedrock mapping. Petrographic and geochemical characteristics of rock types based on Stage 1 (2002) and Stage 2 (2003) surface data. SKB P-04-87, Svensk Kärnbränslehantering AB.
- Stephens M B, Fox A, La Pointe P, Simeonov A, Isaksson H, Hermanson J, Öhman J, 2007.** Geology Forsmark. Site descriptive modelling Forsmark stage 2.2. SKB R-07-45, Svensk Kärnbränslehantering AB.
- Stephens M B, Bergman T, Isaksson H, Petersson J, 2008.** Bedrock geology Forsmark. Modelling stage 2.3. Description of the bedrock geological map at the ground surface. SKB R-08-128, Svensk Kärnbränslehantering AB.
- Stephens M B, Ripa M, Lundström I, Persson L, Bergman T, Ahl M, Wahlgren C-H, Persson P-O, Wickström L, 2009.** Synthesis of the bedrock geology in the Bergslagen region, Fennoscandian Shield, south-central Sweden. Uppsala: Geological Survey of Sweden. (Serie Ba 58)
- Stille H, Fredriksson A, Widing E, Åhrling G, 1985.** Bergmekaniska beräkningar – FEM-analys av silo med anslutande tunnlar. SKB SFR 85-05, Svensk Kärnbränslehantering AB. (In Swedish.)
- Strömgren M, Brydsten L, 2008.** Digital elevation models of Forsmark. Site descriptive modelling, SDM-Site Forsmark. SKB R-08-62, Svensk Kärnbränslehantering AB.
- Strömgren M, Lindgren F, 2011.** Mapping of reed in shallow bays. SFR-Site Forsmark. SKB P-11-09, Svensk Kärnbränslehantering AB.

**Svensson U, Kuylenstierna H-O, Ferry M, 2010.** DarcyTools version 3.4 – concepts, methods and equations. SKB R-07-38, Svensk Kärnbränslehantering AB.

**Söderbäck B (ed), 2008.** Geological evolution, palaeoclimate and historical development of the Forsmark and Laxemar-Simpevarp areas. Site descriptive modelling, SDM-Site. SKB R-08-19, Svensk Kärnbränslehantering AB.

**Tröjbom M, Grolander S, 2010.** Chemical conditions in present and future ecosystems in Forsmark – implications for selected radionuclides in the safety assessment SR-Site. SKB R-10-27, Svensk Kärnbränslehantering AB.

**Tröjbom M, Nordén S, 2010.** Chemistry data from surface ecosystems in Forsmark and Laxemar-Simpevarp. Site specific data used for estimation of CR and  $K_d$  values in SR-Site. SKB R-10-28, Svensk Kärnbränslehantering AB.

**Tröjbom M, Söderbäck B, 2006.** Chemical characteristics of surface systems in the Forsmark area. Visualisation and statistical evaluation of data from shallow groundwater, precipitation, and regolith. SKB R-06-19, Svensk Kärnbränslehantering AB.

**Tröjbom M, Söderbäck B, Johansson P-O, 2007.** Hydrochemistry in surface water and shallow groundwater. Site descriptive modelling, SDM-Site Forsmark. SKB R-07-55, Svensk Kärnbränslehantering AB.

**Tullborg E-L, Drake H, Sandström B, 2008.** Palaeohydrogeology: a methodology based on fracture mineral studies. Applied Geochemistry 23, 1881–1897.

**Walger E, Ludvigson J-E, Gentzsch B, 2011.** Site investigation SFR. Evaluation of selected interference tests and pressure responses during drilling at SFR. SKB P-10-43, Svensk Kärnbränslehantering AB.

**Werner K, Lundholm L, Johansson P-O, 2009.** Platsundersökning Forsmark. Installation av pegelrör och grundvattenrör i våtmarker och sjön Tjärnpussen. SKB P-09-17, Svensk Kärnbränslehantering AB. (In Swedish, with abstract in English.)

**Westman P, Wastegård S, Schoning K, Gustafsson B, Omstedt A, 1999.** Salinity change in the Baltic Sea during the last 8,500 years: evidence causes and models. SKB TR-99-38, Svensk Kärnbränslehantering AB.

**Zangerl C, Evans K F, Eberhardt E, Loew S, 2008.** Normal stiffness of fractures in granitic rock: a compilation of laboratory and in-situ experiments. International Journal of Rock Mechanics and Mining Sciences 45, 1500–1507.

**Öhman J, 2010.** Site investigation SFR. Hydrogeologic modelling of SFR v 0.1. Influence of the ridge on the flow fields for different target volumes. SKB R-09-43, Svensk Kärnbränslehantering AB.

**Öhman J, Follin S, 2010a.** Site investigation SFR. Hydrogeological modelling of SFR. Data review and parameterisation of model version 0.1. SKB P-09-49, Svensk Kärnbränslehantering AB.

**Öhman J, Follin S, 2010b.** Site investigation SFR. Hydrogeological modelling of SFR. Model version 0.2. SKB R-10-03, Svensk Kärnbränslehantering AB.

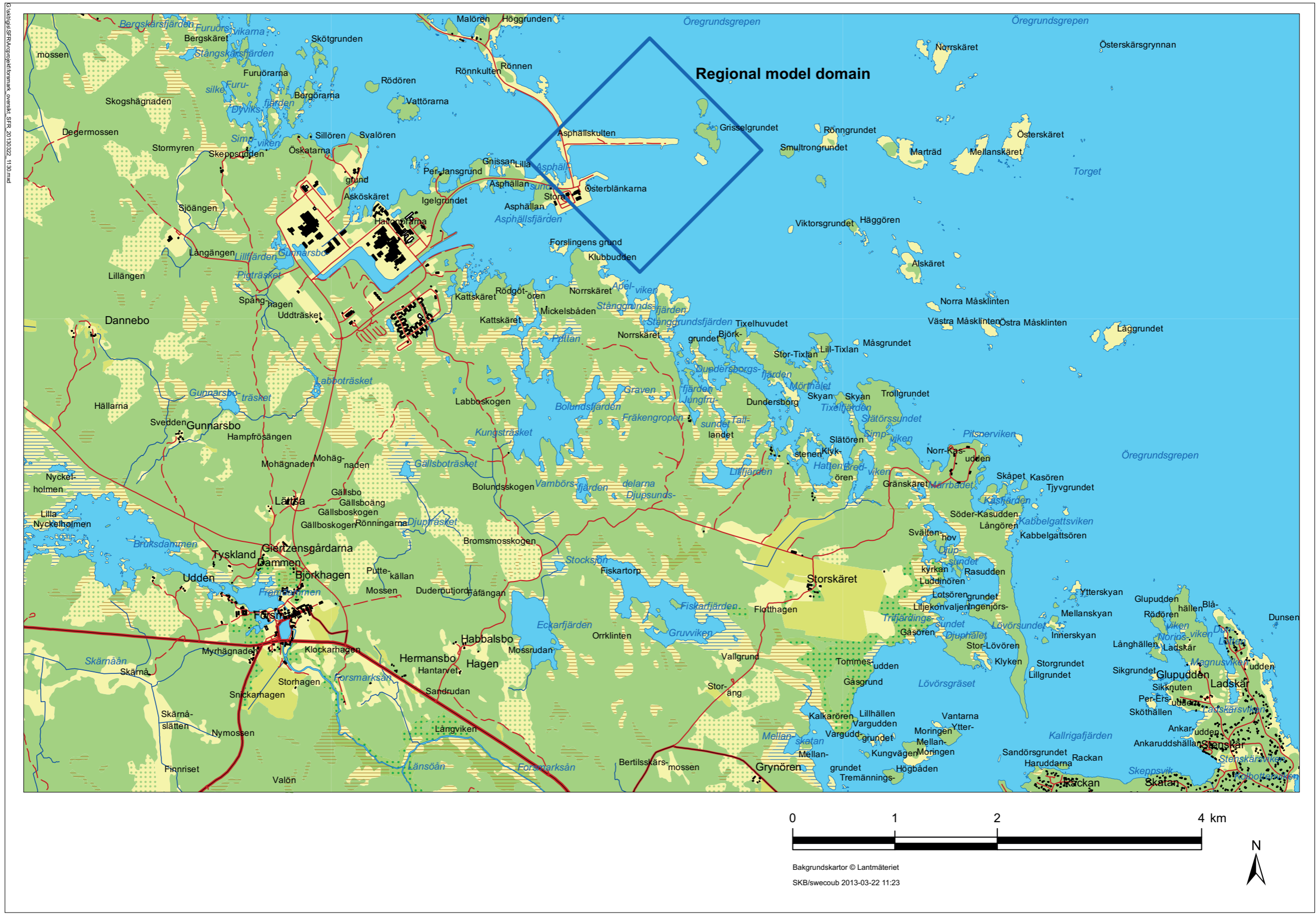
**Öhman J, Bockgård N, Follin S, 2012.** Site investigation SFR. Bedrock hydrogeology. SKB R-11-03, Svensk Kärnbränslehantering AB.

**Öhman J, Follin S, Odén M, 2013.** Site investigation SFR. Bedrock hydrogeology – Groundwater flow modelling. SKB R-11-10, Svensk Kärnbränslehantering AB.

#### Unpublished documents

SKBdoc id, version	Title	Issuer, year
1233642 ver 1.0	SFR Kontrollprogram. Bergkontroll. Bergkontrollgruppens årsrapport 2009. Huvudrapport	Vattenfall Power Consultant AB, 2010
1233647 ver 1.0	SFR – Registrering av grundvattentryck under 2009	Geosigma AB, 2010

Map of the Forsmark and SFR area



### List of abbreviations

This appendix contains explanations of abbreviations and acronyms used by SKB and occurring in this report. Definition of terms that are of basic importance for the modelling and description of the SFR model volumes are provided in Section 1.6.5.

1D	One-dimensional
2D	Two-dimensional
3D	Three-dimensional
AD	Anno Domini.
AMS	Anisotropy of Magnetic Susceptibility
ATP	Adenosine-Tri-Phosphate.
BC	Before Christ.
BIPS	Borehole Imaging Process System; down-hole video camera system providing oriented images of the borehole.
BLA	<i>Bergsal för Lågaktivt Avfall</i> ; Rock vault for low-level waste.
BMA	<i>Bergsal för Medelaktivt Avfall</i> ; Rock vault for intermediate-level waste.
Boremap	SKB's core mapping methodology including inspection of both the drill core and oriented images of the borehole provided by BIPS.
BRT	<i>Bergsal för ReaktorTankar</i> ; Rock vault for reactor vessels.
BT	Access tunnel to the existing SFR facility.
BTF	<i>BetongTankFörvar</i> ; Rock vault for concrete moulds.
DEM	Digital Elevation Model.
DFN	Discrete Fracture Network.
DT	Access tunnel to the existing SFR facility.
DZ	Deformation Zone
EC	Electrical Conductivity
FFM	Identification code prefix for a deterministically modelled fracture domain at Forsmark (SKB 2008b).
FWH	Fresh Water Head,
HCD	Hydraulic Conductor Domain; represents deterministic deformation zones.
HFM	Percussion-drilled borehole in the Forsmark site investigation
HFR	Percussion-drilled borehole at SFR.
HRD	Hydraulic Rock Domain; represents the less fractured rock in between deterministic deformation zones.
HSD	Hydraulic Soil Domain; represents the regolith, i.e. the unconsolidated material on top of the bedrock.
HTHB	<i>HydroTestutrustning för HammarBorrhål</i> ; equipment used for hydraulic characterisation in boreholes by open hole pumping tests.
K	Hydraulic conductivity [L/M]
$K_d$	Partitioning coefficient for sorption [ $L^3/M$ ]
KFM	Cored borehole in the Forsmark site investigation.
KFR	Cored borehole at SFR.
M3	Multivariate mixing and mass balance calculation programme.
MIKE SHE	Numerical modelling tool for surface hydrogeological modelling.
NBT	<i>Nedre ByggTunnel</i> ; lower construction tunnel at SFR.
NEP	Net Ecosystem Production.
PCA	Principal Component Analysis; statistical method for analysing groundwater compositions.
PDZ	Possible Deformation Zone (see also Section 1.6.5).
PFL	Posiva Flow log; equipment used for hydraulic characterisation in boreholes by difference flow logging pumping tests.
PHREEQC	Numerical modelling tool for chemical speciation, batch reaction, one-dimensional transport, and inverse geochemical calculations.
pmC	Percent modern Carbon.
PSU	<i>Projekt SFR Utbyggnad</i> ; The SFR extension project.
PWH	Point Water Head
QA	Quality Assurance
QD	Quaternary Deposits.
RDM	Regolith Depth and stratigraphy Model.

RFM	Identification code prefix for a deterministically modelled rock domain in the Forsmark SDM
RFR	Identification code prefix for a deterministically modelled rock domain in the PSU SDM
RHB 70	Coordinate system used for elevation; see Section 2.6.
RT90	Coordinate system used for x- and y directions; see Section 2.6.
RMR	Classification system for empirical characterisation of rock mechanics properties.
RQD	Rock Quality Designation numbers; xxxxxxxx
RVS	Rock Visualisation System; SKB's tool for modelling and visualisation of the 3D geometry of geological entities.
SAR08	The most recent safety assessment of the existing SFR facility (SKB 2008c).
SARG	SFR extension Application Review Group
SBA	Shallow Bedrock Aquifer structures; horizontal to gently dipping structures in the uppermost part of the bedrock.
SDE GIS	SKB's database for geographic information.
SDM	Site Descriptive Model.
SHI	Single-hole interpretation; an integrated interpretation of geological and geophysical data from a borehole that gives rise to an essentially 1D model for rock units and possible deformation zones along the borehole.
Sicada	SKB's database for primary site investigation data.
SKBdoc	SKB's internal documentation database.
SMHI	Swedish Meteorological and Hydrological Institute.
T	Transmissivity [ $L^2/T$ ].
tDZ	Possible tunnel deformation zone (see also Section 1.6.5).
UCS	Uniaxial Compressive Strength
WATEQ4F	Thermodynamic database.
V-SMOW	Vienna Standard Mean Ocean Water; a water standard defining the isotopic composition of water (IAEA 1995).
ZFM	Identification code prefix for a deterministically modelled deformation zone at Forsmark (SKB 2008b).

## Tables with references to primary data

Specifications of quality-assured data that were available for use in the site descriptive modelling work are compiled in tables in this appendix. Table A3-1 contains geological and geophysical data, Table A3-2 hydrogeological data and Table A3-3 hydrogeochemical data. A list of full references is provided at the end of this appendix.

**Table A3-1. Available geological and geophysical bedrock data and their treatment in SFR model version 1.0.**

Data specification	Reference to data report	Reference in Sicada/GIS	Usage in version 1.0 analysis/modelling
<b>Bedrock mapping – outcrop data</b>			
Rock type, rock type distribution and ductile deformation	Stephens et al. 2003	AP PF400-02-011	Input to RD modelling
	Bergman et al. 2004	AP PF400-02-011	
	Bedrock geological map, Forsmark version 1.1	AP PF400-02-011	
	Bedrock geological map, Forsmark version 1.2	AP PF400-02-011	
	Revised bedrock geological map, Forsmark version 2.2	AP PF400-02-011	
	Revised bedrock geological map, Forsmark version 2.3	AP PF400-02-011	
	Stephens et al. 2008a		
<b>Ground geophysical data and lineament interpretation</b>			
Petrophysical and <i>in situ</i> gamma-ray spectrometric data from rock types	Mattsson et al. 2003	AP PF400-02-011	Input to RD modelling
	Isaksson et al. 2004a	AP PF400-02-047	
	Isaksson et al. 2004b	AP PF400-02-011 AP PF400-02-047	
High-resolution ground magnetic measurements	Isaksson et al. 2006a	AP PF400-05-082	Identification of magnetic lineaments and input for RD and DZ modelling
	Isaksson et al. 2006b	AP PF400-06-034	
	Isaksson et al. 2007	AP PF400-06-034	
Interpretation of topographic, bathymetric and helicopter-borne geophysical data. Lineament assessment	Isaksson et al. 2004c	AP PF400-02-047	Identification of magnetic lineaments and input for RD and DZ modelling
	Isaksson and Keisu 2004	AP PF400-02-047	
Correlation between seismic refraction, lineaments and DZ	Isaksson 2007		Input to DZ modelling
reflectors identified during reflection seismic survey	Balu and Cosma 2005		Input to DZ modelling
	Cosma et al. 2006		
	Cosma et al. 2003		
	Juhlin et al. 2002	AP PF400-03-84	
	Juhlin and Bergman 2004	AP PF400-03-84	
	Juhlin and Palm 2005	AP PF400-04-78	
<b>Data from cored boreholes from the construction of SFR</b>			
Technical data	Hagkonsult 1982a	–	Siting and orientation of the boreholes in the modelling work
	Hagkonsult 1983	–	
	Carlsson et al. 1986	–	
	Keisu and Isaksson 2004	AP PF400-02-048	
Geophysical logging and petrophysical data (KFR01, KFR02, KFR03, KFR04, KFR05, KFR19, KFR20)	Christiansson and Magnusson 1985a	–	Data used in geological SHI and input for RD and DZ modelling
	Christiansson and Magnusson 1985b	–	
	Mattsson 2009	AP SFR-09-009	
Older geological mapping including fracture logging	Hagkonsult 1983	–	Input to rock type coding according to SKB:s current nomenclature
	Christiansson and Magnusson 1985a	–	
	Christiansson and Magnusson 1985b	–	
	Christiansson 1986	–	

Data specification	Reference to data report	Reference in Sicada/GIS	Usage in version 1.0 analysis/modelling
Updated geological mapping and rock type coding	Petersson and Andersson 2011	AP SFR-07-004	Used in geological SHI and as input to RD and DZ modelling
	Petersson et al. 2011	AP SFR-09-014 AP SFR-09-020 AP SFR-09-028	
Geological SHI	Petersson et al. 2011	AP SFR-09-014 AP SFR-09-020 AP SFR-09-028	Input for RD and DZ modelling
	Petersson et al. 2009a	AP SFR-07-005	
<b>Data from cored and percussion boreholes from the period 2006 to 2009</b>			
Technical data (HFM34, HFM35, HFR101, HFR102, HFR105, HFR106, KFM11A, KFR27, KFR101, KFR102A, KFR102B, KFR103, KFR104, KFR105, KFR106)	Claesson et al. 2007	AP PF400-06-006 AP PF400-06-025	Siting and orientation of the boreholes in the modelling work
	Claesson and Nilsson 2007	AP PF400-06-027	
	Nilsson and Ullberg 2008	AP SFR-08-001	
	Nilsson and Ullberg 2009a	AP SFR-08-001 AP SFR-08-002	
	Nilsson and Ullberg 2009b	AP SFR-08-011	
	Nilsson and Ullberg 2009c	AP SFR-08-002 AP SFR-08-020	
	Nilsson G 2009a	AP SFR-09-015	
	Nilsson G 2009b	AP SFR-09-004	
Radar and BIPS logging (HFM34, HFM35, HFR101, HFR102, HFR105, HFR106, KFM11A, KFR27, KFR101, KFR102A, KFR102B, KFR103, KFR104, KFR105, KFR106)	Gustafsson and Gustafsson 2006a	AP PF400-06-046	Data used in borehole mapping (BIPS) and in geological SHI (radar logging) with a focus on the identification of brittle deformation zones. Input for both RD and DZ modelling
	Gustafsson and Gustafsson 2006b	AP PF400-06-046	
	Gustafsson and Gustafsson 2007	AP PF400-06-092	
	Gustafsson and Gustafsson 2008	AP SFR-08-003	
	Gustafsson and Gustafsson 2009a	AP SFR-08-017	
	Gustafsson and Gustafsson 2009b	AP SFR-09-011 AP SFR-09-019	
Geophysical logging, petrophysical data and interpretation of geophysical data (HFM34, HFM35, HFR101, HFR102, HFR105, HFR106, KFM11A, KFR27, KFR101, KFR102A, KFR102B, KFR103, KFR104, KFR105, KFR106)	Nielsen and Ringgaard 2007a	AP PF400-06-050	Data used in the borehole mapping and in geological SHI. Input for both RD and DZ modelling
	Nielsen and Ringgaard 2007b	AP PF400-06-103	
	Nielsen and Ringgaard 2008	AP SFR-08-004	
	Nielsen and Ringgaard 2009a	AP SFR-08-018	
	Nielsen and Ringgaard 2009b	AP SFR-09-010	
	Nielsen and Ringgaard 2009c	AP SFR-09-018	
	Mattsson and Keisu 2007a	AP PF400-06-074	
	Mattsson and Keisu 2007b	AP PF400-07-018	
	Mattsson and Keisu 2009a	AP SFR-08-010	
	Mattsson and Keisu 2009b	AP SFR-08-010 AP SFR-08-019	
	Mattsson and Keisu 2010	AP SFR-09-017	
	Boremap mapping (HFM34, HFM35, HFR101, HFR102, HFR105, HFR106, KFM11A, KFR27, KFR101, KFR102A, KFR102B, KFR103, KFR104, KFR105, KFR106)	Döse and Samuelsson 2007	
Petersson et al. 2007		AP PF400-06-094	
Döse 2009		AP SFR-08-006	
Döse et al. 2009a		AP SFR-08-006	
Döse et al. 2009b		AP SFR-08-015	
Winell et al. 2009a		AP SFR-09-001	
Winell et al. 2009b		AP SFR-08-028	
Winell 2009		AP SFR-09-012	
Winell 2010a		AP SFR-09-027	
Winell 2010b		AP SFR-09-027	
Geological SHI (HFM34, HFM35, HFR101, HFR102, HFR105, HFR106, KFM11A, KFR27, KFR101, KFR102A, KFR102B, KFR103, KFR104, KFR105, KFR106)		Carlsten et al. 2007	AP PF400-07-016
	Petersson et al. 2009b	AP SFR-08-009	
	Petersson et al. 2009c	AP SFR-08-009	
	Petersson et al. 2009d	AP SFR-08-009	
	Petersson et al. 2009e	AP SFR-08-009	
	Petersson et al. 2010b	AP SFR-09-026	
	Petersson et al. 2010a	AP SFR-09-026	



Data specification	Reference to data report	Reference in Sicada/GIS	Usage in version 1.0 analysis/modelling
<b>Data from tunnel mapping</b>			
Geological tunnel mapping and interpretation of fracture zones	Christiansson and Bolvede 1987	–	Input to modelling in proximity of the SFR facility
	Berglund 2009	AP SFR-07-007	
<b>Previous models</b>			
SFR structural models	Carlsson et al. 1985	–	Input to DZ modelling of zones H2, 3, 6, 8 and 9
	Carlsson et al. 1986	–	
	Christiansson 1986	–	
	Axelsson and Mærsk Hansen 1997	–	
Forsmark SDM versions and stages 0, 1.1, 1.2, 2.1, 2.2 and 2.3. SDM-Site Forsmark	SKB 2002	The approved models are stored in the SKB model database	Conceptual understanding and comparison
	SKB 2004		
	SKB 2005		
	SKB 2006		
	Olofsson et al. 2007		
	Fox et al. 2007		
	Stephens et al. 2007		
	Stephens and Skagius 2007		
	Sandström et al. 2008		
	Stephens et al. 2008b		
SKB 2008b			
SFR SDM version 0	SKB 2008a	–	Introduction to available data
SFR geological model 0.1	Curtis et al. 2009	AP SFR-08-021	Input to the SFR DZ model

**Table A3-2. Available hydrogeological bedrock data and their treatment in SFR model version 1.0**

Data specification	Reference to data report	Reference in Sicada/GIS	Usage in version 1.0 analysis/modelling	
<b>Data from cored and precussion boreholes from the construction of SFR</b>				
Single-hole hydraulic tests	Hagkonsult 1982b	–	Input to HCD modelling	
	Arnefors and Carlsson 1985	–		
	Carlsson et al. 1985	–		
	Andersson et al. 1986	–		
Carlsson et al. 1986	–			
<b>Data from cored and precussion boreholes from the period 2006 to 2009</b>				
Boremap mapping (KFR27, KFR101, KFR102A, KFR102B, KFR103, KFR104, KFR105, KFR106)	Döse 2009	AP SFR-08-006	Input to HRD and HCD modelling	
	Döse et al. 2009a	AP SFR-08-006		
	Döse et al. 2009b	AP SFR-08-015		
	Winell et al. 2009a	AP SFR-09-001		
	Winell et al. 2009b	AP SFR-08-028		
	Winell 2009	AP SFR-09-012		
	Winell 2010a	AP SFR-09-027		
Differential flow logging (PFL) (KFR27, KFR101, KFR102A, KFR102B, KFR103, KFR104, KFR105, KFR106)	Pekkanen et al. 2008	AP SFR-08-007	Input to HRD and HCD modelling	
	Kristiansson and Väisäsvaara 2008	AP SFR-08-016		Input to modelling of deterministic Shallow Bedrock Aquifer (SBA) structures
	Hurmerinta and Väisäsvaara 2009a	AP SFR-08-25		
	Hurmerinta and Väisäsvaara 2009b	AP-SFR-08-030		
	Väisäsvaara 2009	AP SFR-09-005		
Kristiansson et al. 2009	AP SFR-09-025			
Impeller flow logging (HTHB) (HFR101, HFR105, HFR106)	Jönsson et al. 2008	AP SFR-08-005	Input to HCD modelling	
	Thur et al. 2009	AP-SFR-09-013	Input to modelling of deterministic Shallow Bedrock Aquifer (SBA) structures	

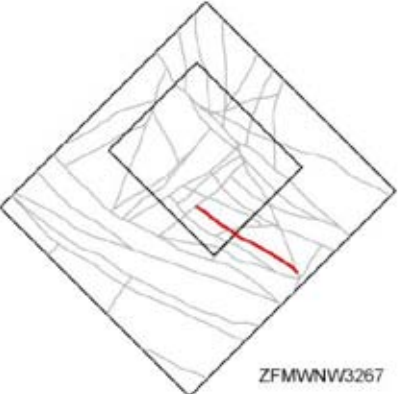
Data specification	Reference to data report	Reference in Sicada/GIS	Usage in version 1.0 analysis/modelling
Injection test (HFR102)	Jönsson et al. 2008	AP SFR-08-005	Input to modelling of deterministic Shallow Bedrock Aquifer (SBA) structures
PFL anomaly linking to Boremap data	Öhman and Follin 2010a	–	Input to HRD and HCD modelling Input to modelling of deterministic Shallow Bedrock Aquifer (SBA) structures
<b>Data from cross-hole (interference) tests</b>			
Interference tests	Arnefors and Carlsson 1985	–	Input to HCD modelling
	Andersson et al. 1986	–	Input to modelling of deterministic Shallow Bedrock Aquifer (SBA) structures
	Carlsson et al. 1986	–	
	Axelsson and Mærsk Hansen 1997	–	
	Walger et al. 2011	AP SFR-10-008	
<b>Groundwater levels</b>			
	Carlsson et al. 1986	–	Input to HCD modelling
	Jönsson 2010	–	Input to modelling of deterministic Shallow Bedrock Aquifer (SBA) structures
	Öhman et al. 2012	–	
<b>Observations within the existing SFR facility</b>			
Geological and hydrogeological tunnel mapping and interpretation of fracture zones	Christiansson and Bolvede 1987	–	Conceptual understanding and comparison Input to modelling of deterministic Shallow Bedrock Aquifer (SBA) structures
Data on performed grouting	Carlsson et al. 1986	–	Conceptual understanding and comparison Input to modelling of deterministic Shallow Bedrock Aquifer (SBA) structures
Tunnel inflow	Carlsson and Christiansson 2007	–	Conceptual understanding and comparison
	Lundin 2010	–	Input to HCD modelling Input to modelling of deterministic Shallow Bedrock Aquifer (SBA) structures
<b>Previous models</b>			
SFR structural models	Carlsson et al. 1985	–	Input to HCD modelling of zones H2, 3, 6, 8 and 9
	Carlsson et al. 1986	–	
	Christiansson 1986	–	
	Axelsson and Mærsk Hansen 1997	–	
SDM-Site Forsmark	SKB 2008b	The approved models are stored in the SKB model database	Conceptual understanding and comparison
Regolith geology	Hedenström et al. 2008	The approved models are stored in the SKB model database	HSD model for groundwater flow modelling
	Bosson et al. 2008		
SFR geological model 1.0	Curtis et al. 2010	?	Input to HRD and HCD modelling
SFR hydrogeochemical model 0.2	Nilsson et al. 2010	?	Conceptual understanding and comparison
SFR hydrogeological model 0.0, 0.1, and 0.2	Odén 2009	?	Input to the SFR HRD and HCD model
	Öhman 2010	?	
	Öhman and Follin 2010a	?	
	Öhman and Follin 2010b	?	

**Table A3-3. Available hydrochemical bedrock data and their treatment in SFR model version 1.0.**

Data specification	Reference to data report	Reference in Sicada/GIS	Usage in version 1.0 analysis/modelling
<b>Groundwater sampling and analyses</b>			
Early SFR boreholes	Nilsson A-C, 2009	AP SFR-08-023	Data used in modelling, Redox modelling
Complementary study	Nilsson K, 2011	AP SFR-10-010	Data used in modelling, Redox modelling
HFR101	Jönsson et al. 2008	AP SFR-08-005	Data used in modelling
HFR105	Jönsson et al. 2008	AP SFR-08-005	Data used in modelling
HFR106	Thur et al. 2009	AP SFR-09-013	Data used in modelling
HFM34	Berg C, 2006	AP PF 400-06-037	Data used in modelling
HFM35	Berg C, 2006	AP PF 400-06-037	Data used in modelling
KFR101 (and KFR02, KFR7A, KFR08, KFR56)	Thur and Nilsson, 2009a	AP SFR-09-003, AP SFR-08-026	Data used in modelling
KFR102A	Thur and Nilsson, 2009b	AP SFR-09-003	Data used in modelling
KFR104	Nilsson et al. 2011	AP SFR-09-029	Data used in modelling
KFR105	Lindquist and Nilsson, 2010	AP SFR-09-022 AP SFR-09-031	Data used in modelling Redox modelling
KFR106	Sandström et al. 2011	AP SFR-09-029	Data used in modelling
KFM11A	Berggölin et al. 2007	AP PF 400-07-004	Data used in modelling
<b>Fracture minerals</b>			
KFR01, KFR08, KFR10, KFR19, KFR7A and KFR105	Sandström and Tullborg, 2011	AP SFR-10-009	Fracture mineralogy and geochemistry. Redox and pH buffer capacity.
KFR106	Sandström et al. 2011	AP SFR-11-002	Fracture minerals incl. uranium Uranium study, redox and pH buffer capacity.
<b>Microbes and gases</b>			
KFR105	Lindquist and Nilsson, 2010	AP SFR-09-022	Data used in modelling
<b>Previous models</b>			
SFR SDM version 0	Laaksoharju and Gurban, 2003	–	Introduction to available data and previous mixing modelling
SFR hydrochemical model 0.1	Nilsson A-C, 2009	AP SFR-08-023	Introduction to available data
SFR hydrochemical model 0.2	Nilsson et al. 2010a	AP SFR-09-008	Explorative analysis and preliminary modell
SFR hydrochemical background report to version 1.0	Gimeno et al. 2011	–	Water-rock interaction and mixing modelling
Forsmark SDM versions 2.2 and 2.3. SDM-Site Forsmark	Laaksoharju et al. 2008 SKB 2008b	The approved models are stored in the SKB model database	Conceptual understanding and comparison

## Properties of deformation zones modelled to intersect the SFR local model volume

The geological and hydrogeological properties of the 28 deformation zones that have been modelled to intersect the SFR local model volume in version 1.0 are summarized in the tables in this appendix.

Deformation zone –zone name	
<p><b>Borehole and tunnel intersections (metres along borehole/tunnel)</b></p> <p>KFRxx: xx–xx m, refers to target interval sec_up and sec_low. (DZxx xx–xx m) refers to corresponding SHI PDZ sec_up and sec_low.</p> <p>Normally target intervals and SHI PDZ intervals in boreholes are identical but, in certain cases, they may differ due to other factors being involved in the overall zone interpretation.</p>	 <p>The regional and local SFR model boundaries shown together with the position of the modelled deformation zones at the ground surface. The zone under consideration is shown in colour.</p>
<p><b>Deformation style, alteration and geometry</b></p> <p><b>Deformation style:</b> Brittle and/or ductile.</p> <p><b>Alteration:</b> Type and degree of alteration.</p> <p><b>Strike/dip (span) right-hand-rule:</b> xxx / xx. The quoted span is a judgement based on a general assessment of all the available data and experience gained from the modelling work.</p> <p><b>Trace length at ground surface (span):</b> xx m. Total length of the deformation zone trace interception with the ground surface without reference to model boundaries. The span is a judgement based on all the available data, in particular a review of the magnetic data with consideration to the lineament continuity and extent.</p> <p><b>Model thickness (span):</b> x m. Distance between the two surfaces that have been modelled to envelop the longest intersection in all the borehole target intercepts (see Figure 5-4 in the main report). This is somewhat different from the method used in the Forsmark site investigation /Stephens et al. 2007/ where, in most cases, the modelling was based on a single or only a limited number of borehole intercepts and the true thickness was calculated from a single borehole intersection or the average of more than one borehole intersection if present. The quoted span is a judgement based on a general assessment of all the available data and experience gained from the modelling work.</p> <p><b>Confidence in existence:</b> Confidence level rated as high (coloured red in the model) /medium (coloured green in the model) /low (coloured grey in the model).</p>	
<p><b>Modelling procedure:</b> A short outline of the basis for the modelled geometry representing the deformation zone.</p>	

## Deformation zone –zone name

### Hydraulic interpretation

**Hydraulic width:** x m. Average hydraulic thickness calculated as the average true thickness (intersection-angle compensated) of all intercepts. For HCDs without intercepts the hydraulic width is taken as 72% of the geologic envelope, based on pooling of HCDs that have intercepts. For HCDs that exist inside SDM-Site Forsmark and where no additional information has been gained from the SFR investigations, the thickness is taken directly from SDM-Site Forsmark.

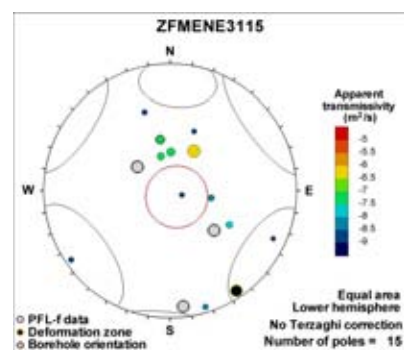
**No of intercepts:** x. Number of intercepts with hydraulic data that are judged representative for the HCD. The number in brackets indicate that additional intercepts exist, but that hydraulic data are unavailable, or judged to be misleading due to junction with other deformation zones that may dominate.

**$T_{\text{eff}}(0)$ :** x m<sup>2</sup>/s. Effective transmissivity at z=0. Calculated as the geometric mean of all intercept transmissivities  $T(z)$  after a depth-trend compensation to z=0. Below,  $T_0$  is short for  $T(z=0)$  or  $T(0)$ .

**Log  $T_{\text{eff}}(0)$ :** x,  $\sigma = x$ . Common logarithm of the effective transmissivity at z=0 and the standard deviation of all log  $T(0)$  values, respectively.

The standard deviation in modeled logarithmic transmissivity values is estimated as  $(\log T_{0,\text{max}} - \log T_{0,\text{min}})/4$  (i.e., assuming that the range in evaluated log  $T_0$  corresponds to  $\pm 2\sigma$ ). For zones with less than 3 intercepts, the standard deviation is assumed equal to 0.55 (indicated by parentheses) taken from the average of zones with more than 3 intercepts.

**Calculation procedure:** A short outline of the basis for the calculation procedure.



Stereogram illustrating PFL-f data orientation coloured and scaled by apparent transmissivity. The term apparent transmissivity is used to emphasise that measurements may be subject to upstream hydraulic chokes. Hard sectors representing fracture set clusters and orientations of boreholes and the modelled deformation zone are included as reference. For further details describing the plotting procedure see below.

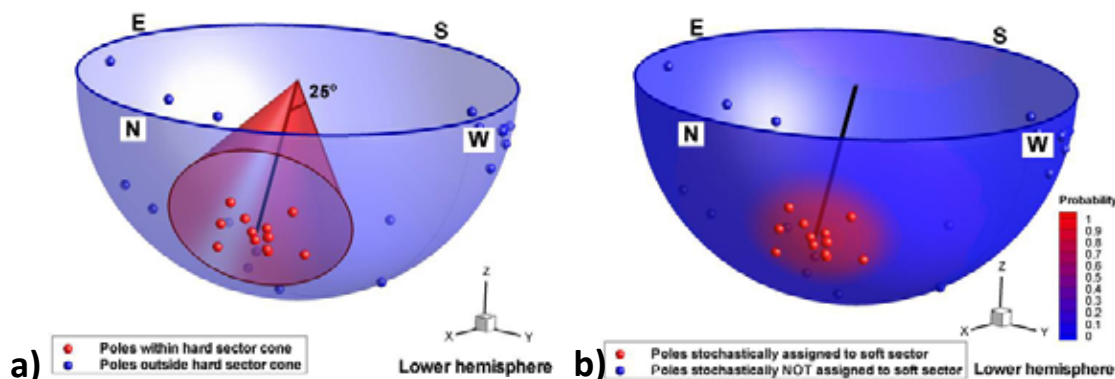
## Fractures in the deformation zone

### General characteristics

**Fracture orientation:** Terzaghi weighted stereograms of open/party open and sealed fractures. The summary stereograms show fractures from one or several borehole target intercepts, if such data are available and have been included in the interpretation. The plots show the clusters of fractures identified by a process of hard and soft sectoring as outlined below. Further details describing this process are reported in /Stephens et al. 2007/. A soft-sector division is difficult to carry out manually. For this reason, clusters are initially approximated in terms of hard sectors (manually) and are transformed into soft sectors (numerically) before Fisher parameterization is calculated.

**Visualisation of hard sector definitions: ZFMENE1061B**  
 Hard sector centre vector: 333°/30°  
 Hard sector solid angle: 25°

**Visualisation of soft sector definitions: ZFMENE1061B**  
 Soft sector mean pole: 332°/30.6°  
 Fisher K: 89.2



*Visualization of principles used; a) a manually hard-sector defined set is transformed into b) a soft sectoring probability field, figure taken from /Stephens et al. 2007/. Note that, for example, the soft sector  $P=0.5$  is defined by the characteristics of the fractures inside the hard sector, and does not necessarily coincide with the initial hard sector solid angle (25°).*

**Fracture frequency:** Mean fracture frequency m<sup>-1</sup> for the deformation zone based on one or several borehole target intercepts. However, data quality is not mixed. If KFR borehole data from the latest drilling campaign are available, they are used exclusively and are not mixed with lower quality HFR or older KFR borehole data. Open/party open and sealed fractures are quoted

## Deformation zone –zone name

separately.

**Fracture mineralogy:** A histogram of mineral coating or mineral filling along fractures inside a deformation zone based on one or several borehole target intercepts. If KFR borehole data from the latest drilling campaign are available, they are used exclusively and not mixed with lower quality HFR or older KFR borehole data. Open/partly open and sealed fractures are shown separately. Where Boremap data from older KFR boreholes without BIPS image are available, broken and unbroken fractures are indicated as undifferentiated grey columns.



Photo of drill core from part of the deformation zone. Generally part of a core zone if such has been identified during the single-hole interpretation. The depth numbers shown at the top of each core box are generally unadjusted measurements (not based on detailed borehole geometry survey) since photography was performed at an early stage prior to the down-hole survey. However, the numbers rarely differ more than one decimetre from the adjusted borehole length.

**BOREHOLE AND TUNNEL INTERCEPT DETAILS- for the named deformation zone**

Borehole intersections for – deformation zone name				
BH	Geometrical Intercept		Target intercept	
	Sec_up BH length (m) [z (-m)]	Sec_low BH length (m) [z (-m)]	Sec_up BH length (m) [z (-m)]	Sec_low BH length (m) [z (-m)]
KFRxx (BH name)	xx= borehole length m [xx= elevation (-masl)]	xx= borehole length m [xx= elevation (-masl)]	xx= borehole length m [xx= elevation (-masl)]	xx= borehole length m [xx= elevation (-masl)]
	Eoh= end or bottom of borehole	BH= borehole	See section 5.1.2 in the main report for the definition of geometrical and target intercepts. In some cases geometrical intercepts are listed without any corresponding target intercepts. This means that the drill core in a borehole in this interval shows no signs of deformation that can be correlated with the specific modelled deformation zone. This may be due to zone heterogeneity where parts of a zone have similar characteristics to the surrounding rock mass.	

**Comment:** Infilled, if necessary.

**SHI DZx xxx–xxx m:** Possible deformation zone (PDZ) in geological single-hole interpretation with a defined sec\_up and sec\_low borehole length. The text description of the drill core and interpreted PDZ character have been extracted from the published SHI report.

**Hydraulic data**

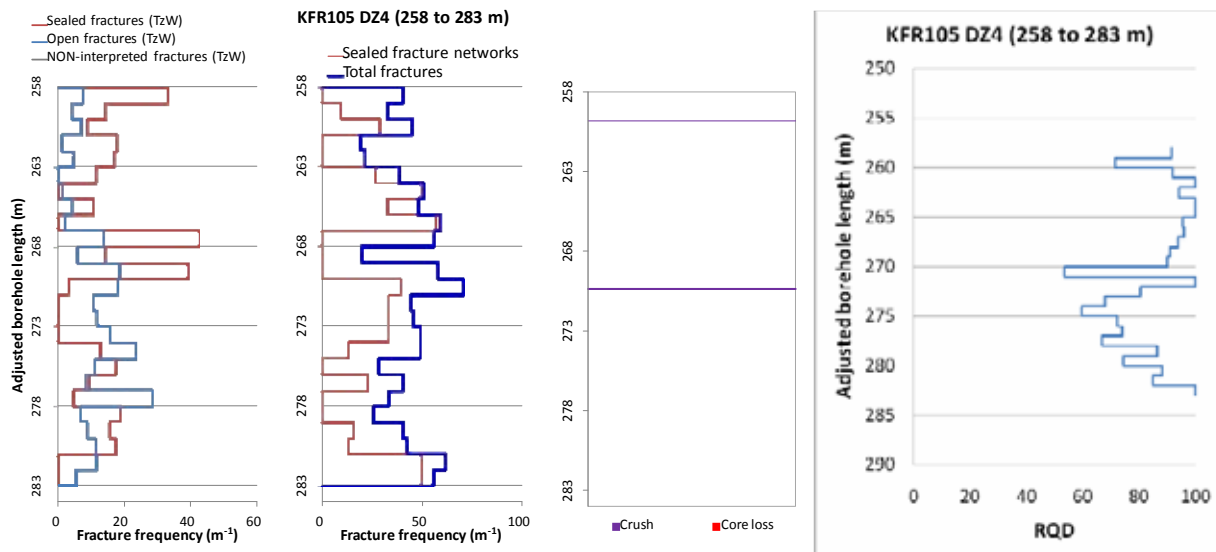
$T = x \text{ m}^2/\text{s}$ . Transmissivity. Interpreted representative values, based on available data partly inside the intercept . Considered uncertain, but necessary to provide a balanced interpretation of the zone (only ZFMNE0870 and ZFMNE3118). Transmissivity values in parenthesis are rejected data values.

$\text{Log } T_0 = x$ . The common logarithm of  $T(z)$  at  $z=0$  ( $= T_0$ ) after a depth-trend compensation.

**Fracture orientation:** Terzaghi weighted stereograms of open/partly open and sealed fractures for the individual specified borehole intercept where oriented fracture data are available).

**Fracture mineralogy:** A histogram of mineral coating or mineral filling along fractures inside a deformation zone based on the individual specified borehole intercept.

**Fracture frequency and RQD plots for the individual specified borehole intercept:**



The first figure shows the Terzaghi-corrected (TzW) frequencies of sealed and open (including partly open) fractures, as well as the Terzaghi-corrected frequencies of broken and unbroken fractures in old SFR boreholes, where BIPS information is lacking and

### Borehole intersections for – deformation zone name

The first figure shows the Terzaghi-corrected (TzW) frequencies of sealed and open (including partly open) fractures, as well as the Terzaghi-corrected frequencies of broken and unbroken fractures in old SFR boreholes, where BIPS information is lacking and a division into open and sealed fractures is not possible, i.e. so-called NON-interpreted fractures, within the modelled deformation zone (DZ) in each borehole. Fracture frequency,  $P_{10}$  (number of fractures/m), was calculated for 1 m bins, starting from (adjusted) SEC\_UP along the DZ. The lowest bin is constrained by the (adjusted) SEC\_LOW and may, therefore, be smaller than 1 m. For example, a DZ defined between 100.5 m to 103.0 m, will be resolved into three bins: 100.5 to 101.5 m, 101.5 to 102.5 m, and 102.5 to 103.0 m. The Terzaghi-weighted  $P_{10}$  for each 1 m bin is calculated as:

$$P_{10} = \frac{\sum \frac{1}{\sin(\max[\alpha, \alpha_{\min}])}}{L}, \text{ minimum bias angle } \alpha_{\min} = 15^\circ (\Leftrightarrow \text{Max TzW} = 3.86)$$

where  $L = 1$  m,  $n$  is the number of fractures inside the bin and  $\alpha$  = maximum dip of the fracture relative to the drill core axis. The minimum bias angle is used to avoid artificial weights for small angles, where the effects of non-zero borehole radius are not negligible

The second figure presents fracture frequency information for sealed fracture networks and all the fractures (total fractures), the latter being defined as open (TzW) + sealed (TzW) + sealed network + crush. The third figure shows the occurrence of crush zone and core loss as actual borehole lengths, i.e. not binned. The Terzaghi weighing has not been implemented for sealed fracture networks and crush zones, since TzW concerns geometric bias owing to the orientation of planar features versus scan line (borehole). The orientation of a sealed fracture network or crush zone, itself, is generally unclear, even if the fractures inside such a structure are defined. Fracture frequency,  $P_{10}$  (number of fractures/m), for a sealed network or crush zone was calculated using the ratio  $1000 \text{ [mm/m]}/d \text{ [mm]}$ , where  $d$  is the piece-length of rock between fractures in the unit m. It is superimposed onto the DZ 1 m bins, by fractional section length inside each bin. For example, a crush with piece length 10 mm extends from 99.0 m to 102.0 m. The crush has a  $P_{10}$  of 100 [1/m]. The first bin in the example above, 100.5 to 101.5 m, will have a crush  $P_{10}$  of 100 [1/m], while the second bin, 101.5 to 102.5 m, will have a crush  $P_{10}$  of 50 [1/m], as only half of the second bin contains crush. Crush  $P_{10}$  is not shown explicitly, but included in the total frequency.

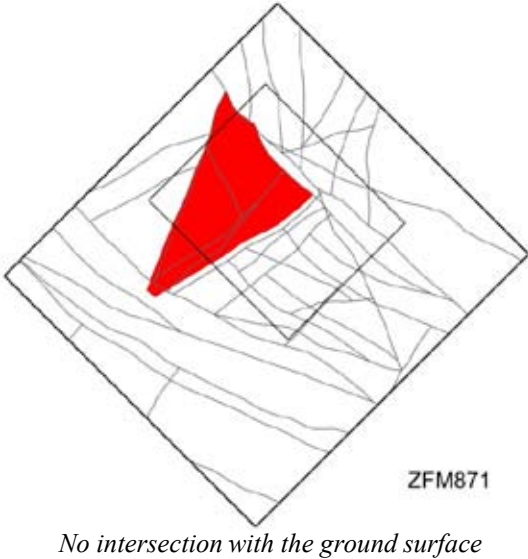
The fourth figure is a standard RQD (Rock Quality Designation) plot of the section of drill core.

### Tunnel intersections for – deformation zone name

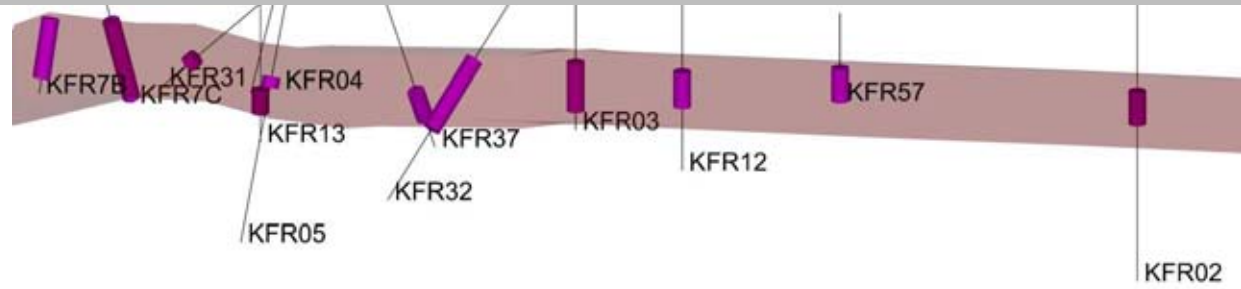
Tunnel	Geometrical intercept		Target intercept		Comment
	Start ch.(m)	End ch. (m)	Start ch.(m)	End ch. (m)	
Tunnel ID	xxx chainage  (x+xxx) Original chainage*	xxx chainage  (x+xxx) Original chainage*	xxx chainage  (x+xxx) Original chainage*	xxx chainage  (x+xxx) Original chainage*	DT = operating tunnel. BT = construction tunnel. See Figure 3-3 for other abbreviations. Chainage refers to tunnel centreline intersections.  * The numbering system used during the construction phase /Christiansson and Bolvede 1987/. These chainages are general zone boundary/tunnel wall intersections.



## Gently dipping deformation zones

<b>Deformation zone ZFM871</b>	
<p><b>Borehole and tunnel intersections (metres along borehole/tunnel)</b></p> <p>KFR02: 114.80–124.45 m (DZ3 114.80–124.45 m)            KFR03: 81.86–95.95 m (DZ4 81.86–95.95 m)            KFR04: 91–100 m            KFR05: 85.00–87.90 m (DZ1 85.00–87.90 m)            KFR7B: 0–17 m (DZ1 0–17 m)            KFR7C: 6–32 m (DZ1 6–32 m)            KFR12: 21.25–31.50 m (DZ1 21.25–31.50 m)            KFR13: 61–68 m (DZ4 61–68 m)            KFR31: 228.76–232.00 m (DZ2 228.76–232.00 m)            KFR32: 163.10–186.10 m (DZ2 163.10–186.10 m)            KFR37: 183.43–193.60 m (DZ2 183.43–193.60 m)            KFR57: 15.85–25.38 m (DZ1 15.85–25.38 m)            NBT: 0+405–0+432 m (tDZ101, tDZ102, tDZ103 and tDZ104 0+405–0+432)</p>	 <p style="text-align: right;">ZFM871</p> <p style="text-align: center;"><i>No intersection with the ground surface</i></p>
<p><b>Deformation style, alteration and geometry</b></p> <p><b>Deformation style:</b> Brittle</p> <p><b>Alteration:</b> Generally red-stained bedrock with fine-grained hematite dissemination, along with local argillization</p> <p><b>Strike/dip (span) right-hand-rule:</b> 074 / 19 (<math>\pm 10</math> / <math>\pm 5</math>)</p> <p><b>Trace length at ground surface:</b> No intercept with the ground surface (see modelling procedure for comment on terminations)</p> <p><b>Model thickness/ model thickness span:</b> 20 m / 1–22 m</p> <p><b>Confidence in existence:</b> High</p>	
<p><b>Modelling procedure:</b> This zone corresponds to zone H2 in earlier SFR models (see, for example, Axelsson and Hansen 1997/). It was renamed ZFM871 in the Forsmark stage 2.2 model /Stephens et al. 2007/. The zone has been modelled in SFR model version 1.0 as an undulating surface passing through a number of borehole control points. There is no corresponding magnetic lineament at the ground surface.</p> <p>Zone ZFM871 has been modelled to terminate at zones ZFMENE3115, ZFMNNE0869, ZFMNW0805A, ZFMNW0805B and ZFMWNW1035. The terminations at the surrounding steeply dipping zones and the resulting limited extent means that the zone no longer has an intersection with the sea bottom and no coincidence with a lineament. The termination at ZFMNNE0869 is particularly uncertain. A possible extension to the north-west is indicated in KFR10 though since this lies close to the meeting point of ZFM871 and ZFMNE0869 the extension has not been implemented. Similarly possible correlations exist in KFR7A, KFR24, KFR25 and KFR38 indicating an extension further to the all north-east. However, all these points lie within the modelled boundaries of the dominant ZFMNW0805A/B modelled deformation zone belt and consequently ZFM871 has been terminated ZFMNW0805A/B. Particular focus was placed on identifying a possible greater extent of the zone to the south-east, beyond ZFMENE3115, using the new borehole information. However, no geological evidence to support a further extent was identified.</p> <p>The zone is interpreted as consisting of a group of parallel oriented, smaller hydraulically conductive structures separated by ordinarily fractured rock. The spread of indications suggest that the structure is complex and has a stepped geometry.</p> <p>/Christiansson 1986/ reports the zone's character is very variable but generally has two to three gently dipping fracture sets, individually recorded zone thicknesses of up to 10 m and a hydraulic thickness varying from 2 to 20 m; the zone is associated with lenses of weathered and highly fractured rock, along with frequent clay-filled joints. The gently dipping fractures, in combination with an increased frequency of steeply dipping fractures, gives rise to the lenses being hydraulically interconnected.</p>	

## Deformation zone ZFM871



Section view of ZFM871 looking down dip to the south (modelled thickness 20m). SHI PDZ sections shown in pink.

## Hydraulic interpretation

**Hydraulic width:** 11.3 m

**No of intercepts:** 19 (4)

**$T_{\text{eff}}(0)$ :**  $6.38 \cdot 10^{-8} \text{ m}^2/\text{s}$

**Log  $T_{\text{eff}}(0)$ :**  $-5.2$ ,  $\sigma = 0.81$

**Calculation procedure:** The zone is interpreted as highly heterogeneous with poor connection to the sea (at least under current open repository conditions). The transmissivity value calibrated by /Holmén and Stigsson, 2001/ is assumed to be representative of the effective hydraulic properties of the zone, while hydraulic borehole data are interpreted to reflect its local-scale heterogeneity. Therefore, the SDM-Site Forsmark depth-trend model is applied to determine  $T_{\text{eff}}(0)$  based on the existing parameterisation of /Holmén and Stigsson, 2001/, which is taken to represent the elevation of the NDB1 tunnel intercept, i.e.,  $\log T_{\text{eff}}(z = -140 \text{ m}) = -5.2$ . Monitored drawdown in KFR27 and KFR104 suggests that it has hydraulic connectivity southeast of ZFMENE3115. Drawdown, hydrochemistry, and local peaks in transmissivity suggests extension to the northeast (beyond ZFMNW0805B), as well as, to the northwest (beyond ZFMNNE0869).

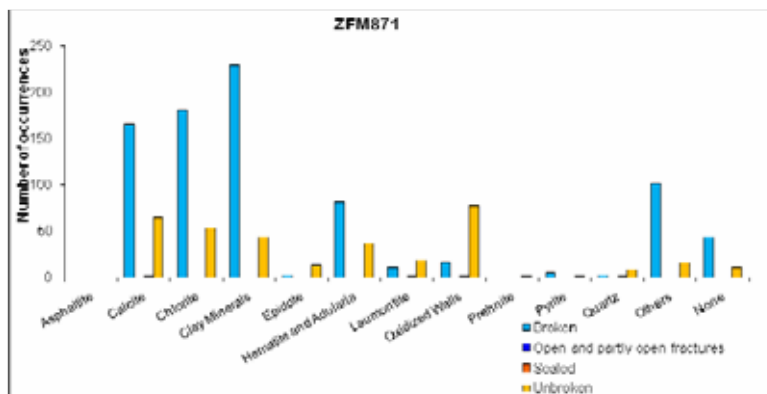
## Fractures in the deformation zone

### General characteristics




**Fracture orientation:** No oriented data available. Construction reports generally include the description of two dominantly gently dipping fracture sets as well as an increase in frequency of steeply dipping fractures /Christiansson and Bolvede 1987/.

**Fracture frequency:** no orientation corrected fracture frequencies are available. See individual older borehole intercepts for a general indication.

**Fracture filling mineralogy:**



## Deformation zone ZFM871

	<p>KFR02 DZ3 (114.80–124.45 m)</p> 
	<p>KFR05 DZ1 (85.00–87.90 m)</p> 
	<p>KFR31 DZ2 (228.76–232.00 m)</p> 
	<p>KFR57DZ1 (15.85–25.38 m)</p>

## Deformation zone ZFM871



## BOREHOLE AND TUNNEL INTERCEPT DETAILS

Borehole intersections for ZFM871				
BH	Geometrical Intercept		Target Intercept	
	Sec_up BH length (m) [z (-m)]	Sec_low BH length (m) [z (-m)]	Sec_up BH length (m) [z (-m)]	Sec_low BH length (m) [z (-m)]
KFR02	109.18 [194.61]	130.15 [215.58]	114.80	124.45
<b>Comment:</b>				
<p><b>SHI DZ3 114.80–124.45 m:</b> Increased frequency of broken fractures, with an average of c. 7 broken fractures/m. Generally high <math>\alpha</math>-angles. Highest frequency of broken fractures in the interval 116.70–117.65 m. Increased frequency of unbroken fractures that form networks in the interval 114.80–116.80 m. Faint to weak oxidation throughout the interval. Predominant minerals in broken fractures are calcite, hematite along with locally minor amounts of clay minerals and in the sealed fracture networks at 114.80–116.80 m adularia, quartz and calcite. Locally vugs in the sealed fracture networks. Pegmatitic granite (101061) and fine- to medium-grained metagranite-granodiorite (101057). Confidence level = 3.</p> <p>Moderate transmissivity of the tested section 81–136 m (<math>9 \cdot 10^{-8}</math> m<sup>2</sup>/s).</p>				
<p><b>Hydraulic data</b></p> <p><math>T = 1.95 \cdot 10^{-7}</math> m<sup>2</sup>/s</p> <p>Log <math>T_0 = -5.8</math></p> <p>Supported by two transient injection tests from 106 to 126 m BHL.</p>				
KFR03	78.33 [160.70]	99.73 [182.10]	81.86	95.95
<b>Comment:</b>				
<p><b>SHI DZ4 81.86–95.95 m:</b> Increased frequency of broken and unbroken fractures, which locally forms sealed networks. Approximately 9 broken fractures/m outside crushed intervals. Varying <math>\alpha</math>-angles with several conspicuous, clay-dominated fractures at angles &lt; 30°. Four minor crushes. Faint to weak oxidation and minor argillization associated with clay-dominated fractures. Predominant fracture minerals are clay minerals, Fe-hydroxide/hematite, chlorite and calcite, and in unbroken fractures also adularia. Distinct decrease in the SPR logging values along the section 85.0–93.0 m. Fine- to medium-grained granite (111058) and pegmatitic granite (101061). Confidence level = 3.</p> <p>Low transmissivity of the section 81–101.6 m (<math>2 \cdot 10^{-8}</math> m<sup>2</sup>/s).</p>				
<p><b>Hydraulic data</b></p> <p><math>T = 2.20 \cdot 10^{-8}</math> m<sup>2</sup>/s</p> <p>Log <math>T_0 = -6.9</math></p> <p>Notably low transmissivity in single pressure-build-up test 81 to 101.6 m BHL.</p>				
KFR04	84.50 [158.81]	eoh [174.26]	91	100
<p><b>Comment:</b> SHI interpreted two possible DZs in KFR04, DZ1 0–3 m and DZ2 14–63 m (BH length) neither of which correlates with ZFM871. However, there are planar chlorite-filled fractures from 86 m onwards and some clay-filled fractures towards the base of the borehole that could be associated with the zone (100.5 m). A target intercept is defined at 91–100 m.</p>				

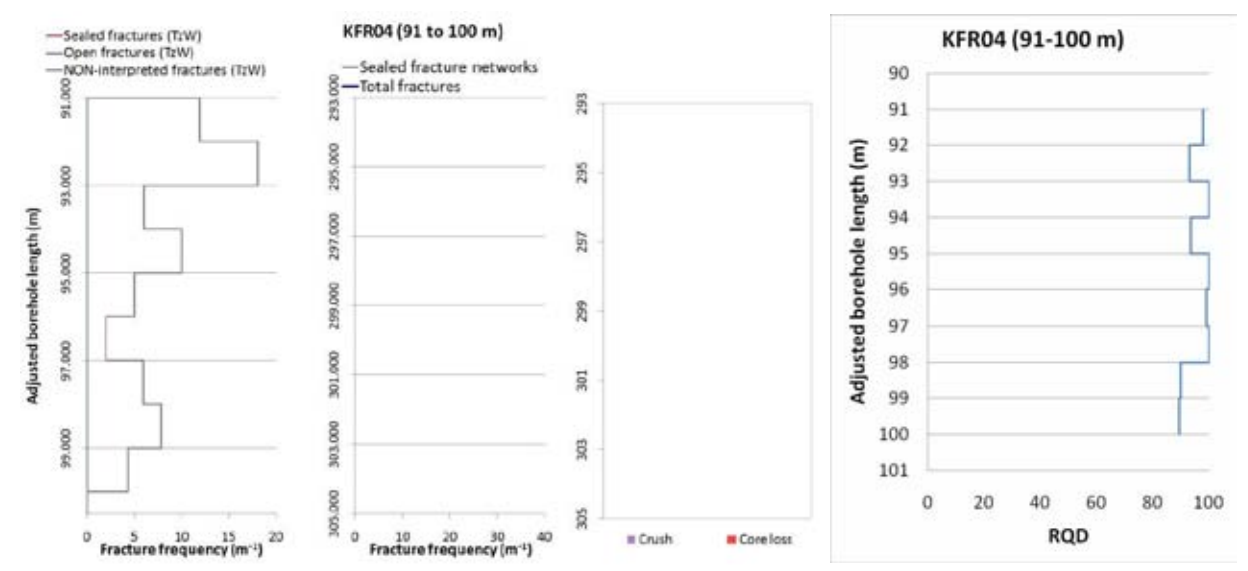
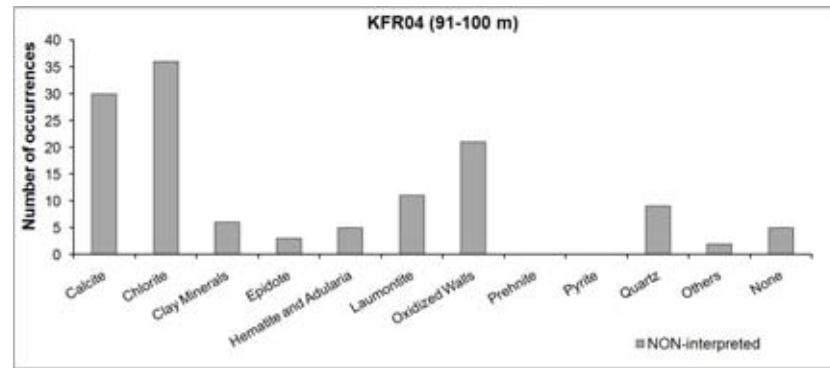
## Borehole intersections for ZFM871

### Hydraulic data

$$T = 5.00 \cdot 10^{-7} \text{ m}^2/\text{s}$$

$$\text{Log } T_0 = -5.6$$

Supported by single pressure-build-up test 84 to 100.5 m BHL.



BH	Geometrical Intercept		Target Intercept	
	Sec_up BH length (m) [z (-m)]	Sec_low BH length (m) [z (-m)]	Sec_up BH length (m) [z (-m)]	Sec_low BH length (m) [z (-m)]
KFR05	76.54 [149.08]	96.27 [167.63]	85.00	87.90

### Comment:

**SHI DZ1 85.00–87.90 m:** Increased frequency of broken fractures, most of them with  $\alpha$ -angles  $> 45^\circ$ . Crushed section at 85.25–86.22 m. Faint to weak oxidation throughout the interval. Predominant fracture minerals are Fe-hydroxide/hematite, calcite, clay minerals and chlorite. Distinct decrease in the SPR logging values along the section 84.2–86.8 m. There is also an anomaly in the fluid temperature data, with its minima at c. 86.6 m, which indicates in or out flow of water. Moderately foliated metagranite-granodiorite (101057). Confidence level = 3.

No hydraulic test data from this section of the borehole.

## Borehole intersections for ZFM871

### Hydraulic data

No data available.

BH	Geometrical Intercept		Target Intercept	
	Sec_up BH length (m) [z (-m)]	Sec_low BH length (m) [z (-m)]	Sec_up BH length (m) [z (-m)]	Sec_low BH length (m) [z (-m)]
KFR7B	0.00 [133.25]	20.39 [152.95]	0	17

**SHI DZ1 0–17 m:** Increased frequency of unbroken and especially broken fractures. Four crushed sections at 0.67–1.01, 4.14–4.33, 14.34–14.88 and 15.98–16.25 m and two core losses at 14.48–14.88 and 15.98–16.25 m. Predominant fracture minerals are calcite, chlorite and clay minerals, locally with hematite/Fe-hydroxide staining.  $\alpha$ -angles are ranging between 43 and 72°. Moderately foliated metagranite-granodiorite (101057) and pegmatitic granite (101061). Confidence level = 3.

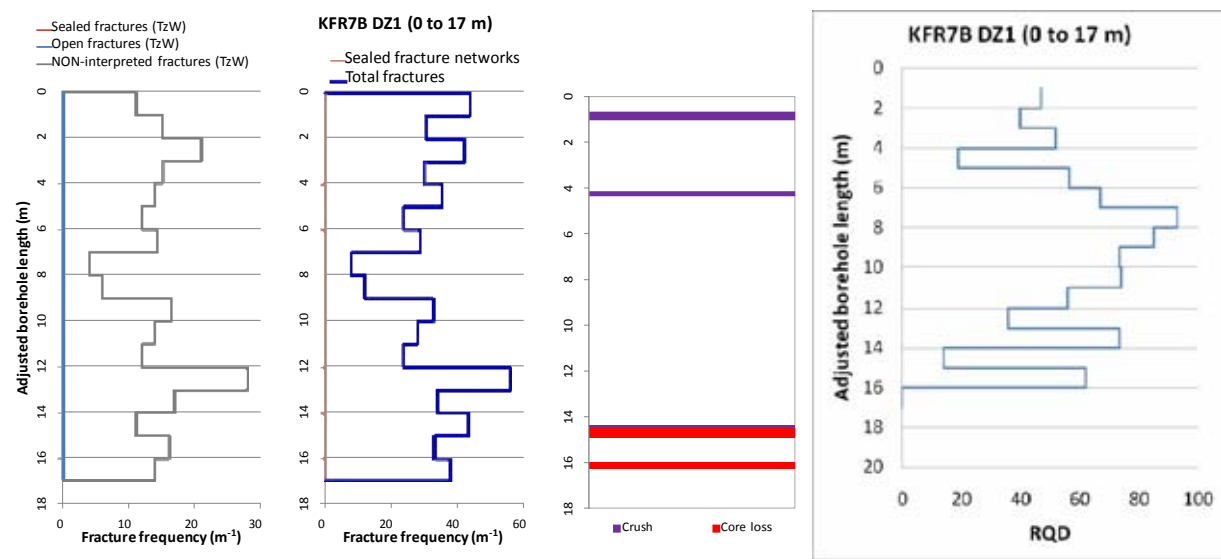
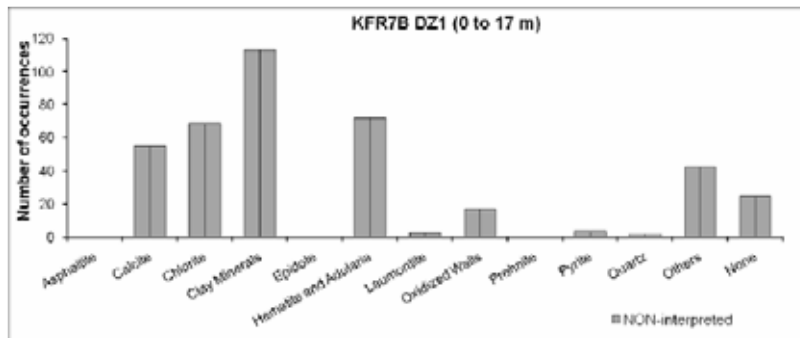
No hydrogeological investigation data from the upper 4 m of the borehole. Moderate hydraulic conductivity of  $1 \cdot 10^{-8}$  m/s in the interval 4–7 m. High hydraulic conductivity of  $2 \cdot 10^{-6}$  m/s in the interval 8–17 m.

### Hydraulic data

$$T = 2.60 \cdot 10^{-5} \text{ m}^2/\text{s}$$

$$\text{Log } T_0 = -4$$

Supported by single pressure build up test 7 to 21 m BHL.



**Borehole intersections for ZFM871**

BH	Geometrical Intercept		Target Intercept	
	Sec_up BH length (m) [z (-m)]	Sec_low BH length (m) [z (-m)]	Sec_up BH length (m) [z (-m)]	Sec_low BH length (m) [z (-m)]
KFR7C	5.91 [138.96]	32.74 [164.16]	6	32

**SHI DZ1 6–32 m:** Increased frequency of unbroken and especially broken fractures. Five crushes in the intervals 7.89–7.95, 8.11–8.19, 8.47–8.50, 9.25–9.40 and 14.67–14.77 m. Predominant fracture minerals are clay minerals, locally accompanied by Fe-hydroxide/hematite discolouration, chlorite and calcite. Most fractures have  $\alpha$ -angles that are moderate (29–74°). Virtually all laumontite-bearing fractures are concentrated in a zone with low  $\alpha$ -angles (9 and 10° for individual fractures) at 6.24–7.15 m length. Locally faint oxidation and minor argillization. Strongly foliated metagranite-granodiorite (101057), fine- to medium-grained granite (111058) and pegmatitic granite (101061). Confidence level = 3.

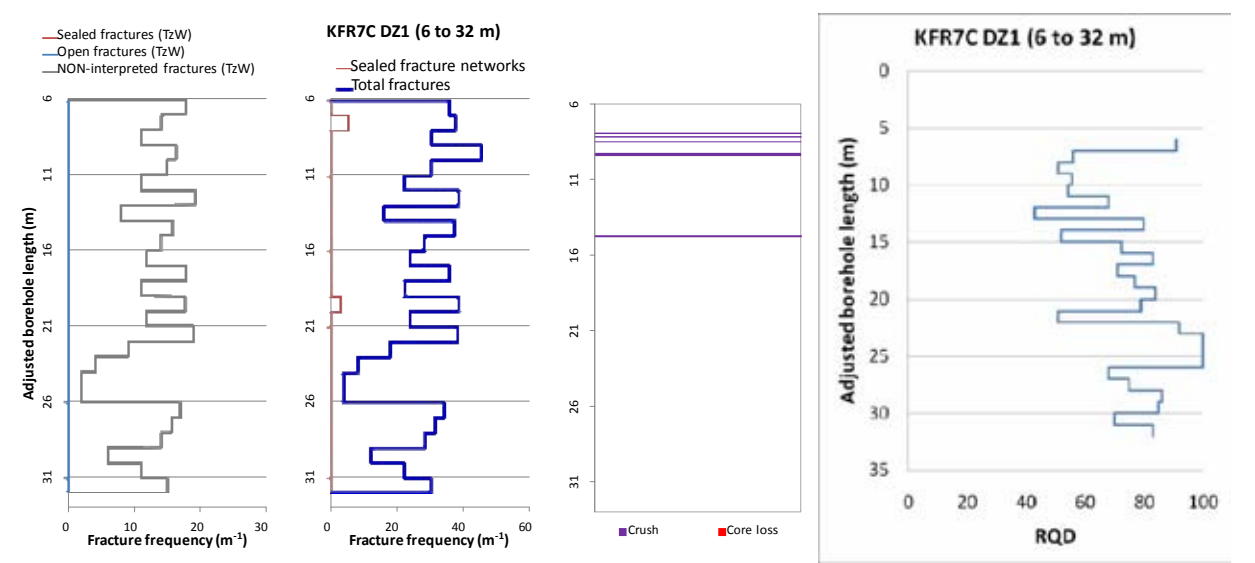
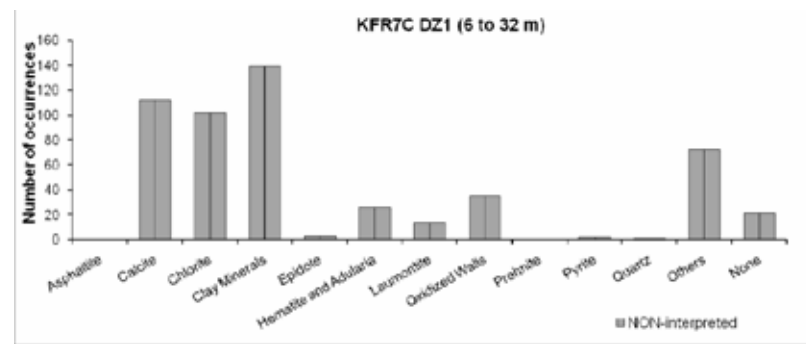
Moderate hydraulic conductivity  $2 \cdot 10^{-8}$  m/s throughout the interval.

**Hydraulic data**

$T = 6.72 \cdot 10^{-7} \text{ m}^2/\text{s}$

$\text{Log } T_0 = -5.5$

Supported by single pressure build up test 6 to 34 m BHL.





**Borehole intersections for ZFM871**

BH	Geometrical Intercept		Target Intercept	
	Sec_up BH length (m) [z (-m)]	Sec_low BH length (m) [z (-m)]	Sec_up BH length (m) [z (-m)]	Sec_low BH length (m) [z (-m)]
KFR12	14.73 [101.85]	36.77 [123.89]	21.25	31.50

**SHI DZ1 21.25–31.50 m:** Increased frequency of broken fractures. The section 24.30–25.64 m is generally crushed.  $\alpha$ -angles > 55°. Weak oxidation throughout the interval. Predominant fracture minerals are clay minerals, Fe-hydroxide/hematite and chlorite. Fine- to medium-grained granite (111058). Confidence level = 3.

Relatively high transmissivity of the section 20.0–33.0 m ( $3 \cdot 10^{-6} \text{ m}^2/\text{s}$ ). The transmissivity of this section is significantly elevated compared with the rest of the tested borehole sections.

**Hydraulic data**

$T = 2.60 \cdot 10^{-6} \text{ m}^2/\text{s}$

$\text{Log } T_0 = -5.1$

Supported by single pressure-build-up test 20 to 33 m BHL.

KFR13	53.36 [176.70]	74.99 [198.33]	61	68
-------	-------------------	-------------------	----	----

**SHI DZ4: 61–68 m:** Increased frequency of unbroken and especially broken fractures. Predominant fracture filling minerals are laumontite, chlorite and calcite. A number of broken fractures with clay minerals are concentrated along the section 60.1–64.5 m length. Their  $\alpha$ -angles range between 42 and 78°. Moderately foliated metagranite-granodiorite (101057) and fine- to medium-grained metagranodiorite-tonalite (101051). Confidence level = 1.

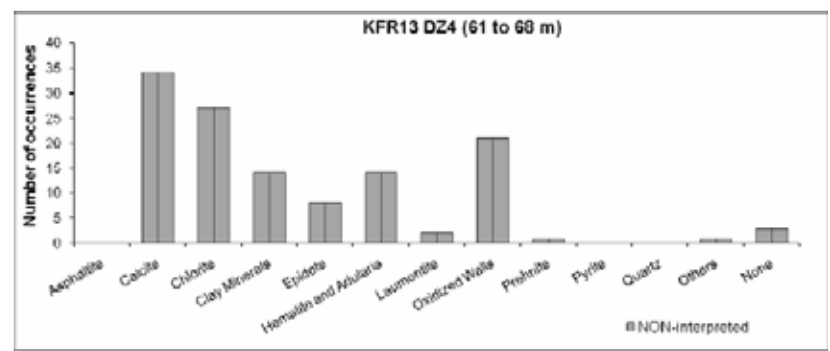
Increased hydraulic conductivity ( $1\text{--}2 \cdot 10^{-7} \text{ m/s}$ ) throughout the interval.

**Hydraulic data**

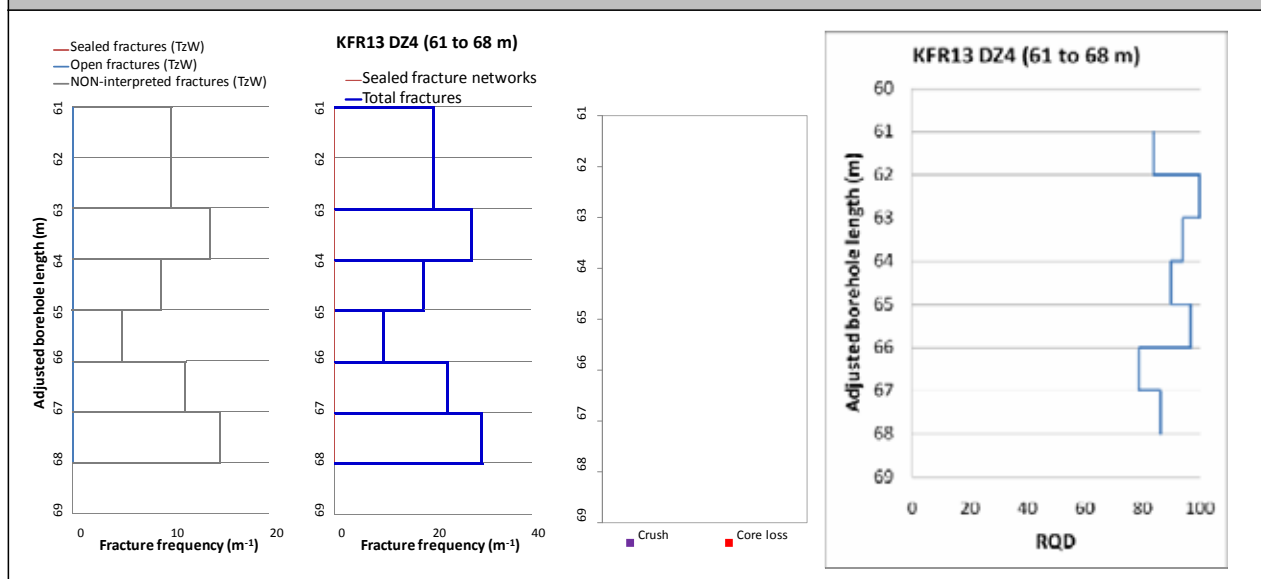
$T = 3.00 \cdot 10^{-6} \text{ m}^2/\text{s}$

$\text{Log } T_0 = -4.7$

Supported by two transient injection tests from 54 to 74 m BHL.



### Borehole intersections for ZFM871



BH	Geometrical Intercept		Target Intercept	
	Sec_up BH length (m) [z (-m)]	Sec_low BH length (m) [z (-m)]	Sec_up BH length (m) [z (-m)]	Sec_low BH length (m) [z (-m)]
KFR31	217.28 [143.72]	eoh [160.73]	228.76	232.00

**SHI DZ2 228.76–232.00 m:** Increased frequency of broken fractures and several crushed intervals.  $\alpha$ -angles generally  $> 45^\circ$  and typically parallel with the tectonic foliation. Generally faint to weak oxidation of the metagranite and faint to weak chloritization of the amphibolites. Predominant minerals in broken fractures are clay minerals, hematite, chlorite and calcite. Fine- to medium-grained metagranite-granodiorite (101057) and amphibolite (102017). Confidence level = 3.

Moderate transmissivity of the interval 204–242 m ( $9 \cdot 10^{-7} \text{ m}^2/\text{s}$ ).

#### Hydraulic data

$$T = 1.81 \cdot 10^{-6} \text{ m}^2/\text{s}$$

$$\text{Log } T_0 = -5.1$$

Poor resolution in hydraulic data. Hydraulic data in the interval 200 to 242.1 m used.

KFR32	161.72 [112.29]	186.25 [130.08]	163.10	186.10
-------	--------------------	--------------------	--------	--------

**SHI DZ2 163.10–186.10 m:** Increased frequency of unbroken fractures and especially broken fractures. More than 10 broken fractures/m throughout the interval.  $\alpha$ -angles generally  $> 45^\circ$ . Locally minor crushes. Weak to medium oxidation throughout the interval and weak to medium chloritization of amphibolites (102017). Predominant minerals in broken fractures are clay minerals, hematite, chlorite and calcite, and in unbroken fractures laumontite. Fine- to medium-grained metagranite-granodiorite (101057) and amphibolite (102017). Confidence level = 3.

High transmissivity of the interval 163–176 m ( $4 \cdot 10^{-5} \text{ m}^2/\text{s}$ ) and moderate transmissivity of the interval 176–187 m ( $2 \cdot 10^{-6} \text{ m}^2/\text{s}$ ).

### Borehole intersections for ZFM871

**Hydraulic data**

$T = 1.20 \cdot 10^{-4} \text{ m}^2/\text{s}$

$\text{Log } T_0 = -3.4$

Single packer data from 157 to 209 m BHL used.

BH	Geometrical Intercept		Target Intercept	
	Sec_up BH length (m) [z (-m)]	Sec_low BH length (m) [z (-m)]	Sec_up BH length (m) [z (-m)]	Sec_low BH length (m) [z (-m)]
KFR37	172.25 [148.38]	200.89 [173.79]	183.43	193.60

**SHI DZ2 183.43–193.60 m:** Increased frequency of broken fractures with an average of c. 10 broken fractures/m outside crushes. Variable  $\alpha$ -angles, but generally  $> 45^\circ$ . Crushed interval at 191.00–192.35 m. Generally weak to medium oxidation. Predominant minerals in broken fractures are clay minerals, hematite/Fe-hydroxide and locally chlorite. Fine- to medium-grained metagranite-granodiorite (101057) and pegmatitic granite (101061). Confidence level = 3.

High transmissivity of the interval 183–194 m ( $4 \cdot 10^{-5} \text{ m}^2/\text{s}$ ). The dominating transmissivity is contained in the in the section 191–194 m.

**Hydraulic data**

$T = 5.42 \cdot 10^{-5} \text{ m}^2/\text{s}$

$\text{Log } T_0 = -3.6$

Supported by high-transmissive data in the interval 183 to 209 m used.

KFR57	6.00 [93.60]	eoh [112.98]	15.85	25.38
-------	-----------------	-----------------	-------	-------

**Comment:**

**SHI DZ1 15.85–25.38 m:** Increased frequency of broken fractures. Varying  $\alpha$ -angles with generally low angles ( $< 30^\circ$ ) in the central part of the interval. Generally faint to moderate oxidation and at 16.80–21.50 m argillization, locally of strong intensity. Predominant minerals in broken fractures are clay minerals. Pegmatitic granite (101061), fine- to medium-grained granite (111058) and amphibolite (102017). Confidence level = 3.

No hydraulic test data from this borehole.

**Hydraulic data**

No data.

Borehole intersections for ZFM871				
BH	Geometrical Intercept		Target Intercept	
	Sec_up BH length (m) [z (-m)]	Sec_low BH length (m) [z (-m)]	Sec_up BH length (m) [z (-m)]	Sec_low BH length (m) [z (-m)]
KFR21	108.57 [108.57]	129.26 [129.26]	–	–
<b>Comment:</b> No drill core available.				
<b>Hydraulic data</b> $T = 1.21 \cdot 10^{-5} \text{ m}^2/\text{s}$ $\text{Log } T_0 = -4.4$ Well-supported by peaking transmissivity in the intercept. Hydraulic data in the interval 115 to 121 m used.				
KFR22	139.98 [121.22]	eoh [138.65]	–	–
<b>Comment:</b> No drill core available.				
<b>Hydraulic data</b> $T = 3.34 \cdot 10^{-6} \text{ m}^2/\text{s}$ $\text{Log } T_0 = -4.9$				
KFR23	81.75 [70.80]	105.07 [90.99]	–	–
<b>Comment:</b> No drill core available.				
<b>Hydraulic data</b> $T = 6.31 \cdot 10^{-5} \text{ m}^2/\text{s}$ $\text{Log } T_0 = -3.9$ Well-supported by peaking transmissivity in the intercept. Hydraulic data in the interval 71 to 107 m used.				
KFR33	158.04 [104.28]	eoh [110.49]	–	–
<b>Comment:</b> No drill core available.				
<b>Hydraulic data</b> $T = 3.90 \cdot 10^{-6} \text{ m}^2/\text{s}$ $\text{Log } T_0 = -4.9$ Supported by single packer data from 156 to 159 m BHL.				

Borehole intersections for ZFM871				
BH	Geometrical Intercept		Target Intercept	
	Sec_up BH length (m) [z (-m)]	Sec_low BH length (m) [z (-m)]	Sec_up BH length (m) [z (-m)]	Sec_low BH length (m) [z (-m)]
KFR80	0.00 [136.00]	13.29 [148.49]	–	–
<b>Comment:</b> No drill core available.				
<b>Hydraulic data</b> No data.				
KFR83	5.28 [90.23]	eoh [98.67]	–	–
<b>Comment:</b> No drill core available.				
<b>Hydraulic data</b> No data.				
KFR10	–	–	–	–
<b>Hydraulic data</b> T = $3.2 \cdot 10^{-5}$ m <sup>2</sup> /s Log T <sub>0</sub> = –4.5 Interpreted as a possible extension of ZFM871 beyond ZFMNNE0869 (from 95.65 m to 107.28 m BHL).				
KFR24	–	–	–	–
<b>Hydraulic data</b> T = $1.93 \cdot 10^{-5}$ m <sup>2</sup> /s Log T <sub>0</sub> = –4.7 Interpreted as a possible extension of ZFM871 beyond ZFMNW0805B (132 to 158 m BHL).				
KFR25	–	–	–	–
<b>Hydraulic data</b> T = $2.02 \cdot 10^{-5}$ m <sup>2</sup> /s Log T <sub>0</sub> = –4.7 Interpreted as a possible extension of ZFM871 beyond ZFMNW0805B (124 m to 154 m BHL).				

Borehole intersections for ZFM871				
BH	Geometrical Intercept		Target Intercept	
	Sec_up BH length (m) [z (-m)]	Sec_low BH length (m) [z (-m)]	Sec_up BH length (m) [z (-m)]	Sec_low BH length (m) [z (-m)]
KFR38	–	–	–	–
<p><b>Hydraulic data</b></p> <p><math>T = 4.2 \cdot 10^{-5} \text{ m}^2/\text{s}</math></p> <p><math>\text{Log } T_0 = -4.4</math></p> <p>Interpreted as a possible extension of ZFM871 beyond ZFMNW0805B (175 m to 185.4 m BHL).</p>				
KFR7A	–	–	–	–
<p><b>Hydraulic data</b></p> <p><math>T = 1.05 \cdot 10^{-4} \text{ m}^2/\text{s}</math></p> <p><math>\text{Log } T_0 = -3.4</math></p> <p>Interpreted as a possible extension of ZFM871 beyond ZFMNW0805B (2 m to 74.7 m BHL).</p>				

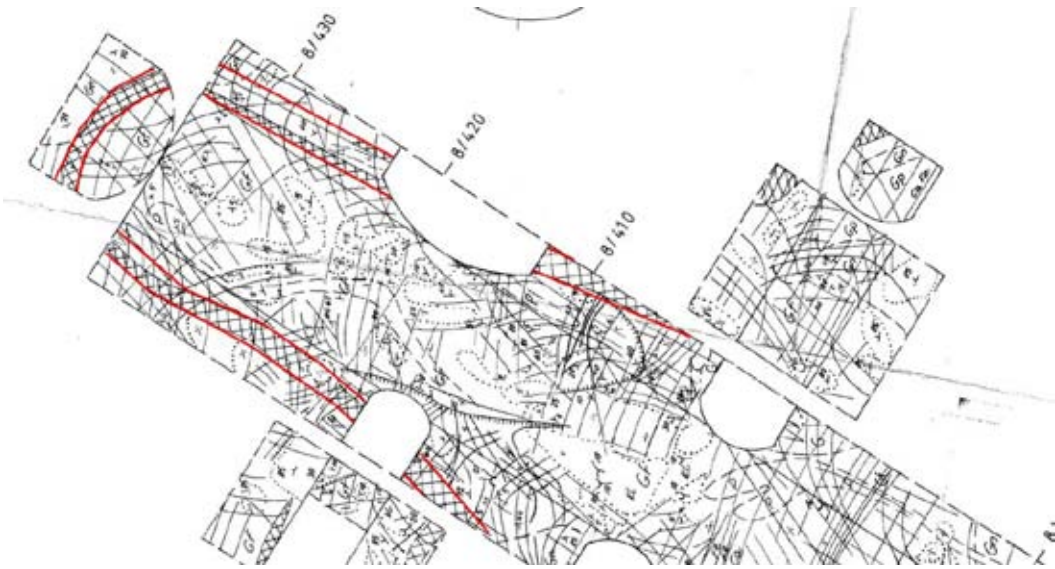
**Tunnel intersections for ZFM871**

Tunnel	Geometrical Intercept		Target Intercept	
	Start ch.(m)	End ch. (m)	Start ch.(m)	End ch. (m)
NBT	0+380	0+432 (End of tunnel)	0+405	0+432

**Comment:** Target intercept defined by (tDZ101, tDZ102, tDZ103 and tDZ104 0+405–0+432) in Appendix 2. 2009/. Control point added at chainage 0+405. Due to the gentle dip and nature of the zone the selected central point, representing the zone position, is approximate


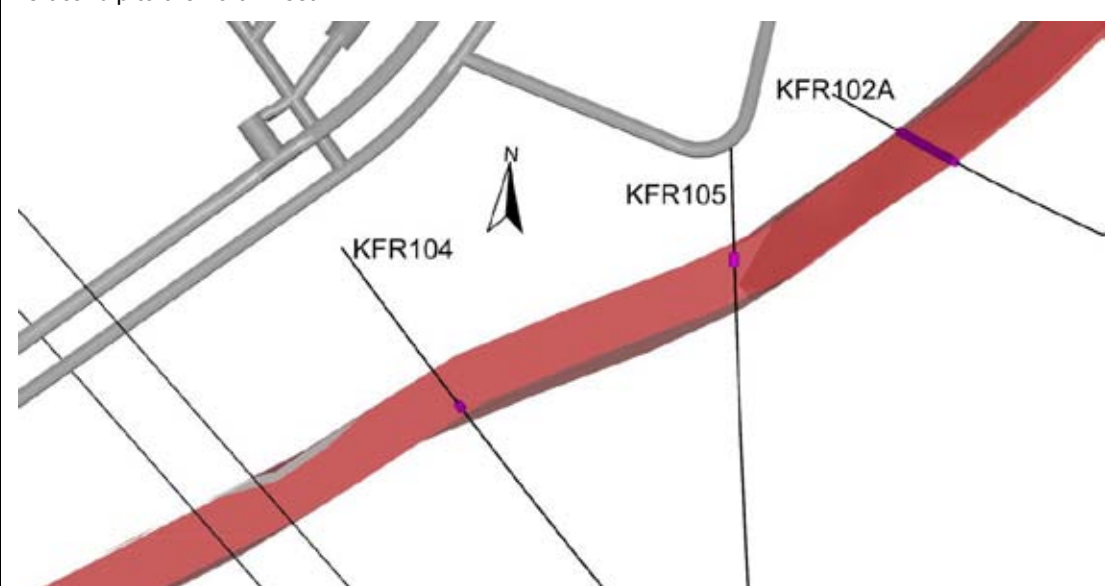
Note: /Axelsson and Hansen 1997/ estimate NBT 8+405 to 8+435 and that the zone also occurs in the connecting rock drainage basin (BB).

The modelled zone geometry also encompasses the rock drainage basin (BB), the support shaft (FS) and nearby niches (connection to the NBT at 0+405) but no detailed survey measurements are available for chainage estimates.



*Position of ZFM871 in the NBT shown by red outline and original cross hatching from detailed mapping drawing –17 of /Christiansson and Bolvede 1987/.*

## Steeply dipping NNE to ENE deformation zones

Deformation zone ZFMENE3115	
<p><b>Borehole and tunnel intersections (metres along borehole/tunnel)</b></p> <p>KFR102A: 422–503 m (DZ3 422–503 m)            KFR104: 149–154 m (DZ2 149–154 m)            KFR105: 45–52 m (DZ1 45–52 m)</p>	
<p><b>Deformation style, alteration and geometry</b></p> <p><b>Deformation style:</b> Brittle. Cohesive breccias present in all BH intercepts</p> <p><b>Alteration:</b> Locally red-stained bedrock with fine-grained hematite dissemination and argillization. Vuggy rock with quartz dissolution at 440.39–440.91, 441.64–441.76, 448.85–458.65, 473.15–474.14 and 478.35–478.42 m in KFR102A DZ3</p> <p><b>Strike/dip (span) right-hand-rule:</b> 236 / 84 (±5 / ±5)</p> <p><b>Trace length at ground surface (span):</b> 793 m (750–850 m)</p> <p><b>Model thickness (span):</b> 28 m (3–30 m)</p> <p><b>Confidence in existence:</b> High</p>	<p><b>Modelling procedure:</b> The position of the zone on the ground surface is based on the lineaments MFM3115G, MSFR08116 and MSFR10001 defined by magnetic minima (Ilsaksson et al. 2007) and SFR model version 1.0) with further extension to the south-west to allow termination at ZFMWNW1035. Forward modelling of magnetic data along profiles 20 and 42 (see Appendix 6) provide weak support for the modelled zone thickness and the sub-vertical dip to the north-west.</p>
	
<p><i>View of ZFMENE3115 looking down dip showing the SHI PDZ intercepts (pink cylinders) in KFR102A, KFR104 and KFR105. It should be noted that the modelled zone thickness of 28 m is based on KFR102A DZ3. An alternative interpretation of DZ3 is that it represents more than one zone and this would result in a reduction of ZFMENE3115 thickness to around 10 m.</i></p>	



## Deformation zone ZFMENE3115

### Hydraulic interpretation

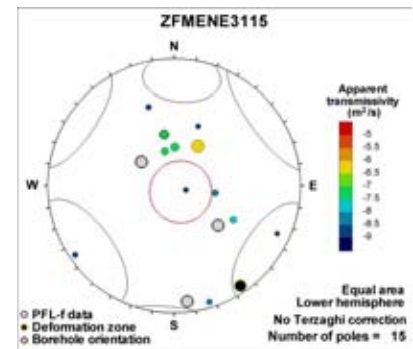
Hydraulic width: 4.8 m

No of intercepts: 3

$T_{\text{eff}}(0)$ :  $3.50 \cdot 10^{-7} \text{ m}^2/\text{s}$

Log  $T_{\text{eff}}(0)$ :  $-6.5$ ,  $\sigma = 0.91$

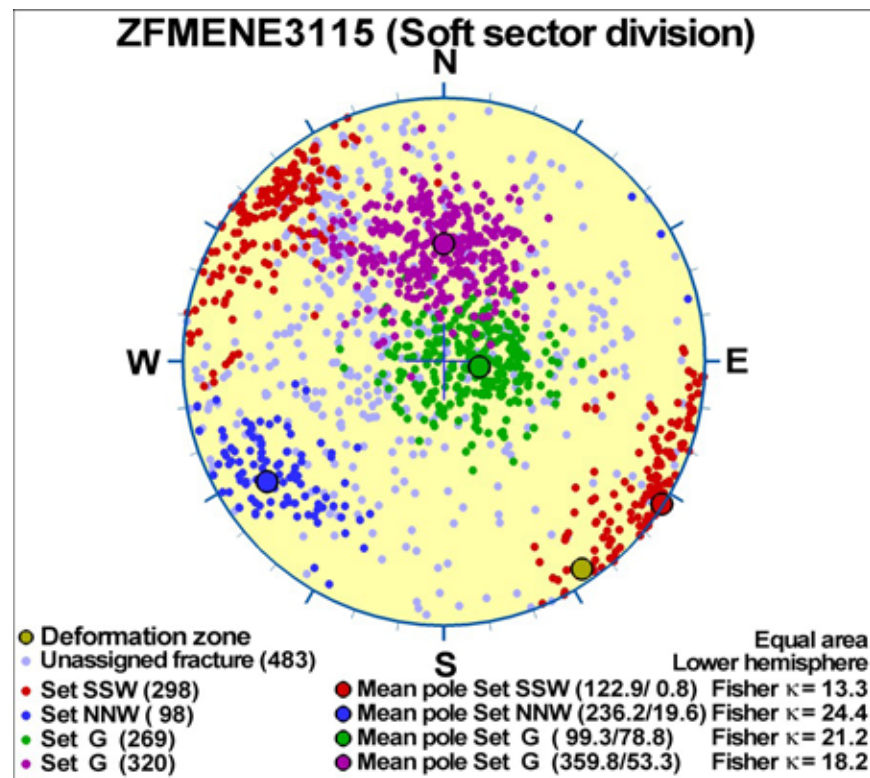
**Calculation procedure:**  $T_{\text{eff}}(0)$  taken as average from all 3 intercepts. The deep intercept in KFR102A is considerably more transmissive than other intercepts of NNE to ENE zones (particularly in context of the assumed depth trend). However, in the other two intercepts, PFL-f data exhibit the typical scattered pattern of rock mass in the Central Block.



## Fractures in the deformation zone

### General characteristics

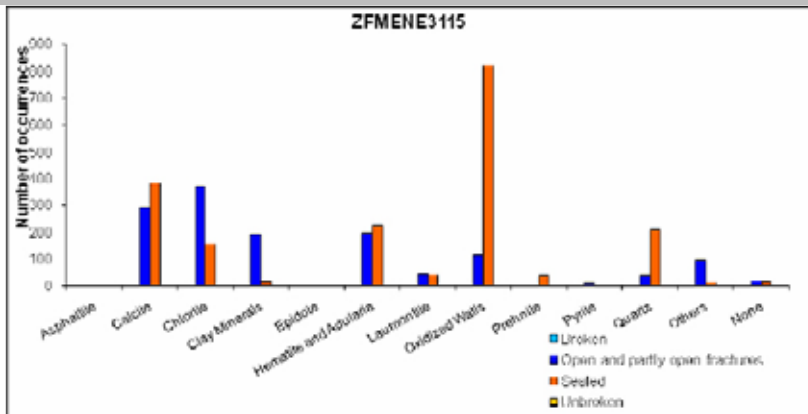
Fracture orientation:



Fracture frequency: Open  $10 \text{ m}^{-1}$ , Sealed  $31 \text{ m}^{-1}$

Fracture filling mineralogy:

## Deformation zone ZFMENE3115



KFR104 DZ2 (149–154 m)



KFR105 DZ1 (45–52 m)



## BOREHOLE AND TUNNEL INTERCEPT DETAILS

Borehole intersections for ZFMENE3115				
BH	Geometrical Intercept		Target Intercept	
	Sec_up BH length (m) [z (-m)]	Sec_low BH length (m) [z (-m)]	Sec_up BH length (m) [z (-m)]	Sec_low BH length (m) [z (-m)]
KFR102A	423.71 [380.72]	503.36 [451.30]	422	503

**SHI DZ3 422–503 m:** Increased frequency of open and sealed fractures in the intervals 422–444 and 461–503 m. Eight crushes with the most extensive at 434.65–435.90 m. Two slickensides. Fracture apertures generally up to 0.5 mm with a few ranging up to 2 mm and a local maximum up to 10 mm. Locally weak to strong oxidation, rarely argillisation, laumontitisation and carbonatitisation. Five intervals with quartz dissolution at 440.39–440.91, 441.64–441.76, 448.85–458.65, 473.15–474.14 and 478.35–478.42 m. Ductile deformation recorded at 466.46–466.09 m (019°/81°) and brittle ductile deformation recorded at 488.86–489.10 m (320°/41°). Predominant minerals in open fractures are chlorite, calcite, hematite, clay minerals, in sealed fractures calcite, quartz, adularia and chlorite and in sealed fracture networks calcite, quartz, chlorite and clay minerals. The entire possible deformation zone is characterised by poor radar penetration. The entire interval 422–503 m is characterized by significantly decreased bulk resistivity, several distinct caliper anomalies and decreased magnetic susceptibility. The most prominent low resistivity anomalies occur in the intervals 434–443, 451–458 and 471–475 m. In the section 450–457 m the density is significantly decreased, c. 2,570 kg/m<sup>3</sup>. Starting at 427 m the fluid temperature is characterized by several anomalies, and this pattern of anomalies continues through out the entire borehole length. Metagranite-granodiorite (101057), pegmatitic granite (101061) and amphibolite (102017). Confidence level = 3.

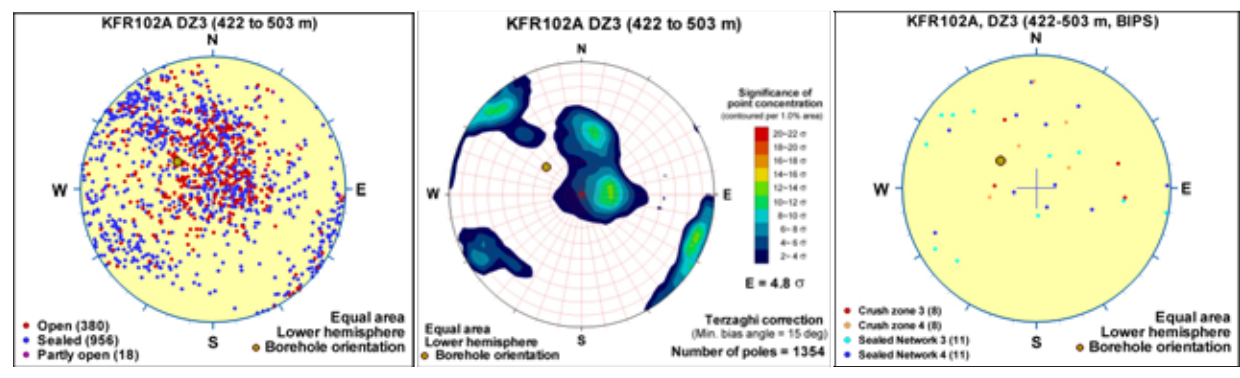
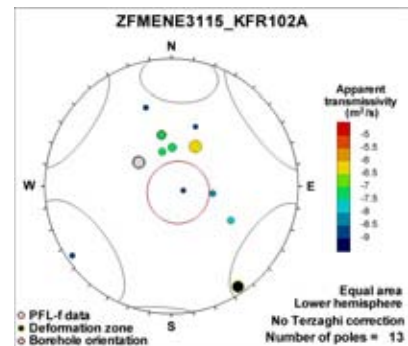
No flow anomalies above 427 m. Increased frequency of flow anomalies in the interval 427–458 m. No flow anomalies below 458 apart from one single flow anomaly at 474 m. The total transmissivity of the section is  $2 \cdot 10^{-6}$  m<sup>2</sup>/s, where the transmissivity is dominated by one single flow anomaly at 427 m ( $T = 1 \cdot 10^{-6}$  m<sup>2</sup>/s) and a number of flow anomalies at the section 435–441 m ( $T = 8 \cdot 10^{-7}$  m<sup>2</sup>/s). The character of the inflow indicates porous rock at 451–458 m.

### Hydraulic data

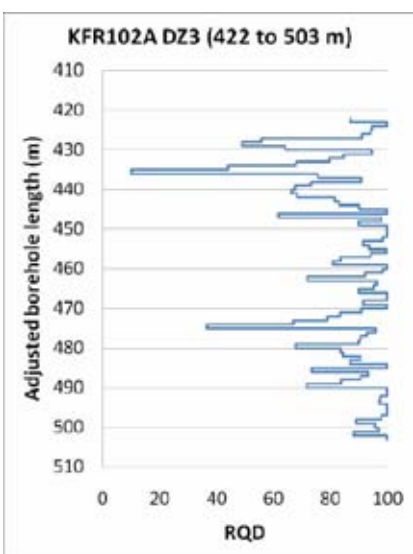
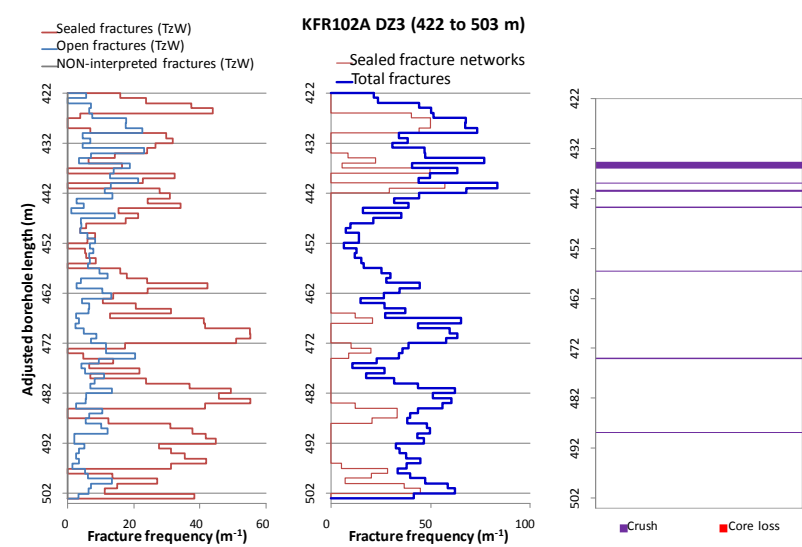
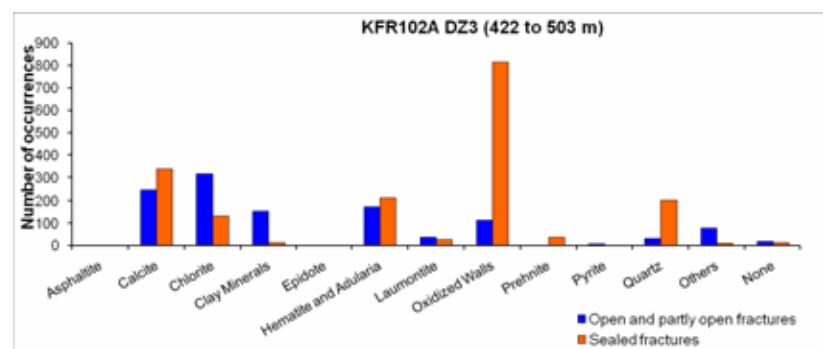
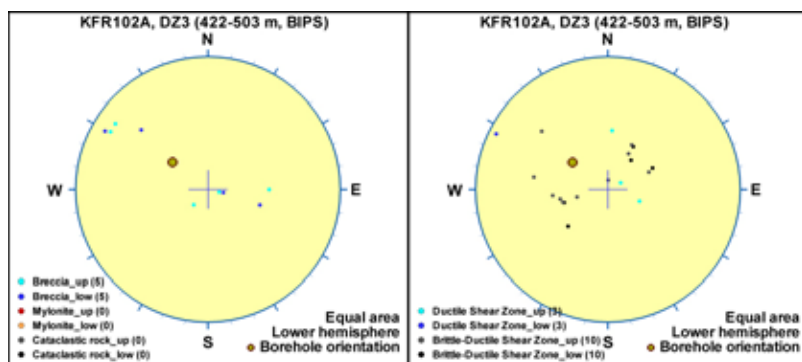
$$T = 1.73 \cdot 10^{-6} \text{ m}^2/\text{s}$$

$$\text{Log } T_0 = -4.1$$

Exceptionally high-transmissive, gently dipping PFL-f for an ENE deformation zone at great depth ( $z < -400$  m elevation). No PFL-f found over a 100 m borehole interval above the intercept. Subject to uncertainty in depth-adjustment. Possibly locally affected by the Northern Belt.



### Borehole intersections for ZFMENE3115



### Borehole intersections for ZFMENE3115

BH	Geometrical Intercept		Target Intercept	
	Sec_up BH length (m) [z (-m)]	Sec_low BH length (m) [z (-m)]	Sec_up BH length (m) [z (-m)]	Sec_low BH length (m) [z (-m)]
KFR104	117.33 [92.42]	168.86 [133.40]	149	154

## Borehole intersections for ZFMENE3115

**SHI DZ2 149–154 m:** Increased frequency of open and sealed fractures. Fractures aperture up to 1 mm. A few moderately altered open fractures. Minor intervals of brecciation at 150.96–151.38 and 153.64–153.80 m. Locally weak to moderate argillization. Predominant minerals in sealed fractures are calcite, chlorite and laumontite and in open fractures are chlorite, calcite and hematite. Low electric resistivity. One distinct radar reflector at the lower end of the interval oriented 105°/15°. Pegmatitic granite (101061), metagranite-granodiorite (101057) and amphibolite (102017). Confidence level = 3.

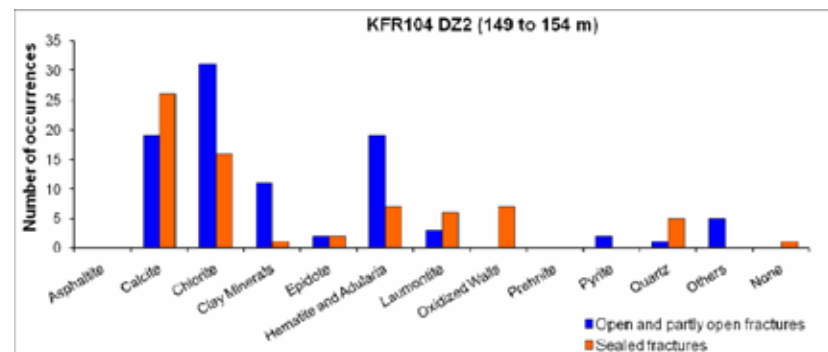
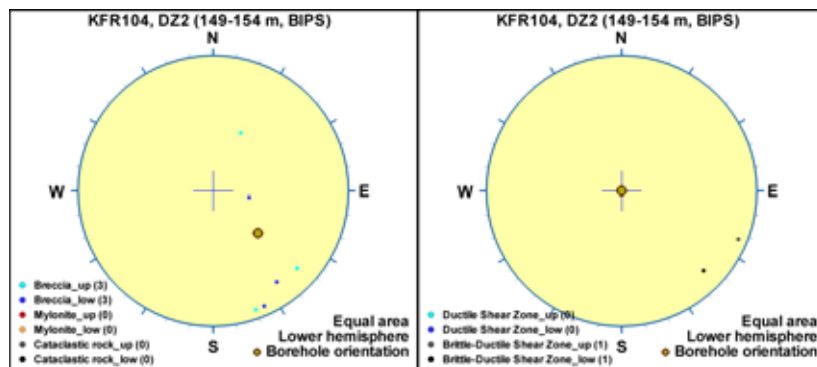
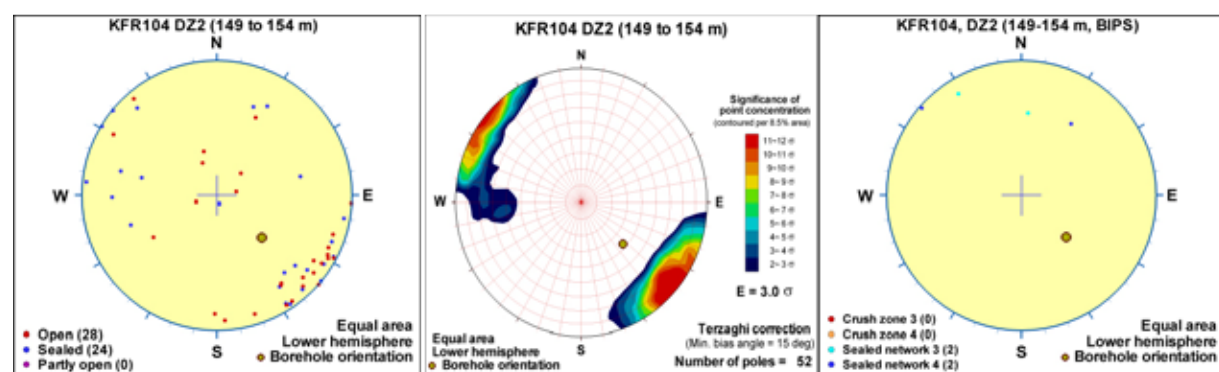
Low transmissivity of the interval ( $4 \cdot 10^{-9} \text{ m}^2/\text{s}$ ).

### Hydraulic data

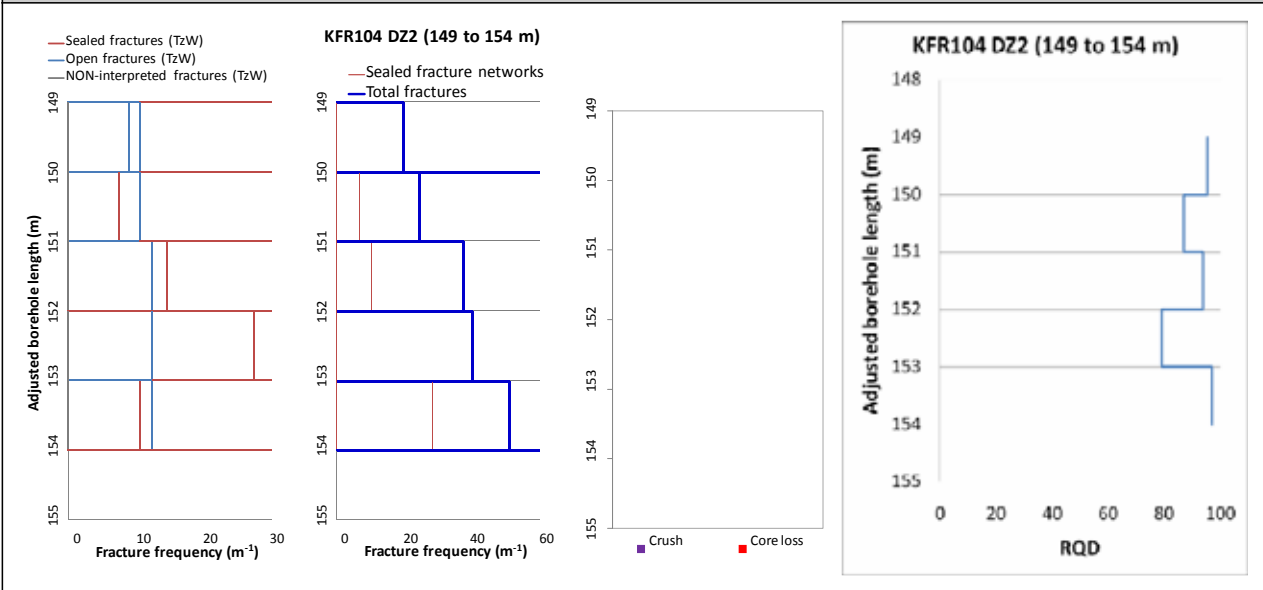
$$T = 8.60 \cdot 10^{-9} \text{ m}^2/\text{s}$$

$$\text{Log } T_0 = -7.6$$

No PFL-f found inside the interval. The detection limit is taken as an upper estimate of the interval transmissivity. Considered typical of Central Block characteristics.



### Borehole intersections for ZFMENE3115



### Borehole intersections for ZFMENE3115

BH	Geometrical Intercept		Target Intercept	
	Sec_up BH length (m) [z (-m)]	Sec_low BH length (m) [z (-m)]	Sec_up BH length (m) [z (-m)]	Sec_low BH length (m) [z (-m)]
KFR105	32.87 [112.53]	62.47 [117.58]	45	52

**SHI DZ1 45–52 m:** Increased frequency of open and sealed fractures and sealed networks. Three minor crushes at 45.58–45.66, 47.97–48.01 and 51.67–51.73 m and one cataclasite at 45.59–45.75 m. Zone cores defined at 45.55–45.85 and 51.65–51.95 m. Fracture apertures in general up to 1mm, with one aperture at 5 mm. Predominant minerals in open fractures are clay minerals, calcite, chlorite and muscovite and in sealed fractures calcite, laumontite and clay minerals. Very local argillization at 45.52–45.75, 49.01–49.04 and 51.67–51.74 m. The entire interval is characterized by several low resistivity anomalies and decreased bulk resistivity (< 1,000 Ohm-m). One radar reflector at 47.6 m, oriented 062°/72° or 282°/54°. Pegmatitic granite (101061). Confidence level = 3.

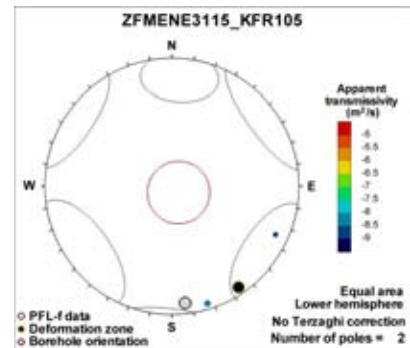
Two low-transmissive flow anomalies at 45.8 m and 49.0 m ( $T = 5 \cdot 10^{-9}$  and  $1 \cdot 10^{-9}$  m<sup>2</sup>/s, respectively). The total transmissivity of the section 43–53 m is about  $1 \cdot 10^{-8}$  m<sup>2</sup>/s.

#### Hydraulic data

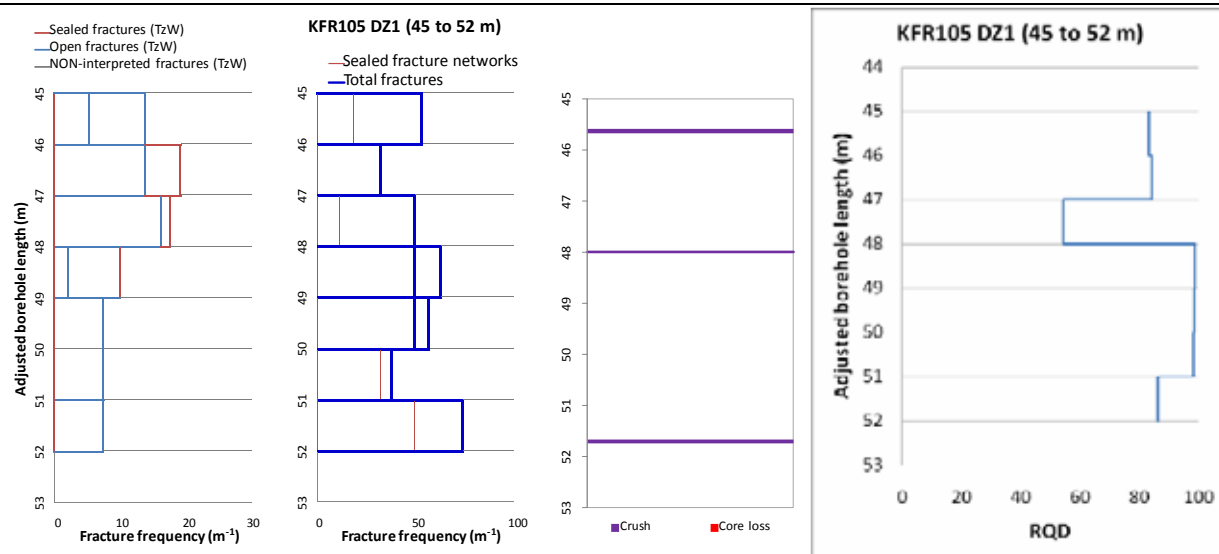
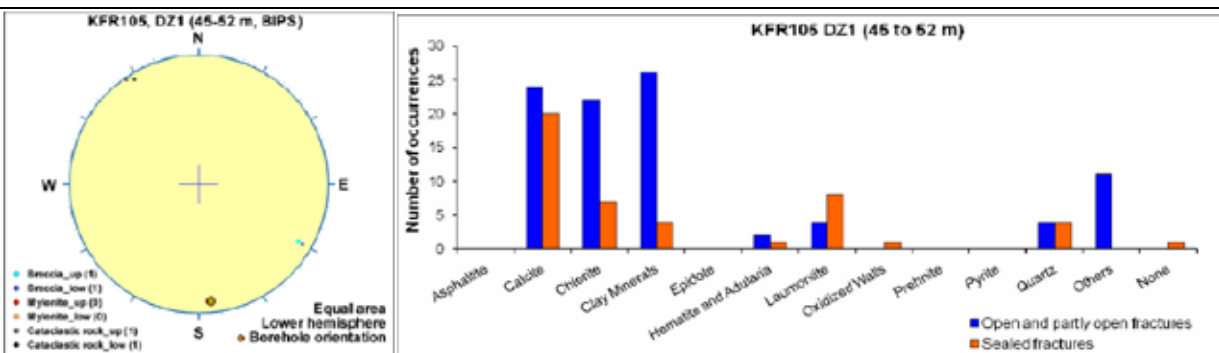
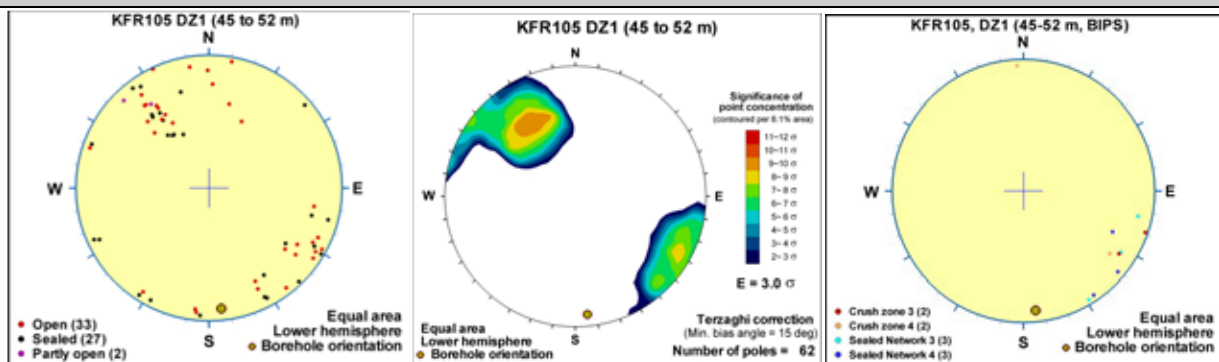
$T = 6.10 \cdot 10^{-9}$  m<sup>2</sup>/s


$\text{Log } T_0 = -7.7$

Little hydraulic support by two PFL-f, which are sub-parallel to the deformation zone.

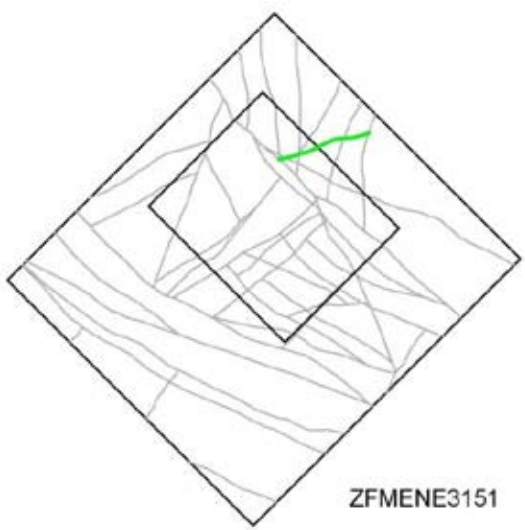


## Borehole intersections for ZFMENE3115



<b>Deformation zone ZFMNE3135</b>	
<p><b>Borehole and tunnel intersections (metres along borehole/tunnel)</b></p> <p>None</p>	
<p><b>Deformation style, alteration and geometry</b></p> <p><b>Deformation style:</b> Brittle (no direct evidence – inferred association with other NE-SW trending deformation zones)</p> <p><b>Alteration:</b> No data</p> <p><b>Strike/dip (span) right-hand-rule:</b> 81 / 90 (±5 / ±10)</p> <p><b>Trace length at ground surface (span) :</b> 368 m (200–380 m)</p> <p><b>Model thickness:</b> 5 m (1% default)</p> <p><b>Confidence in existence:</b> Medium</p>	
<p><b>Modelling procedure:</b> Based on magnetic lineament MSFR08113 in SFR model version 1.0 that is a modification of lineament MFM3135G in Forsmark model stage 2.3 /Isaksson et al. 2007/.</p>	
<b>Hydraulic interpretation</b>	
<p><b>Hydraulic width:</b> 3.6 m</p> <p><b>No of intercepts:</b> None</p> <p><b><math>T_{\text{eff}}(0)</math>:</b> <math>1.92 \cdot 10^{-7} \text{ m}^2/\text{s}</math></p> <p><b>Log <math>T_{\text{eff}}(0)</math>:</b> -6.7, <math>\sigma = (0.55)</math></p> <p><b>Calculation procedure:</b> <math>T_{\text{eff}}(0)</math> taken as pooled average of the NNE to ENE set (only based on new data).</p>	
<b>Fractures in the deformation zone</b>	
<b>General characteristics</b>	
<p><b>Fracture orientation:</b> No data</p> <p><b>Fracture frequency:</b> No data</p> <p><b>Fracture filling mineralogy:</b> No data</p>	



<b>Deformation zone ZFMENE3151</b>	
<p><b>Borehole and tunnel intersections (metres along borehole/tunnel)</b></p> <p>None</p>	
<p><b>Deformation style, alteration and geometry</b></p> <p><b>Deformation style:</b> Brittle (no direct evidence – inferred association with other ENE-WSW trending deformation zones)</p> <p><b>Alteration:</b> No data</p> <p><b>Strike/dip (span) right-hand-rule:</b> 74 / 90 (±5 / ±10)</p> <p><b>Trace length at ground surface (span) :</b> 421 m (300–470 m)</p> <p><b>Model thickness:</b> 5 m (1% default)</p> <p><b>Confidence in existence:</b> Medium</p>	
<p><b>Modelling procedure:</b> The position of the zone at the ground surface is based on a modification to the magnetic lineament MSFR08005 (SFR modelling work). The lineament was originally inferred to cross ZFMNW0805A and to continue a short distance on the western side of the zone. This extension was not considered likely conceptually and the zone was terminated against ZFMNW0805A. The number from the associated, Forsmark stage 2.3 lineament MFM3151G /Isaksson et al. 2007/ has been maintained for traceability between the different versions of the lineament interpretation.</p> <p>Forward modelling of magnetic data along profiles 7, 8 and 34 (see Appendix 6) support the inferred vertical dip of the inferred zone, whereas profile 9 indicates a very steep dip to the north-west.</p>	
<b>Hydraulic interpretation</b>	
<p><b>Hydraulic width:</b> 3.6 m</p> <p><b>No of intercepts:</b> None</p> <p><b>T<sub>eff</sub>(0):</b> <math>1.92 \cdot 10^{-7} \text{ m}^2/\text{s}</math></p> <p><b>Log T<sub>eff</sub>(0):</b> -6.7, <math>\sigma = (0.55)</math></p> <p><b>Calculation procedure:</b> T<sub>eff</sub>(0) taken as pooled average of the NNE to ENE set (only based on new data).</p>	
<b>Fractures in the deformation zone</b>	
<b>General characteristics</b>	
<p><b>Fracture orientation:</b> No data</p> <p><b>Fracture frequency:</b> No data</p> <p><b>Fracture filling mineralogy:</b> No data</p>	

## Deformation zone ZFMENE8031

### Borehole and tunnel intersections (metres along borehole/tunnel)

None

### Deformation style, alteration and geometry

**Deformation style:** Brittle (no direct evidence – inferred association with other ENE-WSW trending deformation zones)

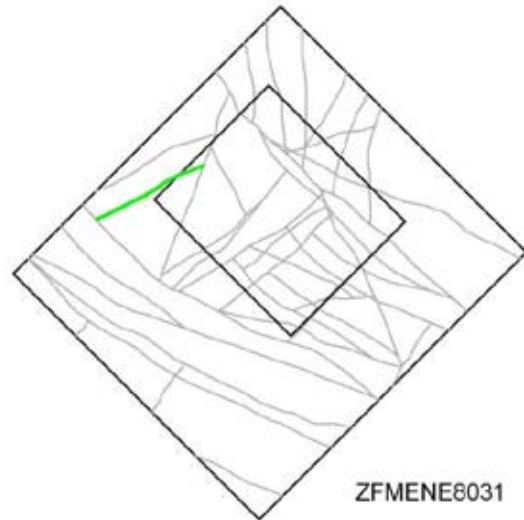
**Alteration:** No data

**Strike/dip (span) right-hand-rule:** 63 / 90 ( $\pm 5$  /  $\pm 10$ )

**Trace length at ground surface:** 537 m (530–670 m)

**Model thickness / model thickness span :** 5 m (1% default)

**Confidence in existence:** Medium



**Modelling procedure:** The position of the zone at the ground surface is based on a modification of the SFR version 1.0 lineament MSFR08031. The DZ trace terminates at ZFMNNE0869 to the NE whereas the lineament extends further to the NE. However, the existence of a zone coupled with the lineament in this position is not supported by tunnel mapping. The DZ trace has a greater extent in the SW where it terminates at ZFMWNW1035, whereas the lineament ends at the general boundary of an area where the magnetic field is "disturbed" and prevents further interpretation.

The initial hypothesis was that the zone dips gently to moderately to the SE. However, any dip between 20 and 70° to the SE would generate a significant intercept in the SFR tunnels and caverns as well as boreholes and nothing significant with such an orientation has been noted. The remaining alternatives are a subvertical to northwards dip. The zone has been modelled as vertical since there is no actual evidence for a northerly dip.

Forward magnetic modelling has been performed along profiles 27, 28, 29 and 30 (see Appendix 6). The anomaly pattern is weak and the results have a high uncertainty. The clearest indicator is from profile 27 where the modelling supports a subvertical dip to the inferred zone. No real indications of orientation can be obtained from profile 28, while profiles 29 and 30 indicate a "slight dip towards the south-east" though the uncertainty is high. The inversion modelling gives no clear indications as regards orientation.

## Hydraulic interpretation

**Hydraulic width:** 3.6 m

**No of intercepts:** None

**$T_{\text{eff}}(0)$ :**  $1.92 \cdot 10^{-7} \text{ m}^2/\text{s}$

**Log  $T_{\text{eff}}(0)$ :** -6.7,  $\sigma = (0.55)$

**Calculation procedure:**  $T_{\text{eff}}(0)$  taken as pooled average of the NNE to ENE set (only based on new data).

## Fractures in the deformation zone

### General characteristics

**Fracture orientation:** No data

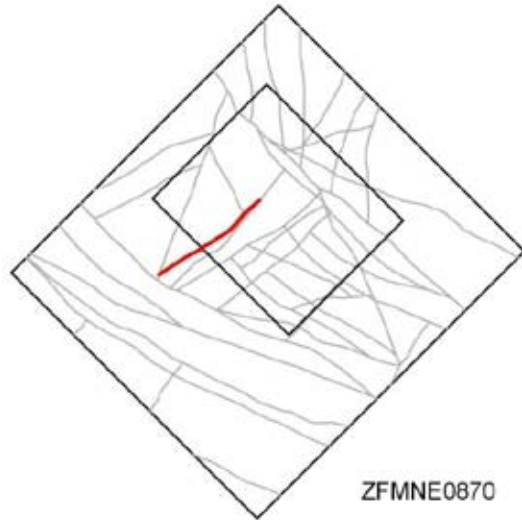
**Fracture frequency:** No data

**Fracture filling mineralogy:** No data

## Deformation zone ZFMNE0870

### Borehole and tunnel intersections (metres along borehole/tunnel)

HFR101: 28–41 m (DZ1 8.04–58 m)  
 KFR02: 32.5–37.5 m (DZ1 32.5–37.5 m)  
 KFR03: 48.00–95.95 m (DZ2 48.00–53.65 m, DZ3 70.42–72.75 m and DZ4 81.86–95.95 m)  
 KFR04: 14–63 m (DZ2 14–63 m)  
 KFR7C: 6.23–7.15 m (DZ1 6–32 m)  
 KFR31: 228.76–232 m (DZ2 228.76–232 m)  
 KFR54: 27–40 m (DZ2 27–40 m)  
 KFR55: 17–38 m (DZ2 8–38 m)  
 KFR68: 71.59–105.13 m (DZ1 71.59–78.11 m and DZ2 102.83–105.13 m)  
 DT: 0+535–0+570 (tDZ40)  
 DT: DT-BT connection tunnel at 0+610 (tDZ40)  
 BT: 0+640–0+690 (tDZ40)  
 BT: 0+888–0+907 (tDZ56)  
 BT: 1+020–1+050 (tDZ66)  
 NBT: 0+352 (tDZ80)  
 STT: 0+810–0+820 (tDZ66)  
 IST: 0+088 (tDZ80)



### Deformation style, alteration and geometry

**Deformation style:** Brittle. Cohesive breccia present in KFR03 DZ2. A possible ductile precursor is recorded by /Carlsson et al. 1986/

**Alteration:** Red-stained bedrock with fine-grained hematite dissemination and locally minor argillization

**Strike/dip (span) right-hand-rule:** 232 / 76 (±5 / 70–90)

**Trace length at ground surface (span):** 559 m (500–730 m)

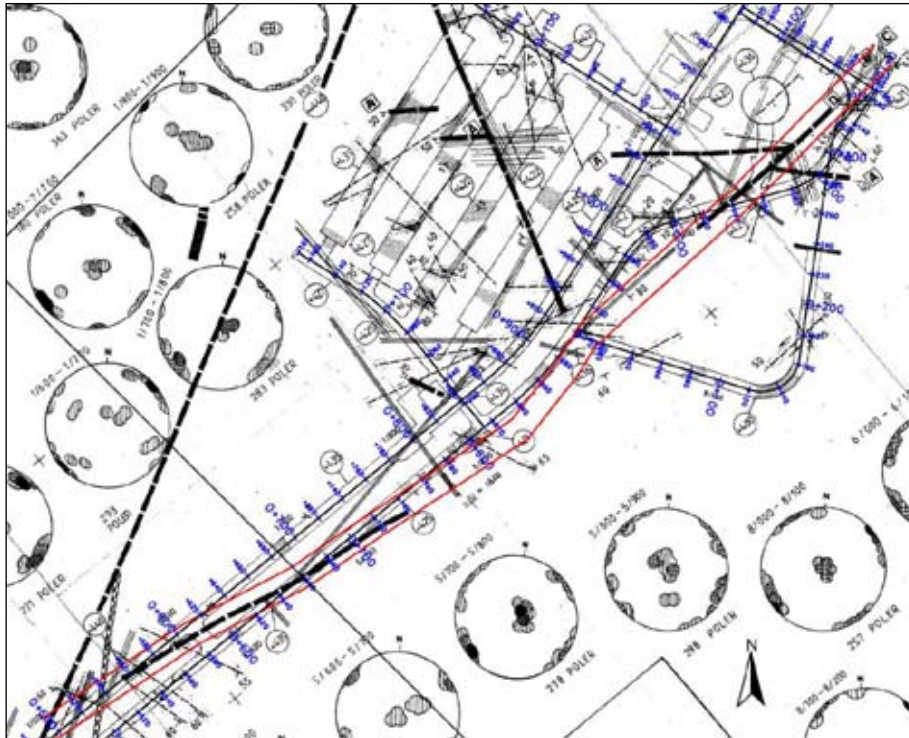
**Model thickness (span):** 16 m (2–20 m)

**Confidence in existence:** High

**Modelling procedure:** This zone corresponds to zone 9 in earlier SFR models (see, for example, Axelsson and Hansen 1997/). It was renamed ZFMNE0870 in the Forsmark stage 2.2 model /Stephens et al. 2007/. It has been remodelled in SFR model version 1.0 to extend from ZFMNW1035 and ZFMNNE0869 in the south-west to ZFMNW0805A/B and ZFMNE3118 in the north-east. The earlier subdivision into two sections (ZFMNE0870A and ZFMNE0870B) with an offset at ZFMWNV3262 has been rejected, based on a lack of support from new borehole data. /Axelsson and Hansen 1997/ state that this zone is, for most of its length, a water-bearing gouge-filled joint. Mylonitization was also recorded and, if correctly interpreted (cataclastic rock?), indicates a ductile origin whilst the clay gouge indicates brittle reactivation. Flush-water loss and water leakage in the BT from 5/640-5/690 were also recorded.

The surface position, based on a projection of tunnel mapping results, lacks a corresponding magnetic lineament and ZFMNE0870 is not crossed by a seismic refraction survey profile. The central part of the zone lies beneath the pier corresponding to an area where the magnetic field is disturbed. The zone has been modelled as an undulating surface based on multiple tunnel intercepts and correlation with borehole SHI results.

## Deformation zone ZFMNE0870



A horizontal section through ZFMNE0870 at general tunnel level,  $-75$  m elevation. The modelled zone position is shown by the two parallel red lines. The earlier interpreted position and extent by /Christiansson and Bolvede 1987/ is seen on the original overview drawing of the tunnel mapping results as bold dashed black lines. The modelled thickness of the zone, 16 m, is based on SHI borehole results.

### Hydraulic interpretation

**Hydraulic width:** 12.0 m

**No of intercepts:** 8 (5)

**$T_{\text{eff}}(0)$ :**  $5.11 \cdot 10^{-7}$  m<sup>2</sup>/s

**Log  $T_{\text{eff}}(0)$  =**  $-6.3$ ,  $\sigma = 0.46$

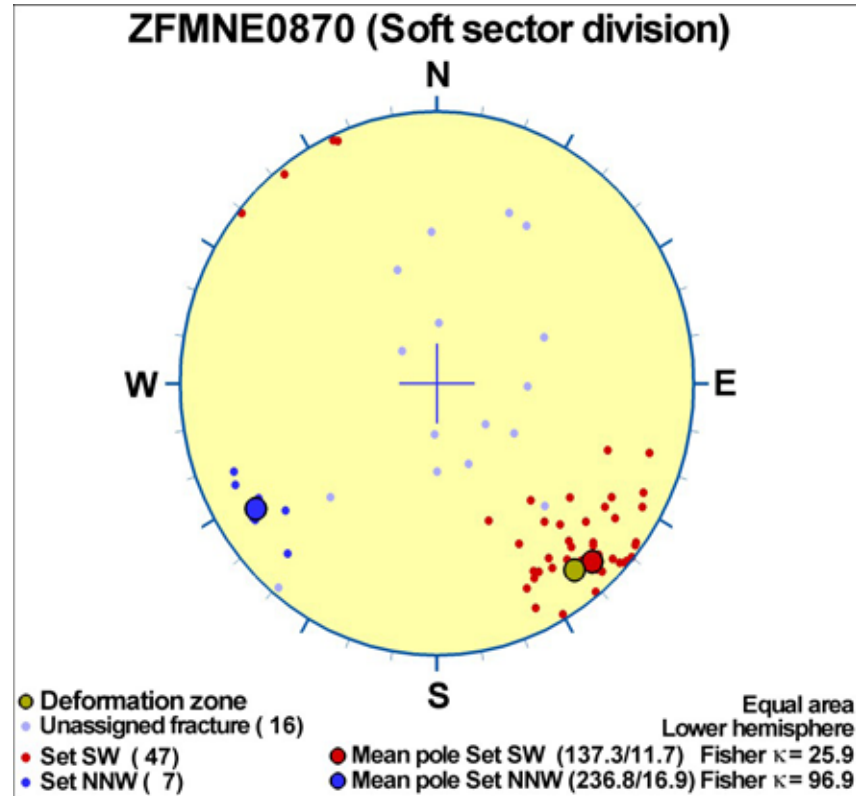
**Calculation procedure:**  $T_{\text{eff}}(0)$  taken as average from all 8 intercepts. Evaluated transmissivity at intercepts are exaggerated by unfavorable borehole orientations, causing long intercepts.

## Deformation zone ZFMNE0870

### Fractures in the deformation zone

#### General characteristics

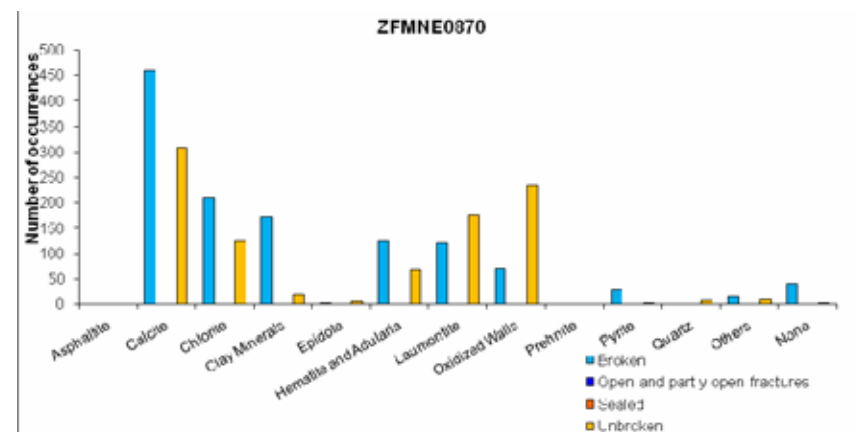
Fracture orientation:



Note that the stereogram only is based on data from HFR101 (28–41 m). The number of points for the NNW set is only 7 and the corresponding low significance of the cluster is described by the Kamb plot presented for the relevant HFR101 borehole section below.

**Fracture frequency:** No orientation corrected data from cored drillholes available. See HFR101 for a general indication.

**Fracture filling mineralogy:**



KFR02 DZ1 (32.5–37.5 m)



## Deformation zone ZFMNE0870



KFR03 DZ2 (48.00–53.65 m)



KFR03 DZ3 (70.42–72.75 m)



KFR03 DZ4 (81.86–95.95 m)



Deformation zone ZFMNE0870

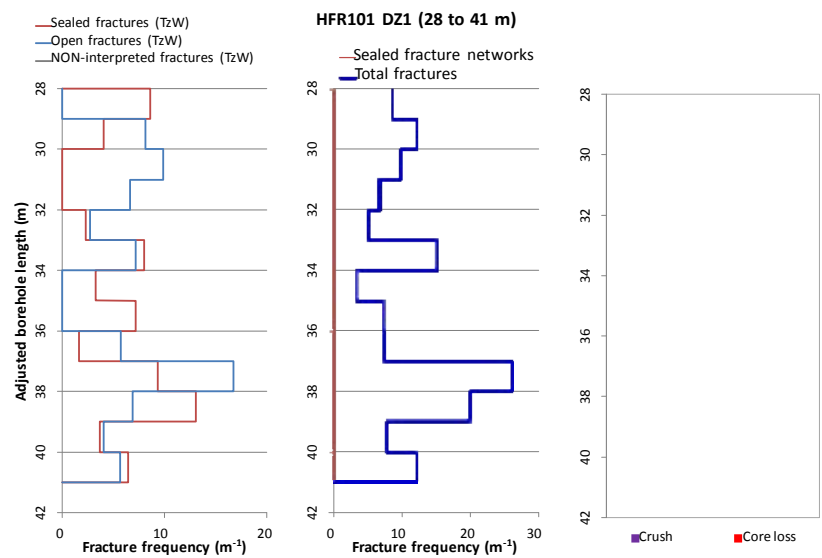
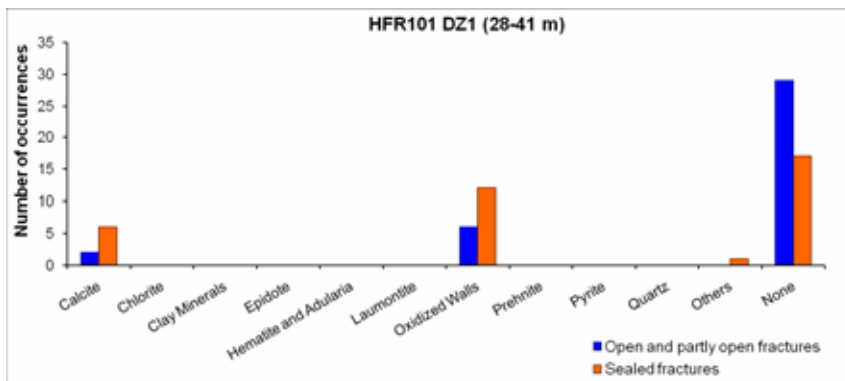
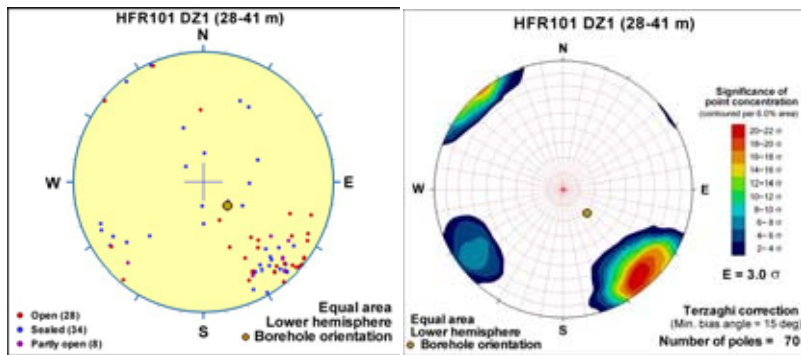


## BOREHOLE AND TUNNEL INTERCEPT DETAILS

Borehole intersections for ZFMNE0870																																																																								
BH	Geometrical Intercept		Target Intercept																																																																					
	Sec_up BH length (m) [z (-m)]	Sec_low BH length (m) [z (-m)]	Sec_up BH length (m) [z (-m)]	Sec_low BH length (m) [z (-m)]																																																																				
HFR101	19.17 [15.39]	46.17 [40.57]	28	41																																																																				
<p><b>Comment:</b> An interval with slightly increased frequency of steeply dipping (&gt; 65°) fractures, striking SW occurs at approximately 28–41 m length. Both sealed and open fractures. Control point added at 33.02 m.</p> <p>(Note DZ1 = 8.04–58 m, see below)</p>			<p><b>HFR101 DZ1 (8.04 to 58 m) Steeply dipping (&gt;65 deg) fractures striking SW (180 to 270 deg)</b></p> <table border="1"> <caption>Fracture Data from Chart</caption> <thead> <tr> <th>Depth (m)</th> <th>Open Fractures</th> <th>Sealed Fractures (Red)</th> <th>Sealed Fractures (Pink)</th> </tr> </thead> <tbody> <tr><td>11</td><td>1</td><td>1</td><td>0</td></tr> <tr><td>14</td><td>1</td><td>0</td><td>0</td></tr> <tr><td>17</td><td>1</td><td>0</td><td>0</td></tr> <tr><td>20</td><td>3</td><td>0</td><td>0</td></tr> <tr><td>23</td><td>1</td><td>1</td><td>0</td></tr> <tr><td>26</td><td>2</td><td>0</td><td>0</td></tr> <tr><td>29</td><td>1</td><td>3</td><td>0</td></tr> <tr><td>32</td><td>1</td><td>1</td><td>1</td></tr> <tr><td>35</td><td>2</td><td>5</td><td>1</td></tr> <tr><td>38</td><td>1</td><td>1</td><td>1</td></tr> <tr><td>41</td><td>1</td><td>2</td><td>1</td></tr> <tr><td>44</td><td>1</td><td>1</td><td>0</td></tr> <tr><td>47</td><td>1</td><td>1</td><td>0</td></tr> <tr><td>50</td><td>0</td><td>1</td><td>0</td></tr> <tr><td>53</td><td>1</td><td>1</td><td>0</td></tr> <tr><td>56</td><td>1</td><td>1</td><td>1</td></tr> </tbody> </table>		Depth (m)	Open Fractures	Sealed Fractures (Red)	Sealed Fractures (Pink)	11	1	1	0	14	1	0	0	17	1	0	0	20	3	0	0	23	1	1	0	26	2	0	0	29	1	3	0	32	1	1	1	35	2	5	1	38	1	1	1	41	1	2	1	44	1	1	0	47	1	1	0	50	0	1	0	53	1	1	0	56	1	1	1
Depth (m)	Open Fractures	Sealed Fractures (Red)	Sealed Fractures (Pink)																																																																					
11	1	1	0																																																																					
14	1	0	0																																																																					
17	1	0	0																																																																					
20	3	0	0																																																																					
23	1	1	0																																																																					
26	2	0	0																																																																					
29	1	3	0																																																																					
32	1	1	1																																																																					
35	2	5	1																																																																					
38	1	1	1																																																																					
41	1	2	1																																																																					
44	1	1	0																																																																					
47	1	1	0																																																																					
50	0	1	0																																																																					
53	1	1	0																																																																					
56	1	1	1																																																																					
<p><b>SHI DZ1 8.04–58 m:</b> Increased frequency of open and sealed fractures. Fracture aperture up to 2 mm. Locally weak to medium oxidation. Significantly decreased bulk resistivity along the entire section and minor caliper anomalies. Metagranite-granodiorite (101057), pegmatitic granite (101061), fine- to medium-grained granite (111058), amphibolite (102017) and felsic to intermediate metavolcanic rock (103076). Confidence level = 3.</p> <p>No flow anomaly in this interval.</p>																																																																								
<p><b>Hydraulic data</b></p> <p><math>T = 1.00 \cdot 10^{-7} \text{ m}^2/\text{s}</math></p> <p><math>\text{Log } T_0 = -6.9</math></p> <p>Below HTHB detection limit. Assumed value, as an upper estimate.</p>																																																																								



## Borehole intersections for ZFMNE0870



Borehole intersections for ZFMNE0870				
BH	Geometrical Intercept		Target Intercept	
	Sec_up BH length (m) [z (-m)]	Sec_low BH length (m) [z (-m)]	Sec_up BH length (m) [z (-m)]	Sec_low BH length (m) [z (-m)]
KFR02	0 [85.43]	60.99 [146.42]	32.5	37.5
<p><b>SHI DZ1 32.5–37.5:</b> Only defined by geophysical data. Distinctly decreased levels in the resistivity and SPR data along the entire interval. In the fluid temperature data there is a significant anomaly centered at c. 34.0 m, which indicates in or out flow of water. Pegmatitic granite (101061), fine- to medium-grained metagranite-granodiorite (101057) and felsic to intermediate metavolcanic rock (103076). Confidence level = 2.</p> <p>Moderate but increased transmissivity of the sections 26–36 m and 36–46 m (<math>7 \cdot 10^{-7}</math> and <math>4 \cdot 10^{-7}</math> m<sup>2</sup>/s, respectively).</p>				
<p><b>Hydraulic data</b></p> <p><math>T = 1.08 \cdot 10^{-6}</math> m<sup>2</sup>/s</p> <p>Log <math>T_0 = -5.4</math></p>				
KFR03	36.39 [118.76]	eoh [183.97]	48	95.95
<p><b>SHI DZ2 48.00–53.65 m:</b> Increased frequency of broken and unbroken fractures. Generally <math>\alpha</math>-angles &gt; 45°. Crushed section at 50.85–51.20 m. A 4 dm long laumontite-sealed breccia at approximately 49.5 m. Generally faint oxidation. Predominant fracture minerals are laumontite, calcite, clay minerals, chlorite and hematite. Distinct decrease in the SPR logging data along the entire interval. Moderately foliated metagranite-granodiorite (101057) and pegmatitic granite (101061). Confidence level = 2.</p> <p>Moderate transmissivity of the section 45–56 m (<math>3 \cdot 10^{-7}</math> m<sup>2</sup>/s).</p>				
<p><b>SHI DZ3 70.42–72.75 m:</b> Slightly increased frequency of broken and unbroken fractures. Generally <math>\alpha</math>-angles &lt; 45°. Faint to weak oxidation and in most of the interval strong laumontization. Predominant fracture minerals are laumontite, hematite/Fe-hydroxide, clay minerals and chlorite. Distinct decrease in the SPR logging values along the entire interval. Fine- to medium-grained granite (111058) and amphibolite (102017). Confidence level = 3.</p> <p>Low transmissivity of the section 57–80 m (<math>4 \cdot 10^{-8}</math> m<sup>2</sup>/s).</p>				
<p><b>SHI DZ4 81.86–95.95 m:</b> Increased frequency of broken and unbroken fractures, which locally forms sealed networks. Approximately 9 broken fractures/m outside crushed intervals. Varying <math>\alpha</math>-angles with several conspicuous, clay-dominated fractures at angles &lt; 30°. Four minor crushes. Faint to weak oxidation and minor argillization associated with clay-dominated fractures. Predominant fracture minerals are clay minerals, Fe-hydroxide/hematite, chlorite and calcite, and in unbroken fractures also adularia. Distinct decrease in the SPR logging values along the section 85.0–93.0 m. Fine- to medium-grained granite (111058) and pegmatitic granite (101061). Confidence level = 3.</p> <p>Low transmissivity of the section 81–101.6 m (<math>2 \cdot 10^{-8}</math> m<sup>2</sup>/s).</p>				
<p><b>Hydraulic data</b></p> <p><math>T = 3.55 \cdot 10^{-7}</math> m<sup>2</sup>/s</p> <p>Log <math>T_0 = -5.8</math></p>				

**Borehole intersections for ZFMNE0870**

BH	Geometrical Intercept		Target Intercept	
	Sec_up BH length (m) [z (-m)]	Sec_low BH length (m) [z (-m)]	Sec_up BH length (m) [z (-m)]	Sec_low BH length (m) [z (-m)]
KFR04	2.73 [79.83]	67.69 [142.57]	14	63

**SHI DZ2 14–63 m:** Increased frequency of broken and unbroken fractures. One crush at 32.60–32.77 m and one breccia at 33.00–33.22 m. Predominant fracture minerals are laumontite and calcite. Registered  $\alpha$ -angles for laumontite-bearing fractures in the interval are generally gently to moderately dipping ( $< 53^\circ$ ). The occurrence of clay minerals is mainly concentrated to two short sections at 20–23 and 32–36 m length, which corresponds to low single point resistivity anomalies (SPR). The  $\alpha$ -angles of these clay filled fractures are moderately to steeply dipping. Generally weak to moderately oxidized. Fine to medium grained granite (111058), amphibolite (102017) and felsic to intermediate metavolcanic rock (103076). Confidence level = 2.

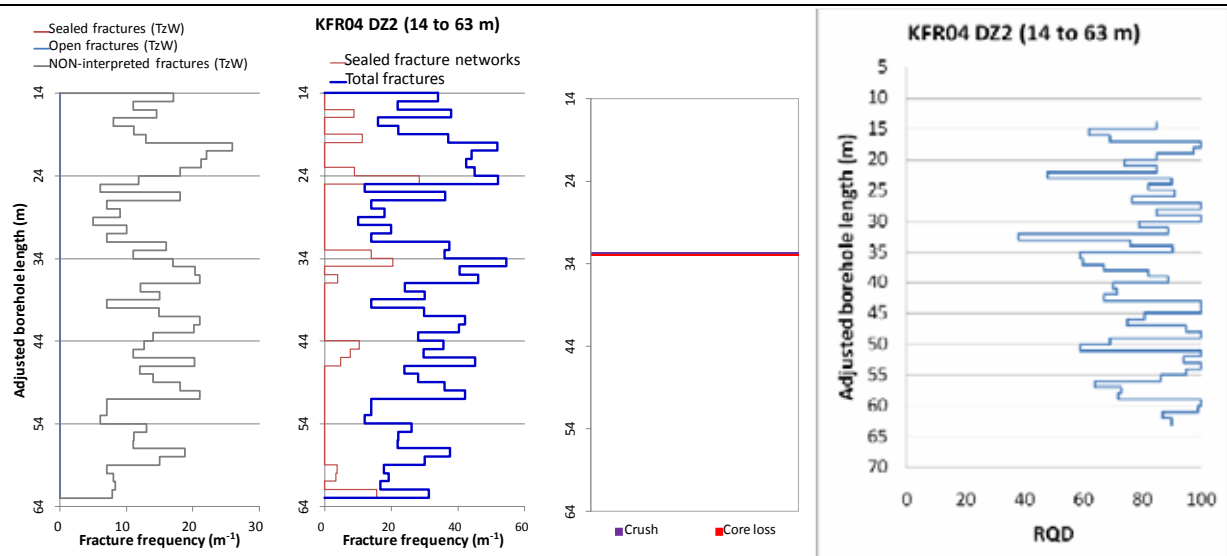
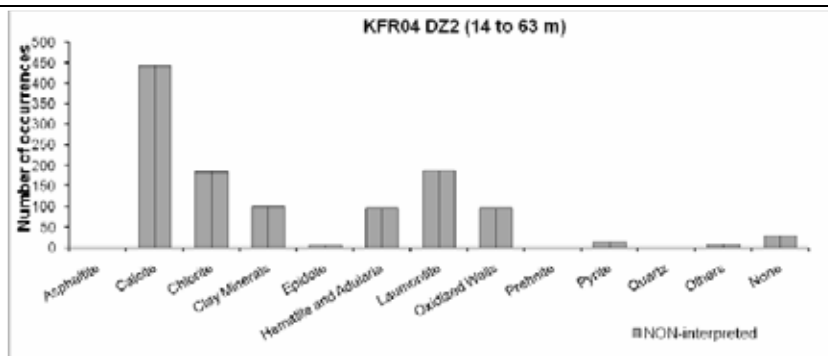
The hydraulic conductivity (measured in sections of about 20–40 m) is low in the whole interval (about  $1 \cdot 10^{-8}$  m/s).

**Hydraulic data**

$T = 1.40 \cdot 10^{-7} \text{ m}^2/\text{s}$

$\text{Log } T_0 = -6.4$

Long intercept due to sub-parallel borehole orientation, interpreted to exaggerate transmissivity. Only packer interval 28 to 43 m BHL used.



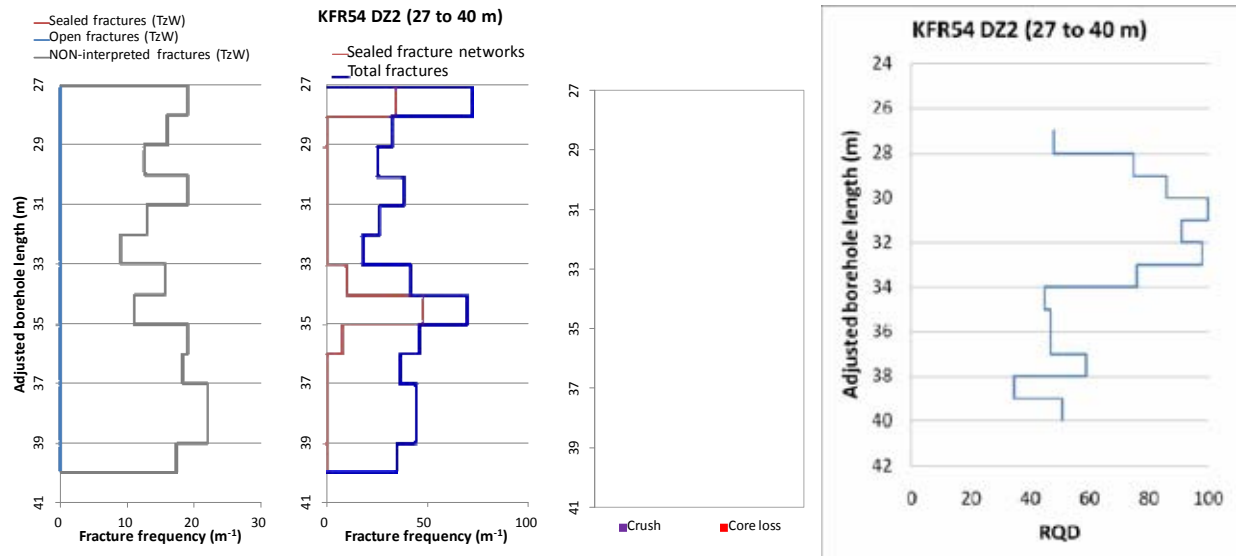
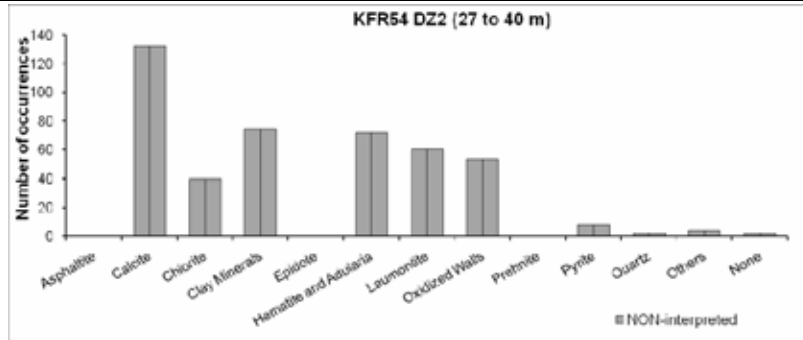
Borehole intersections for ZFMNE0870				
BH	Geometrical Intercept		Target Intercept	
	Sec_up BH length (m) [z (-m)]	Sec_low BH length (m) [z (-m)]	Sec_up BH length (m) [z (-m)]	Sec_low BH length (m) [z (-m)]
KFR7C	0.00 [133.40]	28.72 [160.39]	6.23	7.15
<p><b>Comment:</b> The intercept is considered to be dominated by ZFM871. However a short section between 6.23–7.15 m contains laumontite filled fractures with low alpha angles that could represent ZFMNE0870.</p>				
<p><b>Hydraulic data</b> Subordinate to ZFM871. Not used.</p>				
KFR31	222.79 [147.50]	eoh [160.73]	228.76	232
<p><b>SHI DZ2 228.76–232.00 m:</b> Increased frequency of broken fractures and several crushed intervals. <math>\alpha</math>-angles generally <math>&gt; 45^\circ</math> and typically parallel with the tectonic foliation. Generally faint to weak oxidation of the metagranite and faint to weak chloritization of the amphibolites. Predominant minerals in broken fractures are clay minerals, hematite, chlorite and calcite. Fine- to medium-grained metagranite-granodiorite (101057) and amphibolite (102017). Confidence level = 3.</p> <p>Moderate transmissivity of the interval 204–242 m (<math>9 \cdot 10^{-7}</math> m<sup>2</sup>/s).</p>				
<p><b>Hydraulic data</b> Assumed subordinate to ZFM871. Not used.</p>				
KFR53	18.72 [89.91]	37.01 [98.33]	–	–
<p><b>Hydraulic data</b> T = <math>2.35 \cdot 10^{-8}</math> m<sup>2</sup>/s Log T<sub>0</sub> = –7.2 Intercept covered by two long, low-transmissive packer data from 17 to 40.6 m.</p>				
KFR54	25.31 [100.37]	42.18 [112.85]	27	40
<p><b>Comment:</b></p> <p><b>SHI DZ2 27–40 m:</b> Increased frequency of broken and to a lesser extent unbroken fractures and sealed networks. Decreased frequency of broken fractures between 28.6–33.7 m. Hematite stained clay minerals are restricted to two intervals of anomalously high fracture frequencies at 26.9–28.2 and 31.1–37.4 m, whereas laumontite mainly is restricted to 28.0–31.2 and 37.3–39.1 m. Both assemblages often include calcite. The chlorite content, on the other hand, is very low relative to that in other parts of the drill core. The <math>\alpha</math>-angles of the clay-bearing fractures are typically dipping gently to moderately (30, 37, 60 and 71°). Generally weak to medium oxidation. Generally strongly foliated metagranite-granodiorite (101057) and one occurrence of pegmatitic granite (101061) in the lower most part of the section. Confidence level = 3.</p> <p>The hydraulic conductivity is low to very low (<math>10^{-9}</math>–<math>10^{-10}</math> m/s).</p>				

### Borehole intersections for ZFMNE0870

#### Hydraulic data

Log  $T_0 = -7^*$

Possible erroneous data indicating  $1 \cdot 10^{-7} \text{ m}^2/\text{s}$ . The value has been included to represent similar low-transmissive data partly inside, or close to other rejected intercepts of ZFMNE0870.



BH	Geometrical Intercept		Target Intercept	
	Sec_up BH length (m) [z (-m)]	Sec_low BH length (m) [z (-m)]	Sec_up BH length (m) [z (-m)]	Sec_low BH length (m) [z (-m)]
KFR55	17.09 [128.84]	42.69 [133.72]	17	38

**Comment:** The quoted target intercept is based on a straightforward geometrical subdivision of DZ2 between ZFMNE0870 and ZFMNE3118. It is not expected that their character can be distinguished.

### Borehole intersections for ZFMNE0870

**SHI DZ2 8–38 m:** Increased frequency of broken and unbroken fractures and sealed networks, especially in the intervals 8–21 m and 32–38 m. Core loss at 17.86–18.51, 19.13–19.37, 33.48–33.60 and 34.89–35.33 m. The most frequent fracture filling minerals, which occur throughout the interval, are calcite, and to some extent chlorite. Fractures with clay minerals as the primary infilling are generally restricted to the interval at 16.8–19.5 m, with  $\alpha$ -angles of 69°. Laumontite ± calcite filled fractures, on the other hand, occur along three intervals at 8.0–12.6, 16.0–16.5 and 20.4–28.1 m length. Two  $\alpha$ -angles are registered in the uppermost (68 and 77°) and three in the lowermost (50, 57 and 65°) intervals. Locally faint to medium oxidation. Strongly foliated metagranite-granodiorite (101057) and one occurrence of fine- to medium-grained granite (111058). Confidence level = 3.

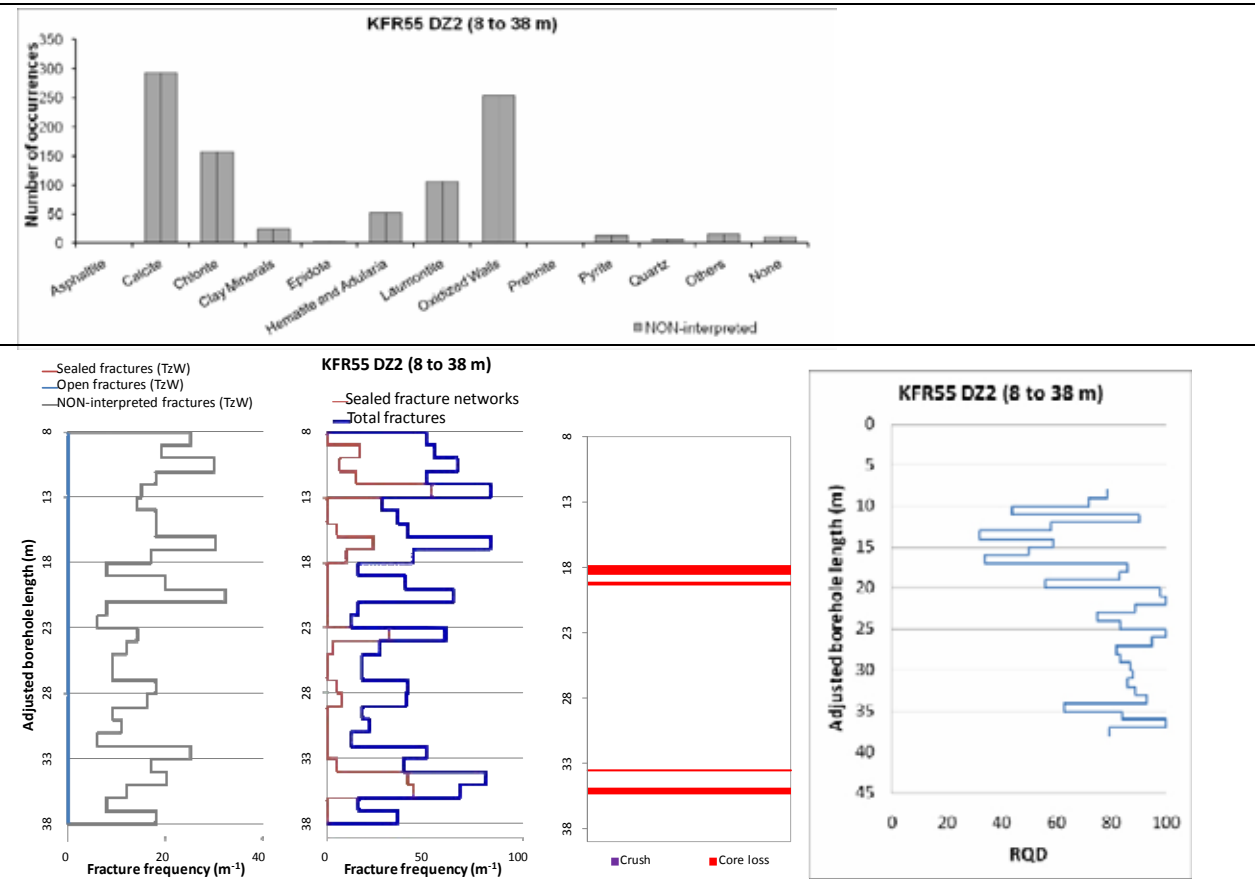
No hydrogeological investigation data from the upper 22 m of the borehole. The hydraulic conductivity is low in the measured section 22–38 m ( $10^{-8}$  m/s).

#### Hydraulic data

$T = 1.70 \cdot 10^{-7} \text{ m}^2/\text{s}$

$\text{Log } T_0 = -6.2$

Covered by single pressure-build up interval from 22 to 39 m BHL.



Borehole intersections for ZFMNE0870				
BH	Geometrical Intercept		Target Intercept	
	Sec_up BH length (m) [z (-m)]	Sec_low BH length (m) [z (-m)]	Sec_up BH length (m) [z (-m)]	Sec_low BH length (m) [z (-m)]
KFR68	60.25 [42.60]	93.99 [66.45]	71.59	105.13
<p><b>Comment:</b> Combined SHI DZ1 and DZ2. Note: KFR68 is interpreted as intercepting the meeting point between ZFMNNE0869 and ZFMNE0870. Since the BH lacks fracture orientation data it is impossible to correlate the PDZ with any specific steeply dipping zone. Thus, the PDZ is taken as target intercept for both ZFMNE0870 and ZFMNNE0869.</p>				
<p><b>SHI DZ1 71.59–78.11 m:</b> Increased frequency of broken fractures, locally also sealed fracture networks. Variable <math>\alpha</math>-angles, but generally <math>&gt; 45^\circ</math>. Locally faint to weak argillization. Weak muscovitization throughout the interval. Predominant minerals in broken and unbroken fractures are clay minerals, calcite and chlorite. Pegmatitic granite (101061) and aplitic metagranite (101058). Confidence level = 3.</p> <p>Transmissivity below the measurement limit (<math>7 \cdot 10^{-7} \text{ m}^2/\text{s}</math>).</p>				
<p><b>SHI DZ2 102.83–105.13 m:</b> Increased frequency of broken fractures and crushes. Variable <math>\alpha</math>-angles. Weak to moderate oxidation throughout the interval. Predominant minerals in broken fractures are clay minerals, chlorite, hematite and calcite. Fine- to medium-grained granite (111058) and pegmatitic granite (101061). Confidence level = 1.</p> <p>Moderate transmissivity of the interval 102.51–105.51 m (<math>8 \cdot 10^{-7} \text{ m}^2/\text{s}</math>).</p>				
<p><b>Hydraulic data</b></p> <p>Subordinate to ZFMNNE0869. Not used.</p>				
KFR7B	20.27 [152.83]	eoh [153.63]	–	–
<p><b>Comment:</b> The geometrical intercept is at the modelled zone margin. No target intercept is defined.</p>				
<p><b>Hydraulic data</b></p> <p>Poor data.</p>				
KFR70	34.91 [24.74]	92.80 [69.92]	–	–
<p><b>Comment:</b> No DZ identified by SHI. Judging from the photographs of the drill cores there is no obvious indication of a possible zone along the geometric intercept. The fracture frequency is generally less than 10 fractures/m and oxidation or other alterations cannot be distinguished. No target intercept has been defined.</p>				
<p><b>Hydraulic data</b></p> <p><math>T = 2.49 \cdot 10^{-6} \text{ m}^2/\text{s}</math>  <math>\text{Log } T_0 = -5.4</math></p>				

Borehole intersections for ZFMNE0870				
BH	Geometrical Intercept		Target Intercept	
	Sec_up BH length (m) [z (-m)]	Sec_low BH length (m) [z (-m)]	Sec_up BH length (m) [z (-m)]	Sec_low BH length (m) [z (-m)]
KFR104	0.00 [2.83]	1.88 [1.29]	–	–
<b>Comment:</b> The geometrical intercept is at the modelled zone margin. No target intercept is defined.				
<b>Hydraulic data</b> Intercept inside borehole casing. Not used.				

Tunnel intersections for ZFMNE0870				
Tunnel	Geometrical Intercept		Target Intercept	
	Start ch.(m)	End ch. (m)	Start ch.(m)	End ch. (m)
DT	0+470	0+600	0+535	0+570
<b>Comment:</b> Target intercept defined by tDZ40 in Appendix 2. Earlier interpreted as 1+530–1+570 /Axelsson and Hansen 1997/.				
DT	DT-BT connection tunnel at 0+610		DT-BT connection tunnel at 0+610	
<b>Comment:</b> Target intercept defined by tDZ40 in Appendix 2. Earlier interpreted as DT-BT connection tunnel at 0+610 /Axelsson and Hansen 1997/.				
BT	0+620	0+780	0+640	0+690
<b>Comment:</b> Target intercept defined by tDZ40 in Appendix 2. Earlier interpreted as 5+640–5+690 /Axelsson and Hansen 1997/.				
BT	0+860	0+925	0+888	0+907
<b>Comment:</b> Connection with NBT. Target intercept defined by tDZ56 in Appendix 2.				
BT	1+017	1+050	1+020	1+050
<b>Comment:</b> Target intercept defined by tDZ66 in Appendix 2. Earlier interpreted as 6+025–6+050 /Axelsson and Hansen 1997/.				
NBT	0+000	0+010	–	–
<b>Comment:</b> Connection with BT.				
NBT	0+350	0+365	0+352	0+352



Tunnel intersections for ZFMNE0870				
Tunnel	Geometrical Intercept		Target Intercept	
	Start ch.(m)	End ch. (m)	Start ch.(m)	End ch. (m)
<p><b>Comment:</b> Target intercept defined by tDZ80 in Appendix 2. Earlier interpreted as 8+290–8+350 (as a branch of zone 9) /Axelsson and Hansen 1997/.</p>				
STT	0+800	0+820	0+810	0+820
<p><b>Comment:</b> Target intercept defined by tDZ66 in Appendix 2.</p>				
IST	0+078	0+095	0+088	0+088
<p><b>Comment:</b> Target intercept defined by tDZ80 in Appendix 2. This location is at the connection between ST and STT an extension of this. Earlier interpreted as 4+090 (as a branch of zone 9) /Axelsson and Hansen 1997/.</p>				

## Deformation zone ZFMNE3112

### Borehole and tunnel intersections (metres along borehole/tunnel)

KFR102A: 302–325 m (DZ2 302–325 m)  
 KFR102B: 173–180 m (DZ4 173–180 m)  
 KFR104: 268–283 m (DZ3 268–283 m)  
 KFR105: 88.5–96.5 m (DZ2 88.5–96.5 m)

### Deformation style, alteration and geometry

**Deformation style:** Brittle. Minor cohesive breccias present in three of the BH intercepts.

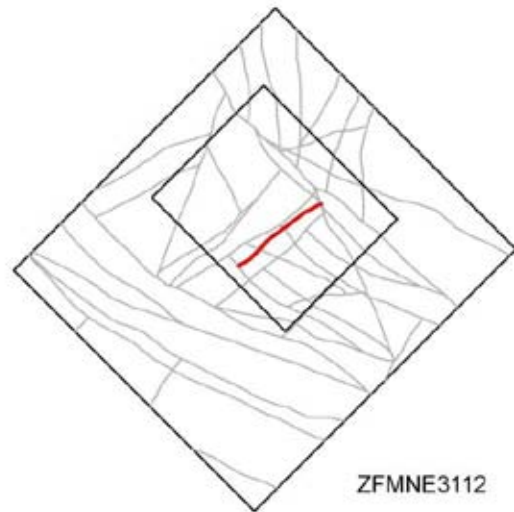
**Alteration:** Generally red-stained bedrock with fine-grained hematite dissemination with minor intervals of laumontization and carbonatization in KFR104 DZ3 and argillization in KFR102A DZ2.

**Strike/dip (span) right-hand-rule:** 233 / 89 ( $\pm 5$  /  $\pm 10$ )

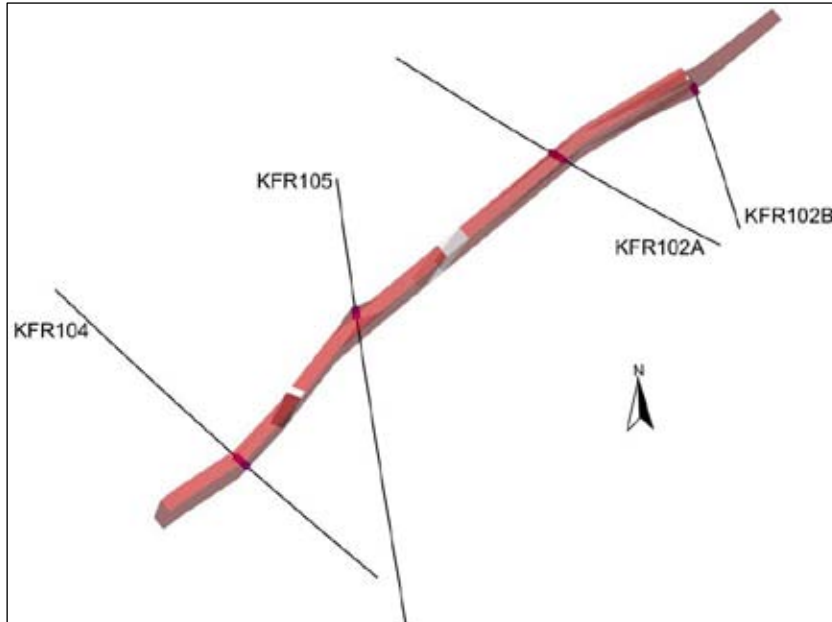
**Trace length at ground surface (span):** 474 m (400–710 m)

**Model thickness (span):** 10 m (5–12 m)

**Confidence in existence:** High



**Modelling procedure:** The position of the zone at the ground surface is based on a projection from the interpreted borehole correlations, with only a weak and partial agreement with the lineament MFM3112G defined by a magnetic minimum /Isaksson et al. 2007/. The central part of this zone lies beneath the pier where the magnetic field is disturbed and hinders lineament interpretation.



*ZFMNE3112 looking down dip. The relevant borehole SHI PDZs are shown as pink cylinders. The modelled zone thickness is 10 m.*

## Deformation zone ZFMNE3112

### Hydraulic interpretation

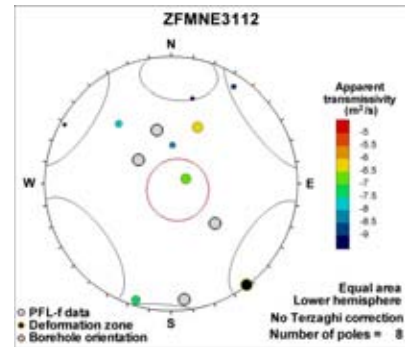
Hydraulic width: 7.4 m

No of intercepts: 4

$T_{\text{eff}}(0)$ :  $2.67 \cdot 10^{-7} \text{ m}^2/\text{s}$

Log  $T_{\text{eff}}(0)$ : -6.6,  $\sigma = 0.62$

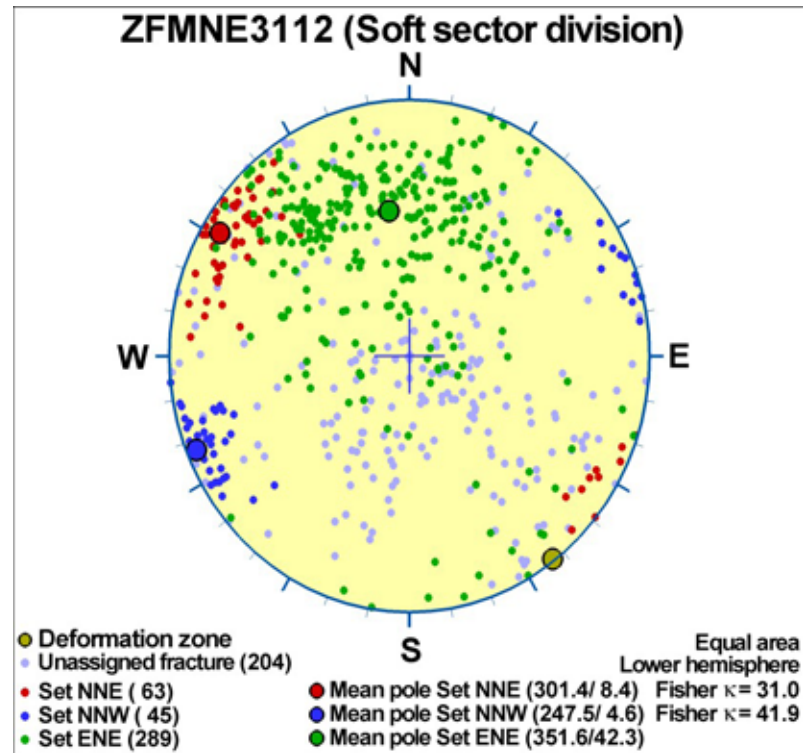
**Calculation procedure:**  $T_{\text{eff}}(0)$  taken as average from all 4 intercepts. More transmissive than other NNE to ENE zones (highest values found close to the Northern Belt). However, in general, the PFL-f data exhibit the typical scattered pattern of rock mass in the Central Block.



## Fractures in the deformation zone

### General characteristics

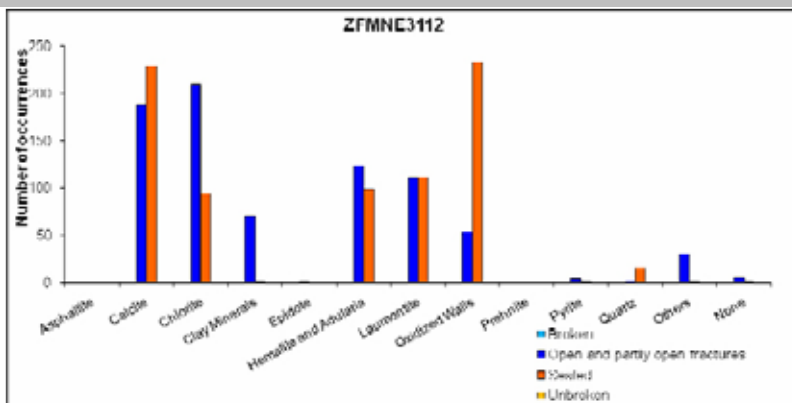
Fracture orientation:



Fracture frequency: Open  $10 \text{ m}^{-1}$ , Sealed  $28 \text{ m}^{-1}$

Fracture filling mineralogy:

## Deformation zone ZFMNE3112



KFR102B DZ4 (173–180 m)



## BOREHOLE AND TUNNEL INTERCEPT DETAILS

Borehole intersections for ZFMNE3112				
BH	Geometrical Intercept		Target intercept	
	Sec_up BH length (m) [z (-m)]	Sec_low BH length (m) [z (-m)]	Sec_up BH length (m) [z (-m)]	Sec_low BH length (m) [z (-m)]
KFR102A	299.70 [269.82]	323.05 [290.81]	302	325

**SHI DZ2 302–325 m:** Increased frequency of open and sealed fractures. Fractures aperture generally less than 0.5 mm. Locally faint to medium oxidation. Predominant minerals in open fractures are chlorite, calcite, hematite, clay minerals and laumontite and in sealed fractures calcite, laumontite, chlorite and adularia. The possible deformation zone core 308–310 m is characterized by two fractures with five mm aperture, three minor crushes, argillisation and clay minerals as predominant mineral in open fractures. Two radar reflectors without orientation at 302 and 311 m, and one oriented reflector at 325 m (033°/83° or 213°/32°). The magnetic susceptibility is decreased along the entire section. In the section 307–310 m the resistivity is significantly decreased and there is also a distinct caliper anomaly. There is another clear low resistivity anomaly in the interval 322–325 m. In the section 312–318 m there is a fluid temperature anomaly indicating the occurrence of a water bearing fracture. Metagranite-granodiorite (101057), fine- to medium-grained granite (111058) and pegmatitic granite (101061). Confidence level = 3.

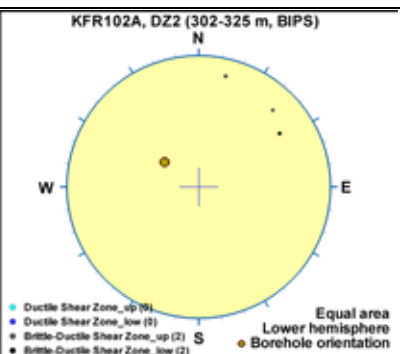
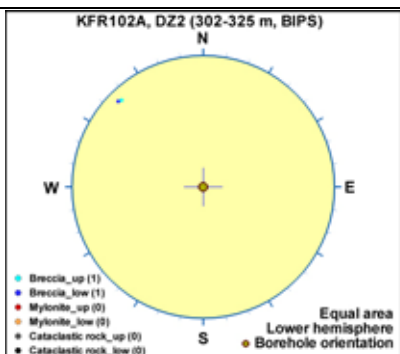
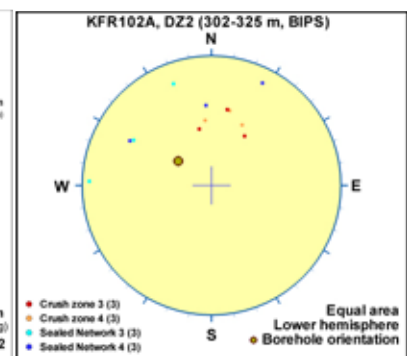
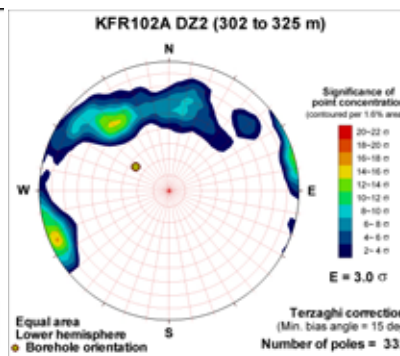
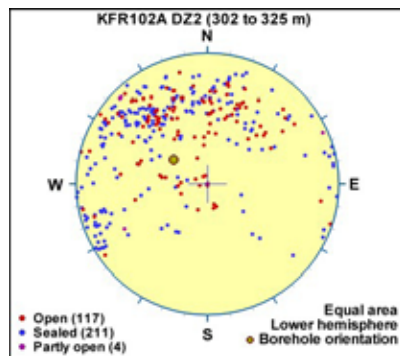
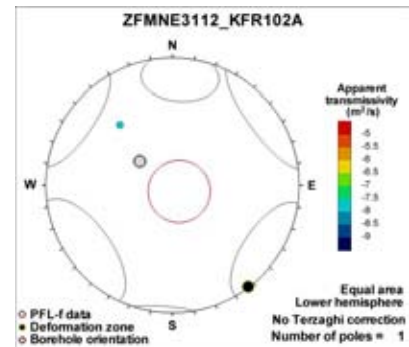
One single medium-transmissive flow anomaly ( $T = 2 \cdot 10^{-8} \text{ m}^2/\text{s}$ ) at 309 m, probably related to one, or both, of the 5 mm aperture fractures. Transmissivity below the measurement limit in the rest of the section.

### Hydraulic data

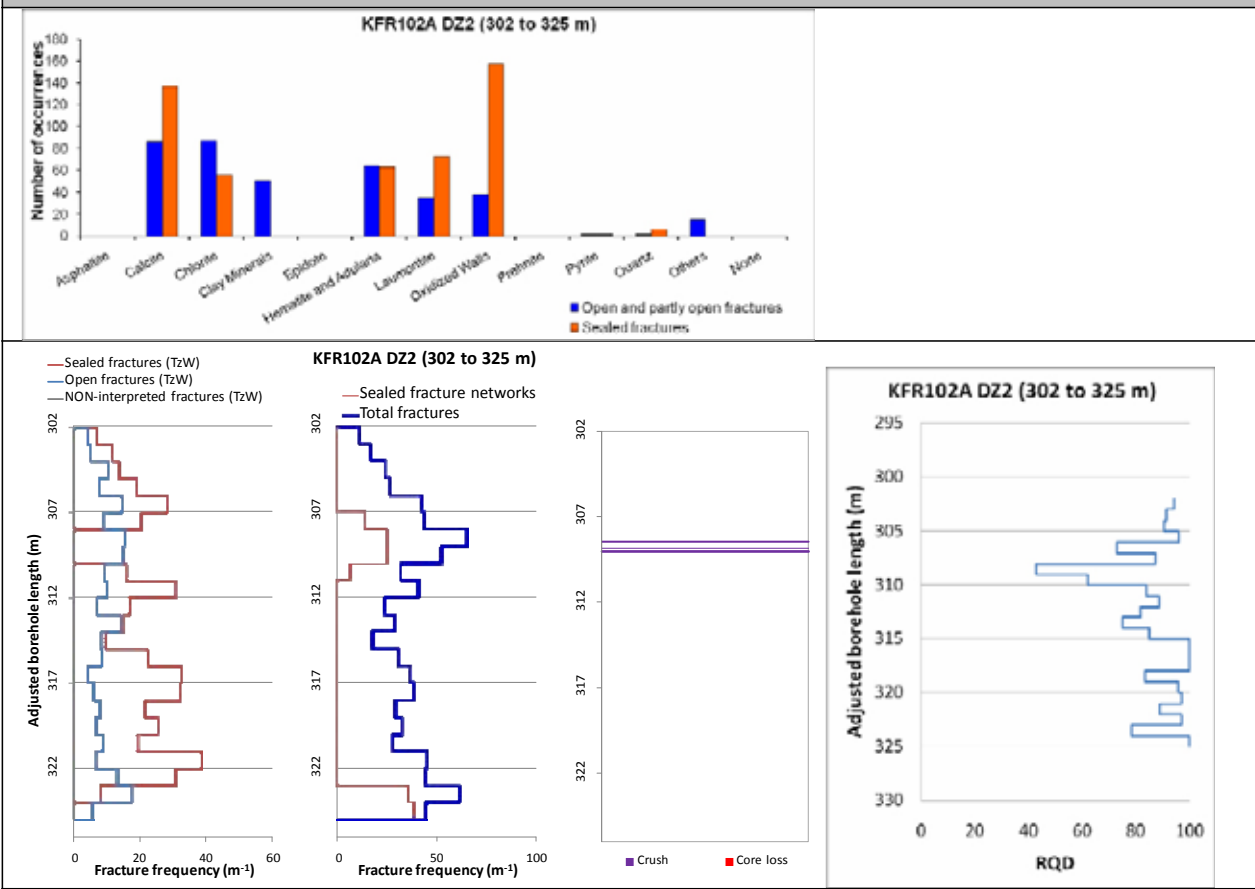
$T = 1.90 \cdot 10^{-8} \text{ m}^2/\text{s}$

$\text{Log } T_0 = -6.5$

Little hydraulic support by single PFL-f, which is sub-parallel to the deformation zone.



### Borehole intersections for ZFMNE3112



BH	Geometrical Intercept		Target intercept	
	Sec_up BH length (m) [z (-m)]	Sec_low BH length (m) [z (-m)]	Sec_up BH length (m) [z (-m)]	Sec_low BH length (m) [z (-m)]
KFR102B	170.32 [135.07]	eoh [180.08]	173	180

**SHI DZ4 173–180 m:** Increased frequency of sealed fractures and sealed fracture networks. Brecciated intervals at 176.01–176.04, 178.92–179.10 and 179.66–179.74 m. Predominant minerals in sealed fractures and sealed fracture networks are calcite, chlorite, laumontite and adularia. Minor interval of medium oxidation. Significantly decreased resistivity and magnetic susceptibility in the interval 172.0–173.5 m. In the remaining part of the section the resistivity and magnetic susceptibility are partly decreased along minor intervals. Pegmatitic granite (101061), metagranite-granodiorite (101057), felsic to intermediate metavolcanic rock (103076), fine- to medium-grained granite (111058) and amphibolite (102017). Confidence level = 3.

An isolated cluster of relatively high-transmissive flow anomalies at 172.0–173.6 m. Total transmissivity of  $2 \cdot 10^{-6} \text{ m}^2/\text{s}$ . No flow logging data below approximately 173.8 m.

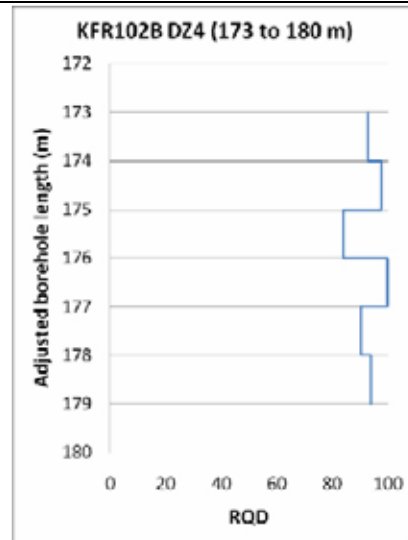
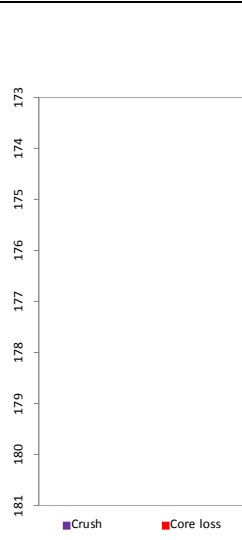
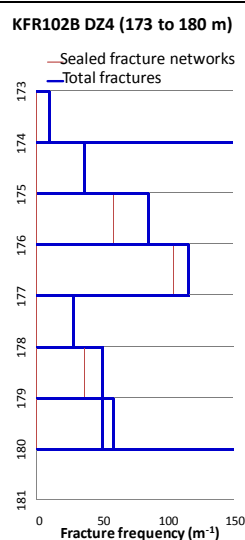
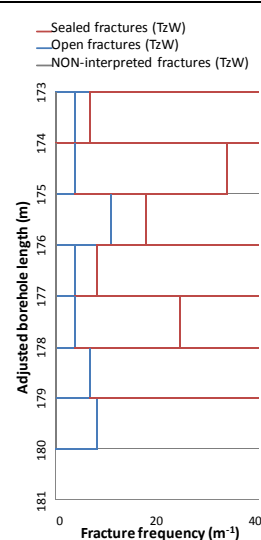
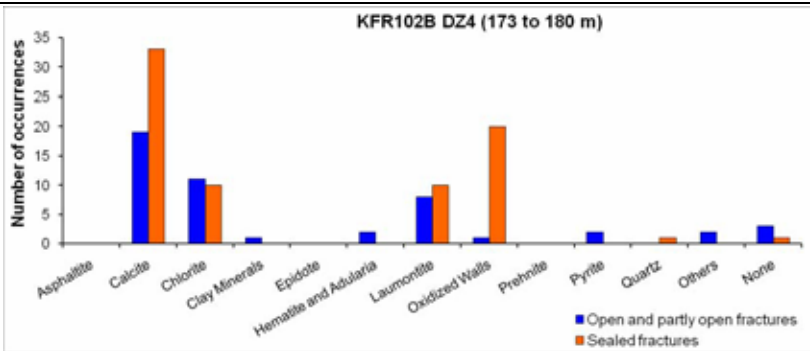
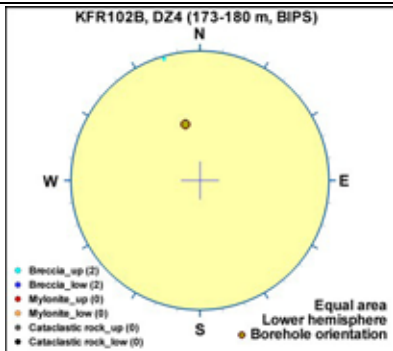
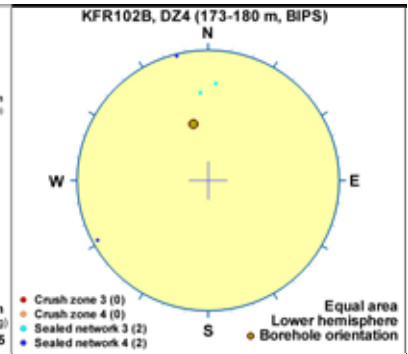
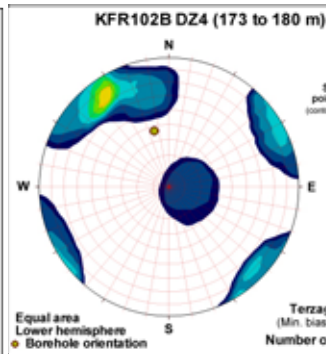
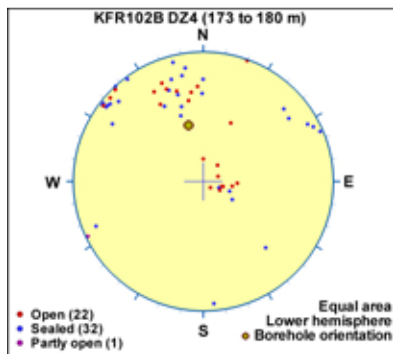
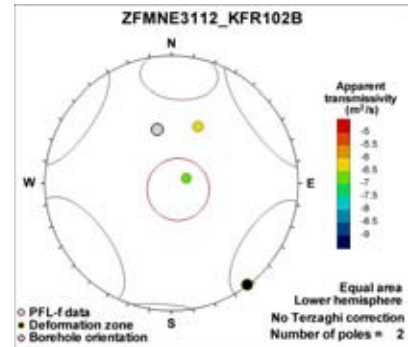
## Borehole intersections for ZFMNE3112

### Hydraulic data

$T = 5.90 \cdot 10^{-7} \text{ m}^2/\text{s}$

$\text{Log } T_0 = -5.6$

Supported by two moderately transmissive, horizontal and gently dipping PFL-f.



**Borehole intersections for ZFMNE3112**

BH	Geometrical Intercept		Target intercept	
	Sec_up BH length (m) [z (-m)]	Sec_low BH length (m) [z (-m)]	Sec_up BH length (m) [z (-m)]	Sec_low BH length (m) [z (-m)]
KFR104	265.84 [209.12]	282.99 [222.33]	268	283

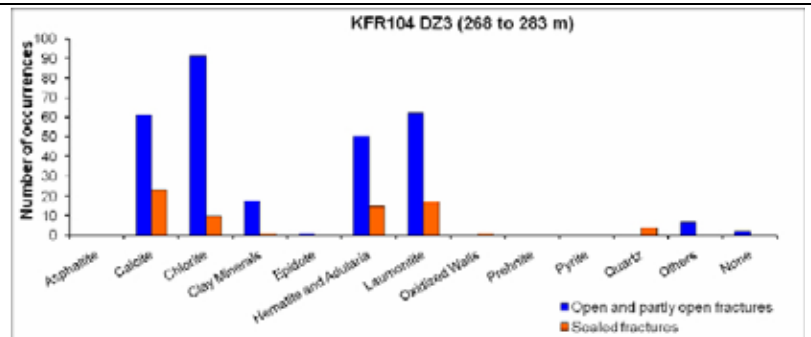
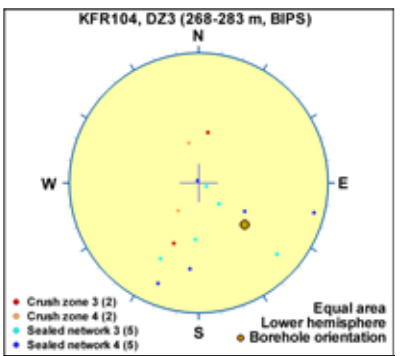
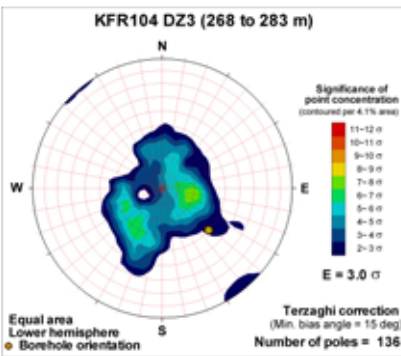
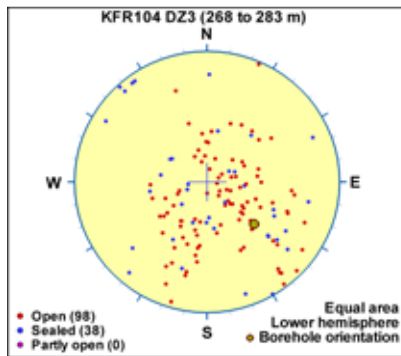
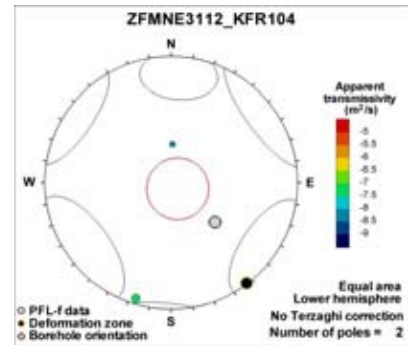
**SHI DZ3 268–283 m:** Increased frequency of open fractures and sealed fracture network. Two crushes at 276.36–276.64 and 277.46–277.75 m. Fracture apertures up to 0.5 mm with a single aperture at 3 mm. Generally weak to moderate oxidation and one interval of carbonatization at 275.06–275.95 m. Predominant minerals in open fractures are chlorite, laumontite, hematite and calcite. Very low electric resistivity and one caliper anomaly. Two radar reflectors of which one is oriented (109°/20° or 232°/85°). Pegmatitic granite (101061), aplitic metagranite (101058), metagranite-granodiorite (101057) and amphibolite (102017). Confidence level = 3.

Two single flow anomalies where the transmissivity of the interval ( $1 \cdot 10^{-7} \text{ m}^2/\text{s}$ ) is dominated by the anomaly at 276 m.

**Hydraulic data**

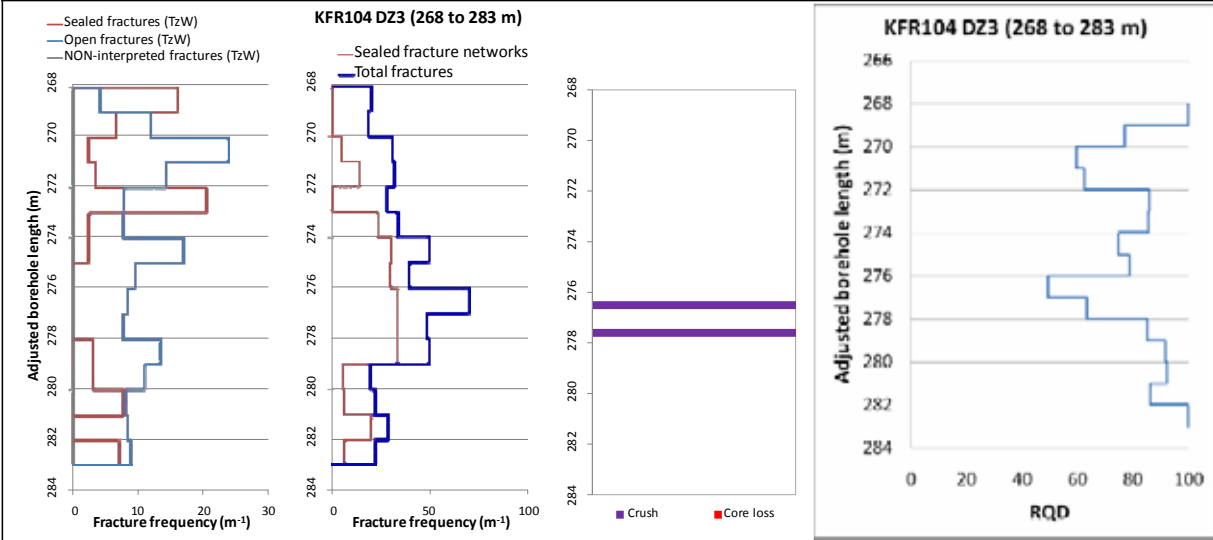
$T = 1.15 \cdot 10^{-7} \text{ m}^2/\text{s}$

$\text{Log } T_0 = -6$





### Borehole intersections for ZFMNE3112



### Borehole intersections for ZFMNE3112

BH	Geometrical Intercept		Target intercept	
	Sec_up BH length (m) [z (-m)]	Sec_low BH length (m) [z (-m)]	Sec_up BH length (m) [z (-m)]	Sec_low BH length (m) [z (-m)]
KFR105	87.69 [121.86]	99.69 [123.87]	88.5	96.5

**SHI DZ2 88.5–96.5 m:** Increased frequency of sealed fractures and sealed networks. Fracture apertures in general up to 0.5 mm. Predominant fracture minerals are calcite, chlorite, adularia and oxidized walls. Generally weakly oxidized. A minor decrease in resistivity along the interval but no other indications in the geophysical logging data. Fine- to medium-grained metagranite-granodiorite (101057) and pegmatitic granite (101061). Confidence level = 3.

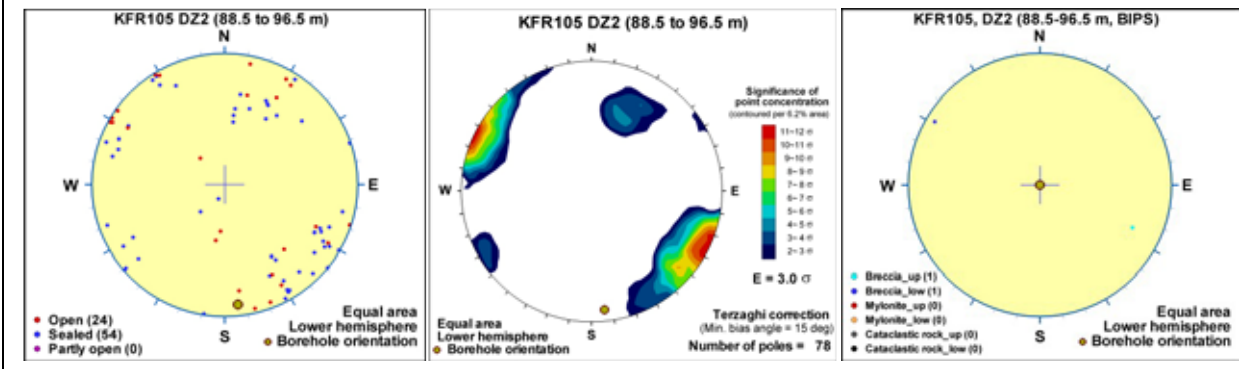
Three low-transmissive flow anomalies at 88.7, 94.9 and 95.7 m. The total transmissivity of the section is very low, about  $2 \cdot 10^{-9} \text{ m}^2/\text{s}$ .

#### Hydraulic data

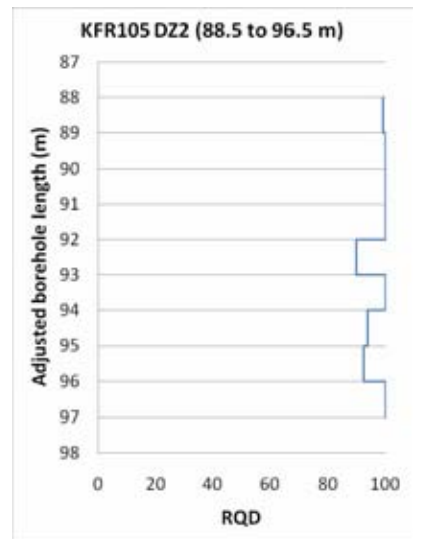
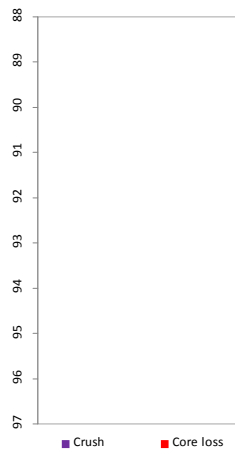
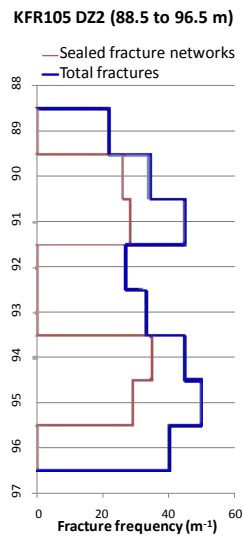
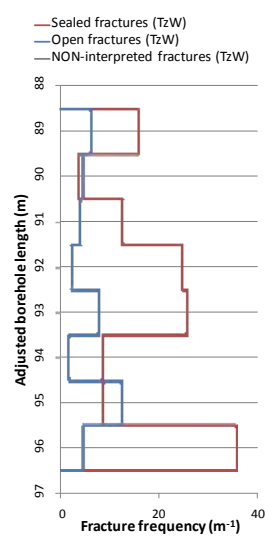
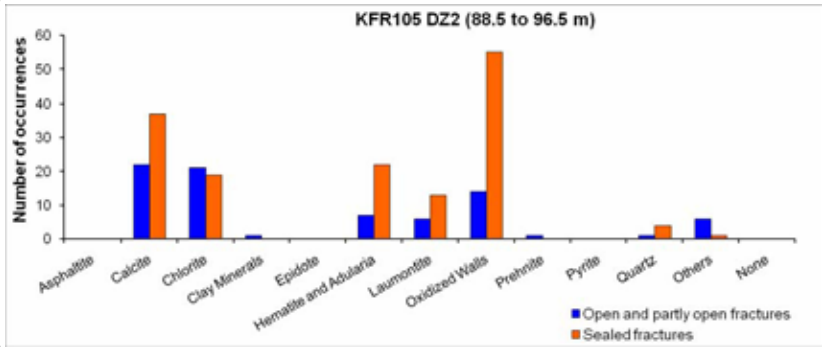
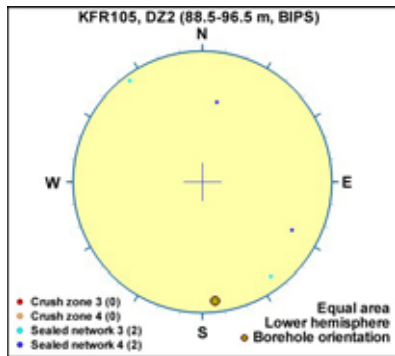
$$T = 2.25 \cdot 10^{-9} \text{ m}^2/\text{s}$$

$$\text{Log } T_0 = -8.1$$

Three low-transmissive PFL-f with scattered orientation. Considered typical pattern of Central Block characteristics (inside as well as outside zones).



## Borehole intersections for ZFMNE3112



## Deformation zone ZFMNE3118

### Borehole and tunnel intersections (metres along borehole/tunnel)

HFR101: 190–202 m (DZ3 190–202 m)  
 KFR13: 47.5–61 m (DZ3 47.5–61 m)  
 KFR54: 0–2.5 m (DZ1 0–2.5 m)  
 KFR55: 8–17 m (DZ2 8–38 m)  
 KFR104: 30–45.5 m (DZ1 30–45.5 m)  
 BT: 1+095 (tDZ73)  
 BT/ST: 1+166 (tDZ73)  
 NBT: 0+055–0+059  
 NBT: 0+295–340 (tDZ73)

### Deformation style, alteration and geometry

**Deformation style:** Brittle. Inferred minor brittle-ductile shear zone at 200.25–200.54 m in HFR101 DZ3. Cohesive breccia in KFR104 DZ1.

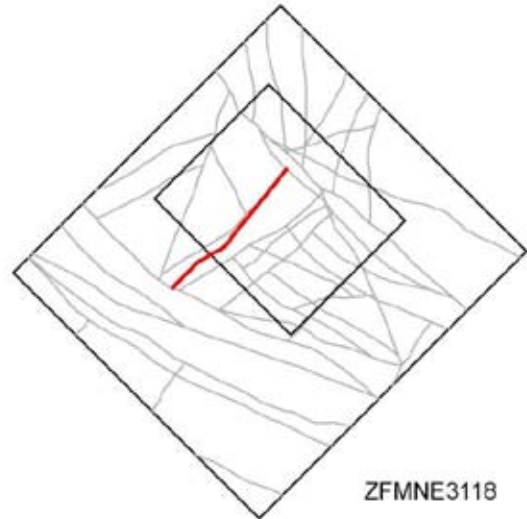
**Alteration:** Locally red-stained bedrock with fine-grained hematite dissemination. Altered vuggy rock with quartz dissolution at 38.30–40.75 m along KFR104 DZ1.

**Strike/dip (span) right-hand-rule:** 44 / 84 (±5 / ±10)

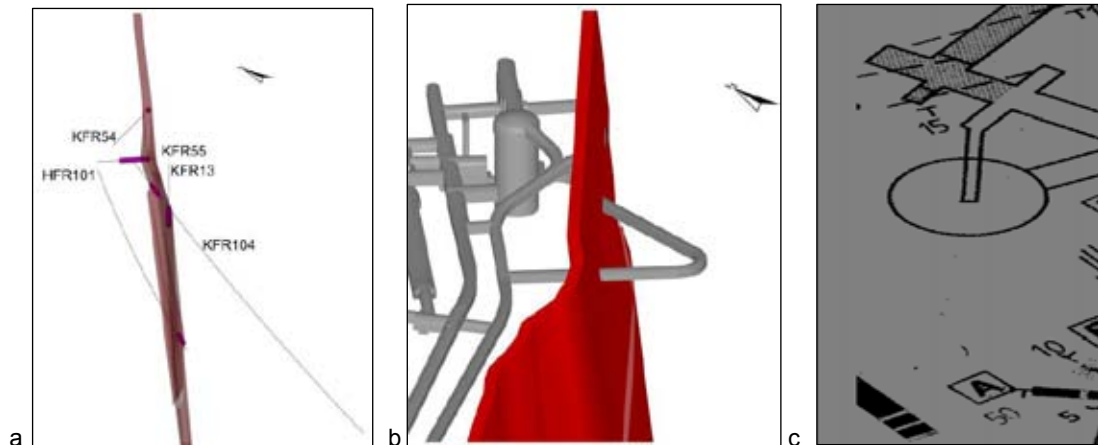
**Trace length at ground surface (span):** 743 m (720–760 m)

**Model thickness (span):** 8 m (2–10 m)

**Confidence in existence:** High



**Modelling procedure:** Modified after zone 12 /Carlsson et al. 1985/. The position of the zone at the ground surface in the south-west coincides with the magnetic lineament MSFR08111 in SFR model version 1.0, itself an update of MFM3118G /Isaksson et al. 2007/. The main central section of the zone lies beneath the pier in an area where the magnetic field is disturbed and hinders lineament interpretation.



- a. The central section of ZFMNE3118 looking along the strike to NE. The relevant SHI PDZs are shown as pink cylinders. Note only part of KFR55 DZ2 correlates with the zone.
- b. ZFMNE3118 looking along the strike to NE showing the tunnel intercept positions.
- c. Overview mapping drawing of the NBT. ZFMNE3118 corresponds to the approximate B alignment.

## Deformation zone ZFMNE3118

### Hydraulic interpretation

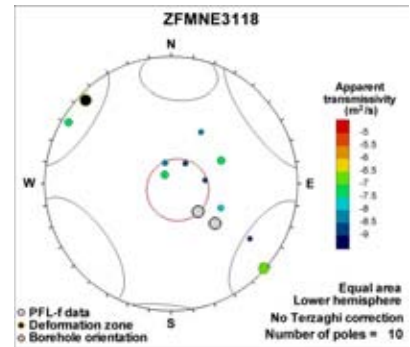
**Hydraulic width:** 6.2 m

**No of intercepts:** 3 (2)

**$T_{\text{eff}}(0)$ :**  $2.38 \cdot 10^{-7}$  m<sup>2</sup>/s

**Log  $T_{\text{eff}}(0)$ :** -6.6,  $\sigma = 0.29$

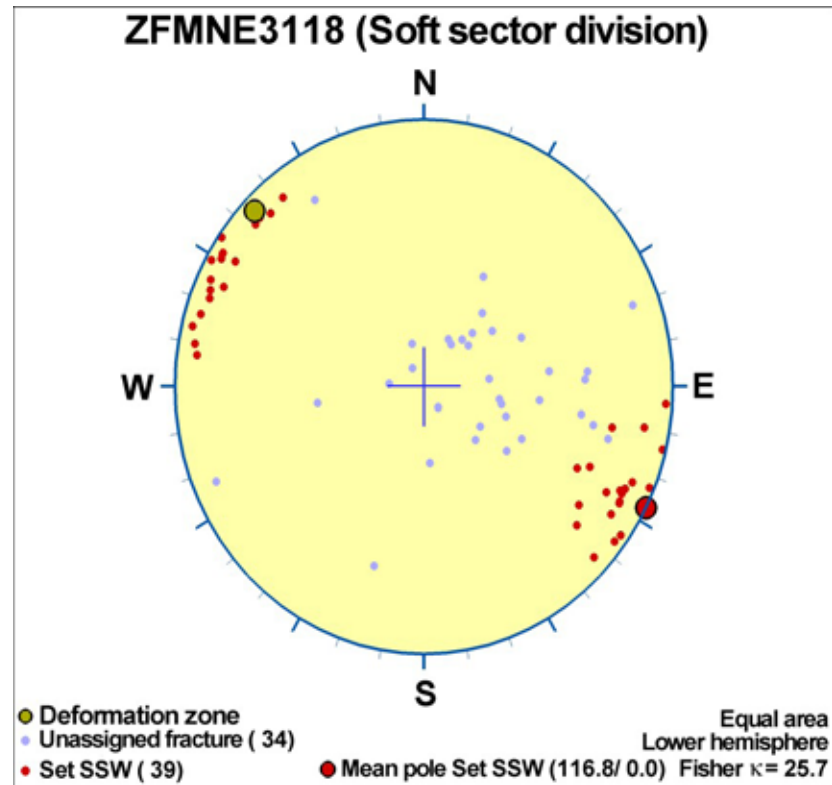
**Calculation procedure:**  $T_{\text{eff}}(0)$  taken as average of all 3 intercepts, weighted by low-transmissive tunnel intercept. Intercepts with the SFR tunnel without record grouting of specific fracture inflow are weighted equal to a single borehole intercept. Such low-transmissive tunnel intercepts were assumed equal to the background conductivity used in /Holmén and Stigsson 2001/ (i.e., the intercept was set to  $T = 6.5 \cdot 10^{-9}$  m/s multiplied by the hydraulic width).



### Fractures in the deformation zone

#### General characteristics

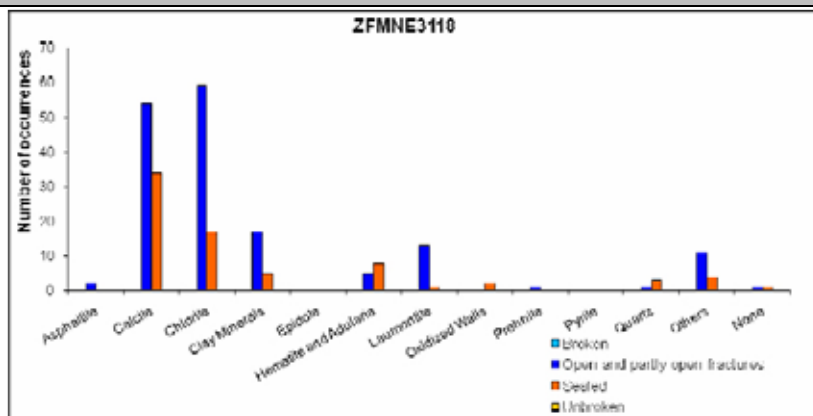
Fracture orientation:



**Fracture frequency:** Open 8 m<sup>-1</sup>, Sealed 23 m<sup>-1</sup>

**Fracture filling mineralogy:**

## Deformation zone ZFMNE3118



KFR104 DZ1 (30–45.5 m)



## BOREHOLE AND TUNNEL INTERCEPT DETAILS

Borehole intersections for ZFMNE3118				
BH	Geometrical Intercept		Target Intercept	
	Sec_up BH length (m) [z (-m)]	Sec_low BH length (m) [z (-m)]	Sec_up BH length (m) [z (-m)]	Sec_low BH length (m) [z (-m)]
HFR101	183.85 [164.70]	203.09 [181.46]	190	202

**SHI DZ3 190–202 m:** Increased frequency of open fractures, sealed fractures and sealed fracture network. Fracture aperture up to 1 mm. Locally weak to medium oxidation. Inferred minor brittle-ductile shear zone at 200.25–200.54 m. Partly decreased bulk resistivity and caliper anomalies. Metagranite-granodiorite (101057), pegmatitic granite (101061) and amphibolite (102017). Confidence level = 1.

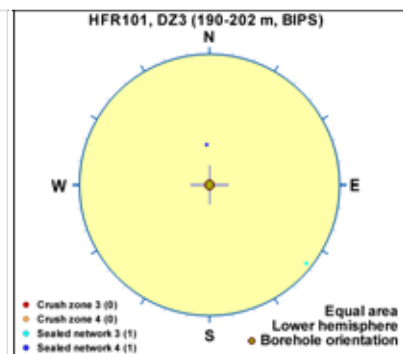
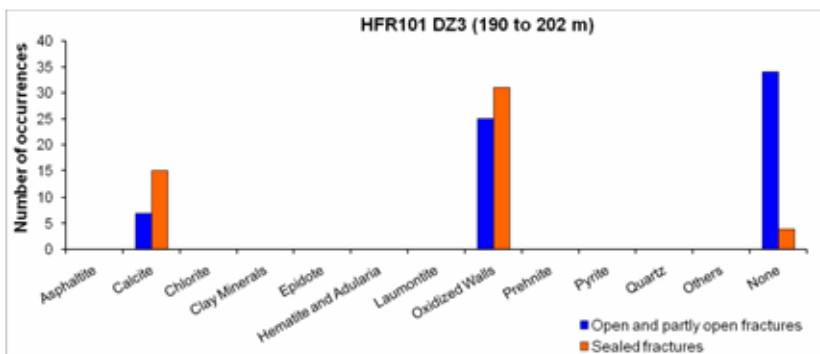
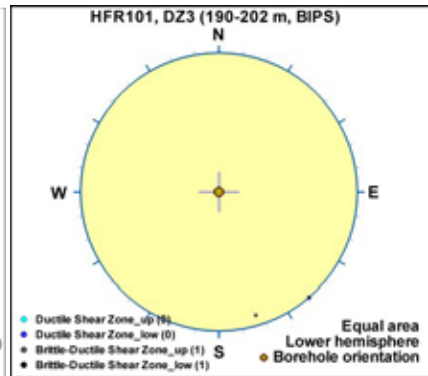
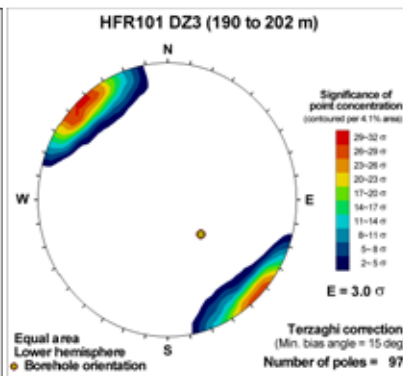
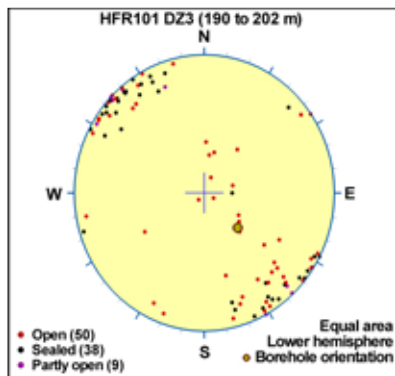
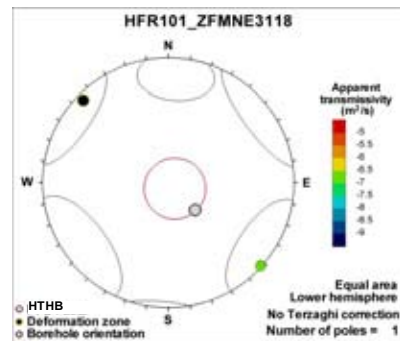
One flow anomaly at 196.0–197.0 m with a moderate transmissivity (about  $3 \cdot 10^{-7} \text{ m}^2/\text{s}$ ). Corresponds to an increased estimated fracture frequency. This is one of the two observed flow anomalies in the borehole.

### Hydraulic data

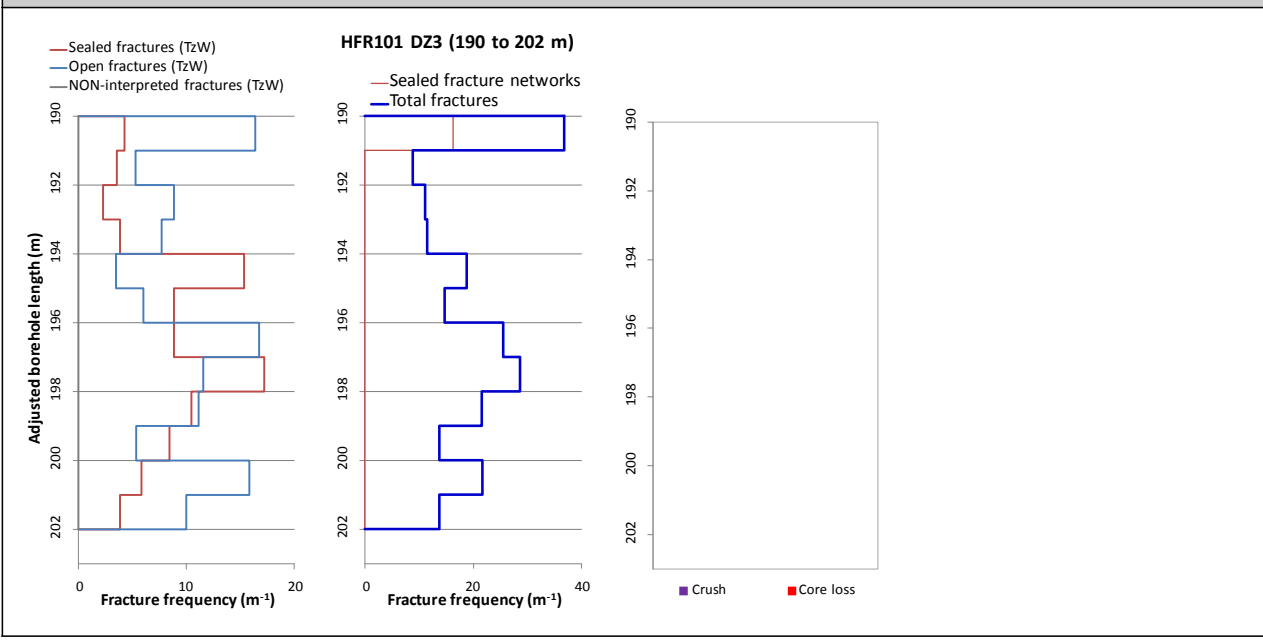
$T = 2.50 \cdot 10^{-7} \text{ m}^2/\text{s}$

$\text{Log } T_0 = -5.8$

Moderate HTHB transmissivity. Estimated HTHB orientation sub-parallel to the zone.



### Borehole intersections for ZFMNE3118



BH	Geometrical Intercept		Target Intercept	
	Sec_up BH length (m) [z (-m)]	Sec_low BH length (m) [z (-m)]	Sec_up BH length (m) [z (-m)]	Sec_low BH length (m) [z (-m)]
KFR13	44.37 [167.71]	eoh [199.94]	47.5	61

**SHI DZ3 47.5–61 m:** Increased frequency of broken and unbroken fractures and sealed networks. Predominant fracture filling minerals are laumontite, chlorite and calcite.  $\alpha$ -angles are generally small. Locally faint to moderate oxidation. Moderately foliated metagranite-granodiorite (101057) and fine- to medium-grained granite (111058). Confidence level = 2.

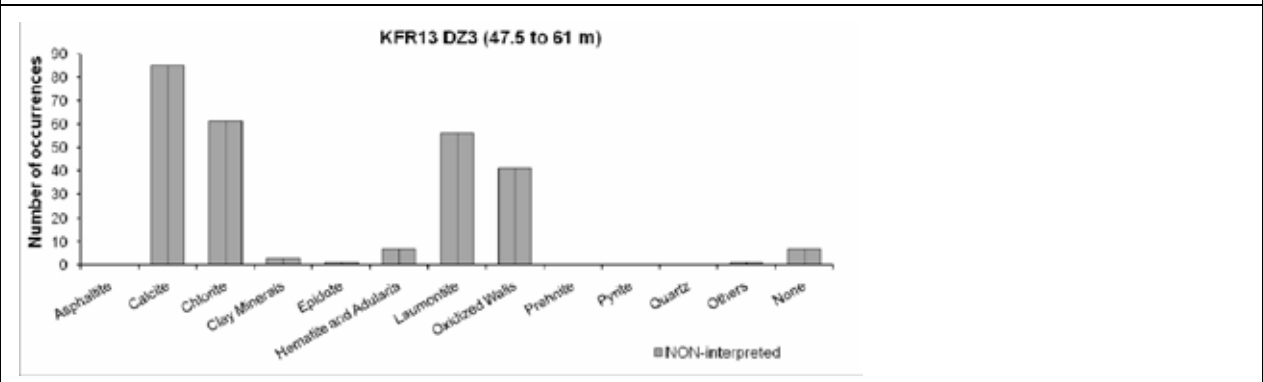
Increased hydraulic conductivity ( $1 \cdot 10^{-7}$  m/s) in the interval 54–61 m.

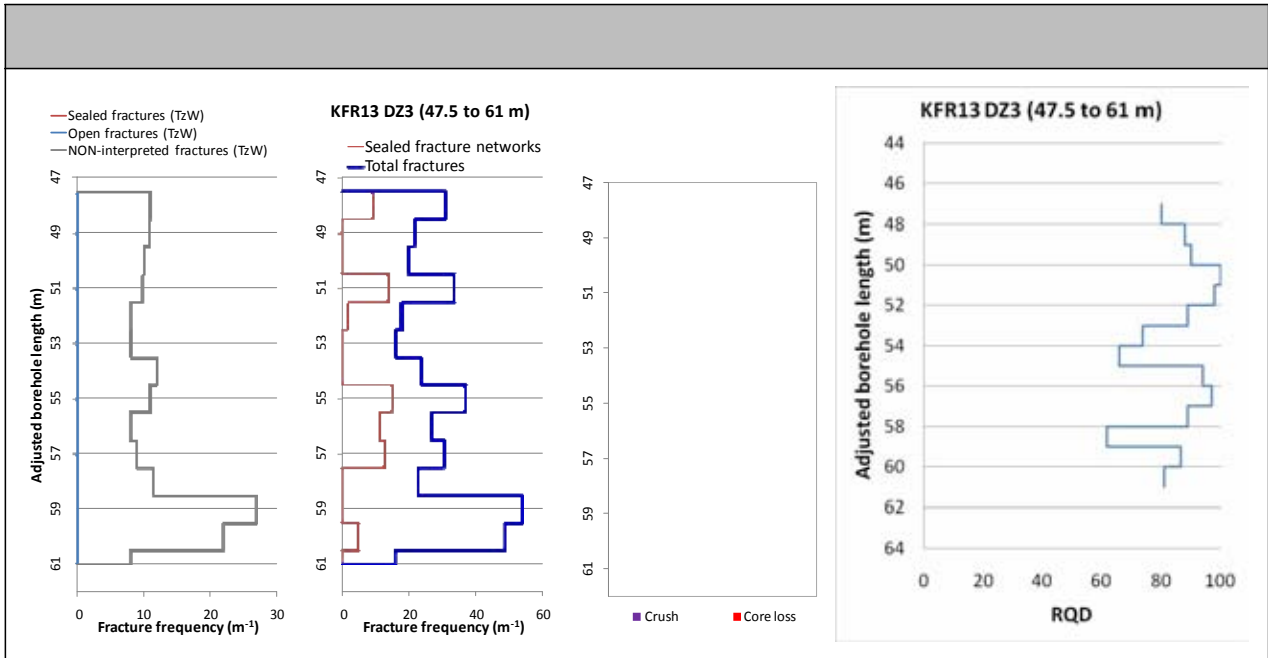
**Hydraulic data**

$T = 3.50 \cdot 10^{-8}$  m<sup>2</sup>/s ( $1.40 \cdot 10^{-6}$  m<sup>2</sup>/s extends into ZFM871)

Log  $T_0 = -7$

Poor data resolution. One of the hydraulic tests partly covers the adjacent ZFM871 intercept. The value has been included to represent similar observations of low-transmissive data partly covering, or found close to ZFMNE3118 intercepts.





BH	Geometrical Intercept		Target Intercept	
	Sec_up BH length (m) [z (-m)]	Sec_low BH length (m) [z (-m)]	Sec_up BH length (m) [z (-m)]	Sec_low BH length (m) [z (-m)]
KFR54	0.00 [81.65]	7.42 [87.14]	0	2.5

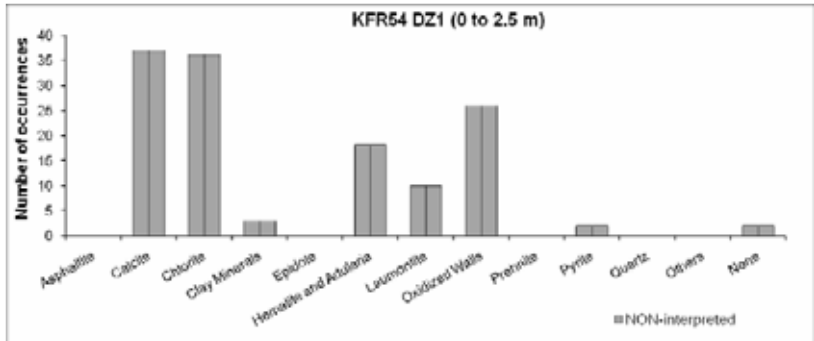
**Comment:**

**SHI DZ1 0–2.5 m:** Increased frequency of broken and unbroken fractures and sealed networks. Predominant fracture minerals are chlorite, calcite and laumontite. Strongly foliated metagranite-granodiorite (101057). Confidence level = 3.

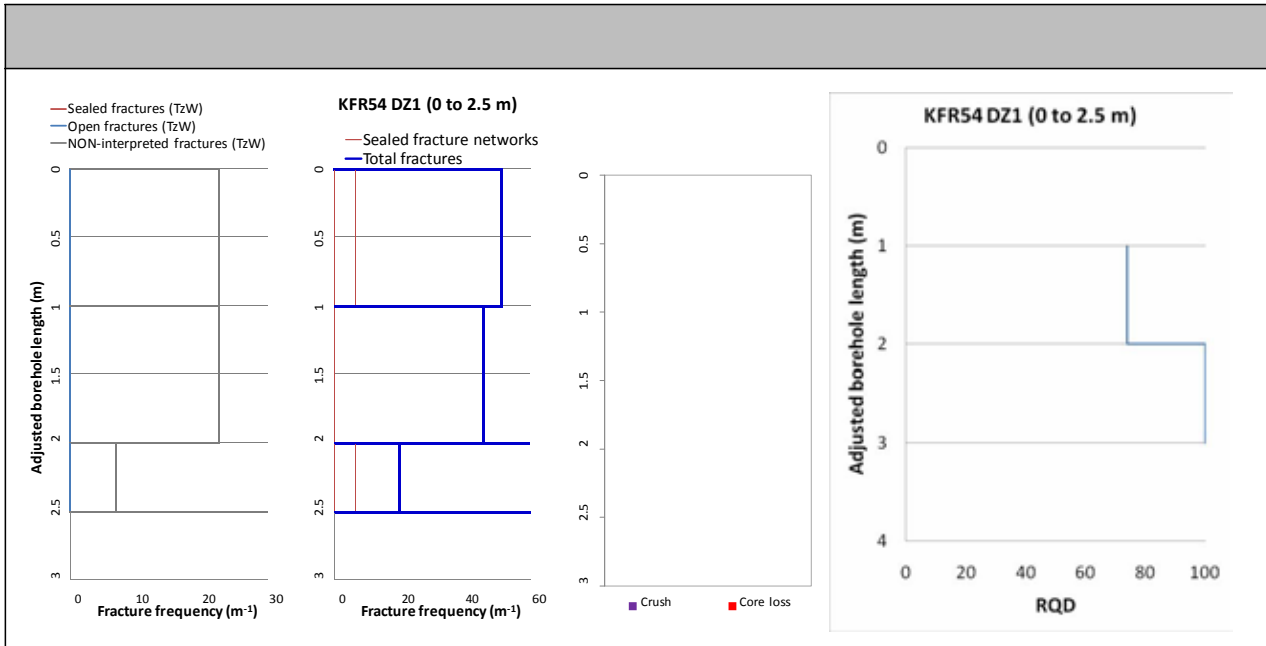
No hydrogeological investigation data from this interval.

**Hydraulic data**

No data ( $T < 1 \cdot 10^{-7} \text{ m}^2/\text{s}$  in surrounding rock).







BH	Geometrical Intercept		Target Intercept	
	Sec_up BH length (m) [z (-m)]	Sec_low BH length (m) [z (-m)]	Sec_up BH length (m) [z (-m)]	Sec_low BH length (m) [z (-m)]
KFR55	8.65 [127.23]	16.80 [128.78]	8	17

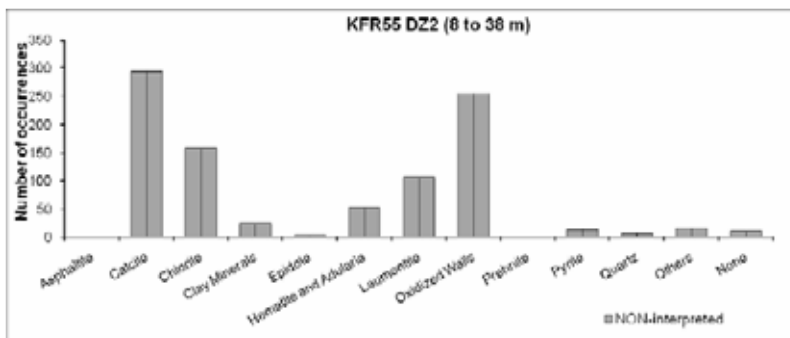
**Comment:** The quoted target intercept is based on a straightforward geometrical subdivision of DZ2 between ZFMNE0870 and ZFMNE3118. It is not expected that their character can be distinguished.

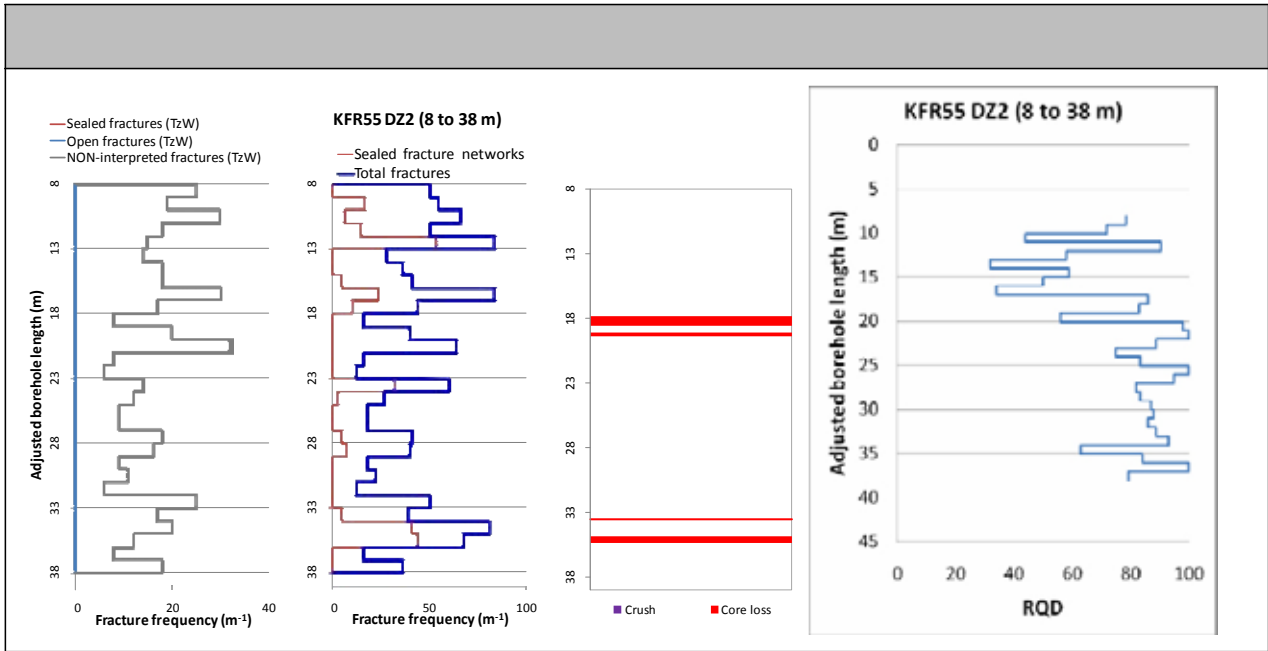
**SHI DZ2 8–38 m:** Increased frequency of broken and unbroken fractures and sealed networks, especially in the intervals 8–21 m and 32–38 m. Core loss at 17.86–18.51, 19.13–19.37, 33.48–33.60 and 34.89–35.33 m. The most frequent fracture filling minerals, which occur throughout the interval, are calcite, and to some extent chlorite. Fractures with clay minerals as the primary infilling are generally restricted to the interval at 16.8–19.5 m, with  $\alpha$ -angles of 69°. Laumontite  $\pm$  calcite filled fractures, on the other hand, occur along three intervals at 8.0–12.6, 16.0–16.5 and 20.4–28.1 m length. Two  $\alpha$ -angles are registered in the uppermost (68 and 77°) and three in the lowermost (50, 57 and 65°) intervals. Locally faint to medium oxidation. Strongly foliated metagranite-granodiorite (101057) and one occurrence of fine- to medium-grained granite (111058). Confidence level = 3.

No hydrogeological investigation data from the upper 22 m of the borehole. The hydraulic conductivity is low in the measured section 22–38 m ( $10^{-8}$  m/s).

**Hydraulic data**

No data ( $T < 1 \cdot 10^{-7}$  m<sup>2</sup>/s in surrounding rock).





BH	Geometrical Intercept		Target Intercept	
	Sec_up BH length (m) [z (-m)]	Sec_low BH length (m) [z (-m)]	Sec_up BH length (m) [z (-m)]	Sec_low BH length (m) [z (-m)]
KFR104	29.73 [21.50]	45.95 [34.72]	30	45.5

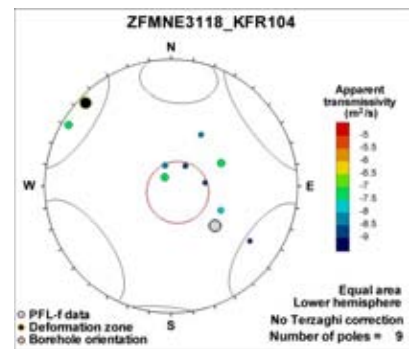
**SHI DZ1 30–45.5 m:** Increased frequency of sealed fracture networks. Faint oxidation in the lower half of the interval and quarts dissolution at 38.30–40.75 m where vugs are filled with calcite. Fracture apertures up to 1 mm with a single aperture at 3 mm. Predominant minerals in sealed fracture networks are chlorite, adularia and hematite. Low electric resistivity. Pegmatitic granite (101061) and metagranite-granodiorite (101057). Confidence level = 1.

Rather high, but not anomalous, transmissivity of the interval ( $2 \cdot 10^{-7} \text{ m}^2/\text{s}$ ).

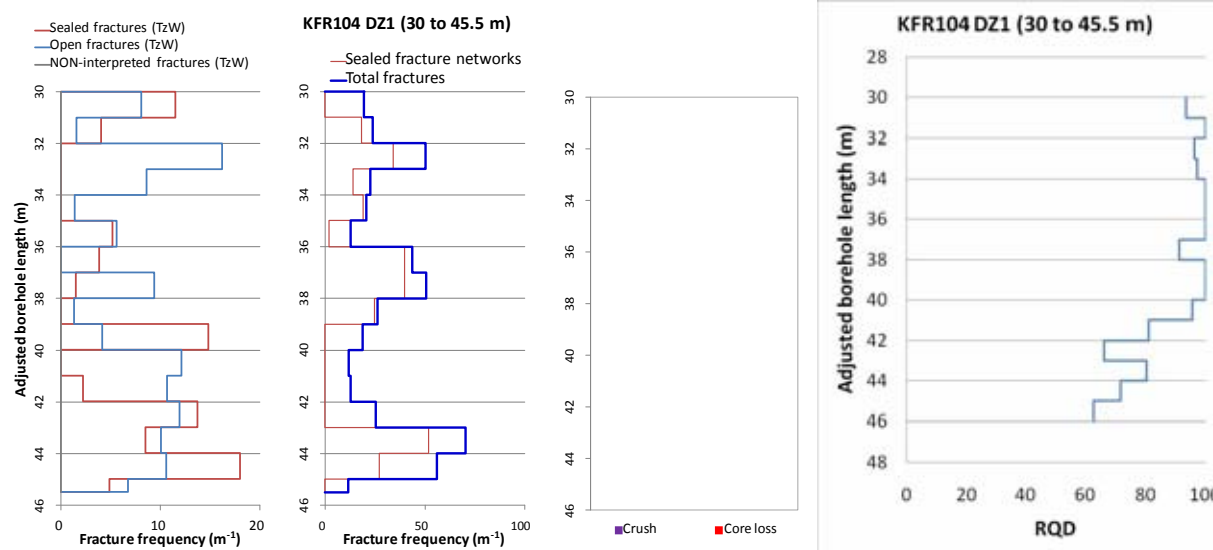
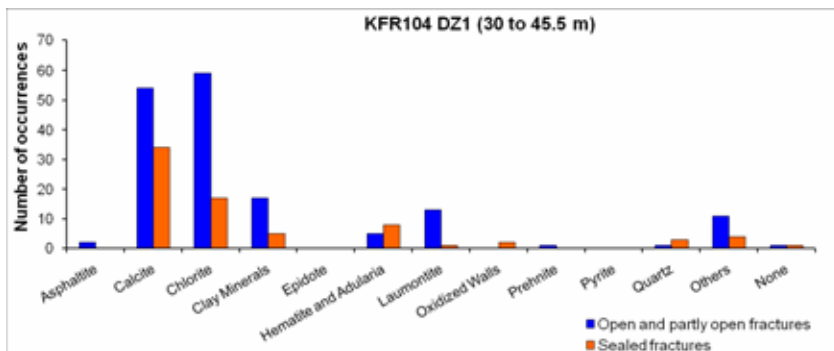
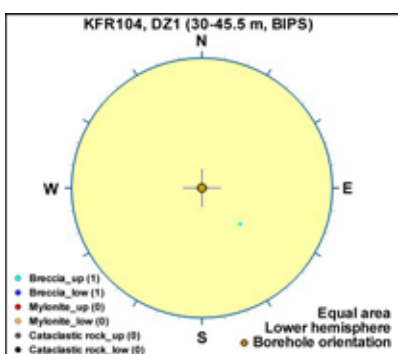
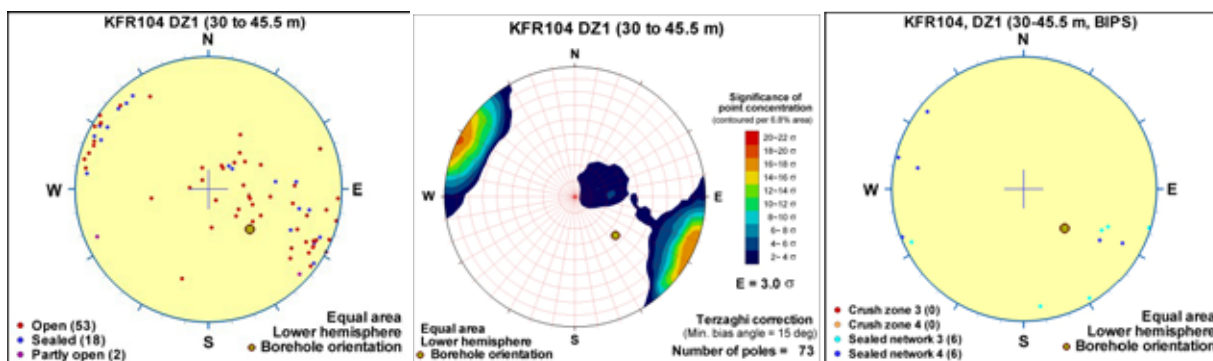
**Hydraulic data**

$T = 1.78 \cdot 10^{-7} \text{ m}^2/\text{s}$

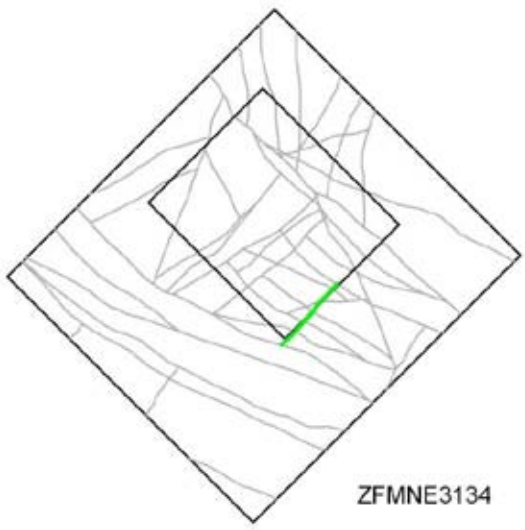
$\text{Log } T_0 = -6.6$



## Borehole intersections for ZFMNE3118



Tunnel intersections for ZFMNE3118				
Tunnel	Geometrical Intercept		Target Intercept	
	Start ch.(m)	End ch. (m)	Start ch.(m)	End ch. (m)
BT	1+075	1+095	1+095	1+095
<b>Comment:</b> Target intercept defined by tDZ73 in Appendix 2.				
BT/ST	1+130	1+166	1+166	–
<b>Comment:</b> Target intercept defined by tDZ73 at 0+88 in ST in Appendix 2.				
NBT	0+055	0+063	0+055	0+059
<b>Comment:</b> Target intercept based on shotcrete coverage marked in the detailed tunnel mapping. Earlier interpreted as zone 12 by /Carlsson et al. 1985/ with an intercept of 8+060.				
NBT	0+295	0+315	0+295	0+340
<b>Comment:</b> Target intercept defined by tDZ73 in Appendix 2.				

<b>Deformation zone ZFMNE3134</b>	
<p><b>Borehole and tunnel intersections (metres along borehole/tunnel)</b></p> <p>None</p>	
<p><b>Deformation style, alteration and geometry</b></p> <p><b>Deformation style:</b> Brittle (no direct evidence – inferred association with other NE-SW trending deformation zones)</p> <p><b>Alteration:</b> No data</p> <p><b>Strike/dip (span) right-hand-rule:</b> 41 / 90 (±5 / ±10)</p> <p><b>Trace length at ground surface (span):</b> 370 m (350–700 m)</p> <p><b>Model thickness:</b> 5 m (1% default)</p> <p><b>Confidence in existence:</b> Medium</p>	
<p><b>Modelling procedure:</b> The position of the zone at the ground surface is based on a linking of lineaments MSFR10005 and MSFR10011 defined by magnetic minima in the SFR model version 1.0, earlier represented by MFM3134G in Forsmark stage 2.3 /Isaksson et al. 2007/. The zone modelled thickness and vertical dip are default values.</p>	
<b>Hydraulic interpretation</b>	
<p><b>Hydraulic width:</b> 3.6 m</p> <p><b>No of intercepts:</b> None</p> <p><b>T<sub>eff</sub>(0):</b> 1.92·10<sup>-7</sup> m<sup>2</sup>/s</p> <p><b>Log T<sub>eff</sub>(0):</b> -6.7, σ = (0.55)</p> <p><b>Calculation procedure:</b> T<sub>eff</sub>(0) taken as pooled average of the NNE to ENE set (only based on new data).</p>	
<b>Fractures in the deformation zone</b>	
<b>General characteristics</b>	
<p><b>Fracture orientation:</b> No data</p> <p><b>Fracture frequency:</b> No data</p> <p><b>Crush zone:</b> No data</p> <p><b>Fracture filling mineralogy:</b> No data</p>	

## Deformation zone ZFMNE3137

### Borehole and tunnel intersections (metres along borehole/tunnel)

KFR102A: 149–161 m (DZ1 149–161 m)  
 KFR102B: 109–114 m (DZ2 109–114 m)  
 KFR104: 382–387 m (DZ4 382–387 m)  
 KFR105: 191–205 m

### Deformation style, alteration and geometry

**Deformation style:** Brittle. Minor cataclasite in KFR104 DZ4

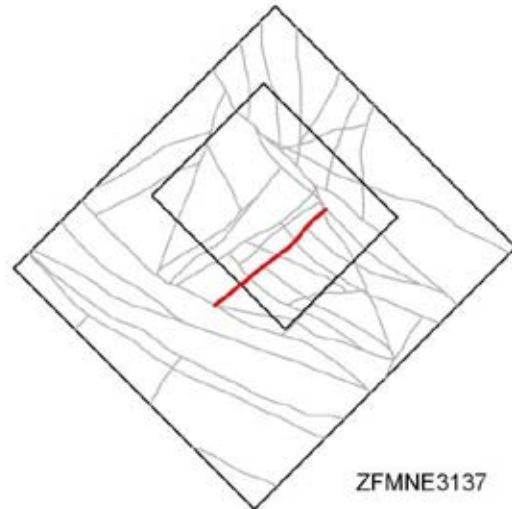
**Alteration:** Locally red-stained bedrock with fine-grained hematite dissemination

**Strike/dip (span) right-hand-rule:** 230 / 90 ( $\pm 5$  /  $\pm 5$ )

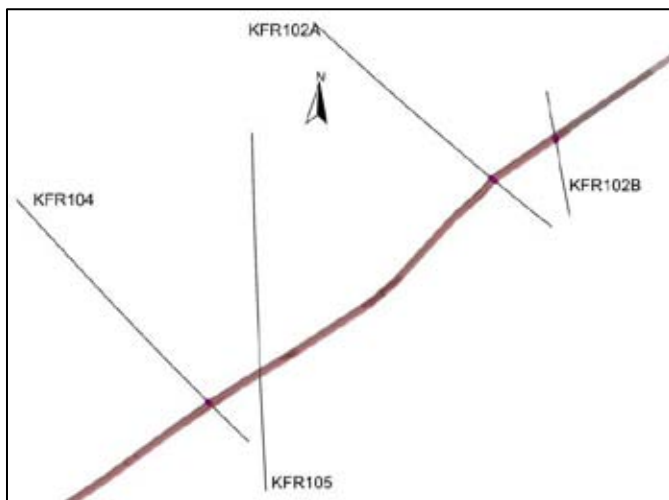
**Trace length at ground surface (span):** 672 m (570–680 m)

**Model thickness (span):** 5 m (1–8 m)

**Confidence in existence:** High



**Modelling procedure:** The position of the zone at the ground surface is based on the magnetic lineament MSFR10004 in SFR model version 1.0, i.e. modified lineament MFM3137G in Forsmark stage 2.3 /Isaksson et al. 2007/, with an extension through the disturbed magnetic area below the pier allowing correlation with new borehole information. Forward modelling of magnetic data along profile 40 (see Appendix 6) supports the modelled vertical dip of the zone.



*ZFMNE3137, top view (dip vertical) in relation to penetrating boreholes. Relevant SHI PDZs are shown as pink cylinders. The modelled zone thickness is 5 m.*

## Deformation zone ZFMNE3137

### Hydraulic interpretation

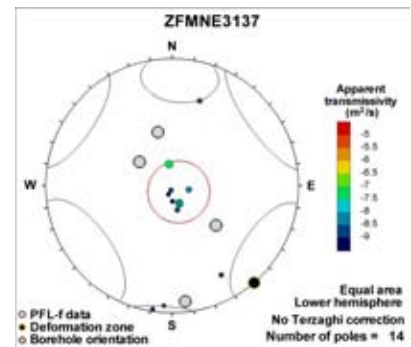
Hydraulic width: 5.0 m

No of intercepts: 4

$T_{\text{eff}}(0)$ :  $5.48 \cdot 10^{-8} \text{ m}^2/\text{s}$

Log  $T_{\text{eff}}(0)$ :  $-7.3$ ,  $\sigma = 0.30$

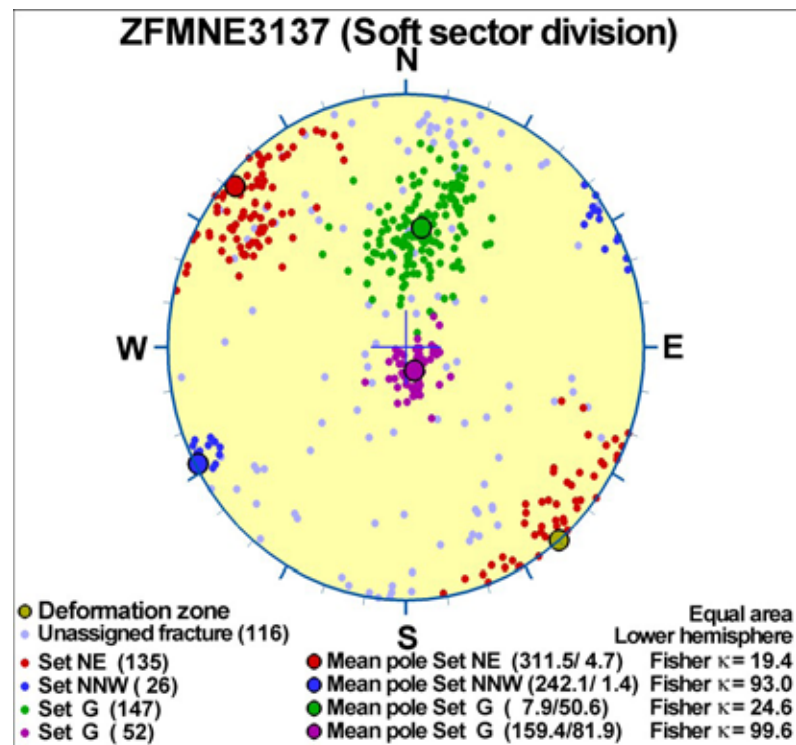
**Calculation procedure:**  $T_{\text{eff}}(0)$  taken as average from all four intercepts. PFL-f data exhibit the typical pattern of rock mass in the Central Block.



## Fractures in the deformation zone

### General characteristics

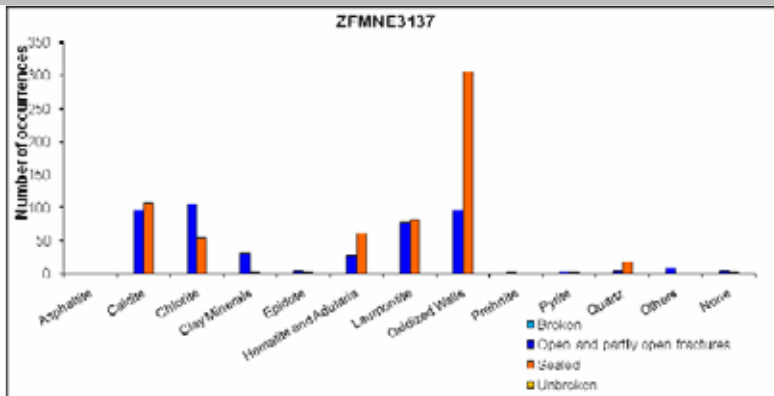
Fracture orientation:



Fracture frequency: Open  $7 \text{ m}^{-1}$ , Sealed  $32 \text{ m}^{-1}$

Fracture filling mineralogy:

## Deformation zone ZFMNE3137



### KFR102A DZ1 (149–161 m)





## BOREHOLE AND TUNNEL INTERCEPT DETAILS

Borehole intersections for ZFMNE3137				
BH	Geometrical Intercept		Target intercept	
	Sec_up BH length (m) [z (-m)]	Sec_low BH length (m) [z (-m)]	Sec_up BH length (m) [z (-m)]	Sec_low BH length (m) [z (-m)]
KFR102A	147.83 [132.22]	160.74 [143.97]	149	161

**SHI DZ1 149–161 m:** Increased frequency of open and particularly sealed fractures. No alteration. Fracture apertures 0.5 mm or less. Predominant minerals in sealed and open fractures are laumontite, adularia, calcite and chlorite. One oriented radar reflector at 154 m (315°/63° or 108°/63°). The magnetic susceptibility is decreased along the entire section. There are no other significant anomalies related to increased fracturing in the geophysical logging data. Metagranite-granodiorite (101057). Confidence level = 2.

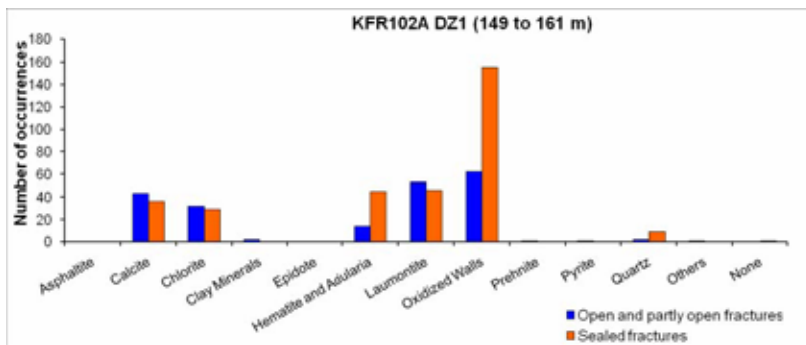
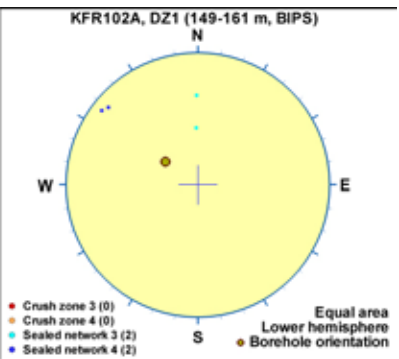
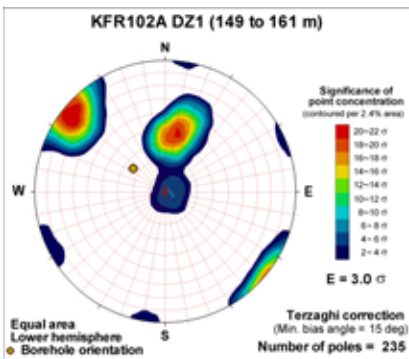
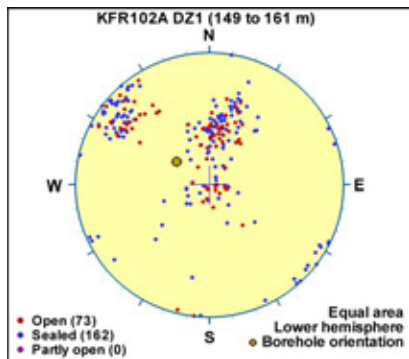
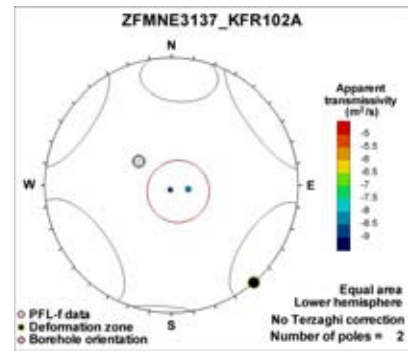
Two flow anomalies and rather low transmissivity of the section ( $T = 1 \cdot 10^{-8} \text{ m}^2/\text{s}$ ).

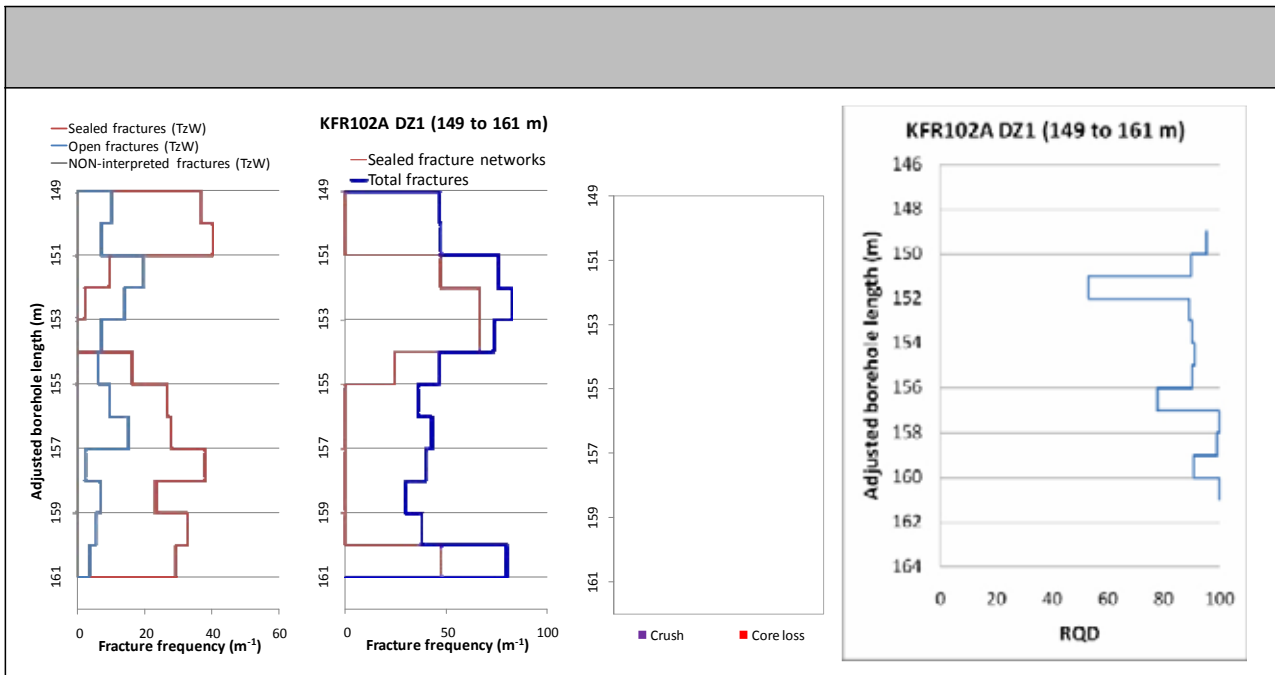
### Hydraulic data

$T = 9.50 \cdot 10^{-9} \text{ m}^2/\text{s}$

$\text{Log } T_0 = -7.4$

Little hydraulic support. Only two low-transmissive, horizontal PFL-f.  
Typical pattern of ENE to NE set.





**Borehole intersections for ZFMNE3137**

BH	Geometrical Intercept		Target intercept	
	Sec_up BH length (m) [z (-m)]	Sec_low BH length (m) [z (-m)]	Sec_up BH length (m) [z (-m)]	Sec_low BH length (m) [z (-m)]
KFR102B	106.92 [84.13]	116.23 [91.63]	109	114

**SHI DZ2 109–114 m:** Increased frequency of open and sealed fractures and sealed fracture networks. Fracture apertures up to 1.5 mm. Locally weak to medium oxidation. Predominant minerals in sealed fractures are calcite, chlorite, laumontite, adularia and quartz and in open fractures chlorite, calcite, laumontite and clay minerals. Significantly decreased resistivity and magnetic susceptibility in the interval 109–111 m. In the remaining part of the section the resistivity and magnetic susceptibility are partly decreased along minor intervals. Metagranite-granodiorite (101057), pegmatitic granite (101061) and amphibolite (102017). Confidence level = 3.

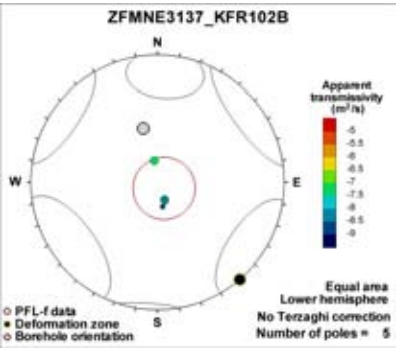
The transmissivity of the interval is about  $1 \cdot 10^{-7} \text{ m}^2/\text{s}$  and is dominated by two flow anomalies at 109.1 and 109.7 m, the latter corresponding to several open fractures.

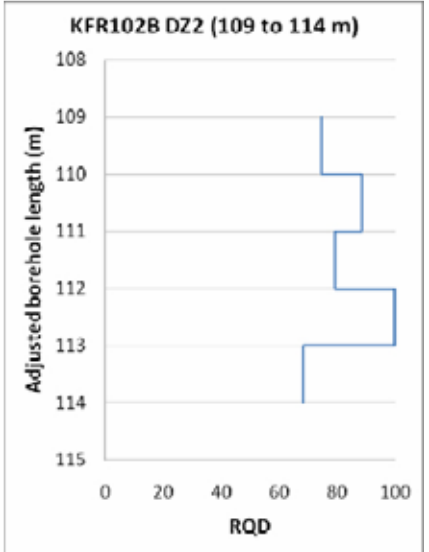
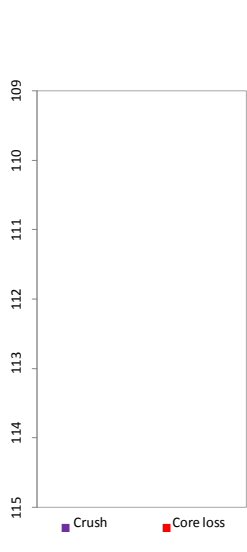
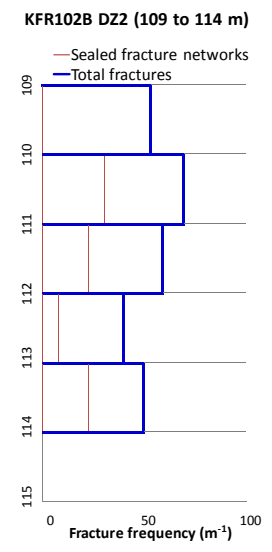
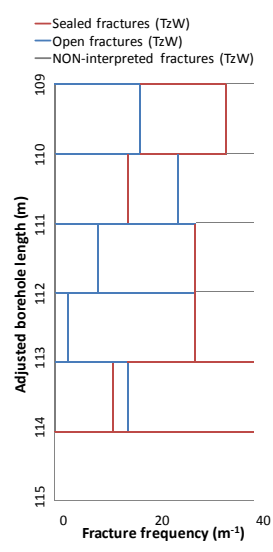
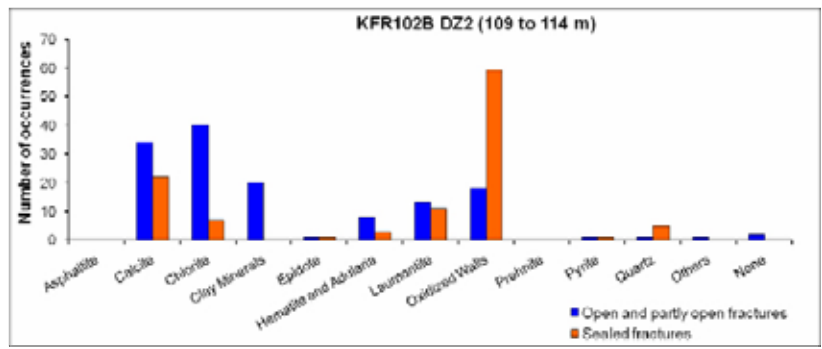
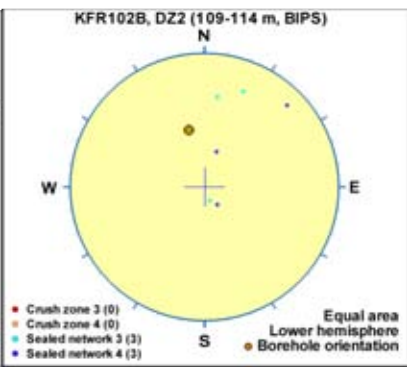
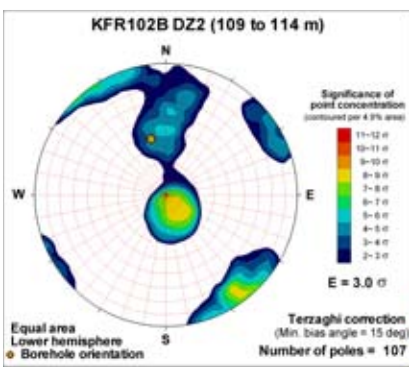
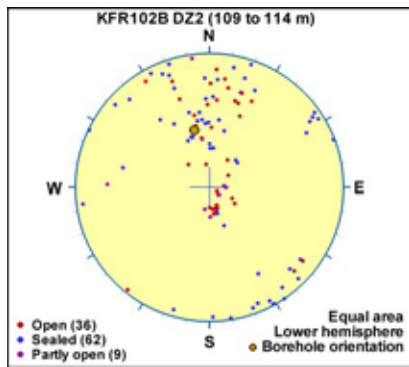
**Hydraulic data**

$T = 1.41 \cdot 10^{-7} \text{ m}^2/\text{s}$

$\text{Log } T_0 = -6.5$

Little hydraulic support. Five moderately transmissive, sub-horizontal PFL-f. Typical pattern of ENE to NE set.





### Borehole intersections for ZFMNE3137

BH	Geometrical Intercept		Target intercept	
	Sec_up BH length (m) [z (-m)]	Sec_low BH length (m) [z (-m)]	Sec_up BH length (m) [z (-m)]	Sec_low BH length (m) [z (-m)]
KFR104	380.85 [296.78]	388.50 [302.51]	382	387

**Comment:**

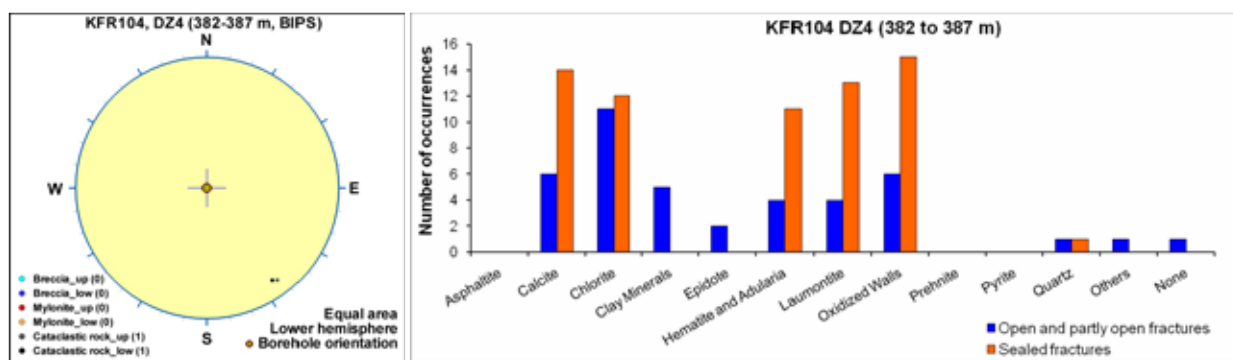
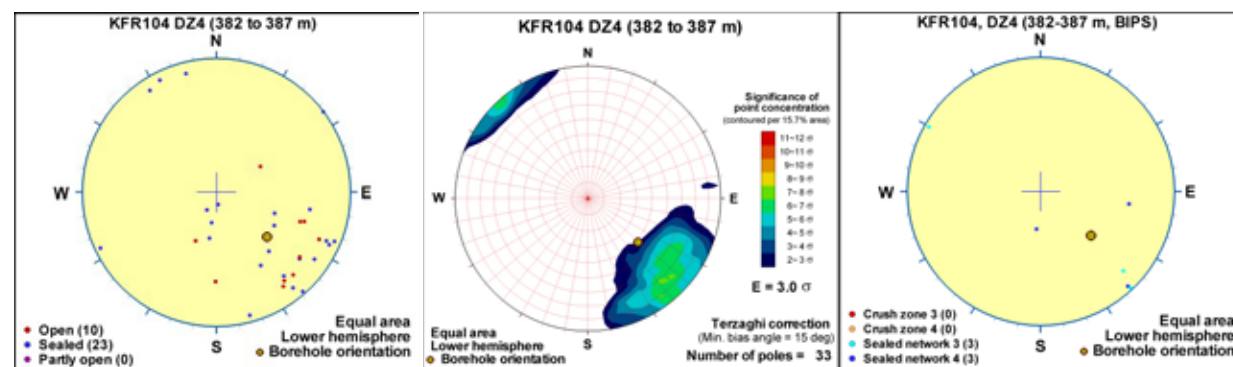
**SHI DZ4 382–387 m:** Increased frequency of sealed fracture networks. One minor cataclasite at 383.34–383.36 m. Locally faint to moderate oxidation. Fracture aperture up to 1mm. Predominant minerals in sealed fracture networks are adularia, laumontite, chlorite and calcite. One minor resistivity anomaly. One oriented radar reflector (216°/70° or 184°/11°). Felsic to intermediate metavolcanic rock (103076) and pegmatitic granite (101061). Confidence level = 3. No flow anomaly and transmissivity below the measurement limit in this interval.

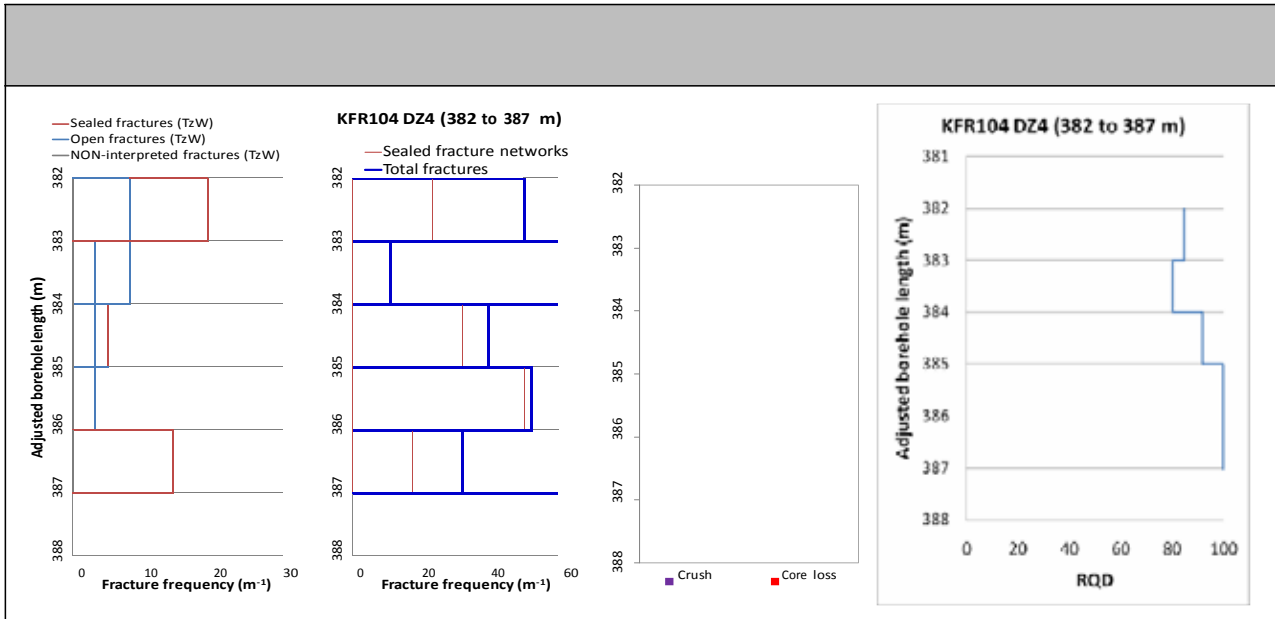
**Hydraulic data**

$T = 1.70 \cdot 10^{-9} \text{ m}^2/\text{s}$

$\text{Log } T_0 = -7.5$

No PFL-f found inside the interval. The detection limit is taken as an upper estimate of the interval transmissivity. Considered typical of Central Block characteristics.





**Borehole intersections for ZFMNE3137**

BH	Geometrical Intercept		Target intercept	
	Sec_up BH length (m) [z (-m)]	Sec_low BH length (m) [z (-m)]	Sec_up BH length (m) [z (-m)]	Sec_low BH length (m) [z (-m)]
KFR105	203.99 [140.86]	209.71 [141.77]	191	205

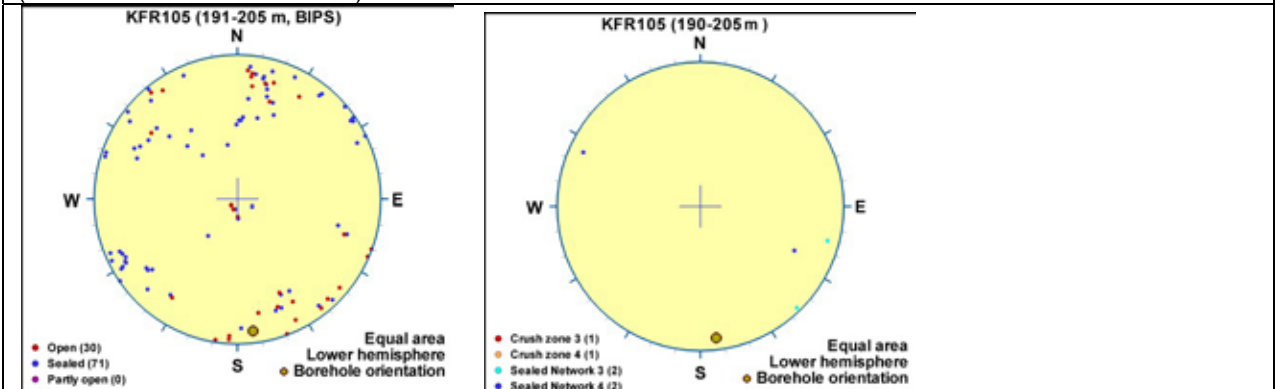
**Comment:** There is no SHI DZ interpreted in the position of the target intercept in KFR105. However, the modelled geometry generates an intercept in KFR105 with a section of core that coincides with an interval of increased frequency of steeply dipping fractures that strike NE at 191 to 193 m length. In addition, two NE-striking sealed networks at 202.7–203.8 and 204.2–204.8 m with piece lengths of 30 and 15 mm, respectively, along with NE-striking crush at 205.0–205.05 m. No control point has been added for this borehole.

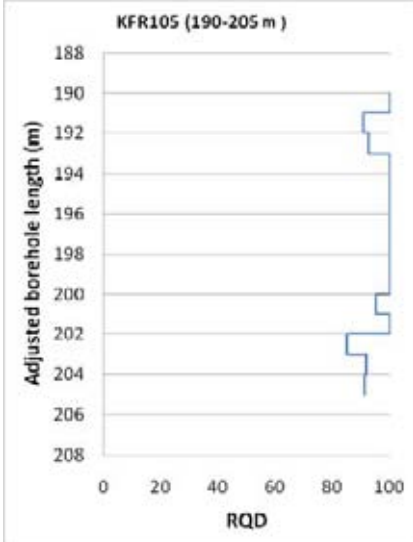
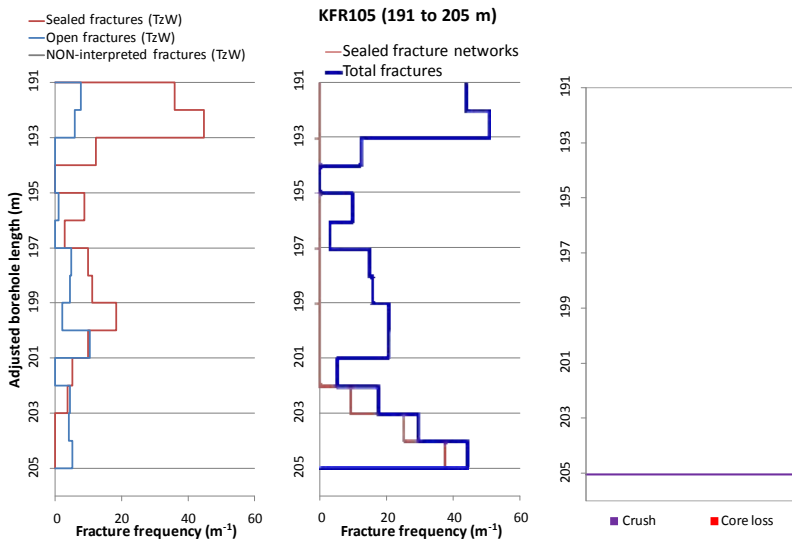
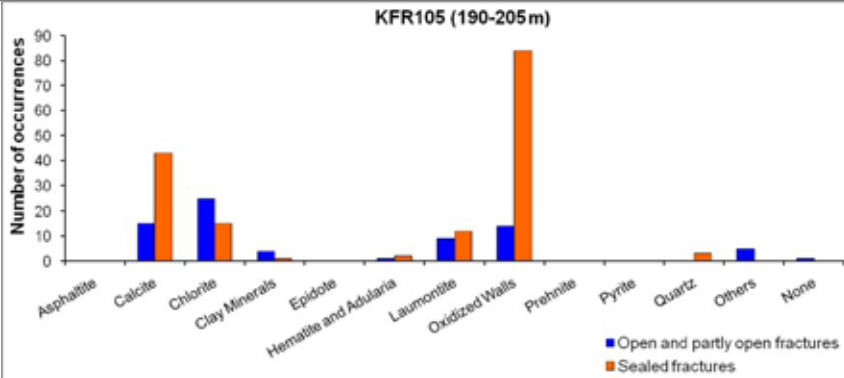
**Hydraulic data**

$T = 5.36 \cdot 10^{-9} \text{ m}^2/\text{s}$

$\text{Log } T_0 = -7.7$

Several low-transmissive PFL-f with scattered orientation. Considered typical pattern of Central Block characteristics (inside as well as outside zones).





## Deformation zone ZFMNNE0869

### Borehole and tunnel intersections (metres along borehole/tunnel)

KFR09: 0–58.7 m (DZ1 0–58.7 m)  
 KFR36: 45–115.5 m (DZ1 45–115.5 m)  
 KFR68: 71.59– 105.13 m (DZ1 71.59–78.11 m and DZ2 102.83–105.13 m)  
 DT 0+430–0+540 (tDZ30 0+430, tDZ31 0+475, tDZ32 0+478 and tDZ34 0+525)  
 BT 0+355–0+450 (tDZ30 0+355, tDZ31 0+400, tDZ32 0+414 and tDZ34 0+450)

### Deformation style, alteration and geometry

**Deformation style:** Brittle. Cohesive breccias present in KFR36 DZ1

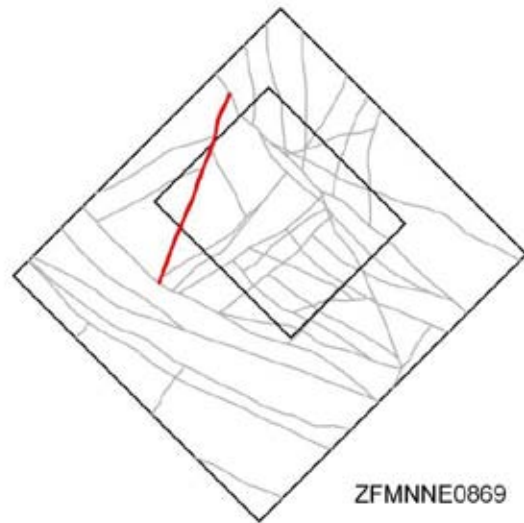
**Alteration:** Red-stained bedrock with fine-grained hematite dissemination

**Strike/dip (span) right-hand-rule:** 201 / 86 ( $\pm 5 / \pm 10$ )

**Trace length at ground surface (span):** 898 m (550–900 m)

**Model thickness (span):** 60 m (20–60 m)

**Confidence in existence:** High

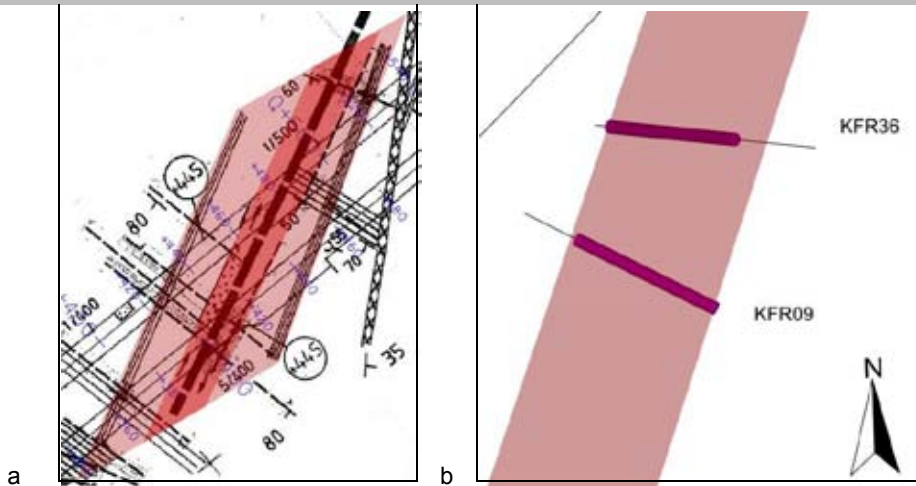


**Modelling procedure:** This zone corresponds to zone 3 in earlier SFR models (see for example /Axelsson and Hansen 1997/). It was renamed ZFMNNE0869 in the Forsmark stage 2.2 model /Stephens et al. 2007/. The position of the central section of the zone at the ground surface is based on the lineament MSFR08089 in SFR model version 1.0 that corresponds to a magnetic minimum. The zone has been extended further to the NNE to terminate against ZFMNW0805A based on the reprocessing and re-evaluation of magnetic data. The NNE termination to ZFMNW0805A is consistent with the extension modelled by /Axelsson and Hansen 1997/, which was adopted subsequently by /Stephens et al. 2007/. However, adjustments to zone ZFMNW0805A have resulted in a minor adjustment of the trace length of zone ZFMNNE0869 at the ground surface compared with that presented in /Stephens et al. 2007/. In the SSE, the zone terminates at the surface at ZFMWNW1035 and at depth at ZFMNW0002.

The orientation 201/86 involves only a slight adjustment compared with earlier models (200/80 in /Stephens et al. 2007/). However, the zone thickness has been modified considerably in accordance with current SKB SHI based methodology. The thickness has been increased from 10 m to 60 m based on the results of the geological SHI from KFR09 and KFR36 and the indications as presented on the tunnel mapping overview drawings, all of which support an increased modelled thickness. The earlier thinner interpretation /Axelsson and Hansen 1997/ did not include the mapped parallel structures shown in the tunnel mapping though the reasoning is not clear. The zone is interpreted to be a composite zone consisting of several narrower high-strain segments (sub-zones) that diverge and converge in a complex pattern /Axelsson and Hansen 1997/. In the tunnels the zone has been reported as associated with moisture, dripping and occasionally running water.

The zone is crossed by four seismic refraction profiles /Keisu and Isaksson 2004/. Two profiles indicate minor low velocity anomalies while velocities generally lie in the range of 4000–5000 m/s. Forward modelling of magnetic data along profile 18 (see Appendix 6) suggests a sub-vertical dip. It should be noted that the width of the anomaly is much narrower than the modelled zone thickness. The anomaly is taken to represent one member of a broader group of sub-parallel, narrow zones represented by the greater modelled thickness.

## Deformation zone ZFMNNE0869



a. Plan view of ZFMNNE0869 as interpreted in the DT and BT tunnels. The possible zone core is shown in dark pink with the bordering damage zones shown in a lighter pink.

b. ZFMNNE0869, looking down dip, as interpreted in KFR36 and KFR09. The relevant SHI PDZs are shown as pink cylinders.

### Hydraulic interpretation

**Hydraulic width:** 41.7 m

**No of intercepts:** 4

**$T_{eff}(0)$ :**  $2.72 \cdot 10^{-5} \text{ m}^2/\text{s}$

**Log  $T_{eff}(0)$ :** -4.6,  $\sigma = 0.28$

**Calculation procedure:**  $T_{eff}(0)$  taken as average from all 4 intercepts.

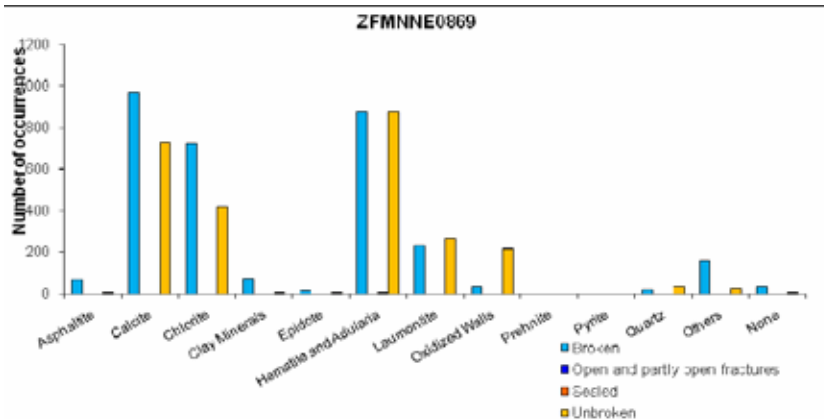
### Fractures in the deformation zone

#### General characteristics

**Fracture orientation:** No orientation fracture data is available

**Fracture frequency:** No orientation corrected data is available. See individual borehole intercepts for general indications.

**Fracture filling mineralogy:**





## Deformation zone ZFMNNE0869

KFR09 DZ1 (0-58.7 m)



## BOREHOLE AND TUNNEL INTERCEPT DETAILS

Borehole intersections for ZFMNNE0869				
BH	Geometrical Intercept		Target Intercept	
	Sec_up BH length (m) [z (-m)]	Sec_low BH length (m) [z (-m)]	Sec_up BH length (m) [z (-m)]	Sec_low BH length (m) [z (-m)]
KFR09	0.00 [77.44]	59.19 [82.60]	0	58.7

**SHI DZ1 0–58.7 m:** Increased frequency of broken and unbroken fractures and sealed networks. Most intensely fractured between 16–58.7 m. Seven minor intervals of crush. Calcite, chlorite, adularia and laumontite, variably discoloured by microscopic hematite, are the most frequent fracture filling minerals. The occurrence of laumontite is, generally restricted to two distinct sections at 0–24 and 40–45 m, and their  $\alpha$ -angles are typically dipping moderately (57–78°). None of the other major mineral phases exhibit such a distinct distribution pattern. Numerous asphalt-bearing fractures have been registered in the length interval 26–61 m. The occurrence of clay mineral fillings is rather scarce. Generally faint to weak oxidation. Felsic to intermediate volcanic rock (103076) with minor occurrences of pegmatitic granite (101061), fine- to medium-grained granite (111058) and amphibolite (102017). Confidence level = 3.

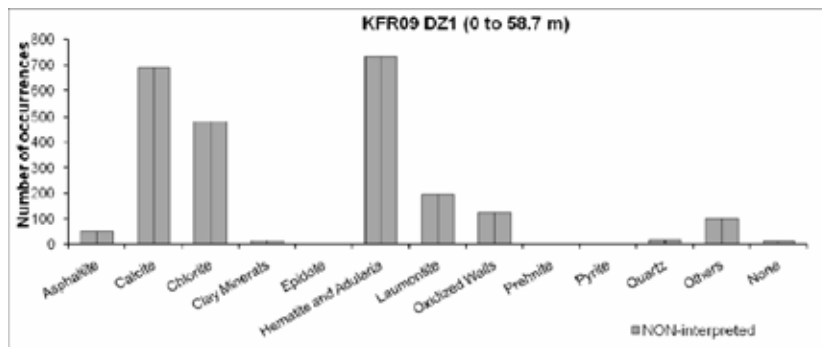
No hydrogeological investigation data from the upper 7 m of the borehole. The hydraulic conductivity (measured in sections of about 20 m) is moderate to high in the whole interval (above  $4 \cdot 10^{-8}$  m/s). The maximum measured hydraulic conductivity is  $2 \cdot 10^{-6}$  m/s in the interval 43–62 m.

### Hydraulic data

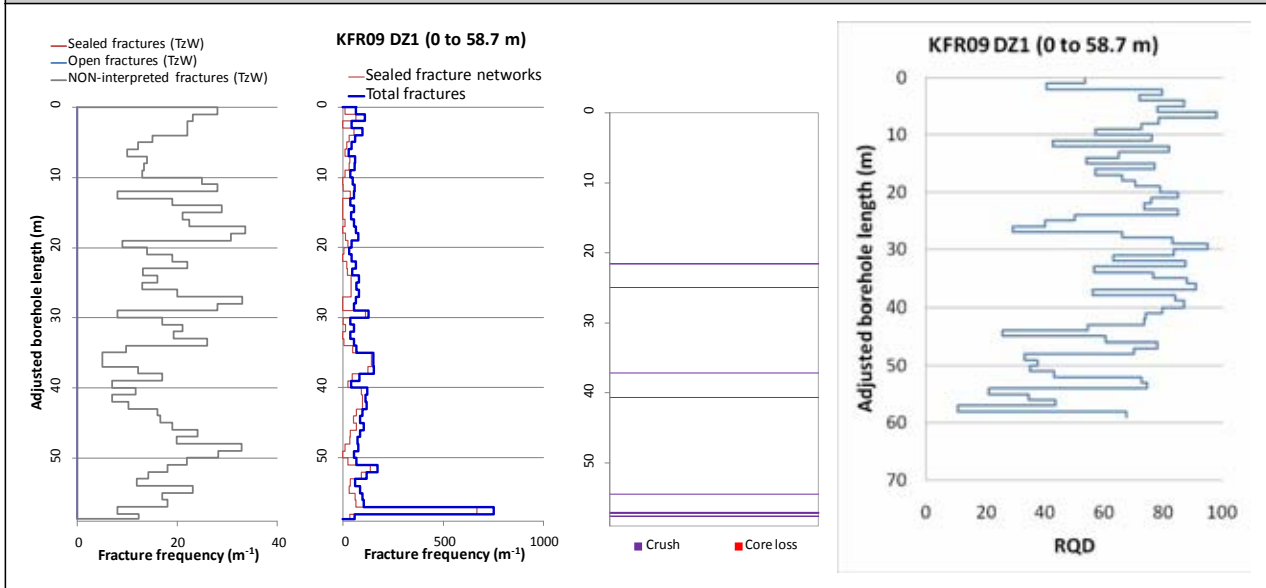
$$T = 4.28 \cdot 10^{-5} \text{ m}^2/\text{s}$$

$$\text{Log } T_0 = -4$$

Highest transmissivity found at the end of the intercept.



### Borehole intersections for ZFMNNE0869



### Borehole intersections for ZFMNNE0869

BH	Geometrical Intercept		Target Intercept	
	Sec_up BH length (m) [z (-m)]	Sec_low BH length (m) [z (-m)]	Sec_up BH length (m) [z (-m)]	Sec_low BH length (m) [z (-m)]
KFR36	27.80 [14.99]	118.84 [80.48]	45	115.5

**SHI DZ1 45–115.5 m:** Increased frequency of broken and unbroken fractures and sealed networks. Decreased frequency of broken fractures between 63.5–70 m, which corresponds to the occurrence of pegmatitic granite. The section between 98–115.5 m is the most highly fractured part, with nine crushed sections. The primary infilling minerals in the interval are adularia, calcite and laumontite, together with trace amounts of hematite. Three breccias at 57.09–57.10, 104.81–105.56 and 107.95–108.04 m occur in the interval.  $\alpha$ -angles are generally small to moderate ( $<67^\circ$ ). In the intensely fractured interval at 44–53 m length, there is a majority of fractures filled by calcite and chlorite, with subordinate amounts of hematite. The interval includes one minor crush zone at 49.11–49.15 m. A distinct peak of broken fractures with adularia and chlorite together with a white unidentifiable mineral that might be kaolinite or a zeolite occurs at 60–62 m. Two  $\alpha$ -angles at 12 and  $30^\circ$  are registered in the interval. Asphaltite-bearing fractures, concentrated to the interval between 105–114 m. Generally faint to weak oxidation through out the possible zone. Strongly foliated metagranite-granodiorite (101057) with occurrences of fine- to medium-grained granite (111058), intermediate metavolcanic rock (103076), pegmatitic granite (101061), amphibolites (102017) and metagabbro-diorite (101033). Confidence level = 3.

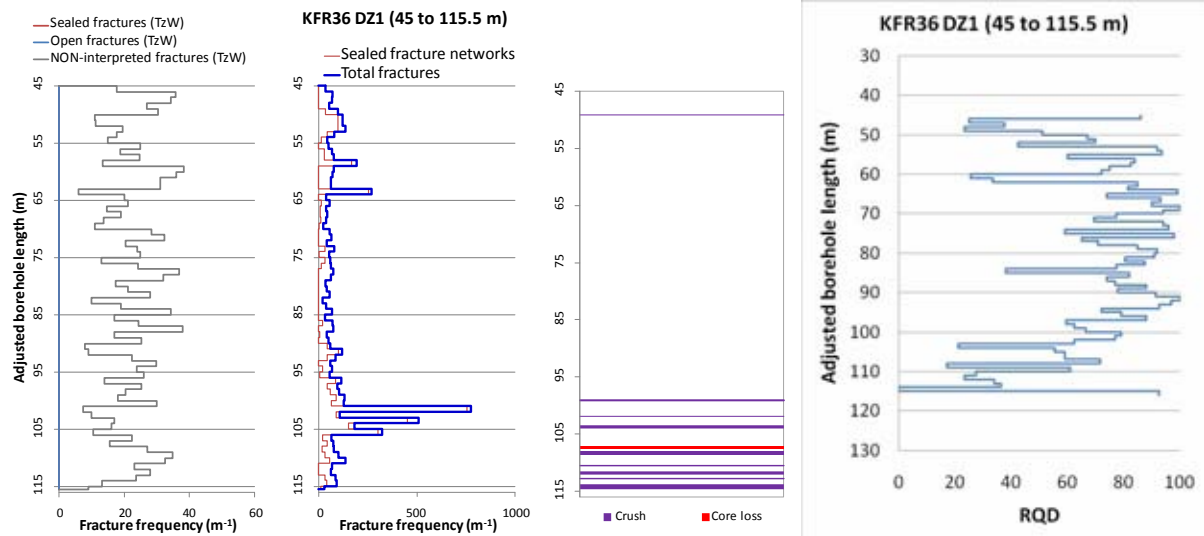
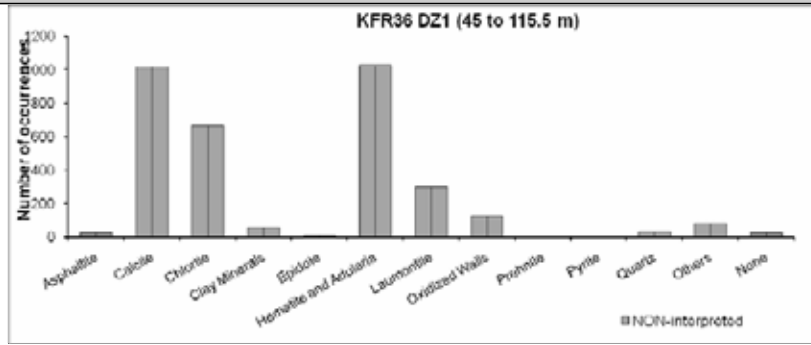
The hydraulic conductivity (measured in 3-m sections) is quite high in the whole interval ( $6 \cdot 10^{-6}$ – $5 \cdot 10^{-8}$  m/s). Hydraulic conductivity above  $1 \cdot 10^{-6}$  m/s at 48–51, 54–57, 96–99 and 102–108 m.

#### Hydraulic data

$$T = 4.09 \cdot 10^{-5} \text{ m}^2/\text{s}$$

$$\text{Log } T_0 = -4.2$$

### Borehole intersections for ZFMNNE0869



BH	Geometrical Intercept		Target Intercept	
	Sec_up BH length (m) [z (-m)]	Sec_low BH length (m) [z (-m)]	Sec_up BH length (m) [z (-m)]	Sec_low BH length (m) [z (-m)]
KFR68	43.94 [31.06]	eoh [90.82]	71.59	105.13

**Comment:** KFR68 is interpreted as intercepting the meeting point between ZFMNNE0869 and ZFMNE0870. Since the BH lacks fracture orientation data, it is impossible to correlate the PDZ with any specific steeply dipping zone. Thus, the PDZs are taken as target intercepts for both ZFMNE0870 and ZFMNNE0869.

**SHI DZ1 71.59–78.11 m:** Increased frequency of broken fractures, locally also sealed fracture networks. Variable  $\alpha$ -angles, but generally  $> 45^\circ$ . Locally faint to weak argillization. Weak muscovitization throughout the interval. Predominant minerals in broken and unbroken fractures are clay minerals, calcite and chlorite. Pegmatitic granite (101061) and aplitic metagranite (101058). Confidence level = 3.

Transmissivity below the measurement limit ( $7 \cdot 10^{-7} \text{ m}^2/\text{s}$ ).

**SHI DZ2 102.83–105.13 m:** Increased frequency of broken fractures and crushes. Variable  $\alpha$ -angles. Weak to moderate oxidation throughout the interval. Predominant minerals in broken fractures are clay minerals, chlorite, hematite and calcite. Fine- to medium-grained granite (111058) and pegmatitic granite (101061). Confidence level = 1.

Moderate transmissivity of the interval 102.51–105.51 m ( $8 \cdot 10^{-7} \text{ m}^2/\text{s}$ ).

### Borehole intersections for ZFMNNE0869

**Hydraulic data**

$T = 4.08 \cdot 10^{-6} \text{ m}^2/\text{s}$

$\text{Log } T_0 = -5.2$

Only three packer data above detection limit (98 to 107 m BHL). Assumed to dominate over ZFMNE0870.

BH	Geometrical Intercept		Target Intercept	
	Sec_up BH length (m) [z (-m)]	Sec_low BH length (m) [z (-m)]	Sec_up BH length (m) [z (-m)]	Sec_low BH length (m) [z (-m)]
KFR10	0.00 [78.30]	97.49 [147.24]	–	–

**Comment:** Judging from the photographs of the drill cores, there is a frequency of broken fractures that locally exceeds 10 fractures/m along the interval 0–97 m. Oxidation of varying degrees occurs frequently throughout the interval 0–97 m. Both the fracture frequency and occurrence of oxidation resembles that for DZ1 in KFR09 and for DZ1 in KFR36, but is generally slightly lower and less conspicuous, respectively. Thus, ZFMNNE0869 may well have its intersection in this interval, but a specific target intercept cannot be defined.

**SHI DZ1 0–5.00 m:** Increased frequency of broken and locally unbroken fractures.  $\alpha$ -angles > 45°. Weak to medium oxidation outside amphibolites. Predominant fracture minerals are chlorite, laumontite, calcite and clay minerals. Moderately foliated metagranite-granodiorite (101057) and amphibolite (102017). Confidence level = 1.

No hydraulic test data from this section of the borehole.

**Hydraulic data**

$T = 3.00 \cdot 10^{-6} \text{ m}^2/\text{s}$

$\text{Log } T_0 = -4.9$

Available hydraulic data in the interval 0 to 86 m BHL used.

### Tunnel intersections for ZFMNNE0869

Tunnel	Geometrical Intercept		Target Intercept	
	Start ch.(m)	End ch. (m)	Start ch.(m)	End ch. (m)
DT	0+430	0+555	0+430	0+540

**Comment:** Target intercept defined by tDZ30 0+430, tDZ31 0+475, tDZ32 0+478, tDZ34 0+525 and tDZ36 0+540 in Appendix 2 of /Curtis et al. 2009/. Clay, crushed rock, alteration, water and injection /Carlsson et al. 1985/.

BT	0+357	0+482	0+350	0+450
----	-------	-------	-------	-------

**Comment:** Target intercept defined by (tDZ30 0+355, tDZ31 0+400, tDZ32 0+414 and tDZ34 0+450) in Appendix 2.

## Deformation zone ZFMNNE3264

### Borehole and tunnel intersections (metres along borehole/tunnel)

None

### Deformation style, alteration and geometry

**Deformation style:** Brittle (no direct evidence – inferred association with other NNE-SSW trending deformation zones)

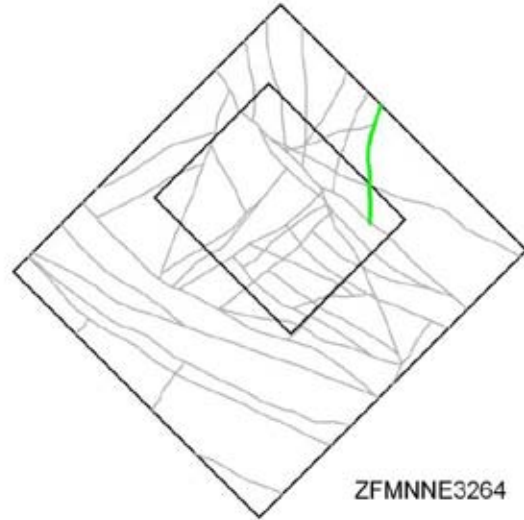
**Alteration:** No data

**Strike/dip (span) right-hand-rule:** 031 / 90 (005–035 / ±10)

**Trace length at ground surface (span):** 1128 m (525–1130 m)

**Model thickness:** 10 m (1% default)

**Confidence in existence:** Medium



**Modelling procedure:** The position of the zone at the ground surface is based on the magnetic lineament MSFR08001 in SFR model version 1.0, itself an update of lineament MFM3264G in Forsmark stage 2.3 /Isaksson et al. 2007/. The stage 2.3 number in the zone name has been maintained for traceability of the zone between different versions of lineament interpretation. Forward modelling of magnetic data along profile 36 (see Appendix 6) weakly supports the inferred vertical dip of the inferred zone, while profile 35 (see Appendix 6) gives a weak indication of a subvertical dip towards the west. The modelled zone thickness is a default value.

### Hydraulic interpretation

**Hydraulic width:** 7.2 m

**No of intercepts:** None

**$T_{\text{eff}}(0)$ :**  $1.92 \cdot 10^{-7}$  m<sup>2</sup>/s

**Log  $T_{\text{eff}}(0)$ :** -6.7,  $\sigma = (0.55)$

**Calculation procedure:**  $T_{\text{eff}}(0)$  taken as pooled average of the NNE to ENE set (only based on new data).

### Fractures in the deformation zone

#### General characteristics

**Fracture orientation:** No data

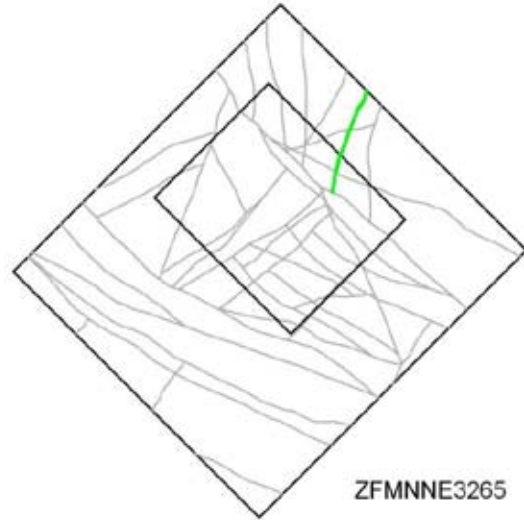
**Fracture frequency:** No data

**Fracture filling mineralogy:** No data

## Deformation zone ZFMNNE3265

### Borehole and tunnel intersections (metres along borehole/tunnel)

None



### Deformation style, alteration and geometry

**Deformation style:** Brittle (no direct evidence – inferred association with other NNE-SSW trending deformation zones)

**Alteration:** No data

**Strike/dip (span) right-hand-rule:** 032 / 90 (015–035 / ±10)

**Trace length at ground surface (span):** 1103 m (475–1103 m)

**Model thickness:** 10 m (1% default)

**Confidence in existence:** Medium

**Modelling procedure:** The position of the zone at the ground surface is based on the magnetic lineament MFM3265G /Isaksson et al. 2007/, itself essentially the same as a linking of lineaments MSFR08002 and MSFR08003 in the SFR model version 1.0 interpretation. The forward modelling of magnetic data along profiles 9, 35 and 36 (see Appendix 6) support the inferred vertical dip of the zone. The modelled zone thickness is a default value.

### Hydraulic interpretation

**Hydraulic width:** 7.2 m

**No of intercepts:** None

**$T_{\text{eff}}(0)$ :**  $1.92 \cdot 10^{-7} \text{ m}^2/\text{s}$

**Log  $T_{\text{eff}}(0)$ :**  $-6.7, \sigma = (0.55)$

**Calculation procedure:**  $T_{\text{eff}}(0)$  taken as pooled average of the NNE to ENE set (only based on new data).

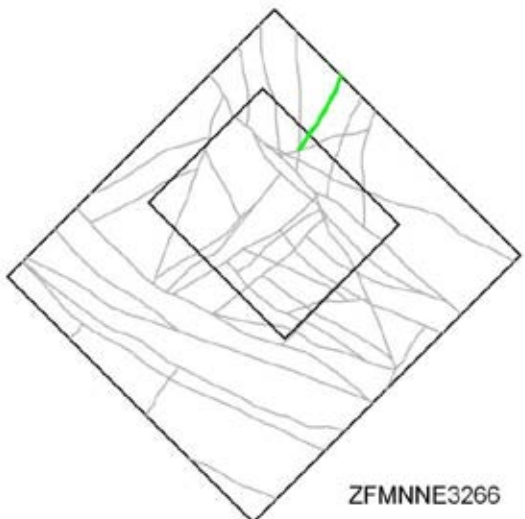
### Fractures in the deformation zone

#### General characteristics

**Fracture orientation:** No data

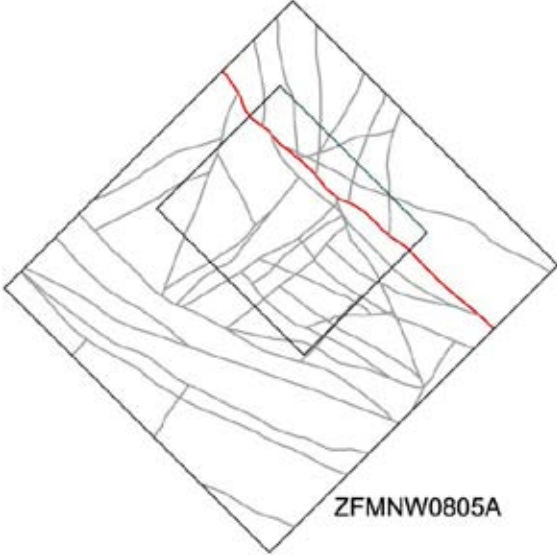
**Fracture frequency:** No data

**Fracture filling mineralogy:** No data

<b>Deformation zone ZFMNNE3266</b>	
<p><b>Borehole and tunnel intersections (metres along borehole/tunnel)</b></p> <p>None</p>	
<p><b>Deformation style, alteration and geometry</b></p> <p><b>Deformation style:</b> Brittle (no direct evidence – inferred association with other NNE-SSW trending deformation zones)</p> <p><b>Alteration:</b> No data</p> <p><b>Strike/dip (span) right-hand-rule:</b> 034 / 90 (025–035 / ±10)</p> <p><b>Trace length at ground surface (span):</b> 1015 m (695–1015 m)</p> <p><b>Model thickness:</b> 10 m (1% default)</p> <p><b>Confidence in existence:</b> Medium</p>	
<p><b>Modelling procedure:</b> The position of the zone at the ground surface is based on the magnetic lineament MFM3266G in Forsmark stage 2.3 /Isaksson et al. 2007/. There has been a very minor update resulting in lineament MSFR08009 in the SFR model version 1.0 interpretation. The stage 2.3 number has been maintained to aid traceability between different versions of the lineament interpretation.</p>	
<b>Hydraulic interpretation</b>	
<p><b>Hydraulic width:</b> 7.2 m</p> <p><b>No of intercepts:</b> None</p> <p><b>T<sub>eff</sub>(0):</b> 1.92·10<sup>-7</sup> m<sup>2</sup>/s</p> <p><b>Log T<sub>eff</sub>(0):</b> -6.7, σ = (0.55)</p> <p><b>Calculation procedure:</b> T<sub>eff</sub>(0) taken as pooled average of the NNE to ENE set (only based on new data).</p>	
<b>Fractures in the deformation zone</b>	
<b>General characteristics</b>	
<p><b>Fracture orientation:</b> No data</p> <p><b>Fracture frequency:</b> No data</p> <p><b>Fracture filling mineralogy:</b> No data</p>	



## Steeply dipping WNW to NW deformation zones

<b>Deformation zone ZFMNW0805A</b>	
<p><b>Borehole and tunnel intersections (metres along borehole/tunnel)</b></p> <p>KFR7A: 43–74.45 m (DZ1 3.5–74.45 m)            KFR08: 41–104.4 m (DZ2 41–104.4 m)            KFR11: 41.45–95.65 m (DZ1 41.45–95.65 m)            KFR101: 242–341.76 m (DZ5 242–341.76 m)</p>	
<p style="text-align: center;"><b>Deformation style, alteration and geometry</b></p> <p><b>Deformation style:</b> Ductile and brittle. Sections of brittle-ductile deformation, including cohesive breccias and cataclasites present in all BH intercepts.</p> <p><b>Alteration:</b> Red-stained bedrock with fine-grained hematite dissemination. Altered vuggy rock with quartz dissolution at 72.55–73.30 and 77.95–79.55 m in KFR08 DZ2, 66.58–67.15 and 70.45–70.60 m in KFR11 DZ1 and 300.76–301.25 m in KFR101 DZ5.</p> <p><b>Strike/dip (span) right-hand-rule:</b> 312 / 82 (±5 / ±5)</p> <p><b>Trace length at ground surface (span):</b> 3643 m (3600→3643 m)</p> <p><b>Model thickness (span):</b> 60 m (30–70 m)</p> <p><b>Confidence in existence:</b> High</p>	
<p><b>Modelling procedure:</b> This zone corresponds to zone 8 in earlier SFR models (see for example /Axelsson and Hansen 1997/). It was renamed ZFMNW0805 in the Forsmark stage 2.2 model /Stephens et al. 2007/ and is referred to as zone ZFMNW0805A in the current SFR model.</p> <p>Zone ZFMNW0805A is a local major zone interpreted as having a length of greater than 3 km /Stephens et al. 2007/. The zone crosses the entire regional model volume. The current interpretation of the zone at the ground surface is based on the magnetic lineaments MFM0805G0, MSFR08095, MSFR10008, MSFR10007, MSFR08033 and MSFR08094 (/Isaksson et al 2007/ and SFR model version 1.0).</p> <p>/Carlsson et al. 1985/ reported that the zone could be identified by seismic investigations. However, the position of the zone does not seem to correspond with any clear low velocity anomalies. The zone was identified in boreholes KFR24 (Kb4) and KFR25 (Kb5) with a dip of 80–90° towards the north-east and a width of 5–10 m. Both /Carlsson et al. 1985/ and /Axelsson and Hansen 1997/ interpreted the zone as dipping steeply to the north-east, with a thickness of 5–15 m (10–45 m including rim zones) /Carlsson et al 1985/. The zone was presented in /Stephens et al 2007/ with an orientation of 134°/90° (uncertainty in strike/dip of ±5°/±10°) and a thickness of 10 m with a span of 10–64 m. The possible deformation zones included in the SHI's reported in the current SFR modelling work are at the base of the boreholes. For this reason, it is inferred that the full thickness of the zone has not been penetrated in these boreholes. The zone has been reported as being characterized by mylonitization, highly fractured rock, alteration and core loss.</p> <p>The modelled zone thickness and orientation show a good fit with the magnetic forward modelling along profiles 2, 3, 31 and the inversion modelling (see Appendix 6). Profiles 4 and 21 also cross ZFMNW0805A and ZFMNW0805B but do not have such a clear correlation due to possible interference from other structures. These two profiles indicate a more sub-vertical pair of structures.</p> <p>The radar reflector at 302 m borehole length in KFR101 has an orientation of 299°/87° which gives a reasonable fit with ZFMNW0805A.</p>	

## Deformation zone ZFMNW0805A

### Hydraulic interpretation

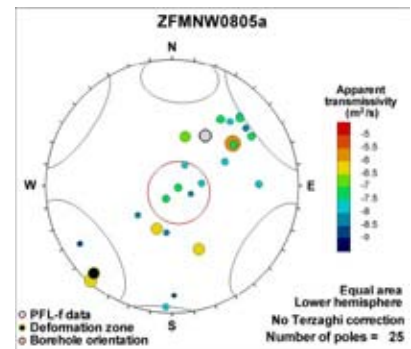
**Hydraulic width:** 37.6 m

**No of intercepts:** 6 (2)

**$T_{\text{eff}}(0)$ :**  $1.83 \cdot 10^{-5} \text{ m}^2/\text{s}$

**Log  $T_{\text{eff}}(0)$ :**  $-4.7$ ,  $\sigma = 0.55$

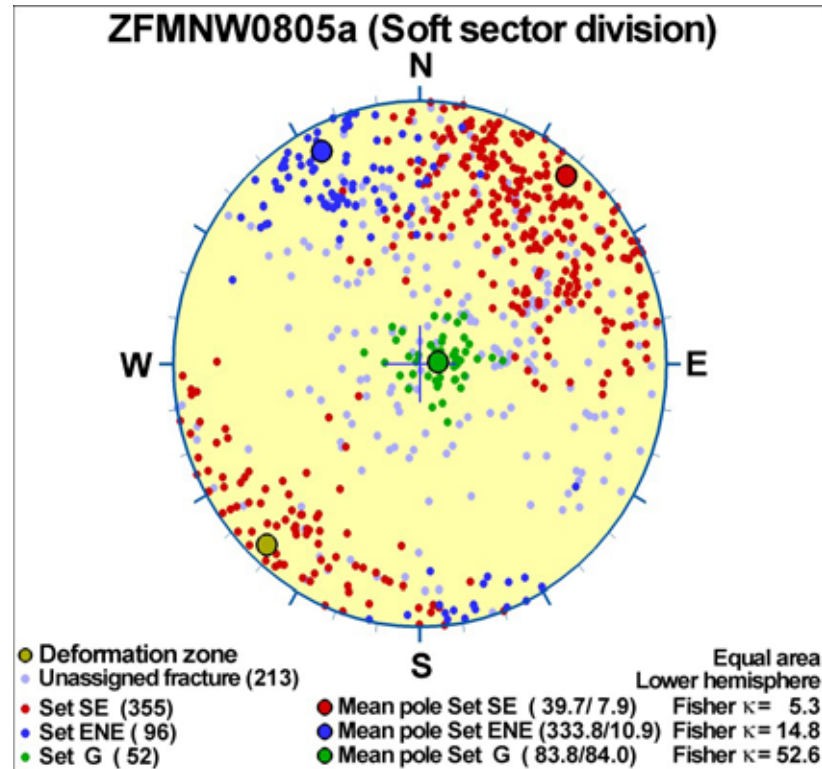
**Calculation procedure:**  $T_{\text{eff}}(0)$  taken as average of all 6 intercepts. Interpreted as a key hydraulic boundary for the hydrogeologic system, associated to the large-scale transmissivity pattern in the vicinity of the Northern Belt. Although the transmissivities are lower than in the Southern Belt, there exist similarities in the PFL-f orientation pattern, predominantly steep NW-striking or gently dipping. Intercepts with the SFR tunnel without record grouting of specific fracture inflow are weighted equal to a single borehole intercept. Such low-transmissive tunnel intercepts were assumed equal to the background conductivity used in /Holmén and Stigsson 2001/ (i.e., the intercept was set to  $T = 6.5 \cdot 10^{-9} \text{ m/s}$  multiplied by the hydraulic width).



## Fractures in the deformation zone

### General characteristics

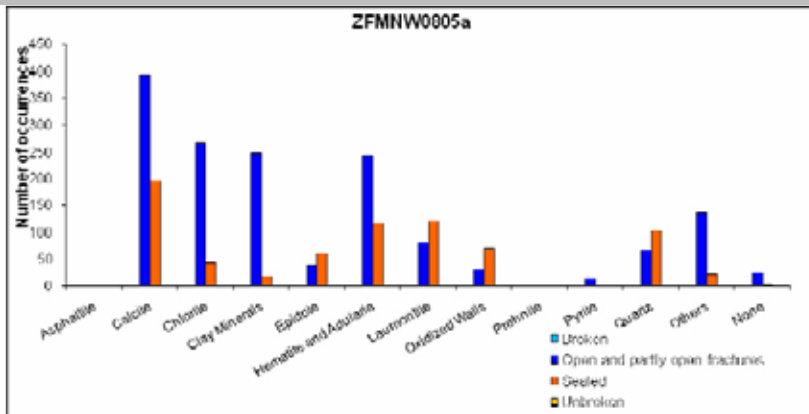
**Fracture orientation:**



**Fracture frequency:** Open  $10 \text{ m}^{-1}$ , Sealed  $31 \text{ m}^{-1}$

**Fracture filling mineralogy:**

## Deformation zone ZFMNW0805A



KFR101 DZ5 292 m–313 m (around fault core position)



## BOREHOLE AND TUNNEL INTERCEPT DETAILS

Borehole intersections for ZFMNW0805A				
BH	Geometrical Intercept		Target Intercept	
	Sec_up BH length (m) [z (-m)]	Sec_low BH length (m) [z (-m)]	Sec_up BH length (m) [z (-m)]	Sec_low BH length (m) [z (-m)]
KFR7A	43.61 [133.81]	eoh [134.89]	43	74.45

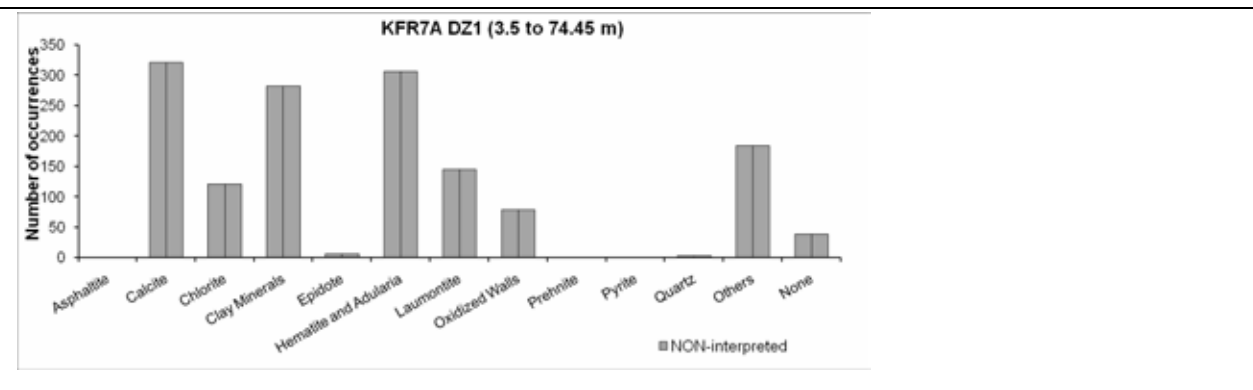
**Comment:** The target interval corresponds to the lower half of DZ1 and the borehole is interpreted not to penetrate the full thickness of the zone. The remainder of DZ1 is interpreted as intercepting ZFMNW0805B.

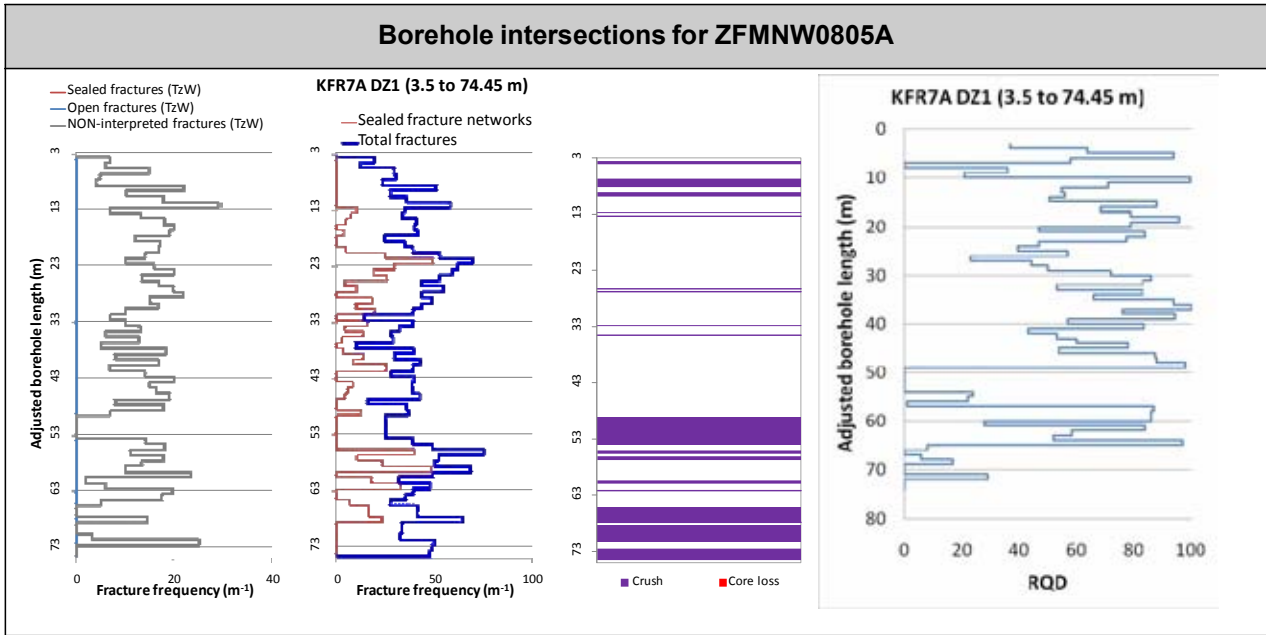
**SHI DZ1 3.5–74.45 m:** Increased frequency of unbroken fractures, sealed networks and especially broken fractures. Nineteen crushes with the most extensive sections at 49.09–74.45 m. Brittle-ductile section characterized by fault breccias and cataclasite at 21–24 m and 64.83–71.29 m. Predominant fracture minerals are clay minerals, calcite and Fe-hydroxide/hematite. The registered  $\alpha$ -angles of clay filled fractures are highly variable, ranging from 0 to 85°. Fractures filled with laumontite form swarms throughout the drill core, with the most extensive occurrence at 56.9–64.8 m length. Most of these fractures have gently dipping  $\alpha$ -angles less than 25°, with a few ranging up to 55° towards the drill core length axis. Moderately to strongly foliated metagranite-granodiorite (101057), pegmatitic granite (101061), aplitic metagranite (101058), fine- to medium-grained granite (111058) and amphibolite (102017). Confidence level = 3.

Low hydraulic conductivity  $6 \cdot 10^{-9}$  m/s in the interval 3.5–19 m. Moderate hydraulic conductivity of  $5 \cdot 10^{-7}$  m/s in the interval 20–47 m. High hydraulic conductivity of  $3 \cdot 10^{-6}$  m/s in the interval 48–74.45 m.

### Hydraulic data

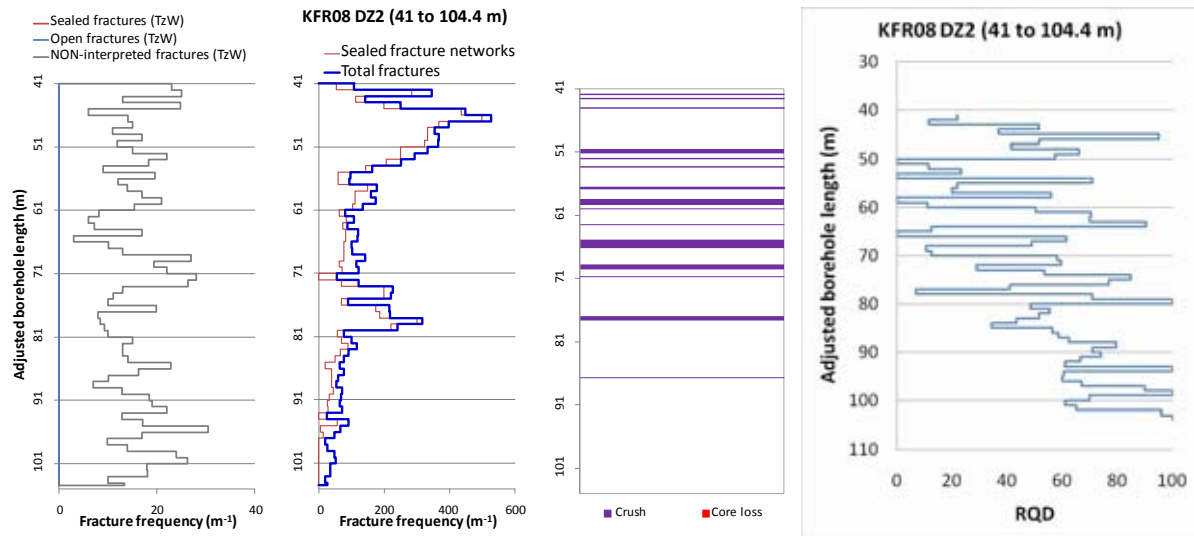
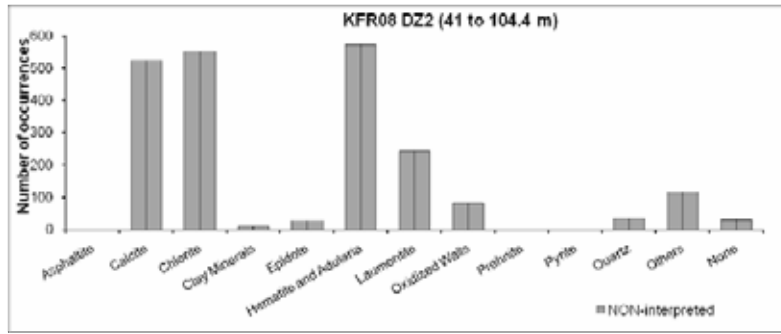
Re-interpreted as possible extension of ZFM871. Not used for ZFMNW0805A.





<b>Borehole intersections for ZFMNW0805A</b>				
<b>BH</b>	<b>Geometrical Intercept</b>		<b>Target Intercept</b>	
	<b>Sec_up BH length (m) [z (-m)]</b>	<b>Sec_low BH length (m) [z (-m)]</b>	<b>Sec_up BH length (m) [z (-m)]</b>	<b>Sec_low BH length (m) [z (-m)]</b>
KFR08	40.32 [89.53]	101.46 [94.86]	41	104.4
<p><b>Comment:</b> /Carlsson et al. 1986/ described the zone in the following manner: rim 41–62 m, core 62–80, rim 80–90 m. <i>Note rim is defined as a zone of increased hydraulic conductivity compared to the general rock mass.</i></p>				
<p><b>SHI DZ2 41–104.4 m:</b> Very high frequency of sealed networks and broken fractures. Nineteen crushed sections. Brittle- to ductile section characterised by fault breccias and cataclasite at 42.25–49.80, 53.83–59.1 and 76–80 m. The predominant fracture filling minerals are calcite, chlorite, laumontite and adularia, typically discoloured by hematite. Registered <math>\alpha</math>-angles for fractures in this interval are variable, but generally moderately dipping. Generally weakly to moderately oxidized with two short sections of quartz dissolution (vuggy rock) at 72.55–73.30 and 77.95–79.55 m. Pegmatitic granite (101061), fine- to medium-grained granite (111058) and moderately foliated metagranite-granodiorite (101057). Confidence level = 3.</p> <p>Moderate hydraulic conductivity (measured in sections of about 20–40 m) of <math>2\text{--}5 \cdot 10^{-7}</math> m/s throughout the interval.</p>				
<p><b>Hydraulic data</b></p> <p><math>T = 1.93 \cdot 10^{-5}</math> m<sup>2</sup>/s</p> <p>Log <math>T_0 = -4.3</math></p>				

### Borehole intersections for ZFMNW0805A



### Borehole intersections for ZFMNW0805A

BH	Geometrical Intercept		Target Intercept	
	Sec_up BH length (m) [z (-m)]	Sec_low BH length (m) [z (-m)]	Sec_up BH length (m) [z (-m)]	Sec_low BH length (m) [z (-m)]
KFR11	32.63 [92.17]	eoh [103.53]	41.45	95.65

**Comment:** /Carlsson et al. 1986/ described the zone in the following manner: rim 42–65 m, core 65–84, rim 84–92 m. Note rim is defined as a zone of increased hydraulic conductivity compared to the general rock mass.

**SHI DZ1 41.45–95.65 m:** Increased frequency of broken fractures. In the section 61.90–92.12 m more highly increased frequency, several crushes, breccias and locally brittle-ductile deformation, particularly at 66.58–74.30 m. Varying  $\alpha$ -angles, but generally  $> 45^\circ$ . A considerable amount of the fractures are parallel with the tectonic foliation. Occurrences of quartz dissolution („vuggy granite”) at 66.58–67.15 and 70.45–70.60 m. Faint to weak oxidation throughout the interval. Predominant fracture minerals are chlorite, calcite, laumontite and in the core of the possible zone clay minerals, asphaltite and quartz. Pegmatitic granite (101061) and fine- to medium-grained granite (111058). Confidence level = 3.

High transmissivity of the section 40.0–98.07 m ( $6 \cdot 10^{-5} \text{ m}^2/\text{s}$ ). The absolutely dominating transmissivity is contained in the in the section 56–98.07 m.

**Borehole intersections for ZFMNW0805A**

BH	Geometrical Intercept		Target Intercept	
	Sec_up BH length (m) [z (-m)]	Sec_low BH length (m) [z (-m)]	Sec_up BH length (m) [z (-m)]	Sec_low BH length (m) [z (-m)]

**Hydraulic data**  
 $T = 5.76 \cdot 10^{-5} \text{ m}^2/\text{s}$   
 $\text{Log } T_0 = -3.8$

KFR101	217.39 [171.55]	334.48 [256.96]	242	341.76
--------	--------------------	--------------------	-----	--------

**Comment:** Note radar reflector at 302 m BH length has an orientation of 299/87 which gives a reasonable fit with ZFMNW0805A.

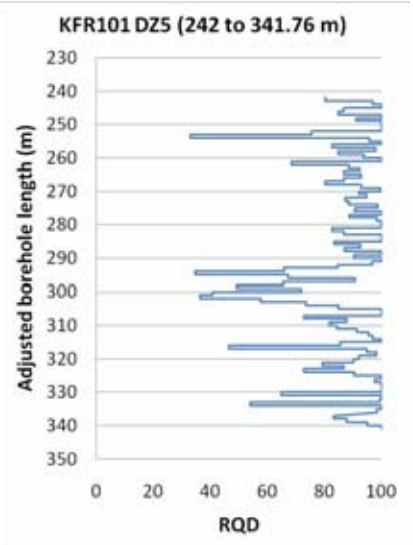
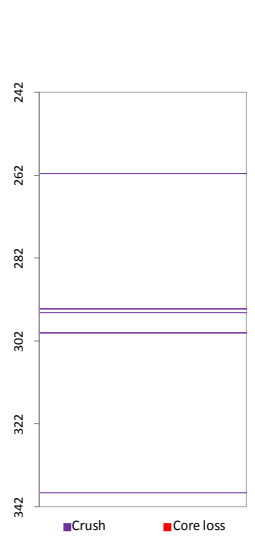
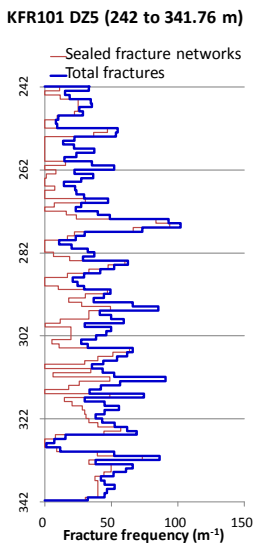
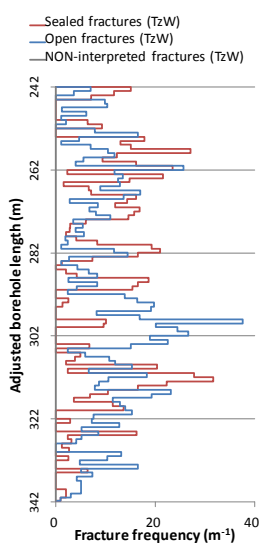
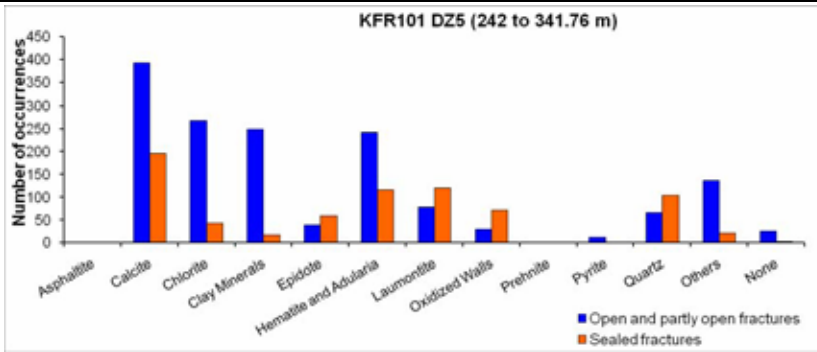
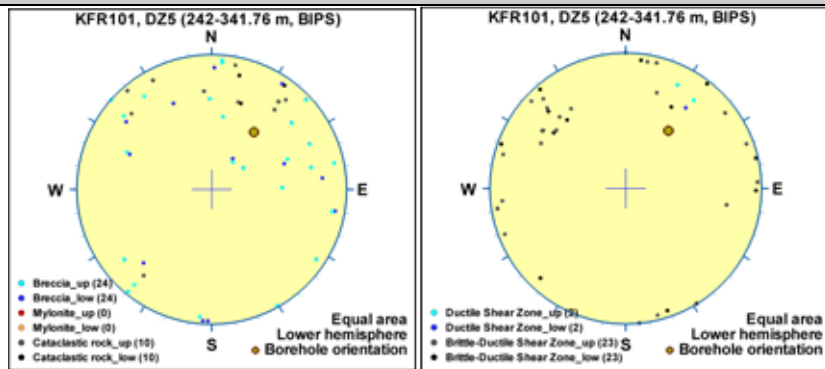
**SHI DZ5 242–341.76 m:** Increased frequency of broken and unbroken fractures and sealed networks. More highly increased frequency of broken fractures at 294–304 m. Five crushed interval at 261.58–261.60, 294.18–294.26, 295.14–295.23, 300.03–300.05 and 338.67–338.71 m. Occasional slickensides. Fractures aperture up to 5 mm. Locally weak to medium oxidation. Interval of vuggy granite affected by argillization at 300.76–301.25 m. Several intervals of breccias, cataclasites and brittle-ductile shear zones, ranging up to a few decimeters in length. One more extensive brittle-ductile shear zones at 326.32–329.91 m. Predominant minerals in sealed fractures are calcite, laumontite, quartz, adularia, epidote and chlorite and in open fractures and crushed intervals calcite, chlorite, clay minerals, hematite, adularia, muscovite, laumontite and quartz. Increased frequency of low resistivity anomalies in the section c. 242–276 m and there is a significant decrease in bulk resistivity in the interval 293–336 m. At 295 m there is one distinct caliper anomaly. Two distinct radar reflector oriented 041°/47°, 296°/16° or 296°/87°, and a prominent radar wave attenuation from c. 290 m to the end of the borehole. Pegmatitic granite (101061), aplitic metagranite (101058), fine- to medium-grained granite (111058), moderately foliated metagranite-granodiorite (101057) and amphibolite (102017). Confidence level = 3.

Increased frequency of flow anomalies in the section, particularly in the interval 294–304 m. No flow anomalies below c. 326 m and no flow logging data available below 332 m. The total transmissivity of the interval is quite high (about  $9 \cdot 10^{-6} \text{ m}^2/\text{s}$ ) where about 90% is concentrated to the interval 294–304 m.

**Hydraulic data**  
 $T = 6.14 \cdot 10^{-6} \text{ m}^2/\text{s}$   
 $\text{Log } T_0 = -4.2$

Well-supported by several PFL-f; the most transmissive at c. 300 m BHL are parallel to the deformation zone. Taken as key evidence for the Northern Belt characteristics.

### Borehole intersections for ZFMNW0805A





Borehole intersections for ZFMNW0805A				
BH	Geometrical Intercept		Target Intercept	
	Sec_up BH length (m) [z (-m)]	Sec_low BH length (m) [z (-m)]	Sec_up BH length (m) [z (-m)]	Sec_low BH length (m) [z (-m)]
KFR23	10.16 [8.80]	11.36 [9.84]	–	–
<p><b>Comment:</b> There is a marginal geometrical intercept with this borehole but no information is available.</p>				
<p><b>Hydraulic data</b> No data.</p>				
KFR24	48.99 [41.08]	156.64 [131.36]	–	–
<p><b>Comment:</b> The earlier quoted position of the zone fits well with the currently modelled position. However, no control point has been added since more weight has been placed on the boreholes that still have drill core available. /Axelsson and Hansen 1997/ report an approximate position of correlation with the zone at 137 m borehole length (385 m level).</p> <p>This borehole has not been assessed during the current modelling phase since no drill core is available for review. /Carlsson et al. 1986/ described the zone in the following manner: rim zone to SW 126–131m, core 131–135 m borehole length. Note rim is defined as a zone of increased hydraulic conductivity compared to the general rock mass.</p>				
<p><b>Hydraulic data</b>  <math>T = 7.50 \cdot 10^{-7} \text{ m}^2/\text{s}</math>  <math>\text{Log } T_0 = -5.8</math>  Part of the intercept (above 132 m BHL) interpreted as possible extension of ZFM871. Hydraulic data in the interval 60 to 132 m used.</p>				
KFR25	50.13 [36.06]	195.09 [140.32]	–	–
<p><b>Comment:</b> No drill core available and therefore no control point has been used from this borehole. The earlier definitions of the zone fall within the current modelled zone boundaries.</p> <p>/Axelsson and Hansen 1997/ report an approximate position of correlation as 174 m borehole length (375 m level). This borehole has not been assessed during the current modelling phase since no drill core is available for review.</p> <p>/Carlsson et al. 1986/ described the zone in the following manner: rim 172–175 m, core 175–184 m, rim 184–188 m. Note rim is defined as a zone of increased hydraulic conductivity compared to the general rock mass.</p>				
<p><b>Hydraulic data</b>  <math>T = 2.20 \cdot 10^{-5} \text{ m}^2/\text{s}</math>  <math>\text{Log } T_0 = -4.3</math>  Hydraulic data in the interval 61 to 195.09 m used, except a midsection of the intercept interpreted as possible extension of ZFM871 (124 m to 154 m BHL).</p>				

Borehole intersections for ZFMNW0805A				
BH	Geometrical Intercept		Target Intercept	
	Sec_up BH length (m) [z (-m)]	Sec_low BH length (m) [z (-m)]	Sec_up BH length (m) [z (-m)]	Sec_low BH length (m) [z (-m)]
KFR56	57.18 [59.48]	eoh [48.72]	–	–
<p><b>Comment:</b> No drill core available and therefore no control point has been used from this borehole. The earlier definition of the zone fall within the current modelled zone boundaries.</p> <p>/Axelsson and Hansen 1997/ report an approximate position of correlation as 68 m borehole length (445 m level). This Intercept is not listed by /Carlsson et al. 1985/</p>				
<p><b>Hydraulic data</b></p> <p><math>T = 5.49 \cdot 10^{-7} \text{ m}^2/\text{s}</math></p> <p><math>\text{Log } T_0 = -6</math></p> <p>Covered by several low-transmissive, pressure-build up data with 3-m spacing.</p>				

## Deformation zone ZFMNW0805B

### Borehole and tunnel intersections (metres along borehole/tunnel)

KFR08: 3–19 m (DZ1 3–19 m)  
 KFR38: 153.60–181.65 m (DZ1 153.60–181.65 m)  
 KFR101: 97–116 m (DZ2 97–116 m)  
 KFR7A: 3.5–43 m (DZ1 3.5–74.45 m)

### Deformation style, alteration and geometry

**Deformation style:** Ductile and brittle. Several minor cohesive breccias, cataclasites and brittle-ductile shear zones along KFR101 DZ2 and KFR7A DZ1.

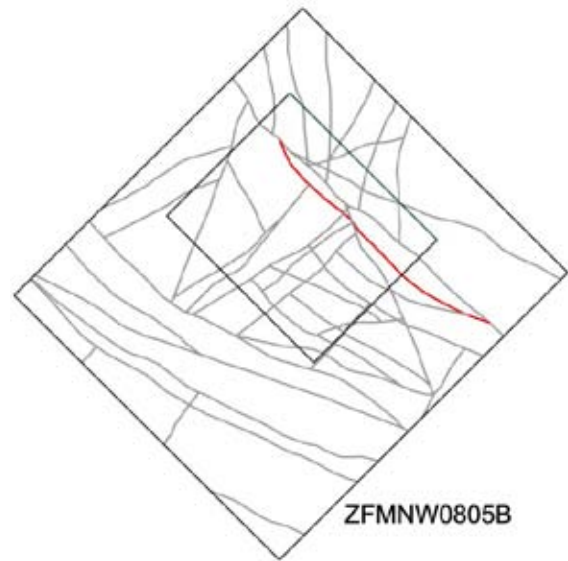
**Alteration:** Red-stained bedrock with fine-grained hematite dissemination, along with chloritization of amphibolite

**Strike/dip (span) right-hand-rule:** 315 / 75 ( $\pm 5$  / 70–90)

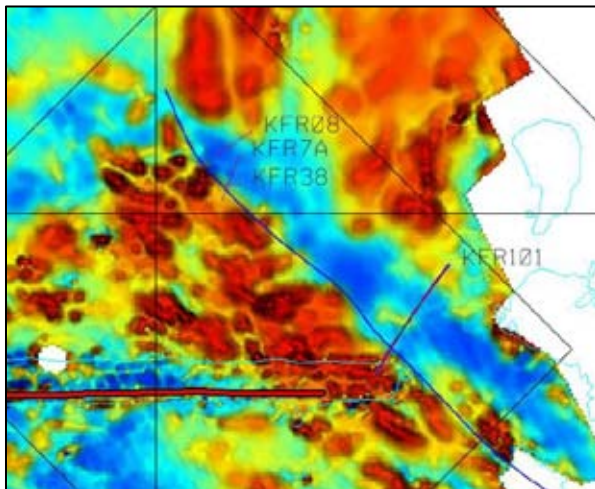
**Trace length at ground surface (span):** 1181 m (1170–1200 m)

**Model thickness (span):** 30 m (5–30 m)

**Confidence in existence:** High



**Modelling procedure:** The position of the zone on the ground surface is based on the magnetic lineaments MFM0805G1, MSFR08104 and MSFR08098 (Isaksson et al. 2007/ and SFR model version 1.0), with further adjustment being made based on borehole data.



*Modified surface position of ZFMNW0805B (blue) shown together with the magnetic map (first vertical derivative of the total field)*

The modelled zone thickness is based on the listed SHI PDZ intervals while the modelled convergence of ZFMNW0805B with ZFMNW0805A at depth within the regional model volume is largely conceptual rather than strictly deterministic, with 3D convergence at depth consistent with the 2D convergence of the inferred zone traces at the ground surface. ZFMNW0805B is considered to form a splay of zone ZFMNW0805A. This interpretation is supported by the similar fracture characteristics along these two zones.

The forward modelling of magnetic data along profile 3 and the inversion modelling (Appendix 6) support the steep dip to the north-east. The magnetic modelling along profile 2 indicates the possibility of a more gently dipping structure possibly lying within the wedge between ZFMNW0805A and ZFMNW0805B. However, this is considered most likely to be a very local feature (see Appendix 6).

An alternative to the geometry presented in the model would be to more strictly follow lineament MFM0805G1 and correlate it with KFR08 DZ2 rather than KFR08 DZ1. Although KFR08 DZ2 is currently inferred as being dominated by ZFMNW0805A, it should be emphasized that DZ1 has a confidence level of 1. Such a modelled zone geometry would also include a more restricted target intercept in KFR7A DZ1. The brittle-ductile deformation style inferred to be associated with ZFMNW0805B is limited to 21–24 m length and it cannot be excluded that some of the brittle deformation outside this interval, at least in part, is alternatively related to zone ZFM871. Such an alternative would

## Deformation zone ZFMNW0805B

eliminate the current geometric intercepts with the SFR tunnels (BT and 1B), where there is no strong evidence to support the presence of the zone. However, heterogeneity along the length of a zone can also adequately account for this feature.

### Hydraulic interpretation

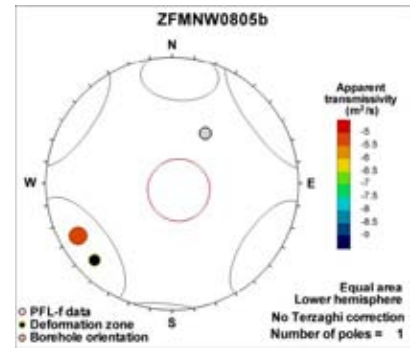
**Hydraulic width:** 21.7 m

**No of intercepts:** 7 (1)

**$T_{eff}(0)$ :**  $3.40 \cdot 10^{-6} \text{ m}^2/\text{s}$

**Log  $T_{eff}(0)$ :** -5.5,  $\sigma = 0.48$

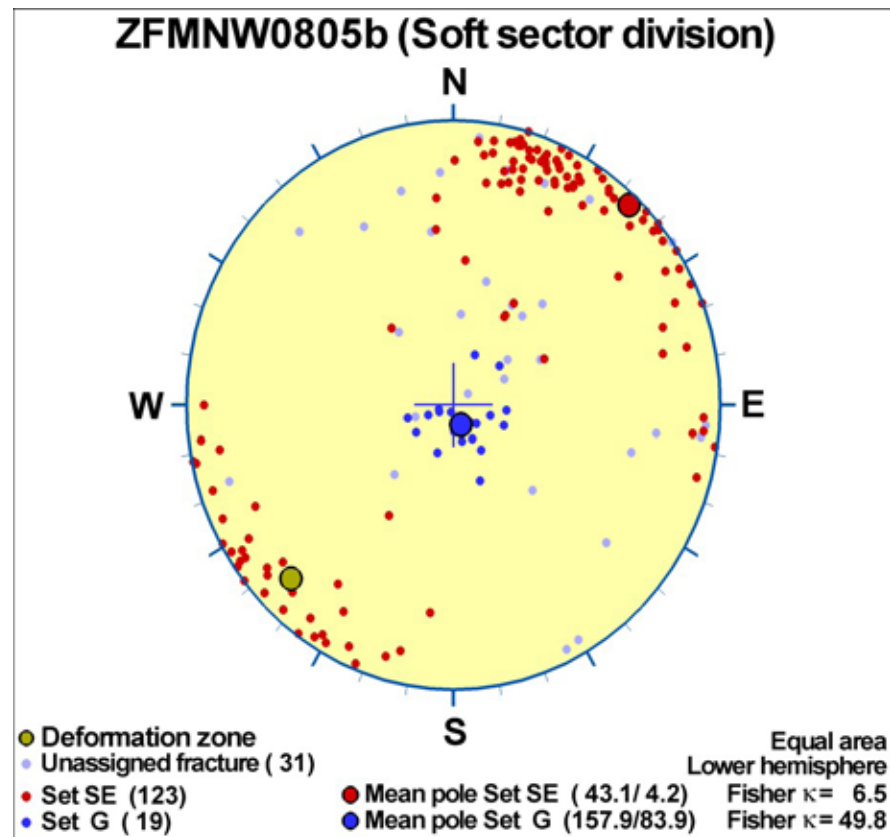
**Calculation procedure:**  $T_{eff}(0)$  taken as average of 7 intercepts and 2 low-transmissive tunnel intercepts. Although only one PFL-f record exists, it is interpreted as part of the hydraulic boundary for the hydrogeologic system, associated to the large-scale transmissivity pattern in the vicinity of the Northern Belt.



### Fractures in the deformation zone

#### General characteristics

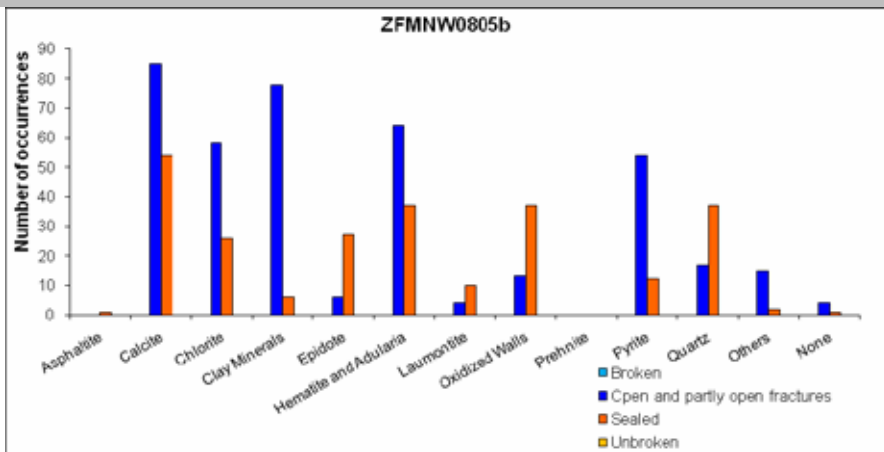
Fracture orientation:



**Fracture frequency:** Open  $13 \text{ m}^{-1}$ , Sealed  $57 \text{ m}^{-1}$

**Fracture filling mineralogy:**

## Deformation zone ZFMNW0805B



KFR101 DZ2 (97-116 m)



## BOREHOLE AND TUNNEL INTERCEPT DETAILS

Borehole intersections for ZFMNW0805B				
BH	Geometrical Intercept		Target Intercept	
	Sec_up BH length (m) [z (-m)]	Sec_low BH length (m) [z (-m)]	Sec_up BH length (m) [z (-m)]	Sec_low BH length (m) [z (-m)]
KFR7A	11.13 [132.68]	43.20 [133.79]	3.5	43.00

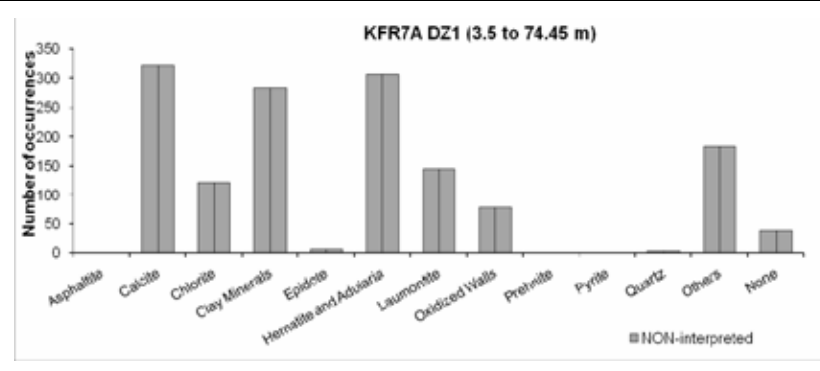
**Comment:** The target interval corresponds to the upper half of DZ1. The remainder of DZ1 is interpreted as intercepting ZFMNW0805A. There is also geometric intercept with ZFM871, which includes the uppermost part of DZ1. The brittle-ductile deformation style inferred to be associated with ZFMNW0805B is limited to 21–24 m length and it cannot be excluded that some of the brittle deformation outside this interval, at least in part, is related to ZFM871, although no target intercept has been defined. Such an alternative interpretation would reduce the zone thickness and hence limit the geometric intercepts with the SFR tunnels (BT and 1B).

**DZ1 3.5–74.45 m:** Increased frequency of unbroken fractures, sealed networks and especially broken fractures. Nineteen crushes with the most extensive sections at 49.09–74.45 m. Brittle-ductile section characterised by fault breccias and cataclasite at 21–24 m and 64.83–71.29 m. Predominant fracture minerals are clay minerals, calcite and Fe-hydroxide/hematite. The registered  $\alpha$ -angles of clay filled fractures are highly variable, ranging from 0 to 85°. Fractures filled with laumontite form swarms throughout the drill core, with the most extensive occurrence at 56.9–64.8 m length. Most of these fractures have gently dipping  $\alpha$ -angles less than 25°, with a few ranging up to 55° towards the drill core length axis. Moderately to strongly foliated metagranite-granodiorite (101057), pegmatitic granite (101061), aplitic metagranite (101058), fine- to medium-grained granite (111058) and amphibolite (102017). Confidence level = 3.

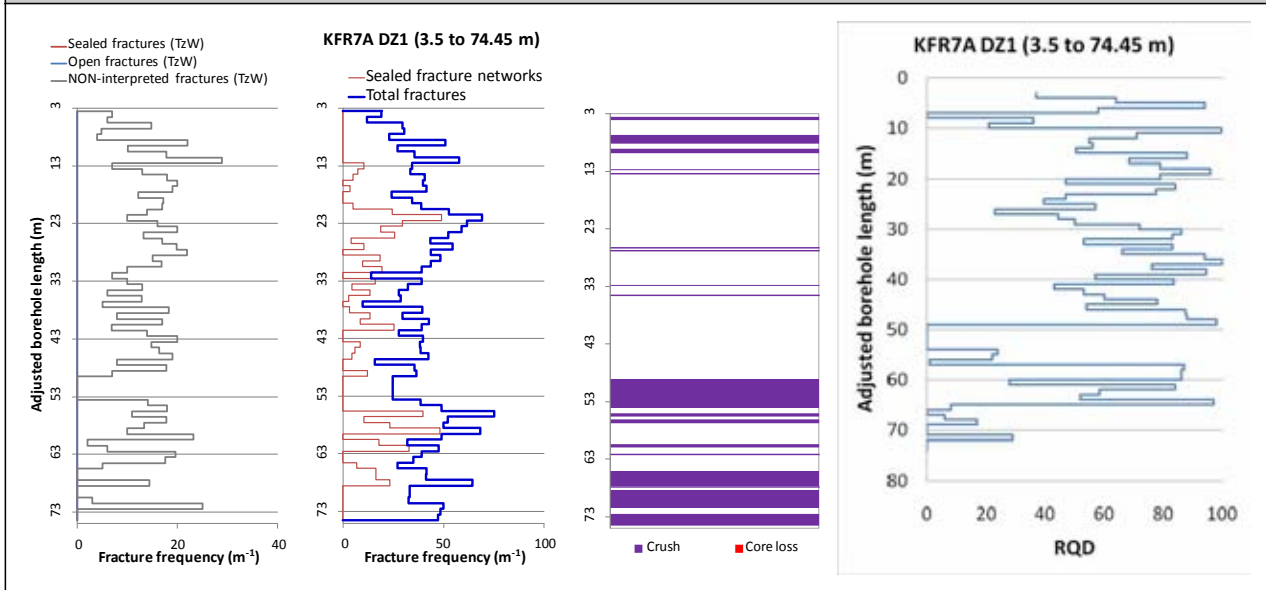
Low hydraulic conductivity  $6 \cdot 10^{-9}$  m/s in the interval 3.5–19 m. Moderate hydraulic conductivity of  $5 \cdot 10^{-7}$  m/s in the interval 20–47 m. High hydraulic conductivity of  $3 \cdot 10^{-6}$  m/s in the interval 48–74.45 m.

### Hydraulic data

Re-interpreted as possible extension of ZFM871. Not used for ZFMNW0805A.



### Borehole intersections for ZFMNW0805B



### Borehole intersections for ZFMNW0805B

BH	Geometrical Intercept		Target Intercept	
	Sec_up BH length (m) [z (-m)]	Sec_low BH length (m) [z (-m)]	Sec_up BH length (m) [z (-m)]	Sec_low BH length (m) [z (-m)]
KFR08	2.8 [86.26]	32.35 [88.84]	3	19

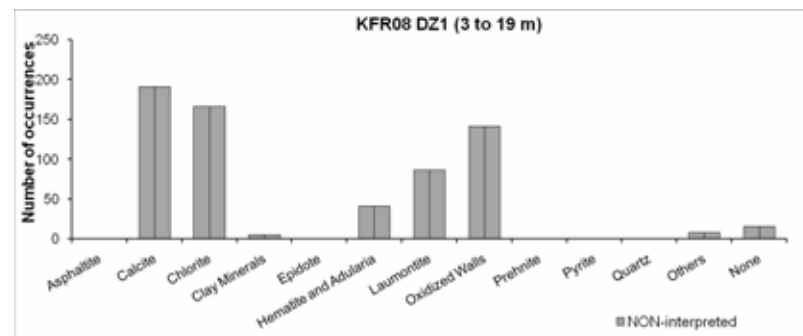
**DZ1 3–19 m:** Increased frequency of broken fractures, sealed networks and especially unbroken fractures. Predominant fracture fillings are chlorite, calcite and laumontite. Registered  $\alpha$ -angles are highly variable between 10 and 81°. Minor weak chloritization and faint oxidation occurs. Moderately to strongly foliated metagranite-granodiorite (101057) and pegmatitic granite (101061). Confidence level = 1.

No hydrogeological investigation data from the upper 6 m of the borehole. Moderate hydraulic conductivity of  $2 \cdot 10^{-8}$  m/s in the section 6–19 m.

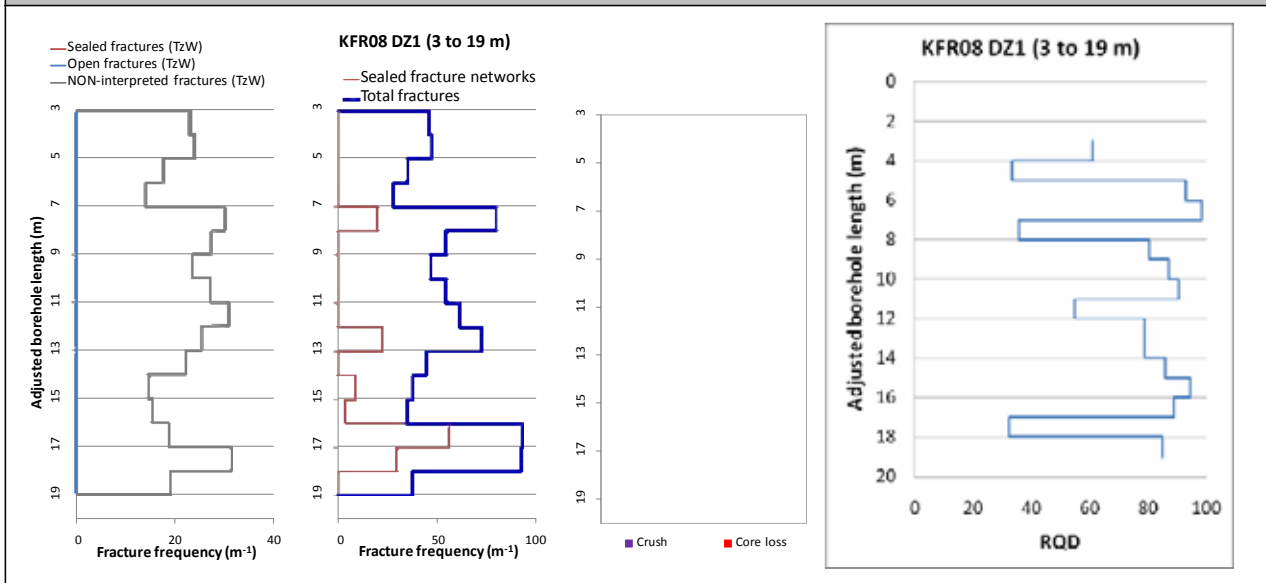
#### Hydraulic data

$$T = 6 \cdot 10^{-7} \text{ m}^2/\text{s}$$

$$\text{Log } T_0 = -5.8$$



### Borehole intersections for ZFMNW0805B



BH	Geometrical Intercept		Target Intercept	
	Sec_up BH length (m) [z (-m)]	Sec_low BH length (m) [z (-m)]	Sec_up BH length (m) [z (-m)]	Sec_low BH length (m) [z (-m)]
KFR38	105.19 [84.31]	eoh [152.04]	153.60	181.65

**DZ1 153.60–181.65 m:** Increased frequency of broken and unbroken fractures. Several crushes, of which the most extensive occurs at 178.90–186.00 m. Generally  $\alpha$ -angles  $> 45^\circ$ . Locally weak oxidation. Amphibolites are consistently weakly chloritized. Predominant minerals in broken fractures are clay minerals, chlorite, hematite, calcite and laumontite and in unbroken fractures laumontite, calcite and hematite. Pegmatitic granite (101061), fine- to medium-grained metagranite-granodiorite (101057), aplitic metagranite (101058) and amphibolite (102017). Confidence level = 3.

High transmissivity of the interval 153–182 m ( $4 \cdot 10^{-5} \text{ m}^2/\text{s}$ ). The dominating transmissivity is contained in the in the section 179–182 m.

**Hydraulic data**

$T = 1.54 \cdot 10^{-6} \text{ m}^2/\text{s}$

$\text{Log } T_0 = -5.6$

Part of the intercept (175 m to 185.4 m BHL) interpreted as possible extension of ZFM871. Hydraulic data in the interval 153 to 175 m used.



**Borehole intersections for ZFMNW0805B**

BH	Geometrical Intercept		Target Intercept	
	Sec_up BH length (m) [z (-m)]	Sec_low BH length (m) [z (-m)]	Sec_up BH length (m) [z (-m)]	Sec_low BH length (m) [z (-m)]
KFR101	80.26 [63.23]	131.55 [104.67]	97	116

**Comment:** Radar reflector at 106 m BH length (316°/87°) has an orientation and position that fits well with ZFMNW0805B.

**SHI DZ2 97–116 m:** Increased frequency of broken and unbroken fractures and sealed networks. One crushed interval at 108.07–108.32 m. Occasional slickensides. Fractures aperture up to 2 mm. Generally weak to medium oxidation. Intervals exceeding a few centimeters of breccia at 108.03–108.51 and of mylonite at 108.51–108.71 and 109.21–109.32 m. Brittle-ductile shear zones at 102.86–102.97 and 107.30–109.64 m. Predominant minerals in sealed fractures are calcite, quartz, adularia, epidote, chlorite and pyrite and in open fractures are calcite, clay minerals, chlorite, pyrite, adularia, hematite and quartz. Significantly decreased resistivity along the entire section and one distinct caliper anomaly at c. 108.5 m. One distinct radar reflector oriented 313°/87° or 331°/30°, and a prominent radar wave attenuation in the interval c. 100–110 m. Moderately foliated metagranite-granodiorite (101057), fine- to medium-grained granite (111058), amphibolite (102017) and pegmatitic granite (101061). Confidence level = 3.

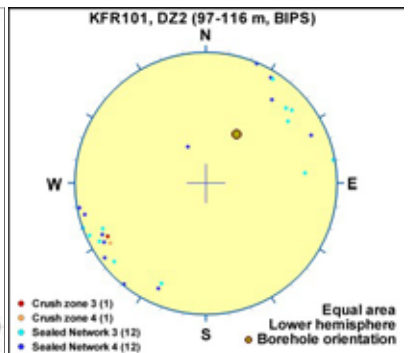
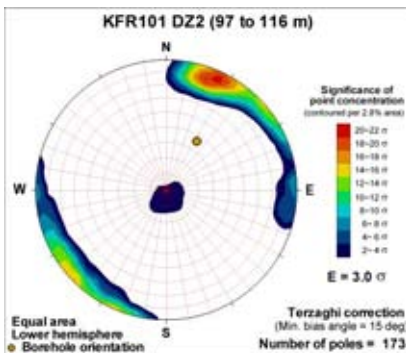
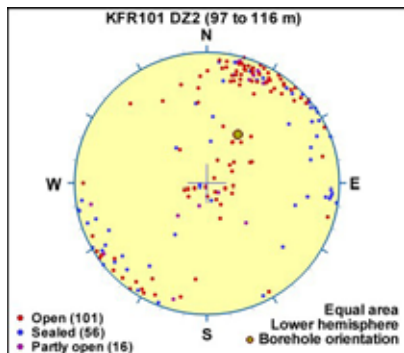
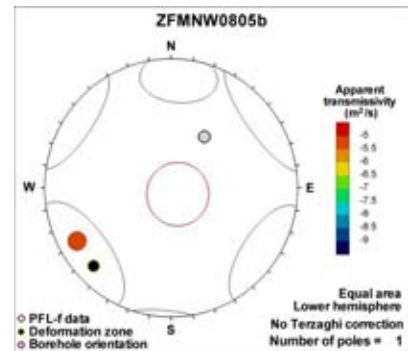
One single high-transmissive flow anomaly (about  $8 \cdot 10^{-6} \text{ m}^2/\text{s}$ ) at c. 108.3 m corresponding to the caliper anomaly.

**Hydraulic data**

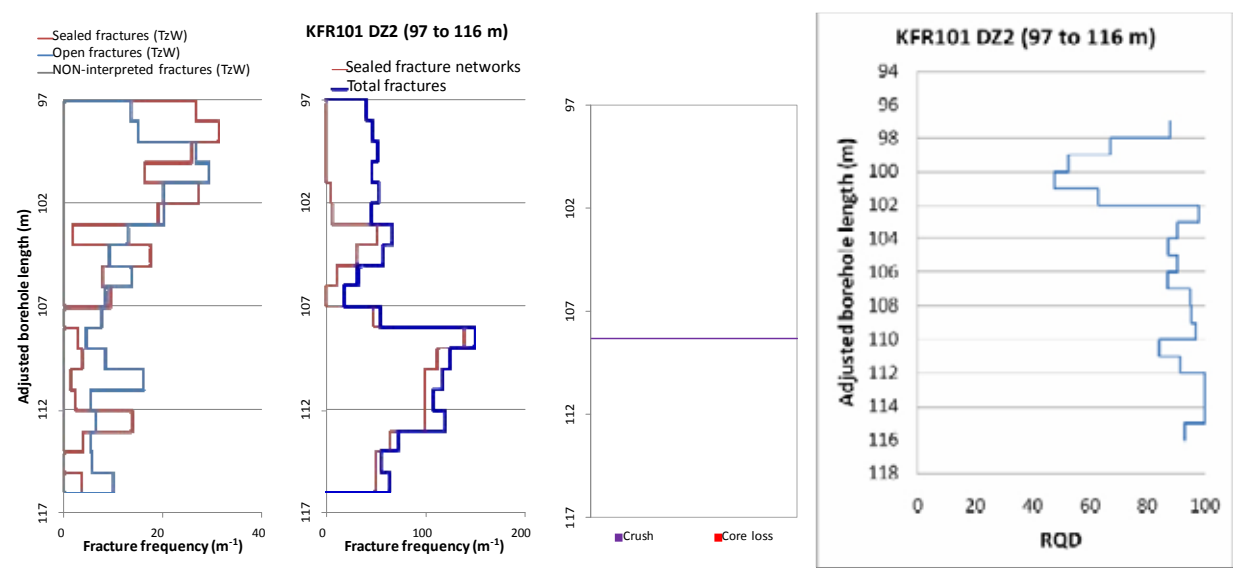
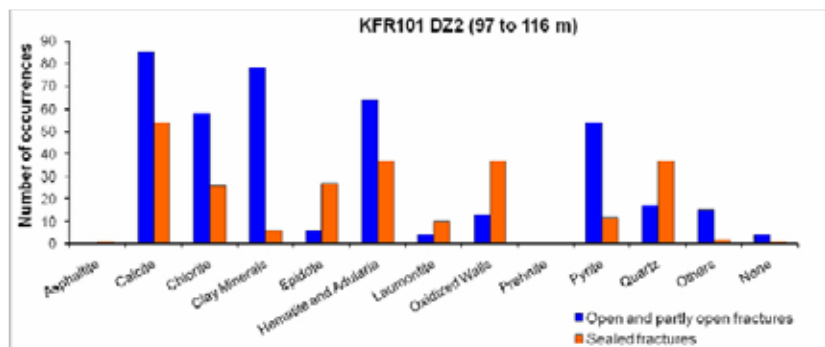
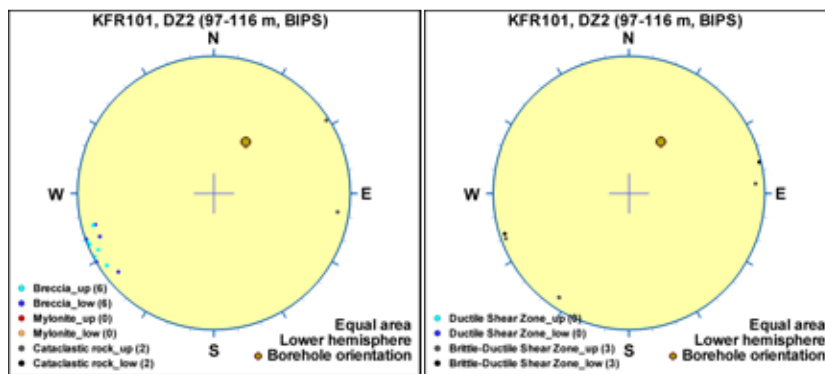
$T = 8.30 \cdot 10^{-6} \text{ m}^2/\text{s}$

$\text{Log } T_0 = -4.7$

Single, distinct, high-transmissive PFL-f parallel to the zone. Taken as key evidence for the Northern Belt characteristics.



### Borehole intersections for ZFMNW0805B



### Borehole intersections for ZFMNW0805B

BH	Geometrical Intercept		Target Intercept	
	Sec_up BH length (m) [z (-m)]	Sec_low BH length (m) [z (-m)]	Sec_up BH length (m) [z (-m)]	Sec_low BH length (m) [z (-m)]
KFR11	0.00 [86.50]	18.77 [89.76]	—	—

**Comment:** Judging from the photographs of the drill cores there is no obvious indication of a zone with the dignity of ZFMNW0805B along the geometric intercept. The only conspicuous feature is an approximately 2 dm long,

**Borehole intersections for ZFMNW0805B**

BH	Geometrical Intercept		Target Intercept	
	Sec_up BH length (m) [z (-m)]	Sec_low BH length (m) [z (-m)]	Sec_up BH length (m) [z (-m)]	Sec_low BH length (m) [z (-m)]

intensely fractured interval with moderate oxidation/laumontization at 16 m length. No target intercept is defined.

**Hydraulic data**

$T = 9.20 \cdot 10^{-6} \text{ m}^2/\text{s}$

$\text{Log } T_0 = -4.7$

Single packer interval 7 to 24 m BHL.

KFR24	0.00 [0.00]	40.81 [34.22]	–	–
-------	----------------	------------------	---	---

**Comment:** No drill core is available for review.

**Hydraulic data**

$T = 1.02 \cdot 10^{-5} \text{ m}^2/\text{s}$

$\text{Log } T_0 = -4.9$

Hydraulic data in the interval 0 to 46 m used.

KFR25	0.00 [0.00]	62.04 [44.62]	–	–
-------	----------------	------------------	---	---

**Comment:** No drill core is available for review.

**Hydraulic data**

$T = 2.68 \cdot 10^{-5} \text{ m}^2/\text{s}$

$\text{Log } T_0 = -4.5$

Hydraulic data in the interval 0 to 61 m used.

KFR56	3.92 [82.83]	44.46 [65.06]	–	–
-------	-----------------	------------------	---	---

**Comment:** No drill core is available for review.

**Hydraulic data**

$T = 2.00 \cdot 10^{-7} \text{ m}^2/\text{s}$

$\text{Log } T_0 = -6.4$

Covered by single, low-transmissive, pressure-build up interval from 10 to 81.7 m BHL (i.e., covering also ZFMNW0805A).

Tunnel intersections for ZFMNW0805B				
BH	Geometrical Intercept		Target Intercept	
	Sec_up BH length (m) [z (-m)]	Sec_low BH length (m) [z (-m)]	Sec_up BH length (m) [z (-m)]	Sec_low BH length (m) [z (-m)]
BT	1+178	1+193	1+182	1+185
<p><b>Comment:</b> Several vertical NNW-SSE striking fractures (approximately 160°/90°) that penetrate the entire tunnel perimeter at 6/182–6/185. Some of the fractures are marked as "damp" in the detailed drawing –11 of /Christiansson and Bolvede 1987/. This is taken as a target intercept for ZFMNW0805B. Note that the extent of the geometric intercept mainly is based on the target intercepts in KFR7A DZ1 and KFR08 DZ1, with confidence level = 1.</p>				
1B	0+023	0+044	–	–
<p><b>Comment:</b> Generally a high frequency of vertical NW-SE striking fractures (approximately 130°/90°) from the connection with IST and onwards towards north. The fracture set is conspicuous in all parts included in detailed drawing –12 of /Christiansson and Bolvede 1987/ and it is not possible to define a specific target intercept. Note that the extent of the geometric intercept mainly is based on the target intercepts in KFR7A DZ1 and KFR08 DZ1, with confidence level = 1.</p>				

## Deformation zone ZFMWNW0835

### Borehole and tunnel intersections (metres along borehole/tunnel)

KFR27: 108–120 m (DZ1 108–120 m) and 323–469 m (DZ2 323–379.5 m, DZ3 389–401 m and DZ4 421–469 m)

### Deformation style, alteration and geometry

**Deformation style:** Brittle. Several minor ductile and brittle-ductile shear zones in KFR27 DZ2, DZ3 and especially DZ4.

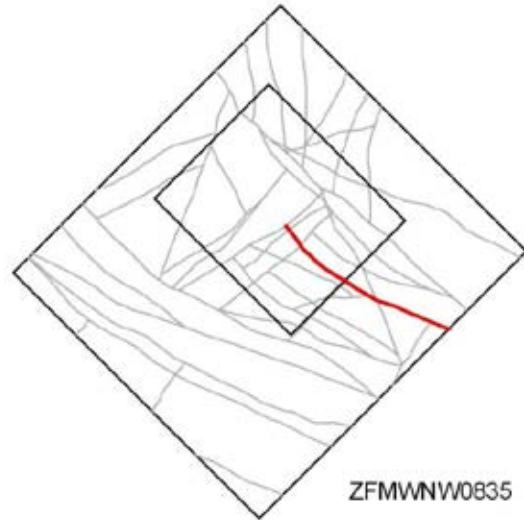
**Alteration:** Locally red-stained bedrock with fine-grained hematite dissemination and argillization. Altered vuggy rock with quartz dissolution at 424.55–428.70, 431.01–451.64 and 457.64–463.08 m in KFR27 DZ4

**Strike/dip (span) right-hand-rule:** 118 / 88 ( $\pm 5$  /  $\pm 10$ )

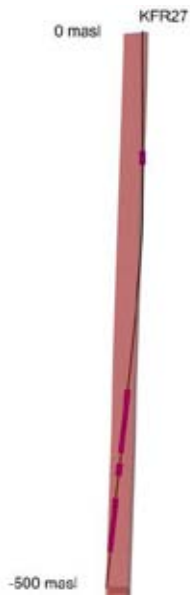
**Trace length at ground surface (span):** 1044 m (1044–1580 m)

**Model thickness:** 21 m (5–22 m)

**Confidence in existence:** High



**Modelling procedure:** The position of the zone on the ground surface is based on a linking of magnetic lineaments MSFR08107 and MSFR08106 (updated from lineament MFM0835BG in Forsmark stage 2.3 /Isaksson et al. 2007/) with a further minor extension to the WNW. The large quoted length range reflects the uncertainty in a further possible extension of the zone to the north-west. Forward modelling of magnetic data along profiles 2 and 44 (see Appendix 6) suggest a steep dip to the north-east whereas inversion modelling supports the more vertical dip.



Section view of ZFMWNW0835 looking along the strike to the WNW, showing intersections with KFR27. The KFR27 SHI PDZs are shown as pink cylinders.

## Deformation zone ZFMWNW0835

### Hydraulic interpretation

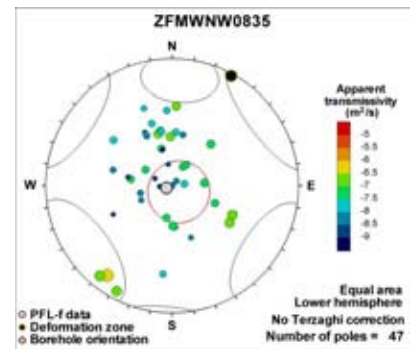
Hydraulic width: 15.1 m

No of intercepts: 1

$T_{\text{eff}}(0)$ :  $6.30 \cdot 10^{-6} \text{ m}^2/\text{s}$

Log  $T_{\text{eff}}(0)$ : -5.2,  $\sigma = 0.71$

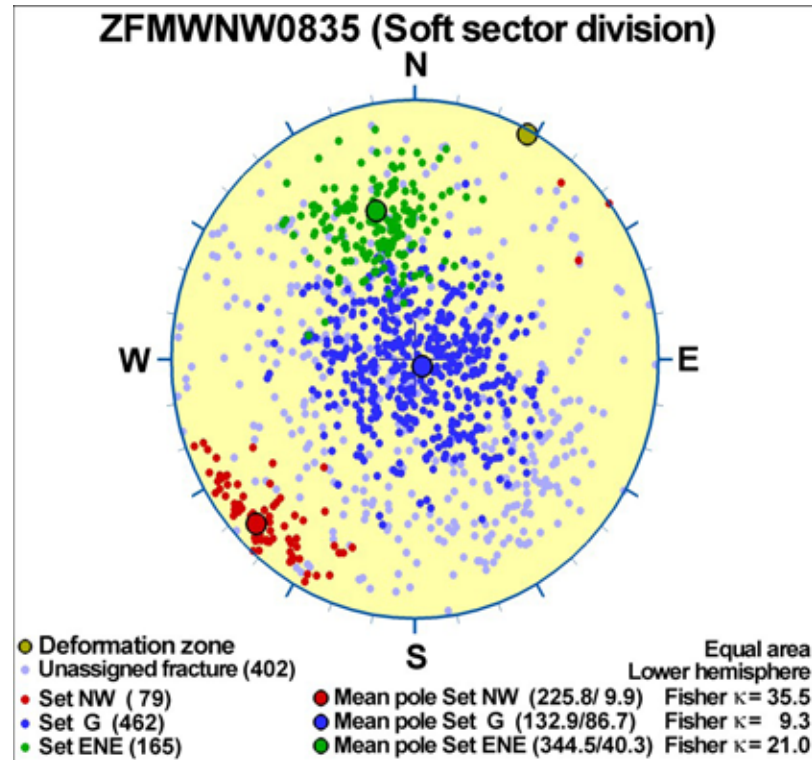
Calculation procedure:  $T_{\text{eff}}(0)$  taken as average of the 2 intercepts in KFR27



### Fractures in the deformation zone

#### General characteristics

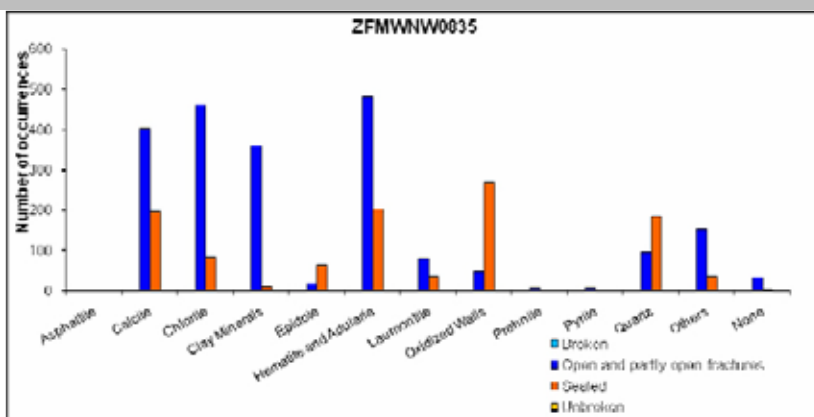
**Fracture orientation:** The apparent dominance of gently dipping fractures is considered to be due to data bias along the more or less vertical borehole KFR27.



Fracture frequency: Open  $14 \text{ m}^{-1}$ , Sealed  $21 \text{ m}^{-1}$

Fracture filling mineralogy:

## Deformation zone ZFMWNW0835



KFR27 DZ2 (323–379.5 m)



**Deformation zone ZFMWNW0835**





## BOREHOLE AND TUNNEL INTERCEPT DETAILS

Borehole intersections for ZFMWNW0835				
BH	Geometrical Intercept		Target Intercept	
	Sec_up BH length (m) [z (-m)]	Sec_low BH length (m) [z (-m)]	Sec_up BH length (m) [z (-m)]	Sec_low BH length (m) [z (-m)]
KFR27	0 [2.87]	153.31 [150.43]	108	120

DZ1 108–120 m: Increased frequency of sealed fractures and sealed fracture networks. Locally weak to moderate oxidation. No core available. Moderate resistivity anomalies. One distinct radar reflector at approximately 118 m. Pegmatitic granite (101061), metagranite-granodiorite (101057) and felsic to intermediate metavolcanic rock (103076). Confidence level = 1.

Medium transmissivity of this interval ( $T = 8 \cdot 10^{-8} \text{ m}^2/\text{s}$ ).

**Hydraulic data**  
See below under DZ4

KFR27 DZ1 (108 to 120 m)

Equal area Lower hemisphere

Number of poles = 104

KFR27 DZ1 (108 to 120 m)

Terzaghi correction (Min. bias angle = 15 deg)

Number of poles = 104

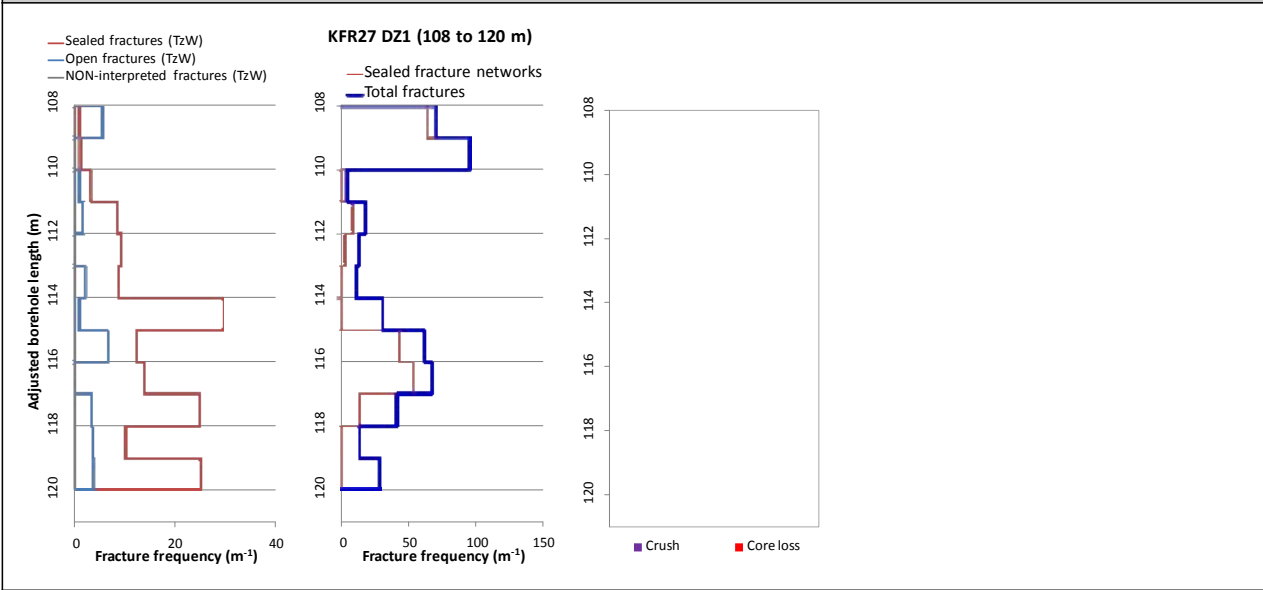
KFR27, DZ1 (108-120 m, BIPS)

Equal area Lower hemisphere

KFR27 DZ1 (108 to 120 m)

Mineral Type	Open and partly open fractures	Sealed fractures
Asphaltite	0	0
Calcite	0	0
Chlorite	0	0
Clay Minerals	0	0
Epistone	0	0
Hematite and Adularia	0	0
Laumontite	0	0
Oxidized Walls	0	0
Prehnite	0	0
Pyrite	0	0
Quartz	0	0
Others	0	0
None	18	55

### Borehole intersections for ZFMWNW0835



### Borehole intersections for ZFMWNW0835

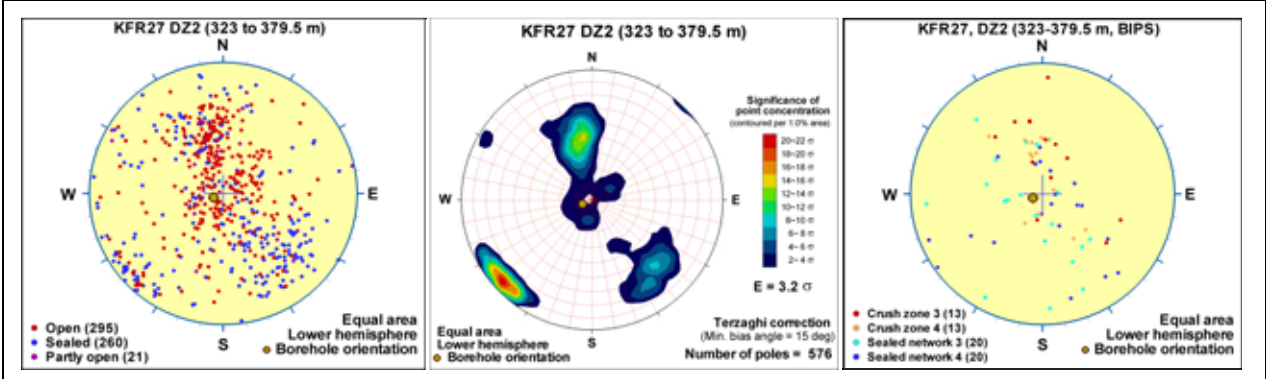
BH	Geometrical Intercept		Target Intercept	
	Sec_up BH length (m) [z (-m)]	Sec_low BH length (m) [z (-m)]	Sec_up BH length (m) [z (-m)]	Sec_low BH length (m) [z (-m)]
KFR27	195.98 [193.06]	470.56 [466.08]	323	469

**SHI DZ2 323–379.5 m:** Several shorter intervals with increased frequency of open and sealed fractures and a more extensive interval in the lower most part of the possible deformation zone. Thirteen crush sections throughout the interval and one minor breccia at 338.51–338.52 m. Fracture aperture up to 1mm. Locally faint to moderate oxidation and faint to weak argillization. Predominant minerals in open fractures are calcite, chlorite, clay minerals and hematite. Low electric resistivity especially in the lower part of the section. A minor deflection in the temperature gradient. Two radar reflectors (352°/01° or 332°/11° and 334°/65° or 154°/53°). Fine- to medium-grained granite (111058), metagranite-granodiorite (101057), pegmatitic granite (101061) and amphibolite (102017). Confidence level = 3.

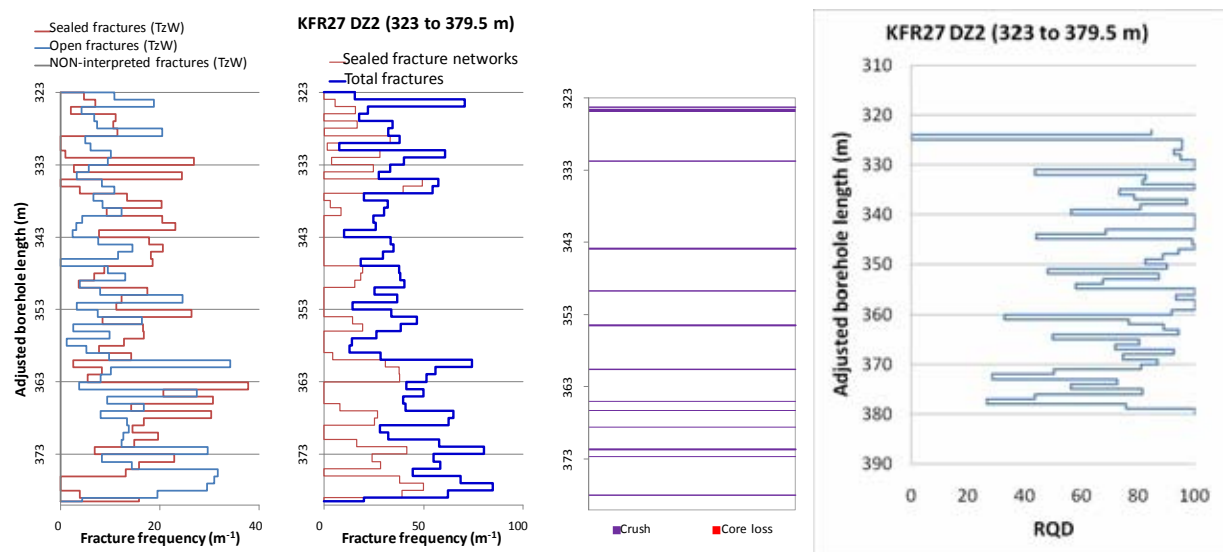
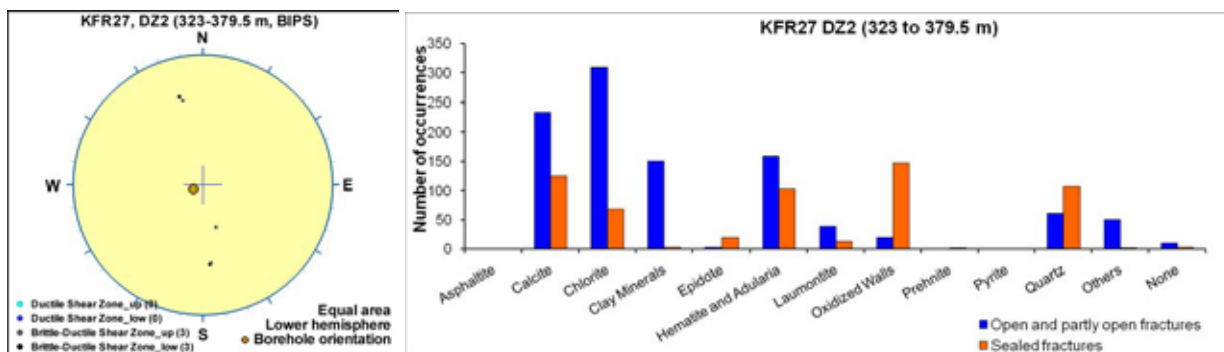
Increased frequency of flow anomalies. The total transmissivity of the interval is  $1 \cdot 10^{-6} \text{ m}^2/\text{s}$ .

#### Hydraulic data

See below under DZ4



## Borehole intersections for ZFMWNW0835

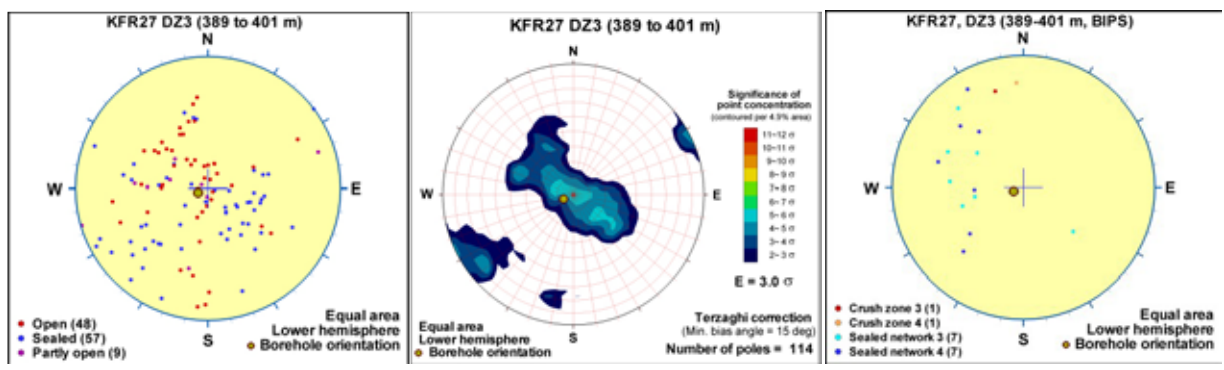


**DZ3 389–401 m:** Increased frequency of sealed and open fractures and sealed fracture networks. One crush at the interval 394.71–394.75 m. Fracture aperture up to 0.5 mm and one single aperture at 3 mm. Generally weak to moderate oxidation. Predominant minerals in open fractures are chlorite, laumontite and clay minerals, in sealed fractures calcite, laumontite and quartz and in the crushed interval chlorite and clay minerals. Moderate resistivity anomalies. Metagranite-granodiorite (101057), pegmatitic granite (101061) and amphibolite (102017). Confidence level = 2.

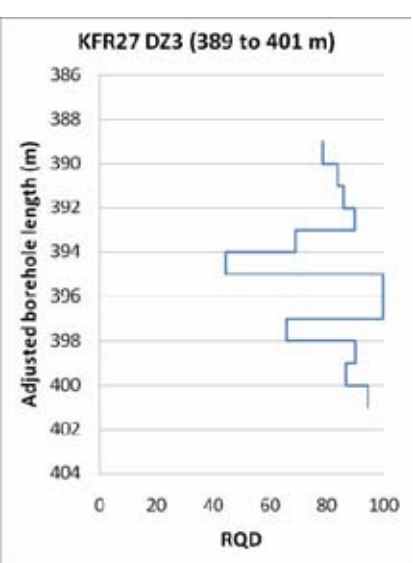
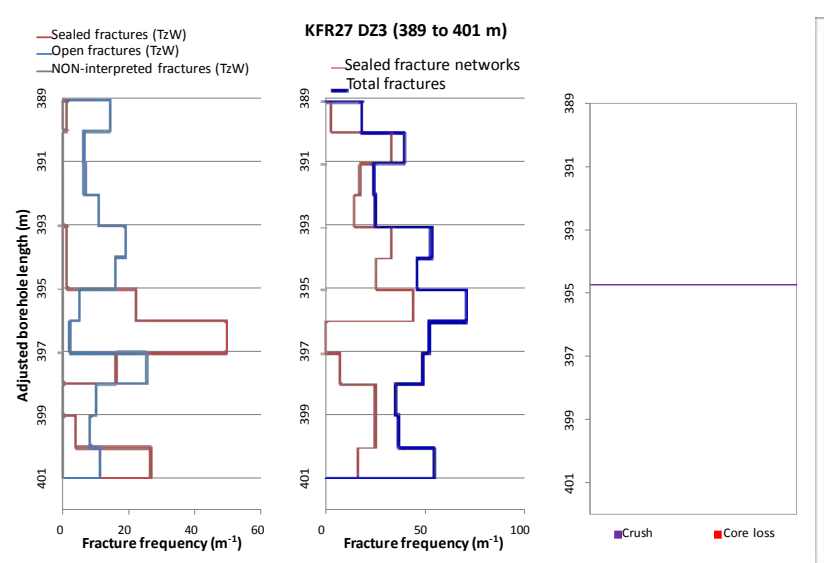
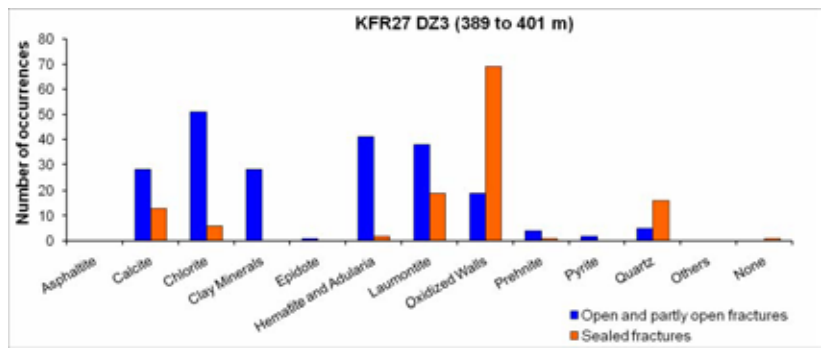
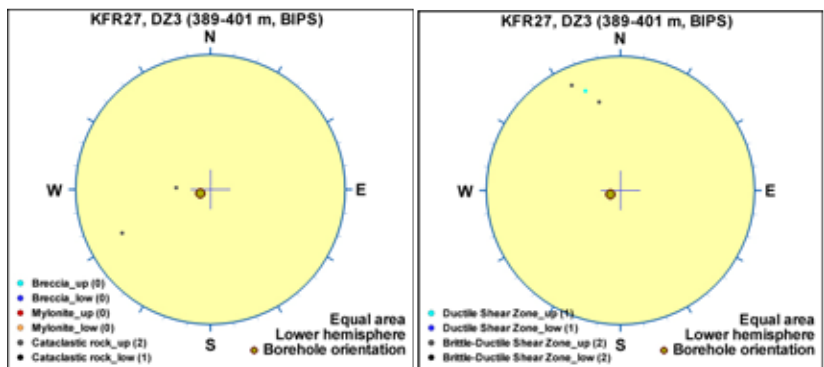
One single low-transmissive ( $T = 1 \cdot 10^{-9} \text{ m}^2/\text{s}$ ) flow anomaly at 392.1 m.

### Hydraulic data

See below under DZ4



## Borehole intersections for ZFMWNW0835



## Borehole intersections for ZFMWNW0835

DZ4 421–469 m: The possible deformation zone can be divided into three different characteristic intervals. The uppermost interval, extending down to c.442 m, is characterized by increased frequency of sealed and especially open fractures. Six crushed sections with a concentration between 431.4–433.5 m. Fracture aperture up to 3 mm. Generally faint to moderate oxidation and faint to strong quartz dissolution. Predominant minerals in open fractures are hematite, calcite, clay minerals and adularia, in sealed fractures adularia, epidote, calcite and quartz and in crushed intervals clay minerals and adularia. Very low resistivity especially in the central part. Several calliper anomalies and a moderate deflection in the temperature gradient. The central sub interval extends from c. 442 m to c. 463 m, is characterized by strong brittle-ductile deformation and intense alteration that includes oxidation, quartz dissolution, argillization, chloritization and epidotization. Three crushes at 446.86–446.91, 448.12–448.14 and 458.30–458.33 m. Several moderately altered open fractures. Apertures ranging up to 2 mm. Predominant mineral in open fractures are clay minerals. The lower most interval, from c.463m, is characterized by increased frequency of sealed and open fractures. A few moderately to strongly altered open fractures. Generally weak oxidation and locally chloritization. Apertures ranging up to 3 mm. Predominant minerals in open fractures are chlorite and clay minerals and in sealed fractures adularia, laumontite and calcite. Very low resistivity especially in the central part. Several calliper anomalies and a moderate deflection in the temperature gradient. Amphibolite (102017), metagranite-granodiorite (101057), fine- to medium-grained granite (111058) and pegmatitic granite (101061). Confidence level = 3.

A cluster of flow anomalies at 410–436 m. The transmissivity is concentrated to the section 423–429 m. No flow anomaly below 436 m. The total transmissivity of the interval is  $4 \cdot 10^{-6} \text{ m}^2/\text{s}$ .

### Hydraulic data

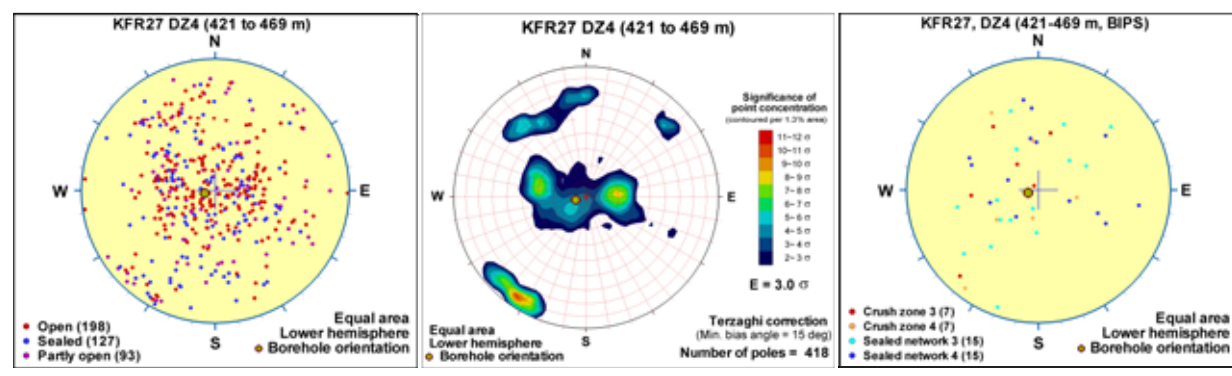
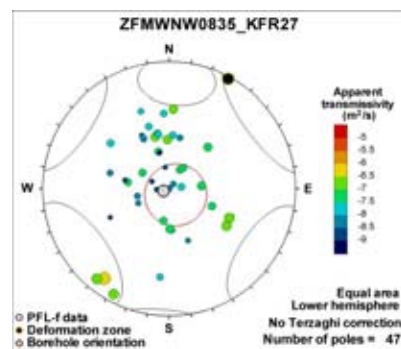
$\log T_0 = -6.6$  and  $-3.8$

Little hydraulic support,  $T = 8.1 \cdot 10^{-8} \text{ m}^2/\text{s}$ , found in the upper intercept (108 to 120 m BHL).

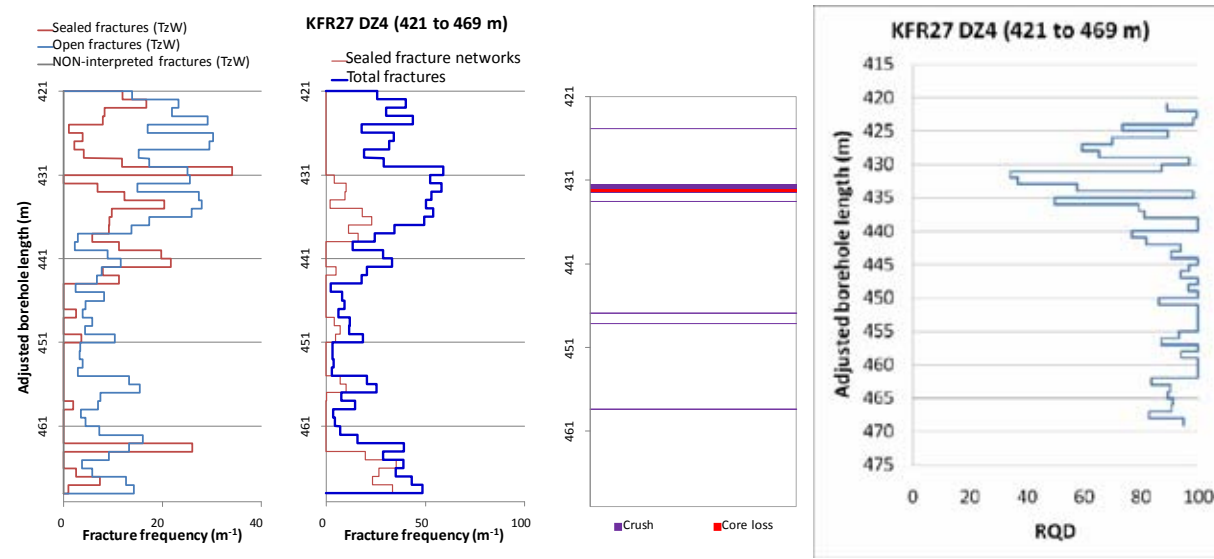
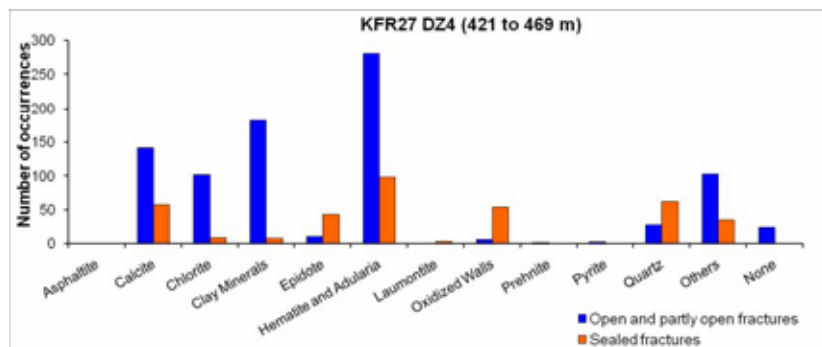
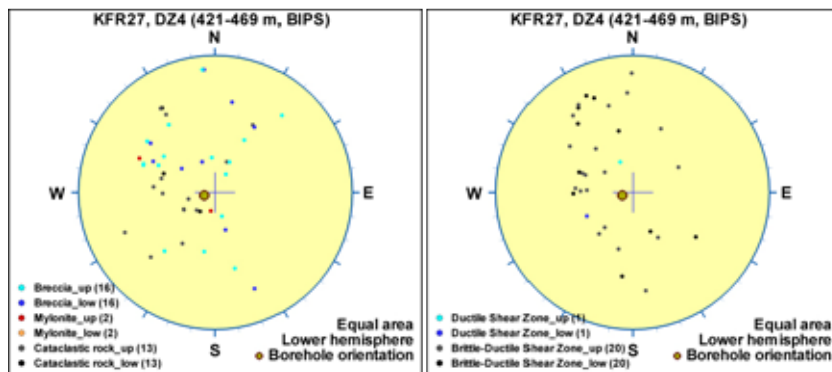
In the long, deep, lower intercept (323 to 469 m BHL) there is strong support from a high frequency of PFL-f data with a total transmissivity of  $3.2 \cdot 10^{-6} \text{ m}^2/\text{s}$ . The total value is dominated by 3 steeply dipping PFL-f at c. 424 m BHL that are sub-parallel to the zone.

This is noticeable from three aspects: 1) The PFL-f data in the borehole are principally sub-horizontal to gently dipping, which is assumed to be a consequence of vertical borehole sampling bias, 2) the midsection (120 to 323 m BHL) of the borehole has a remarkable lack of PFL-f records, although it is understood to be closely aligned to the outside the zone, and 3) in terms of depth-adjusted transmissivity, the contrast between the two target intercepts is three orders of magnitude:  $\log T_0$  is  $-6.6$  and  $-3.8$  for the upper and lower intercepts, respectively.

The borehole has a strong drawdown peak at c. 250 m BHL, which coincides with a potential extension of ZFM871 beyond its modeled termination against ZFMENE3115.



## Borehole intersections for ZFMWNW0835



## Deformation zone ZFMWNW0836

### Borehole and tunnel intersections (metres along borehole/tunnel)

None

### Deformation style, alteration and geometry

**Deformation style:** No data

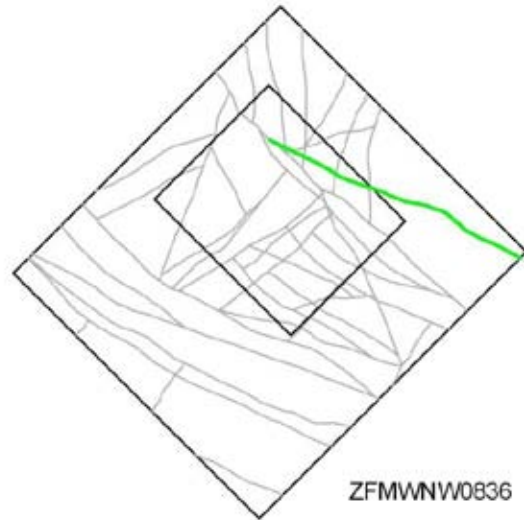
**Alteration:** No data

**Strike/dip (span) right-hand-rule:** 117 / 90 ( $\pm 5$  /  $\pm 10$ )

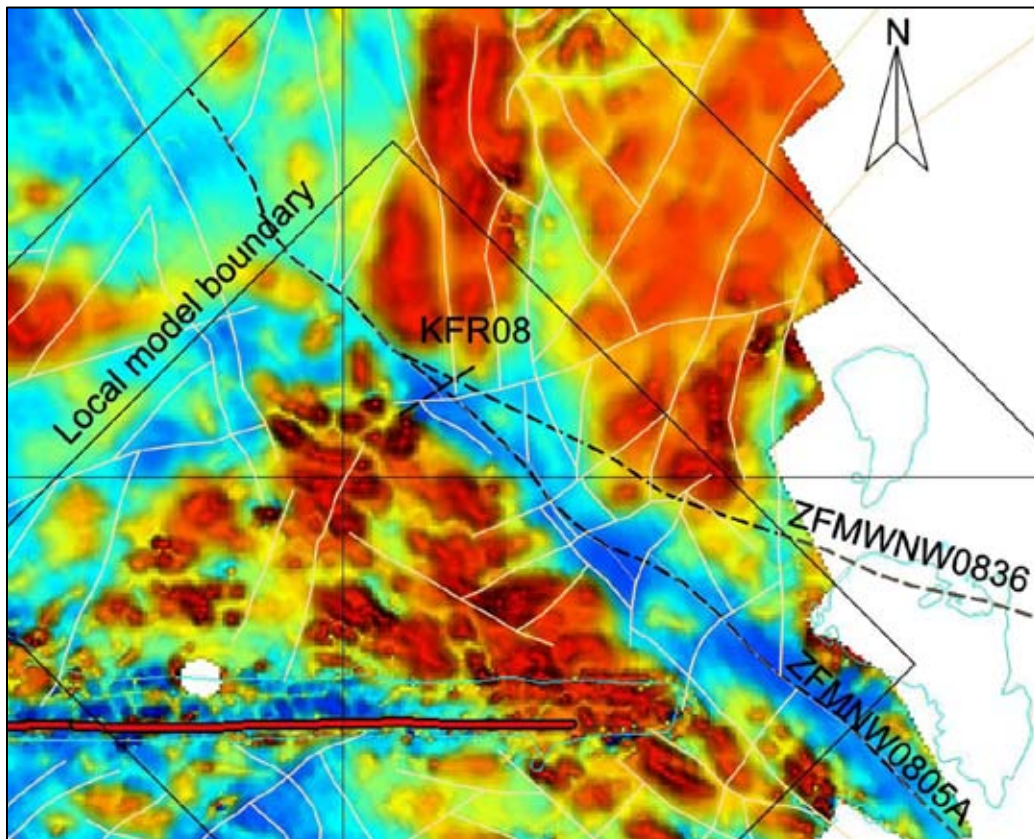
**Trace length at ground surface (span):** 4868 m (4868→4868 m)

**Model thickness:** 50 m (1% default)

**Confidence in existence:** Medium



**Modelling procedure:** The surface position of the zone is based on magnetic lineaments MFM0836G, MSFR08007 and MSFR10010 (Isaksson et al 2007/ and SFR model version 1.0). The zone has been given a significant extension to the north-west compared with the lineament, to allow a better fit with the concept that the zone is a splay of ZFMNW0805A. The extension is not in any conflict with the magnetic data (see below).



Map of the first vertical derivative of the magnetic total field, the deformation zone ground surface traces for ZFMWNW0836 and ZFMNW0805A, and the SFR version 1.0 lineaments, with a focus on the local model area where the ZFMWNW0836 zone trace diverges from the lineaments.

The zone is associated with two geometrical borehole intercepts. In KFR08 the geometrical intercept fits well with the magnetic surface data and the SHI (DZ1 41–104 m). However, KFR08 DZ1 is currently interpreted as being dominated by ZFMNW0805A. No drill core or SHI is available for KFR25. Since there is no confidently supportive borehole or tunnel information, the zone is only assigned a medium confidence.

## Deformation zone ZFMWNW0836

### Hydraulic interpretation

**Hydraulic width:** 36.0 m

**No of intercepts:** 0 (2)

**$T_{\text{eff}}(0)$ :**  $7.92 \cdot 10^{-8}$  m<sup>2</sup>/s

**Log  $T_{\text{eff}}(0)$ :** -7.1,  $\sigma = (0.55)$

**Calculation procedure:** Two rejected intercepts. Value taken from SDM-Site Forsmark.

### Fractures in the deformation zone

#### General characteristics

**Fracture orientation:** No data

**Fracture frequency:** No data

**Fracture filling mineralogy:** No data

## BOREHOLE AND TUNNEL INTERCEPT DETAILS

### Borehole intersections for ZFMWNW0836

BH	Geometrical Intercept		Target Intercept	
	Sec_up BH length (m) [z (-m)]	Sec_low BH length (m) [z (-m)]	Sec_up BH length (m) [z (-m)]	Sec_low BH length (m) [z (-m)]
KFR08	46.04 [90.03]	104.12 [95.10]	–	–

**Comment:** Geometrical intercept fits well with the magnetic surface data and the SHI (DZ2 41–104 m). However, KFR08 DZ2 is currently interpreted as being dominated by ZFMNW0805A.

#### Hydraulic data

Assumed subordinate to ZFMNW0805A. Not used

KFR25	64.07 [46.08]	144.25 [103.76]	–	–
-------	------------------	--------------------	---	---

**Comment:** No core available

#### Hydraulic data

Assumed subordinate to ZFMNW0805A. Not used



## Deformation zone ZFMWNW3262

### Borehole and tunnel intersections (metres along borehole/tunnel)

KFR103: 180–182.5 m (DZ3 180–182.5 m)  
 KFR106: 67–73 m (DZ3 67–73 m)

### Deformation style, alteration and geometry

**Deformation style:** Brittle. Minor ductile and brittle-ductile shear zones present in KFR106 DZ3 and KFR103 DZ3, respectively

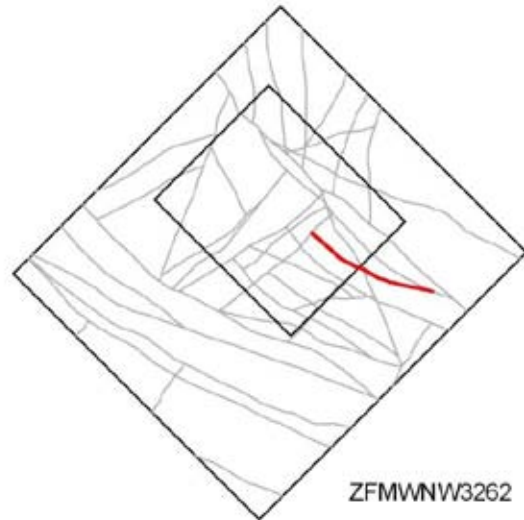
**Alteration:** Locally red-stained bedrock with fine-grained hematite dissemination

**Strike/dip (span) right-hand-rule:** 116 / 86 ( $\pm 10$  /  $\pm 10$ )

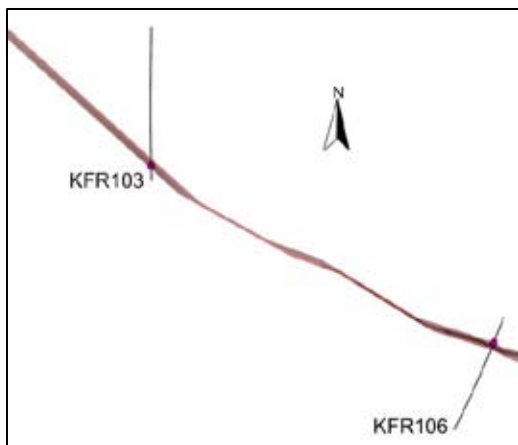
**Trace length at ground surface (span):** 610 m (300–1000 m)

**Model thickness (span) :** 2 m (<1–3 m)

**Confidence in existence:** High



**Modelling procedure:** The position of the zone on the ground surface is based on magnetic lineament MSFR08105 in SFR model version 1.0, itself a modification of lineament MFM3262G from /Isaksson et al. 2007/. The earlier number has been retained in the zone name to assist traceability. There has been an extension to the WNW, through an area where the magnetic field is disturbed, to allow termination at zone ZFMNE3137. Thickness is based on the SHI PDZ borehole intercepts. Forward modelling of magnetic data along profile 2 (Appendix 6) indicates a very steep dip to the north-east whereas inversion modelling indicates a vertical to sub-vertical dip towards the south-west that corresponds to the modelled geometry.



*ZFMWNW3262, looking down dip (sub-vertical) with the relevant SHI PDZs shown as pink cylinders. The modelled zone thickness is 2 m.*

## Deformation zone ZFMWNW3262

### Hydraulic interpretation

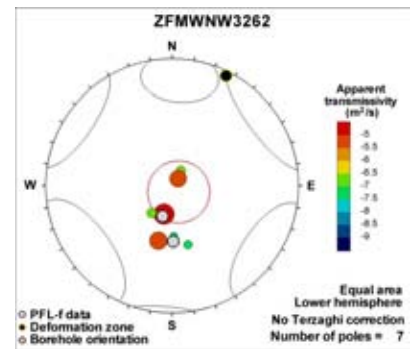
Hydraulic width: 1.4 m

No of intercepts: 2

$T_{eff}(0)$ :  $2.80 \cdot 10^{-5} \text{ m}^2/\text{s}$

Log  $T_{eff}(0)$  -4.6,  $\sigma = (0.55)$

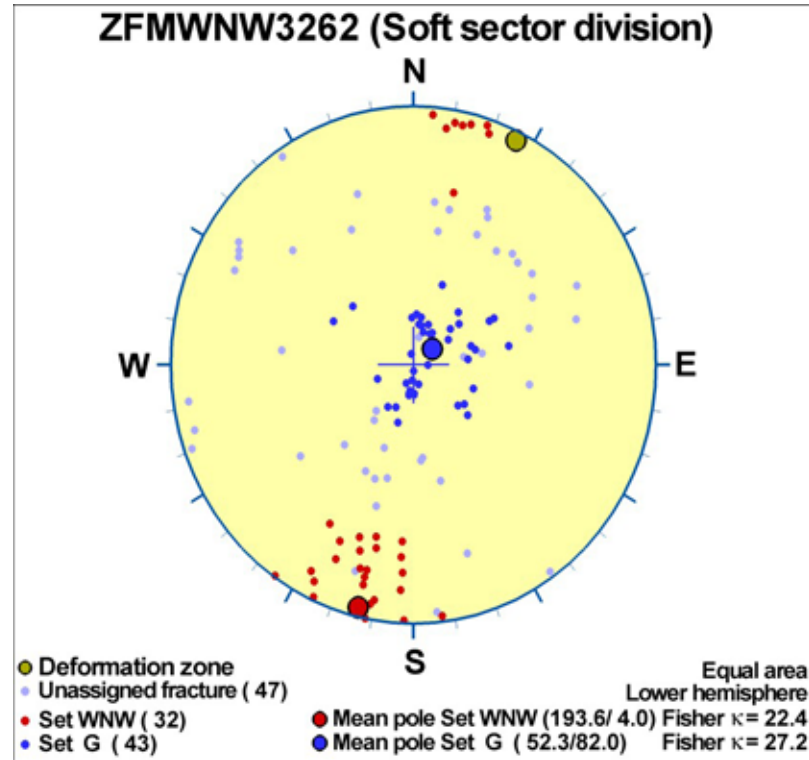
Calculation procedure: Average of both intercepts.



### Fractures in the deformation zone

#### General characteristics

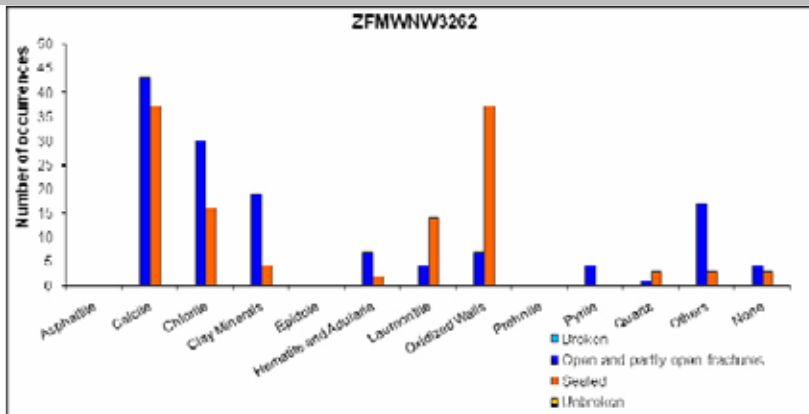
Fracture orientation:



Fracture frequency: Open  $19 \text{ m}^{-1}$ , Sealed  $20 \text{ m}^{-1}$

Fracture filling mineralogy:

## Deformation zone ZFMWNW3262



KFR106 DZ3 (67–73 m)



### BOREHOLE INTERCEPT DETAILS

#### Borehole intersections for ZFMWNW3262

BH	Geometrical Intercept		Target Intercept	
	Sec_up BH length (m) [z (-m)]	Sec_low BH length (m) [z (-m)]	Sec_up BH length (m) [z (-m)]	Sec_low BH length (m) [z (-m)]
KFR103	178.46 [141.30]	183.59 [145.39]	180	182.5

**DZ3 180–182.5 m:** Increased frequency of open fractures and two crushed intervals at 180.69–180.73 and 181.89–182.01 m. Three intervals of core loss at 181.16–181.22, 181.28–181.40 and 181.96–182.00 m. Fracture apertures 0.5 mm or less. Faint to moderate oxidation. Predominant minerals in open fractures and crushed intervals are chlorite, calcite, clay minerals, iron hydroxide and muscovite. Significantly decreased bulk resistivity and magnetic susceptibility along the entire section. Metagranite-granodiorite (101057), pegmatitic granite (101061) and amphibolite (102017). Confidence level = 3.

An isolated cluster of flow anomalies at 180.7–187.9 m. The flow anomalies correspond to crushes and core losses. Total transmissivity of  $1 \cdot 10^{-5} \text{ m}^2/\text{s}$ .

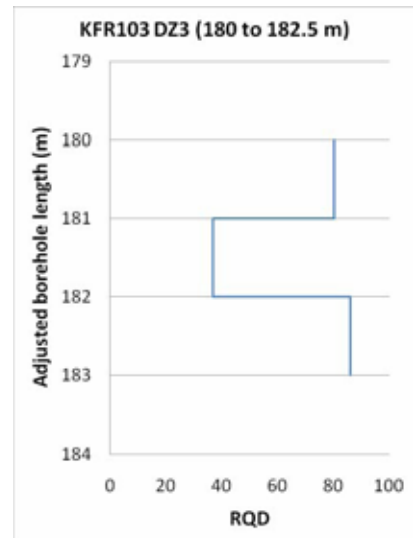
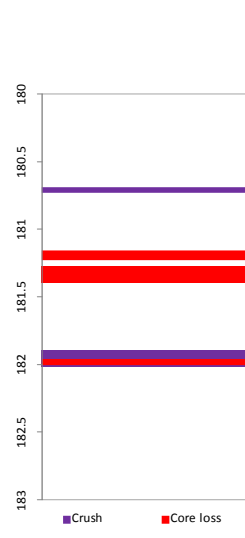
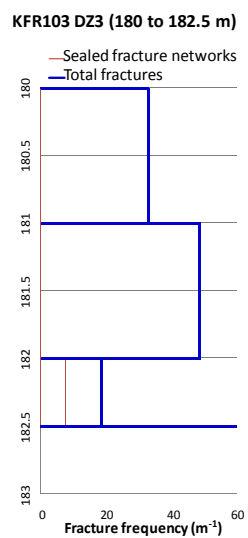
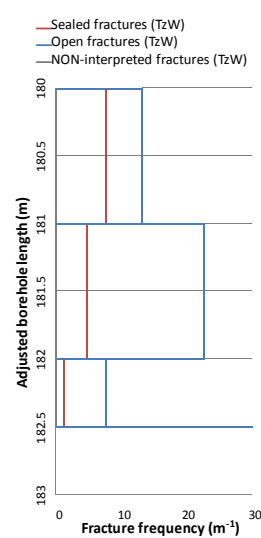
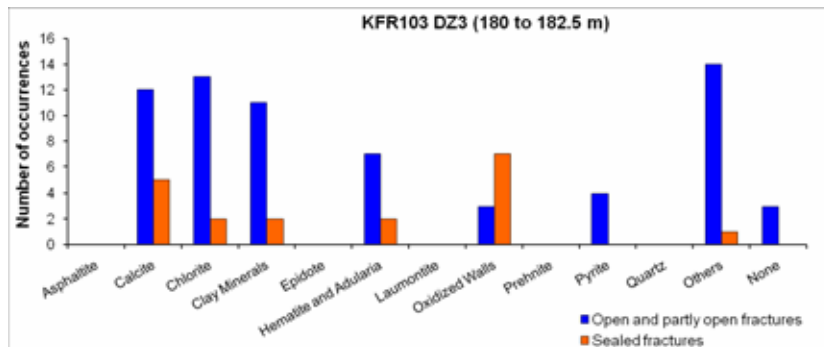
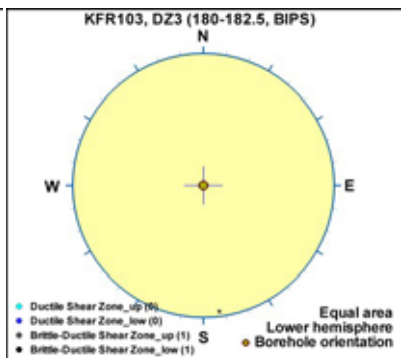
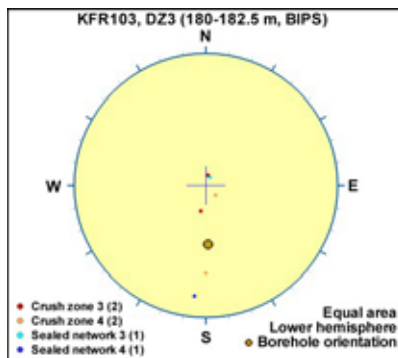
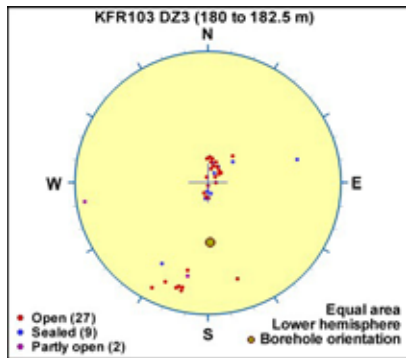
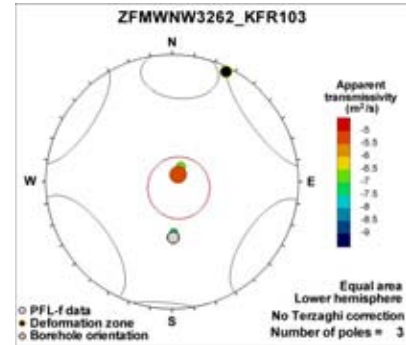
## Borehole intersections for ZFMWNNW3262

### Hydraulic data

$T = 5.08 \cdot 10^{-6} \text{ m}^2/\text{s}$

$\text{Log } T_0 = -4.7$

Three sub-horizontal to gently dipping, high-transmissive PFL-f.  
Alternatively modelled as SBA3,4,5.



### Borehole intersections for ZFMWNW3262

BH	Geometrical Intercept		Target Intercept	
	Sec_up BH length (m) [z (-m)]	Sec_low BH length (m) [z (-m)]	Sec_up BH length (m) [z (-m)]	Sec_low BH length (m) [z (-m)]
KFR106	67.04 [61.90]	73.35 [69.69]	67	73

**DZ3 67–73 m:** Locally increased frequency of open and sealed fractures. One minor crush at 69.58–69.61 m and one ductile shear zone at 69.45–70.19 m (256°/44°). Fracture apertures generally between 0.5 and 1.5mm with one example up to 12 mm. No alteration. Predominant minerals in open fractures are calcite, chlorite, clay minerals, laumontite and oxidized walls. In sealed fractures calcite, oxidized walls, laumontite and chlorite. One radar reflector interpreted without orientation at 72 m. A few narrow low resistivity anomalies and one distinct fluid temperature anomaly, that in combination indicate the occurrence of water bearing fractures. Metagranite-granodiorite (101057), felsic to intermediate metavolcanic rock (103076) and pegmatitic granite (101061). Confidence level = 3.

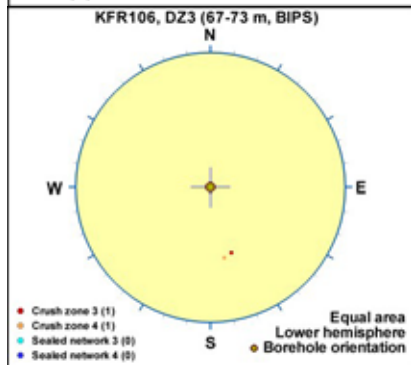
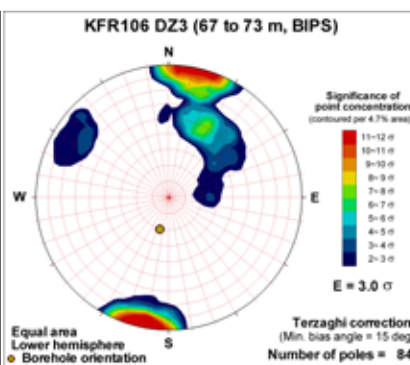
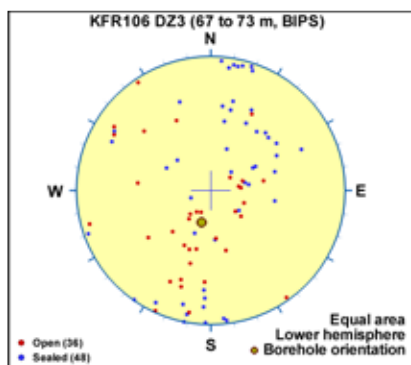
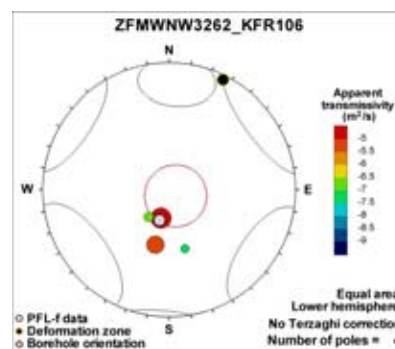
Very high transmissivity of the interval 68–73 m. A number of flow anomalies, with the dominating anomaly at 68.3 m. The total transmissivity of the section is  $3 \cdot 10^{-5} \text{ m}^2/\text{s}$ .

#### Hydraulic data

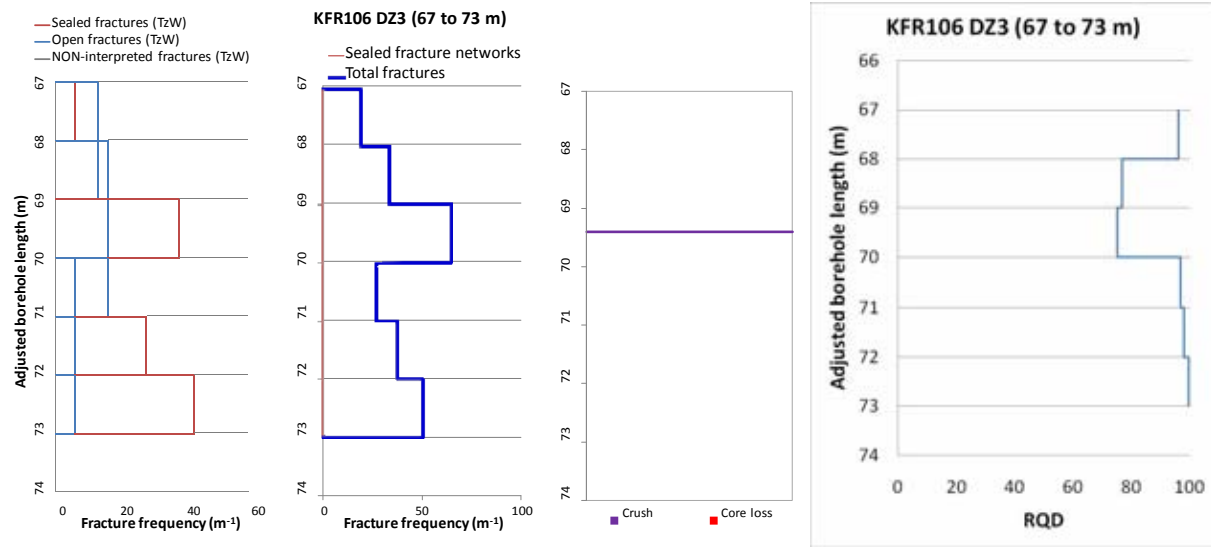
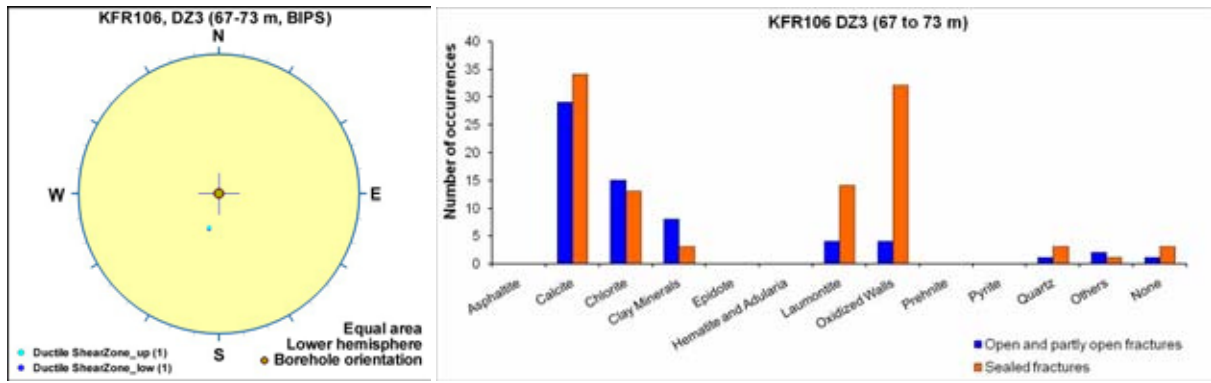
$T = 1.96 \cdot 10^{-5} \text{ m}^2/\text{s}$

$\text{Log } T_0 = -4.4$

Three sub-horizontal to gently dipping, high-transmissive PFL-f. Alternatively modelled as SBA3,4,5.



## Borehole intersections for ZFMWNW3262



## Deformation zone ZFMWNW3267

### Borehole and tunnel intersections (metres along borehole/tunnel)

KFR104: 396–454.57 m (DZ5 396–405 m and DZ6 447–454.57 m)  
 KFR105: 258–283 m (DZ4 258–283 m)

### Deformation style, alteration and geometry

**Deformation style:** Brittle. Minor cohesive breccia and cataclasite in target intercept along KFR104

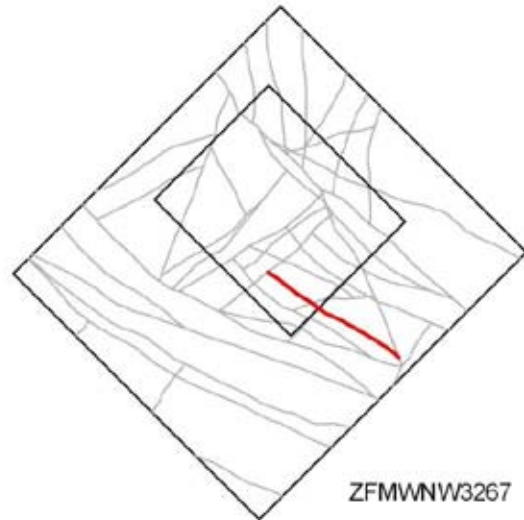
**Alteration:** Locally red-stained bedrock with fine-grained hematite dissemination, argillization, laumontitization and epidotization

**Strike/dip (span) right-hand-rule:** 122 / 90 ( $\pm 5 / \pm 10$ )

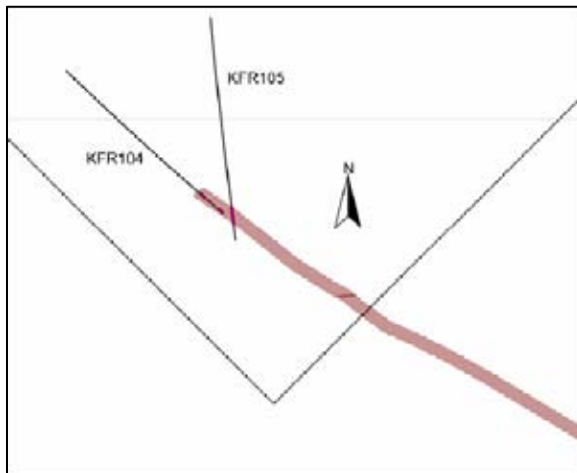
**Trace length at ground surface (span):** 698 m (500–1000 m)

**Model thickness (span):** 18 m (2–20 m)

**Confidence in existence:** High



**Modelling procedure:** In the current SFR model version 1.0, this zone is based on a modification of the Forsmark stage 2.3 lineament MFM3267G /Isaksson et al. 2007/. In the SFR model version 0.1 lineament interpretation, this lineament was replaced by MSFR08121 and MSFR08115. The dip of the zone is based on a link with the borehole interceptions in KFR104 and KFR105. The forward modelling of magnetic data along profile 1 (see Appendix 6) data suggests a sub-vertical to a very steep dip to the north-east, while profile 39 modelling suggests a vertical dip.



Plan view of ZFMWNW3267 with the relevant SHI PDZs shown as pink cylinders. The modelled zone thickness is 18 m.

## Hydraulic interpretation

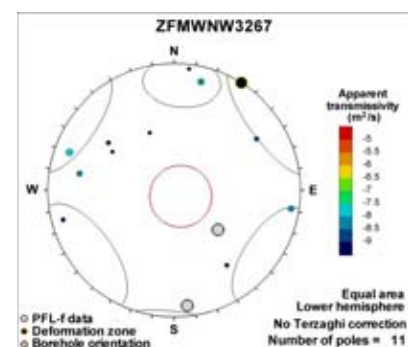
**Hydraulic width:** 12.3 m

**No of intercepts:** 2

**$T_{\text{eff}}(0)$ :**  $2.13 \cdot 10^{-7} \text{ m}^2/\text{s}$

**Log  $T_{\text{eff}}(0)$ :**  $-6.7$ ,  $\sigma = (0.55)$

**Calculation procedure:** Average of both intercepts. PFL-f data exhibit the typical pattern of rock mass in the Central Block.

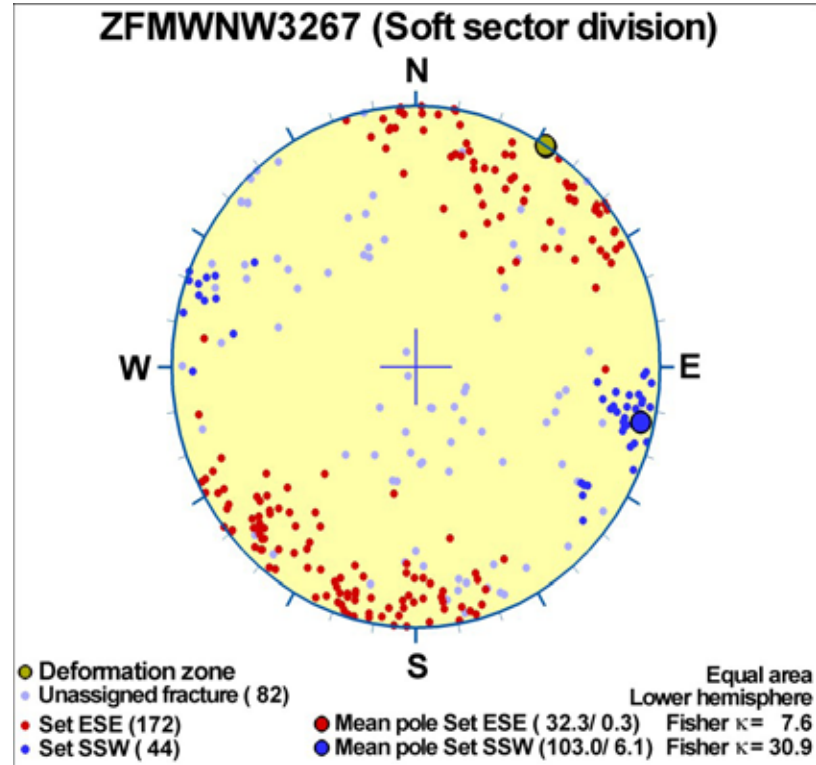


# Deformation zone ZFMWNW3267

## Fractures in the deformation zone

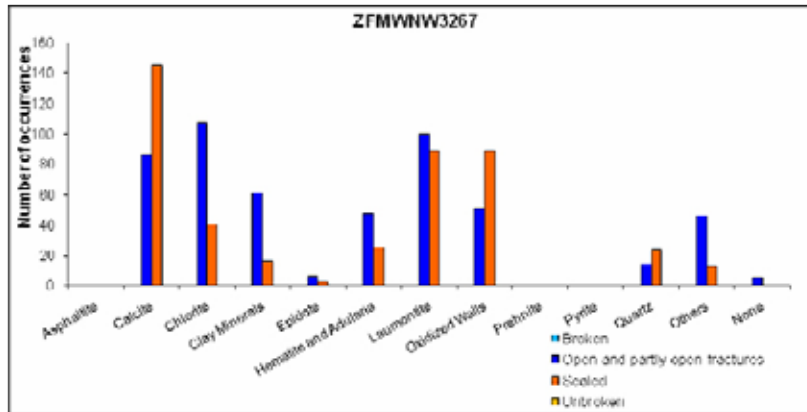
### General characteristics

Fracture orientation:



Fracture frequency: Open  $10 \text{ m}^{-1}$ , Sealed  $26 \text{ m}^{-1}$

Fracture filling mineralogy:



KFR105 DZ4 (258-283 m)





# Deformation zone ZFMWNW3267



## BOREHOLE AND TUNNEL INTERCEPT DETAILS

Borehole intersections for ZFMWNW3267				
BH	Geometrical Intercept		Target Intercept	
	Sec_up BH length (m) [z (-m)]	Sec_low BH length (m) [z (-m)]	Sec_up BH length (m) [z (-m)]	Sec_low BH length (m) [z (-m)]
KFR104	388.50 [302.51]	eoh [351.72]	396	454.57

**Comment:** Fracture plots show that NW striking fractures dominate the interval between DZ5 and DZ6.

**DZ5 396–405 m:** Increased frequency of open fractures. One minor cataclasite along the lower limit of the possible zone at 400.39–400.41 m. Fracture apertures up to 2 mm. Several moderately altered open fractures. Varying degrees of argillization and epidotization in the lower half of the interval. Predominant minerals in open fractures are clay minerals, chlorite and calcite. Low electric resistivity and one minor caliper anomaly. Pegmatitic granite (101061) and amphibolite (102017). Confidence level = 3.

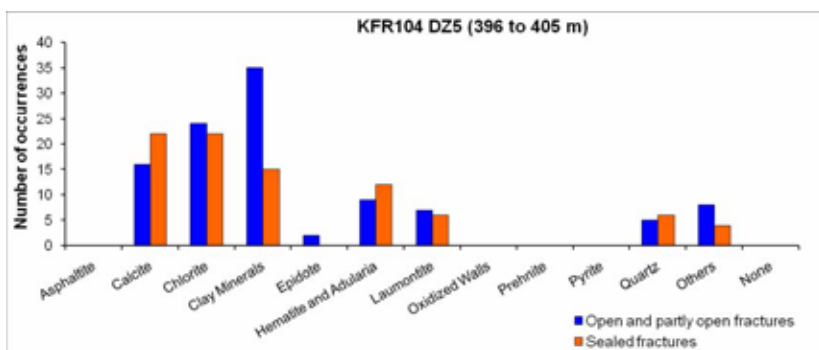
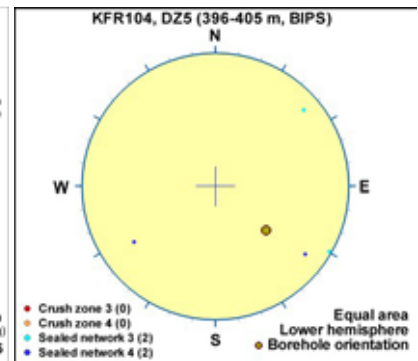
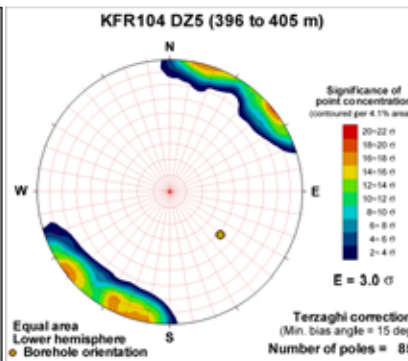
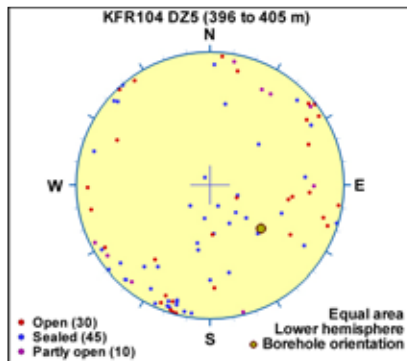
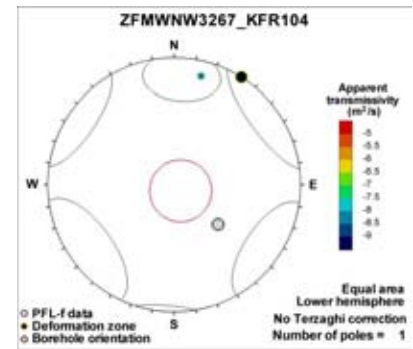
One single flow anomaly ( $T = 1 \cdot 10^{-8} \text{ m}^2/\text{s}$ ) at 405 m. This is the only flow anomaly in the borehole below 350 m.

### Hydraulic data

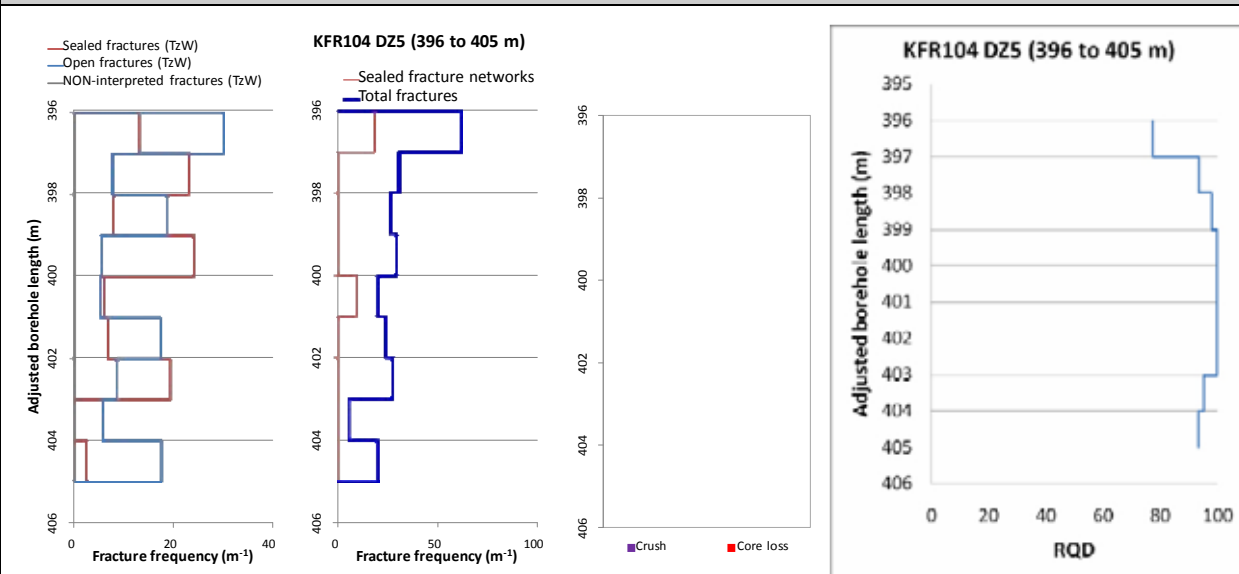
$T = 1.10 \cdot 10^{-8} \text{ m}^2/\text{s}$

$\text{Log } T_0 = -6.6$

Little hydraulic support by single PFL-f, which is sub-parallel to the deformation zone. Considered typical pattern of Central Block characteristics (inside as well as outside zones).

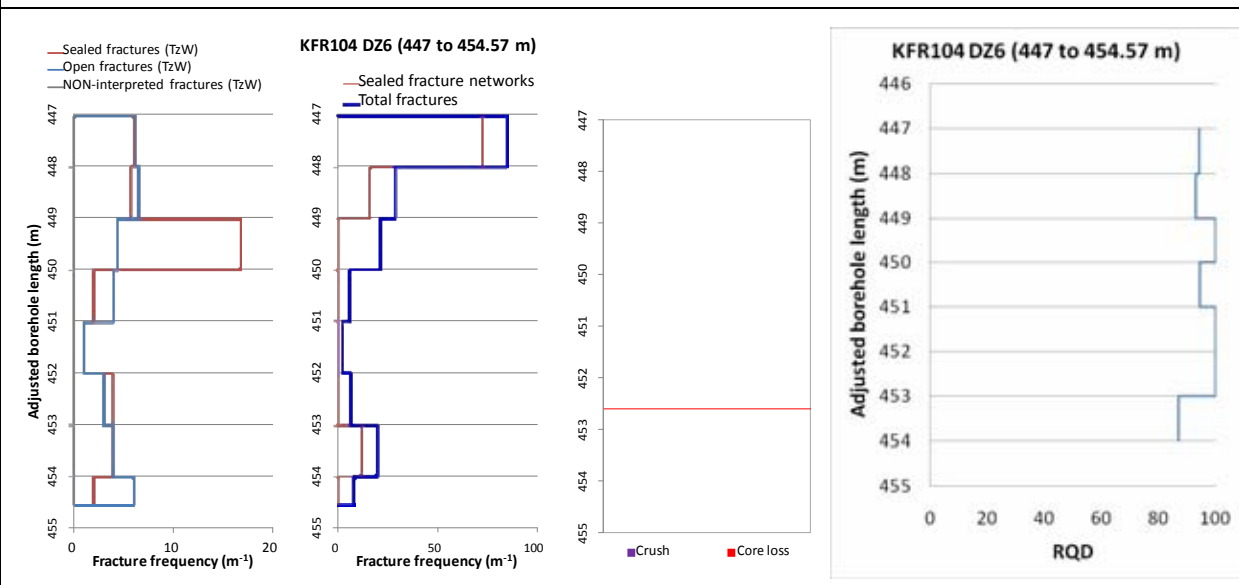
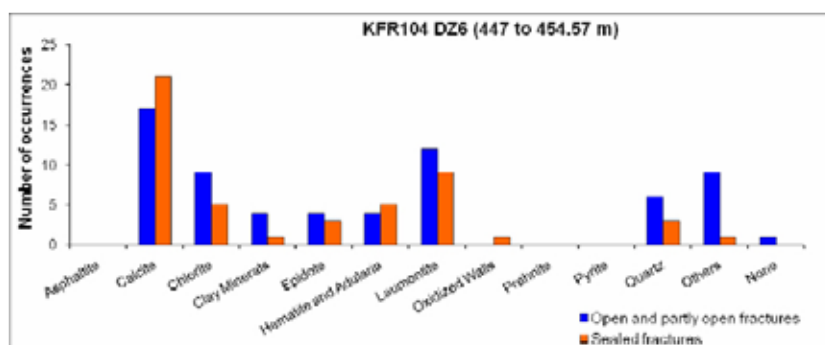


### Borehole intersections for ZFMWNW3267



**DZ6 447–454.57 m:** Increased frequency of sealed fractures and sealed fracture network in the upper half of the interval. One brecciated interval at 452.97–453.05 m. Locally faint to strong oxidation and laumontization. No BIPS image of the interval. Predominant minerals in sealed fractures are laumontite, calcite and chlorite. Low electric resistivity and one major caliper anomaly. Fine to medium grained granite (111058), pegmatitic granite (101061) and metagranite-granodiorite (101057). Confidence level = 3.

No hydraulic data from this interval.



### Borehole intersections for ZFMWNW3267

BH	Geometrical Intercept		Target Intercept	
	Sec_up BH length (m) [z (-m)]	Sec_low BH length (m) [z (-m)]	Sec_up BH length (m) [z (-m)]	Sec_low BH length (m) [z (-m)]
KFR105	257.84 [149.34]	282.99 [153.16]	258	283

**DZ4 258–283 m:** Increased frequency of open fractures and especially sealed fractures along with sealed fracture networks. Two minor crushes at 259.80–259.82 and 270.31–270.38 m. Zone core defined at 279.7–281.0 m. Fracture apertures in general up to 0.5 mm. Very local moderate to strong oxidation and moderate laumontite alteration. Predominant fracture minerals in open fractures are laumontite, chlorite, calcite, oxidized walls, hematite and clay minerals and in sealed fractures laumontite, calcite and oxidized walls. Several significant low resistivity anomalies (< 2,000 Ohm-m), and two distinct anomalies in the fluid temperature data indicating water-bearing fractures. In the section 278–286 m there are significant caliper anomalies. One radar reflector at 268.6 m oriented 316°/33° or 039°/45°. Pegmatitic granite (101061), fine- to medium-grained metagranite-granodiorite (101057) and felsic to intermediate metavolcanic rock (103076). Confidence level = 3.

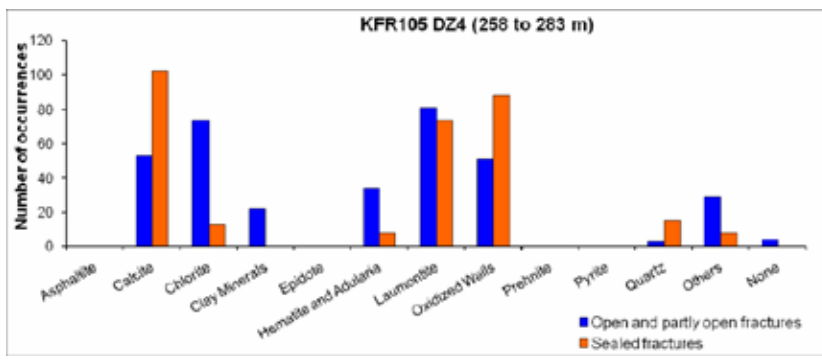
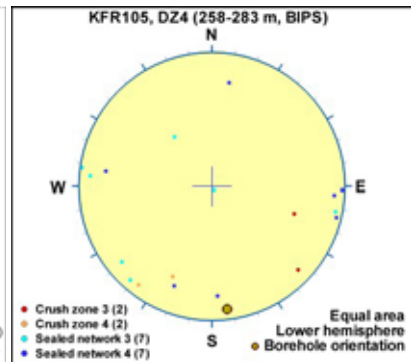
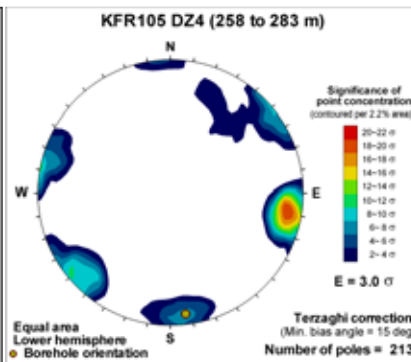
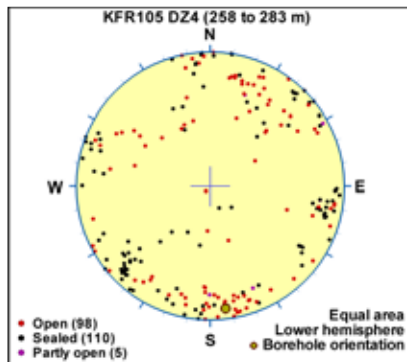
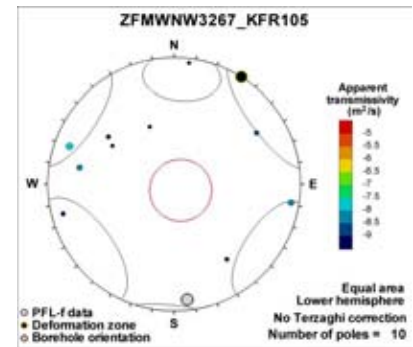
Low transmissivity of the section ( $T = 4 \cdot 10^{-8} \text{ m}^2/\text{s}$ ). The main flow anomaly is located at 267.3 m.

#### Hydraulic data

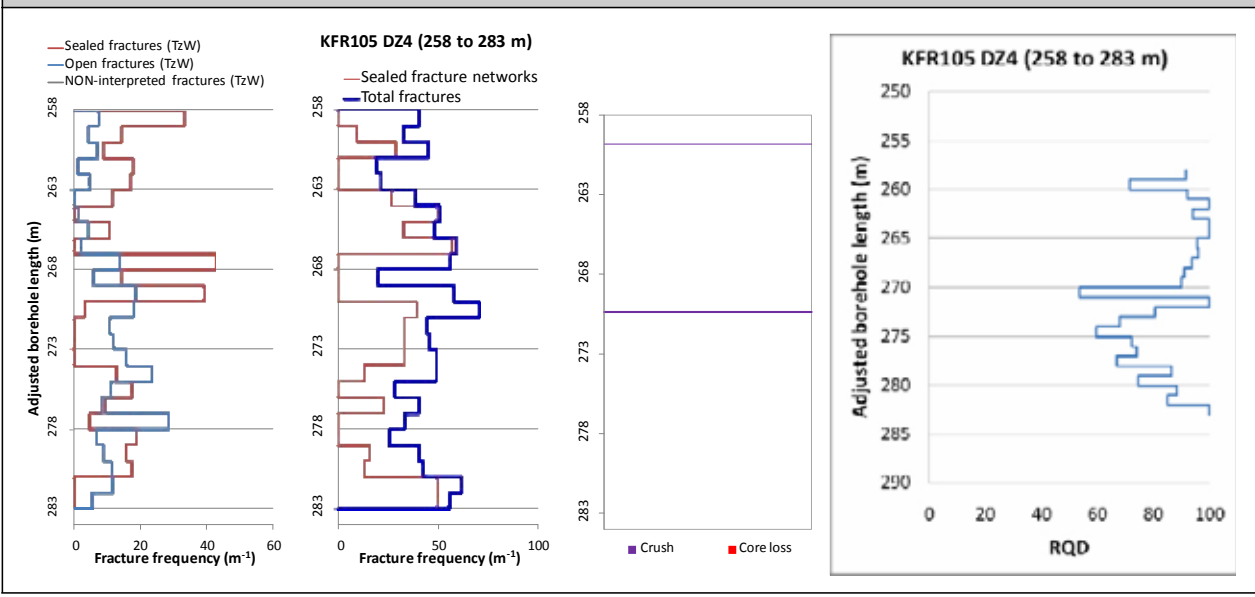
$$T = 4.10 \cdot 10^{-8} \text{ m}^2/\text{s}$$

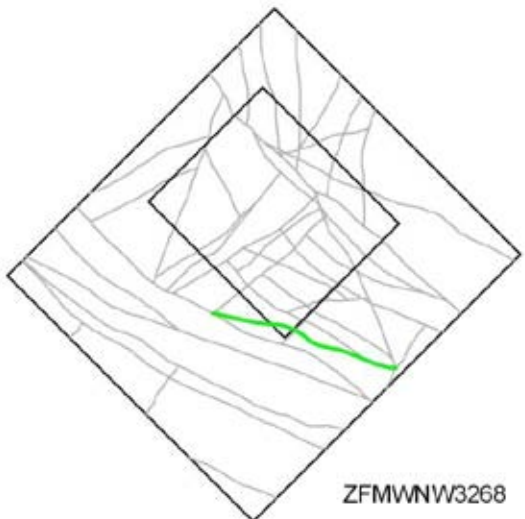
$$\text{Log } T_0 = -6.7$$

Several low-transmissive PFL-f with scattered orientation. Considered typical pattern of Central Block characteristics (inside as well as outside zones).



### Borehole intersections for ZFMWNW3267



<b>Deformation zone ZFMWNW3268</b>	
<p><b>Borehole and tunnel intersections (metres along borehole/tunnel)</b></p> <p>None</p>	
<p><b>Deformation style, alteration and geometry</b></p> <p><b>Deformation style:</b> Ductile and brittle (no direct evidence – inferred association with other WNW-ESE trending deformation zones)</p> <p><b>Alteration:</b> No data</p> <p><b>Strike/dip (span) right-hand-rule:</b> 109 / 90 (±5 / ±10)</p> <p><b>Trace length at ground surface (span):</b> 861 m (700–870 m)</p> <p><b>Model thickness:</b> 5 m*</p> <p><b>Confidence in existence:</b> Medium</p>	
<p><b>Modelling procedure:</b> The position of the zone at the ground surface is based on magnetic lineament MSFR80006 (SFR model version 1.0), itself an update of lineament MFM3268G /Isaksson et al. 2007/, with a further extension to the WNW to allow termination at ZFMNE3137 and ZFMWNW1035. The vertical dip is a default value.</p> <p>*The modelled thickness is a 1% default value based on the traceable zone length of 709 m. However, in the model the zone geometry has been extended to terminate at ZFMWNW1035 to ensure connectivity giving an rvs modelled length of 861 m.</p>	
<b>Hydraulic interpretation</b>	
<p><b>Hydraulic width:</b> 3.6 m</p> <p><b>No of intercepts:</b> None</p> <p><b>T<sub>eff</sub>(0):</b> 1.44 · 10<sup>-6</sup> m<sup>2</sup>/s</p> <p><b>Log T<sub>eff</sub>(0):</b> -5.8, σ = (0.55)</p> <p><b>Calculation procedure:</b> T<sub>eff</sub>(0) taken as pooled average of the WNW to NW set (only based on new</p>	
<b>Fractures in the deformation zone</b>	
<b>General characteristics</b>	
<p><b>Fracture orientation:</b> No data</p> <p><b>Fracture frequency:</b> No data</p> <p><b>Fracture filling mineralogy:</b> No data</p>	

## Deformation zone ZFMWNW8042

### Borehole and tunnel intersections (metres along borehole/tunnel)

KFR105: 170.8–176 m (DZ3 170.8–176 m)

### Deformation style, alteration and geometry

**Deformation style:** Brittle

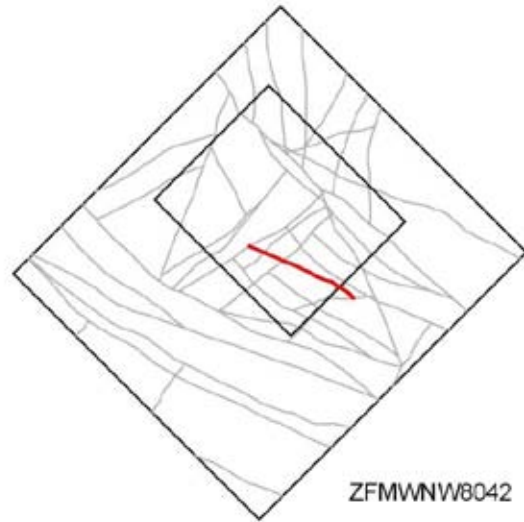
**Alteration:** Locally red-stained bedrock with fine-grained hematite dissemination and chloritization of amphibolite.

**Strike/dip (span) right-hand-rule:** 116 / 89 (±5 / ±10)

**Trace length at ground surface (span):** 524 m (250–800 m)

**Model thickness (span):** 5 m (1–7 m)

**Confidence in existence:** High



**Modelling procedure:** The position of the zone at the ground surface is based on magnetic lineament MSFR08042 (SFR model version 1.0) with a further extension to the WNW to allow termination at ZFMENE3115. The zone thickness is based on the borehole intercept and the dip is based on linking the lineament to the borehole intercept. Forward modelling of magnetic data along profiles 12 and 44 supports the vertical dip and limited thickness of the zone, while inversion modelling suggests a very steep dip to the north-east (see Appendix 6)

## Hydraulic interpretation

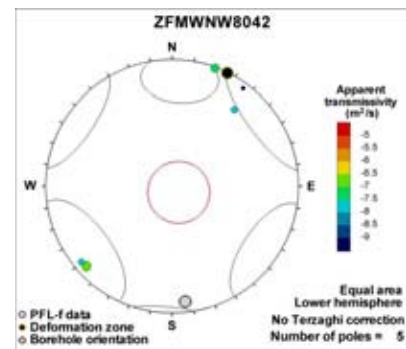
**Hydraulic width:** 4.3 m

**No of intercepts:** 1

**$T_{\text{eff}}(0)$ :**  $1.05 \cdot 10^{-6} \text{ m}^2/\text{s}$

**Log  $T_{\text{eff}}(0)$ :** -6.0,  $\sigma = (0.55)$

**Calculation procedure:** Single intercept used. The zone is well-supported by sub-parallel PFL-f data.

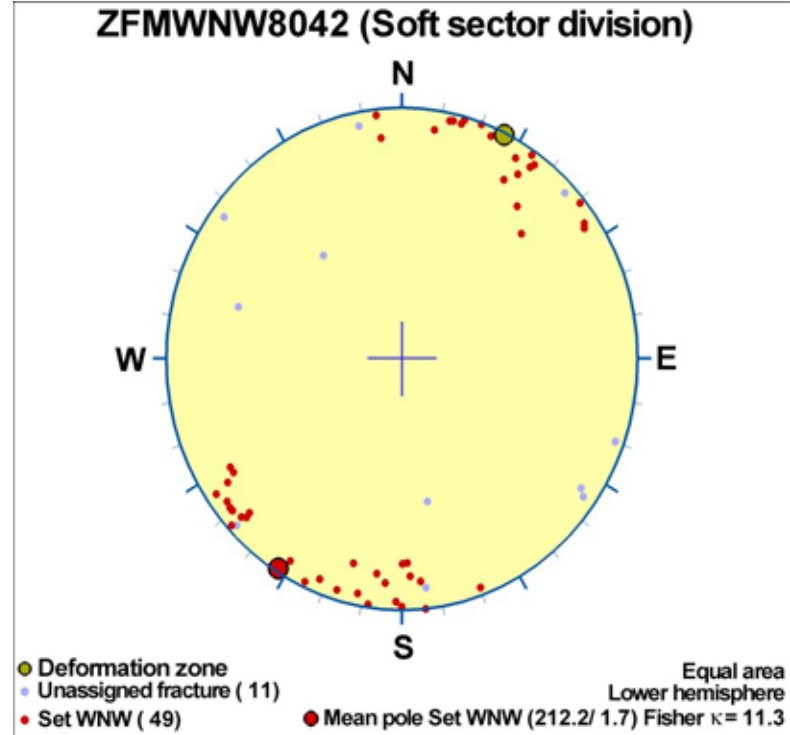


## Deformation zone ZFMWNW8042

### Fractures in the deformation zone

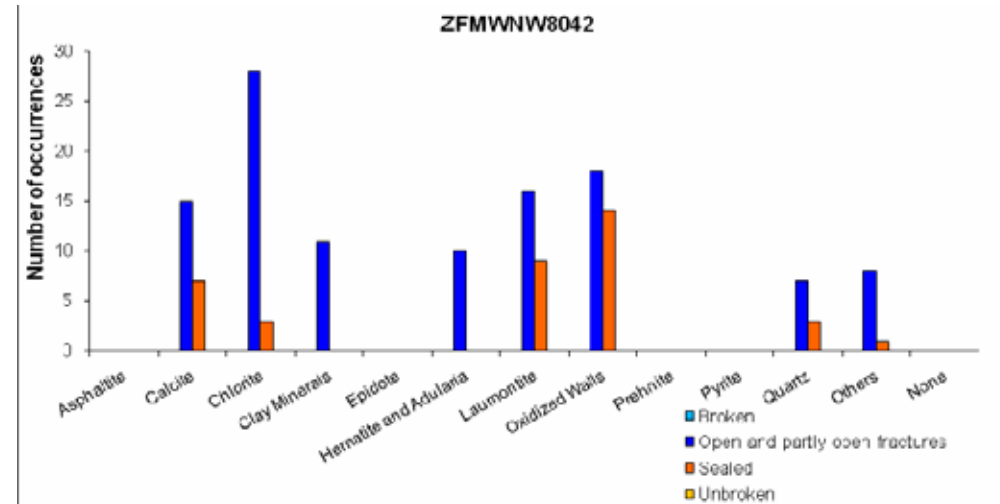
#### General characteristics

Fracture orientation:



Fracture frequency: Open 14 m<sup>-1</sup>, Sealed 55 m<sup>-1</sup>

Fracture filling mineralogy:



KFR105 DZ3 (170.8–176 m)



**Deformation zone ZFMWNW8042**



## BOREHOLE AND TUNNEL INTERCEPT DETAILS

Borehole intersections for ZFMWNNW8042				
BH	Geometrical Intercept		Target Intercept	
	Sec_up BH length (m) [z (-m)]	Sec_low BH length (m) [z (-m)]	Sec_up BH length (m) [z (-m)]	Sec_low BH length (m) [z (-m)]
KFR105	170.49 [135.48]	176.34 [136.42]	170.8	176

**SHI DZ3 170.8–176 m:** Increased frequency of sealed and open fractures and sealed networks. Zone core defined at 172.5–173.4 m. One minor crush at 172.82–172.86 m and one breccia at 173.11–173.19 m. Fracture apertures in general up to 0.5 mm. Predominant fracture minerals in open fractures are chlorite, oxidized walls, laumontite, calcite and clay minerals and in sealed fractures laumontite, calcite and oxidized walls. Local faint to moderate oxidation and chloritization. The section 172–176 m is characterized by significantly decreased bulk resistivity, < 1,000 Ohm-m in the zone core and a distinct anomaly in the fluid temperature data indicating a water bearing fracture. One distinct radar reflector at 173.6 m oriented 270°/38°. Felsic to intermediate metavolcanic rock (103076) and pegmatitic granite (101061). Confidence level = 3.

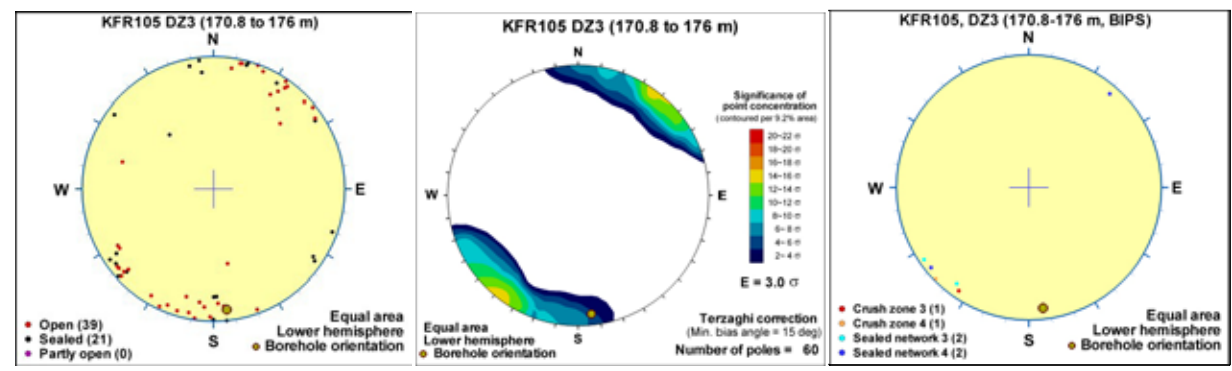
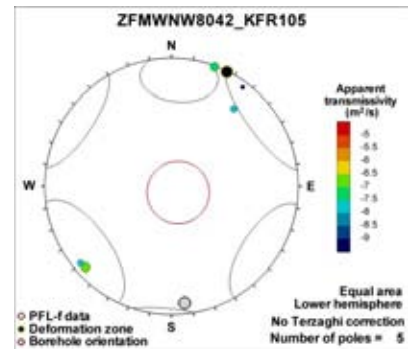
Increased frequency of flow anomalies, the two most significant at 172.7 and 173.0 m. The total transmissivity of the section is moderate, about  $3 \cdot 10^{-7} \text{ m}^2/\text{s}$ .

### Hydraulic data

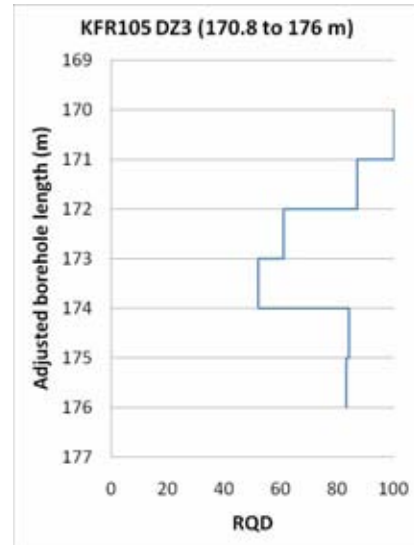
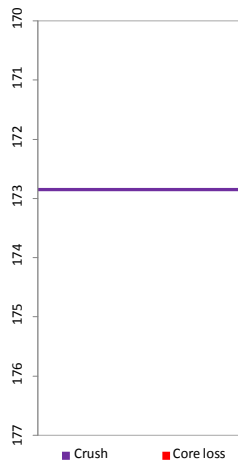
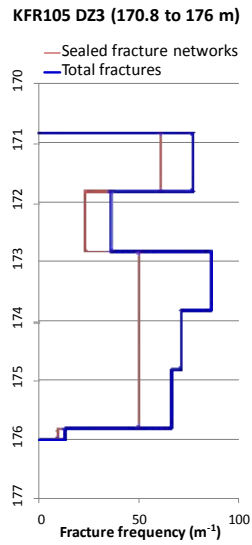
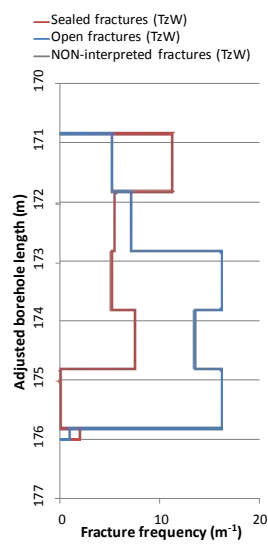
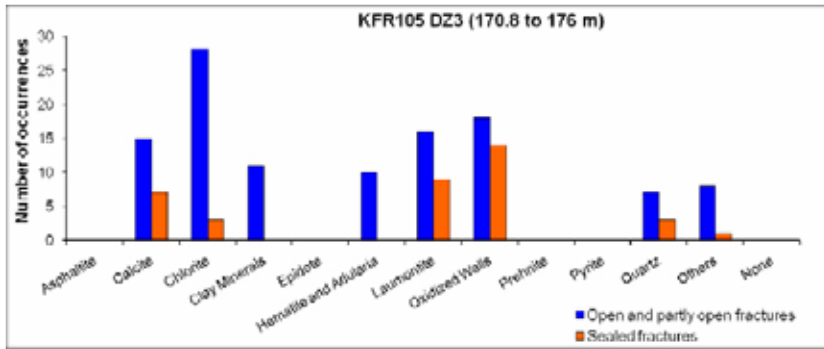
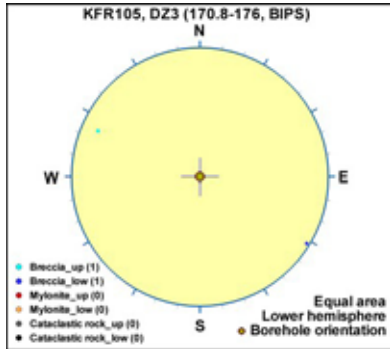
$T = 2.74 \cdot 10^{-7} \text{ m}^2/\text{s}$

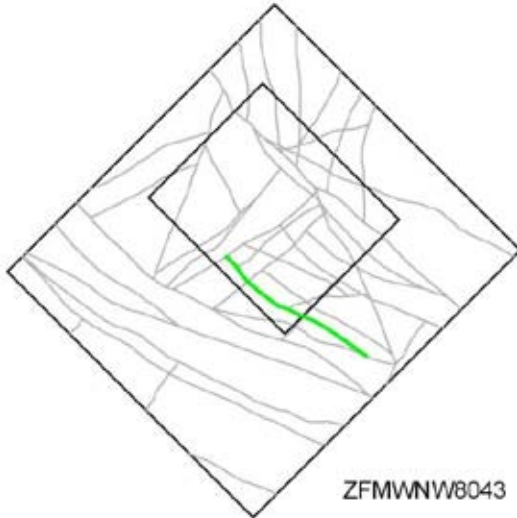
$\text{Log } T_0 = -6$

Five moderately transmissive PFL-f that are sub-parallel to the zone.

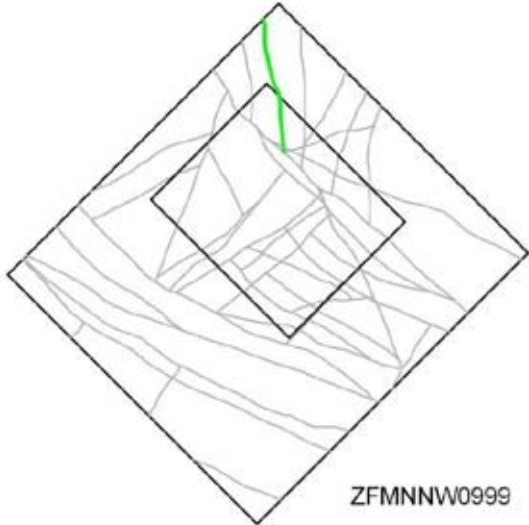


## Borehole intersections for ZFMWNW8042



<b>Deformation zone ZFMWNW8043</b>	
<p><b>Borehole and tunnel intersections (metres along borehole/tunnel)</b></p> <p>None</p>	
<p><b>Deformation style, alteration and geometry</b></p> <p><b>Deformation style:</b> Brittle (no direct evidence – inferred association with other neighbouring WNW-ESE trending deformation zones)</p> <p><b>Alteration:</b> No data</p> <p><b>Strike/dip (span) right-hand-rule:</b> 124 / 90 (±5 / ±10)</p> <p><b>Trace length at ground surface (span):</b> 775 m (625–925 m)</p> <p><b>Model thickness:</b> 10 m (1% default)</p> <p><b>Confidence in existence:</b> Medium</p>	
<p><b>Modelling procedure:</b> The position of the zone at the ground surface is based on version 1.0 magnetic lineament MSFR10002 that replaces version 0.1 lineaments MSFR08043 and MSFR08045. The earlier number has been kept in the zone name to assist traceability between different model versions. The modelled dip and thickness are default values.</p>	
<b>Hydraulic interpretation</b>	
<p><b>Hydraulic width:</b> 7.2 m</p> <p><b>No of intercepts:</b> None</p> <p><b>T<sub>eff</sub>(0):</b> <math>3.06 \cdot 10^{-7} \text{ m}^2/\text{s}</math></p> <p><b>Log T<sub>eff</sub>(0):</b> -6.5, <math>\sigma = (0.55)</math></p> <p><b>Calculation procedure:</b> T<sub>eff</sub>(0) taken as pooled average of the WNW to NW set (only based on new data).</p>	
<b>Fractures in the deformation zone</b>	
<b>General characteristics</b>	
<p><b>Fracture orientation:</b> No data</p> <p><b>Fracture frequency:</b> No data</p> <p><b>Crush zone:</b> No data</p> <p><b>Fracture filling mineralogy:</b> No data</p>	

## Steeply dipping NNW to N-S deformation zones

<b>Deformation zone ZFMNNW0999</b>	
<p><b>Borehole and tunnel intersections (metres along borehole/tunnel)</b></p> <p>None</p>	
<p><b>Deformation style, alteration and geometry</b></p> <p><b>Deformation style:</b> No data</p> <p><b>Alteration:</b> No data</p> <p><b>Strike/dip (span) right-hand-rule:</b> 170 / 90 (<math>\pm 5 / \pm 10</math>)</p> <p><b>Trace length at ground surface (span):</b> 692 m (692--&gt;692 m)</p> <p><b>Model thickness:</b> 5 m (1% default)</p> <p><b>Confidence in existence:</b> Medium</p>	
<p><b>Modelling procedure:</b> ZFMNNW0999 is based on the magnetic lineament MFM0999G in the Forsmark stage 2.3 interpretation /Isaksson et al. 2007/. The zone has a length of 692 m terminating at ZFMNNW0805A in the south and extending outside of the regional model area to the north, where MFM0999G terminates at lineament MSFR08078 in the SFR model version 1.0 (an update of Forsmark stage 2.3 lineament MFM3149G in /Isaksson et al. 2007/). The modelled zone geometry results in an intersection in KFR08 SHI DZ2. However, this interval is inferred as being dominated by ZFMNNW0805A and no exclusive evidence for the existence of ZFMNNW0999 has been identified. For this reason, ZFMNNW0999 has been classed as medium confidence. The general thickness and vertical to sub-vertical dip are supported by the forward modelling of magnetic data along profiles 5 and 6 (see Appendix 6).</p>	
<b>Hydraulic interpretation</b>	
<p><b>Hydraulic width:</b> 3.6 m</p> <p><b>No of intercepts:</b> None</p> <p><b><math>T_{\text{eff}}(0)</math>:</b> <math>1.76 \cdot 10^{-8} \text{ m}^2/\text{s}</math></p> <p><b>Log <math>T_{\text{eff}}(0)</math>:</b> <math>-7.8, \sigma = (0.55)</math></p> <p><b>Calculation procedure:</b> Rejected intercept. Value taken from pooled average of NNW group in SDM-Site Forsmark.</p>	
<b>Fractures in the deformation zone</b>	
<b>General characteristics</b>	
<p><b>Fracture orientation:</b> No data</p> <p><b>Fracture frequency:</b> No data</p> <p><b>Fracture filling mineralogy:</b> No data</p>	

**BOREHOLE AND TUNNEL INTERCEPT DETAILS**

Borehole intersections for ZFMNNW0999				
BH	Geometrical Intercept		Target Intercept	
	Sec_up BH length (m) [z (-m)]	Sec_low BH length (m) [z (-m)]	Sec_up BH length (m) [z (-m)]	Sec_low BH length (m) [z (-m)]
KFR08	75.72 [92.62]	81.46 [93.12]	-	-
<p><b>Comment:</b> This interval is inferred as being dominated by ZFMNNW0805A and no exclusive evidence for the existence of ZFMNNW0999 has been identified.</p>				

## Deformation zone ZFMNNW1034

### Borehole and tunnel intersections (metres along borehole/tunnel)

HFR106: 158–182 m (DZ2 158–162 m and DZ3 177–182 m)  
 KFR101: 13.72–88 m (DZ1 13.72–88 m)  
 KFR106: 256–266 m (DZ7 256–266 m)

### Deformation style, alteration and geometry

**Deformation style:** Brittle, including minor cohesive breccias. Inferred brittle-ductile shear zone registered in HFR106 DZ3. Ductile and brittle-ductile shear zones present in KFR101 DZ1.

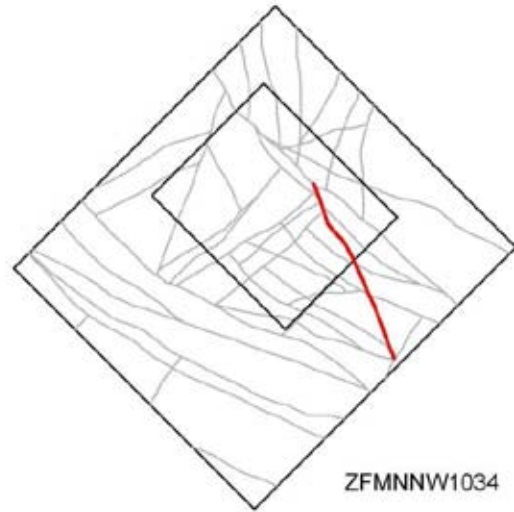
**Alteration:** Locally red-stained bedrock with fine-grained hematite dissemination. Very locally argillization and epidotization

**Strike/dip (span) right-hand-rule:** 337 / 78 ( $\pm 5$  /  $\pm 10$ )

**Trace length at ground surface (span):** 883 m (880–1130 m)

**Model thickness (span):** 17 m (5–20 m)

**Confidence in existence:** High



**Modelling procedure:** Based on magnetic lineament MFM1034G in Forsmark stage 2.3 /Isaksson et al. 2007/ that has been adjusted slightly and updated as lineaments MSFR08100 and MSFR08101 in SFR model version 1.0. Further modification took place in the modelling work at the north-west end, based on information from KFR101 DZ1, where the zone passes through the magnetically disturbed pier area. The general thickness and steep dip to the north-east are supported by the forward modelling of magnetic data along profile 2 (see Appendix 6).

## Hydraulic interpretation

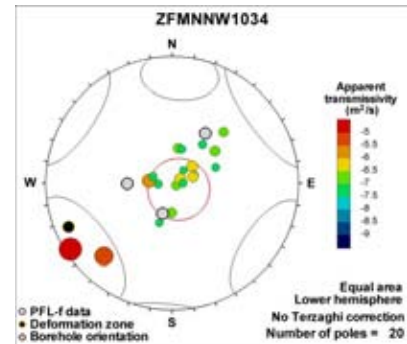
**Hydraulic width:** 13.7 m

**No of intercepts:** 3

**$T_{\text{eff}}(0)$ :**  $3.74 \cdot 10^{-5} \text{ m}^2/\text{s}$

**Log  $T_{\text{eff}}(0)$ :**  $-4.4$ ,  $\sigma = 0.27$

**Calculation procedure:**  $T_{\text{eff}}(0)$  taken as average from all 3 intercepts. Interpreted as a key hydraulic boundary for the hydrogeologic system, associated to the large-scale transmissivity pattern in the vicinity of the Northern Belt. Although the transmissivities are lower than in the Southern Belt, there exist similarities in the PFL-f orientation pattern, predominantly steep NW-striking or gently dipping.

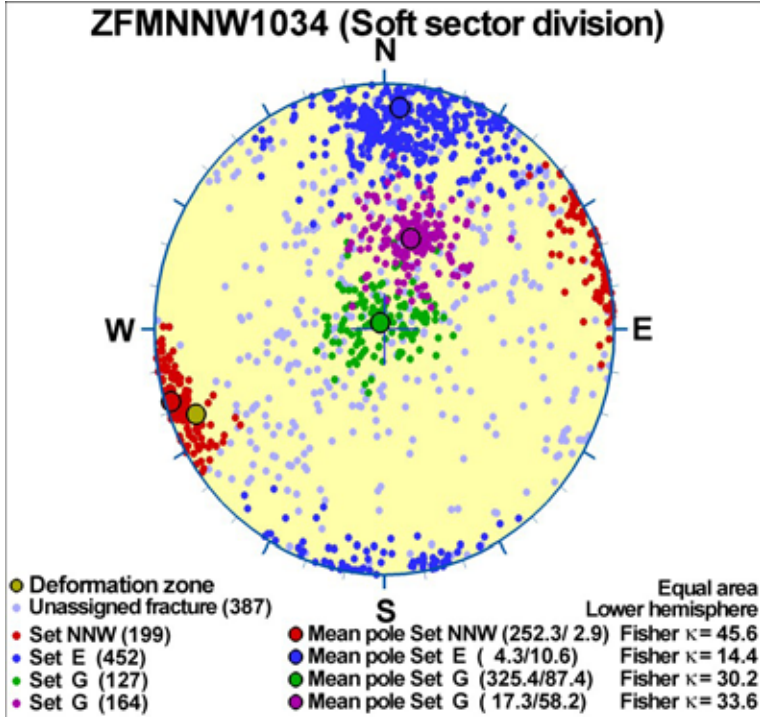


# Deformation zone ZFMNNW1034

## Fractures in the deformation zone

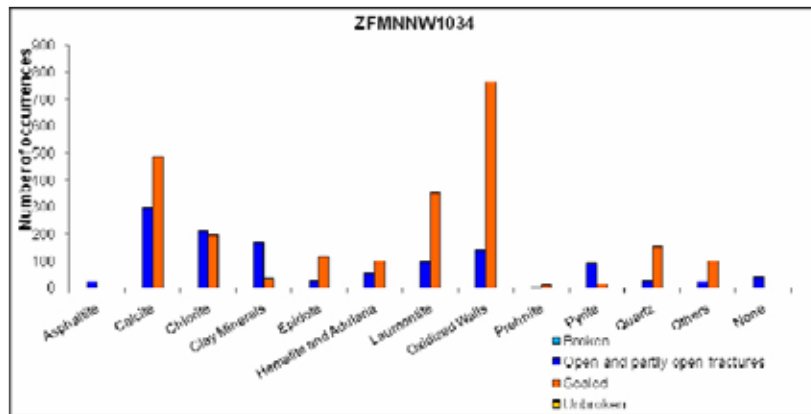
### General characteristics

Fracture orientation:



Fracture frequency: Open 9 m<sup>-1</sup>, Sealed 43 m<sup>-1</sup>

Fracture filling mineralogy:



KFR106 DZ7 (256–266 m)





## Deformation zone ZFMNNW1034

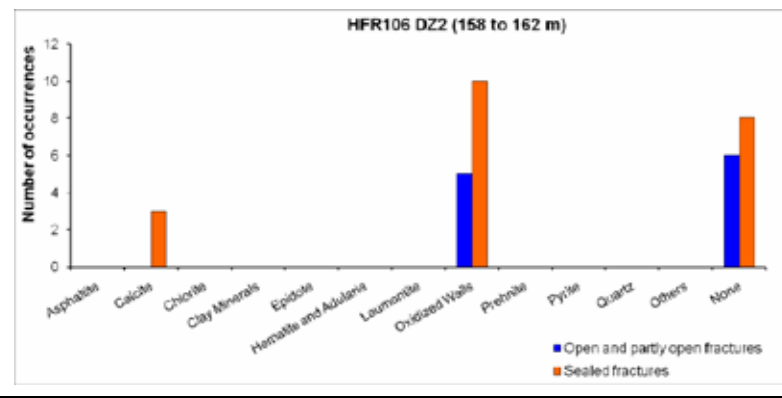
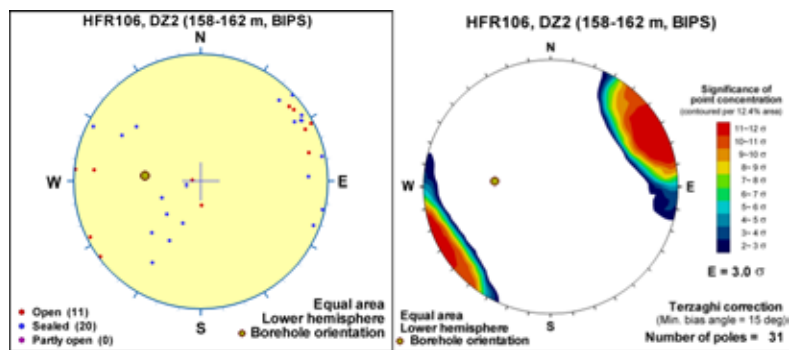


## BOREHOLE AND TUNNEL INTERCEPT DETAILS

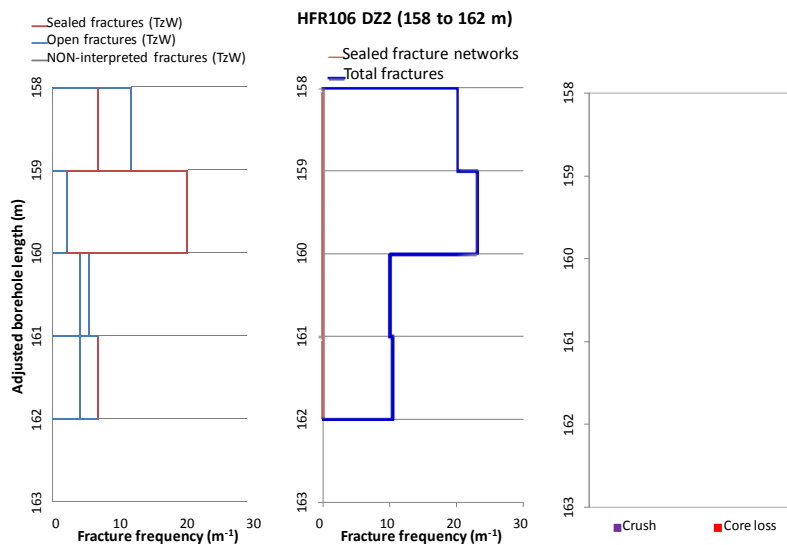
Borehole intersections for ZFMNNW1034				
BH	Geometrical Intercept		Target intercept	
	Sec_up BH length (m) [z (-m)]	Sec_low BH length (m) [z (-m)]	Sec_up BH length (m) [z (-m)]	Sec_low BH length (m) [z (-m)]
HFR106	136.61 [110.02]	179.79 [144.56]	158	182

**SHI DZ2 158–162 m:** No clear indications in the BIPS-image. However, there is a distinct decrease in the bulk resistivity and there are significant caliper anomalies. Metagranite-granodiorite (101057), pegmatitic granite (101061) and felsic to intermediate metavolcanic rock (103076). Confidence level = 1.

No flow anomaly observed in this section (however, there may be flow below the lower measurement limit which was relatively high in this case).



## Borehole intersections for ZFMNNW1034



**SHI DZ3 177–182 m:** Distinct increase in fracture frequency. One brittle-ductile shear zone at 178.05 m ( $322^\circ/88^\circ$ ) –178.27 m ( $331^\circ/84^\circ$ ) and one breccia at 178.39 m ( $332^\circ/82^\circ$ ) –178.74 m ( $326^\circ/82^\circ$ ). Fracture apertures generally 0.5 to 2 mm, with one example of 8 mm. Locally weak oxidation. At 179.0 m borehole length there is one narrow low resistivity anomaly, one caliper anomaly and a minor but distinct fluid temperature anomaly, that in combination indicate the occurrence of water bearing fractures. Metagranite-granodiorite (101057), pegmatitic granite (101061). Confidence level = 3.

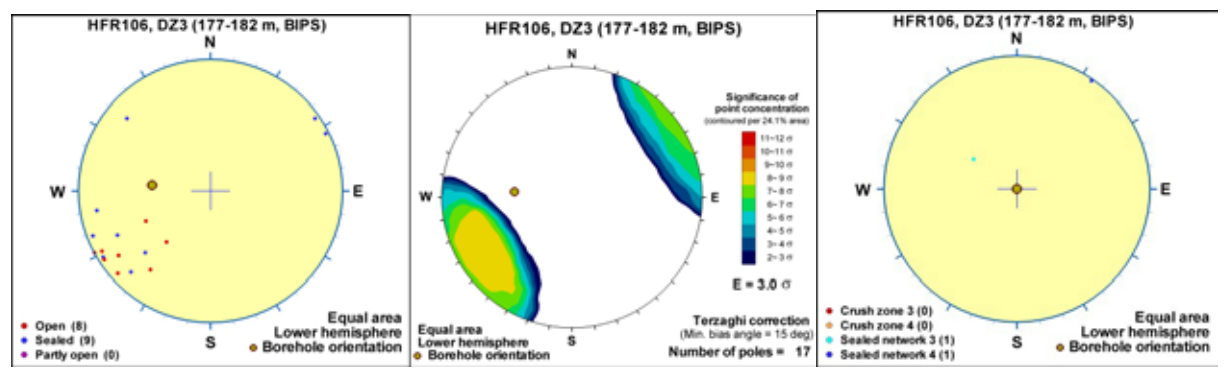
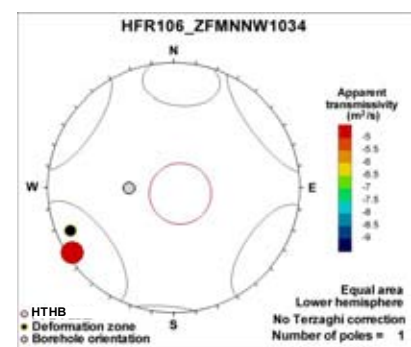
One flow anomaly at 177.3–178.5 m. The transmissivity of the section is very high,  $2 \cdot 10^{-5} \text{ m}^2/\text{s}$ .

### Hydraulic data

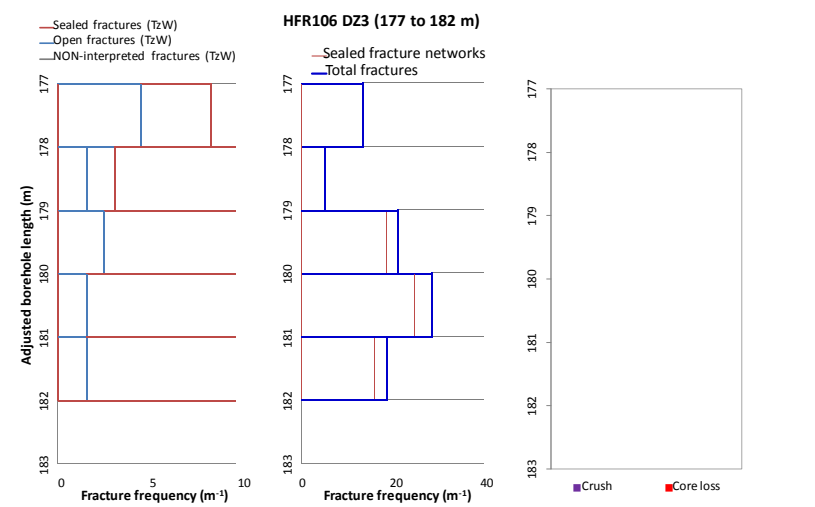
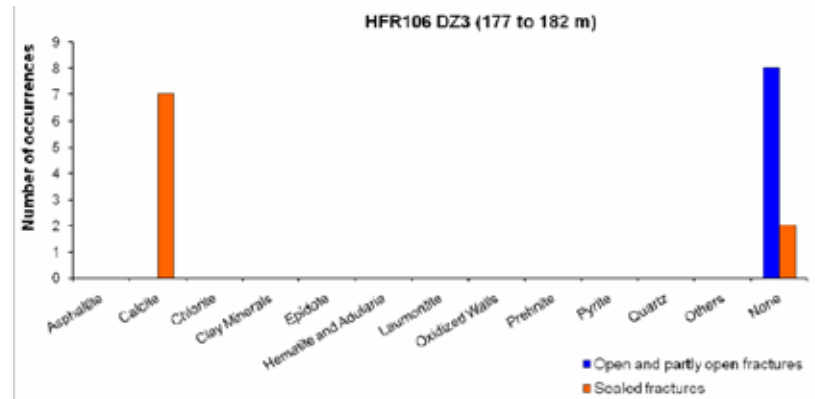
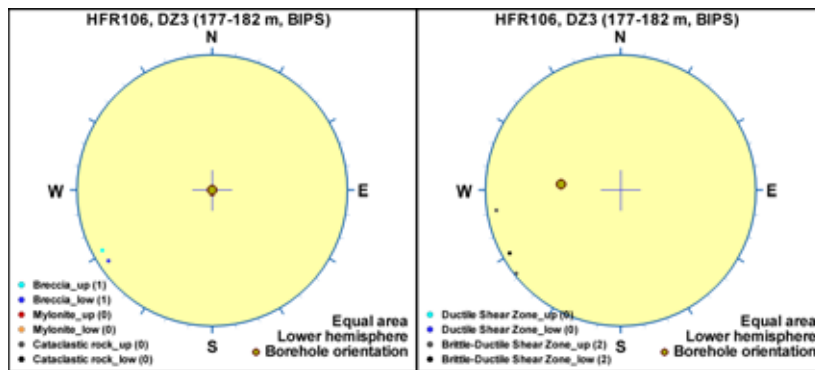
$$T = 2.10 \cdot 10^{-5} \text{ m}^2/\text{s}$$

$$\text{Log } T_0 = -4.1$$

Distinct, high-transmissive HTHB with an estimated orientation parallel to the zone. Taken as key evidence for the Northern Belt characteristics. Estimation of HTHB orientation is highly uncertain.



### Borehole intersections for ZFMNNW1034



BH	Geometrical Intercept		Target intercept	
	Sec_up BH length (m) [z (-m)]	Sec_low BH length (m) [z (-m)]	Sec_up BH length (m) [z (-m)]	Sec_low BH length (m) [z (-m)]
KFR101	8.42 [4.50]	79.85 [62.90]	13.72	88

## Borehole intersections for ZFMNNW1034

**SHI DZ1 13.72–88 m:** Increased frequency of open fractures, sealed fracture networks and especially sealed fractures. Occasional slickensides. Fractures aperture up to 1.5 mm. Locally faint to medium oxidation. Several minor intervals (< 1 dm) of breccias, cataclasites, mylonite and brittle-ductile shear zones. Predominant minerals in sealed fractures are calcite, laumontite, chlorite, quartz and epidote, and in open fractures are calcite, chlorite, clay minerals, laumontite and pyrite. Decreased resistivity in the section c. 30–50 m and one distinct caliper anomaly at c. 33 m. The magnetic susceptibility is increased along the entire interval defining the deformation zone. Moderately foliated metagranite-granodiorite (101057), amphibolite (102017), pegmatitic granite (101061) and felsic to intermediate metavolcanic rock (103076). Confidence level = 3.

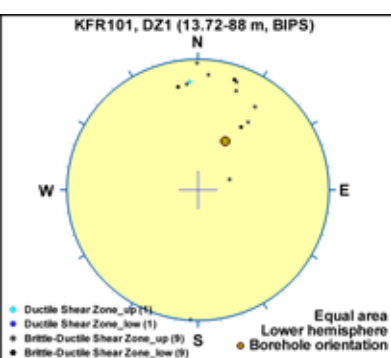
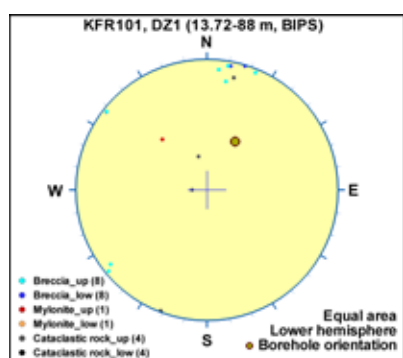
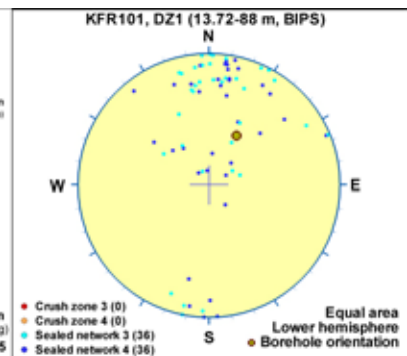
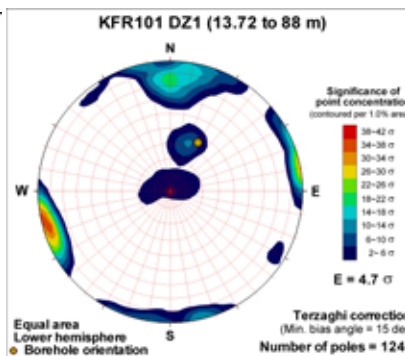
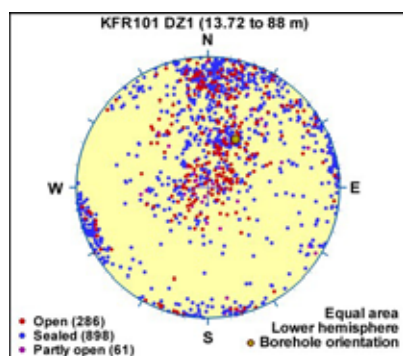
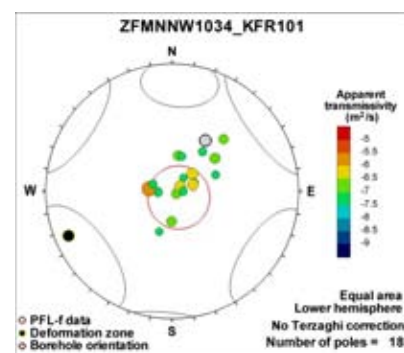
Increased frequency of flow anomalies in the section 14–65 m but no flow anomalies below 65 m. The total transmissivity of the interval is quite high (about  $5 \cdot 10^{-6} \text{ m}^2/\text{s}$  if the dominating flow at the lower edge of the casing is removed). The caliper anomaly at c. 33 m corresponds to a single high-transmissive flow anomaly.

### Hydraulic data

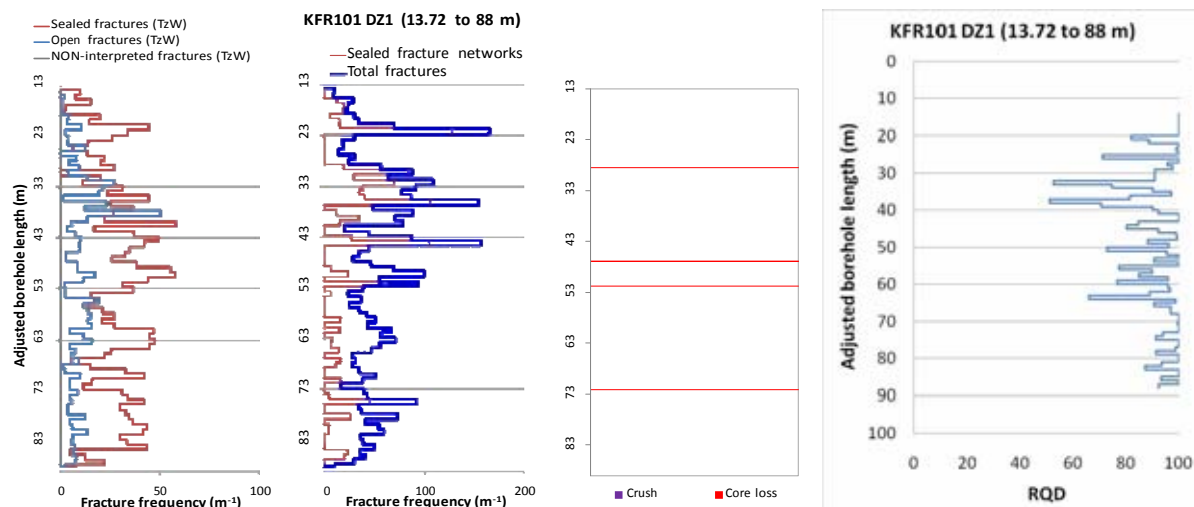
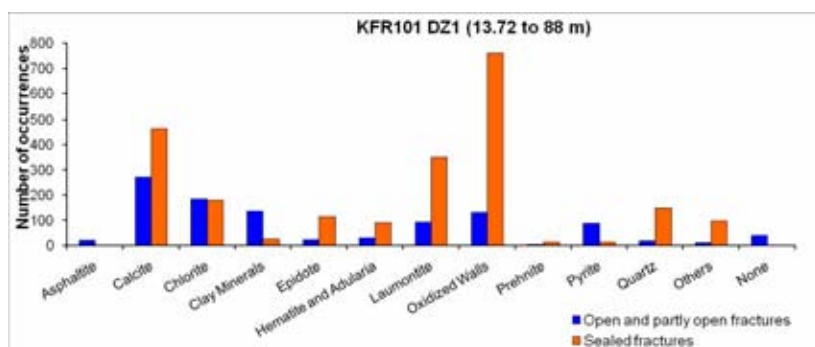
$$T = 4.97 \cdot 10^{-6} \text{ m}^2/\text{s}$$

$$\text{Log } T_0 = -5.2$$

Several sub-horizontal to gently dipping PFL-f, which is typical of the shallow rock.



### Borehole intersections for ZFMNNW1034



### Borehole intersections for ZFMNNW1034

BH	Geometrical Intercept		Target intercept	
	Sec_up BH length (m) [z (-m)]	Sec_low BH length (m) [z (-m)]	Sec_up BH length (m) [z (-m)]	Sec_low BH length (m) [z (-m)]
KFR106	200.93 [187.19]	271.05 [252.67]	256	266

**SHI DZ7 256–266 m:** Increased frequency of sealed and locally open fractures. One crush at 263.16–263.31 m, and one breccia at 263.29 m (294°/55°) – 263.91 m (327°/70°). Fracture apertures generally 0.5 mm or less, locally up to 3 mm. Locally faint to weak oxidation, faint argillization and faint epidotization. Dominating minerals in sealed fractures are calcite, chlorite, clay minerals, oxidized walls, quartz, epidote and hematite; in open fractures clay minerals, calcite, chlorite and hematite. Three radar reflectors of which one is oriented at 262 m (330°/81°). Significantly decreased bulk resistivity, one significant caliper anomaly and a minor, but distinct fluid temperature anomaly. Metagranite-granodiorite (101057) and pegmatitic granite (101061). Confidence level = 3.

One high-transmissive flow anomaly at 262.7 m. The transmissivity of the section is  $8 \cdot 10^{-6} \text{ m}^2/\text{s}$ .

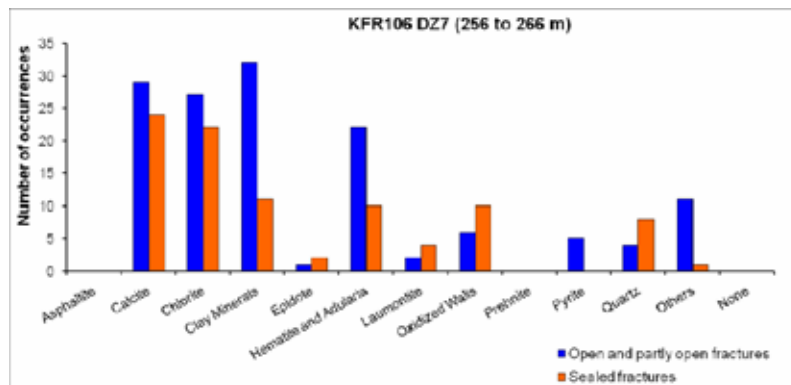
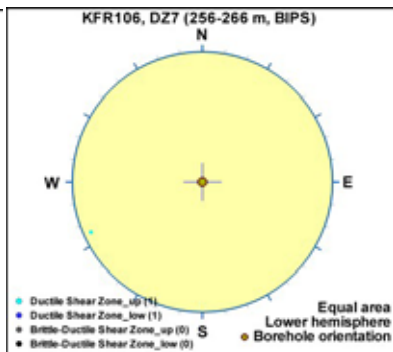
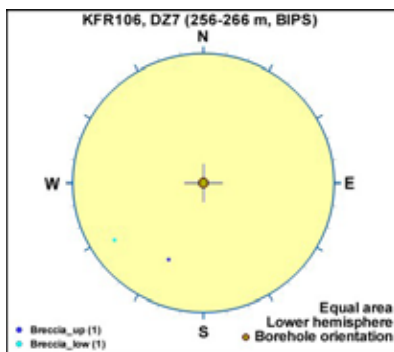
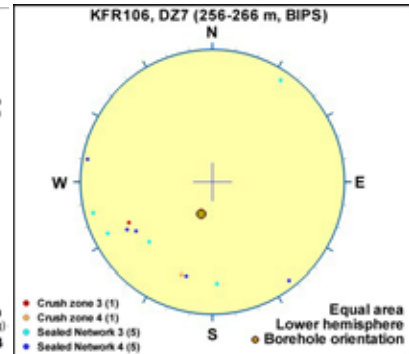
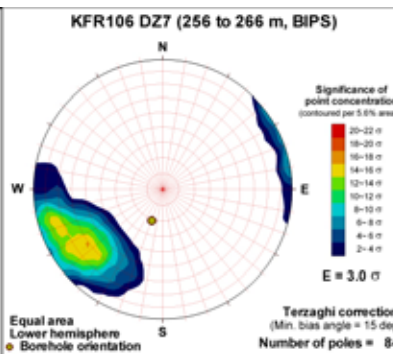
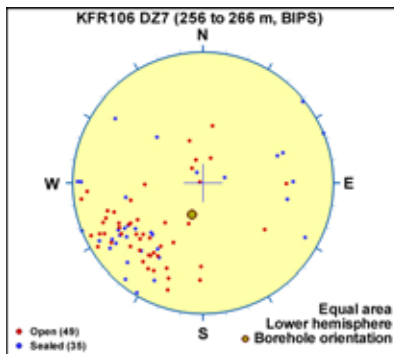
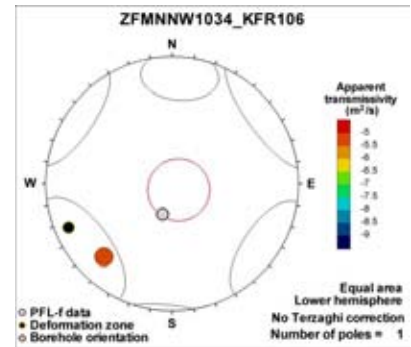
## Borehole intersections for ZFMNNW1034

### Hydraulic data

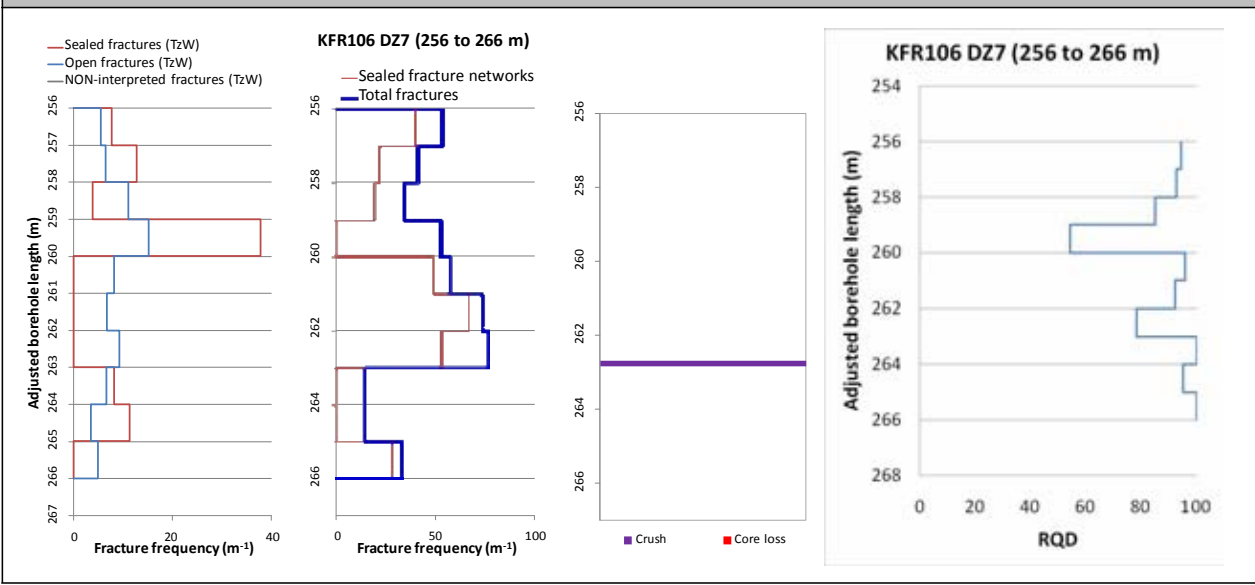
$$T = 7.60 \cdot 10^{-6} \text{ m}^2/\text{s}$$

$$\text{Log } T_0 = -4.1$$

Single, distinct, high-transmissive PFL-f parallel to the zone. Taken as key evidence for the Northern Belt characteristics.



### Borehole intersections for ZFMNNW1034

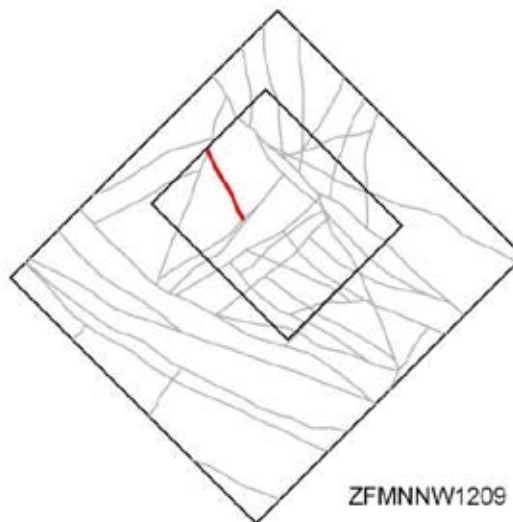




## Deformation zone ZFMNNW1209

### Borehole and tunnel intersections (metres along borehole/tunnel)

KFR35: 32.7–70 m (DZ1 32.7–70 m)  
 DT: 0+930 (tDZ59 0+930)  
 BT: 0+893  
 1 BTF: 0+100 (tDZ59 0+100)  
 2 BTF: 0+078 to 0+080 (tDZ59 0+080 and tDZ126 0+078)  
 BLA: 0+055 to 0+060 (tDZ59 0+060 and tDZ126 0+055)  
 BMA: 0+030 (tDZ59 0+030)



### Deformation style, alteration and geometry

**Deformation style:** Brittle, including minor cohesive breccias and cataclasites present in KFR35 DZ1.

**Alteration:** Locally red-stained bedrock with fine-grained hematite dissemination.

**Strike/dip (span) right-hand-rule:** 151 / 83 ( $\pm 10$  /  $\pm 10$ )

**Trace length at ground surface (span):** 341 m (340–400 m)

**Model thickness (span):** 18 m (2–18 m)

**Confidence in existence:** High

### Modelling procedure:

This zone corresponds to zone 6 in earlier SFR models (see, for example, Axelsson and Hansen 1997/). It was renamed ZFMNNW1209 in the Forsmark stage 2.2 model /Stephens et al. 2007/. In the same manner as that carried out in Forsmark stage 2.2 /Stephens et al. 2007/, the zone has essentially been adopted from the earlier geological model for SFR by /Axelsson and Hansen 1997/. The surface position is based on a combination of magnetic lineament and tunnel mapping results. The zone is crossed by a single seismic refraction profile /Keisu and Isaksson 2004/. However, it does not have a seismic refraction anomaly associated with it, probably due to its diffuse character.

The extent of the zone at the ground surface is based on a modification to the Forsmark stage 2.3 magnetic lineament MFM3114G /Isaksson et al. 2007/. A further extension to the south-east was examined. However, although possible correlation is suggested by the fracture patterns of KFR104 DZ5 and KFR105 DZ4 and DZ5, the resulting projected surface trace does not fit well with the magnetic data. In addition, HFR102 should intercept the zone at an intermediary position and there is no PDZ recorded in this BH. For this reason, the southern extension is possible, but is only weakly supported and has not been implemented.

Based on inspection of the tunnel mapping results and their visualization in RVS, the existence of this apparently „well established“ zone reported in /Axelsson and Hansen 1997/ and earlier reports is difficult to follow as a single discrete structure. It is judged most likely to be a group of loosely associated thin discontinuous structures with a similar trend spread out over a thickness of around 18 m. The evidence quoted in the northernmost BMA cavern by /Axelsson and Hansen 1997/ shows a structure that dips steeply (c. 70°) to the NE, whereas indicators in the other caverns (BLA, 2BTF and 1 BTF) are more consistent and dip steeply to the west. Modelling work has adopted the steep dip to the west. The existence of the same structure in the DT is uncertain, while extension of the DT structure as a fracture swarm along the BT is present but was discounted in earlier work /Axelsson and Hansson 1997/.

The modelled geometry has been kept simple based on a partial agreement with the magnetic lineament MFM3114G, three control points from BLA, 2BTF and 1BTF, along with the SHI DZ1 in KFR35, giving a dip of 83° towards west. The zone has been modelled with a thickness of 18 m to correlate with the thickness indicated by the geological SHI DZ1 in KFR35 and the geometrical spread of the individual, gouge-filled fractures. Individually mapped tunnel locations yield earlier recorded thicknesses between 0.5 and 2 m. Similar and parallel, clay-filled fractures have been reported to the north of the defined zone /Christiansson 1986/. As pointed out in the main text in this report, estimates of zone thickness in the earlier SFR work were underestimated according to current SKB methodology.

## Deformation zone ZFMNNW1209

### Hydraulic interpretation

Hydraulic width: 15.8 m

No of intercepts: 2

$T_{\text{eff}}(0)$ :  $1.28 \cdot 10^{-6}$  m<sup>2</sup>/s

Log  $T_{\text{eff}}(0)$ : -5.9,  $\sigma = (0.55)$

**Calculation procedure:**  $T_{\text{eff}}(0)$  taken as average from both 2 intercepts. The zone is interpreted as highly heterogeneous, and therefore it is conditioned also at its intersections with the four disposal facilities.

### Fractures in the deformation zone

#### General characteristics

**Fracture orientation:** No data

**Fracture frequency:** See KFR35 DZ1 for general indication of fracture frequency (no Terzaghi correction)

**Fracture filling mineralogy:** See KFR35 DZ1 below

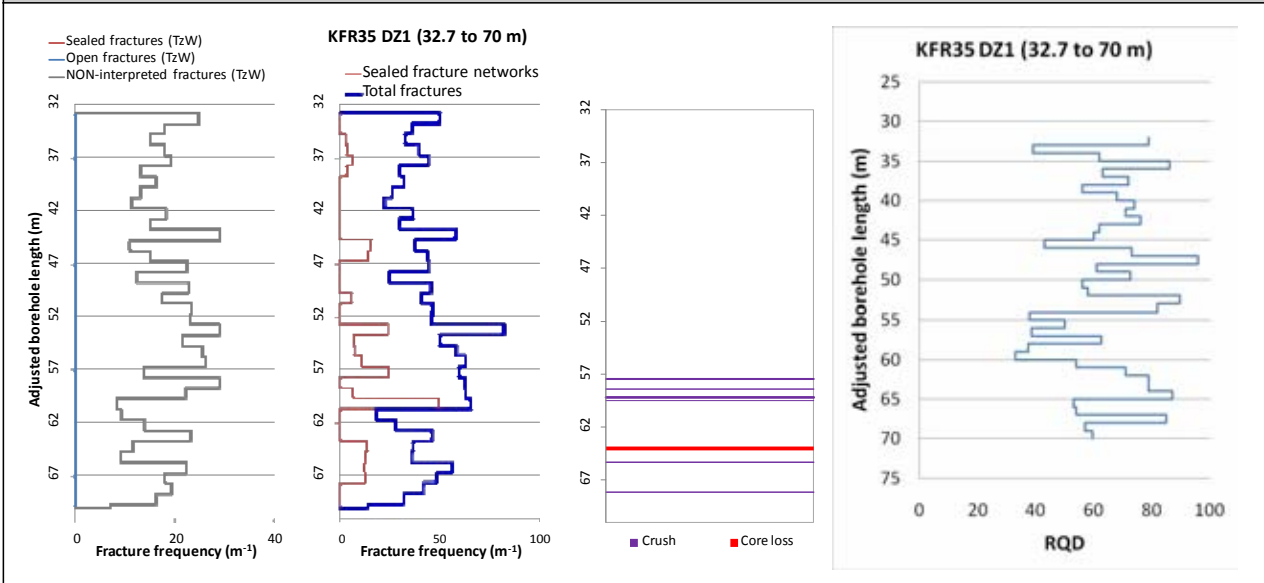
KFR35 52–70 m



## BOREHOLE AND TUNNEL INTERCEPT DETAILS

Borehole intersections for ZFMNNW1209																																
BH	Geometrical Intercept		Target Intercept																													
	Sec_up BH length (m) [z (-m)]	Sec_low BH length (m) [z (-m)]	Sec_up BH length (m) [z (-m)]	Sec_low BH length (m) [z (-m)]																												
KFR35	32.90 [20.65]	71.04 [50.49]	32.7	70																												
<p><b>SHI DZ1 32.7–70 m:</b> Increased frequency of broken and unbroken fractures and sealed networks. Six crushed intervals in the lower part of the section (57.37–68.15 m). Three intervals at 44.83–46.07, 55.92–56.01 and 60.37–61.60 m include fault breccias and cataclasite. Predominant fracture minerals are adularia, calcite and quartz. <math>\alpha</math>-angles are generally small to moderate (21–61°). Asphaltite, typically associated with calcite, is more or less limited to this section. Occurrence of a black unknown mineral that resembles asphaltite is registered in the interval between 20.1 and 71.6 m. Locally faint to weak oxidation. One minor core loss at 63.84–64.15 m. Pegmatitic granite (101061) with occurrences of felsic to intermediate metavolcanic rock (103076), fine- to medium-grained granite (111058) and strongly foliated metagranite-granodiorite (101057). Confidence level = 3.</p> <p>Hydraulic conductivity (measured in 3-m sections) above the lower measurement limit (<math>1.7 \cdot 10^{-8}</math>) in the intervals 36–39 and 54–63 m. Hydraulic conductivity slightly above <math>1 \cdot 10^{-6}</math> m/s at 54–60 m.</p> <p><b>Hydraulic data</b>  <math>T = 1.09 \cdot 10^{-5} \text{ m}^2/\text{s}</math>  <math>\text{Log } T_0 = -4.8</math></p> <p>Supported by 3 packer data above detection limit, 54 to 63 m BHL. The interval is also intersected by the possible stress-release structure SBA7.</p>																																
<p style="text-align: center;"><b>KFR35 DZ1 (32.7 to 70 m)</b></p> <table border="1"> <caption>Approximate data from the bar chart</caption> <thead> <tr> <th>Mineral</th> <th>Number of occurrences</th> </tr> </thead> <tbody> <tr><td>Asphaltite</td><td>~20</td></tr> <tr><td>Calcite</td><td>~450</td></tr> <tr><td>Chlorite</td><td>~100</td></tr> <tr><td>Clay Minerals</td><td>~150</td></tr> <tr><td>Epidote</td><td>~10</td></tr> <tr><td>Hematite and Adularia</td><td>~200</td></tr> <tr><td>Laumontite</td><td>~10</td></tr> <tr><td>Oxidized Walls</td><td>~50</td></tr> <tr><td>Prehnite</td><td>~20</td></tr> <tr><td>Pyrite</td><td>~20</td></tr> <tr><td>Quartz</td><td>~100</td></tr> <tr><td>Others</td><td>~50</td></tr> <tr><td>None</td><td>~50</td></tr> </tbody> </table>					Mineral	Number of occurrences	Asphaltite	~20	Calcite	~450	Chlorite	~100	Clay Minerals	~150	Epidote	~10	Hematite and Adularia	~200	Laumontite	~10	Oxidized Walls	~50	Prehnite	~20	Pyrite	~20	Quartz	~100	Others	~50	None	~50
Mineral	Number of occurrences																															
Asphaltite	~20																															
Calcite	~450																															
Chlorite	~100																															
Clay Minerals	~150																															
Epidote	~10																															
Hematite and Adularia	~200																															
Laumontite	~10																															
Oxidized Walls	~50																															
Prehnite	~20																															
Pyrite	~20																															
Quartz	~100																															
Others	~50																															
None	~50																															

### Borehole intersections for ZFMNNW1209



### Borehole intersections for ZFMNNW1209

BH	Geometrical Intercept		Target Intercept	
	Sec_up BH length (m) [z (-m)]	Sec_low BH length (m) [z (-m)]	Sec_up BH length (m) [z (-m)]	Sec_low BH length (m) [z (-m)]
KFR33	46.19 [26.87]	114.64 [74.24]	–	–

**Comment:** /Axelsson and Hansen 1997/ approximate position of correlation was 465 m level. /Carlsson et al. 1986/ quote direct BH lengths and these have been judged a more reliable indicator of the zones interpreted position in the borehole (67–72 m). They describe the character in terms of mylonitization, crushed rock, highly fractured and alteration.

#### Hydraulic data

$$T = 6.00 \cdot 10^{-8} \text{ m}^2/\text{s}$$

$$\text{Log } T_0 = -7$$

The only data above detection limit in the interval are assigned to the possible stress-release structure SBA7. Remaining data below detection limit ( $6.00 \cdot 10^{-8} \text{ m}^2/\text{s}$ ).

### Tunnel intersections for ZFMNNW1209

Tunnel	Geometrical Intercept		Target Intercept	
	Start ch.(m)	End ch. (m)	Start ch.(m)	End ch. (m)
DT	0+920	0+945	0+930	0+930

**Comment:** Target intercept defined by tDZ59 in Appendix 2.

1/920 Sheet fractured rock. Shotcrete before mapping /Carlsson et al. 1985/

**Tunnel intersections for ZFMNNW1209**

Tunnel	Geometrical Intercept		Target Intercept	
	Start ch.(m)	End ch. (m)	Start ch.(m)	End ch. (m)
BT	0+885	0+907	0+893	0+893

**Comment:** Additional possible low confidence observation based on detailed drawing –09 /Christiansson and Bolvede 1987/

5/890 to a lesser degree sheet fractured rock /Carlsson et al. 1985/

NBT	0+000	0+010	-	-
-----	-------	-------	---	---

**Comment:**

1 BTF	0+090	0+117	0+100	0+100
-------	-------	-------	-------	-------

**Comment:** Target intercept defined by tDZ59 in Appendix 2.

2 BTF	0+070	0+090	0+078	0+080
-------	-------	-------	-------	-------

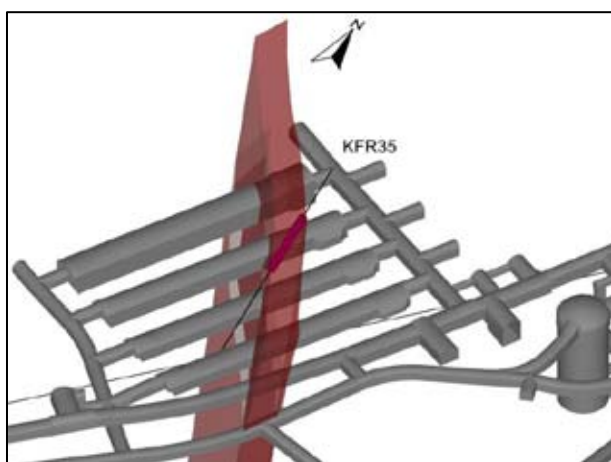
**Comment:** Target intercept defined by tDZ59 and tDZ126 in Appendix 2.

BLA	0+048	0+068	0+055	0+060
-----	-------	-------	-------	-------

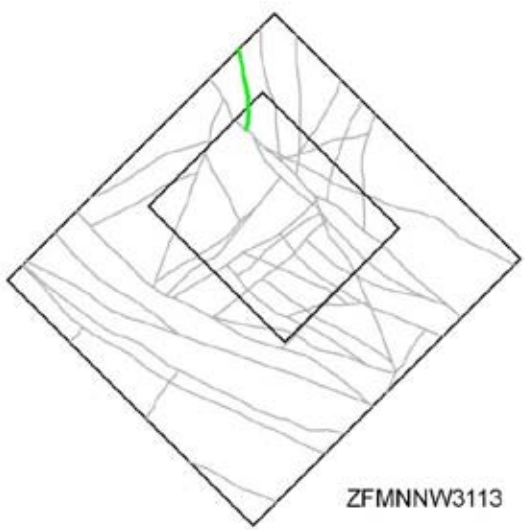
**Comment:** Target intercept defined by tDZ59 and tDZ126 in Appendix 2.

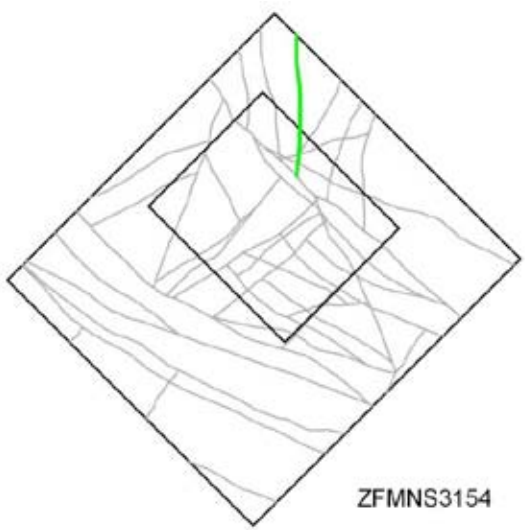
BMA	0+030	0+055	0+030	0+030
-----	-------	-------	-------	-------

**Comment:** Target intercept defined by tDZ59 in Appendix 2.



ZFMNNW1209 crossing the rock caverns and intercepted by KFR35 as it appears in the model (left) and the original overview mapping /Christiansson and Bolvede 1987/. The zone is modelled with a thickness of 18 m based on KFR35 SHI.

<b>Deformation zone ZFMNNW3113</b>	
<p><b>Borehole and tunnel intersections (metres along borehole/tunnel)</b></p> <p>None</p>	
<p><b>Deformation style, alteration and geometry</b></p> <p><b>Deformation style:</b> No data</p> <p><b>Alteration:</b> No data</p> <p><b>Strike/dip (span) right-hand-rule:</b> 173 / 90 (170–180 / ±10)</p> <p><b>Trace length at ground surface (span):</b> 376 m (360–380 m)</p> <p><b>Model thickness:</b> 5 m (1% default)</p> <p><b>Confidence in existence:</b> Medium</p>	
<p><b>Modelling procedure:</b> The position of the zone at the ground surface is based on magnetic lineament MSFR08079 in SFR model version 1.0, being a very minor revision of lineament MFM3113G in Forsmark stage 2.3 /Isaksson et al. 2007/. The earlier number has been maintained for traceability purposes in different lineament interpretations. The modelled thickness and dip are default values.</p>	
<b>Hydraulic interpretation</b>	
<p><b>Hydraulic width:</b> 3.6 m</p> <p><b>No of intercepts:</b> None</p> <p><b>T<sub>eff</sub>(0):</b> <math>1.76 \cdot 10^{-8} \text{ m}^2/\text{s}</math></p> <p><b>Log T<sub>eff</sub>(0):</b> -7.8, <math>\sigma=(0.55)</math></p> <p><b>Calculation procedure:</b> Taken from SDM-Site Forsmark, pooled average of NNW group.</p>	
<b>Fractures in the deformation zone</b>	
<b>General characteristics</b>	
<p><b>Fracture orientation:</b> No data</p> <p><b>Fracture frequency:</b> No data</p> <p><b>Fracture filling mineralogy:</b> No data</p>	

<b>Deformation zone ZFMNS3154</b>	
<p><b>Borehole and tunnel intersections (metres along borehole/tunnel)</b></p> <p>None</p>	
<p><b>Deformation style, alteration and geometry</b></p> <p><b>Deformation style:</b> No data</p> <p><b>Alteration:</b> No data</p> <p><b>Strike/dip (span) right-hand-rule:</b> 180 / 90 (<math>\pm 5</math> / <math>\pm 10</math>)</p> <p><b>Trace length at ground surface (span):</b> 757 m (500–760 m)</p> <p><b>Model thickness:</b> 10 m (1% default)</p> <p><b>Confidence in existence:</b> Medium</p>	
<p><b>Modelling procedure:</b> The position of the zone at the ground surface is based on the magnetic lineament MFM3154G /Isaksson et al. 2007/. This lineament was subsequently broken up and modelled at a higher resolution as lineaments MSFR08012, MSFR08013, MSFR08014 and MSFR08015 during SFR model version 1.0. The SFR model version 1.0 interpretation is considered as equally valid as the earlier stage 2.3 interpretation. However, the latter suits more favourably the DZ modelling resolution in the SFR regional model and, for this reason, the earlier name has been maintained. Forward modelling of magnetic data along profiles 5 and 6 (see Appendix 6) supports the earlier assumed vertical dip of the zone. The modelled thickness and dip of the zone are default values.</p>	
<b>Hydraulic interpretation</b>	
<p><b>Hydraulic width:</b> 7.2 m</p> <p><b>No of intercepts:</b> None</p> <p><b><math>T_{\text{eff}}(0)</math>:</b> <math>3.74 \cdot 10^{-5} \text{ m}^2/\text{s}</math></p> <p><b>Log <math>T_{\text{eff}}(0)</math>:</b> <math>-4.4</math>, <math>\sigma = (0.55)</math></p> <p><b>Calculation procedure:</b> Assumed similar to ZFMNNW1034, based on location and orientation.</p>	
<b>Fractures in the deformation zone</b>	
<b>General characteristics</b>	
<p><b>Fracture orientation:</b> No data</p> <p><b>Fracture frequency:</b> No data</p> <p><b>Fracture filling mineralogy:</b> No data</p>	

## DFN parameters suggested for usage in the SFR extension project

The suggested hydrogeological DFN model parameterisation for PSU modelling purposes is presented in Table A5-1. The depth trend in flowing fracture characteristics is numerically represented by dividing the SFR model domain into three depth intervals: the shallow, repository, and deep domains (Table A5-1). Five fracture sets are parameterised in each of these depth domains. Three steeply dipping fracture sets are referred to by strike: East-West (EW), Northwest (NW), and Northeast (NE). Two fracture sets are referred to by dip: gently dipping (Gd) and subhorizontal (Hz). The orientation model for the fracture sets is defined by mean poles and the spread around the mean pole. Set mean poles are determined as trend (Tr) and plunge (Pl), and the dispersion around the mean pole is defined by the univariate Fisher concentration parameter,  $\kappa$ . It is noted that these names are symbolic and that the magnitudes of the Fisher concentration parameters are moderate, which means there is an overlap between the sets in a probabilist sense.

The fracture intensity,  $P_{32}$  ( $m^2/m^3$ ), is defined as fracture area per volume for a given interval in fracture size. The intensity provided in Table A5-1 refers to the size range bounded by the minimum fracture radius,  $r_0$  (m), assumed to be equal to the borehole radius (c. 0.038 m), and the maximum fracture radius,  $r_{max}$  (m), corresponds to the resolution level of the deterministic geological model /Curtis et al. 2010/ (c. 169 m). Fracture size is assumed to follow the power-law distribution, defined by the scaling exponent,  $k_r$ . The parameter  $k_r$  determines the proportion between small and large fractures and is relatively uncertain, as it cannot be directly measured from borehole investigations. It has a strong influence on the connectivity of the fracture system, and is therefore estimated by means of a connectivity analysis approach (see /Öhman and Follin 2010b/). The connectivity analysis relies on an assumed relationship between fracture transmissivity,  $T$  ( $m^2/s$ ), and fracture radius,  $r$  (m). A direct relationship, i.e. without a random component, was assumed of the form  $T = a \cdot r^b$ , where  $a$  is the transmissivity of a one-metre radius fracture and  $b$  is a scaling exponent.

Deterministically modelled deformation zones provide an additional source of information for the size distribution of steeply dipping sets. This alternative method is referred to as the tectonic continuum approach (Table 1; details in /Öhman and Follin 2010b/).

**Table A5-1. Hydrogeological DFN model parameterisation based on connectivity analysis and tectonic continuum, respectively /Öhman et al. 2012/.**

		Connectivity analysis						Tectonic continuum			
Set intensity <sup>2)</sup>		Orientation <sup>3)</sup>				Shape	( $T = a r^b$ )	Shape	(T = a r <sup>b</sup> )		
<b>Shallow domain (z &gt; 60 m RHB 70)</b>											
Set	$P_{32}$	Tr	Pl	Fisher $\kappa$	$k_r$	a	b	$k_r$	a	b	
EW	2.32	4.8	13.9	10.1	3.2 <sup>4)</sup>	$2.1 \cdot 10^{-8}$	1.3	2.694	$1.6 \cdot 10^{-9}$	1.25	
NW	0.99	233.8	7.2	13.7	3.2 <sup>4)</sup>	$5.3 \cdot 10^{-8}$	1.3	2.626	$3.3 \cdot 10^{-9}$	1.2	
NE	1.31	125.4	1.8	13.7	3.45	$1.8 \cdot 10^{-8}$	1.0	2.778	$1.2 \cdot 10^{-9}$	1.0	
Gd	1.79	339.1	87	7.2	2.79	$2.1 \cdot 10^{-8}$	1.09	2.79	$2.1 \cdot 10^{-8}$	1.09	
Hz	0.96	127.5	83.7	41.9	2.6	$9.8 \cdot 10^{-8}$	1.32	2.60	$9.8 \cdot 10^{-8}$	1.32	
<b>Repository domain<sup>1)</sup> (<math>60 \geq z &gt; 200</math> m RHB 70)</b>											
Set	$P_{32}$	Tr	Pl	Fisher $\kappa$	$k_r$	a	b	$k_r$	a	b	
EW	1.44	4.8	13.9	10.1	3.1 <sup>4)</sup>	$2.1 \cdot 10^{-9}$	1.1	2.63	$7.9 \cdot 10^{-11}$	1.4	
NW	0.81	233.8	7.2	13.7	3.0 <sup>4)</sup>	$1.1 \cdot 10^{-8}$	1.1	2.596	$1.3 \cdot 10^{-9}$	1.1	
NE	1.00	125.4	1.8	13.7	3.3 <sup>4)</sup>	$2.2 \cdot 10^{-9}$	1.3	2.752	$8.6 \cdot 10^{-11}$	1.35	
Gd	1.21	339.1	87	7.2	2.72	$4.0 \cdot 10^{-9}$	0.8	2.72	$4.0 \cdot 10^{-9}$	0.8	
Hz	0.95	127.5	83.7	41.9	2.55	$8.5 \cdot 10^{-10}$	1.35	2.55	$8.5 \cdot 10^{-10}$	1.35	



**Deep domain<sup>1)</sup> (200 ≥ z > 1,100 m RHB 70)**

Set	P <sub>32</sub>	Tr	Pl	Fisher κ	k <sub>r</sub>	a	b	k <sub>r</sub>	a	b
EW	1.06	4.8	13.9	10.1	3.2 <sup>4)</sup>	3.6·10 <sup>-9</sup>	1.6	2.585	7.1·10 <sup>-13</sup>	2.5
NW	0.67	233.8	7.2	13.7	3.15 <sup>4)</sup>	4.7·10 <sup>-9</sup>	1.13	2.597	1.5·10 <sup>-10</sup>	1.31
NE	1.03	125.4	1.8	13.7	3.2 <sup>4)</sup>	1.9·10 <sup>-9</sup>	1.0	2.75	1.6·10 <sup>-10</sup>	1.25
Gd	1.49	339.1	87	7.2	2.7	2.7·10 <sup>-10</sup>	1.6	2.7	1.4·10 <sup>-10</sup>	1.7
Hz	0.75	127.5	83.7	41.9	2.75	1.9·10 <sup>-9</sup>	1.15	2.75	1.3·10 <sup>-9</sup>	1.25

<sup>1)</sup> The boundary between the repository and deep domains is changed to -200 m elevation, based on taking data characteristics and borehole coverage into account. In the v. 0.2 model, the boundary was set at -245 m elevation, based on the preliminary geometrical modelling of ZFM871 (SFR geological model v.0.1).

<sup>2)</sup> The intensity of open fractures reflects the size interval  $r_0$  to  $r_{max}$ . The smallest modelled deterministic zones are on the order of 300 m (SFR geologic model v.1.0), corresponding to a radius of 169 m. Stochastic open fractures are therefore assumed to have a maximum radius of  $r_{max} = 169$  m. The smallest fracture modelled is set equal to the borehole radius,  $r_0 = 0.038$  m.

<sup>3)</sup> Global orientation model used for all three depth domains. The same orientation model is used in both the connectivity analysis and the tectonic continuum approach.

<sup>4)</sup> Adjusted  $k_r$ , relative to the preliminary hydro-DFN v. 0.2 /Öhman and Follin 2010b/.

## Final deformation-zone parameterisation

This appendix presents the final parameterisation of deformation-zone transmissivity inside the SFR Regional model domain (Table A6-1). With the exception of ZFM871, the final values are reproduced from Table 3-2 in Öhman et al. (2013). The recommended parameterisation of ZFM871 is presented below.

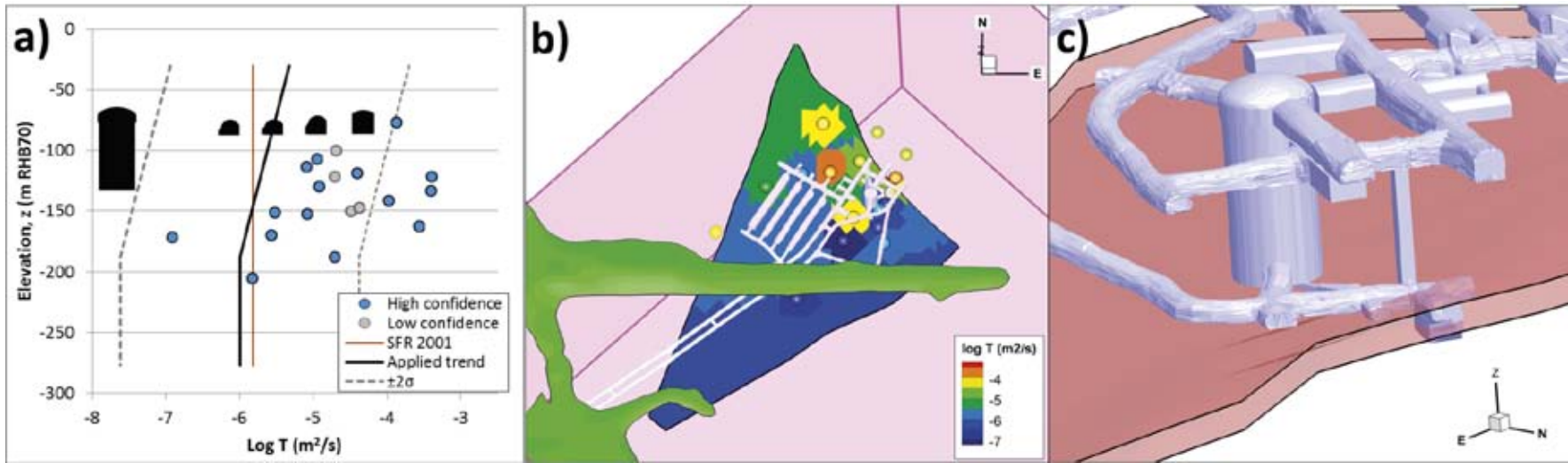
### Representativeness of available data for a parameterisation of ZFM871

Recent interference tests and hydrochemistry data indicate that ZFM871 is highly heterogeneous, with local channelling and compartmentalised volumes of stagnant water. Therefore, historic transmissivity data interpreted from hydraulic tests carried out in boreholes drilled during the construction of SFR probably reflect local hydraulic characteristics. According to Holmén and Stigsson (2001), the measured inflow to the SFR tunnel, where ZFM871 intercepts the tunnel, may be assumed to be a better data source for the average, effective transmissivity value of ZFM871,  $T_{\text{eff}}$ .

### Recommended parameterisation for ZFM871

The following parameterisation approach was applied:

- 1) The depth-dependency model for ZFM871,  $T_{\text{eff}}(z)$ , is no different than the model assumed for all the other zones, see Equation (7-3).
- 2) The effective transmissivity,  $T_{\text{eff}}(0)$ , is defined to match the effective value, as calibrated by Holmén and Stigsson (2001), at the tunnel intercept elevation (c. -140 m). However, a minimum value of  $10^{-6}$  m<sup>2</sup>/s is employed.
- 3) The standard deviation,  $\sigma_{\log T_{\text{eff}}}$ , is based on hydraulic data at borehole intercepts, following the principles of Follin (2008).



**Figure A6-1.** Applied transmissivity parameterisation for ZFM871; a) Applied trend (black line) matched to the effective transmissivity in the SFR 2001 model (brown line), calibrated by /Holmén and Stigsson, 2001/ at the SFR tunnel intercept, and b) triangulated surface representing ZFM871, conditioned at borehole intercepts, and c) close-up of the intercept in the NDB tunnel (c. -140 m). Four intercepts outside the geologically modelled termination of ZFM871 (grey dots marked as “low confidence” discussed in Appendix A of /Öhman et al. 2013/).

**Table A6-1. Final deformation-zone parameterisation inside the SFR Regional model domain.**

Deformation zone	Hydraulic width <sup>1)</sup>	No. intcps <sup>2)</sup>	No. cond. points <sup>6)</sup>	$T_{\text{eff}}(0)^{7)}$ (m <sup>2</sup> /s)	log $T_{\text{eff}}(0)$	Standard deviation $\sigma(\log T_{\text{eff}}(0))^{5)}$	Basis for determining $T_{\text{eff}}(0)$
ZFM871	11.3	19 (4)	15	6.38E-6	-5.19	0.81	
ZFMA1	40.0	None	None	1.59E-5	-4.8	(0.55)	Taken from SDM-Site Forsmark
ZFMB10	7.2	None	None	1.59E-5	-4.8	(0.55)	Assumed equal to ZFMA1 (i.e., taken from SDM-Site Forsmark)
ZFMENE3115	4.8	3	3	3.50E-7	-6.5	0.91	Taken as average of all 3 intercepts.
ZFMENE3135	3.6	None	None	1.92E-7	-6.7	(0.55)	Taken as pooled average of the NNE to ENE set (only based on new data)
ZFMENE3151	3.6	None	None	1.92E-7	-6.7	(0.55)	Taken as pooled average of the NNE to ENE set (only based on new data)
ZFMENE8031	3.6	None	None	1.92E-7	-6.7	(0.55)	Taken as pooled average of the NNE to ENE set (only based on new data)
ZFMENE8034	7.2	None	None	1.92E-7	-6.7	(0.55)	Taken as pooled average of the NNE to ENE set (only based on new data)
ZFMNE0870	12.0	8 (5)	7	5.11E-7	-6.3	0.46	Taken as average of all 8 intercepts. Evaluated transmissivity at intercepts are exaggerated by unfavourable borehole orientations, causing long intercepts.
ZFMNE3112	7.4	4	4	2.67E-7	-6.6	0.62	Taken as average of all 4 intercepts.
ZFMNE3118	6.2	3 (2)	3 (1)	2.38E-7	-6.6	0.29	Taken as average of all 3 intercepts, weighted by low-transmissive tunnel intercept <sup>3)</sup> .
ZFMNE3134	3.6	None	None	1.92E-7	-6.7	(0.55)	Pooled average of the NNE to ENE set (only based on new data)
ZFMNE3137	5.0	4	4	5.48E-8	-7.3	0.30	Taken as average of all 4 intercepts.
ZFMNNE0725	12.0	None	None	1.11E-4	-4.0	(0.55)	Taken from SDM-Site Forsmark
ZFMNNE0869	41.7	4	4	2.72E-5	-4.6	0.28	Taken as average of all 4 intercepts
ZFMNNE2308	15.0	None	None	8.26E-7	-6.1	(0.55)	Taken from SDM-Site Forsmark
ZFMNNE3130	3.6	None	None	1.92E-7	-6.7	(0.55)	Taken as pooled average of the NNE to ENE set (only based on new data)
ZFMNNE3264	7.2	None	None	1.92E-7	-6.7	(0.55)	Taken as pooled average of the NNE to ENE set (only based on new data)
ZFMNNE3265	7.2	None	None	1.92E-7	-6.7	(0.55)	Taken as pooled average of the NNE to ENE set (only based on new data)
ZFMNNE3266	7.2	None	None	1.92E-7	-6.7	(0.55)	Taken as pooled average of the NNE to ENE set (only based on new data)
ZFMNNW0999	3.6	0 (1)	None	1.76E-8	-7.8	(0.55)	Rejected intercept. Value taken as pooled average of NNW group in SDM-Site Forsmark
ZFMNNW1034	13.7	3	3	3.74E-5	-4.4	0.27	Taken as average of all 3 intercepts.
ZFMNNW1209	15.8	2	2 (4)	1.28E-6	-5.9	(0.55)	Taken as average of both 2 intercepts. The zone is interpreted as highly heterogeneous.
ZFMNNW3113	3.6	None	None	1.76E-8	-7.8	(0.55)	Taken from SDM-Site Forsmark, pooled average of NNW group
ZFMNS3154	7.2	None	None	3.74E-5	-4.4	(0.55)	Assumed similar to ZFMNNW1034, based on location and orientation.
ZFMNW0002	50.0	1 (2)	1	2.45E-5	-4.6	(0.55)	Rejected intercept. Value taken from SDM-Site Forsmark
ZFMNW0805A	37.6	6 (2)	6	1.83E-5	-4.7	0.55	Taken as average of all 6 intercepts.
ZFMNW0805B	21.7	7 (1)	7 (2)	3.40E-6	-5.5	0.48	Taken as average of 7 intercepts and 2 low-transmissive tunnel intercepts <sup>3)</sup> .

Deformation zone	Hydraulic width <sup>1)</sup>	No. intcps <sup>2)</sup>	No. cond. points <sup>6)</sup>	$T_{\text{eff}}(0)^{7)}$ (m <sup>2</sup> /s)	log $T_{\text{eff}}(0)$	Standard deviation $\sigma(\log T_{\text{eff}}(0))^{5)}$	Basis for determining $T_{\text{eff}}(0)$
ZFMWNW0001	108.0	3 (9)	3	1.32E-4	-3.9	0.56	Taken as average from 3 intercepts: KFR71, HFM34, and KFM11A render $T_{\text{eff}}(0) = 1.3 \times 10^{-3}$ m <sup>2</sup> /s or $\log T_{\text{eff}}(0) = -2.9$ . The value was lowered one order of magnitude as a result of flow simulations.
ZFMWNW0813	72.7	1	1 (1)	1.16E-6	-5.9	(0.55)	KFM11A, weighted by low-transmissive tunnel intercept <sup>3)</sup>
ZFMWNW0835	15.1	1	2	6.30E-6	-5.2	0.71	Taken as average of the 2 intercepts in KFR27
ZFMWNW0836	36.0	0 (2)	None	7.92E-8	-7.1	(0.55)	Two rejected intercepts. Value taken from SDM-Site Forsmark
ZFMWNW1035	10.8	2 (2)	4	1.08E-5	-5.0	0.64	Only two intercepts used: HFM35, HFR105. This renders $T_{\text{eff}}(0) = 1.1 \times 10^{-4}$ m <sup>2</sup> /s or $\log T_{\text{eff}}(0) = -4.0$ . The value was lowered one order of magnitude as a result of flow simulations.
ZFMWNW1056	10.0	None	None	7.92E-8	-7.1	(0.55)	Taken from SDM-Site Forsmark
ZFMWNW3259	49.0	1	1 (1)	5.18E-6	-5.3	(0.55)	KFM11A, weighted by low-transmissive tunnel intercept <sup>3)</sup>
ZFMWNW3262	1.4	2	2	2.80E-5	-4.6	(0.55)	Average of both intercepts
ZFMWNW3267	12.3	2	2	2.13E-7	-6.7	(0.55)	Average of both intercepts.
ZFMWNW3268	3.6	None	None	1.44E-6	-5.8	(0.55)	Taken as pooled average of the WNW to NW set (only based on new data).
ZFMWNW8042	4.3	1	1	1.05E-6	-6.0	(0.55)	Single intercept used. The zone is well-supported by sub-parallel PFL-f data.
ZFMWNW8043	7.2	None	None	3.06E-7	-6.5	(0.55)	Taken as pooled average of the WNW to NW set (only based on new data).

- 1) Average hydraulic thickness calculated as the average true thickness (intersection-angle compensated) of all intercepts. For HCDs without intercepts the hydraulic width is taken as 72% of the geologic envelope, based on pooling of HCDs that have intercepts. For HCDs that exist inside SDM-Site Forsmark and where no additional information has been gained from the SFR investigations, the thickness is taken directly from SDM-Site Forsmark.
- 2) Number of intercepts with hydraulic data that are judged representative for the HCD. The number in brackets indicate that additional intercepts exist, but that hydraulic data are unavailable, or judged to be misleading due to junction with other deformation zones that may dominate.
- 3) Intercepts with the SFR tunnel without record grouting of specific fracture inflow are weighted equal to a single borehole intercept. Such low-transmissive tunnel intercepts were assumed equal to the background conductivity used in /Holmén and Stigsson 2001/ (i.e., the intercept was set to  $T = 6.5 \times 10^{-9}$  m/s multiplied by the hydraulic width).
- 4) Reported transmissivity values in /Holmén and Stigsson 2001/. These values do not refer to  $T_0$ , as no depth trend was implemented in the SFR 2001 model. Approximately 0.4 should be added to these log T-values for direct comparison to the  $T_0$ -concept (i.e., extrapolated from the SFR depth level).
- 5) Following the established SKB methodology /Follin 2008/, the standard deviation in modelled logarithmic transmissivity values is estimated as  $(\log T_{0,\text{max}} - \log T_{0,\text{min}})/4$  (i.e., assuming that the range in evaluated log  $T_0$  corresponds to  $\pm 2\sigma$ ). For zones with less than 3 intercepts, the standard deviation is assumed equal to 0.55 (indicated by parentheses) taken from the average of zones with more than 3 intercepts.
- 6) Number of conditional points for the particular HCD. The number in brackets indicates additional intercepts with the SFR tunnel that have no record of inflow. Low-transmissive tunnel intercepts were set equal to the background conductivity used in /Holmén and Stigsson 2001/ (i.e., set to  $T = 6.5 \times 10^{-9}$  m/s multiplied by the hydraulic width).
- 7) Calculation of ground-surface transmissivity,  $T_{\text{eff}}(0)$ , is described in the comment field. In principle, Equation (7-2) is applied for zones with available intercepts; see Table A-1 and Table A-3 in Öhman et al. (2013). Pooled deformation zone-set statistics, or values from SDM-Site Forsmark, are applied to zones without intercepts. However, ZFMWNW1035, ZFMWNW0001, and ZFM871 have reduced  $T_0$ -values, based on results of Model Exercise M6.